ADVANCED EXERGY ANALYSIS OF HIGH TEMPERATURE FUEL CELL SYSTEMS

Arend de Groot

ADVANCED EXERGY ANALYSIS OF HIGH TEMPERATURE FUEL CELL SYSTEMS

Proefschrift

ter verkrijging van de graad van doctor
aan de Technische Universiteit Delft,
op gezag van de Rector Magnificus prof. dr.ir. J.T. Fokkema
voorzitter van het College voor Promoties,

in het openbaar te verdedigen op maandag 12 januari 2004 om 15:30 uur

door
Arend DE GROOT

werktuigkundig ingenieur
geboren te Apeldoorn

Dit proefschrift is goedgekeurd door de promotoren:
Prof. ir. R.W.J. Kouffeld
Prof. dr. ir. H.J. Veringa

Samenstelling promotiecommissie:

Rector Magnificus,	voorzitter
Prof. ir. R.W.J. Kouffeld,	Technische Universiteit Delft, promotor
Prof. dr. ir. H.J. Veringa,	Universiteit Twente, promotor
Prof. ir. J. Grievink,	Technische Universiteit Delft
Prof. dr. G.G. Hirs,	Universiteit Twente
Prof. dr. ir. J.R. Selman,	Illinos Institute of Technology, V.S.
Prof. dr. ir. J.H. de Wit,	Technische Universiteit Delft
Dr. S.B. van der Molen,	Energieonderzoek Centrum Nederland (ECN), Petten

ir. N. Woudstra heeft als begeleider in belangrijke mate aan de totstandkoming van het proefschrift bijgedragen.

Published by:
the Energy research Centre of the Netherlands (ECN)
Petten, the Netherlands
ECN-R-03-002

Key words:
Fuel cells, modelling, exergy analysis, flow sheeting, system analysis

voor mijn ouders:
Jan P. de Groot en Gerda de Groot-Meijer

The research presented in this thesis was partly funded by the Stichting Technische Wetenschappen (**STW**).

The financial and academic support from the Energy Research Center of the Netherlands (**ECN**) has been instrumental in producing this thesis.

SUMMARY

In this thesis the performance of high temperature fuel cell systems is studied using a new method of exergy analysis. The thesis consists of three parts:

- In the first part a new analysis method is developed, which not only considers the total exergy losses in a unit operation, but which distinguishes between different types of exergy losses;
- The second part describes the development of a fuel cell model. A detailed model is used to determine the relevant aspects of the performance of the fuel cell. Using this knowledge, a simpler model for the off-design performance of a fuel cell is designed for the system calculations.
- In the last part the advanced exergy analysis method is used to compare different high temperature fuel cell system configurations. The focus is on understanding the effect of changes in the conceptual design on the performance of the system. The value of the exergy analysis method is discussed and the main factors influencing the system efficiency are identified.

The fuel cell is a single component in a complex system. As this study, and earlier studies on fuel cell systems show, the design of the fuel cell system largely determines the efficiency of the system. To achieve a high efficiency a high degree of integration is necessary. But a high degree of integration generally tends to make optimisation of systems difficult. The focus of this thesis is on therefore on:

- Identifying how the interaction between subsystems in the fuel cell system affects straightforward optimisation;
- Identifying how exergy analysis can be used in the optimisation process.

Exergy analysis

In the fuel cell system exergy losses in a component or unit operation may be the result of one or more processes with their specific driving forces. In the method developed in this thesis 5 such driving forces are distinguished in the fuel cell system :

- temperature difference → heat transfer;
- pressure difference → mass flow;
- difference in concentration → mixing (isothermal);
- difference in chemical potential → chemical reactions;
- difference in electrical potential → electrical current.

If only one driving force plays a role in a unit operation, calculating the total exergy loss is sufficient. However, if the processes in a unit operation are determined by more than one driving force, it is necessary to determine which part of the total exergy loss can be attributed to each of the separate causes. In this thesis, methods are developed to calculate these losses separately. The first method is 'sequential modelling', where a complex process is considered as a series of process occurring sequentially. For example the combustion process can be considered as a process where in the first step fuel and oxidant are mixed and in the second step reaction takes place. In other cases processes cannot be separated in this way and a more detailed model is required. In the fuel cell system this is the case for the reformer and the fuel cell itself.

The system analysis shows that the losses as a result of heat transfer and the losses as a result of chemical reactions are of particular interest in the fuel cell system. Different graphical methods to analyse these losses are discussed. Diagrams which can be used to analyse the losses as a result of heat transfer are the value and pinch-value diagram. Chemical reactions are more difficult to analyse, because they generally occur simultaneously with other processes as heat transfer, friction and mixing. The concept of the equilibrium temperature is introduced to clarify exergy losses in chemical reactions. Using the equilibrium temperature, makes it possible to visualize the chemical reaction in a 'value diagram' as well. However, this method is useful only for a limited class of reactions and another more general method is developed to visualize the losses in (electro-)chemical reactions in those cases where no chemical equilibrium temperature can be determined. This method considers separately the change in exergy of the process flows and the exergy supplied to the process in the form of heat or power. For both quantities a separate generalized Carnot factor (=exergy/energy ratio) is calculated. Using these Carnot factors, complex processes involving chemical reactions and heat transfer can be represented in a Carnot factor- enthalpy diagram. These diagrams play an important role in the analysis of the losses in the fuel cell system in the system analysis of the fuel cell systems.

Fuel cell modelling

A detailed model for the fuel cell is developed. The model calculates the current density (distribution) along the fuel cell. Other phenomena which are included in the model are the heat transfer in the hardware and from the hardware to the process flow and chemical reactions occurring in the fuel cell. The full concentration and temperature profiles are calculated by the model. The most important output parameters for the system calculations are the compositions and temperatures at the outlet of the fuel cell (cathode and anode).
The detailed fuel cell model is used to analyse several fuel cell configurations and types: MCFC and SOFC, co- and counter-flow, external and internal reforming. The objective is to understand which characteristic parameters have a large influence on the fuel cell performance. This knowledge can be used to simplify the fuel cell model for use in system calculations. Specifically two essential parameters are identified which characterise the temperature distribution in the fuel cell:

- The effective temperature is a measure for the average temperature at which the electrochemical reaction takes place. Analysis of the calculation results of the detailed model shows that the combination of temperature and current density distribution is important. This leads to the definition of the 'effective temperature'.
- The temperature approach is the difference between the maximum temperature in the fuel cell and the outlet temperature of the cathode flow. Because the fuel cell is cooled by the cathode flow, the outlet temperature of the cathode flow determines how much heat can be removed from the fuel cell. The calculations show that, if a maximum temperature is assumed for the hardware, the outlet temperature (i.e. the temperature approach) depends on the operating characteristics (e.g. fuel utilisation, cell voltage).

The temperature approach and the effective temperature are essential parameters because both have a large impact on the system calculations. The temperature approach determines how much air is needed to cool the cell stack. The effective temperature is a measure for the performance of the fuel cell stack.
A simplified model of the fuel cell is developed for the system calculations. The main simplification in the model is that the processes in the fuel cell (electrochemical and chemical reactions) are calculated at a constant temperature. Therefore the simplified model (or isothermal model) does not require iterative procedures to solve for the temperature and

current density distributions. Using the detailed model, the performance of the fuel cell at different off-design conditions (different values of the cell voltage and fuel utilisation) is studied. Subsequently it is shown that using simple correlations for the temperature approach and the effective temperature, the performance predicted with the simplified off-design model, corresponds well with the performance predicted using the detailed model.

Systems analysis
In the last part the calculation results for a large number of SOFC and MCFC system configurations are analysed. The method of detailed exergy analysis, which distinguishes different causes of exergy losses, is used to identify the main mechanisms of losses in the fuel cell system. The most important conclusion is that heat transfer is the dominant cause of exergy losses. The fuel cell generates electrical power and heat. The heat represents a substantial part of the total exergy (power+heat) 'generated'. More heat is generally much available than the amount of heat required in the system (e.g. for reformer steam production or preheating the anode and cathode gas). There is therefore a 'heat surplus' in the system. In both the SOFC and the MCFC systems exergy losses as a result of heat transfer are responsible for approximately half of the exergy losses. To improve the system efficiency, reducing the losses as a result of heat transfer is necessary.
The key components in the fuel cell system are the components in which the fuel is converted: the fuel cell, the reformer and the combustor. The exergy losses in these components are small, but changes in the process within these components have large consequences for the system performance, as the comparison a large number of system configurations shows. Reducing the exergy losses as a result of heat transfer requires optimising the processes in these components.

The detailed analysis of the system calculations in this thesis also leads to a distinction between the intended or primary effect of a change in the process design and the secondary effects. Comparison of the different configurations clearly indicates that even simple changes in process design or changes in process parameters generally result in a number of secondary effects. In many cases the secondary effects largely off-set the primary effect.
It is in identifying the secondary effects that exergy analysis plays an important role. Because the calculated efficiencies are often the cumulative result of a number of different effects, it is difficult to identify what changes occur by considering the energy inputs and outputs. But by determining the exergy losses and comparing the exergy losses in different configurations, it is possible to determine where the changes in the system occur and to quantify them. The method of splitting exergy losses into different types of losses, as introduced in this thesis is a particularly powerful method. Firstly because it makes it possible to detect changes in the process which are more difficult to recognize by considering the total exergy losses. Secondly, by identifying the cause of the losses, it is easier to trace the underlying changes in the process which cause the exergy losses. Understanding how changes in one part of the system affect the system as a whole is the key to optimising the system. Detailed exergy analysis offers a systematic approach to identifying these changes.

TABLE OF CONTENTS

PART III: SYSTEMS ANALYSIS

CHAPTER 1
GENERAL INTRODUCTION

Design and analysis of fuel cell systems

In this thesis the performance of high temperature fuel cell systems is studied using a new method of exergy analysis. The thesis consists of three parts:

- In the first part a new analysis method is developed, which not only considers the total exergy losses in a unit operation, but which distinguishes between different types of exergy losses (**part I: Exergy analysis**);
- The second part describes the development of a fuel cell model. A detailed model is used to determine the relevant aspects of the performance of the fuel cell. Using this knowledge, a simpler model for the off-design performance of a fuel cell is designed for the system calculations (**part II: Fuel Cell Model**).
- In the last part the advanced exergy analysis method is used to compare different high temperature fuel cell system configurations. The focus is on identifying the effect of changes in the conceptual design on the performance of the system. The value of the exergy analysis method is discussed and the main factors influencing the system efficiency are identified (**part III: Systems Analysis**).

Two types of high temperature fuel cells are considered. The molten carbonate fuel cell (MCFC) and the solid oxide fuel cell (SOFC). The operating principle of a fuel cell is simple. The process flows, fuel and air, are supplied separately to the fuel cell. In the fuel cell hydrogen and oxygen from these flows react directly to produce electricity and heat. However, even if the operating principle of the fuel cell is simple, to operate the fuel cell requires a complex system. Feed flows have to be pre-heated to high temperatures (600°C or even 850°C). Components which are harmful for the fuel cell, for example sulphur components, have to be reduced to low levels. On the other hand the reactants, hydrogen and oxygen (and in the case of the MCFC CO_2 as well), should be present in high concentrations to increase the performance of the fuel cell. Pressurisation increases the performance of the fuel cell as well. The fuel cell system should be designed to condition the feed flows in an efficient manner. At the same time achieving a high efficiency for the total system requires effective recovery of energy flows [de Groot, 1998]. For example the heat from the outlet flows is use to heat the feed flows, the power generated by expanding the off-gasses in a pressurized system is used to compress the incoming gas flows and off-gas from the fuel cell can be used to provide heat to the reformer. As a result, the fuel cell becomes part of a complex system of heat exchanges, compressors, reactors and other unit operations.
As this study and earlier studies on fuel cell systems (e.g. [Patel, 1983], [Dicks, 1990]) show, the design of the balance-of-plant largely determines the efficiency of the system. However, a high degree of integration generally makes optimisation of systems challenging. The focus of this thesis is on therefore on identifying how the high degree of integration affects straight-forward optimisation and how exergy analysis can be used in optimising the system.
How should the fuel cell system be designed? The strong interaction between components in the system due to the high degree of integration, makes it difficult to determine on forehand what the optimum configuration of the system will be. The 'simple' approach to optimisation is to carry out a large number of system calculations, in order to determine how each of the relevant parameters and different system configurations will effect the performance of the system. But there are important limitations to this approach in the case of highly integrated

systems. The amount of parameters which can or should be varied is generally large, which makes it impossible to optimize the system fully. Furthermore, input data or correlations used in the system calculation change (for example as a result of developing technology or insights into the technology). The 'empirical approach' offers little knowledge on how the outcome of the optimisation can change and will often require redoing the evaluation with the new data. It is therefore necessary to complement the type of studies indicated above, with studies which focus more fundamentally on understanding the mechanisms which underlie the optimisation of the systems. In this thesis such a detailed analysis is made of high temperature fuel cell systems using exergy analysis. Rather than trying to determine the optimal configuration, the objective of this study is to identify what phenomena influence the optimisation process.

The role of exergy analysis (I)

The concept of exergy analysis is based on the second law of thermodynamics. Although the concept of exergy has been introduced much earlier and its "correct" application has been a source of heated debate, interest in the use of exergy analysis has been boosted in the 90's by the development of flow sheeting programs, which make it possible to calculate the exergy flows and losses in a system in a fairly routine manner. However, although the calculation of exergy flows and losses may be considered standard procedure, it is not always clear how an exergy analysis can contribute to optimising a process. In this thesis the use of exergy analysis as a tool for process optimisation is taken a step further by developing a method which also identifies to which type of irreversibility or irreversibilities each loss can be attributed. By clarifying the causes of the losses, it becomes simpler to assess the way in which the losses can be reduced and the extent to which they can be reduced. In **Chapter 2** the fundamentals of exergy analysis are treated and the correlations are developed for calculating the exergy losses and values. In **Chapter 3** a new method is discussed which distinguishes different causes of exergy losses. Furthermore methods of representing the exergy losses in diagrams are discussed.

The fuel cell model (II)

Although the fuel cell is only one of the components in the fuel cell system, the performance of the fuel cell influences the performance of the total system strongly. However, modelling the fuel cell is complex. A large number of different phenomena occur in the fuel cell: chemical and electrochemical reactions, heat transfer, mass transfer, etc. There is a strong interaction between all processes. For example, all of these processes are influenced strongly by the temperature and on the temperature distribution in the cell. As a result, the rate of the processes occurring in the fuel cell is generally distributed non-uniformly. A detailed model of the fuel cell therefore not only describes the local phenomena in the fuel cell, but also calculates the distribution of the parameters: temperature profiles, concentration profiles, etc. Solving the mathematical model analytically is not possible if the local processes are described in some detail as in the model developed here. In order to solve the fuel cell model a numerical method is required. Such a model is not well suited for carrying out system calculations. System calculations involve highly iterative procedures to calculate all the process flows in the system. Correspondingly, in the course of one system calculation, the fuel cell model is called many times. Use of a detailed model as described above in a system calculation will therefore require extreme calculation times. More fundamentally, convergence of system calculations is always an issue, especially for systems with a high degree of integration as fuel cell systems. Therefore a robust model is required for these type of calculations while the detailed model is very sensitive to variations in input parameters.

For system calculations therefore a highly simplified fuel cell model is required.
In **Chapter 4** the development of a detailed model is described, which can be used to calculate both the output parameters (e.g. outlet concentrations) as the distribution of relevant parameters over the cell (e.g. a current density distribution or temperature profile). In **Chapter 5** the calculation results for this model are discussed for different stack configurations: SOFC and MCFC, external and internal reforming, co-flow and counter-flow. Based on the results of detailed model, in **Chapter 6** such a simplified model is developed, which can be used in the system calculations.

Systems Analysis (III)
The application selected for analysis is natural gas fuelled units for industrial combined heat and power. Natural gas is the most logical fuel for high temperature fuel cell systems because it is widely available primary fuel and can be used in the fuel cell system relatively simple. Natural gas can be used either directly (internal reforming) or by using a reformer to convert the natural gas to hydrogen rich synthesis gas (external reforming). Furthermore, the current electricity generation capacity in the Netherlands is based largely on natural gas.
However, where the economy-of-scale dictates very large scale production for the current state-of-the-art technology (for example gas fired combined steam and gas turbine cycles and coal gasification), the economy of scale is not as strong for the fuel cell system. The efficiencies which are expected for large scale systems (>100 MW) are not much higher than the efficiencies in the 1...2 MW range. Therefore one of the most interesting applications is in the latter range, where the system can be used for combined heat and power. Heat demand in the industry consists primarily of process steam. Therefore the starting points selected for the systems considered in this thesis are:

- natural gas fuelled;
- nominal electrical power: 1 MW
- conditions process steam: 180 °C/10 bar

System calculations have been carried out using the flow sheeting program CYCLE-TEMPO, developed at Delft University of Technology. Two base case configurations (SOFC and MCFC) are discussed in **Chapter 7**. The detailed exergy analysis developed in the first part of the thesis is used to identify which factors limit the system efficiency. In the calculations the detailed fuel cell model developed in second part of the thesis is used to calculate the performance for these base case configurations.
Rather than carry out a large number of calculations for a wide range of applications (the 'empirical approach'), a detailed analysis of a limited number of configurations is carried out. Different configurations for SOFC systems are considered in **Chapter 8**. Several configurations are evaluated to determine how the mayor exergy losses identified in the base case calculations can be reduced: cathode off-gas recycling, pressurising the system, increasing the fuel utilisation and internal reforming are analysed. A similar series of calculations of MCFC systems is discussed in **Chapter 9**. The objective of these calculations and the subsequent analysis is to determine how the major exergy losses identified in the base case systems can be reduced.

PART I:

"Exergy Analysis"

INTRODUCTION I:
THE ROLE OF EXERGY ANALYSIS

The efficiency of a system is the ratio between the useful energy output of the system and the energy input to the system (for example in the form of fuel). The 'balance' of the energy (input minus useful output) leaves the system in a form which cannot be recovered, for example as sensible heat in the cooling water or sensible and latent heat in the flue gas stack. These are the energy losses of the system. The objective of optimising the system is in general to find the system configuration which (taking into account restraints with respect to cost and technical limitations) minimizes the energy losses.
The first law of thermodynamics for a steady-state energy system (*energy in = energy out*) can be used to determine which losses occur in the system: how much heat is lost with the cooling water, how much energy does the flue gas contain. This type of energy analysis considers only the energy flows going in and out of the system: the system is treated as a black-box. Therefore energy analysis is of limited value when it comes to identifying and quantifying the processes within the system which lead to these losses. To learn more of the process within this black-box, it is important to take into account the "quality" of energy. The second law of thermodynamics states that in each energy conversion, as a result of the irreversibility of the process(es), the quality or the value of the energy decreases (although the quantity remains constant in accordance to the first law). The closer a process is to reversibility, the smaller the losses will be. The second law therefore offers a clear objective for optimising the system: minimising the losses as a result of irreversibility.
It turns out to be very useful, in analysing second law losses in technical systems, to use the concept of *exergy* to quantify the value of energy. The exergy of a process flow or energy flow is defined as the amount of power which could be produced from the flow in an ideal technical process. Using the exergy concept in the analysis of the fuel cell systems provides a powerful tool. In the **Chapter 2** some of the basic principles of the concept of exergy and correlations for calculating exergy values and exergy losses will be reviewed shortly. Using these correlations, the exergy losses in all the process steps in the fuel cell system can be determined.
In the ideal energy system no degradation of energy occurs, i.e. the system operates reversibly. However, in any real energy conversion system, a driving force is necessary. For example, heat transfer only occurs as a result of a temperature difference and a mass will only flow from one point to another if there is a difference in pressure. These driving forces are necessary for the process to occur in a finite time interval and geometry, but also introduce irreversibility into the system[a]. In a single process step different types of driving forces may cause the exergy losses. To know how the exergy losses can be reduced, it is essential to know to what extent each of the separate driving forces contributes to the total exergy loss. In **Chapter 3** different types of irreversible processes which play a role in the fuel cell system are identified. Subsequently methods are developed to attribute the loss in each component of the fuel cell system to different types of irreversibilities. Generating this information is useful to focus the exergy analysis more specifically on identifying how the process can be improved, as will be shown in **part III**.

---

[a] In the design of an energy system the size of these driving forces is subject to optimisation. A large driving force will in general lead to compact components and reduced investment cost. But a large driving force will also lead to large losses in the components of the energy system and consequently lower efficiencies.

TABLE OF CONTENTS I

CHAPTER 2
CALCULATING EXERGY LOSSES AND EXERGY FLOWS

2.1 INTRODUCTION

Analysis of energy systems is based on thermodynamics as the study of energy transformations, the conversion of one form of energy into another form. Thermodynamics uses two axioms which are known as the first and second law of thermodynamics. The first law, commonly known as the *law of conservation of energy*, postulates that the change of the (internal) energy of a system, is equal to the net energy supplied to the system. Or for a steady state system (for which the internal energy does not change), that total energy supplied to the system is equal to total energy delivered by the system. Optimising the system therefore focusses on maximising the energy which can used and on minimising the energy "losses" of the system: energy flows which cannot be recovered usefully. First law analysis can identify where in a system these energy losses occur and how they depend on the design of the system. However, where the losses are caused and how the losses can be reduced does not follow from the analysis. To learn more about the process within the system, the analysis should be based on the second law of thermodynamics as well.
The 2nd law of thermodynamics states, that although the amount of energy stays the same in any conversion step, irreversibility of processes always leads to degradation of energy. One of the ways in which the second law can been formulated is: *' work can be completely transformed into heat, but heat can only be transformed partially into work '*. Through the introduction of the concept of entropy it is possible to quantify how large the irreversibility is in a specific process step. For technical systems the loss as a result of irreversibility can be translated to a more practical concept of exergy. The exergy of an energy or process flow is defined as the theoretical amount of work which can be produced by bringing the flow in equilibrium with the surrounding environment in a reversible process. This reflects very well the 'value' which the energy or process flow represents. By calculating the exergy losses it is possible to determine how reversible a process step is. Studying the exergy losses in the fuel cell system makes it possible to determine not only the size of these losses, but also where the losses occur. In this chapter the basic principles and correlations will be treated.

In **Section 2.2** the first and second law of thermodynamics are used to define two concepts: lost work and exergy. Subsequently the calculation of differences in exergy between two thermodynamic states is treated. Because of its importance in the fuel cell systems the exergy losses as a result of (electro-)chemical reactions are treated separately in **Section 2.3**. Both enthalpy and exergy are relative variables, *ie* only the difference in enthalpy or exergy between two states is defined. To be able to define the enthalpy (energy) or exergy of a process flow, it is necessary to define a reference state at which the enthalpy respectively the exergy is equal to zero. The selection of a reference state and the method for calculating absolute values for the enthalpy are treated in **Section 2.4**. The corresponding definition of a reference state for the calculation of exergy values and the calculation of those values is the subject of **Section 2.5**.

2.2 ENERGY AND EXERGY

2.2.1 The first law of thermodynamics: energy balances for closed and open systems

A closed system is a system where no mass is exchanged across the system boundary to or from the surroundings: only energy flows across the boundary can occur. The first law of thermodynamics or the law of 'conservation of energy' applied to a closed system, states the relation between the energy flows to the system and the change of state of that system. A closed system is schematically represented in figure 2.1-a. Energy is always transferred to and from a system in the form of heat (**Q**) or in the form of work (**W**). The first law of thermodynamics for a closed system, states that the total amount of energy does not change in the process. That is, the total energy transferred to a system is equal to the increase of the internal energy of the system. The internal energy of the system in the initial state is indicated with $\mathbf{U}_1$ and in the final state with $\mathbf{U}_2$. The first law or the energy balance for the transition from state 1 to state 2, can than be written as:

$$\mathbf{Q} - \mathbf{W} = \mathbf{U}_2 - \mathbf{U}_1 \qquad (2.1)$$

Here $\mathbf{Q} - \mathbf{W}$ is the total energy supplied to the system and $\mathbf{U}_2 - \mathbf{U}_1$ the change of energy in the system. The sign convention which has been used in the equation and in figure 2.1 is that heat **Q** is considered positive if transferred to a system and work **W** is considered positive if performed by the system[b]. This sign convention will be used consistently in this thesis.
In a fuel cell system the components (heat exchangers, pumps, reactors) are not closed systems but open systems, in which mass is transferred to and from the system. The schematic representation of such a system is given in figure 2.1-b.

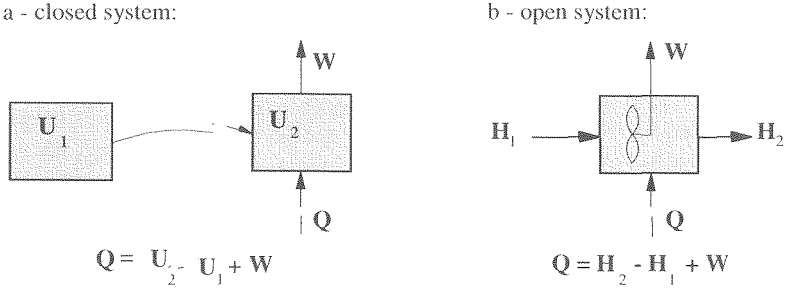

Figure 2.1: Energy balances for a closed system and an open system

Only steady-state systems are considered. The first law applied to an open steady-state system does not consider the change in energy between two moments in time ($t_1 \rightarrow t_2$), as in the closed system, but the change in energy of the process flows between inlet (1) and outlet (2). The energy of the process flows consists of the internal energy U. Other types of energy may be relevant as well, e.g. the kinetic energy of the process flow or the potential energy if the differences in height are significant. However, for the type of system which will be considered the kinetic and potential energy can be neglected. The change in energy of the

[b] This sign convention is logical for cycles which use heat to produce power (power plants, gas turbines). As power generation is the main aim of a fuel cell system this convention is used. However, other sign conventions are used in other areas.

process flows is therefore $\mathbf{U}_2 - \mathbf{U}_1$.
The work which is supplied to the process in figure 2.1-b consists of two parts. The **W** indicated in the figure is the 'technical work' which is generated by the process flow and transferred to or from the system. In the figure this is represented by the shaft of a gas turbine. The surrounding atmosphere also performs work on the process flow. At the inlet the process flow with volume **V** is transferred to the system under a pressure p. This pressure 'displaces' the volume $\mathbf{V}_1$ and therefore work $p_1\mathbf{V}_1$ is work which is performed on the system. Similarly $p_2\mathbf{V}_2$ is the work which is performed by the system. The work $p\mathbf{V}$ which is performed on or by the process flows is indicated as the volumetric work. The total energy for the open system is:

$$\mathbf{Q} - (\mathbf{W} + p_2\mathbf{V}_2 - p_1\mathbf{V}_1) = \mathbf{U}_2 - \mathbf{U}_1$$

In most cases the interest is only in the technical work. To eliminate the volumetric work from the energy balance, the state variable "enthalpy" has been defined with the symbol **H**:

$$\mathbf{H} = \mathbf{U} + p\mathbf{V}$$

Substituting the internal energy U by the enthalpy **H** eliminates the volumetric work from the energy balance, giving the most common form for the energy balance for an open steady-state system:

$$\mathbf{Q} = \mathbf{H}_2 - \mathbf{H}_1 + \mathbf{W} \qquad (2.2)$$

2.2.2 Conversion of heat into work

It is impossible to convert heat fully into work. This is one formulation of the second law of thermodynamics. A very important question is therefore, which fraction of the heat can be converted into work. Consider a steady-state process which uses heat to produce work (a heat engine). In figure 2.2 such a heat engine is shown. To produce the work, heat $\mathbf{Q}_1$ is used by the heat engine at temperature T_1. The heat is used to produce work **W**, which according to the second law is smaller than the heat ($\mathbf{W}<\mathbf{Q}$). In order to satisfy the energy balance over the heat engine[c], a second flow of heat is necessary. This flow, indicated as $\mathbf{Q}_2$ in figure 2.2, flows from the system at temperature T_2. The shaded rectangles T_1 and T_2 represent heat reservoirs[d].
The maximum amount of work which can be produced using the amount of heat $\mathbf{Q}_1$ depends on the temperature at which the heat is available (T_1) and the temperature at which it can be removed from the system (T_2). According to the Carnot principle, the maximum amount of work which can be produced from $\mathbf{Q}_1$ is equal to:

$$\mathbf{W}_{max} = \mathbf{Q}_1 \left(1 - \frac{T_2}{T_1} \right) \qquad (2.3)$$

The term between brackets is the fraction of the heat $\mathbf{Q}_1$ which can be converted into work using the two heat reservoirs in figure 2.2. and is indicated as the Carnot efficiency:

---

[c] Because the system is steady-state, the internal energy of the system does not change and the total energy supplied to the system must be zero.

[d] Heat reservoirs are idealized sources and sinks for heat where heat can be supplied to or extracted from without changing the temperature of the reservoir.

$$f = 1 - \frac{T_2}{T_1} \qquad (2.4)$$

Note that for the work performed by the system in figure 2.2 to be positive, the temperature of the heat supplied (T_1) must be higher than the sink temperature (T_2). As the ratio becomes closer to unity, i.e. the temperature difference between the hot (1) and cold (2) reservoirs becomes smaller, the Carnot efficiency decreases.
The maximum amount of work does not depend on the process in which the heat is partially converted into work. However, it can be shown that any process which renders the maximum amount work, must be a reversible process[c] [Smith & van Ness]. In a similar manner it can be shown that all reversible processes must have the same efficiency, i.e. the Carnot efficiency.

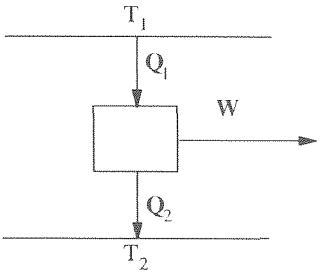

Figure 2.2: A heat engine working between the heat reservoirs T_1 and T_2 to produce work W

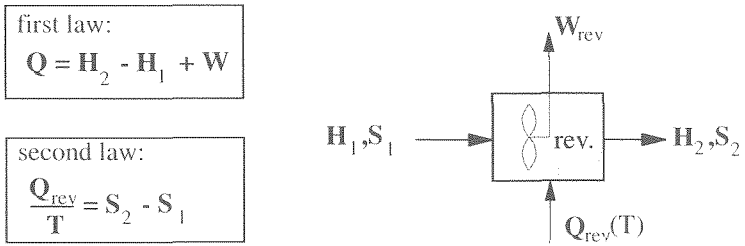

Figure 2.3: First and second law of thermodynamics for a reversible process in a steady-state open system

2.2.3 Lost work and exergy losses

Any real process is irreversible and consequently has a lower efficiency than the reversible process which leads to the same change in state. How irreversibly an actual process occurs, can be determined by comparing the real process with the reversible process. In figures 2.3 and 2.4 a reversible and an irreversible process are shown. The change in state between inlet (1) and outlet (2) is the same in both processes. The reversible process produces an amount of work W_{rev}, which is referred to as the reversible work. The actual process produces

[c] A process is reversible if a process is possible in which all mass and energy the flows to and from the system are in the opposite direction. A real system is never completely reversible.

work a smaller amount of work which will be denoted as **W**. For the change of state from (1) to (2), the energy increase of the process flows is equal to ($\mathbf{H}_2$ - $\mathbf{H}_1$). The work which is produced by the process is equal to the heat supplied to the system minus the increase in energy of the process flows. Rewriting equation (2.2):

$$\mathbf{W} = \mathbf{Q} - (\mathbf{H}_2 - \mathbf{H}_1) \tag{2.5}$$

The maximum amount of work can be generated if the process is reversible. This amount of is work indicated as the reversible work $\mathbf{W}_{rev}$ and the corresponding amount of heat as the reversible heat $\mathbf{Q}_{rev}$ To calculate the maximum amount of heat which can be supplied to the process, $\mathbf{Q}_{rev}$, it is necessary to introduce another property of state: the "entropy" with the symbol "S". The entropy of the process flow in figures 2.3 and 2.4 changes from $\mathbf{S}_1$ to $\mathbf{S}_2$. As any standard thermodynamics text will indicate, the amount of heat absorbed by the reversible process is determined by the change in entropy. The reversible heat can be calculated from:

$$\mathbf{S}_2 - \mathbf{S}_1 = \frac{\mathbf{Q}_{rev}}{\mathbf{T}} \tag{2.6}$$

However, for any real, irreversible process which results in the same change of state (1→ 2) the work and heat supplied to the system will be different from the work and heat in the reversible system. The irreversible process is indicated in figure 2.4

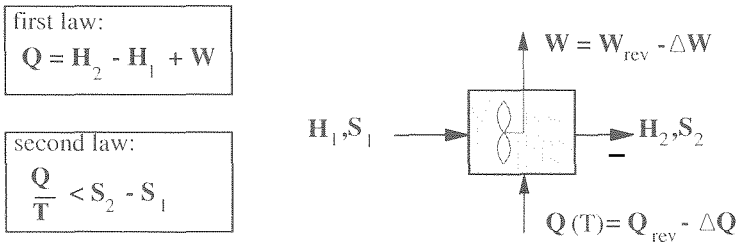

Figure 2.4: First and second law of thermodynamics for an open, steady-state system in a irreversible system

The work produced by the irreversible process is smaller than W_{rev}. The difference will be denoted as the "lost work" ΔW. Because the change of state is the same for the reversible process in figure 2.3 and the irreversible process in figure 2.4, the change in enthalpy ($\mathbf{H}_1$ - $\mathbf{H}_2$) is the same in both cases. Therefore **Q** in the irreversible process is smaller than $\mathbf{Q}_{rev}$. The first law (equation 2.5) indicates that the difference between the heat supplied to the reversible and the irreversible process will be equal to the difference between the work supplied in the reversible and the irreversible process (although of opposite sign). In other words, ΔW in figure 2.4 is equal to ΔQ.
Equation 2.6 is not valid for the irreversible process. To generalize the equation for both reversible and irreversible processes, the irreversible entropy increase $\Delta \mathbf{S}_{irr}$ is introduced. This quantity is always positive (>0).

Using the concept of the irreversible entropy increase, the change in entropy in the real process can be written as:

$$S_2 - S_1 = \frac{Q}{T} + \Delta S_{irr} \tag{2.7}$$

The irreversible entropy increase can be used to calculate ΔQ:

$$\Delta Q = T \Delta S_{irr} \tag{2.8}$$

And the difference in work performed by the reversible process and the irreversible process, previously defined as the lost work, can be calculated from the irreversible entropy increase as well:

$$\Delta W = T \Delta S_{irr} \tag{2.9}$$

ΔS_{irr} is larger than zero for a real, irreversible process and equal to zero for a reversible process. As the lost work is proportional to ΔS_{irr}, the irreversible entropy increase (or entropy generation) is a measure for the irreversibility of the process. However, for technical systems, a more useful measure for the irreversibility can be introduced than the lost work.
The lost work indicates how much more work could have been produced in a process resulting in the same change of state from 1 to 2 indicated in figure 2.4. Or, if the work is supplied to the process (eg. if figure 2.4 represents a compressor), with how much less work the same change of state could have been achieved. Therefore the lost work is a measure of the 'cost' of the irreversibility of a process. However, the difference between the reversible and the irreversible process is not only the difference in work output ΔW. If the real process produces less work it also consumes less heat. And this amount of heat ΔQ represents an amount of value as well. To quantify the "net" losses as a result of irreversibility, both the lost work and the lower heat requirement for the process have to be taken into account the heat.
To compare the value of the heat ΔQ to the lost work, the amount of work which could be produced from this heat should be determined. In general, the work which can be produced from an amount of heat depends on the temperature at which the heat is available. The work equivalent of ΔQ can be calculated from the Carnot efficiency (see equation 2.4). While the temperature (T_1) at which the heat is available is determined by the process, the temperature of the available sink for heat is not a characteristic of the process. However, the calculation of the amount of work which can be produced from ΔQ requires that the temperature of the available heat sink (T_2) for the rejected heat is determined as well.
For technical systems, the natural sink for heat is formed by the environment (air, water). Therefore a logical starting point for the calculation of the amount of work which can be produced from a quantity of heat for technical systems, is that the temperature of the heat sink (T_2) for the imaginary heat engine in figure 2.2 is equal to the temperature of the environment (T_o). The maximum work which can be produced from the heat using the environment as a sink for heat, is known as the exergy E_Q of the heat [Rant] and is calculated from:

$$E_Q = Q\left(1 - \frac{T_o}{T}\right) \tag{2.10}$$

The loss as a result of irreversibility in the real process, can be quantified more exactly using the exergy of the heat. The actual process produces ΔW less work than the reversible process with the same change of state 1→2. At the same time, the reversible process consumes ΔQ less heat. This heat, using the environment as a heat sink, could be used to produce an amount of work equal to the exergy of this heat. The net difference between the reversible and the

irreversible process is therefore equal to the lost work $\Delta \mathbf{W}$ minus the exergy of $\Delta \mathbf{Q}$. This 'net lost work' is called the exergy loss $\Delta \mathbf{E}_L$ of the irreversible process:

$$\Delta \mathbf{E}_L = \Delta \mathbf{W} - \Delta \mathbf{Q} \left(1 - \frac{T_o}{T} \right)$$

Both $\Delta \mathbf{W}$ and $\Delta \mathbf{Q}$ are equal to the $T \Delta \mathbf{S}_{irr}$ (see equations 2.8 and 2.9). This leads to the following expression for the exergy loss in an irreversible process in an open, steady-state system:

$$\Delta \mathbf{E}_L = T_o \Delta \mathbf{S}_{irr} \tag{2.11}$$

This equation is a general definition of the exergy loss ΔE_L in a process. It shows the fundamental relationship between exergy loss and entropy generation. However, to calculate the exergy loss the exergy balance discussed below will be used.

2.2.4 The exergy balance of a process

To any process in an open steady-state system, energy is supplied in the form of heat $\mathbf{Q}$ and/or in the form of work $\mathbf{W}$. The energy supplied to the system corresponds to a certain amount of exergy. The exergy of the energy which is supplied to a process in the open system is:

$$\mathbf{E} = \mathbf{E}_Q + \mathbf{E}_W$$

The exergy of the heat $\mathbf{Q}$ is defined as the amount of work which could be produced from this heat using the environment as a heat reservoir. More in general, the exergy of any energy flow can be defined as the amount of work it represents, using the environment as a heat sink. The exergy of the heat is defined by equation (2.10). The exergy of the work produced by the process is (by definition) equal to the work itself ($\mathbf{E}_W$=W). Therefore the exergy of the energy flows to process in the open system is equal to:

$$\mathbf{E} = \mathbf{Q} \left(1 - \frac{T_o}{T} \right) + \mathbf{W} \tag{2.12}$$

Substituting equations (2.5) for the work $\mathbf{W}$ and (2.7) for the heat, the exergy supplied to the process is equal to:

$$\mathbf{Q} \left(1 - \frac{T_o}{T} \right) + \mathbf{W} = \mathbf{H}_2 - \mathbf{H}_1 - T_o (\mathbf{S}_2 - \mathbf{S}_1) + T_o \Delta \mathbf{S}_{irr}$$

The last term on the right-hand side is the exergy loss in the irreversible process. The equation can therefore be rewritten to:

$$\mathbf{Q} \left(1 - \frac{T_o}{T} \right) + \mathbf{W} = (\mathbf{H}_2 - T_o \mathbf{S}_2) - (\mathbf{H}_1 - T_o \mathbf{S}_1) + \Delta \mathbf{E}_L \tag{2.13}$$

The above equation shows that the exergy which is supplied to the irreversible process by the energy flows depends only on the exergy loss in the process and on the change of the state of the process flows. This leads to the introduction of a new variable of state for the process

flow, the "exergy" with symbol "**E**":

$$\mathbf{E} = \mathbf{H} - T_o\mathbf{S} \tag{2.14}$$

The exergy change for the process flow in the open system in figure 2.4 therefore becomes:

$$\mathbf{E}_2 - \mathbf{E}_1 = \mathbf{H}_2 - \mathbf{H}_1 - T_o(\mathbf{S}_2 - \mathbf{S}_1) \tag{2.15}$$

The exergy of heat has been defined as maximum amount of work that can be produced from the heat using the environment as a heat sink. Correspondingly the exergy E of a process flow can be defined as the maximum amount of work that can be produced from the flow, using the environment as a sink for both mass and heat. To determine the maximum amount of work for the process, the process flow in the final state of this process (H_o and S_o) must have zero work potential with respect to the environment, i.e. be in equilibrium with the environment. A definition of the exergy of a process flow is the following:
"*The exergy of an energy carrier indicates how much work can be produced in a reversible process which takes place in an open and steady-state system using only the environment as a heat sink and where the energy carrier at the end of the process is in complete equilibrium with the environment.*" [Lier, 1977].

Using the exergy of the process flow **E**, equation (2.13) simplifies to:

$$Q\left(1 - \frac{T_o}{T}\right) - \mathbf{W} = \mathbf{E}_2 - \mathbf{E}_1 + \Delta\mathbf{E}_L \tag{2.16}$$

This equation can be considered as the "exergy balance" for an irreversible process in an open steady-state system:

exergy supplied to the process = exergy increase of the process flows - exergy loss

In figure 2.5 the exergy balance is represented schematically. If the exergy balance is used to calculate the exergy loss in the process in an open steady-state system, equation (2.16) can be rewritten to:

$$\Delta\mathbf{E}_L = Q\left(1 - \frac{T_o}{T}\right) - \mathbf{W} - (\mathbf{E}_2 - \mathbf{E}_1) \tag{2.17}$$

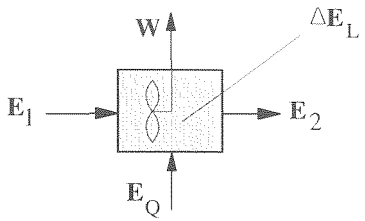

Figure 2.5: 'Exergy balance' for an open, steady-state system

2.3 CHANGE IN EXERGY IN CHEMICAL REACTIONS

2.3.1 Calculating the change in composition as a result of chemical reactions

Although the number of components in a fuel cell system in which chemical or electrochemical reactions occur is small (the combustor, the reformer and the fuel cell), the influence of the losses in these components on the rest of the system is very large. Therefore the change in exergy of a process flow as a result of chemical reactions will be investigated in more detail in this section. The results will be used in chapter 3 to calculate the exergy losses in a specific chemical reaction for systems with more than one reaction. The exergy losses as a result of a chemical reaction are considered in the open, steady-state system. Furthermore in this section the chemical reaction is considered as an isothermal process (no change in temperature and a constant pressure is assumed). In any chemical reaction there are chemical species which are consumed (reactants) and chemical species which are formed from the reactants (products). Characteristic for the chemical reaction is that the reactants are consumed and the products are created in fixed ratios. The numbers which represent the fixed ratios between the products and reactants are called the stoichiometric coefficients and indicated as ν_i. The stoichiometric coefficients for product species are defined positive and the stoichiometric coefficients for reactants negative. Using ν_j to indicate the stoichiometric coefficients of component X_j a general notation for a chemical reactions is:

$$|\nu_1|\,X_1 + |\nu_2|\,X_2 + \ldots \rightarrow |\nu_i|\,X_i + |\nu_{i+1}|\,X_{i+1} + \ldots$$

In a chemical reaction all species, product and reactant, have zero charge. In an electro-chemical reaction charged species (ions) are involved and the total charge of the reactants and products is not necessarily equal: for every mole reacted a fixed number of electrons can be either produced or consumed in the reaction. This stoichiometric number for the electrons is indicated by z. The notation for chemical reactions can be expanded to include electrochemical reactions:

$$|\nu_1|\,X_1 + |\nu_2|\,X_2 + \ldots \rightarrow |\nu_i|\,X_i + |\nu_{i+1}|\,X_{i+1} + \ldots \pm z\,e^-$$

A conventional way of representing the composition of a gas flow, is by using mole fractions. For the calculations involving changes in composition as a result of chemical reactions it is more convenient of use the mole vector $\underline{n}$, which uses the number of moles for each component rather than the fractions. The change in number of moles for each of the components as a result of a chemical reaction is proportional to the stoichiometric coefficient of the component. If n_i is the number of moles of component i, then Δn is the change in the number of moles as a result of the chemical reactions. In m is the number of chemical species in the system, then the ratios in the changes in the number of moles of the separate components are determined by the stoichiometric coefficients:

$$\frac{\Delta n_1}{\nu_1} = \frac{\Delta n_2}{\nu_2} = \ldots = \frac{\Delta n_m}{\nu_m}$$

This ratio indicates how many moles of each component is consumed or produced, i.e. how far a reaction proceeds. The variable is defined as the change of the reaction coordinate ε:

$$\Delta\varepsilon = \frac{\Delta n_i}{\nu_i} \qquad \text{for any } i=1\ldots m \qquad (2.18)$$

The change of the composition as a result of the chemical reaction is therefore fixed by a

single parameter ($\Delta\varepsilon$) instead of by the concentrations or mole fractions of the species involved. If more reactions occur in the system, several reaction coordinates (one for every chemical reaction) can be defined. If the number of reactions is equal to ℓ, the change in the number of moles of component i is given by:

$$\Delta n_i = \sum_{k=1}^{\ell} \nu_{k,i} \cdot \Delta\varepsilon_k \qquad \text{for } i = 1 \ldots n \tag{2.19}$$

The change in the total number of moles as a result of is given by:

$$\Delta n = \sum_{k=1}^{\ell} \Delta\nu_k \cdot \Delta\varepsilon_k \tag{2.20}$$

where $\Delta\nu_k$ is the change in the total number of moles, i.e.:

$$\Delta\nu_k = \sum_{i=1}^{n} \nu_{i,k} \tag{2.21}$$

In figure 2.6 the schematic representation of a chemical reaction is given.
Different chemical components (for example components A, B) enter the system. The number of moles for these components are $n_{1,A}$ and $n_{1,B}$ respectively. As a result of the chemical reaction the number of moles of the components change. In the example given in figure 2.6 the following reaction occurs:

$$A + B \rightarrow C$$

which leads to the flows $n_{2,A}$, $n_{2,B}$ and $n_{2,C}$ leaving the system.
Note that the process flow to the reactor is one single flow and the partial pressures which are considered are the partial pressures of the pre-mixed reactants and the mixture of products. Therefore the losses in the system are purely the losses of the chemical reaction and not the losses in the mixing process (see **Section 3.2**).

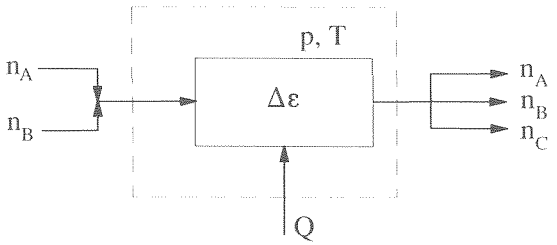

Figure 2.6: Mass and energy flows over the system boundary (---) of a system in which a chemical reaction occurs

The change in exergy for the reaction can be calculated using the general equation based on the exergy change for a steady-state open process (equation 2.15):

$$\Delta\mathbf{E} = \Delta\mathbf{H} + T_o \Delta\mathbf{S}$$

To calculate the change of the exergy in the a chemical process as in figure 2.6, the quantities $\Delta\mathbf{H}$ and $\Delta\mathbf{S}$ have to be calculated.

2.3.2 Calculating the change in exergy as a result of chemical reactions

Enthalpy of reaction

Because no work is delivered by the general chemical reaction in figure 2.6, according to the first law for the steady-state open system (equation 2.2) the heat which is transferred from the system (**Q**) is equal to the change in enthalpy:

$$\mathbf{Q} = \mathbf{H}_1 - \mathbf{H}_2$$

The enthalpy change as a result of the reaction in an isothermal reaction is therefore equal to the heat produced in the reaction and indicated as the heat of reaction. To calculate the enthalpy change, use is made of the reaction enthalpy $\Delta_r h$. This is the heat of reaction if 1 mole of the "characteristic" component reacts. For example, the heat or reaction for the combustion reaction of hydrogen [$H_2 + \frac{1}{2}O_2 \rightarrow H_2O$] will be given per mole H_2, the heat of reaction for the reforming reaction [$CH_4 + H_2O \rightarrow 3H_2 + CO$] per mole CH_4, etc. Using the reaction coordinate introduced in the previous section, the reaction enthalpy per mole can be defined by [Smith&Van Ness]:

$$\Delta_r h \equiv \left(\frac{d\mathbf{H}}{d\varepsilon} \right)_{p,T} \tag{2.22}$$

where the indices p and T indicate that the derivative is taken at constant pressure and temperature. Using the reaction enthalpy the heat which is generated/consumed in the reaction is equal to:

$$\Delta\mathbf{H} = \Delta_r h \, \Delta\varepsilon \tag{2.23}$$

If more than one reaction occurs, the total enthalpy change for the isothermal reactions is the sum of the enthalpy changes of the separate reactions and can be written as:

$$\Delta\mathbf{H} = \sum_{k=1}^{f} (\Delta_r h)_k \, \Delta\varepsilon_k \tag{2.24}$$

If the reaction enthalpy $\Delta_r h$ is negative, heat is produced by the system and the reaction is called an "exothermal" reaction. The negative $\Delta\mathbf{H}$ indicates a decrease of the chemical energy of the flow(s). The chemical energy is converted into heat. If the reaction enthalpy is positive heat is used to increase the chemical energy of the flow(s) and the reaction is indicated as "endothermal".

The enthalpy h_i is the enthalpy of the pure species i at temperature T (**Appendix 1**). Due to the selection of the reference for the calculation of the enthalpies h_i (**Section 2.4**), the reaction enthalpy (for homogeneous gas phase reactions) can be calculated simply from the enthalpy of the pure species:

$$\Delta_r h = \sum \nu_i \, h_i \tag{2.25}$$

Entropy of reaction

Analogous to the reaction enthalpy, the reaction entropy can be defined by:

$$\Delta_r s = \left(\frac{d\mathbf{S}}{d\varepsilon} \right)_{p,T} \tag{2.26}$$

However, $\Delta_r s$ depends on the partial pressure of the components and therefore on ε. As a result the value of $\Delta_r s$ will change from in- to outlet as a function of the concentrations. Therefore the change in entropy as a result of the reaction can only be given for the infinitesimal reaction $d\varepsilon$ in which the change in entropy equals:

$$dS = \Delta s_r(\varepsilon)\, d\varepsilon \tag{2.27}$$

and the total entropy for a process is found by this equation:

$$\Delta S = \int_{\varepsilon_{in}}^{\varepsilon_{out}} \Delta_r s(\varepsilon)\, d\varepsilon \tag{2.28}$$

The reaction entropy can be calculated from the entropy of the pure species s_i in the same way as the enthalpy (see equation 2.25):

$$\Delta_r s = \sum \nu_i s_i \tag{2.29}$$

Here s_i is the entropy of the species at the partial pressure at which the component is present in the gas (**Appendix 1**). The entropy of the component in the mixture is the sum of two terms. The first is the entropy of component i at standard pressure p^o which is denoted as s_i^o which depends only on the temperature. The second term takes into account the partial pressures of the component. The entropy of the component i at the partial pressure in the gas, is therefore equal to:

$$s_i = s_i^o - R \ln\left(\frac{p_i}{p^o}\right) \tag{2.31}$$

If this expression for the entropy of component i is used in the equation for the reaction entropy (2.29), the reaction entropy becomes equal to:

$$\Delta_r s = \sum \left(\nu_i s_i^o - R \ln (p_i)^{\nu_i}\right) \tag{2.32}$$

Similar to the expression for the entropy of component i, the entropy of reaction can be written as the sum of the entropy change at standard pressure ($p_i=p^o$) and the term which takes into account the partial pressures of the components:

$$\Delta_r s = \Delta_r s^o - \Delta_r s^p$$

with the standard entropy of reaction equal to:

$$\Delta_r s^o = \sum \nu_i s_i^o \tag{2.33}$$

and the influence of the partial pressures reflected by:

$$\Delta_r s^p = R \sum \ln (p_i)^{\nu_i} \tag{2.34}$$

Exergy of reaction

Using the equations for the reaction enthalpy and the reaction entropy, it is now possible to calculate the reaction exergy. In analogy to the definition of the reaction entropy, the reaction exergy can be defined as the increase of the exergy of the process flow as a result of the chemical reaction in an isothermal steady-state process:

$$\Delta_r e = \left(\frac{d\mathbf{E}}{d\varepsilon} \right)_{p,T} \tag{2.35}$$

For an infinitesimal change of the composition, the change in exergy, using the general equation for the exergy change of a process flow (2.15), becomes:

$$d\mathbf{E} = d\mathbf{H} - T_o d\mathbf{S}$$

As a result of the chemical reaction, which proceeds by the infinitesimal small change in the reaction coordinate $d\varepsilon$, the exergy of the flow[f] changes from **E** to **E+dE** and the change of the exergy is given by:

$$d\mathbf{E} = \Delta_r e(\varepsilon)\, d\varepsilon \tag{2.36}$$

Using equations (2.23) and (2.27) the exergy change as a result of the chemical reaction equals:

$$\Delta_r e\, d\varepsilon = \Delta_r h\, d\varepsilon - T_o \Delta_r s\, d\varepsilon$$

The reaction exergy is therefore equal to:

$$\Delta_r e = \Delta_r h - T_o \Delta_r s \tag{2.37}$$

Using equations (2.25) and (2.32) this can be rewritten to:

$$\Delta_r e = \sum \nu_i (h_i - T_o s_i^o) + T_o \sum \ln (p_i)^{\nu_i} \tag{2.38}$$

Again the total exergy change is found by integration of:

$$\Delta_r \mathbf{E} = \int_{\varepsilon_{in}}^{\varepsilon_{out}} \Delta e(\varepsilon)\, d\varepsilon \tag{2.39}$$

2.4 CALCULATING THE ENERGY OF PROCESS FLOWS

In the previous section, the calculation of change of the enthalpy (**H**) and the exergy (**E**) of the process flow in a steady-state open process has been treated. Although in the equation the values of the enthalpy and exergy of the process flows ($\mathbf{H}_i$, $\mathbf{E}_i$, etc) were used, only the differences between the value at the outlet and inlet are required in the calculations. Using the increase in enthalpy of the process flow ($\Delta\mathbf{H}$) and the increase in exergy ($\Delta\mathbf{E}$) all absolute values can be eliminated from the equations in the previous section. Although it is not necessary to use the enthalpy and exergy values for most calculations, there are several applications which do require the calculation of the value of **H** or **E** for a process flow. For example, values are required in order to:

- define efficiencies for energy systems and their components or subsystems;
- make energy and exergy flow diagrams;
- quantify energy and exergy flows to the environment, eg. flue gas stack losses.

Working with values requires the definition of a reference or zero state at which the value of the enthalpy or exergy is fixed. The reference system used for the calculation of the enthalpy

---

[f] the exergy of the process flow is a property of state (as **H** and **S**) once the temperature of the environment is fixed

of a process flow is comparable to the reference system used for the calculation of exergy values. In both cases the composition of the environment (air) is used as a starting point. Because the calculation of the energy of a process flow is much simpler, the reference state for the enthalpy calculation will be treated first.

2.4.1 Requirements for a reference state for the calculation of the enthalpy

The energy balance for a steady-state process in an open system is (equation 2.2):

$$\mathbf{Q} = \mathbf{W} + (\mathbf{H}_2 - \mathbf{H}_1)$$

The enthalpy is a variable for which only the change is defined (and can be measured) and not the value itself. In order to make a quantitative analysis, a reference state or zero state is required. In an energy system typical process flows are air, natural gas, flue gas, synthesis gas, etc. A process flow generally consists of a mixture of (chemical) components. In this thesis, for the calculation of the enthalpy of such process flows, the flows are considered as ideal mixtures [Smith & van Ness]. In that case the enthalpy of an ideal gas mixture can be defined as the sum of the enthalpies of the separate components. If x_i is the mole fraction of component i in the process flow and n is the total number of moles, than the number of moles for component i is given by:

$$n_i = x_i\, n \tag{2.40}$$

Using the molar or specific enthalpy h_i for component i [kJ/mole], the total enthalpy of the process flow is equal to:

$$\mathbf{H} = \sum n_i\, h_i \tag{2.41}$$

To be able to work with an value **H** a reference state has to be defined for the components, at which the value of the enthalpy is specified. This reference state is specified by the temperature T^*. Because ideal gas correlations are used, the enthalpy does not depend on the pressure. The enthalpy of component i is equal to the sum of the (measurable) difference in enthalpy between the actual and the reference conditions (Δh_i) and the selected value at reference conditions (h_i^*):

$$h_i(T) = \Delta h_i(T) + h_i^*(T^*)$$

In principle it is possible to choose the reference state for each of the components i in the system separately. This is practical if the composition of the flows in the system does not change. However, such a choice of the reference state does not automatically fulfill the equations for the calculation of the reaction properties $\Delta_r h$ and $\Delta_r s$ (equations 2.25 and 2.29).

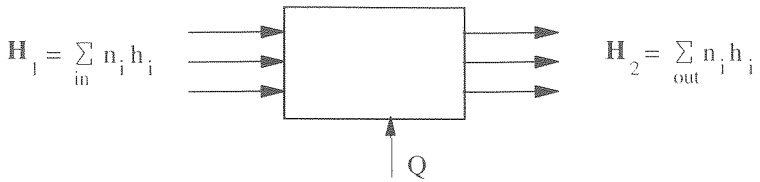

Figure 2.7: Calculation of the enthalpy change of the process flows from the enthalpy of the component in the mixture for an isothermal system with chemical reactions

More general, it is desirable to choose the reference values for h_i^* in such a way that the change of the enthalpy of the process flows in the system represented in figure 2.7 can be calculated directly from the enthalpy of the components as well:

$$\mathbf{H}_2 - \mathbf{H}_1 = \sum_{out} n_i h_i - \sum_{in} n_i h_i \qquad (2.42)$$

It is not possible to choose the components for which the enthalpy is fixed completely arbitrarily. If for example the enthalpy for the components O_2 en H_2O is fixed at reference conditions, the enthalpy of H_2 is determined as well, because the combustion reaction of H_2 has a known enthalpy of reaction. Requirement for the complete and unambiguous determination of the enthalpy of all components present in the system is:

- The number of fixed environment components is equal to the number of chemical elements present in the system (C, H, O, N, S, Ar, etc);
- Every element in the system is present in at least one of the environment components.

2.4.2 Different reference states for systems with chemical reactions

Reference state starting from the elements

A convenient choice of the reference state, in which the enthalpy and entropy of reaction can be determined directly from the properties of the pure components h_i and s_i will simplify the calculations considerably. A system which satisfies this criterion and is widely accepted in the chemical thermodynamics is based on setting the enthalpies of the elements in molecular form (O_2, N_2, C, etc.) equal to zero at standard conditions (at 25 °C and 1 bar) . By setting the enthalpies of compounds (H_2O, CO_2, etc) at the same conditions (25 °C and 1 bar) equal to the enthalpy of reaction from the elements the enthalpy change calculated value of $\mathbf{H}_2$ - $\mathbf{H}_1$ is correct for systems in which chemical reactions occur. The enthalpy of reaction from the elements at 25 °C and 1 bar is the formation enthalpy at standard conditions $\Delta_f h_i^o$.

$h_i^* = 0$ for the elements

$= \Delta_f h_i^o$ for all other components

Note that this reference state fulfills the requirement for a complete and unambiguous determination of all enthalpies automatically. Setting the enthalpy of the elements equal to zero at standard conditions and the enthalpy of all other chemical components equal to the formation enthalpy, leads to a consistent system. The values of the enthalpy can be used to calculate the enthalpy differences and the heat and work from the energy balance over the component or energy system. This way of defining the values for the enthalpy is very convenient and widely used, in particular in the chemical thermodynamics.

Reference state starting from the environment components

At the beginning of this section the use of values of the enthalpy for the calculation of efficiencies and construction of energy flow diagrams, was indicated as one of the reasons for calculating the value of the enthalpy. However, the indicated method is not suited for these purposes. Components representing a high energy content, for example fuel components as H_2 and C, are set zero because they are elements. As a result highly negative values for the enthalpy are calculated for other compound components, for example CO_2 and H_2O, which are abundant in the environment.

In order to arrive at a practical system for technical systems, the enthalpy of the components at the reference conditions should reflect the energy value of the component: fuel components (H_2, CH_4) should have a high value, components present in the environment, (H_2O, O_2, CO_2 and N_2) should have a low value. Therefore, the enthalpies of the components that are present in significant amounts in the environment are set equal to zero[g]. These components are indicated as the environment components. To fulfill the conditions formulated in **Section 2.4.1**, for every element present in the system, one environment is selected.

Reference state starting from the elements

If the energy of the elements are set to zero, the chemical enthalpy of H_2 is determined from the combustion reaction ($H_2 + ½ O_2 \rightarrow H_2O$). The heat which is release if 1 mole of H_2 is combusted at 25 °C is 242 kJ. Because no power is generated (**W**=0), the energy balance for the system is (equation 2.2):

$$\mathbf{Q} = \mathbf{H}_2 - \mathbf{H}_1 = -242 \text{ kJ/mole}$$

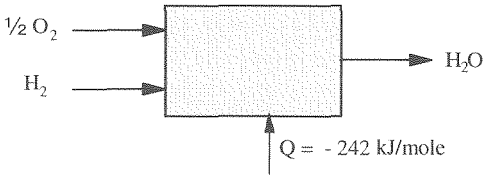

(**Q** is positive if supplied to the system, see section 2.2). If 1 mole H_2 reacts with ½ mole O_2 to one mole H_2O, the enthalpy change between inlet and outlet becomes:

$$\mathbf{H}_2 - \mathbf{H}_1 = h_{H_2O} - h_{H_2} + 0.5\, h_{O_2} = 242 \text{ kJ/mole}$$

Therefore the enthalpies at standard temperature (25 °C) become:

H_2	=	0	kJ/mole
O_2	=	0	kJ/mole
H_2O	=	-242	kJ/mole

For the reference temperature again the temperature of the environment is used. In the Netherlands 15 °C is the most commonly used temperature for the environment and this value has been used in this thesis[h].

The enthalpy of all other components can be calculated from the reaction of these components from the environment components. Condensing components, most importantly H_2O, form a complication as they occur in the environment both in the liquid and in the gas phase. As liquid water has a lower energy level than water vapour, setting the enthalpy of liquid water at p_0 and T_0 equal to zero seems preferable. By setting the enthalpy of liquid water equal to zero negative calculated values for the enthalpy are avoided. The energy calculated in this manner is indicated as the higher heating value (HHV). Based on the historical development, in Europe the calculation of the energy of process flows setting the enthalpy of the water in the gas phase equal to zero is widely accepted. This calculation method is based on the assumption that the latent heat or condensation heat of water (in flue gas) is not recoverable in an economic manner. The energy calculated using the zero state for

---

[g] Note that constituents of air have been used as the environment components. More elaborate systems have been developed for the exergy calculation (see **Section 2.5**), but for practical technical systems the air is the most relevant reference.

[h] Because this temperature is used to calculate for example how much heat is lost through the flue gas stack (see **Chapter 7** and further), this choice of temperature more relevant to technical systems is preferred over the 25 °C used in the calculation standard formation enthalpies

water in the gas phase is indicated with the lower heating value (LHV). Both methods are used in **Chapter 7** and further. For use in energy flow diagrams negative values of energy flows must be avoided and the HHV is used. On the other hand the LHV is used for calculating efficiencies, as is the customary procedure in Europe.

Reference state starting from the environment components

If the environment components are the reference components, the combustion reaction ($H_2 + \frac{1}{2} O_2 \rightarrow H_2O$) is used to calculate the chemical enthalpy of H_2. If 1 mole H_2 reacts with ½ mole O_2 to 1 mole H_2O, the enthalpy change between inlet and outlet is again equal to:

$$\mathbf{H}_2 - \mathbf{H}_1 = h_{H_2O} - h_{H_2} + 0.5\, h_{O_2} = 242 \text{ kJ/mole}$$

But now O_2 and H_2O are environment components and their enthalpies have been set to zero. Therefore the enthalpy of H_2 at environment temperature (15 °C) become:

O_2 = 0 kJ/mole
H_2O = 0 kJ/mole
H_2 = +242 kJ/mole

This is a more practical reference system, because the absolute value of the enthalpy of hydrogen in this system therefore corresponds to the combustion heat. The enthalpy values for hydrogen (and other fuel components) can be used directly to calculate efficiencies, etc.

Table 2.1: Different systems for the zero state the enthalpy: the table indicates for which components the enthalpy is set zero at standard conditions

	standard chemical	(HHV) (technical)	(LHV) (technical)
temperature T_o	25 °C	15 °C	15 °C
pressure p_o	1 bar	1.013 bar	1.013 bar
element defined by			
C	C(s)	CO_2	CO_2
H	H_2	H_2O(l)	H_2O(g)
O	O_2	O_2	O_2
N	N_2	N_2	N_2
S	S(s)	SO_2	SO_2
Cl	Cl_2	Cl_2	Cl_2
Si	Si(s)	SiO_2	SiO_2

2.4.3 Thermo-mechanical and chemical energy

The enthalpy of the process flow can be determined from the enthalpies of the components in the flow. Using the above expression for the enthalpy of component i gives the following expression for the enthalpy of the process flow:

$$\mathbf{H} = \sum n_i \Delta h_i(T) + \sum n_i h_i^* \qquad (2.43)$$

The first term of this equation is the energy which is released if the process flow is cooled (or

heated) to reference temperature and expanded to the standard temperature, i.e. the enthalpy difference between the process flow at actual (p,T) and standard conditions (p_o, T_o). This enthalpy value is indicated as the thermo-mechanical enthalpy $\mathbf{H}^{tm}$:

$$\mathbf{H}^{tm} = \sum n_i \Delta h_i(T) \tag{2.44}$$

If the environment definition based on the components in the environment is used, the second term in equation (2.43) is the energy which is released if the components of the process flow as a result of chemical reactions are converted to components in environment (e.g. oxidation of H_2 to H_2O) and is consequently indicated as the chemical enthalpy $\mathbf{H}^{ch}$:

$$\mathbf{H}^{ch} = \sum n_i h_i^{\circ} \tag{2.45}$$

The convenience of the selected reference state is that the chemical enthalpy which is calculated with this equation now corresponds to the heating value of the process flow.

2.5 CALCULATING THE EXERGY OF PROCESS FLOWS

2.5.1 A reference state for the calculation of exergy

As for the enthalpy, use of the exergy value of a process flow is convenient in analysis of energy systems. Similar to the enthalpy therefore a reference state will be defined. The definition of the exergy of the process flow (**Section 2.2**) states (implicitly) that the exergy of a process flow is zero if the process flow is in equilibrium with the environment. Equilibrium is the absence of (resultant) driving forces [Smith & van Ness]. As there are different driving forces, there are also different aspects of equilibrium or partial equilibria. With respect to the equilibrium of a process flow with the environment, three driving forces play a role:

- Temperature differences;
- Pressure differences ;
- Concentration differences.

Absence of the respective driving forces is indicated with respectively thermal, mechanical and chemical equilibrium. A definition of the reference state therefore consists of a reference temperature, pressure and composition [Meijer, 1993]. For the temperature of the environment 15 °C has been selected for the calculation of the enthalpy of a flow and this value will be used for the exergy calculation as well. For the value of the environment pressure 1 atmosphere or 1.013 bar has been selected. The reference composition will be discussed in the next section.

2.5.2 Composition of the environment

In the actual environment for a technical system (atmosphere, water, earth crust), the different subsystems are not in equilibrium: oceans, rivers and the air have different temperatures, none of the subsystems is in chemical equilibrium, etc. However, for a process flow to be in equilibrium with the environment, as required by the exergy definition, implies an environment in equilibrium with itself. In order to be able to calculate a value for the exergy of a process flow, an artificial environment must be defined. An extensive literature exists on the requirements for such a reference state and a wide range of definitions have been proposed. Some definitions have been proposed which differ strongly from the main stream of definitions. As an example the reference state has been calculated based on the assumption of equilibrium between the atmosphere and the part of the earth's crust [Ahrends]. The

resulting reference state deviates strongly from the actual atmosphere, in particular as a result of the low O_2 concentration. Specifically for energy systems an environment definition based on an average flue gas composition has been proposed [Riekert]. Differences between other proposals are much smaller.

For a technical system, the reference state must assign every process flow an exergy value that matches as close as possible the 'real' value. Just as for the enthalpy of a component, the reference state must assign a high value to a fuel stream while the value of the flue gas flow should be low. In general the proposed environment definitions use the earth's atmosphere as a starting point. As explained in **Section 2.4**, every component which is specified in the definition of the environment defines one element in the system or in the process flow. For energy systems, the most important elements (C, H, O and N) are found in significant quantities in the atmosphere (although not necessarily in elemental form). In almost all reference states proposed in literature the four main elements (C, H, O and N) are defined by the main constituents of air: CO_2, H_2O, O_2 and N_2.

The main difference with respect to the specification of these components is the way in which the zero state for water is defined. In several definitions the partial pressure of the water is below the vapour pressure (as is the case in the actual atmosphere (cf. [Szargut]). If liquid water is added to the definition (as done by [Gaggioli]), this leads to an over-defined system. If water in both liquid and gas phase has an exergy equal to zero, the definition is based on fully saturated air as equilibrium between gas and liquid has to be assumed (cf. [Baehr, 1978], [Munsch]).

Larger difference exist in the manner in which other elements which do not or rarely occur in the atmosphere are defined in the different reference systems. Elements which do not occur in the atmosphere and can play a role in energy systems are for example S (sulphur) and Si (silicium). However, within the framework of this thesis, in which only natural gas fuelled systems are studied, the exergy of these components is of little influence as their concentrations are very low. In [Meijer, 1993] different environment definitions are compared and a choice is made for the definition based on [Baehr, 1978] which is shown in table 2.2. The concentration water in this environment definition is based on humid air (relative =100%). The environment composition has been corrected for the selected temperature (15 °C).

Table 2.2: Environment definition p=1.013 bar at T=25 ° C based on [Baehr, 1978], adapted for T=15°C by [Meijer, 1993].

environment definition	concentration [mol/mol]	
components	T_0 = 15 °C	T_0 = 25 °C
N_2	0.7678	0.7565
O_2	0.2060	0.2030
Ar	0.0091	0.0090
CO_2	0.0003	0.0003
H_2O	0.0168	0.0312

The exergy of a process flow, is equal to the change in exergy if the flow is brought to equilibrium with the (defined) environment. This process, consisting of several steps, is illustrated in figure 2.8. The exergy flow is first brought to thermal equilibrium by cooling or heating the flow to environment temperature. The process flow is then said to be in thermal equilibrium with the environment. In the second step the pressure of the process flow is brought to the environment pressure through an isothermal expansion or compression step. The exergy difference between the process flow at the initial or system conditions (p,T) and the environment conditions (p_o en T_o) is indicated as the thermo-mechanical or physical exergy ΔE^{tm}. Subsequently in a third step the process flow is brought to chemical equilibrium with the environment. Chemical equilibrium with the environment can be defined as the state in which the chemical potential μ is the same for all the components in the environment and in the process flow[i]. The exergy change in this third step is indicated as the chemical exergy (E^{ch}). The exergy of the process flow which is determined using this procedure, is equal to the sum of the thermo-mechanical and the chemical exergy:

$$\mathbf{E} = \Delta \mathbf{E}^{tm} + \mathbf{E}^{ch} \tag{2.46}$$

The thermo-mechanical exergy, as the difference in exergy between two states, can be calculated directly using equation (2.15):

$$\Delta \mathbf{E}^{tm} = \mathbf{H}(p,T,\underline{x}) - \mathbf{H}(p_o,T_o,\underline{x}) - T_o(\mathbf{S}(p,T,\underline{x}) - \mathbf{S}(p_o,T_o,\underline{x})) \tag{2.47}$$

where p, T and x are the pressure, temperature and composition of the process flow and p_o and T_o are the reference pressure and temperature.

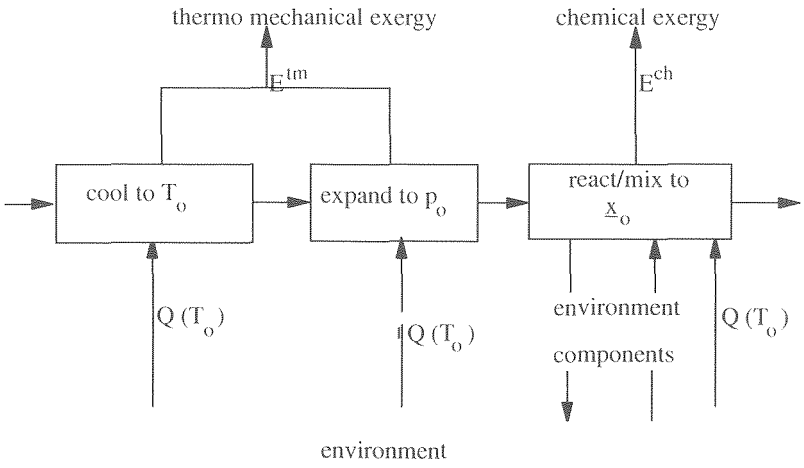

Figure 2.8: Imaginary reversible process in which a process flow is brought to equilibrium with the environment.

[i] If a component is present in the environment definition, the chemical potential is determined by the partial pressure in the defined environment. For components which are not present in the definition, the chemical potential is determined by the chemical reaction by which the component can be created from the environment components (see **Section 2.5.4**).

2.5.4 Calculation of the chemical exergy

The calculation of the chemical exergy is much more complex. The aim of the calculation is to determine the exergy of a mixture at environment conditions p_o and T_o and composition of the process flow x_o. The general method for this calculation is given in this section. A detailed description of the equations used for calculating the chemical exergy of a flow is given in **Appendix 2**. The starting point for the calculation method is the exergy of the components which form the reference environment. These components are indicated as the environment components and their exergy has been set equal to zero at environment conditions, i.e. at environment temperature and at the partial pressure at which they occur in the environment. The partial pressure of the environment components depends on the environment pressure and the concentration of the components in the environment (x_o). The environment temperature and pressure are used in the calculation as the reference conditions (T_o, p_o)

The process flow for which the exergy at reference conditions (p_o, T_o) is calculated, can consist of components which are present in the environment and other components (which can be formed from these components). The components which occur in the process flow are indicated as the system components. The concentration of these components is given by x_s. T_o, p_o, x_o and x_s are the input data for the calculation of the exergy of the process flow at reference conditions. There are different ways in which the exergy of the process flow can be calculated. The method which is used to calculate the exergy values in this thesis has been implemented in the flow sheeting program CYCLE-TEMPO for the system calculations (**part III**). This very flexible method has been reported previously by [Meijer, 1993].

The method is clarified using a numerical example given in **Appendix 2**. In this example the calculation of the exergy of an equimolar mixture of CH_4 and N_2 is considered. Here the global method, illustrated in figure 2.9, will be explained.

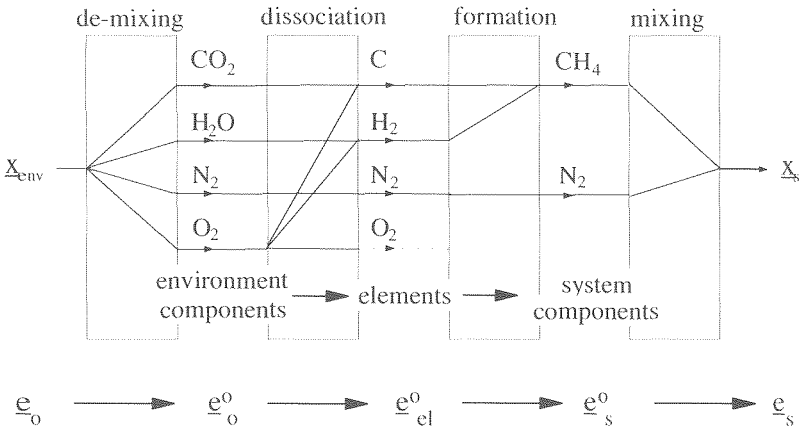

*Figure 2.9: Procedure for the calculation of the exergy of a process flow at reference conditions (in **Appendix 2** the complete calculation is elaborated)*

Exergy of the environment component at partial pressure
Starting point for the exergy calculation is the exergy of the environment components. By definition the exergy of the environment components at the partial pressure at which they are present in the environment is equal to zero because they are in equilibrium with the environment. In the given example CO_2, O_2, H_2O and N_2 are the environment and there concentrations are given in table 2.2. The exergy of an environment component i at the partial pressure in the environment (*eg.* O_2 at 0.2 bar) is indicated as $e_{o,i}$, where "e" indicates the molar or specific exergy [kJ/mole].

Exergy of the environment component at environment pressure: de-mixing
Because the exergy of the environment components at their partial pressure is known ($e_{o,i}=0$),, the exergy of the environment components at the reference pressure can be calculated. The exergy of the pure environment component (*eg.* O_2 at 1.013 bar) is indicated as $e^o_{o,i}$ for environment component i where the superscript "o" indicates exergy is determined for the component at pressure p^o. The exergy of the pure environment component is determined in the first step in figure 2.9 indicated as the de-mixing step.

Exergy of the elements at environment pressure: dissociation reaction
Subsequently, the exergy of the pure environment components can be used to calculate the exergy of the elements at the same conditions (p_o, T_o). In this second step, the environment components 'dissociate' into there elements (in molecular form). The exergy of the elements is denoted with $e^o_{el,k}$ for element k, where "el" indicates the exergy of an element. The exergy of the elements at reference pressure can be determined from the exergy of the pure environment components calculated in the preceding step, and the formation (= reversed dissociation) reaction exergies of the environment components.

Exergy of the system component at reference pressure: formation reactions
In the third step in figure 2.9 the exergy of the elements at reference conditions is used to determine the exergy of the system components at reference conditions $e^o_{s,i}$ for system component i, where the subscript "s" indicates a system component.. In this case the formation reactions for the system components are used to calculate the exergy of the system components.

Exergy of the system component at partial pressure: mixing
Finally, the exergy of the process flow is the sum of the exergies of the components at their partial pressures. Therefore the exergy of the pure components is used to calculate the exergy of the system components at partial pressure ($e_{s,i}$ for system component i).

CHAPTER 3:
CAUSES OF EXERGY LOSSES

3.1 INTRODUCTION

The total exergy loss for the process in a unit operation (heat exchanger, compressor, reactor, etc.) is calculated from the exergy balance over the unit operation. Using the correlations developed in the previous chapter, the energy and exergy flows can be determined as well as the exergy losses in all unit operations in the system. In many cases, in a single unit operation in a fuel cell system or another type of energy conversion system, more than one process occurs. Consider for example the mixing of two process flows. In this simple process the losses may be caused by several separate mechanisms. Firstly, the difference in composition will result in exergy losses. Secondly, if the flows have different temperatures, "heat transfer" from the hot to the cold flow to equilibrate the temperatures will lead to losses as well. Finally friction will lead to a pressure drop over the mixing process, leading to a third type of losses. The exergy losses calculated with the exergy balance, do not indicate which part is due to the change in composition, which part to the change in temperature and which to the pressure drop. Other unit operations which are used in a fuel cell system in which more than one type of loss occurs are for example a heat exchanger, in which both heat transfer and friction will occur, a reformers in which exergy losses as a result of heat transfer, friction, chemical reactions and as a result of mixing will play a role, etc. In order to indicate how the exergy losses can be reduced, it is important to identify the causes of the exergy losses, in particular if more than one driving force plays a role. This means not only calculating the total exergy loss, but determining which part of the total exergy loss is due to which cause. In this chapter a method is developed which does not only take into account the total exergy loss in a unit operation, but takes into account the different cause of the exergy losses in a unit operation. The main issue is to separate the different contributions to the total exergy loss. In some cases, the different processes occurring in a unit operation can be considered as independent steps. In that case, the exergy losses can be separated by considering the processes to occur sequentially. This method is therefore indicated as "sequential modelling". For the more complex unit operations (the fuel cell, the reformer) sequential modelling is not possible and other methods are required.

In **Section 3.2** a classification of the different causes of exergy losses is proposed and the different types of losses are investigated separately. Subsequently in **Section 3.3** unit operations in which more than one cause or driving force occurs are considered. Sequential modelling and correlations for separating the exergy losses in these unit operations are developed in this section. In **Section 3.4** the exergy losses as a result of chemical reactions are considered in more detail. Using the concept of the 'equilibrium temperature' a more physical interpretation of exergy losses in chemical reactions is discussed. Finally in **Section 3.5** some graphical methods to analyse the processes within the black-box are developed

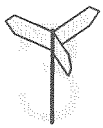

3.2.1 Identification of the types of exergy losses in the fuel cell system

The first step is to identify which driving forces play a role in the fuel cell system. There is not a systematic procedure available to identify the driving forces which play a role. Several researchers have attempted to develop this type of system, for example [Rogener], [Bauer] and [Klenke]. However, these approaches are highly theoretical and can not be readily used for an exergy analysis of an actual system. Therefore the driving forces in the fuel cell system have been identified by making a list of unit operations which are present in this energy system and identifying the causes of the exergy losses for each of these unit operations. This leads to a set of five driving forces that play a role in the fuel cell system.

Table 3.1: Types of losses and driving forces for the processes occurring in a fuel cell system

cause of loss	driving force	symbol	flow
heat transfer	temperature difference	ΔT	heat
friction	pressure difference	Δp	mass
mixing	difference in concentration	Δc	mass
chemical reactions	difference in chemical potential	$\Delta \mu$	mass
~~electrical~~	~~difference in electrical potential~~	~~ΔV~~	~~charge~~

- *heat transfer*:

The driving force for heat transfer is a temperature difference[j]. As will be shown, the role of the losses as a result of heat transfer is very important in the fuel cell system. This type of losses will be indicated as "heat transfer losses" even though actual heat transfer may not be the occur (in the case of non-isothermal mixing, for example);

- *friction:*

A large number of process flows is required to operate the system: fuel, air, flue gasses, steam, recycle flows, etc. The driving force that is required to move the flows is the difference in pressure between points in the system. The corresponding losses will be indicated as "friction losses";

- *mixing:*

If two process flows are mixed, losses may occur because of the difference in temperature of both flows, because of the pressure drop caused by mixing and because of the difference in composition between the flows. The first two types of losses have already been identified as heat transfer losses and friction losses respectively. The losses as a result of the difference in composition are a separate category and will be indicated as the "mixing losses". The driving force for the mixing process is the difference in concentration (partial pressure) of the components of the process flows;

- *chemical reactions:*

An important role in the fuel cell system is played by chemical reactions, for example in the fuel cell, in the reformer, etc. For the corresponding "chemical losses" the driving force for a

[j] the heat flow is proportional to ΔT. However, the exergy loss is proportional to the difference in $1/T$. It can be argued that $\Delta(1/T)$ is the driving force for heat transfer.

chemical reaction is determined by the chemical equilibrium of the reaction. If the reaction is far out of equilibrium, the driving force is large. If the reaction is in equilibrium, the driving force is zero. Therefore the difference in chemical potential, which indicates how far the chemical reaction is out of equilibrium, can be considered as the driving force;

- *electrical losses:*

In two different unit operations in the fuel cell system a difference in electrical potential plays a role. In the DC/AC-converter, which converts the DC-power generated by the fuel cell into AC-power, and in the fuel cell itself. In both cases the difference in electrical potential can be considered as the driving force. The exergy losses in this group, will be indicated as the "electrical losses".

All losses in the system can be attributed to one of these five driving forces and therefore the classification is complete. However, the classification which has been used is not absolute. It is possible to define the types of losses differently. To illustrate this the electrical loss in the fuel cell may be considered. The losses which are the result of the electrochemical reaction, are indicated as electrical losses in this classification. A more detailed examination of the processes occurring in the electrode and electrolyte shows that 'non-electrical' processes, eg. transport processes and chemical reactions, may contribute to the polarisation losses. Therefore, if the losses are considered at a more detailed level, this may lead to a different classification. However, it should be kept in mind that whether or not a classification is 'correct' is determined solely by the fact if it is useful or not in the analysis of an energy system. Such a 'common-sense' starting-point is necessary to prevent endless theoretical discussions on the 'correct' way to define exergy and related concepts. The chosen classification helps to clarify the exergy losses in the **part III** ("System Analysis") and is therefore useful. In the next section the different types of losses are investigated separately.

3.2.2 Losses as a result of heat transfer

Heat transfer takes place in many unit operations in the fuel cell system. Most importantly heat is transferred to and from the fuel and air flows. Furthermore heat transfer takes place in the waste heat boiler or steam generator. Heat transfer plays an important role in other unit operations than heat exchangers as well, for example in the reformer and the fuel cell.
If an amount of heat dQ is transferred, the exergy loss can be calculated from [van Lier, 1977]:

$$dE_L^{ht} = T_o \frac{\Delta T}{(T_1 + \Delta T) T_1} dQ \qquad (3.1)$$

where T_1 is the temperature of the primary medium[k]. ΔT is the temperature difference between the primary (T_1) and secondary medium (T_2) and T_o the temperature of the environment. From equation (3.1) it is evident that the exergy loss as a result of heat transfer increases with the amount of heat transferred (dQ) and with the temperature difference between primary and secondary medium ΔT. The exergy loss becomes smaller as the average temperature at which the heat is transferred becomes smaller. In a heat exchanger the temperatures T_1 and T_2 are not constant. The temperatures change (gradually) as a result of heat transfer: $T_1=f_1(Q)$ and $T_2=f_2(Q)$.

[k] The primary medium is the medium receiving the heat, the secondary medium donates the heat.

To calculate the total exergy loss as a result of heat transfer in a heat exchanger, equation (3.1) can be integrated from 0 to Q:

$$\Delta \mathbf{E}_L^{ht} = \int_0^Q T_o \frac{\Delta T}{(T_1 + \Delta T) T_1} |d\mathbf{Q}| \qquad (3.2)$$

In figure 3.1 the temperature of the process flow against the amount of heat transferred is given for two types of heat exchangers: co-flow and counter-flow. If a constant heat capacity c_p is assumed for both flows, the temperature profiles are linear, as indicated in figure 3.1. dQ and ΔT can both be written as functions of T_1. dQ is equal to (see figure 3.1 for the notation[1]):

$$|d\mathbf{Q}| = Q \frac{dT_1}{(T_{1,2} - T_{1,1})}$$

and the secondary temperature as function of the primary temperature becomes:

$$T_2 = \frac{(T_1 - T_{1,1})}{(T_{1,2} - T_{1,1})} \cdot (T_{2,2} - T_{2,1}) + T_{2,1}$$

By eliminating dQ and $\Delta T(=T_2-T_1)$ in the integral (equation 3.2), for constant c_P the following equation can be derived for the exergy loss as a result of heat transfer:

$$\Delta \mathbf{E}_L^{ht} = T_o \mathbf{Q} \left(\frac{\ln(\frac{T_{1,2}}{T_{1,1}})}{T_{1,1} - T_{1,2}} + \frac{\ln(\frac{T_{2,2}}{T_{2,1}})}{T_{1,1} - T_{2,1}} \right) \qquad (3.3)$$

This equation can be used to estimate the exergy loss as a result of heat transfer, for example if the exergy losses can not be determined from equation (2.17) because more than one process occurs. A condition is that the temperature profiles are approximately linear.

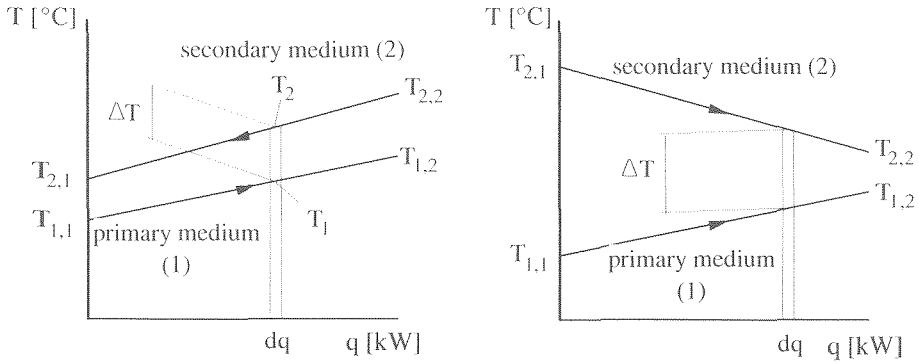

Figure 3.1: Temperature profiles for heat transfer in counter and co-flow assuming constant values for the heat capacity (c_p) for both flows

[1] Note that the second subscript of the temperature refers to the inlet of the primary side. This convention is used to make it possible to use one equation for the exergy losses of both co- and counter flow heat exchange

3.2.3 Losses as a result of friction

Friction losses in technical systems lead to pressure drops over the unit operations in a system. In general these have to be overcome by using a compressor or pump in the system. The work that has to be supplied to the fluid to overcome the pressure loss is the lost work as a result of friction. The general equation for lost work is (see equation 2.9):

$$\Delta \mathbf{W} = T \Delta \mathbf{S}_{irr}$$

The exergy loss however also takes into account the heat which is generated in the process. This heat represents an exergy equal to $(1-T_0/T)\ \Delta W$. The exergy loss as a result of friction is therefore equals:

$$\Delta \mathbf{E}_L^{fr} = \frac{T_o}{T} \Delta \mathbf{W}$$

At higher temperatures, a larger part of the exergy supplied to the fluid in the form of work, can be recovered in the form of heat. This has been expressed as the loss factor T_O / T [van Lier, 1977].The loss factor is equal to 1 at environment temperature where all the exergy of the work supplied is lost and decreases at higher temperatures where a larger part of the exergy can be recovered.
To calculate the exergy loss again a different approach is used. Equation 2.7 shows that for an adiabatic process (Q=0) the entropy change is equal to the entropy generation ($\Delta \mathbf{S}=\Delta \mathbf{S}_{irr}$). The expression for the lost work in the adiabatic process simplifies to:

$$\Delta \mathbf{W} = T \Delta \mathbf{S}$$

The entropy change for Q=0 and W=0 for an ideal gas is equal to [Smith&van Ness]:

$$\Delta \mathbf{S} = n R \ln\left(\frac{p_1}{p_2}\right) \tag{3.4}$$

This leads to the following expressions for lost work:

$$\Delta \mathbf{W} = n R T \ln\left(\frac{p_1}{p_2}\right) \tag{3.5}$$

and the exergy loss:

$$\Delta \mathbf{E}_L^{fr} = n R T_o \ln\left(\frac{p_1}{p_2}\right) \tag{3.6}$$

The work which must be supplied (by the compressor or pump) to the fluid for a given entropy increase $\Delta \mathbf{S}_{irr}$, increases at higher temperature (see equation 3.5). But the exergy loss does not depend on the temperature (equation 3.6). As a result for ideal gasses the exergy loss as a result of friction does not depend on the temperature, only on the pressure ratio p_1/p_2. Again this equation will be used to calculate the exergy loss as a result of friction if more than one process occurs simultaneously. The use of lost work or exergy loss in system calculations with be discussed in **part III**.

The general equation for the exergy change of the process flows in an open system is equation (2.15):

$$\Delta \mathbf{E} = \Delta \mathbf{H} - T_o \Delta \mathbf{S}$$

The schematic mixing process is shown in figure 3.2. Two process flows (flow 0 and flow 1) are mixed to a single flow (flow 2). The process is adiabatic (**Q**=0) and no work is performed on or by the system (**W**=0). Therefore, the change in enthalpy must be zero (Δ**H**=0) as well according to the energy balance (equation 2.2). In that case, the exergy change of the process flow is equal to:

$$\Delta \mathbf{E} = - T_o \Delta \mathbf{S}$$

If no energy is exchanged with the environment, the exergy loss is equal to the decrease in exergy of the process flow (Q=0 and W=0 in equation 2.17):

$$\Delta \mathbf{E}_L = - \Delta \mathbf{E}$$

and therefore:

$$\Delta \mathbf{E}_L = T_o \Delta \mathbf{S}$$

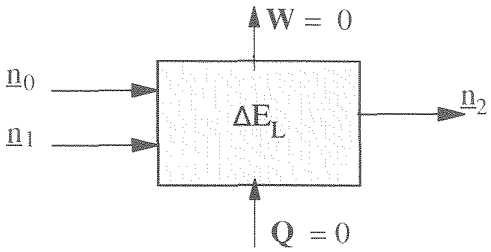

Figure 3.2: Adiabatic mixing of two process flows in an open, steady-state system

Consider the system in figure 3.2 where two flows are mixed. n_0 and n_1 denote the total number of moles, the number of moles for each (chemical) component i (for i=1,m) is denoted by $n_{0,i}$ and $n_{1,i}$ respectively. For the mixed flow at the outlet the notations are n_2 for the total number of moles and $n_{2,i}$ for the number of moles per component.
The entropy of an ideal mixture is the summation of the entropy of the components at there partial pressures [Smith & Van Ness]. The change in entropy of the process flow as a result of the pressure drop can be written as:

$$\Delta \mathbf{S} = \sum_{i=1}^{m} (n_{2,i}\, s_{2,i}) - \sum_{i=1}^{m} (n_{0,i}\, s_{0,i}) - \sum_{i=1}^{m} (n_{1,i}\, s_{1,i}) \qquad (3.7)$$

If s_i^o denotes the entropy of component i at standard conditions, the entropy of a component at the partial pressure p_i is equal to:

$$s_i = s_i^o + R \ln p_i \qquad (3.8)$$

Using equations (3.7) and (3.8) to calculate the difference in entropy for the mixing process, the expression for the exergy loss becomes:

$$\Delta E_L^{mx} = T_o \sum_{i=1}^{m} \left[n_{i,2}(s_i^o + R \ln p_{i,2}) - n_{i,0}(s_i^o + R \ln p_{i,0}) - n_{i,1}(s_i^o + \ln p_{i,1}) \right] \qquad (3.9)$$

Because no chemical reactions occur, the total number of moles for each component i is the same at in and outlet. In other words the number of moles in equals the number of moles out, for i=1,m:

$$n_{i,2} = n_{i,0} + n_{i,1} \qquad (3.10)$$

Therefore for all i=1,m:

$$n_{i,2}\, s_i^o - n_{i,0}\, s_i^o - n_{i,1}\, s_i^o = 0$$

As a result, the standard entropy s_i^o can be eliminated from equation (3.9):

$$\Delta E_L^{mx} = R T_o \sum_{i=1}^{m} \left[n_{i,2} \ln p_{i,2} - n_{i,0} \ln p_{i,0} - n_{i,1} \ln p_{i,1} \right] \qquad (3.11)$$

Substituting $\ln p_i = \ln x_i + \ln p$ (because the gas is considered ideal):

$$E_L^{mx} = R T_o \left[\sum_{i=1}^{m} \left[n_{i,2} \ln x_{i,2} - n_{i,0} \ln x_{i,0} - n_{i,1} \ln x_{i,1} \right] + \sum_{i=1}^{m} \left[n_{i,2} \ln p - n_{i,0} \ln p - n_{i,1} \ln p \right] \right]$$

Again using equation (3.10) the last term can be eliminated. For all i=1,m:

$$n_{i,2} \ln p - n_{i,0} \ln p - n_{i,1} \ln p = 0$$

Rewriting gives the following expression for the exergy loss as a result of isothermal mixing:

$$\Delta E_L^{mx} = T_o \sum_{i=1}^{m} \left[n_{i,0} \ln \left(\frac{x_{i,2}}{x_{i,0}} \right) + n_{i,1} \ln \left(\frac{x_{i,2}}{x_{i,1}} \right) \right] \qquad (3.12)$$

3.2.5 Losses as a result of chemical reactions

Similar to the treatment in the previous sections, the losses as a result of chemical reactions are considered for the case of an open, steady-state system. In many cases the chemical reaction occurs at the same time as the mixing process. For example if natural gas is combusted, in general the air and fuel are mixed and react in a combustion zone. For the analysis of the causes of exergy losses, the losses as a result of mixing and as a result of the chemical reaction can be separated. In this section only the chemical reaction is of interest and therefore the reactant flow is assumed to be 'pre-mixed', as shown in figure 3.3.
The starting point for the calculation of the exergy loss as a result of a chemical reacion is the general expression which was derived for the exergy loss in an open, steady-state system (equation 2.17):

$$\Delta E_L = -Q \left(1 - \frac{T_0}{T} \right) + W - \Delta E$$

The process considered occurs at constant pressure and temperature. Furthermore no work is produced in the chemical reaction (W=0). Energy to or from the process occurs only in the

form of heat. Therefore the energy balance (equation 2.2) for the chemical reaction becomes $\Delta H=Q$. Substituting this and the general expression for the exergy change of the process flow ($\Delta E=\Delta H-T_0\Delta S$) in the exergy balance leads to:

$$\Delta E_L = -\Delta H\left(1-\frac{T_0}{T}\right) - \Delta H + T_0\Delta S$$

or:

$$\Delta E_L^{ch} = -\Delta H\frac{T_0}{T} + T_0\Delta S \qquad (3.13)$$

Using the Gibbs energy ($G = H - TS$) equation (3.13) can be rewritten to:

$$\Delta E_L^{ch} = -\frac{T_0}{T}\Delta G \qquad (3.14)$$

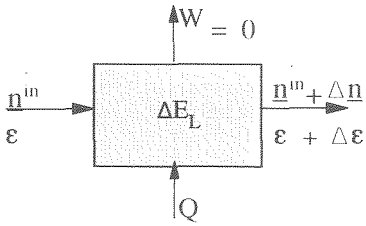

Figure 3.3: Chemical reaction in an open, steady-state system at constant pressure and temperature

In figure 3.3 an open steady-state process in which a chemical reaction occurs is represented. The chemical reaction leads to a change in composition from n^{in} to n^{out}. The change in composition, Δn, can be characterized using the reaction coordinate ε [mole]. This variable was introduced in **Section 2.3.1** to characterize the change in composition using a single variable. The reaction coordinate $\Delta\varepsilon$ is useful because, as shown in **Section 2.3.2**, it can also be used to calculate changes in thermodynamic properties. The change in the Gibbs energy is equal to [Smith & Van Ness]:

$$\Delta G = \Delta_r g\ \Delta\varepsilon$$

The exergy loss is therefore equal to:

$$\Delta E_L^{ch} = -\frac{T_0}{T}\Delta_r g\ \Delta\varepsilon \qquad (3.15)$$

Evidently the exergy loss in the chemical reaction is proportional to the change in the Gibbs energy. This is not wholly unexpected as the criterion for chemical equilibrium is the minimization of the Gibbs energy (see **Section 3.4**). Equilibrium is the absence of a driving force. Exergy losses are an immediate result of the presence of a driving force. Therefore a relation between the Gibbs energy change and exergy losses seems logical. A second remark which can be made is that the previously defined loss factor (T_0/T) is apparent in equation 3.14. In the case of friction, the exergy loss can be calculated from the lost work using the loss factor. The loss factor indicates which part of the lost work is definitively lost (T_0/T) and which part of the lost work could be recovered by utilising the heat which is generated ($1-T_0/T$). In equation (3.14) the loss factor has the same meaning. It can be shown

that (for example [Daubert]) that in a chemical reaction which produces work directly (for example a electrochemical reaction in a fuel cell!) the maximum amount of work which the reaction can produce corresponds to ΔG. Because the chemical reaction produces no work, ΔG can be considered completely as lost work. And equation (3.14) shows that the exergy loss is again *lost work x loss factor.*

3.2.6 Electrical losses

Voltage losses occur in the fuel cell system in two locations, in the fuel cell and in the DC/AC-converter. The voltage losses in the DC/AC-converter result in a lower electrical AC power output than is DC power supplied to the converter by the fuel cell. The ratio between both is indicated as the converter efficiency. In the DC/AC converter, where the heat which is generated is not recovered the exergy loss is equal to the lost work. The exergy loss in the previous section, based on the common approach in thermodynamic text books, is calculated over a non-specified time interval Δt, i.e. in [kJ] instead of [kJ/s] which would be more appropriate for steady-state open systems. Equations for the electrical loss include the current (electrical charge/unit time). As a result, in the equation for the voltage loss the time interval Δt is explicitly used. If the voltage loss as a result of the resistance in the DC/AC-converter is ΔV, the exergy loss is equal to:

$$\Delta \mathbf{E}_L^{el} = I \cdot \Delta V \, \Delta t$$

A similar correlation is valid for the losses in an electrical motor or in the generator. In the fuel cell, however, the irreversible heat generated in the electrochemical process is recovered and should be taken into account in the exergy balance. The work which is generated in the fuel cell over a period of time Δt is equal to:

$$\mathbf{W} = V \, I \Delta t$$

If the fuel cell operates reversible, the voltage V is equal to the reversible voltage V_{rev} and the work which is generated in this case is equal to:

$$\mathbf{W}_{rev} = V_{rev} \, I \, \Delta t$$

Introducing the voltage loss $\Delta V = V_{rev} - V$, the lost work $\Delta \mathbf{W}$ in the fuel cell is equal to:

$$\Delta \mathbf{W} = \mathbf{W}_{rev} - \mathbf{W} = \Delta V \, I \, \Delta t$$

The lost work $\Delta \mathbf{W}$ is converted into heat at the high operating temperature of power. To calculate the actual exergy, the loss factor (T_o/T) should be applied. Considering the process at constant temperature, the exergy loss in the electrochemical reaction becomes:

$$\Delta \mathbf{E}_L^{el} = \frac{T_o}{T} \Delta V \, I \, \Delta t \qquad (3.16)$$

3.3 CALCULATION OF DIFFERENT TYPES OF EXERGY LOSSES

3.3.1 Separating the exergy losses as a result of the different driving forces

In the third part of this thesis, 'System Analysis', the results of the thermodynamical system calculations for different fuel cell systems are discussed. In a system calculation, the energy flows and the conditions of the process flows are calculated. Using these data and the

expression which was derived in **Chapter 2** (equation 2.17), the exergy loss can be calculated in every unit operation of the system:

$$\Delta \mathbf{E}_L = \mathbf{Q}\left(1 - \frac{T_0}{T}\right) - \mathbf{W} - (\mathbf{E}_2 - \mathbf{E}_1)$$

The exergy loss which is calculated in this manner, is the total exergy loss, i.e the sum of:

- heat transfer loss;
- friction losses;
- mixing losses;
- chemical losses;
- electrical losses.

In **Section 3.2** the exergy losses are calculated for each of these processes. However, in each case discussed in the previous section, it is assumed that only one process occurs in the unit operation. As indicated, in many of the unit operations in the fuel cell system more than one cause of exergy losses can be found. For example, in a heat exchanger exergy losses occur due to heat transfer and friction. The exergy losses in a heat exchanger can therefore be reduced by either by decreasing the temperature difference between the process flow or by decreasing the pressure drop between in- and outlet. Which of these measures will contribute most to reducing the exergy losses, will depend on the size of the respective losses. It is therefore important therefore to know the contributions of the friction losses and the losses as a result of heat transfer to the total loss in the heat exchanger. Two methods are used in this thesis to separate the different types of exergy losses. The two methods are indicated as "sequential modelling" and "detailed modelling" respectively.

3.3.2 Sequential models to separate the different types of exergy losses

In sequential modelling the process is considered as a series of steps which occur one after another. In each of these different steps only one type of loss occurs. The exergy loss in each step is calculated by considering the step as a black box. This procedure, which will be described in more detail below, is only possible if the exergy losses in the different processes are independent. Consider for example the heat exchanger in which losses occur as a result of heat transfer and friction. In **Section 3.2** the following expression for the exergy losses as a result of heat transfer is given (equation 3.2):

$$\Delta \mathbf{E}_L^{ht} = \int_0^Q T_0 \frac{\Delta T}{(T_1 + \Delta T) T_1} |d\mathbf{Q}| \qquad (3.2)$$

An expression for the exergy loss as a result of friction was derived (equation 3.6):

$$\Delta \mathbf{E}_L^{fr} = n R T_0 \ln\left(\frac{p_{in}}{p_{out}}\right)$$

If the process flow on one side of the heat exchanger is considered (either the primary or the secondary flow), the process flow undergoes two changes. As the process flow passes through the heat exchanger:

- the pressure decreases as a result of friction;
- the temperature changes as a result of heat transfer.

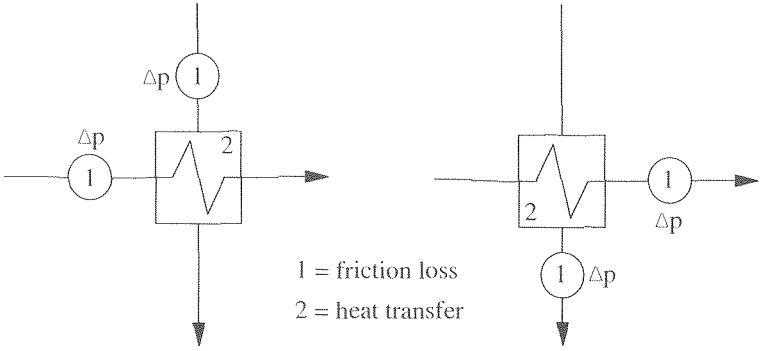

Figure 3.4: Sequential modelling of heat transfer and friction losses

These processes occur at the same time. However, in the expression for the exergy loss as a result of friction the temperature does not appear. Therefore exergy loss as a result of friction is evidently independent of the temperature[m]. Consequently, for the calculation of the exergy loss, it is not important whether the pressure decreases mainly near the inlet, near the outlet or whether the pressure drop occurs uniformly over the heat exchanger. In all of these cases the exergy loss as a result of friction will be the same. Therefore the exergy loss in the heat exchanger can be calculated by assuming that the pressure drop and the heat transfer process are separate steps. This is indicated in figure 3.4. The exergy losses can be calculated for the adiabatic pressure drop Δp (step 1) for both flows using equation (3.6). The exergy loss as a result of heat transfer (step 2) can be calculated considering the heat exchanger in figure 3.4 as a black box. If the pressure drop is considered to occur at the outlet, as indicated in the diagram on the right-hand side in figure 3.4, the calculated loss for each of these steps will not change

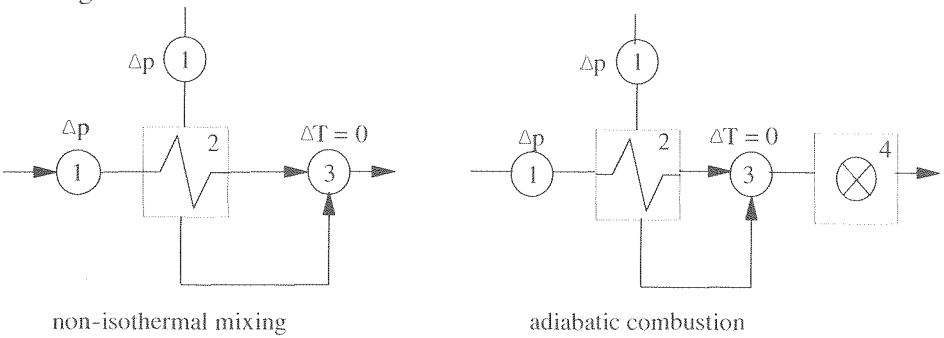

non-isothermal mixing adiabatic combustion

Figure 3.5: Two other examples of sequential modelling to separate exergy losses as a result of different driving forces

In figure 3.5 two other important processes are shown for which the exergy losses are separated using sequential modelling. The first process (left-hand side) is non-isothermal mixing, the second is combustion, which in the fuel cell system refers to the combustion of anode off-gas. Sequential modelling is based on the fact that different types of exergy losses

[m] due to the assumption that the gas behaves as an ideal gas, dH/dT does not depend on pressure

are in most cases independent. This is true for the process of mixing. For the isothermal process with negligible pressure drop, in **Section 3.2** the following correlation was developed (equation 3.12) for the exergy loss:

$$\Delta E_L^{mix} = T_o \sum_{i=1}^{n} \left[n_{i,0} \ln\left(\frac{x_{i,2}}{x_{i,0}}\right) + n_{i,1} \ln\left(\frac{x_{i,2}}{x_{i,1}}\right) \right]$$

In this equation only the number of moles n and mole fractions x_i occur. Therefore the loss as a result of mixing is independent of both pressure and temperature. Using the fact that the mixing process is independent of both pressure and temperature, the complex process can be separated into three steps, as indicated in figure 3.5:

(1) friction;
(2) heat transfer;
(3) mixing (isothermal: $\Delta T=0$).

Another unit operation for which the exergy losses are separated by sequential modelling is the combustor. In this unit operation fuel and air (or other oxidant) are mixed and the pre-mixed process flow is combusted. The process is schematically represented in the diagram on the right-hand side of figure 3.5. The mixing step may involve any of the three steps mentioned above. The exergy losses in this combustion process can be determined in the simplest way considering this last step as a black-box.

3.3.3 Detailed models to separate the different types of exergy losses

The sequential method requires that the exergy losses in the complex process in a unit operation are, or can be considered as, independent. This is not the case for all unit operations. In the fuel cell system there are two important unit operations in which the different process steps can not be separated by sequential modelling: the reformer and the fuel cell. As a result, for these unit operations a more detailed calculation is required. In particular the exergy losses as a result of heat transfer and as a result of the chemical and electrochemical reaction are difficult to separate. An example can illustrate this.
In figure 3.6 sequential modelling is used to calculate the exergy losses for a chemical reactor in three different configurations. The process flow consists of 1 mole CH_4 and 1 mole H_2O. In

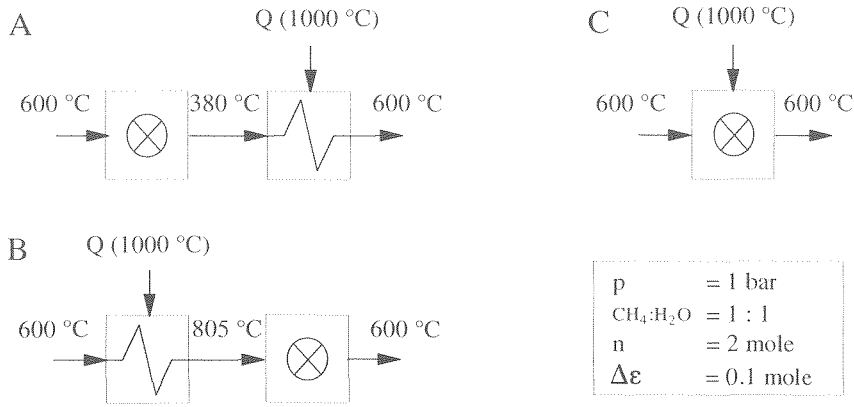

Figure 3.6: Three different options for modelling a reaction with heat transfer sequentially.

the reactor the reforming reaction occurs ($CH_4 + H_2O \rightarrow 3H_2 + CO$) in which 10% of methane is converted ($\Delta\varepsilon$=0.1 mole). The heat Q is supplied at 1000 °C. The temperature at the both inlet and outlet is 600 °C. The heat Q is used solely for the reforming reaction.
Three cases have been calculated:

A - The mixture reacts adiabatically in the reactor, in which the temperature drops to 380 °C. In the next step the heat is supplied to reheat the process flow to 600 °C;

B - The mixture is first heated to 805 °C and then reacts adiabatically in the reactor, which has an outlet temperature of 600 °C;

C - The reaction and heat transfer are simultaneous: the heat is supplied during the reaction keeping the temperature at 600 °C;

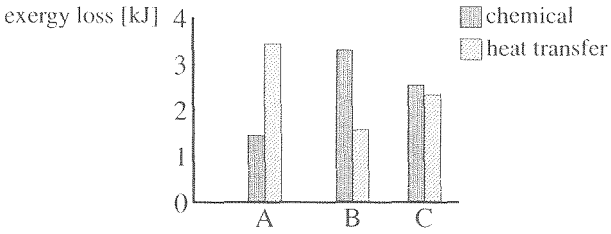

Figure 3.7: Distribution of the exergy losses (per mole CH_4) as a result of the chemical reaction and heat transfer for the three cases shown in figure 3.6

In all three cases the total exergy loss is the same (considering the process as a black-box, the same flows go in and out of the process). However, the distribution of these losses is different. This is shown in figure 3.7. This graph shows the exergy losses as a result of the chemical reaction and heat transfer separately. The average temperature difference for heat transfer is 510 °C for case A, 300 °C for case B and 400 °C for case C (see figure 3.6). The difference in average temperature leads to different values for the exergy loss as a result of heat transfer. In case A the exergy loss as a result of heat transfer is much larger than in case B. Case C lies between both other cases. The three cases considered correspond to different assumptions with respect to the process within the reactor. If, in the given example, the temperature profile in the reactor is linear (dT/dQ is constant), the exergy loss distribution is approximated by case C. If the reaction occurs very fast and heat transfer is the slower step, the distribution of loss can be approximated with case A and if the reaction kinetics are slow and heat transfer is fast case B will be the closest approach for the distribution of losses.
The example shows that the different approximations lead to different results with respect to the distribution of exergy losses. For those unit operations where different process are closely linked the black-box approach is therefore not sufficient. It is necessary to know with some accuracy the temperature and concentration profiles within the process. In the fuel cell system there are two unit operations for which the sequential modelling does not yield good results. These unit operations are the reformer and the fuel cell. In the case of the reformer, the heat which is used in the reforming reaction is transferred from the flue gas to the catalyst bed. Heat transfer and chemical reaction are therefore directly coupled. In the fuel cell the losses in the electrochemical reaction depend strongly on the temperature distribution in the fuel cell. Consequently, for these unit operations the exergy losses can not be separated by splitting the process in subsequent steps (e.g. electrochemical reactions followed by heat transfer).
For both unit operations a detailed model has been made. These models determine

temperature profiles within the reformer and fuel cell, respectively. These temperature profiles can be used to determine which part of the exergy losses is due to heat transfer and which part is due to the chemical and electrochemical reactions. For the fuel cell a detailed model is developed for the system calculations (see **part II**) . The data which this model generates can be used to calculate the exergy losses. For the reformer a black-box model is used in the system calculations. A more detailed model has been developed specifically to calculate the exergy losses. This model is described in **Appendix 3**. The detailed models are used to distinguish the different types of exergy loss in both unit operations. As illustrated in figure 3.8, not all losses are calculated in the detailed model. In the case of the reformer, the exergy losses as a result of friction and as a result of mixing (steam + natural gas) are calculated a priori. The detailed model is then used to calculate separately the losses as a result of heat transfer and as a result of the chemical reactions. In the fuel cell the friction losses are calculated separately as well. The detailed model is used to calculate the losses as a result of heat transfer and as a result of the chemical and the electrochemical reactions.

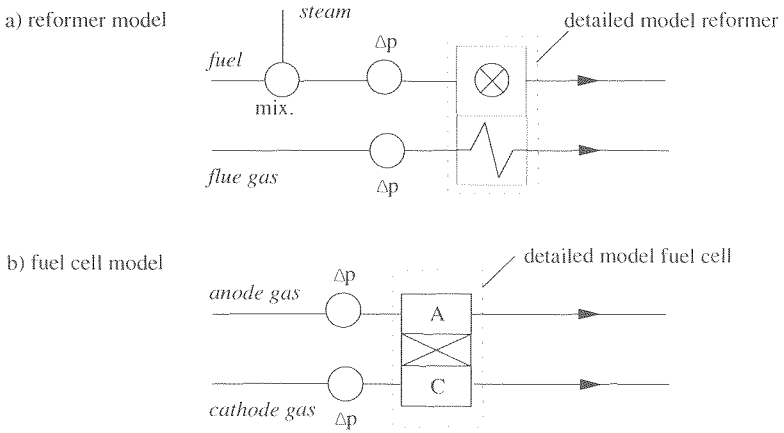

Figure 3.8: The role of the detailed model in determining the exergy losses per type for the reformer and the fuel cell

Calculation of the different types of exergy losses for the reformer

The exergy losses in the reformer depend on concentrations and temperature. As these vary from in- to outlet along the reformer, the exergy losses will vary as well. Therefore the exergy loss calculation is based on the calculated profiled of temperature and concentrations. For the calculation of these profiles in the reformer model, the reformer is divided into subsections (figure 3.9). For each of these subsections all thermodynamical data are calculated. The data which are relevant for the calculation of the exergy losses in the reformer are:

- $\Delta\varepsilon_r$ = change in reaction coordinate for the reforming reaction in the catalyst bed;
- $\Delta\varepsilon_s$ = change in reaction coordinate shift reaction in the catalyst bed;
- T_b = temperature of the catalyst bed
- T_{fg} = temperature of the flue gas channel;
- ΔQ = heat transferred from the flue gas to the catalyst bed.

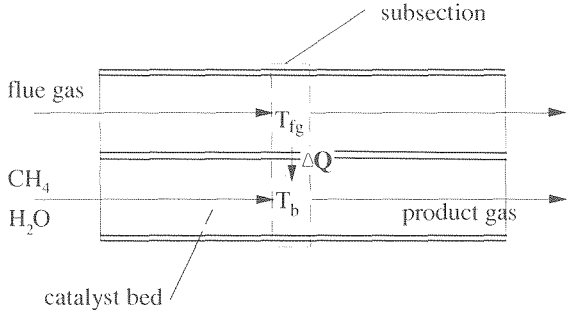

*Figure 3.9: A subsection of the reformer defined for the calculation of temperature and concentration profiles (for the model see **Appendix 3**)*

Each of these variables is calculated for all subsections. Using these data the exergy losses in the subsection can be calculated using the equations developed in **Section 3.2**.

Heat transfer
The loss as a result of heat transfer can be calculated using equation (3.1). Using the temperature of the catalyst bed T_b (primary) and flue gas T_{fg} (secondary) and the heat transferred in the subsection ΔQ, the exergy loss equals:

$$\Delta E_L^{ht} = \frac{T_o}{T_b} \frac{\Delta T}{T_{fg}} \Delta Q \qquad (3.17)$$

where ΔT is the difference between the flue gas temperature T_{fg} and the bed temperature T_b.

Chemical reactions
The exergy loss as a result of the chemical reactions requires calculating the Gibbs energy of reaction for both the shift reaction $\Delta_r g_s$ and the reforming reaction $\Delta_r g_r$ (see **Section 3.2**). Both reactions occur at bed temperature T_b. The exergy loss as a result of both chemical reactions combined can be calculated using equation (3.15):

$$\Delta E_L^{ch} = - \frac{T_o}{T_b} \left(\Delta_r g_r \, \Delta \varepsilon_r + \Delta_r g_r \, \Delta \varepsilon_s \right) \qquad (3.18)$$

Calculation of the exergy losses per type of process for the fuel cell

The detailed model of the fuel cell is split into subsections as well (figure 3.10). In the fuel cell model a subsection contains three elements for which the temperature and other properties are calculated: the anode and the cathode channel and the electrolyte (the model is described extensively in **Chapter 4**). The subsection parameters which are relevant for the calculation of the exergy losses are:

- V^j = cell voltage for the subsection;
- I^j = current for the subsection;
- $\Delta^j \varepsilon_e$ = change in reaction coordinate for the electrochemical reaction;
- $\Delta^j \varepsilon_r$ = change in reaction coordinate for the reforming reaction;
- $\Delta^j \varepsilon_s$ = change in reaction coordinate for the shift reaction;
- $T^j{}_a$ = temperature anode channel;

- T^j_e = temperature of the electrolyte;
- $\Delta^j \mathbf{Q}_a$ = heat transferred from the electrolyte to the anode gas flow;
- $\Delta^j \mathbf{Q}_c$ = heat transferred from the electrolyte to the cathode gas flow

Using these calculated values the exergy losses for every process can be determined.

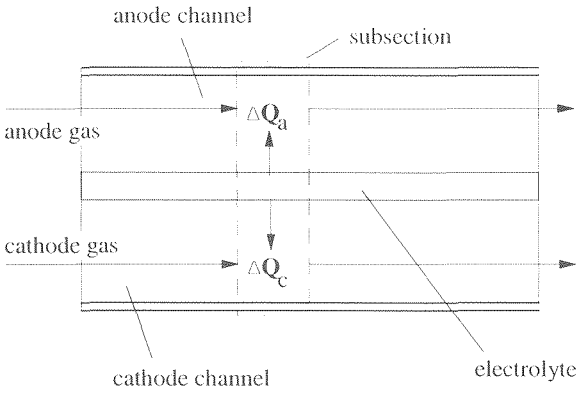

Figure 3.10: A subsection or sub cell of the fuel cell defined for the calculation of temperature and concentration profiles (see chapter 4)

Heat transfer

The exergy losses as a result of heat transfer are calculated separately for the anode channel and the cathode channel. If ΔT_m (m=a,c) is the temperature difference between the electrolyte and the process flow in the channel (anode, cathode), then the loss for heat transfer from the electrolyte to the cathode can be calculated using:

$$\Delta \mathbf{E}_L^{ht,c} = \frac{T_o}{T_e} \frac{\Delta T_c}{T_c} \Delta \mathbf{Q}_c \tag{3.19}$$

and the loss as a result of heat transfer to the anode from:

$$\Delta \mathbf{E}_L^{ht,a} = \frac{T_o}{T_e} \frac{\Delta T_a}{T_a} \Delta \mathbf{Q}_a \tag{3.20}$$

Chemical

The exergy losses as a result of chemical reactions can be calculated in the same manner as the corresponding losses in the reformer. In calculating the losses in the reformer, the assumption was made, that the shift and the reforming reactions occur at the average bed temperature in the subsection. Correspondingly the temperature at which the reactions occur in the fuel cell is assumed to be equal to the electrolyte temperature T_e. The exergy loss as a result of chemical reactions are therefore equal to:

$$\Delta \mathbf{E}_L^{ch} = - \frac{T_o}{T_e} \left(\Delta_r g_r \, \Delta \varepsilon_r + \Delta_r g_s \, \Delta \varepsilon_s \right) \tag{3.21}$$

Electrical
Finally the losses as a result of charge transfer in the fuel cell are caused by polarisation and ohmic losses in the fuel cell are given by:

$$\Delta E_L^{el} = \frac{T_o}{T_c} \Delta V I \Delta t \qquad (3.22)$$

3.4 CHEMICAL EQUILIBRIUM AND EXERGY LOSSES

3.4.1 Chemical equilibrium

For each process which occurs in the fuel cell system, a driving force has been identified. For heat transfer this is a difference in temperature, for mixing processes a difference in concentration, etc. This driving force is important because it determines both the rate of the reaction and the (exergy) losses in the process. In most cases this driving force is readily interpreted: it easy to understand that a larger temperature difference will lead to a larger heat flow, a larger potential difference will lead to a higher current, etc. The driving force which is difficult to understand is the chemical potential: the driving force for the chemical reaction. In this section a more physical interpretation of the exergy losses in a chemical reaction is developed. The basis of this discussion is the equilibrium temperature. Using the equilibrium temperature, the exergy losses as a result of a chemical reaction can be interpreted in a manner comparable to the losses as a result of heat transfer. First the concept of chemical equilibrium will be considered.

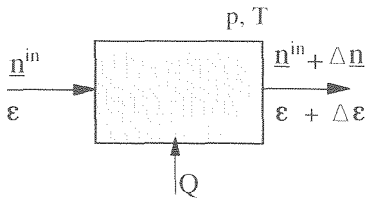

Figure 3.11: Isothermal system in which the composition changes as a result of a chemical reaction

In figure 3.11 the general representation of a chemical reaction in a steady-state, open system is given. The inlet composition is given by the vector n^{in} [mole]. If the outlet composition is given by the vector $\underline{n}$, the number of moles for component i at the outlet is equal to:

$$n_i = n_i^{in} + \Delta n_i$$

The change in number of moles for component i, Δn_i, depends on the chemical reaction. Using the reaction coordinate introduced in **Section 2.3**, the outlet concentration can be written as function of the reaction coordinate:

$$n_i = n_i^{in} + \nu_i \Delta\varepsilon \qquad (3.23)$$

Using the number of moles at the inlet n^{in} and the stoichiometric coefficient $\Delta\nu$ ($= \Sigma\nu_i$) for the total reaction, the total number of moles ($n = \Sigma n_i$) at the outlet is equal to:

$$n = n^{in} + \Delta\nu \Delta\varepsilon \qquad (3.24)$$

For a steady-state, open system, the chemical equilibrium is determined by the Gibbs energy **G**. If the reaction is in equilibrium at the outlet, the Gibbs energy of the flow will be minimal (e.g. [Smith & Van Ness]). The system is considered at constant pressure and temperature: the Gibbs energy depends only on the composition, i.e. on the reaction coordinate. Therefore the chemical reaction is in equilibrium at the outlet if:

$$\frac{d\mathbf{G}(\varepsilon)}{\varepsilon} = 0$$

The Gibbs energy for a process flow is equal to:

$$\mathbf{G} = \mathbf{H} - T\mathbf{S}$$

If g_i^o denotes the entropy of component i at standard conditions, the Gibbs energy of a component at the partial pressure p_i is equal to (e.g. [Smith & van Ness]):

$$g_i = g_i^o - RT \ln p_i$$

For an ideal gas mixture the Gibbs energy therefore can be calculated from:

$$\mathbf{G} = \sum_{i=1}^{m} n_i g_i^o + RT \sum_{i=1}^{m} n_i \ln p_i \qquad (3.25)$$

where g_i^o is the Gibbs energy for the pure species at standard pressure p^0 and at temperature T. The partial pressure of component i, assuming ideal gas behaviour, can be calculated from:

$$p_i = \frac{n_i}{n} p$$

Using the expressions for n_i (equation 3.23) and n (equation 3.24) the second term on the right hand side can be rewritten to:

$$n_i \ln p_i = (n_i^{in} + \nu_i \Delta\varepsilon)(\ln(n_i^{in} + \nu_i \Delta\varepsilon) - \ln(n^{in} + \Delta\nu\Delta\varepsilon) - \ln p)$$

The Gibbs energy **G** of the outlet flow in figure 3.11 can therefore be written as a function of the change in reaction coordinate ε and the inlet flow n^{in}:

$$\mathbf{G} = \sum_{i=1}^{m} (n_i^{in} + \nu_i \Delta\varepsilon) g_i^o + RT \sum_{i=1}^{m} (n_i^{in} + \nu_i \Delta\varepsilon) \ln (n_i^{in} + \nu_i \Delta\varepsilon)$$

$$- RT (n^{in} + \Delta\nu\varepsilon)(\ln(n^{in} + \Delta\nu\varepsilon) - \ln p) \qquad (3.26)$$

As an example the reforming reaction will be considered. As before, the system is a steady-state, open system. The inlet flow consists of an stoichiometric (1:1) mixture of H_2O and CH_4. The reforming reaction is given by:

$$CH_4 + H_2O \rightleftarrows 3\,H_2 + CO$$

The composition at the outlet can be characterized by the reaction coordinate ε. If ε=0, no chemical reaction has occurred and no H_2 and CO are present. On the other hand ε=1 indicates conversion of 1 mole of CH_4 (i.e. full conversion of CH_4 and H_2O) which results in an outlet flow of 3 mole H_2 and 1 mole CO. For all values of ε between 0 and 1 the outlet flow consists of a mixture of CH_4, H_2O, H_2 and CO.
Using equation (3.26) the Gibbs energy of the process flow at the outlet of the system has

been calculated as a function of ε for the conditions 600 °C and 1 bar. The result is shown in figure 3.12. For the given inlet composition and conditions, the reaction is in equilibrium if the reaction coordinate is 0.47 mole. To calculate the exact equilibrium value the derivative of the Gibbs energy is used. This leads to the definition of the fourth reaction property (see **Section 2.3.2**), the reaction Gibbs energy:

$$\Delta_r g = \left(\frac{d\,G}{d\,\varepsilon} \right)_{p,T} \tag{3.27}$$

The criterion for chemical equilibrium is:

$$\Delta_r g(\varepsilon) = 0 \tag{3.28}$$

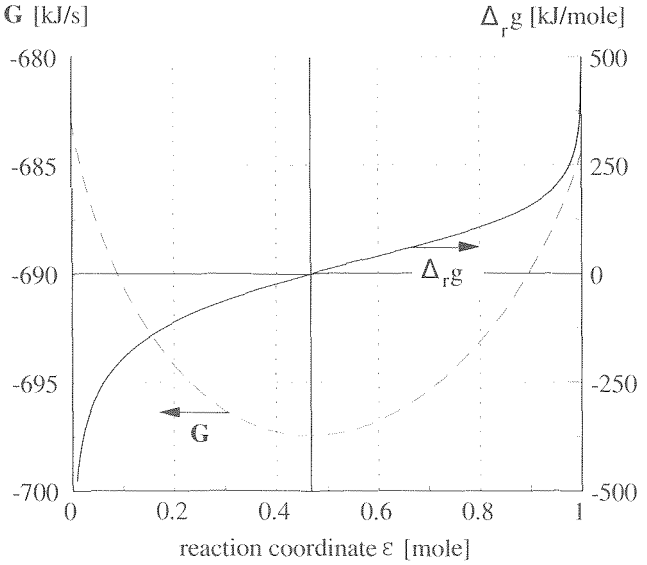

*Figure 3.12: Gibbs energy (**G**) and Gibbs energy of reaction ($\Delta_r g$) at the outlet of the system as a function of the reaction coordinate ε (i.e. as function of the conversion): p=1 bar, T=600 °C for an initial composition 1 mole CH_4 and 1 mole H_2O*

Using the expressions derived for the reaction enthalpy and the reaction entropy, the expression for the reaction Gibbs energy is equal to:

$$\Delta_r g = \sum \nu_i g_i^{o} + RT \sum \ln (p_i)^{\nu_i} \tag{3.29}$$

In the same way as the expression for the Gibbs energy G, this expression can be written as a function of the reaction coordinate:

$$\Delta_r g(\varepsilon) = \sum_{i=1}^{m} \nu_i g_i^{o} + RT \sum_{i=1}^{m} \nu_i \ln (n_i^{in} + \nu_i \Delta\varepsilon) - RT\,\Delta\nu (\ln (n^{in} + \Delta\nu\,\Delta\varepsilon) + \ln p) \tag{3.30}$$

In figure 3.13 the equilibrium mole fraction CH_4 for the reforming reaction is shown, based on the initial composition in figure 3.12 (1 mole H_2O and 1 mole CH_4) as a function of the temperature for several different pressures. On the left Y-axis the mole fraction CH_4 in the equilibrium composition is indicated, on the right the corresponding reaction coordinate ε. As

can be seen in the figure, at high temperature the mole fraction CH_4 approaches zero and correspondingly the reaction coordinate approaches unity. The reaction coordinate approaches 0 if the temperature approaches infinity. The behaviour is asymptotic: the value $\varepsilon=1$ is never reached. In other words, it is not possible to convert CH_4 or H_2O ($\varepsilon=0$) fully by an equilibrium reaction. In the same way it is not possible to convert all H_2 or CO ($\varepsilon=0$) by lowering the temperature: $\varepsilon=0$ is theoretically achieved at absolute zero (T = 0 K).

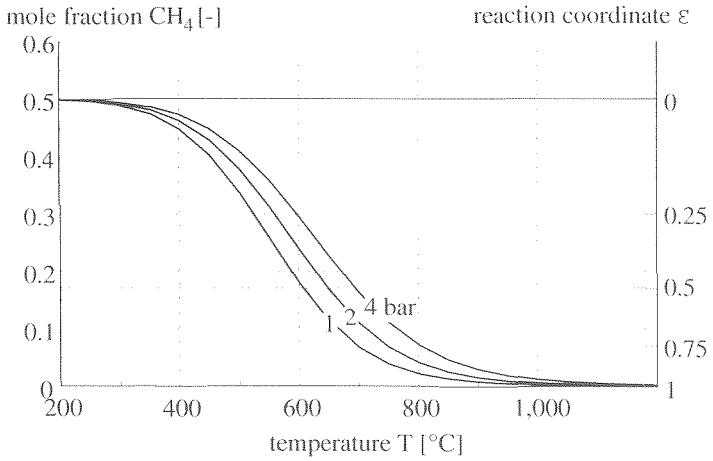

Figure 3.13: Equilibrium CH_4 mole fraction as a function of pressure and temperature : p=1 bar, T=600 °C for an initial composition 1 mole CH_4 and 1 mole H_2O

3.4.2 Influence of the equilibrium on the exergy losses in a reaction

The Gibbs energy of reaction can be considered as the driving force for the chemical reaction. In **Section 3.2** an expression was derived for the exergy loss as a result of this driving force:

$$\Delta \mathbf{E}_L = -\frac{T_o}{T}\Delta \mathbf{G} \tag{3.31}$$

In figure 3.14 the Gibbs energy and Gibbs reaction energy are shown again for the case where 1 mole H_2O and 1 mole CH_4 are supplied to the open steady-state system at 600 °C and 1 bar. The reaction coordinate corresponding to this composition is indicated in figure 3.14 as ε_{in}. The driving force for the reaction is large at first. As the value of reaction coordinate becomes closer to the equilibrium value, the driving force becomes smaller. The same is valid for the exergy loss per mole which can be calculated from:

$$\left(\frac{d\mathbf{E}_L}{d\varepsilon}\right) = -\frac{T_o}{T}\Delta_r g \tag{3.32}$$

As the composition approaches equilibrium, the driving force reduces to zero and consequently the specific exergy loss becomes zero. The same is true for the rate with which the reaction will occur. In a 'real' isothermal reactor it therefore is not possible to reach equilibrium. Due to the decrease of the rate of the reaction to zero at equilibrium, this would require an infinitely large reactor. Therefore in figure 3.14 the reaction coordinate for the

outlet flow (ε_{out}) is smaller than the equilibrium value (ε_{eq}). The total exergy loss in the chemical reaction from ε_{in} to ε_{out} is equal to:

$$\Delta E_L = \frac{T_0}{T} \int_{\varepsilon_{in}}^{\varepsilon_{out}} \Delta_r g(\varepsilon)\, d\varepsilon \qquad (3.33)$$

This is proportional to the area which has been shaded in figure 3.14.

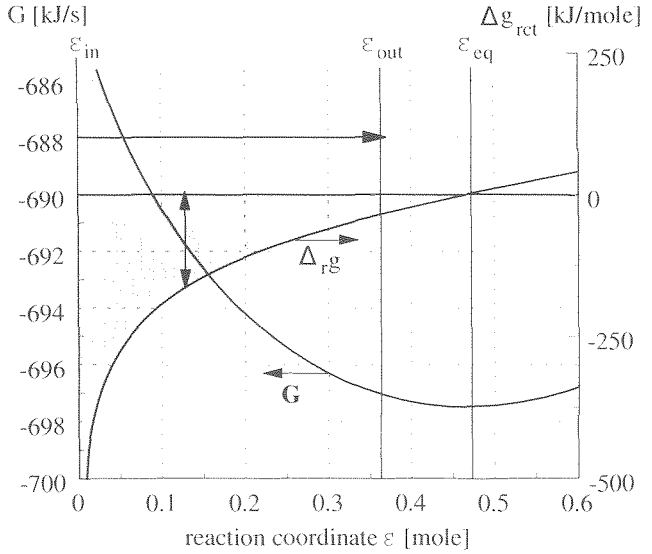

Figure 3.14: Graph showing the driving force ($\Delta_r g$) and the resulting exergy losses (area x T_0/T) *for a chemical reaction for the case where 1 mole H_2O and 1 mole CH_4 are supplied to the open steady-state system at 600 °C and 1 bar.*

3.4.3 The equilibrium temperature

The reaction Gibbs energy $\Delta_r g$ can be used to indicate how far out-of-equilibrium a process flow is. If the reaction is far from equilibrium the reaction Gibbs energy will be large. Consequently the specific exergy losses (i.e. per mole converted) will be large as well. If the reaction approaches equilibrium, both the reaction Gibbs energy and the exergy losses will tend to zero. In determining the equilibrium state in the previous section, the equilibrium state was (implicitly) defined as the state with that composition for which the system is in equilibrium at given pressure and temperature. If so defined, a process flow can only achieve equilibrium if the components react to the equilibrium composition. However, it is also possible to achieve equilibrium by changing the temperature of the process flow at constant composition.
This is illustrated in figure 3.15. Consider an open system in which the reforming reaction can occur. The inlet conditions are indicated by (1) in figure 3.15. The composition at ε=0 corresponds to the initial composition of 1 mole CH_4 + 1 mole H_2O used in the previous section. The composition at state (1) in figure is characterized by the reaction coordinate ε=0.2 and the temperature of 800 °C. The curve represents those points (ε, T) for which the

mixture is in equilibrium (note that this graph is a rotated image of the line for 1 bar in figure 3.13). The mixture reaches chemical equilibrium if the composition changes at constant temperature to the composition corresponding to ε=0.92. The change in reaction coordinate from 0.2 to 0.92 and the corresponding change in composition $\Delta \underline{n}$ is indicated in figure 3.15 by the process 1→2. On the other hand, the outlet flow is also in equilibrium if the composition in (1) is frozen ($\Delta\varepsilon$=0) and the temperature is lowered to 520 °C. This process is indicated in figure 3.15 by the process 1→2'. Instead of achieving equilibrium because the process flow has reacted to the equilibrium composition, the process flow is in equilibrium because the temperature has been lowered to the equilibrium temperature corresponding to the inlet composition

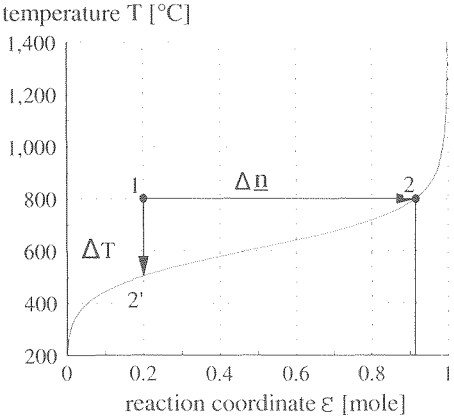

Figure 3.15: Achieving equilibrium by a change in composition Δn (equilibrium composition) and by a change in temperature ΔT (equilibrium temperature)

In **Section 2.2** the losses in the irreversible process were determined by comparing the irreversible process to an imaginary reversible process. Using the equilibrium temperature such a reversible process can be constructed for a class of chemical reactions (as will be shown in **Section 3.5**, not for all chemical reactions). This is shown in figure 3.16 for a reforming reaction in an open system. The state at the inlet is represented by (1) and the outlet state is equal to (2).
The reaction, which occurs irreversibly, is represented in figure 3.16 by 1→2. Alternatively the change of state from 1 to 2 can be achieved by the process 1→2'→2"→2. In this process the input flow is first cooled down to the equilibrium temperature. This process is reversible if the heat is transferred from the process at ΔT=0. Subsequently the chemical reaction proceeds gradually in such a way that the temperature of the process flow corresponds to the equilibrium temperature for every value of ε until the outlet composition is achieved. The chemical reaction can be considered as a series of semi-equilibrium states through which the process flow passes. If the composition corresponds to the outlet composition, the reaction is 'frozen' and the process flow is reheated to the outlet temperature (again at ΔT=0). If heat is supplied to and removed from the system at the temperature of the process flow at each intermittent state, the process is completely reversible. In **Section 3.5** this process will be used to develop a graphical representation of the exergy losses in the chemical reaction.
The equilibrium temperature can be calculated from the equilibrium condition:

$$\Delta \mathbf{G} = \Delta \mathbf{H} - T\Delta \mathbf{S} = 0$$

Replacing T by the equilibrium temperature T_{eq}, the following must be valid:

$$T_{eq} = \frac{\Delta \mathbf{H}}{\Delta \mathbf{S}} \tag{3.34}$$

Because the change in **H** and **S** is due to the change in the reaction coordinate, ΔH ($=\Delta_r h \cdot \Delta\varepsilon$) and ΔS ($=\Delta_r s \cdot \Delta\varepsilon$) can be replaced by the reaction enthalpy and entropy:

$$T_{eq} = \frac{\Delta_r h}{\Delta_r s} \tag{3.35}$$

Note that $\Delta_r h$ and $\Delta_r s$ are the enthalpy and entropy of reaction at equilibrium temperature. Consequently the calculation of the equilibrium temperature with equation (3.35) is always iterative.

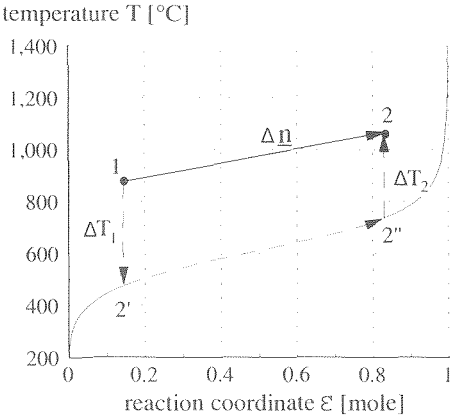

Figure 3.16: A reversible route (1-2'-2"-2) for a chemical reaction using the equilibrium temperature

The exergy loss in a chemical reaction depends on the degree to which the reaction is out-of-equilibrium. In this section two approaches have been considered. First it was shown that the exergy losses increase as the compositions differs more from the equilibrium composition (see figure 3.14). The second approach is consider how much the temperature at which a reaction occur differs from the equilibrium temperature. In that case the exergy loss can be interpreted in terms of heat transfer. The exergy loss in an exothermal reaction occurs because the heat is removed from the reaction at a lower temperature than the equilibrium temperature. In an endothermal reaction exergy losses are due to the difference between the temperature at which the heat is supplied and the temperature at which the reaction is in equilibrium. In the next section this approach will be elaborated.

3.5 GRAPHICAL METHODS TO REPRESENT EXERGY LOSSES

The amount of data which comes out of an exergy analysis is very large. Consequently, the method which is used to represent the losses is as important as the method to calculate the exergy losses. One way to make the data easily accessible is the use of graphs. In this chapter some methods will be presented to visualize exergy losses. Two types of diagrams will be considered. The first type is the value diagram. This diagram is developed for representing the losses as a result of heat transfer [van Lier]. Using the approach developed in **Section 3.4** based on the equilibrium temperature, this diagram can be extended to include losses as a result of chemical reactions. Not all types of chemical reactions can be represented in a value diagram. Therefore a more general type of diagram is introduced as well.

3.5.1 Value diagram for heat transfer

Heat transfer is the most important cause of exergy losses in the fuel cell system, as is shown in **part III** "System Analysis". Characteristic for heat transfer losses is that they occur in many locations in the fuel cell system in different heat exchangers and other unit operations. To be able to compare the losses in different unit operations in an energy conversion system the value diagram was developed [Lier, 1992]. This diagram is based on the Q,T-diagram in which the temperature at which heat is transferred to and from the process flows is represented.

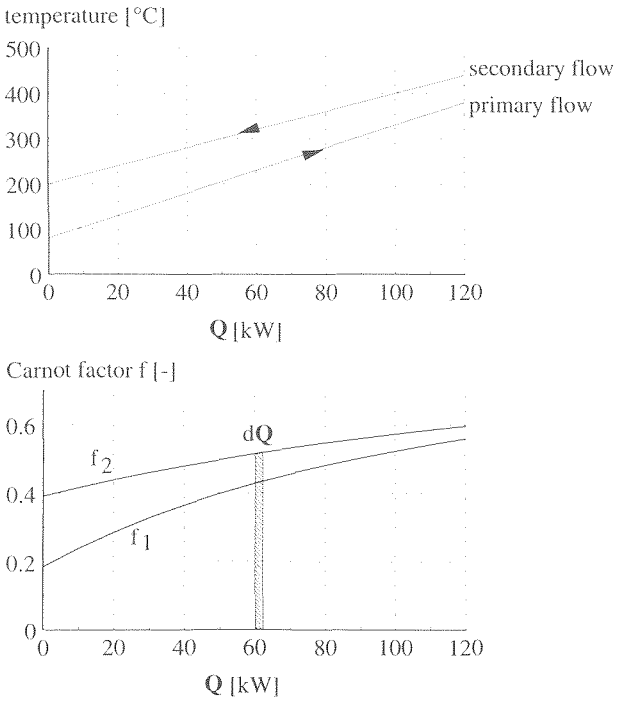

Figure 3.17: Example of a Q,T-diagram (top) and corresponding value diagram (bottom) for a heat exchanger

A simple example of such a Q,T-diagram is given in figure 3.17 for a single heat exchanger. In the given example the cold flow or primary flow heats up from 80 °C to 380 °C. The heat for this temperature increase is supplied by the secondary or hot flow, which cools down from 430 °C to 200 °C. The amount of heat which is exchanged (120 kW) between the hot and the cold flow in the heat exchanger is indicated on the X-axis The Q,T-diagram shows the temperature difference between the two process flows exchanging heat. This temperature difference is the driving force for heat transfer and consequently determines the exergy losses as a result of heat transfer. However, these exergy losses are not proportional to the temperature difference, but to the difference between $1/T_p$ and $1/T_s$. According to equation (3.2) the exergy losses as a result of heat transfer are equal to:

$$\Delta \mathbf{E} = \int T_o \frac{\Delta T}{T_s T_p} \, d\mathbf{Q}$$

were p indicates the primary flow which receives heat and s the secondary flow which supplies the heat. The equation can be rewritten to:

$$\Delta \mathbf{E}_L = \int \left(\frac{T_o}{T_p} - \frac{T_o}{T_s} \right) d\mathbf{Q}$$

Using the Carnot factor f , with $f_s = 1 - T_o/T_s$ and $f_p = 1 - T_p/T_2$, this can be simplified to:

$$\Delta \mathbf{E}_L = \int \left(f_s - f_p \right) d\mathbf{Q} \qquad (3.36)$$

In the value diagram, the lower graph in figure 3.17, instead of the temperature of the two process flows, the Carnot factors are represented as a function of the heat which is transferred. In that case the area which lies under the primary curve equals the exergy of the heat which is transferred to the primary medium:

$$\Delta \mathbf{E}_p = \int f_p \, d\mathbf{Q}$$

Likewise the area which lies under the secondary curve will be equal to the exergy of the heat which is transferred from the secondary medium:

$$\Delta \mathbf{E}_s = \int f_s \, d\mathbf{Q}$$

The area which lies between the two curves corresponds to the value calculated using equation (3.2) and therefore must equal the exergy loss as a result of heat transfer. This diagram, a slightly modified version of the 'value' diagram [van Lier, 1992] will be used extensively in the system analysis in **part III**.

3.5.2 The value diagram for chemical reactions

The basis of the value diagram is the difference in exergy of the same amount of heat as it is transferred from a process flow and absorbed by another process flow at a lower temperature. In **Section 3.4** the exergy losses as a result of a chemical reaction are interpreted in a similar way. Exergy losses in a chemical reaction occur due to the difference in the value of the exergy of the heat at the temperature at which it is actually supplied and the exergy value of the heat if this heat is supplied to the process at equilibrium temperature. Using the concept of the equilibrium temperature, a reversible route for a chemical reaction can be conceived. This reversible route consists of three steps: (a) reversible heating/cooling of the mixture at constant composition to the equilibrium temperature, (b) the reaction occurs slowly going

through a series of equilibrium states until the outlet composition is obtained, (c) reversible reheating/cooling to the outlet temperature (cf. figure 3.16). In figure 3.18 the irreversible and the reversible process are shown for a reforming reaction in a Q,T-diagram. The curves in figure 3.18 are calculated curves based on the following starting-points:

- An initial methane/steam ratio of 2.5;
- 96% methane conversion;
- Inlet temperature 500 °C;
- Outlet temperature of 850 °C.

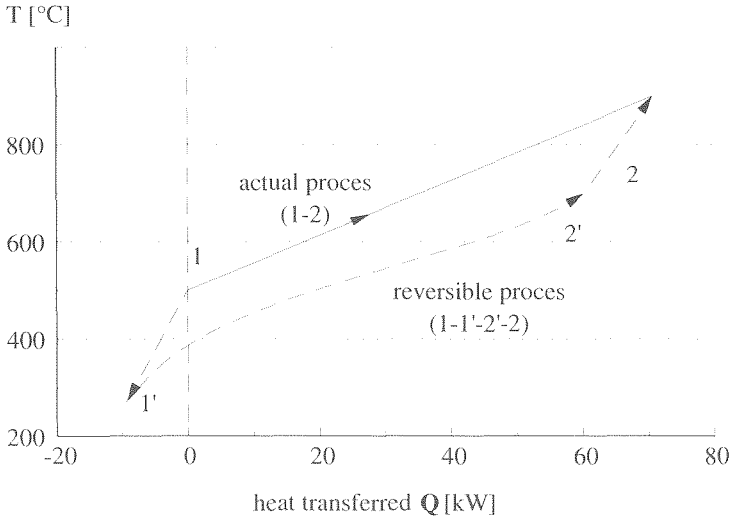

Figure 3.18: Comparison of an actual and a reversible reforming process routes in a Q,T-diagram

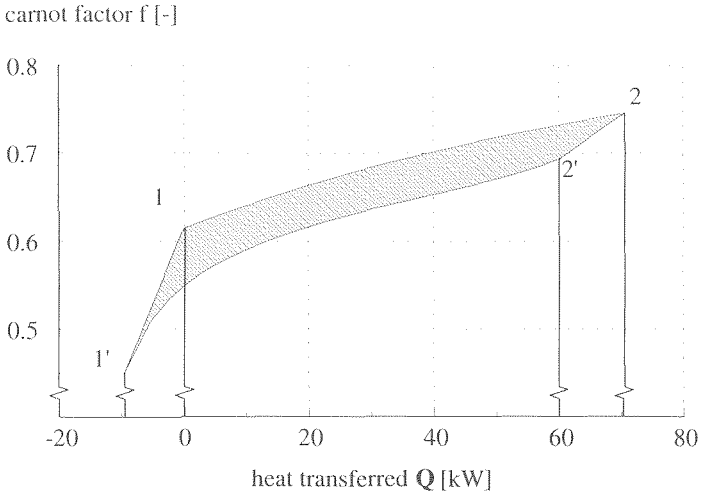

Figure 3.19 Value diagram for the reforming process corresponding the Q,T-diagram in figure 3.18

The irreversible (actual) process is given by 1-2 which is an (assumed) linear temperature profile (i.e. dT/dQ is constant). The reversible route is given by 1-1'-2'-2: after cooling the gas to equilibrium temperature corresponding to the inlet concentration (1-1'), the reforming reaction proceeds slowly going through a series of equilibrium states (1'-2') until the outlet composition is achieved and the gas is reheated to the outlet temperature (2'-2).

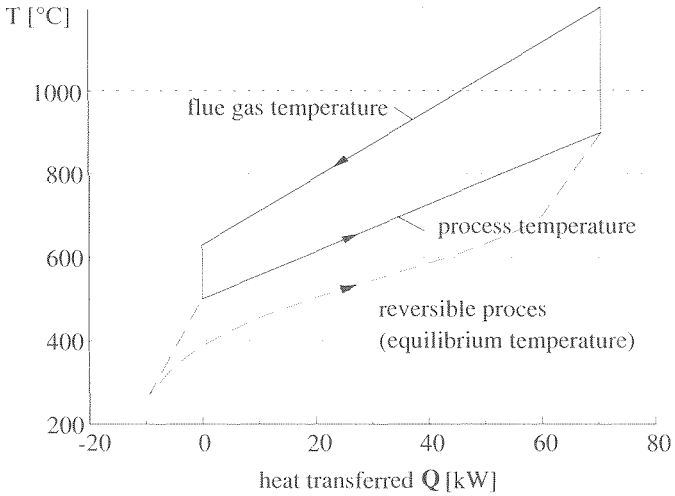

Figure 3.20: Q,T-diagram for the reforming process showing both the comparison of reversible and irreversible reaction routes and the heat transfer to the catalyst bed

Based on the Q,T-diagram in figure 3.18 the value diagram for the processes can be constructed (figure 3.19) by using $f=1-T_0/T$ instead of the temperature T on the Y-axis. The area which lies under the curve 1-2 is the amount of exergy which is actually supplied to the process. The exergy which has to be supplied to the reversible process is equal to the area below the curve 1'-2'-2 minus the exergy corresponding to the area below 1-1', which is exergy which is recovered initially (more exergy is recovered in cooling from 1 to 1' than has to be supplied from 2' to 2). The difference between the exergy required by the reversible and the irreversible process therefore corresponds to the area enclosed by the two curves 1-1'-2'-2 and 1-2 is equal to the exergy loss as a result of the chemical reaction.
An advantage of this diagram is that it is now possible to compare two different types of exergy losses: exergy losses as a result of heat transfer and exergy losses as a result of chemical reactions in one diagram. In the Q,T-diagram in figure 3.20 the cooling curve has been added the temperature profile of the flue gas flow which supplies heat to the catalyst bed is added to the curves for the reversible and the irreversible reforming process. The assumed inlet temperature for the flue gas is 1200 °C and the outlet temperature 630 °C (these values are representative for the values which are used/calculated in the system calculations in **part III**).
Converting this diagram to a value diagram by replacing temperature T by the Carnot factor f, results in the diagram shown in figure 3.21, which shows both types of losses in one and the same figure. This makes it possible to compare the contributions of both driving forces easily.

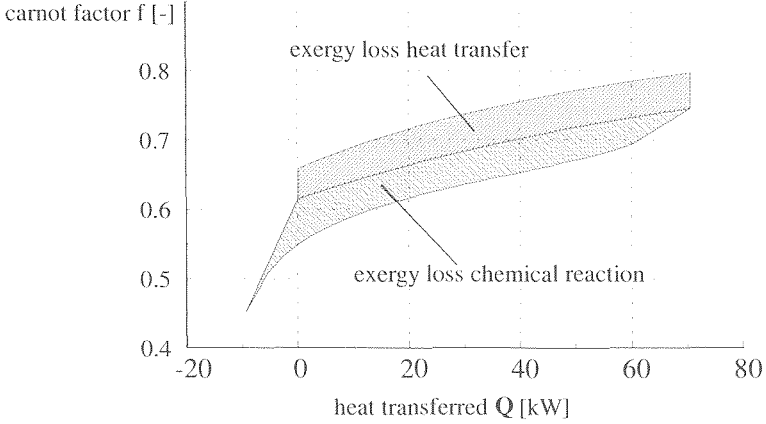

Figure 3.21: A value diagram for the reforming process corresponding the Q,T-diagram in figure 3.20

.

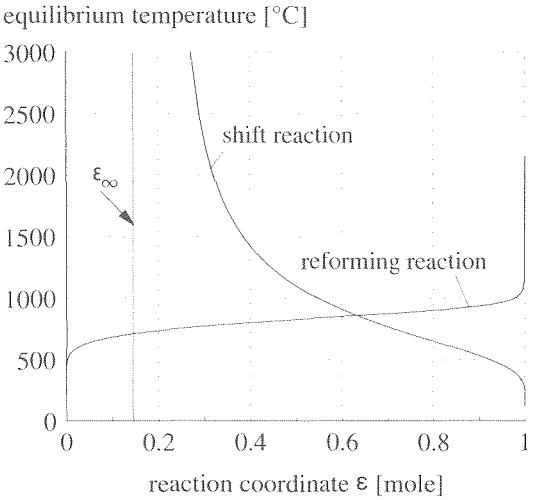

Figure 3.22 Equilibrium temperature for the shift reaction (ε =0 corresponds to $CO:H_2O$=1:1, ε=1 corresponds to $CO_2:H_2$=1:1) and reforming reaction (ε=0 corresponds to $CH_4:H_2O$=1:1, ε=1 corresponds to $H_2:CO$=3:1)

In figure 3.22 the equilibrium for the reforming reaction is shown. At high temperatures CH_4 is consumed to produce H_2:

$$CH_4 + H_2O \rightarrow 3H_2 + CO$$

To convert all CH_4 (ε=1), the temperature would have to approach infinity:

$$\lim_{\varepsilon \to 1} T_{eq} = \infty$$

On the other hand, decreasing the temperature in the equilibrium state, leads to production of CH_4 according to:

$$CH_4 + H_2O \leftarrow 3H_2 + CO$$

To convert all H_2 (and CO) into CH_4, in this case requires the equilibrium temperature approaches absolute zero or:

$$\lim_{\varepsilon \to 0} T_{eq} = 0$$

The figure shows a characteristic of the reforming reaction which is very important if use is made of value diagrams to represent chemical reactions: for every composition on the interval $\varepsilon = \langle 0,1 \rangle$ an equilibrium temperature exists. Therefore, a reversible process is always possible.
Contrarily, for the shift reaction this is not apparent. Starting with a composition corresponding to $\varepsilon=1$ (i.e. an equi-molar mixture of CO_2 and H_2) the temperature at which the heat has to be supplied has to be higher as the reaction proceeds to CO and H_2O as can be seen from figure 3.22. The shift reaction is exothermal, i.e. the equilibrium temperature decreases as H_2 is produced and CO is consumed. To convert all CO, the temperature of the (equilibrium) reaction should become equal to 0 K. On the other side, converting all the H_2 into CO through the shift reaction by increasing the temperature is not possible. The equilibrium temperature approaches infinity at a value of ε which is not equal to zero. It is not possible to let the reaction proceed below this value (i.e. convert more CO_2+H_2 into CO+H_2). The boundary value is indicated in figure 3.22 as ε_∞. For the *reforming reaction* all values for the reaction coordinate can be achieved as equilibrium conversions by adapting the temperature, because:

$$\lim_{T_{eq} \downarrow 0} \varepsilon = 0 \qquad \text{and} \qquad \lim_{T_{eq} \uparrow \infty} \varepsilon = 1$$

But for the *shift reaction* only values below ε_∞ can be achieved because:

$$\lim_{T_{eq} \downarrow 0} \varepsilon = 1 \qquad \text{and} \qquad \lim_{T_{eq} \uparrow \infty} \varepsilon = \varepsilon_\infty$$

For the shift reaction it is not true that for every composition on the interval $\varepsilon = \langle 0,1 \rangle$ an equilibrium temperature exists. Therefore, the reaction can only be represented in a value diagram in a limited range.
A second, more practical limitation of the diagram, is that the thermodynamic data used to calculate the equilibrium temperature are only valid in a limited range (for the JANAF data used in this thesis, for example, the limits are approximately 0-2000 °C (depending on the species). The equilibrium temperature will therefore in many cases exceed the range where the thermodynamic data are valid.
For all practical purposes the value diagram can only be used for specific conditions. A more generalized diagram will be developed in the following section.

3.5.3 The Carnot factor - enthalpy (f,H) diagram

The value diagram for chemical reactions is useful because it uses the difference in temperature between the reversible and the irreversible process and visualizes the reversible process. However, for a chemical reaction it is not always possible to determine a reversible route in the indicated manner. Therefore, the graphical presentation developed in the previous

section can only be used for equilibrium reactions and in this section a more general graphical method to visualize the exergy losses in the chemical reaction will be developed based on the Carnot factor. This approach is similar to the ones proposed by Ishida ([1986], [1998] and [Yamamoto, 1997]) and Le Goff ([1990], [1997]). For the exergy analysis an (isothermal) chemical reaction can be considered as two-step process (see **Section 3.4**). In the first process the heat of reaction is supplied to the process and in the second step the heat of reaction is 'absorbed' by the chemical reaction[n]. Separately the exergy of the heat which is supplied to the chemical reaction and the exergy change ΔE of the process flow can be calculated. The exergy loss ΔE_L is the difference between both.
The exergy of the heat can be calculated from equation (2.10):

$$d\mathbf{E}_Q = d\mathbf{Q}\left(1 - \frac{T_o}{T}\right)$$

The term between brackets in this equation is indicated as the **Carnot factor of the heat**:

$$f_Q \equiv 1 - \frac{T_o}{T} \qquad (3.37)$$

and, as can be seen from the equation for $d\mathbf{E}_Q$, the Carnot factor of the heat corresponds to:

$$f_Q = \frac{d\mathbf{E}_Q}{d\mathbf{Q}}$$

or, if the process occurs at a constant temperature:

$$f_Q = \frac{\mathbf{E}_Q}{\mathbf{Q}} \qquad (3.38)$$

The Carnot factor is a measure for the quality of the heat, i.e. a indicator for the ratio between the exergy of the heat (useful energy) and the energy of the heat. It is useful, as will be shown in the course of this chapter, to define the Carnot factor in a more general manner as the ratio between the exergy and energy:

$$\mathbf{f} \equiv \frac{\mathbf{exergy}}{\mathbf{energy}}$$

It is possible, using such a generalized Carnot factor, to define a **Carnot factor for the process flow $\mathbf{f_p}$**. The energy increase of a process flow (energy balance for an open, steady-state system) is equal to ΔH. The exergy increase of the process flow is ΔE. Therefore Carnot factor for the process flow is:

$$f_p \equiv \frac{\Delta \mathbf{E}}{\Delta \mathbf{H}} \qquad (3.39)$$

For the chemical reaction the exergy balance is:

exergy loss = exergy supplied with the heat - exergy increase of the process flows

---

[n] The direction of the heat flows is different for the exothermal reaction, but this does not alter the line of reasoning

or:

$$\Delta E_L = -Q\left(1 - \frac{T_0}{T}\right) - \Delta E$$

If the process occurs at a constant temperature, this equation can be rewritten using the Carnot factors defined by equations (3.38) and (3.39):

$$\Delta E_L = -\Delta H \cdot (f_Q - f_p)$$

If the temperature changes during the process, the equation becomes:

$$\Delta E_L = \int_{H_1}^{H_2} (f_p - f_Q)\, dH \qquad (3.40)$$

The general exergy balance for a process in the steady-state, open system (equation 2.17) considers the exergy increase of the process flows as well as the exergy of the energy flows. In such an open system energy is transferred to and from the system either in the form of heat (Q) and or work (W). A generalized **Carnot factor of the energy flow f_e** can be defined. f_e is equal to the ratio of the net exergy flow to the system and the net energy flow to the system:

$$f_e = \frac{E_Q - W}{\Delta H} \qquad (3.41)$$

This simplifies to equation (3.38) if only heat is exchanged between system en environment. The generalized form of equation (3.40) is therefore:

$$\Delta E_L = \int_{H_1}^{H_2} (f_p - f_e)\, dH \qquad (3.42)$$

This equation can be used to visualize exergy losses in the Carnot factor-enthalpy diagram (next section). To calculate the Carnot factor of the energy flow, equation (3.41) can be used. The calculation of the Carnot factor for the process flow is based on the general equation (3.39). For a system with constant composition (no chemical or electrochemical reactions), assuming ideal gas behaviour, ΔS is given by:

$$\Delta S = n \int_{T_1}^{T_2} \frac{c_V}{T}\, dT - n R \ln \frac{p_2}{p_1} \qquad (3.43)$$

If the composition of the process flow changes the reaction properties (**Section 2.3.2**) can be used to calculate the Carnot factor. If a reaction occurs the change of the exergy of the process flow, for an infinitesimal change of the reaction coordinate $d\varepsilon$ at temperature T and p according to equation (2.36) is equal to:

$$dE = \Delta_r e(\varepsilon)\, d\varepsilon$$

The energy increase required for the reaction is equal to the change in enthalpy, which according to equation (2.23) is corresponds to:

$$dH = \Delta_r h(\varepsilon)\, d\varepsilon$$

Now the Carnot factor for the process flow can be calculated as the ratio between change in exergy and change in energy as a result of the chemical reaction:

$$f_p = \frac{\Delta_r e}{\Delta_r h}$$

Or using $\Delta_r e = \Delta_r h - T_o \Delta_r s$ this equation can be rewritten to:

$$f_p = 1 - T_o \frac{\Delta_r s}{\Delta_r h} \qquad (3.44)$$

Two Carnot factors have been defined for the general case through equations (3.37) and (3.39). In the remaining part of this section some examples of f,H-diagrams specifically for chemical reactions will be discussed to illustrate the use of the Carnot factor to visualize losses. However, the Carnot factor can be used for other processes as well. In **part III** for example, the Carnot factor will be used to visualize the exergy losses in a fuel cell.
For any chemical reaction the two relevant Carnot factors are:

- The Carnot factor which characterizes the **energy** which is supplied in the form of heat to the process. The Carnot factor depends on the temperature and is calculated using equation (3.37);
- The chemical reaction leads to a change in exergy and a change in energy of the **process flow**. The exergy change in the chemical reaction can be characterized by the Carnot factor, which depends on the conditions (p,T) and composition (described by the reaction coordinate ε). The Carnot factor is calculated using equation (3.39).

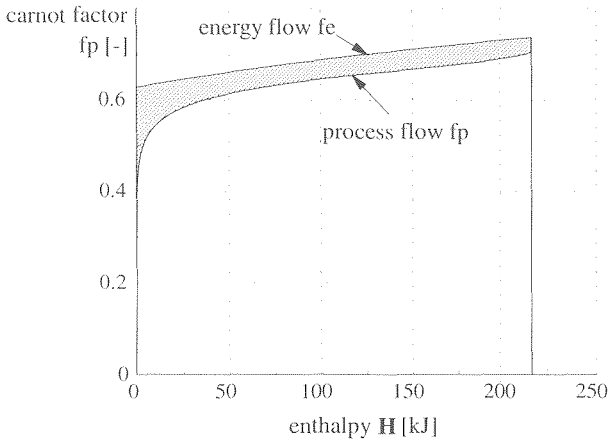

Figure 3.23: f,H-diagram for the reforming reaction calculated assuming a linear temperature profile in the catalyst bed, an initial composition of CH_4:H_2O = 1:2.5 and 96% conversion

3.5.3.1 The f,H-diagram for the reformer

To illustrate the use of the Carnot factor, once again the reforming process will be considered. Calculations are based on the same assumptions which were used to construct the value

diagram for the reforming reaction in the previous section:

- initial composition consisting of CH_4:H_2O = 1: 2.5
- methane conversion 96%
- linear temperature profile (dT/dH) in the catalyst bed (500 °C - 850 °C).

No work is performed on or by the system. The change in enthalpy (dH) therefore corresponds to the heat transferred to the catalyst bed (dQ). The Carnot factor for the energy supplied to the system is calculated from the assumed temperature profile (equation 2.4). The Carnot factor for the process flow is calculated from the general equation (3.39). By plotting the Carnot factors f_e and f_p against the change in enthalpy of the process figure 3.23 results (the change in enthalpy used in the graph is equal to the heat transferred to the process is because W=0).

The upper curve represents the heat supplied to the process. The exergy of this heat is equal to the area which lies under the curve. The lower curve represents the Carnot factor of the process flow and correspondingly the area under the curve is equal to the exergy increase or the process flow. The area between the curves therefore is equal to the exergy losses (see equation 3.42)

3.5.3.2 Shift reaction

A second example of a chemical reaction for which the f,H-diagram is constructed, is the shift reaction. In **Section 3.5.2** an essential difference between the reforming reaction and shift was discussed. For a mixture of the reactants/products of the reforming reaction for every composition an equilibrium temperature exists. However, it was shown that this is not the case for the shift reaction. This point can be clarified by considering the Carnot factor for the process flow. In figure 3.24 the Carnot factor for the two reactions are shown as a function of the reaction coordinate (the corresponding diagram showing the equilibrium temperature was shown in figure 3.22). Following the curve for the shift reaction and starting from the right hand side of the diagram H_2O+CO is formed. As the shift reaction proceeds

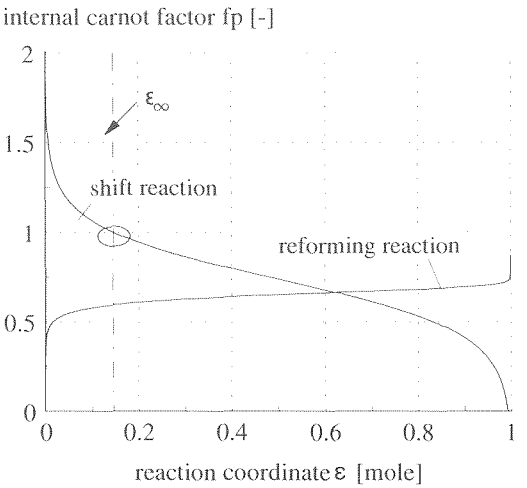

Figure 3.24: Carnot factor for the process flow for the shift (ε=0 corresponds to $CO:H_2O$=1:1, ε=1 corresponds to $CO_2:H_2$=1:1) and the reforming reaction (ε=0 corresponds to $CH_4:H_2O$=1:1, ε=1 corresponds to $H_2:CO$=3:1)

from ε=1 in the direction of ε=0, the Carnot factor of the process increases. That means that the ratio between exergy and energy of the heat supplied to the chemical reaction increases. If energy is supplied to the process in the form of heat only, this means that the temperature of the heat has to increase to obtain a further conversion ($H_2+CO_2 \rightarrow H_2O+CO$). If energy is supplied in the form of heat, the amount of exergy supplied to the process is never larger than the amount of energy and the Carnot factor will therefore always be less than unity. Therefore it is not possible to let a chemical reaction proceed if the Carnot factor is larger than unity (f_p >1).

In figure 3.24 this occurs at ε=0.14, which correspond to the asymptotic behaviour of the equilibrium temperature indicated in figure 3.22. To convert more H_2+CO_2 to H_2O+CO by supplying heat of a higher temperature is not possible. A Carnot factor >1 seems strange. However, consider for example an electrochemical conversion which is endothermal (Q>0) and produces work (W>0). The reversible or almost reversible electrochemical oxidation of carbon is an example of such a process (characterized by $|\Delta G|>|\Delta H|$). In that case the work produced by the system is larger than the net ΔH and f becomes larger than unity.

Note that the Carnot factor calculated for the reforming reaction in contrast is smaller than unity over the whole range of reaction. This agrees with the fact that an equilibrium temperature could be determined of the whole interval ε=[0,1].

In **Section 3.5.2** this lead to the conclusion that the exergy losses as a result of the shift reaction can not always be shown in a value diagram. However, the using the Carnot factor, it is possible to show these losses In figure 3.25 the f,H-diagram for a shift reaction is shown. The curves are calculated using the following starting points:

- Initial composition $CO:H_2O=1:1$;
- Process temperature 600 °C;
- Final composition is the equilibrium composition.

In the diagram the lower curve in this case represents the heat which is rejected by the process. As a constant temperature is assumed for the process, the Carnot factor of the energy (f_e) is constant ($1-T_o/T$). The shift reaction proceeds from ε=0 ($CO+H_2O$) to equilibrium at

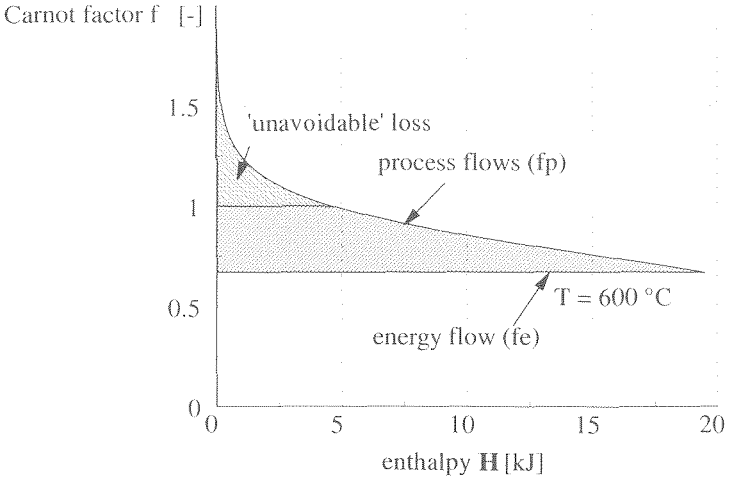

Figure 3.25: f,H-diagram for the shift reaction calculated assuming a constant temperature (600 °C), an initial composition of $CO:H_2O=1:1$, T=600 °C and assuming equilibrium at the outlet

600 °C. As the reaction proceeds, the Carnot factor of the process flow decreases. The reaction is exothermal: heat is produced. The exergy loss is due to the fact that the exergy of the heat which is produced in the reaction is lower than the exergy decrease of the process flow. Two facts are important in this diagram. The first is the fact that the exergy losses become smaller as the reaction proceeds (f_p-f_e becomes smaller) This is logical as the driving force (ΔG, see **Section 3.4**, figure 3.14) decreases as a result of the reaction and becomes zero as the process flow achieves equilibrium (corresponding to 62 % CO conversion). Secondly, at the start of the reaction, the Carnot factor of the process flow is substantially higher than 1. As indicated it is not possible to let the reaction proceed in the opposite direction by supplying heat, because the Carnot factor for heat is always smaller than unity. If the reaction occurs in the opposite direction the reaction can only be reversible if the exergy change in the reaction equals the exergy 'produced', i.e. the exergy of the energy which is released. However, if the process is a chemical reaction the energy is released in the form of heat (f_e<1). If f_p is larger than 1, the reaction is therefore always irreversible. Therefore the exergy loss in figure 3.25 has been divided into a part which could be recovered (f_p < 1) and a part which cannot be recovered in a chemical reaction ($f_p \geq 1$)[o].

3.5.3.3 Combustion of methane

A final example of the combustion of methane will be considered using the f,H-diagram. The combustion of a mixture of methane and nitrogen (CH_4:N_2=0.86:0.14) with air (O_2:N_2=0.2:0.8) is calculated (the fuel simulates the composition of Dutch Slochteren gas). The Carnot factor of the process flow f_p has been calculated and is shown in figure 3.26.

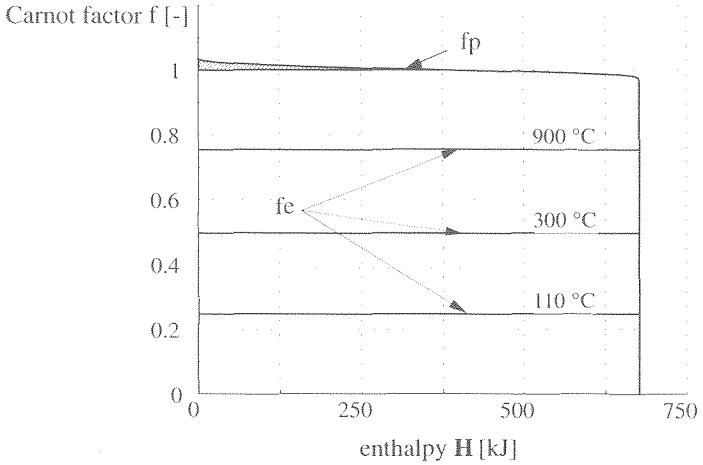

Figure 3.26: Analysis of the combustion of methane with air based on the calculated Carnot factor of the process flow f_p. Carnot factor for the energy flow shown for different temperatures of energy recovery

[o] This is an approximation because f_p has been calculated at process temperature (600 °C), cf. the closing remarks in **Section 3.5.2**

The area in figure 3.26 below the f_p curve and below the line f_p=1 is the exergy which could in principle be recovered in the form of heat. This exergy has been roughly divided into 4 equal parts, which show the influence of the average temperature at which the heat is recovered on the exergy efficiency of the combustion process. If the average temperature is 110 °C, the efficiency is approximately 25%. To increase this efficiency to 50% the average temperature of heat recovery should be 300 °C and 75% efficiency is achieved if the average temperature is 900 °C.

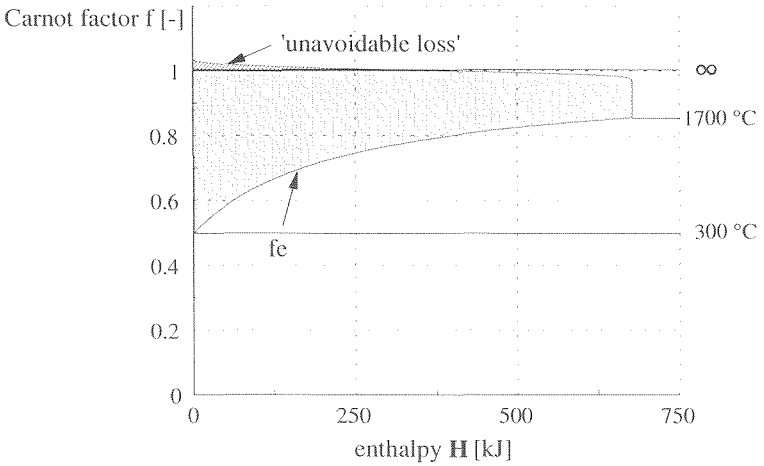

Figure 3.27: Analysis of the adiabatic combustion of methane with air based using preheated air and fuel (300 °C, λ=1.2)

In the normal combustion process, the process flow consists of a mixture of reactants (natural gas/air) at the inlet which is (gradually) converted to flue gas. The heat of reaction is released to this process flow. During the process the temperature of the process flow increases. The f,H-diagram for a combustion process in which the heat is transferred to the flue gas is shown in figure 3.27. The temperature profile (dT/dH) is calculated for the process flow assuming an adiabatic process an and inlet temperature of the process flows of 300 °C. The outlet temperature is calculated (1700 °C). Due to the decrease of f_p but mainly the increase of f_e as the reaction proceeds, the specific exergy losses (exergy loss per amount of energy converted) are much higher at the start than at the end of the combustion process. The figure shows that approximately one third of the exergy in the fuel is lost as a result of the chemical reaction and is 'recovered' in the flue gas.
If the energy in the flue gas is subsequently used in a process to produce power, for example in a steam cycle or a gas turbine, further losses will occur. To determine the role of the combustion process in the total exergy losses in the complete energy conversion system have to be considered. In these chapters methods for calculating exergy and exergy losses and for representing these losses graphically have been developed considering only the separate steps in the process. In **part III** these methods will be used to make the analysis for such the complete energy conversion system.

DISCUSSION I
'EXERGY ANALYSIS'

To analyse the performance of different fuel cell system configurations in the last part of this thesis, an advanced exergy analysis method is used. The theoretical framework and the equations used to calculate the exergy losses in the fuel cell system have been derived in these first chapters.
The degree of irreversibility in a steady-state process, can be determined by comparing the actual process with a reversible process leading to the same change of state of the process flows. This leads to the definition of "Lost work", as the amount of work produced less by the irreversible process than by the reversible process (**Section 2.2**). The lost work method however, does not take into account that less heat is required for the irreversible process than for the reversible process. If the environment is considered as the sink of heat, as is a logical choice for technical systems, the value of the heat is defined as the "Exergy": the work potential relative to the environment. The exergy 'balance' for a steady state process is derived:

exergy losses = exergy supplied to the process with the energy flows
- the change in exergy of the process flows

Explicitly separating exergy of the process flows and of the energy flows helps understanding complex processes, e.g. exergy losses in chemical reactions and is the basis for graphical methods developed in **Chapter 3**.
To calculate the net loss of work potential, or the "exergy loss", for a steady-state process, equation 2.17 is derived:

$$\Delta E_L = Q\left(1 - \frac{T_o}{T}\right) - W - \Delta E$$

To calculate the exergy loss, the change (Δ) in exergy between inlet and outlet has to be calculated. The general equations for the calculation of the change in energy (enthalpy) and exergy in a system where the composition changes as a result of chemical reactions is described (**Section 2.3**). Using a absolute values for these properties (**H**, **E**) is required for example when efficiencies are defined or for making energy and exergy flow diagrams. The use of absolute values for the energy and exergy of a process flow requires the use of a reference state. For the calculation of the value of the properties, a reference state is selected. For the calculation of the energy relative to the selected reference state, standard thermodynamic correlations are sufficient (**Section 2.4**). For the calculation of the exergy **E** relative to this environment, a new method is developed (**Section 2.5**)
The total exergy loss in a unit operation may be the result of one or more processes with their specific driving forces (**Section 3.2**). In the method developed in this thesis 5 such driving forces are distinguished in the fuel cell system :

- temperature difference → heat transfer;
- pressure difference → mass flow;
- difference in concentration → mixing (isothermal);
- difference in chemical potential → chemical reactions;
- difference in electrical potential → electrical current.

If only one driving force plays a role in a unit operation, calculating the total exergy loss is sufficient. However, if the processes in a unit operation are determined by more than one driving force, it is useful to determine which part of the total exergy loss can be attributed to each of the separate causes. In **Section 3.3** methods are developed to calculate these losses separately. The first method is 'sequential modelling', where a complex process is considered as a series of process occurring sequentially. For example the combustion process can be considered as a process where in the first step fuel and oxidant are mixed and in the second step reaction takes place. However, in some cases processes cannot be separated in this way. This is the case for the reforming process, where chemical reactions and heat transfer are closely linked. Another example in the fuel cell system is the fuel cell itself, where the electrochemical, chemical reactions and heat transfer are inseparable by with a black-box approach. In such cases a model which determines the process within the black-box is necessary. To calculate the different types of exergy losses within the fuel cell, the model developed in **part II** is used. For the reformer a separate model was developed to separate the losses as a result of heat transfer and chemical reactions.

Of particular interest in the fuel cell system are the losses as a result of heat transfer and the losses in chemical reactions. Heat transfer plays an important role in all energy systems. Chemical reactions are difficult to analyse because they generally occur simultaneously with other processes as heat transfer, friction and mixing. The losses in the chemical reactions and heat transfer are analysed in more detailed.

The concept of the equilibrium temperature is introduced in **Section 3.4** to clarify exergy losses in chemical reactions. The equilibrium temperature is the temperature at which a chemical reaction occurs reversibly. Using the equilibrium temperature, exergy losses can be interpreted more easily. For example in the reforming reaction the equilibrium temperature can be considered as the minimum temperature at which heat has to be supplied to the process. The exergy losses in the chemical reaction occur because the actual process occurs at a higher temperature. And therefore heat of a higher temperature (=higher exergy value) than necessary is used to achieve the chemical conversion.

This interpretation of the losses in the chemical reaction, which is based on the exergy balance in the form given above, makes it possible to visualize the chemical reaction in a 'value diagram' (**Section 3.5**). The value diagram can be used to visualize the losses as a result of heat transfer. The heated and cooled flow are shown and areas in this diagram represent the exergy losses. The value diagram is adapted for visualising exergy losses in chemical reaction using the equilibrium temperature.

However, this method is useful only for a limited class of reactions. In many cases no equilibrium temperature can be determined. Another method is developed to visualize the losses in (electro-)chemical reactions in those cases where no chemical equilibrium temperature can be determined. This method considers separately the change in exergy of the process flows and the exergy supplied to the process in the form of heat or power. For both quantities a separate generalized Carnot factor (=exergy/energy ratio) is calculated. Using these Carnot factors, complex processes involving chemical reactions and heat transfer can be represented in a Carnot factor- enthalpy diagram. These diagrams play an important role in the analysis of the losses in the fuel cell system in **part III**.

PART II:

"Fuel Cell Modelling"

INTRODUCTION II
A FUEL CELL MODEL FOR SYSTEM CALCULATIONS

A system calculation basically consists of the calculations of all mass and- energy flows in the system. A model of the fuel cell for use in system calculations therefore should calculate the mass and energy flows to and from the fuel cell stack. The mass flows for the fuel cell stack are the anode flow (fuel flow) and the cathode flow (which supplies O_2 and in the case of the MCFC CO_2 to the fuel cell). The relevant thermodynamic data of these flows are the temperatures, pressures and compositions at the in- and outlet of the fuel cell.

Detailed model
A large number of phenomena occur in the fuel cell: chemical and electrochemical reactions, heat transfer, mass transfer, etc. There is a strong interaction between the processes in the cell. For example, the rate of each of the processes (chemical reactions, electrochemical reactions, heat transfer, etc) depends on the local temperature. On the other hand, each of these processes in turn influences the temperature. This leads to a large number of equations which have to be solved simultaneously to calculate the local parameters (e.g. temperature, current density, composition). Furthermore, for any type of cell, the rate of the processes occurring in the cell is distributed non-uniformly. The model of the fuel cell therefore not only describes the local phenomena in the fuel cell, but also calculates the distribution of the parameters: temperature profiles, concentration profiles, etc.
In **Chapter 4** the development of a detailed model is described, which can be used to calculate both the output parameters (e.g. outlet concentrations) as the distribution of relevant parameters over the cell (e.g. a current density distribution or temperature profile). This model is used for two purposes. Firstly the calculation of local temperatures and compositions enables the calculation of exergy losses in the different processes occurring in the cell. This is required for the method of exergy analysis which is developed in **part I**. The second objective of the fuel cell model is the use of the model in the system calculations in **part III**. However, using the model directly in the system calculations is not possible and a two step approach is used.

Simplified model
Solving the mathematical model analytically is not possible if the local processes are described in some detail as in the model developed in **Chapter 4**. In order to solve the fuel cell model iterative numerical methods are required. The resulting model is not well suited for carrying out system calculations. System calculations involve highly iterative procedures to calculate all the process flows in the system. Correspondingly, in the course of one system calculation, the fuel cell model is called many times. Use of a detailed model as described above in a system calculation will lead to extreme calculation times. More fundamentally, the stability (convergence) of such a model is a problem, especially for systems with a high degree of integration as fuel cell systems. A robust model is required for these type of calculations while the detailed model is very sensitive to variations in input parameters. For system calculations therefore a highly simplified fuel cell model is required. In **Chapter 5** the calculation results for the detailed model are discussed for different stack configurations: SOFC and MCFC, external and internal reforming, co-flow and counter-flow. In **Chapter 6** a simplified model is developed. The effect of simplifying the fuel cell model is evaluated by comparing the results of the simplified model with the detailed model.

TABLE OF CONTENTS II (continued)

CHAPTER 4
A DETAILED MODEL FOR THE FUEL CELL

4.1 INTRODUCTION

The fuel cell model developed in this chapter is used to identify which phenomena are important to include in a model that is used for system analysis. Therefore, the model should be able to help understand the fundamental relationships between the parameters which are relevant to the system calculations:

- How does a change in fuel utilisation affect the efficiency of the fuel cell?
- Does the methane content of the anode gas at the cell inlet influence the temperature of the cathode off-gas at the outlet?
- How do the inlet concentrations affect efficiency and power density?

The main objective of the detailed fuel cell model is to understand how the operating parameters influence the performance of the fuel cell. In evaluating whether the necessary simplifying assumptions in the model are permitted, this objective for the fuel cell model should be kept in mind.

The main process in a fuel cell is the electrochemical reaction. In this reaction the hydrogen supplied through the anode flow, and the oxygen (and also the CO_2 in the case of a MCFC) from the cathode flow react. As a result of the reactions, an electrical potential difference builds up between the electrodes of the fuel cell. Because the cells within a fuel cell 'stack' are electrically connected in series, a large potential difference results between the end-plates of the fuel cell stack (the top and bottom cell). When an electrical current flows through the external load, the fuel cell delivers electrical power. To enable the electrochemical reaction several other processes occur: electricity is transported through the electrodes, ions are transported through the electrolyte and reactants and products of the reactions diffuse through the porous electrodes. Other processes are not directly related to the electrochemical reaction. Different chemical reactions may occur in the fuel cell, which may consume or generate heat as well. This heat, and the heat generated in the electrochemical reaction is removed from the fuel cell by the cathode and anode flow by convection and radiation. A detailed model of the fuel cell will include a wide range of phenomena: charge transfer in electrodes and separator, transport of ions through the electrolyte, electrochemical reactions and chemical reaction, heat transfer, mass transport, etc. All these processes occur with varying intensity in different parts of the cell. Key parameters, for example temperatures and compositions, will vary over the cell. A full model for the fuel cell will therefore include both a description of the local phenomena as well as describe the key parameters as a function of the location in the cell (eg. the temperature distribution).

Section 4.2 discusses which phenomena are included in the model and which are the key in- and output parameters for the fuel cell model. In **Section 4.3** the most important correlations used for the calculations of the local processes (rate of reaction, heat transfer, etc.) are reviewed. A consistent and complete set of equations for the subcell is given in **Section 4.4.** How the distribution of temperatures and compositions over the cell are calculated is discussed in **Section 4.5**.

4.2.1 Input data and output data for the fuel cell model

A schematic representation of a fuel cell is given in figure 4.1. The anode gas (fuel) and cathode gas (oxidant) are supplied separately to the fuel cell. As a result of (electro-) chemical reactions, compositions and temperatures of both process flows change and electrical power (P_e) is generated by the fuel cell. The outlet flows are the (partially) exhausted anode off-gas and cathode off-gas. The main component in the fuel cell is the PEN-layer[a], which consists of a cathode, an electrolyte and an anode. This is the active component in which the electrochemical and chemical reactions take place, in which the electrical power is generated, etc. The second essential element in the fuel cell is the separator plate or interconnect. The separator plate has three functions:

- to connect the two cells in series electrically;
- to form the separate channels through which the anode and cathode gas can flow;
- to separate the anode and the cathode compartment.

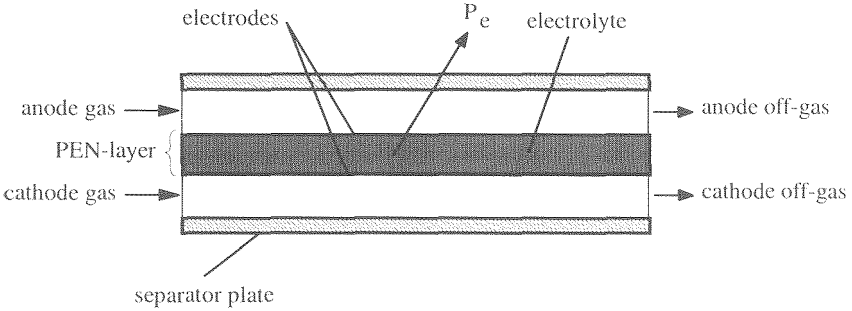

Figure 4.1: Schematic representation of a fuel cell

The most relevant processes which play a role in the fuel cell are:

- the electrochemical reactions;
- chemical reactions;
- heat transfer.

Models for the fuel cell can describe the processes occurring in the fuel cell in varying detail. As a minimum requirement for a fuel cell model it has to calculate the mass and energy balances over the fuel cell. The fuel cell model uses the mole flows (φ) and conditions (compositions $\underline{x}$ and temperature T) of the inlet as input data. The mass flows, compositions and temperatures at the outlet are calculated output data. Although for system calculations other combinations of input and output are often more useful, for simplicity the detailed model described in this chapter is such an 'inlet-to-outlet' model.

All thermodynamic data of the inlet flows (anode gas and cathode gas) have to be specified: the mole flows (φ [mole/s]), temperatures and pressures at the (anode and cathode). The composition of these flows is defined by specifying the mole fractions x_i for each component i. As figure 4.2 indicates, the mole fractions are treated as a vector ($\underline{x}$, with the elements $x(i)=x_i$). Other input data required by the fuel cell model are the cell and stack geometry. This includes for example the number of cells, cell area, channel diameters. It also includes the

[a] PEN =Positive electrode+Electrolyte + Negative electrode

data required to calculate the chemical and electrochemical processes: catalyst activities, ohmic resistance, etc. Evidently, which data are required will depend on the detail with which the processes in the fuel cell are modelled.
The electrical performance of the fuel cell is characterized by the electrical power which is generated in the fuel cell. The operating point for the fuel cell can be defined by specifying the generated power, the current delivered by the fuel cell or the cell voltage. Only one of these parameters can be selected independently for the calculations (see **Section 4.3**). In the fuel cell model the cell voltage (V) is specified to define the operating point for the fuel cell. Based on the complete data for the process flows (inlet and outlet flows), other parameters can be calculated, for example the cell current I and the electrical power P_e generated by the stack. Figure 4.2 gives an overview of in -and output for the fuel cell model.

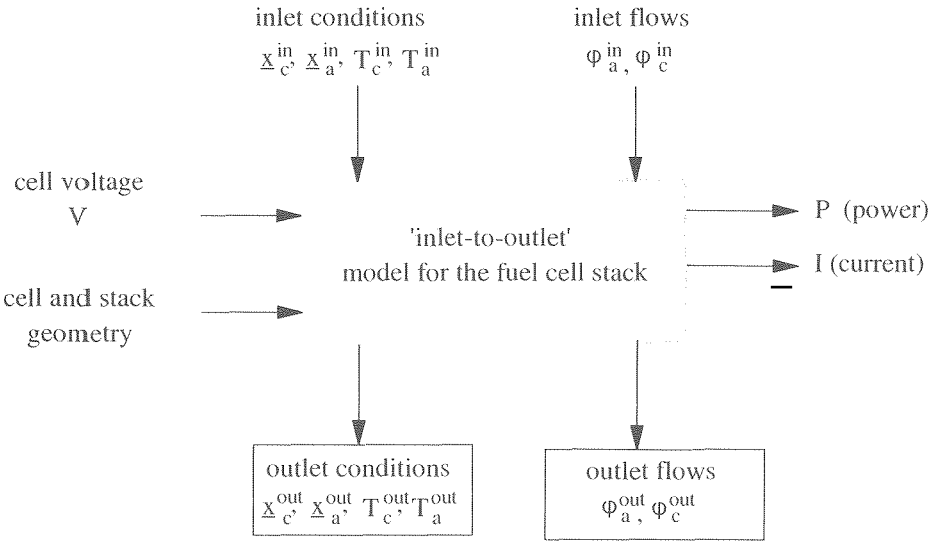

Figure 4.2: Basic inlet-to-outlet model for the fuel cell

4.2.2 From a 3-D stack model to a 1-D single cell model

A single fuel cell can only generate limited power. Therefore a fuel cell module always consists of a large number of single cells. Different geometries are possible for the cell element and for joining together a large number of fuel cells into a module. The fuel cell is a 3-dimensional system, which typically would require for example finite element techniques to model. Many such models have been described in literature. Examples of rigorous 3-D models for solid oxide fuel cells have been discussed among others by Erdle [1991], Karoliussen [1993], Achenbach [1994] and Recknagle [2003]. 3-D models for molten carbonate fuel cell stacks have been discussed by He, [1994] and Selman [1990]. The 3-D models give useful information for designing fuel cell stacks. However, these models lack the flexibility required for analysing the influence of different operating parameters on the performance of the fuel cell. Therefore, in view of the objective of the fuel cell model in this thesis, a less rigorous type of fuel cell model is required. In this section, the fuel cell configuration is selected and several assumptions are made to simplify the model.

- *Flat plate type or planar cells are considered.* The basic active element (PEN-layer) of a

fuel cell module in that case consists of a flat plate with anode gas flowing on one side of the plate and cathode gas on the other. For the molten carbonate fuel cell (MCFC) all cells are of the planar type. There are different types of SOFC stacks. The most important SOFC types are the tubular cell and the planar (flat plate). Although currently the tubular type is further developed, the planar type has an important advantage with respect to the manufacturing cost [Snowdon, 1991, Itoh, 1994, Romero, 1996]. Therefore this type as been selected.[b]

- *Idealized fuel cell stack.* Conditions for different cells in a stack may vary. In particular flows and temperatures may show a non-uniform distribution over the stack. Manifolding and inlet effects will result in different behaviour for each cell. A detailed model of the stack therefore should reflect how the uneven distribution of these parameters affects the performance of a real stack. There are two reasons why these effects are not incorporated in the fuel cell model developed in this chapter:
  - The fuel cell model developed here is not used (for example) to evaluate manifolding design, but to evaluate the effects of the more general parameters of the fuel cell;
  - Results from stack tests suggest that deviations from the uniform distribution of temperature and flows over the stack can be strongly reduced by adapting the stack design (see for example the results reported by ERC [Maru, 1992],[Farooque, 1994] and IHI [Kakihara,1994])

  Therefore in this thesis the stack is modelled as an ideal stack. A ideal stack, is a stack which consists of a large number of cells which operate under the same conditions (flows, temperatures). Evidently, this strongly simplifies the stack model because only one fuel cell element has to be modelled in detail.
- *Limitation to co-flow and counter-flow models*: Anode and cathode gas flow on different sides of the PEN-layer. The relative direction of the anode and cathode flow determine the flow configuration of planar fuel cell stacks: co-flow, counter-flow, cross-flow. Based on other evaluations of the differences between these types of cells (e.g. [Selman]), the additional modelling effort required to cross-flow cells is not justified for the current purpose. The detailed model has only been developed for co- and counter-flow cells.

A final general assumptions is that the calculations are based on the average pressure. The pressure drop over the fuel cell stack will typically be for example 2%-5% of the inlet pressure. This leads to a minor effect on the chemical and electrochemical reactions, which depend on the partial pressures of the reacting species. The exact profile of the pressure loss over the channels in the direction of the flow is therefore not taken into account[c].

Based on the assumptions listed above, it will be sufficient to model the fuel cell as a large number of repeating single cell elements. The flow direction in the single cell element is indicated as the x-direction (figure 4.3). As a result of the processes occurring in the fuel cell (reactions, heat transfer), compositions and temperatures will change in the x-direction. The detailed model therefore has to calculate the concentration and temperature profiles along the cell in the x-direction (even though the mole flows, concentrations and temperatures at the outlet of the fuel cell may be the only output from the model).

---

[b] For the type of calculations which are performed in **Chapters 5** and **6**, the difference between planar and tubular cells is not essential.

[c] The pressure loss over the fuel cell is an important effect in the system calculation, because the pressure loss influences the required power for the air and recycle blowers (see part III, "System Analysis").

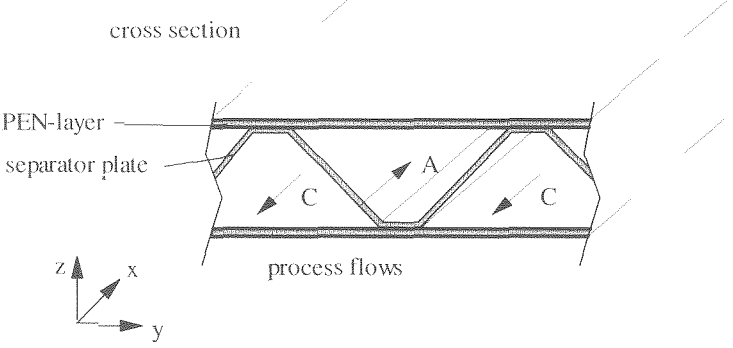

Figure 4.3 An example of a flat plate cell with corrugated separator plate

4.2.3 Main processes in the cross-section

Which are the processes which have to be taken into account in the fuel cell model to calculate the changes along the cell? As indicated the average pressure between in- and outlet is used in the fuel cell model. Therefore the thermodynamic state of the gas flows in a given cross-section is determined by the concentrations and temperatures (the cross-section is the y-z plane, see figure 4.3). Changes in temperature and concentration along the cell in flow direction, are due to several processes occurring in the cross-section of the cell. The most important processes are:

- electrochemical and chemical reactions in and on the PEN-layer;
- heat transfer (e.g. convection) from the PEN-layer and separator plate to the process flows;
- conductive heat transfer within the PEN-layer and the separator plate;
- mass transport from the PEN-layer to the process flows and within the process flows.

In the next section the specific assumptions used in modelling each of these processes will be discussed in detail. Based on the assumptions discussed in this section, the general characteristics of the fuel cell model discussed in this chapter can be summarized as follows:

- A fuel cell model considers a single, repetitive fuel cell element.
- The input for the fuel cell model are the inlet flows, concentrations and temperatures, the cell voltage and the geometry of the fuel cell.
- Outlet flows and conditions and the cell current I are calculated.
- The model describes the (electro-)chemical reactions and heat transfer within the fuel cell. Temperature and concentration profiles along the cell in flow direction are calculated.

4.3 SINGLE CELL MODEL

Many different geometries can be conceived for the fuel cell. The type of geometry represented in figure 4.3, where the separator plate or interconnect has a corrugated form, is an example of a specific geometry. A general characteristic of all concepts is the PEN-layer, with on one side the air electrode or cathode and on the other side a fuel electrode or anode. The (ion-conducting) electrolyte between both electrodes is the defining element for each type of fuel cell. A second general characteristics is that all fuel cells have some sort of separator plate which forms the channels through which the anode and cathode gas can flow and the electric conductor between two adjoining cells. The fuel cell model therefore has to

describe how processes as electrochemical reactions, chemical reactions and heat transfer take place in a generalized fuel cell consisting of a PEN-layer and a separator plate forming the channels for the process flows. For each of these processes, the starting points will be discussed separately in the following sections. The assumption which are made are explicitly valid only for high temperature fuel cells (MCFC and SOFC).

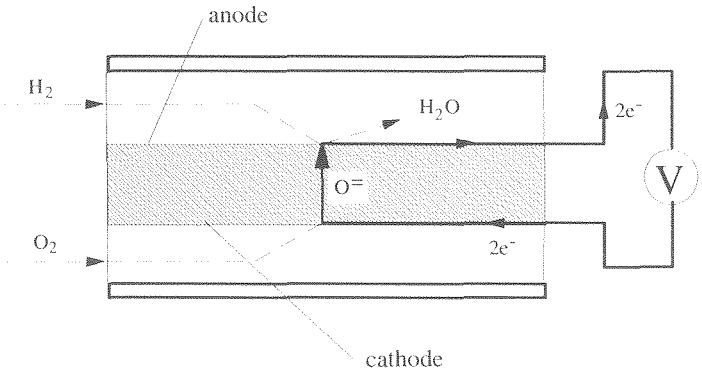

Figure 4.4: Principle of electrochemical reaction in the solid oxide fuel cell

4.3.1 Calculation of the power generated by the electrochemical reaction

In the fuel cell the combustion reaction $H_2 + ½O_2 \rightarrow H_2O$ is split into two half reactions. As these reactions involve electrons as reactants or products, these reactions are electrochemical reactions. In the SOFC for example (see figure 4.4), the hydrogen (H_2) reacts with an oxygen ion ($O^=$) at the anode and two electrons are released:

$$H_2 + O^= \rightleftharpoons H_2O + 2e^-$$

The electrons pass through the external electrical load and return to the fuel cell cathode where oxygen is reduced, absorbing the two electrons in the second half reaction:

$$½O_2 + 2e^- \rightleftharpoons O^=$$

In order to close the circuit, charge transfer (-) is required from the cathode to the anode. This charge transfer is achieved by transport of ions. In the case of the SOFC the charge is transferred by the $O^=$ ions. The different steps in this process (electron transport through the cathode electrode, reduction of O_2 to $O^=$-ions, transport of ions through the electrolyte, the reaction of H_2 with $O^=$, electron transport through the anode) can be considered as a series of steps which have to occur to enable the overall reaction:

$$H_2 + ½O_2 \rightleftharpoons H_2O$$

In the MCFC the charge transfer through the electrolyte is achieved by the transport of $CO_3^=$ ions from the cathode to the anode and the half reactions become:

$$H_2 + CO_3^= \rightleftharpoons H_2O + CO_2 + 2e^-$$

and:

$$\tfrac{1}{2}O_2 + CO_2 + 2e^- \rightleftharpoons CO_3^=$$

As a result of the electrochemical half reactions at both electrodes, an electric potential difference builds up between anode (-) and cathode (+). This potential difference is indicated as the cell potential or cell voltage V. The efficiency of the fuel cell and the power that the fuel cell generates is directly related to the cell voltage.
In the ideal case, the cell voltage is equal to the **reversible voltage** or **Nernst potential** V_{rev}. The reversible cell voltage represents the case that no losses occur in the electrochemical reaction. In a real fuel cell however, there is always a difference between the reversible voltage V_{rev} and the actual cell voltage V. This difference, ΔV, can be considered as the driving force for the electrochemical reaction.

$$V = V_{rev} - \Delta V \tag{4.1}$$

In general for flat plate type cells, the voltage losses which occur in (the plane of) the electrodes as a result of resistance are much smaller than the losses occurring in the electrochemical reaction or as a result of transport of ions in the electrolyte[d]. Therefore the voltage drop in the electrodes in the direction of the process flows can be considered negligible. This leads to the assumption that the cell voltage is constant in the whole cell, V=V(x). The reversible cell voltage on the other hand depends on the partial pressures of the reactants and on the temperature. Therefore, as the reversible voltage (and the voltage drop) vary along the cell and the cell voltage does not, we write:

$$V = V_{rev}(x) - \Delta V(x)$$

The dependency of the reversible voltage on the temperature and on the partial pressures of the reactants and products in the electrochemical reaction is given by the Nernst equation [Hirschenhoffer]. For the SOFC the Nernst equation equals:

$$V_{rev} = V_{rev}^{o}(T) - \frac{RT}{zF} \ln\left(\frac{p_{H_2,a}\, p_{O_2,c}^{\frac{1}{2}}}{p_{H_2O,c}} \right) \tag{4.2}$$

The Faraday constant F is defined as the (electrical charge) of one mole of electrons. z is the number of electrons produced in the electrochemical half reactions per mole hydrogen (z=2). V_{rev}^{o} is the standard reversible voltage. This corresponds to the theoretical voltage an ideal fuel cell would deliver if all the reactants and products are present at standard state (at a partial pressure of 1 bar [Smith & van Ness]). As equation (4.2) indicates, the standard reversible voltage depends on the temperature only. The second term in the equation is a correction for the actual partial pressure of the reactants and products. In the case of the SOFC, the relevant partial pressures are the hydrogen pressure at the anode (H_2,a) and the partial pressures of oxygen and water at the cathode: (O_2,c and H_2O,c respectively). For the MCFC, CO_2 plays a role at the cathode and anode as a reactant and product respectively. Correspondingly for the calculation of the reversible voltage of the MCFC the partial pressures of CO_2 appear in the Nernst equation as well:

$$V_{rev} = V_{rev}^{o}(T) - \frac{RT}{zF} \ln\left(\frac{p_{H_2,a}\, p_{O_2,c}^{\frac{1}{2}}\, p_{CO_2,c}}{p_{H_2O,c}\, p_{CO_2,a}} \right) \tag{4.3}$$

[d] although this is not true for all fuel cell designs, for example see [Bossel, 1992-a]

Using the Nernst equation the reversible cell voltage can be determined. To calculate the cell voltage, the parameter which is linked directly to the efficiency and the power output of the fuel cell, the voltage drop has to be calculated. The voltage drop in most cases corresponds to 30-50% of the Nernst voltage and is therefore an important effect in the fuel cell model.

Effective cell resistance

The voltage difference $\Delta V(x)$ can be considered as the driving force for the electrochemical reaction. The current density therefore increases with increasing voltage drop. The voltage characteristics of a fuel cell are generally given as a curve of the voltage (V) against the current density (i). The schematic representation of such a i-V curve is shown in figure 4.5. The general form for such a curve is discussed extensively in literature (eg. [Vetter], [Hirshenhoffer]). At low current density the voltage loss is dominated by the activation losses, which leads to a sharp increase in the voltage drop in this region ('I', in figure 4.5). At higher current density ('II') the effect of the ohmic and quasi-ohmic losses is dominant and the slope of the i-V curve becomes constant. At even higher current density ('III') the role of transport of reactants and products becomes increasingly important and as a result the slope of the i-V curve increases. Corresponding to this classification of losses, the voltage loss can be written as:

$$\Delta V = \Delta V_{pol,\,act} + \Delta V_{pol,\,trans} + \Delta V_{ohmic}$$

However, this expression is of limited practical value for predicting the voltage drop in the fuel cell. There are theoretical equations for all different types of losses and limitations. But even a simple approach based on the different reaction and transport mechanisms leads to a large number of parameters which have to be fitted. However, the model can be strongly simplified by lumping the losses by linearizing the voltage drop:

- The linearization is justified by the fact that the measured i-V curves for high temperature fuel cell do not show the deviation from linear behaviour as strongly as the schematic curve in figure 4.5 (e.g. [Larminy & Dicks], [Hirschenhoffer]). In particular the effect of activation polarisation at low current density is much less pronounced than shown in figure 4.5. Therefore the assumption is justified that the open cell voltage (V at i=0) corresponds to the reversible cell voltage V_{rev} at i=0.
- The current density range which is relevant to practical cell operation is much more limited than shown in figure 4.5. Low values of the current density lead to high investment cost per kW (the fuel cell is operated at a low power density). More importantly for linearization, high current densities lead to low efficiencies. The operating range for the fuel cell therefore more or less corresponds to the range indicated as (II) in figure 4.5, where the ohmic losses are dominant and the linearization of the voltage losses gives the smallest deviation.

For the calculations in the fuel cell model in this thesis voltage losses are assumed to be proportional to the current density. Linearization of the i-V curve leads to the following expression for the cell voltage:

$$V = V_{rev}(x) - i(x) \cdot R_{\square} \qquad (4.4)$$

where the subscript '□' indicates that $R_{\square}$ refers to the area specific resistance, i.e. with the unit [ohm·m^2] instead of [ohm]. The cell resistance will generally depend on the temperature and partial pressures in cross-section x. In **Appendix 4** the equations which have been used for $R_{\square}$ are discussed.

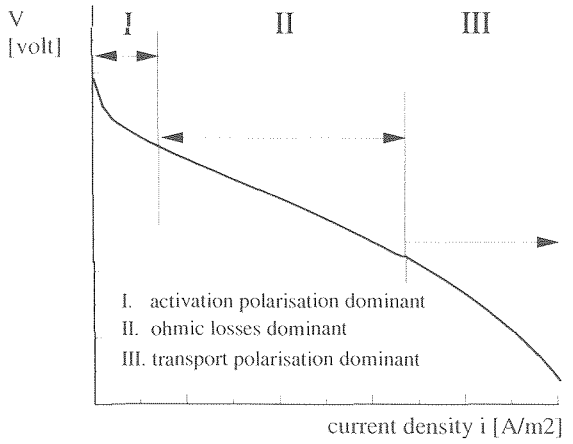

Figure 4.5: Schematic representation of the i-V curve for a fuel cell

The current density i is the current per unit area:

$$i(x) = \frac{dI}{dA} \tag{4.5}$$

For the definition of dA in this equation the idealized version of the separator plate shown in figure 4.6 is used. The actual separator plate (compare for example figure 4.3) covers part of the electrode area. As a result, the transport of species from the process flows to the electrodes is hindered and the active area of the cell is reduced. The form of the separator plate therefore influences the performance of the fuel cell. Some estimates have been made to determine the influence of the separator plate, e.g. on the reduction in effective area (eg. [Statoil]). However, this has not been taken into account as a separate effect in the model. The effective cell resistance $R_{\square}$ is considered to correspond to the total area (or apparent area as is sometimes called) instead of the effective area.
The current can be calculated from Faraday's law. For every mole of hydrogen which reacts in the electrochemical reaction, 2 moles of electrons are released. Because hydrogen can be produced within the fuel cell from other components, the total amount of hydrogen which can react in the electrochemical reaction is determined by the amount of hydrogen and other fuel components which can react to produce hydrogen. Taking into account CO and CH_4 as possible fuel components (cf. **Section 4.3.2**) this leads to the definition of the hydrogen equivalent flow:

$$\varphi_{eq,H_2} = \left(\varphi_{H_2} + \varphi_{CO} + 4\varphi_{CH_4}\right) \tag{4.6}$$

The charge of one mole of electrons is equal to the Faraday constant (F=96485 C/mole). If $\varphi^{in}_{eq,H2}$ is the hydrogen equivalent flow at the inlet, the maximum current which can be produced in the fuel cell equals:

$$I_{max} = 2 \cdot F \cdot \varphi^{in}_{eq,H_2}$$

However, in the fuel cell not all the fuel is converted. Generally the fuel utilisation, i.e. the fraction of fuel converted in the fuel cell (U_F), lies between 70% and 90%.Taking into

account the fuel utilisation U_F the expression for the current becomes:

$$I_F = 2 \cdot F \cdot \varphi^{in}_{eq,H_2} \cdot U_F$$

The electrolyte always shows a small conductivity to electrons as well, which causes a short circuit flow of electrons directly from the anode to the cathode. As a result, the effective current will be somewhat less than the theoretical current (I_F). The ratio between the actual and the theoretical current is called the Faraday efficiency:

$$\eta_F = \frac{I}{I_F}$$

The model assumes short circuit currents to be negligible ($I=I_F$) and therefore the current produced by the fuel cell is equal to:

$$I = 2 \cdot F \cdot \varphi^{in}_{eq,H_2} \cdot U_F \qquad (4.7)$$

This is an acceptable assumption for high temperature fuel cells. Summarising the 'electrochemical model', there are basically two relevant dependencies:

- The current in the fuel cell is linked to the changes in composition by Faradays law and the specification of the fuel utilisation U_F;
- The cell voltage depends on the reversible cell voltage, which can be calculated from the Nernst equation, and on the voltage drop. For the voltage drop the model assumes a linear correlation with the current (or more specifically in equation (4.4) the current density). The cell resistance is introduced to calculate the voltage drop in the model.

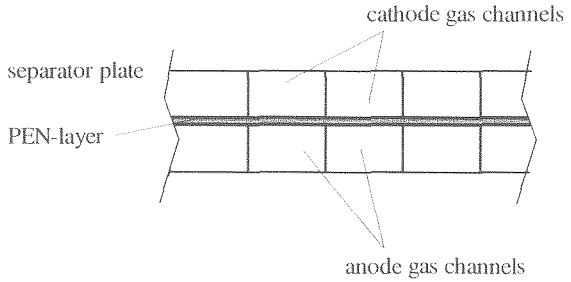

Figure 4.6: Simplified geometry for the fuel cell model assuming an idealized separator plate

4.3.2 Chemical reactions in the fuel cell

Besides the electrochemical reactions, different chemical reactions play a role in the fuel cell. The shift and reforming reactions are the main reactions determining the change in composition along the cell (at the anode side). The fuel cell model has to calculate the rate of reaction for both. The rates of reaction depend on the partial pressures of the reactants and on the temperature. For the calculation of the rate of reaction, the bulk concentrations have been used. The temperature for which equilibria and rates have been calculated is the temperature in the PEN-layer (see section 4.3.3)

Shift reaction
In both MCFC and SOFC CO can be oxidized directly at the anode. However, it seems that the polarisation in the CO oxidation will be slightly higher than in the oxidation of H_2. CO

can also be converted indirectly through the shift reaction. CO reacts to hydrogen in the shift reaction:

$$CO + H_2O \rightarrow H_2 + CO_2$$

Subsequently the hydrogen reacts in the electrochemical reaction. The shift reaction appears to be very fast in both types of high temperature fuel cells and as a result the shift reaction is practically at equilibrium. It is therefore likely, that the main route of oxidation of CO is through the shift reaction: CO is converted to H_2 and H_2 is converted in the electrochemical reaction. In order to determine the effect of the rate of the shift reaction, both equilibrium and kinetics have been modelled.

Reforming reaction
The reforming reaction is a very important reaction because of the large amount of heat which is consumed in the reaction and its strong influence on the hydrogen concentration. In the reforming reaction hydrogen is produced from methane:

$$CH_4 + H_2O \rightarrow 3\ H_2 + CO$$

For the fuel cell model a distinction must be made between external and internal reforming fuel cells.

- In external reforming systems, the methane is largely converted before the fuel is fed to the fuel cell. The conversion of methane in the reformer upstream of the fuel cell is very high (97 to 99%) and consequently the amount of methane in the fuel gas is small[e]. In the MCFC the conditions (600-700 °C, 1-5 bar) are favourable for the formation of methane (i.e. the reverse of the methane reforming reaction). Although some evidence indicates that this reaction does occur, the reaction appears to proceed slowly in absence of a catalyst. Consequently, the reforming reaction has not been included in the external reforming MCFC model. Due to the much higher operating temperatures in the SOFC, virtually all methane present will be converted in the reforming reaction at equilibrium. Because the nickel anode material is a good catalyst for the reforming reaction at this temperature, the reaction can be modelled as an equilibrium reaction for the external reforming SOFC.
- In the internal reforming fuel cell the concentration CH_4 in the anode gas is much higher and consequently the importance of the reforming reaction is much larger. Again there is an important difference between both types of high temperature fuel cells. At the high operating temperature in the SOFC, the reforming reaction is sufficiently catalysed by the anode material. The high rate of the reaction under actual cell conditions can lead to a strong local cooling effect which can induce thermal stresses. The correlations used in the model are based on a kinetic expression for the rate of reaction. If the kinetics of the reaction are very fast in an area of the cell, equilibrium modelling has been used. In the MCFC a separate catalyst is required to promote the reforming reaction. Furthermore the conditions (600-700 °C) in the MCFC favour a more gradual conversion of methane. However, the same kinetic/equilibrium modelling approach has been found to give good results.

Carbon forming reactions
There is another group of reactions which may occur in the fuel cell: coking reaction, ie.

---

[e] due to the high H_2O/CH_4 ratio at the inlet and the large increase in number of moles in the reforming reaction the methane content of the anode gas substantially less than 1 mole%

reactions in which carbon is formed. Carbon formation is detrimental to the performance of the fuel cell because it hinders the transport of reactants to the electrode/electrolyte interface and can mechanically damage the cell ([Mogensen, 1990], [Larminy & Dicks]). Whether carbon formation occurs, depends on:

- The thermodynamic equilibrium;
- The kinetics of the reactions.

It is not important to know how much carbon is formed (i.e. the rate for these reactions). But it is important to know if carbon will be formed. Therefore the model checks whether conditions favourable to carbon formation occur. A general theory predicting carbon formation on basis of kinetics is not available. The model estimates the possibility of carbon deposition on basis of the equilibrium of the carbon deposition reactions (Boudouard, methane-cracking). A safety factor is used to give a margin for the reaction kinetics.
The higher hydrocarbons will form carbon more easily than methane. Although tolerance to hydrocarbons in small concentrations has been established [Pigeaud, 1994], it is not clear whether the higher hydrocarbons in the natural gas (C_2H_6, C_3H_8, etc) will lead to carbon formation or not. Therefore the use of a pre-reformer has been assumed on all system calculations of internal reforming systems. No check on the carbon formation from higher hydrocarbons has been included in the fuel cell model.
The way in which each of the reactions is taken into account in the fuel cell model for the different types of fuel cells is summarized in table 4.1.

Table 4.1: Calculation of the rate of reaction for the chemical reactions in the fuel cell model

	reforming	reforming reaction	shift reaction	methane cracking
MCFC	external	not included in model	both equilibrium and kinetic models included	check on carbon deposition using a 'safety factor'
	internal	kinetic/equilibrium model		
SOFC	external	equilibrium model	both equilibrium and kinetic models included	
	internal	kinetic/equilibrium model		

4.3.3. Heat transfer model

The temperatures of the process flows changes along the cell as a result of the chemical and electrochemical reactions. Each of these reactions takes place on a specific location in the cross section of the cell. For example, the chemical reactions are catalysed on the surface of the electrodes. But heat generated as a result of electronic and ionic charge transfer will be generated within the materials of electrolyte, electrodes and separator. Due to the highly porous character of these electrodes and the small thickness of all components the reactions can be considered to occur in the PEN-layer assuming a constant temperature in the PEN-layer.
The basis for the calculation of the change in temperature of the anode and cathode flow is the energy balance over a small part of the fuel cell. As figure 4.7 indicates, a length of cell dx is considered. Within this infinitesimal distance, the heat dQ_a is transferred to the anode and the heat dQ_c to the cathode flow. In the cell element electrical power P_e is generated. The length of cell dx, with the system boundaries indicated in figure 4.7 with 'I', is an adiabatic stationary, open system and therefore the energy balance over the cell element corresponds to:

$$0 = dP_e + dH_a + dH_c \quad (4.8)$$

where dH indicates the change in enthalpy of the process flow between inlet and outlet of the control volume 'I'. Note that the energy balances are not based on energy [kJ] (as in **part I**) but on energy flows [kW]. Hence the notation dQ instead of d**Q** and the use of P_e instead of W_e in **part II.**

Heat generation

The heat which is produced in the electrochemical and chemical reactions results in an increase of the thermal energy over the subcell. However, as a result of the chemical and electrochemical reactions the chemical energy of the process flows decreases. Therefore the heat which is generated in the PEN-elements and absorbed by the process flows does not appear explicitly in the energy balance over the subcell ('I' in figure 4.7).

To be able to determine the heat which is generated in the PEN-element explicitly the energy balance over this system is considered (indicated in figure 4.7 as 'II'). The PEN-element is also a stationary open system: the flow into the system consists of the species which react and the process flows out of the system are the reaction products. The temperature in the PEN-element is assumed to be constant (T_c). The enthalpy of the reactants and products crossing the system boundary ('II') is calculated at this temperature as well. The energy balance over the PEN-element is:

$$dQ = dP_e + dH \quad (4.9)$$

where:

dP_e	=	the electrical work produced in the subcell;
dH	=	the enthalpy difference between the reactant into the PEN-element (reactant) and from the PEN-element to the process flows (products) at temperature T_c;
dQ	=	heat absorbed (Q>0) or generated (Q<0) in the PEN-element.

In the fuel cell model heat is generated in the PEN-element as a result of:

- the (overall) electrochemical reaction (e);
- the shift reaction (s);
- the reforming reaction (r).

The total heat generated in the PEN-element of the subcell therefore equals:

$$dQ = dQ_e + dQ_s + dQ_r \quad (4.10)$$

Heat transfer from PEN layer to the process flows

Because the model assumes the total heat is generated within the PEN-element, the model has to describe how this heat is transferred from the PEN-element. The gas flows (anode and cathode) cool the cell. Therefore all heat is ultimately transferred to the process flows. Figure 4.8 shows the relevant modes of heat transfer in the fuel cell. A distinction is made between heat transfer in the cross-section and heat transfer in the direction of the process flows. The most important heat transport mechanism in the x-direction (i.e. in the direction of the flow) is heat convection by the gas flows (Q_6). Heat transport in the direction of the gas flows by the hard ware (separator and PEN layer) is much smaller (Q_5), but has been taken into account in the model as well. However, accurately modelling the heat transfer in the cross section from the PEN layer to the gas flows is more critical to the calculated temperature profiles.

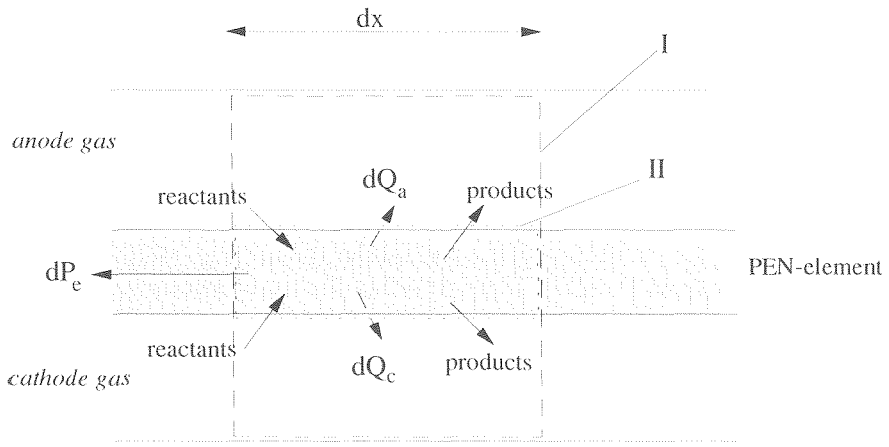

Figure 4.7: Energy and mass flows over the system boundary of a cell element with infinitesimal cell length dx ('I') and the PEN layer within the cell element

As indicated in figure 4.8, heat can be transported directly from the PEN layer (where the heat is generated) to the process flows (Q_1). The heat transfer mechanism in that case is convection. Given the relatively small channel diameters radiative heat transfer from the PEN element to the gas flow is negligible compared to the convective heat transfer. The heat generated in the PEN element can also be transferred from the PEN layer to the gas flow through the separator plate. In that case heat is transferred first from the PEN-layer to the separator plate (Q_4) and subsequently from the hardware to the process flows (Q_2).

heat transfer in the cross-section (y-z plane)

Q_1 = convection PEN -> gas

Q_2 = convection separator -> gas

Q_3 = radiation PEN -> separator

Q_4 = conduction PEN -> separator

heat transfer in the flow direction (x)

Q_5 = convection in gas flow

Q_6 = conduction in PEN

Q_7 = conduction separator plate

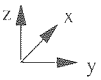

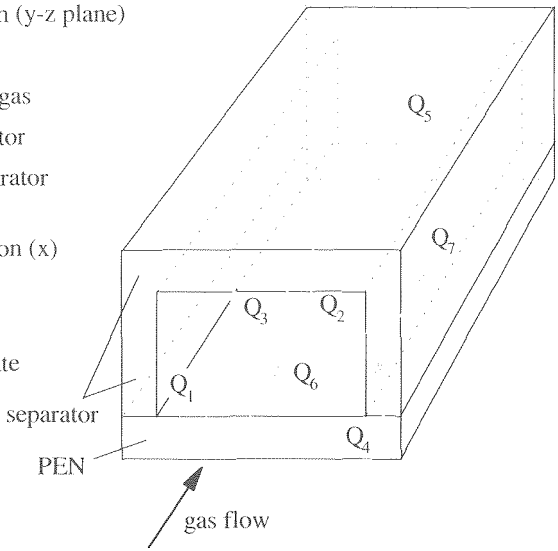

Figure 4.8: Main modes of heat transfer from the PEN element in the fuel cell

Figure 4.8 also shows two ways in which heat is transferred from the PEN layer to the separator plate. The first mechanism is by conductive heat transfer in the cross section (Q_4). Secondly radiative heat transfer may also play a role in reducing the temperature difference between PEN layer and separator plate (Q_3) . Good heat conductivity in the cross-section tends to minimize temperature differences between the separator plate and the PEN-layer. In **Appendix 5** it is shown that the heat conductivity of the separator plate is much higher than heat transfer coefficients for heat convection from the separator plate to the process flows. Therefore assuming that in a cross section the temperature in the separator plate and the temperature of the PEN layer are the same is an acceptable simplification. Heat transfer is therefore calculated assuming a uniform temperature T_e in the cross-section of the cell. As a result, the only mode of heat transfer in the cross section taken into account in the model is convective heat transfer from the hardware (PEN layer + separator plate).
Summarising the starting points for the model for heat transfer in the fuel cell:

- Heat is generated by electrochemical and chemical reactions in the PEN-layer;
- The PEN-layer and separator plate are assumed to have the same temperature in a cross-section of the fuel cell;
- Only convective heat transfer from hardware to gas flows (cross-section), convective heat transfer by the gas flow (x-direction) and conductive heat transfer in the hardware (x-direction) have to be taken into account explicitly in the model;
- The temperature in the cross-section is characterised to 3 values:
  $T_e(x)$ = electrolyte temperature (= temperature PEN-layer and separator plate) ;
  $T_a(x)$ = temperature of the anode, to calculate heat transfer from PEN to anode flow;
  $T_c(x)$ = temperature of the cathode, to calculate heat transfer from PEN to cathode flow.

The other modes of heat transfer (heat convection and heat conduction in x-direction) are depend on the gradient dT_m/dx, for each of these temperatures.

4.3.4 Using reaction coordinates to calculate the composition in a cross-section

The compositions of the process flows play a role in all calculations: the calculations of electrochemical and chemical reactions, the calculation of the heat balances, heat transfer, etc. To simplify describing the changes in composition along the cell, use is made of the previously defined **reaction coordinates (Section 2.3.1)**. A reaction coordinate ε indicates the number of mole/s which are converted in a reaction[f]. Because more than one reaction occurs, the progress of reaction k is denoted by ε_k. By definition ε_k is zero at the inlet of the fuel cell. Again note that the reaction coordinate ε in the fuel cell model is defined using the mole flows φ where in **Chapters 2** and **3** the reaction coordinate ε was defined in [mole]. The mole flow of component i at the inlet of the fuel cell is equal to φ_i^{in}. The stoichiometric coefficient for the reaction k and component is given by $\nu_{i,k}$ The mole flow for component i at cross-section x can then be given by:

$$\varphi_i(x) = \varphi_i^{in} + \sum_k \nu_{i,k} \cdot \varepsilon_k(x) \quad \text{for k=1...m} \qquad (4.11)$$

[f] the maximum corresponds to the maximum (mole/s) which can be converted in the reaction taking into account the presence of other components and stoichiometry of the reaction [Daubert]

Three reactions are important in the fuel cell (as discussed in **Section 4.2**) and correspondingly three reaction coordinates are defined:

- ε_e for the electrochemical reaction;
- ε_s for the shift reaction;
- ε_r for the reforming reaction.

The use of reaction coordinates has two advantage.

- Using the reaction coordinates introduces a standard manner of describing the changes in compositions in submodels. Normally the electrochemical submodel calculates the number of moles (hydrogen) consumed in the electrochemical reaction, the chemical submodel calculates the concentrations at the subcell outlet and the thermal submodel uses the number of moles CH_4 consumed to calculate the heat of the reforming reaction. Using the reaction coordinates, therefore introduces a uniform in- and output for all submodels.
- Secondly, the number of variables required to describe the compositions is equal to the number of reactions, which is much smaller than the number of components . Therefore a much compacter notation is possible using reaction coordinates instead of mole fractions, by using matrix notation.

The three reaction coordinates are written as a vector.

$$\underline{\varepsilon} = \begin{bmatrix} \varepsilon_e \\ \varepsilon_s \\ \varepsilon_r \end{bmatrix} \tag{4.12}$$

The compositions in the cross-section are defined as vectors as well. Seven chemical components are taken into account in the model. Besides the components in the electrochemical and chemical reactions, nitrogen is included. This leads to the following composition vectors:

$$\underline{\varphi}_a = \begin{bmatrix} \varphi_{a,H_2} \\ \varphi_{a,CO} \\ \varphi_{a,H_2O} \\ \varphi_{a,CO_2} \\ \varphi_{a,CH_4} \\ \varphi_{a,O_2} \\ \varphi_{a,N_2} \end{bmatrix} \quad \text{and:} \quad \underline{\varphi}_c = \begin{bmatrix} \varphi_{c,H_2} \\ \varphi_{c,CO} \\ \varphi_{c,H_2O} \\ \varphi_{c,CO_2} \\ \varphi_{c,CH_4} \\ \varphi_{c,O_2} \\ \varphi_{c,N_2} \end{bmatrix} \tag{4.13}$$

The reaction coordinates determine the mole flows in the cross-section. To calculate the composition the matrices $\mathbf{N}_a$ and $\mathbf{N}_c$ are defined in which the elements are the stoichiometric coefficients. As shown in **Section 2.3.1** the stoichiometric coefficient $\nu_{i,k}$ correlates the composition change ($\Delta\varphi_i$) for component i as a result of reaction k. The stoichiometric matrix $\mathbf{N}$ is therefore defined by the elements:

$$\mathbf{N}(k,i) = \left[\nu_{i,k}\right] \tag{4.14}$$

In **Appendix 6**, the stoichiometric matrices $\mathbf{N}_a$ and $\mathbf{N}_c$ are determined for both MCFC and SOFC. The composition in the cross-section in the anode flow can now be calculated by:

$$\underline{\varphi}_a(x) = \mathbf{N}_a \underline{\varepsilon}(x) + \underline{\varphi}_a^{in} \tag{4.15}$$

and:

$$\underline{\varphi}_c(x) = \mathbf{N}_c \underline{\varepsilon}(x) + \underline{\varphi}_c^{in} \tag{4.16}$$

Using these equations and notations, the composition at cathode and anode side of the fuel cell can be described with only three independent variables: the three reaction coordinates.

4.4. EQUATIONS FOR THE SUBCELL MODEL

4.4.1 The subcell model

As a result the processes occurring in the cross-section of the cell (described in the previous section) temperatures and compositions change along the fuel cell. The fuel cell model therefore does not only calculate in- and outlet values of these parameters. The model also calculates the profiles for the main variables in the fuel cell: temperatures, concentrations, current density. To calculate those profiles the fuel cell stack is split into a large number of subcells. The number of subcells is chosen large enough to enable the assumption that the temperatures, process flow compositions, mass flows, etc, may be approximated by an average value in a subcell[g]. By calculating the temperatures and compositions in each subcell, the temperature and concentration profiles along the cell are calculated. The iterative procedures for calculation the temperature and concentration profiles will be discussed in the next **Section 4.5**. In this section the equations for calculating the values of and changes in the main parameters for the subcell are discussed.
In the fuel cell a number of processes occur simultaneously. As indicated in the previous section, the most important processes are:

- the electrochemical reaction;
- chemical reactions;
- mass and heat transfer between process flows and hardware.

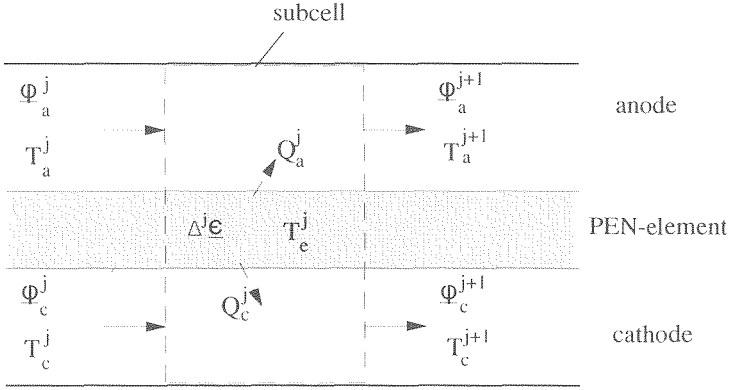

Figure 4.9: Key parameters in the subcell model from inlet (j) to outlet (j+1)

[g] The required number of subcells depends strongly on the type of cell which is modelled and can be varied accordingly (see **Chapter 5**). In most cases a non-uniform distribution of subcells is used.

Each subcell uses the outlet conditions (temperature, concentrations, mole flows) of the previous subcell as the input for the calculations. Therefore the input data for each subcell are the following parameters at the inlet of the subcell (**j**):

T^j_a = temperature of the anode flow
T^j_c = temperature of the cathode flow
φ^j_a = mole composition anode flow
φ^j_c = mole composition cathode flow

The corresponding values for the outlet of the subcell (**j+1**) are calculated. The submodel actually calculates the changes for the main parameter in each subcell. The simplified calculation using reaction instead of changes in composition has been introduced in **Section 4.3**. Accordingly the changes in composition over the subcell are calculated from:

$$\underline{\varphi}^{j+1}_a = \mathbf{N}_a \Delta \underline{\varepsilon}^j + \underline{\varphi}^j_a \tag{4.17}$$

and:

$$\underline{\varphi}^{j+1}_c = \mathbf{N}_c \Delta \underline{\varepsilon}^j + \underline{\varepsilon}^j_a \tag{4.18}$$

In the next sections the calculation of the change of the following independent parameters for each subcell will be discussed:

$\Delta^j\varepsilon_e$ change in reaction coordinate for electrochemical reaction is determined by the current density in the subcell (**Section 4.4.2**)

$\Delta^j\varepsilon_s$, $\Delta^j\varepsilon_r$ change in reaction coordinates for the shift and the reforming reaction are calculated based on equilibrium and/or kinetic data (**Section 4.4.3**);.

ΔT^j_a, ΔT^j_c the increase in temperature of anode and the cathode flow in the subcell are calculated from the energy balance over the subcell and heat transfer correlations (**Section 4.4.4**)

All chemical and electrochemical processes are considered to occur at the temperature of the electrolyte (T^j_e).

4.4.2 Calculation of the change of the electrochemical reaction coordinate in the subcell

The current in the subcell can be calculated from Faraday's law. For every mole of hydrogen which reacts in the electrochemical reaction, 2 moles of electrons are released. The mole flow hydrogen reacting in the electrochemical reaction is linked to the previously defined hydrogen equivalent flow (equation 4.6):

$$\varphi_{eq,H_2} = \left(\varphi_{H_2} + \varphi_{CO} + 4\varphi_{CH_4}\right)$$

Applying Faraday's law to subcell j, the generated current equals:

$$I^j = 2 \cdot F \, \Delta^j \varphi_{eq,H_2} \tag{4.19}$$

where F is the Faraday constant and $\Delta^j\varphi_{eq}$ the change of the hydrogen equivalent flow in the subcell. The change in the reaction coordinate for the electrochemical reaction is defined as the number of mole/s H_2 converted in the subcell and therefore:

$$\Delta^j \varepsilon_e = \Delta^j \varphi_{eq,H_2}$$

Linking the reaction coordinate for the electrochemical reaction directly to the current generated in the subcell eliminates the mole fractions:

$$\Delta^j \varepsilon_e = \frac{I^j}{2 \cdot F} \tag{4.20}$$

The driving force for the current in the subcell is the voltage drop. Linearizing the voltage drop (see **Section 4.3**) leads to the following expression for the current density the subcell:

$$i^j \cdot R_\square = V^j_{rev} - V \tag{4.21}$$

Combining equations (4.20) and (4.21) an expression for the change in reaction coordinate as a function of the cell voltage can be derived. Using the subcell area $\Delta^j A$ and the current density ($i^j = I^j/\Delta^j A$) instead of the current for the subcell, the expression for the change of the reaction coordinate in the subcell becomes:

$$\Delta^j \varepsilon_e = \frac{V^j_{rev} - V}{2 \cdot F \cdot R^j_\square} \Delta^j A \tag{4.22}$$

The reversible voltage, as can be seen from the Nernst equation (4.2), depends on the temperature, pressure and the composition at the anode and cathode. In calculating the reversible voltage for subcell j, the average partial pressure for the components (H_2, O_2, etc) and average temperature over the subcell is used in equation (4.2). The values of $R^j_\square$ are also evaluated for the average values for the subcell.

4.4.3 Chemical reactions in the subcell

In order to determine the composition at the outlet of the subcell, it is necessary to calculate the changes in the two other reaction coordinates:

- $\Delta^j \varepsilon_s$ for the shift reaction;
- $\Delta^j \varepsilon_r$ for the reforming reaction.

For the two chemical reactions included in the model, i.e. the shift and the reforming reaction, the calculation of the rate of the reaction in the subcell depends on the case which is modelled. In principle there are three options for modelling the chemical reactions:

- *the rate of the reaction is negligible*:
  An example is the reforming reaction in external reforming MCFC. If the rate of reaction is zero, the reaction coordinate for the subcell is zero as well:

  $$\Delta^j \varepsilon_k = 0$$

- *the kinetics of the reaction are fast:*
  In this case the composition will correspond to the equilibrium composition. In the most calculations the shift reaction is considered to be fast enough to assume chemical equilibrium. Whether or not the reforming reaction can be considered as an equilibrium reaction depends on the type of fuel cell modelled and the configuration of the stack. The calculation of $\Delta^j \varepsilon_k$ assuming equilibrium will be treated in **Section 4.4.3.1**.
- *the kinetics of the reaction are slow*
  If the rate of reaction is determined by the kinetics, the reaction will occur too slow to achieve equilibrium. In that case the change in the reaction coordinate $\Delta^j \varepsilon_k$ is calculated using (empirical) correlations for the rate of reaction. For both the shift and the reforming reactions the correlations for $\Delta \varepsilon_k$ are developed in **Section 4.4.3.2**.

4.4.3.1 Calculating the reaction coordinates assuming chemical equilibrium

In the fuel cell model, two different chemical reactions are modelled (shift and reforming reaction). Different methods of calculation are used when the chemical equilibrium composition of a single reaction has to be calculated and when calculating the chemical equilibrium composition of two simultaneous chemical reactions.

Calculating the equilibrium of a single reaction
The equilibrium composition for a single reaction is calculated in the following cases:
- The rate of the other reactions is considered negligible (for example the reforming reaction in the external reforming MCFC);
- The rate of one of the reactions is determined by the reaction kinetics.

To calculate the equilibrium composition for a single reaction, methods can be found in thermodynamics textbooks. The standard method (based on ΔG) is used to calculate the equilibrium constant K. If the composition is in chemical equilibrium for reaction k, the partial pressures will satisfy the expression using the equilibrium constant K_k:

$$K_k = \prod_{i=1}^{n} (p_i)^{\nu_{i,k}} \tag{4.23}$$

In the fuel cell model the reaction coordinate $\Delta^j\varepsilon_k$ is used to characterise the composition. As shown in **Appendix 7**, the partial pressures at the outlet of the subcell can be written as functions of the inlet composition and the changes in reaction coordinates. By introducing these expressions in the general equation (4.23) a method is developed to solve $\Delta^j\varepsilon_k$ from equation (4.23) directly. This leads to a general expression of the form:

$$b_0 + b_1\Delta^j\varepsilon_k + b_2(\Delta^j\varepsilon_k)^2 + b_3(\Delta^j\varepsilon_k)^3 + b_4(\Delta^j\varepsilon_k)^4 = 0 \tag{4.24}$$

As shown in **Appendix 7** the coefficients b_0 ... b_4 in this expression depend only on:
- the inlet composition φ^j of the subcell;
- the equilibrium constant K_k;
- the total pressure p.

In the appendix the equations for the coefficients b_0 ... b_4 are determined for the both the shift and the reforming reaction. This method of calculating the reaction rate is used in the fuel cell model if a single reaction is modelled as an equilibrium reaction.

Calculating the equilibrium of a two simultaneous reactions
In many other cases however, the equilibrium of both shift and reforming reactions has to be determined. In principle the equilibrium for two simultaneous reactions can be calculated using the equilibrium constants. This calculation is called the 'series reactor' method [Daubert]. However, due to the interactions between the two reactions, convergence of this calculation can be very slow. Because the equilibrium calculation is used many times (for every subcell in every iteration, see **Section 4.5**), a faster calculation is required.
Methods for solving simultaneous chemical reactions are available in literature. An example is the method based on minimization of the Gibbs energy using the Lagrange multipliers [Gordon & McBride]. Although this is a very powerful method, it introduces a large number of degrees of freedom because the method is based on the mole balances instead of the specific reactions. The number of unknowns which have to be solved is much larger than for example in the series reactor method, where only two variables are solved (i.e. both reaction coordinates $\Delta\varepsilon_k$).

Therefore a new method has been developed by the author which combines the advantages of both abovementioned methods. Like the series reactor method, the method makes explicit use of the reactions (which limits the number of variable to be solved) but the method is much faster than the series reaction method because it also takes into account the interaction of the different reactions. This 'linearization method' is described in detail in **Appendix 8**. Only the main points will be discussed below.
Just as in the calculation of equilibrium for the single reaction, use is made of the differential $\partial G/\partial \varepsilon_k$ for the reaction k:

$$g_k^1 = \frac{\partial G(\Delta\varepsilon_k)}{\partial \varepsilon_k} \qquad \text{for } k=1..\ell \tag{4.25}$$

G is the total Gibbs energy at the outlet of the cell written as a function of the change of the reaction coordinate. In the linearization method the second derivatives of the Gibbs energy to the reaction coordinates are used as well. The second derivatives represent the change of the equilibrium composition of reaction **k** as a result of the change of the reaction coordinate of reaction **m**. These cross-coefficients therefore reflect the interactions between the different reactions, which makes the method superior to the series reactor method.
The second derivatives are:

$$g_{k,m}^2 = \frac{\partial^2 G(\Delta\varepsilon_k)}{\partial \varepsilon_k \, \partial \varepsilon_m} \qquad \text{for } k,m=1..\ell \tag{4.26}$$

Expressions for g^1 and g^2 as a function of $\Delta^j\varepsilon_k$ are determined in **Appendix 9**. The Gibbs energy of the anode flow at the outlet of the fuel cell element depends on the reaction coordinates ($\Delta^j\varepsilon_k$ for $k=1..\ell$). The reaction k is in equilibrium at the outlet of the subcell if the Gibbs energy with respect to that reaction is at its minimum. Therefore the criterion for equilibrium of reactions 1 to ℓ is the set of equations:

$$g_k^1(\Delta^j\varepsilon_k) = 0 \qquad \text{for } k=1..\ell$$

In the fuel cell model the method is used to solve the equilibrium for the shift reaction and for the reforming reaction simultaneously ($\ell=2$). In **Appendix 8** it is shown that the reaction coordinates can be estimated by solving:

$$\begin{bmatrix} g_{ss}^2(0) & g_{sr}^2(0) \\ g_{rs}^2(0) & g_{rr}^2(0) \end{bmatrix} \begin{bmatrix} \Delta^j\varepsilon_s^* \\ \Delta^j\varepsilon_r^* \end{bmatrix} = - \begin{bmatrix} g_s^1(0) \\ g_r^1(0) \end{bmatrix} \tag{4.27}$$

where g^1 and g^2 are the first and second derivatives of G depending only on φ^j

4.4.3.2 Calculating the change of the reaction coordinates based on reaction kinetics

If the rate of a chemical reaction is insufficient to achieve equilibrium, the rate of the reaction is controlled by the reaction kinetics. To model the progress of the reaction, use can be made of empirical or semi-empirical expressions for the kinetics. The rate of the reaction is defined as the number of moles per second which react on a certain area. If the rate is denoted by r, the rate of reaction k can be calculated from the reaction coordinate by:

$$r_k^j = \frac{\Delta^j\varepsilon_k}{\Delta^j A} \tag{4.28}$$

where $\Delta^j A$ is the surface of the electrode on one side of the PEN-layer and $\Delta^j \varepsilon_k$ the change in reaction coordinate [mole/s] for the reaction. In most correlations in literature the specific rate r' is given (in [mole/s per kg catalyst]). If a A_r is the catalyst loading [kg/m^2], the average specific rate of reaction $r^{'j}$ for subcell j is equal to:

$$r_k'^j = \frac{1}{A_r} \cdot \frac{\Delta^j \varepsilon_k}{\Delta^j A} \tag{4.29}$$

If the area of the subcell is given by $\Delta^j A$, then the change of the reaction coordinate is calculated from:

$$\Delta^j \varepsilon_k = A_r \cdot \Delta^j A \cdot r'^j \tag{4.30}$$

The correlations used for the specific rates of reaction r'_k for the reaction playing a role in the fuel cell model will be discussed below.

a) Specific rate of reaction for the reforming reaction MCFC

The main reaction to be modelled is the reforming reaction, as the rate of this reaction influences the processes in the fuel cell to a large extent due to the highly endothermic nature of the reaction. In the MCFC, the catalyst is mounted in the anode gas channel. Therefore the amount of catalyst is a design parameter in the fuel cell model (in the SOFC the anode material itself (Ni-YSZ) is the catalyst and the amount of catalyst is determined by the electrode thickness).
In the literature on steam reforming and the literature on internal reforming MCFC's several relations for the rate of reforming can be found. One of the first semi-empirical relations found in the general literature on reforming is the relation given by [Akers & Camp, 1955]:

$$r_r' = k_0 e^{-E_A/RT} p_{CH_4}$$

where k_0 is the frequency factor and E_A is the activation energy. Although this relation is useful for describing the reforming reaction in an out-of-equilibrium situation, close to equilibrium it has limited validity. A great number of improved relations has been suggested which incorporate the equilibrium condition. Good agreement with experimental data have been achieved for MCFC [Willemski, 1985] using:

$$r_r' = k_0 e^{-E_A/T} \left(p_{CH_4} - \frac{p_{H_2}^3 p_{CO}}{p_{H_2O} K_r}\right) \tag{4.31}$$

Ding [1997] indicates that the equation compares well with experimental data over a wide range of steam/carbon ratios. Different catalysts correspond to different values of k_0 and E_a. Equation (4.31) is also based on equilibrium as can be seen from the criterion for the chemical equilibrium (see **Appendix 7**). If K_r^* is defined as the actual value of the ratio:

$$K_r^* = \frac{p_{H_2}^3 p_{CO}}{p_{CH_4} p_{H_2O}}$$

and K_r is the equilibrium constant, then the criterion for equilibrium is $K_r^* = K_r$ and equation (4.31) can be rewritten to:

$$r_r' = k_0 e^{-E_A/T} p_{CH_4} \left(1 - \frac{K_r'}{K_r}\right) \qquad (4.32)$$

For the calculation of the reforming rate in the fuel cell model for internal reforming MCFC stacks, the following data have been used [Willemski, 1985]:

A_r = 500 [kg/m^2]
k_0 = 0.01 mole/(kg atm)
E_A = 4000 kJ/mole

This expression has been used in the fuel cell model for the MCFC calculations.

b) Specific rate of reaction for the reforming reaction SOFC

In the SOFC the temperature is much higher than in the MCFC and the reaction equilibrium lies towards complete conversion of methane. In this case the reaction rate is determined purely by the kinetics of the reaction. A second difference with the MCFC is that the anode material itself (Ni-YSZ) serves as a catalyst. The amount of catalyst is therefore given and the catalyst loading can be calculated from the anode properties[h]. Several studies have been made to develop empirical correlations. For purely empirical correlations, valid for a limited range of conditions, the rate of reaction is often expressed as:

$$r_r' = k_0 e^{-E_A/T} p_1^{a_1} \cdot p_2^{a_2} \ldots$$

where the parameters p_i are the partial pressures of the reactants and product and the coefficients a_i are the reaction orders. For the SOFC Lee [1987] investigated a range of different Ni-YSZ pellets and fitted the data to:

$$r_r' = k_0 \cdot e^{-E_A/T} \cdot p_{CH_4}^{a_1} \cdot p_{H_2O}^{a_2} \qquad (4.33)$$

Lee determined the reaction orders to be $a_1 = 1$ while a_2 varied between -1.25 and -1.28 for different types of pellets. Corresponding values for k_0=0.68 [mole CH_4/(g-Ni s)] and E_A=11830 [kJ/mole] were determined. More recently work at Statoil (N) has shown much higher reforming rates [Odegard, 1994]. In experiments under varying steam/carbon ratios (S/C =1..3) no influence of the water partial pressure on the reforming rate was detected (β=0). The results were fitted by with k_0=3.11 [mole CH_4/(g-Ni s)] and E_A=7400 [kJ/mole], a_1 =0 and a_2 = 1.25. Reforming rates 50 to 100 times higher than found with the Lee-correlation are calculated. The high reforming rates are supported by the work done at British Gas [Parsons, 1992] which correspond more closely with the values calculated with the correlation published by Odegard. Therefore the Statoil correlation has been used for the SOFC model.

c) Specific rate of reaction for the shift reaction

With regard to the rate of the shift reaction no kinetic data exist. The reaction is so fast, that the assumption in fuel cell models is that the equilibrium composition is achieved at the outlet of the cell element. The influence of the rate of the shift reaction on the calculated power and

---

[h] For example (see [Hinseveld, 1989]) for a 35 µm anode, using a density of 4.5 g/cm3 the catalyst loading A_r is equal to 1.575 x 10^{-3} [kg/m^2].

the efficiency of the fuel cell is small. From the point of view convergence of the numerical solution the rate of the shift reaction is relevant. If the incoming fuel is not in equilibrium, the shift reaction will, in the case of equilibrium modelling, achieve equilibrium in the first subcell. If this subcell is very small, this leads to an unrealistically high heat flux in the first subcell. Therefore the reaction has been modelled using a 'general purpose' equation which calculates the rate of the shift reaction in the inlet zone based on the difference between the equilibrium composition and the actual composition at the inlet of the subcell. The calculation uses the difference between K_s, the equilibrium constant for the shift reaction, and K_s^*, the mass action for the shift reaction, which is calculated from the actual partial pressures of the components at the inlet of the subcell:

$$K_s^* = \frac{P_{H_2} P_{CO_2}}{P_{H_2O} P_{CO}}$$

Analogously to the expression for the reforming rate (4.32) the rate of the shift reaction can be written as:

$$r_s' = k_s \left(1 - \frac{K_s^*}{K_s}\right) \qquad (4.34)$$

$1 - K^*/K$ indicates how far the reaction is from equilibrium (when $K_s^* = K_s$). Because no representative data are available for k_s, a value for k_s has been estimated by assuming the shift reaction will be in equilibrium within 5% of the cell length (x/L=0.05). Sensitivity analysis showed the results of the fuel cell model are not sensitive to large variations in the value of k_s.

4.4.4 Heat transfer in the subcell

The objective of this section is to define the set of equations required to calculate the temperatures of the anode and the cathode flow at the outlet of the fuel subcell. The temperatures at the inlet of the subcell are T_a^j and T_c^j respectively (see figure 4.9). The temperature increase over the subcell at the anode side is denoted by $\Delta^j T_a$ and the outlet temperature is therefore equal to:

$$T_a^{j+1} = T_a^j + \Delta^j T_a \qquad (4.35a)$$

The corresponding equation for the cathode side is:

$$T_c^{j+1} = T_c^j + \Delta^j T_c \qquad (4.35b)$$

To calculate the temperatures in the subcell, it is necessary (1) to calculate how much heat is generated in the PEN-layer in the subcell and (2) how the heat is transferred from the PEN-layer to the process flows.

Calculation of the heat generated in the subcell

First the calculation of the heat which is generated in the PEN-layer of one subcell will be discussed. In the fuel cell model heat is generated in the PEN-element as a result of:

- the (overall) electrochemical reaction (e);
- the shift reaction (s);
- the reforming reaction (r).

The total heat flow transferred from the PEN-element to the process flows equals:

$$Q^j = Q_e^j + Q_s^j + Q_r^j \tag{4.36}$$

For the chemical reactions W=0 and therefore the energy balance becomes Q=ΔH. The heat generated by the chemical reactions in the PEN-element corresponds to the enthalpy change as a result of the chemical reaction. The heat generated by the shift reaction is equal to (see equation (2.23), **Section 2.3.2**):

$$Q_s^j = \Delta_r h_s \Delta^j \varepsilon_s \tag{4.38}$$

while the heat generated by the reforming reaction equals:

$$Q_r^j = \Delta_r h_r \Delta^j \varepsilon_r \tag{4.39}$$

To calculate the heat generated by the electrochemical reaction in the PEN-element, the electrical power which is generated by the system should be taken into account. The energy balance using energy flows (kW instead of kJ) becomes:

$$Q = \Delta H + P$$

and the energy balance over the subcell for the electrochemical reaction therefore equals:

$$Q_e^j = \Delta_r h_e \Delta^j \varepsilon_e + P_e^j \tag{4.40}$$

The amount of power generated in the subcell can be calculated from the cell voltage and the cell current: P=I·V. Using equation (4.20) to calculate I from the reaction coordinate for the electrochemical reaction gives:

$$P_e^j = I V = z F \Delta^j \varepsilon_e V \tag{4.41}$$

Correspondingly the heat generated in the electrochemical reaction becomes:

$$Q_e^j = (\Delta_r h_e + z F V) \Delta^j \varepsilon_e \tag{4.42}$$

reversible heat Q_{rev}

The total heat which is generated in the electrochemical reaction (equation 4.42) is partly due to irreversibilities. The amount of heat generated (and therefore the amount of cooling required, see part III) can be reduced by reducing the (voltage) losses. However, even if the process is reversible, part of the chemical energy which is converted, will be converted into heat. To reduce (or increase) this amount of heat, other measures are possible. Therefore the reversible and irreversible part of the heat generated in the electrochemical reaction will be calculated separately. Consider the case that the electrochemical reaction in the PEN-element is reversible. In that case the cell voltage will be equal to the reversible cell voltage V_{rev}:

$$P_{rev,e}^j = z F V_{rev} \Delta^j \varepsilon_e$$

The energy balance for the reversible process in the subcell is:

$$Q_{rev,e}^j = \Delta H + P_{rev,e}^j$$

Consequently the heat generated in the reversible reaction is equal to:

$$Q^{j}_{rev,e} = (\Delta_r h_e + z F V_{rev}) \Delta^j \varepsilon_e \qquad (4.43)$$

It can be shown [e.g. Daubert] that the reversible voltage is directly linked to the reaction Gibbs energy of the electrochemical reaction $\Delta_r g_e$:

$$V_{rev} = - \frac{\Delta_r g_e}{z F}$$

To calculate the heat which is generated in the reversible electrochemical reaction, the expression for the reversible work can be substituted into equation (4.43):

$$Q^{j}_{rev,e} = (\Delta_r h_e - \Delta_r g_e) \Delta^j \varepsilon_e$$

or

$$Q^{j}_{rev,e} = T_e \Delta_r s_e \Delta^j \varepsilon_e \qquad (4.44)$$

This is the well known expression $T\Delta S$ for the heat produced in a reversible process (equation 2.6). For the calculations in **Chapters 5** and further equation (4.44) has been used to calculate the reversible heat.

irreversible heat Q_{irr}
The heat which is generated as a result of the electrochemical reaction is always larger than Q_{rev} because of the irreversibility of the process or the voltages losses. The heat which is generated as a result of the voltage losses is indicated as the irreversible heat $Q_{irr,e}$. This heat can be calculated by combining equations (4.42) and (4.43), which leads to:

$$Q^{j}_{irr,e} = z F \left(V_{rev} - V \right) \Delta^j \varepsilon_e$$

or, using ΔV as introduced in **Section 4.3.1**:

$$Q^{j}_{irr,e} = z F \Delta V \Delta^j \varepsilon_e \qquad (4.45)$$

A logical result, as ΔV is introduced as the loss term or irreversibility in the electrochemical reaction.

Calculation of the temperature increase over the subcell
The heat Q which is generated in the PEN-element by the chemical and electrochemical is transferred from the PEN-element either by convection to the process flows or by conduction to an adjoining PEN-element. The following heat flows have to be calculated in the subcell

- Convective heat flow from the subcell to the anode flow;
- Convective heat flow from the subcell to the cathode flow;
- In-plane conductive heat flow from the subcell to the adjoining subcell (j+1);
- In-plane conductive heat flow from the subcell from the adjoining subcel (j-1).

Basic equations
The calculation of the temperatures in the subcell uses only a limited number of basic equations. The heat balances over the gas flow are used to calculate the temperatures changes over the subcell are

$$Q = m c_p \Delta T \qquad (4.46)$$

Overall heat transfer coefficients are used to calculate heat transfer from the hardware (PEN and separator) to the process flows (using the sign convention discussed in **Section 2.2**):

$$Q = -\alpha \Delta A \, (T_c - T) \tag{4.47}$$

The basic equation for conductive heat transfer through the hardware in x-direction is:

$$\frac{dQ}{dx} = C_\lambda \frac{d^2 T_c}{dx^2} \tag{4.48}$$

where C_λ is the sum of the heat conductivities of the separate cell components (anode, cathode, electrolyte, separator plate). If $A_{cs,i}$ is the cross sectional area of component i, the effective heat conductivity is equal to:

$$C_\lambda = \sum_{comp.} A_{cs,i} \lambda_i$$

Equations for the subcell

Based on the assumption discussed in **Section 4.3**, the heat which is produced in the PEN-layer in the subcell (Q^j) is transferred either to process flow at the anode (Q_a^j) or the cathode (Q_c^j) or by conduction to the adjacent subcells, for which the net effect is equal to $Q_\lambda^{j+1} - Q_\lambda^j$. The heat balance over the PEN layer (see the boundary indicated as **II** in figure 4.7) in the subcell is:

$$0 = Q^j + Q_a^j + Q_c^j + Q_\lambda^{j+1} + Q_\lambda^{j-1} \tag{4.49}$$

where:

Q_a^j: convective heat flow from the subcell to the anode flow
Q_c^j: convective heat flow from the subcell to the cathode flow
Q_λ^{j+1}: in-plane conductive heat flow to the subcell from the adjoining subcell (j+1)
Q_λ^{j-1}: in-plane conductive heat flow to the subcell from the adjoining subcell (j-1)

The heat transferred to the anode and cathode flow is calculated using equation (4.47) and the difference between the electrolyte temperature and the average temperature of the process flow in the subcell:

$$Q_a^j = \alpha_a \cdot (T_e^j - (T_a^j + \tfrac{1}{2}\Delta^j T_a)) \cdot \Delta A \tag{4.50}$$

$$Q_c^j = \alpha_c \cdot (T_e^j - (T_c^j + \tfrac{1}{2}\Delta^j T_c)) \cdot \Delta A \tag{4.51}$$

These correlations for heat transfer use the bulk temperature of the gas flow. The heat transfer coefficients α_a and α_c can be calculated from the dimensionless Nusselt number defined as:

$$Nu = \frac{\alpha d_h}{\lambda}$$

where d_h is the hydraulic diameter and λ is the heat conductivity of the gas. In the channels of the fuel cell, the flow past the inlet zone, is laminar. The situation in the cross-section of the fuel cell is best represented by the assumption of constant heat flux and constant temperature in the cross section perpendicular to the flow. A constant Nusselt number is assumed for this case based on the work of [Bossel, 1990-b]. The value (α=3.6) has been taken from Hinseveld [1980]. The method for calculating the thermal conductivity of the gasses and corresponding heat transfer coefficients given in **Appendix 1**.

If c_P is the total heat capacity of the process flow, than the increase in temperature (equation 4.46) at the anode and cathode must also be equal to:

$$\Delta^j T_a = \frac{Q_a^j}{\varphi_a \cdot c_{P_a}} \tag{4.52}$$

$$\Delta^j T_c = \frac{Q_c^j}{\varphi_c \cdot c_{P_c}} \tag{4.53}$$

Heat conduction from the adjacent subcells is calculated using the average temperature gradient (heat absorbed by the system is positive, cf. **Section 2.2**). Assuming uniformly sized subcells (with a lenght Δx), the average temperature gradient between subcell j and j+1 is equal to:

$$Q_\lambda^{j+1} = C_\lambda \frac{(T_e^{j+1} - T_e^j)}{\Delta x} \tag{4.54}$$

and between subcell j-1 and j:

$$Q_\lambda^{j-1} = C_\lambda \frac{(T_e^{j-1} - T_e^j)}{\Delta x} \tag{4.55}$$

Equations (4.49) - (4.55) form a set of 7 equations from which 7 unknowns can be solved:

- Convective heat flows: Q_a^j and Q_c^j
- Conductive heat flows: $Q^{j+1}{}_\lambda$ and $Q^{j-1}{}_\lambda$
- Temperatures: T_e^j, T_a^j and T_c^j

The system can be solved numerically. However a different approach is used in the fuel cell model. First the amount of heat generated in the subcell Q^j is calculated. In the next calculation step the net amount of heat exchanged with the adjacent subcells (ΔQ_λ) is calculated, using the temperature difference ($T_e^j - T_e^{j+1}$) from the previous main iteration (see **Section 4.5**). Q_a^j and Q_c^j are eliminated by substituting the expressions (4.50) and (4.51) in the heat balance for the PEN element (equation 4.49). Eliminating T_e^j, T_a^{j+1} and T_c^{j+1} using equations (4.51), (4.52) and (4.53) leads to explicit correlations for ΔT_a^j and ΔT_c^j. To simplify the notations we introduce

$$B_a = \frac{\varphi_a c_{P_a} - \frac{1}{2}\alpha_a \Delta^j A}{\varphi_a c_{P_a} \alpha_a \Delta^j A}$$

and

$$B_c = \frac{\varphi_c c_{P_c} - \frac{1}{2}\alpha_c \Delta^j A}{\varphi_c c_{P_c} \alpha_c \Delta^j A}$$

B_a and B_c depend only on the heat transfer coefficients (α_a, α_c), the heat capacities ($c_{P,a}$, $c_{P,c}$), the subcell area ΔA^j and the mole flows φ_a^j and φ_b^j (all are parameters in the equations (4.49)-(4.53)).

Using these notations, the explicit equations for ΔT_a^j and ΔT_c^j become:

$$\Delta T_a^j = \frac{(-Q^j - \Delta Q_\lambda)\, B_c + T_c^j - T_a^j}{n_a\, c_{p_a} (B_a + B_c)} \tag{4.54a}$$

and:

$$\Delta T_c^j = \frac{(-Q^j - \Delta Q_\lambda)\, B_a + T_c^j - T_a^j}{n_c\, c_{p_c} (B_a + B_c)} \tag{4.54b}$$

4.5 INTEGRATED MODEL OF THE FUEL CELL

The fuel cell model divides the length of a cell into a large number of subcells. The equations discussed in the previous section can be used to calculate the change of the following independent parameters for each subcell:

$\Delta^j\varepsilon_e$ = change in reaction coordinate for electrochemical reaction in subcell j;
$\Delta^j\varepsilon_s$ = change in reaction coordinate for the shift reaction in subcell j;
$\Delta^j\varepsilon_r$ = change in reaction coordinate for the reforming reaction in subcell j.
ΔT^j_a = temperature increase of anode flow in the subcell [K]
ΔT^j_c = temperature increase of the cathode flow in the subcell [K]

Furthermore the average electrolyte temperature T_e^j is defined for each subcell.

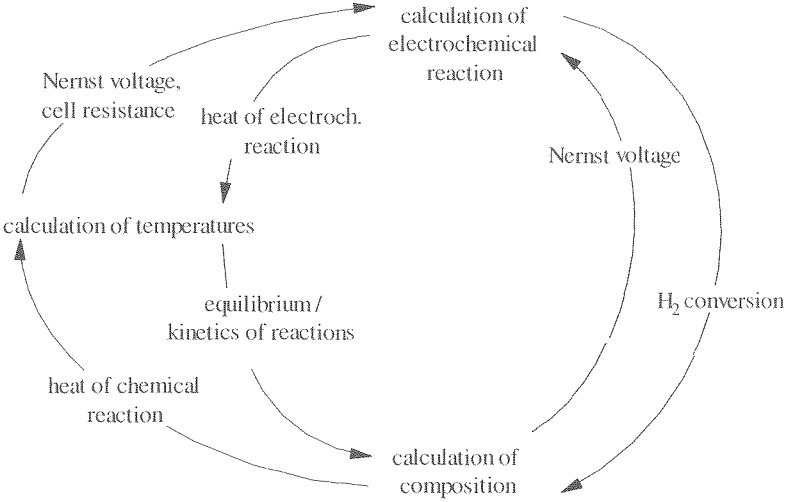

Figure 4.10: Interaction between the different calculations in the subcell model

If the compositions and temperatures at the inlet of the subcell are known, the outlet compositions and temperatures for the subcell can be calculated using these variables. This leads to a straight-forward procedure where the output of the subcell calculation is used as input in the calculation of the next subcell.

However, the problem is that the different calculations are closely linked. This is illustrated in figure 4.10:

- The rate of the electrochemical reaction depends on the (hardware) temperature in the subcell (T_c^j) through the Nernst voltage and the cell resistance;
- The temperature increase in the subcell depends on the amount of heat which is generated in the electrochemical and chemical reactions;
- The heat produced in the chemical reactions is a function of the compositions at the anode and cathode and consequently as well on the hydrogen conversion in the electrochemical reaction;
- The Nernst voltage driving the electrochemical reaction depends on the average compositions in the subcell;
- Equilibrium and the kinetics of the chemical reactions are a function of the temperature as well.

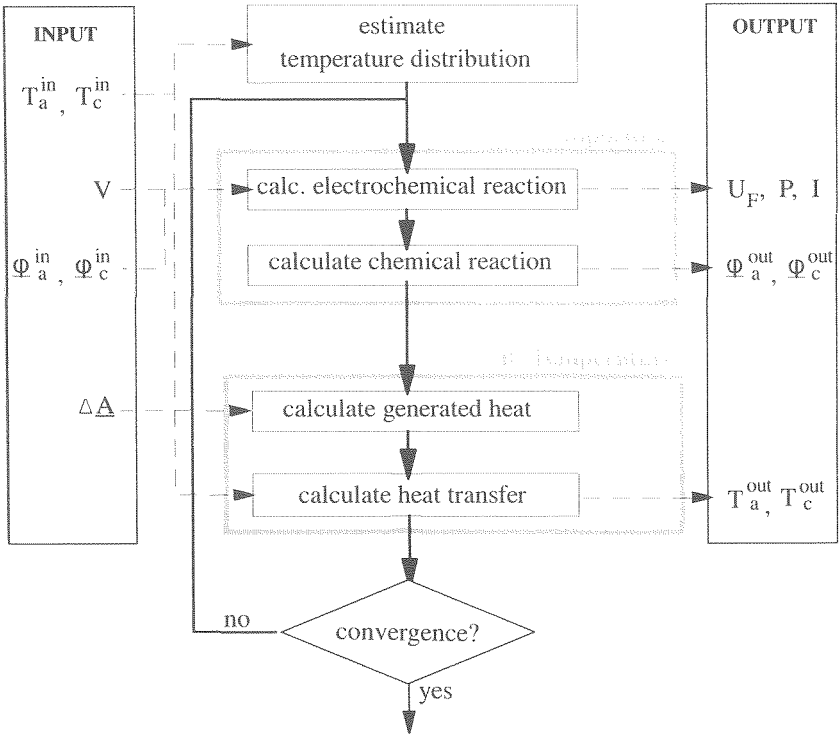

Figure 4.11: Iterative calculation of the composition along the cell and the temperature distribution in the fuel cell model

In the fuel cell model the approach is to calculate the composition and the temperature iteratively. The procedure is shown in figure 4.11.

- *Calculation of compositions*
  First, the temperature is estimated for each subcell (j=1:n). Based on an estimated temperature distribution in the fuel cell, electrochemical reaction and the corresponding cell current and cell voltage are calculated. Subsequently, the change in composition as a result of chemical reactions is calculated. This leads to composition profiles along the cathode and anode.
- *Calculation of temperature distribution*
  Subsequently the heat which is generated in the chemical and electrochemical reactions is calculated and the new temperature distribution is calculated using calculated heats of reaction from the chemical and the electrochemical reaction.

The whole procedure, illustrated in figure 4.11, is repeated until convergence is reached. Convergence is reached if the change in calculated temperature between two iterations for each subcell is smaller than 0.001 K. The two steps, calculating the composition along the cell (figure 4.12) and the calculation of the temperature distribution (see figure 4.13) are discussed in more detail below.

A. Calculation of the composition along the cell

In figure 4.12 the calculation procedure for the compositions for each subcell (j=1 to n) is given. For the first subcell the inlet composition is given by the inlet composition specified the fuel cell:

$$\underline{\varphi}_a^1 = \underline{\varphi}_a^{in} \quad \text{and:} \quad \underline{\varphi}_c^1 = \underline{\varphi}_c^{in}$$

Therefore the temperature T_e^j is used as an input variable in the calculation of the composition. To calculate the current density, the model also uses the area for each subcell (ΔA^j), which can be chosen freely. The same is the case for the calculation of the reaction coordinates for the chemical reactions, $\Delta\varepsilon_s^j$ and $\Delta\varepsilon_r^j$, which uses the temperature to calculate equilibria and kinetics and the cell area for the kinetics as well. Which correlations are used for the chemical reactions depend on the specific case which is modelled (MCFC/SOFC, external/internal reforming: see **Section 4.4.3**). By definition, because the conversion for each reaction is zero at the inlet, the reaction coordinate vector at the inlet equals:

$$\underline{\varepsilon}^{in} = \begin{bmatrix} 0 \\ 0 \\ 0 \end{bmatrix}$$

For each of the subcells, the reaction coordinates at the outlet are calculated using:

$$\underline{\varepsilon}^{j+1} = \underline{\varepsilon}^j + \begin{bmatrix} \Delta\varepsilon_e^j \\ \Delta\varepsilon_s^j \\ \Delta\varepsilon_r^j \end{bmatrix}$$

Using the reaction coordinates the outlet concentrations for each subcell can be calculated using equations (4.17) and (4.18). This procedure is repeated for each of the n subcells to calculate the composition along the cell.

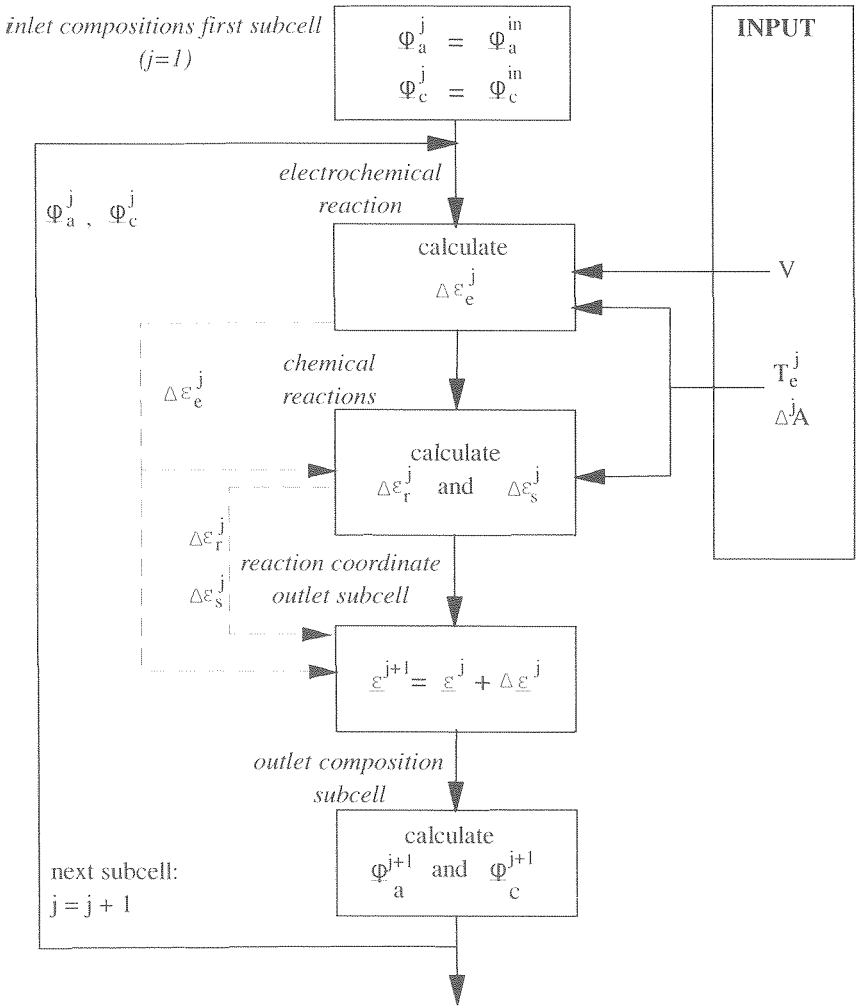

Figure 4.12: Iterative calculation of the compositions and reaction coordinates in each cell using the temperatures in each cell

B. Temperature distribution

The calculation of the temperature distribution follows the steps indicated in figure 4.13. The temperatures of the process flows at the inlet of the first subcell are equal to the inlet temperatures (T_a^{in} and T_c^{in}). The amount of heat generated in the subcell is calculated, the amount of heat generated in the electrochemical reaction (Q^j_{rev} and Q^j_{irr}) and the amount of heat generated in the chemical reactions (Q^j_r and Q^j_s).The model uses the reaction coordinates to calculate the generated heat. In the next step the corresponding compositions are used to calculate the relevant heat transfer properties for the subcell (c_p, α, λ). Subsequently the hardware temperature (T_a^j) and outlet temperatures for the subcell (T_a^{j+1} and T_c^{j+1}) are calculated using equations (4.35) and (4.54).

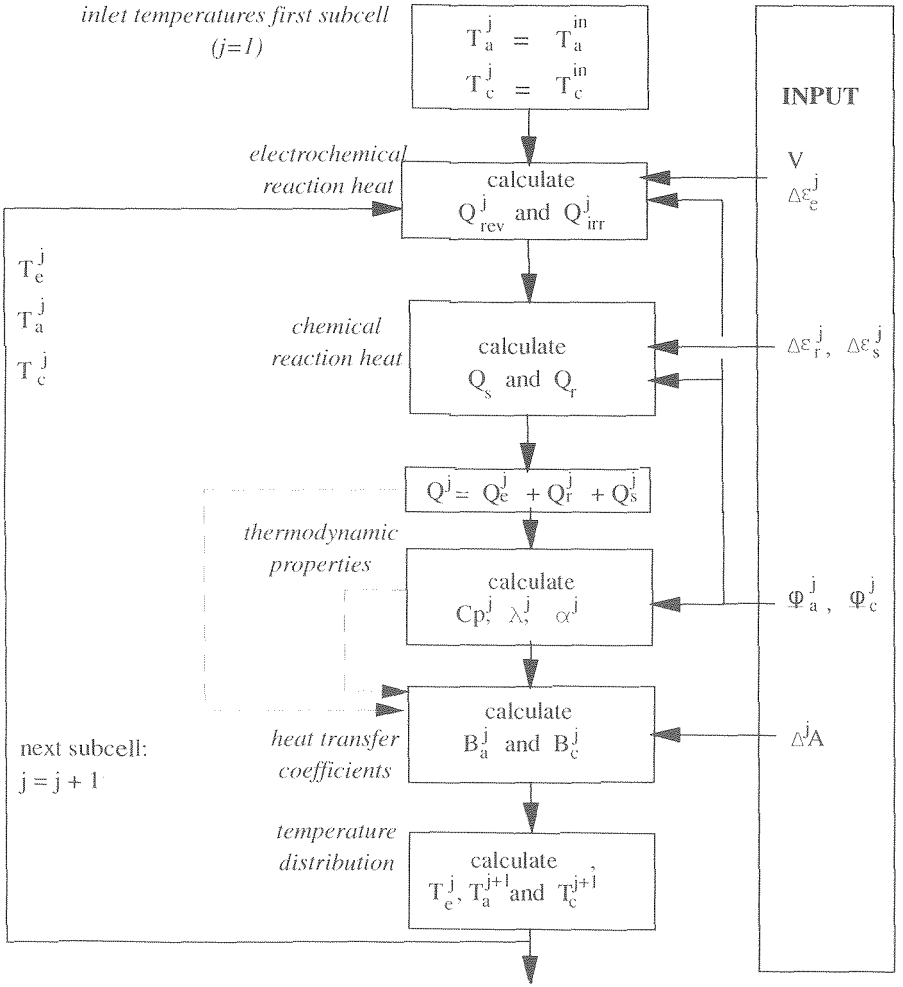

Figure 4.13: Iterative calculation of the temperatures in each cell using the compositions and reaction coordinates in each cell

Using the reaction coordinates the outlet concentrations for each subcell can be calculated using equations (4.17) and (4.18). This procedure is repeated for each of the n subcells to calculate the composition along the cell.

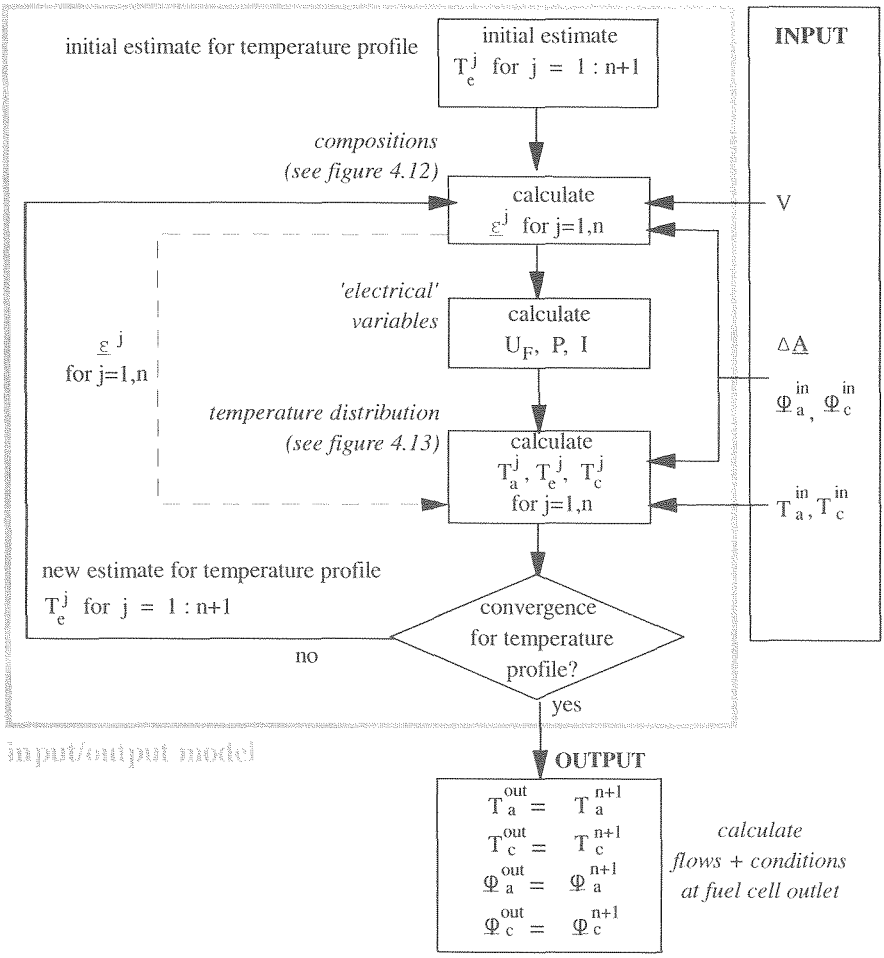

Figure 4.12: Iterative calculation of the compositions and reaction coordinates in each cell using the temperatures in each cell

CHAPTER 5
ANALYSIS OF THE CALCULATION RESULTS FOR THE DETAILED FUEL CELL MODEL

5.1 INTRODUCTION

The detailed fuel cell model described in **Chapter 4** is used to develop a simple model, which can be used in system calculations. The detailed model is used in two ways in the development of the simple model. In **Chapter 6** the results of the detailed model are compared to the results calculated with the simple model. The detailed model is therefore used to 'validate' the simple model. However, to make a simpler model, it is important to understand first which phenomena determine the performance of the fuel cell. To that end, in this chapter, the calculation results of the detailed model are analysed.
Five different sets of calculations have been carried out using the detailed model. Separate comparisons are made for MCFC and SOFC. Because the characteristics of internal and external reforming cells are very different, the results for these two types are compared separately as well. Furthermore different flow patterns (co-flow vs. counter-flow) are modelled. Co-flow in combination with external reforming has the advantage of the smallest temperature gradients [Selman, 1990] and this approach has been adopted for the external reforming fuel cells in this study. For internal reforming fuel cells the use of a co-flow configurations has a number of disadvantages. Most notably the temperature in the zone where the endothermic reforming reaction takes place may become unacceptably low. The counter-flow configuration may therefore be more appropriate for internal reforming fuel cells, although concepts with different flow patterns have been developed ([Murashi, 1994], [Kraaij, 1998]). In this study only counter-flow is considered for internal reforming fuel cells. An external reforming MCFC with a counter-flow configuration has been included to simplify the comparison of the internal reforming (counter-flow) and external reforming (co-flow) configurations.

In **Section 5.2** the starting-points and input data used in the calculations for the different fuel cell configuration is discussed. Subsequently the calculation results for each of the configurations[i)] discussed above are analysed:

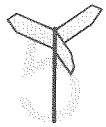

- co-flow external reforming MCFC (*mcoe*) }
- counter-flow external reforming MCFC (*mcne*) } in **Section 5.3**
- co-flow external reforming SOFC (*scoe*) }

- counter-flow internal reforming MCFC (*mcni*) }
- counter-flow internal reforming SOFC (*scni*) } in **Section 5.4**

[i] for the names the following convention has been used: m=MCFC, s = SOFC. External reforming cells may be co-flow (xcoe) or counter-flow (xcne). Internal reforming cells (xcni) are all counter-flow

5.2 STARTING POINTS AND INPUT DATA FOR THE CALCULATIONS

The input used for the different calculations corresponds largely with the input data specified for the "input/output' fuel cell model developed in the previous chapter (cf. figure 4.2). Cell geometry, cell voltage V, inlet concentrations ($\underline{x}_a^{in}$ and $\underline{x}_c^{in}$) and temperatures (T_a^{in} and T_c^{in}) are specified. However, in the system calculations (in part III) two data, which are calculated in the input/output model, are generally specified. These are the fuel utilisation (U_F) and the maximum temperature (T_e^{max}) in the stack (these will be discussed in more detail below). Values for both parameters are generally dictated by the fuel cell stack design and are therefore fixed and not of calculated. The inlet flows φ_a and φ_c, which were specified in the input/output model are calculated to sattisfy the conditions for U_F and T_e^{max} respectively. Figure 5.1 hows the procedure and the input and output for the model

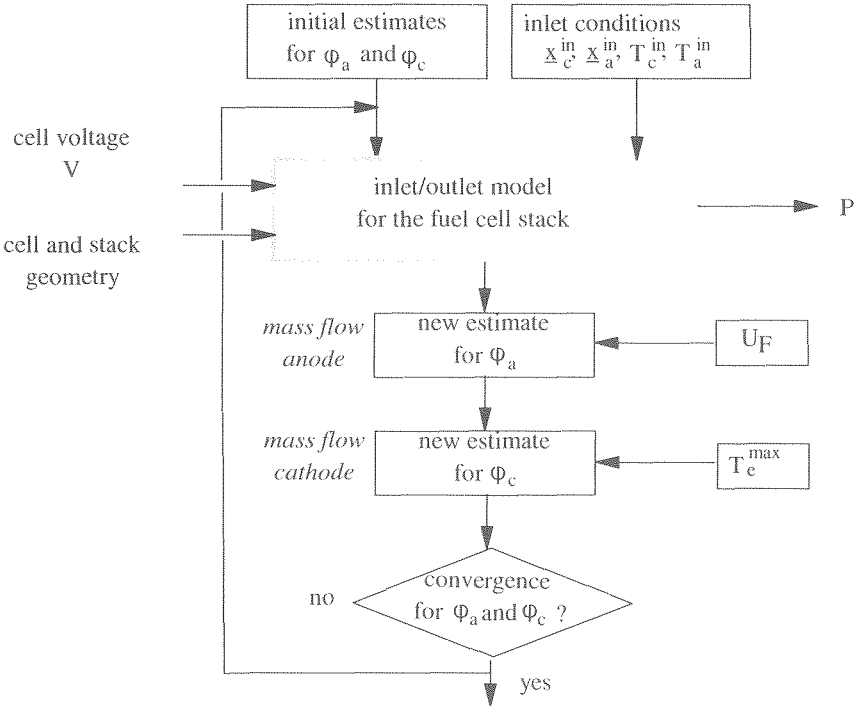

Figure 5.1: Input/output and calculating procedure for the fuel cell calculations in this chapter

5.2.1 Geometrical data

The geometrical data specifies the dimensions of the fuel cell (cell and stack geometry) as well as the characteristics required to calculate the local current densities, reaction rates, etc, for example kinetic data and cell resistance. The most important geometrical data used in the calculations for this chapter are discussed below. An overview is given in table 5.1.

Stack area

For the MCFC, the calculations are based on the full scale flat plate type fuel cell which is considered as the most appropriate design for commercial technology. A stack area of 1 m^2 has been used. This corresponds to the state-of-the-art and a further scale-up of the cell area does not seem to have many advantages.

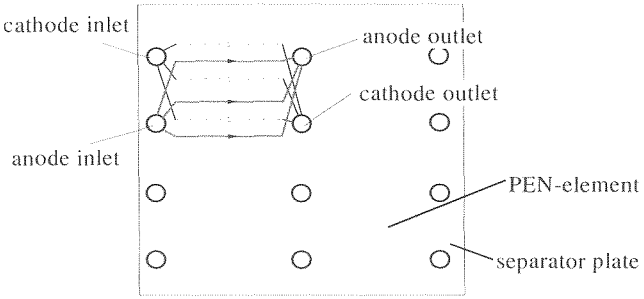

Figure 5.2: Schematic of the modelled planar SOFC using multiple PEN elements in one layer

For the SOFC, the calculations are base on the metallic plate separator type developed by Siemens ([Beie, 1998]). One of the main problems in (planar) SOFC's, is the difficulty of producing large scale PEN-elements. In the metallic separator plate technology, this is solved by combining multiple PEN-elements into 1 metallic separator plate. The detailed fuel cell model calculates the process in one of these PEN-elements. As stated in the introduction to chapter 4, an ideal stack is assumed, in which the reactants are fed to all the cells in the stack from the manifolds at equal conditions (concentrations, pressure, temperature). For the SOFC stack, this assumption is also used for the PEN elements within one layer. One stack is assumed to consist of 9 PEN-elements in one layer which all operate under equal conditions. The principle of a multiple-PEN layer is shown in figure 5.2. For these calculations the size of the cells is 0.25 x 0.25 m^2. This represents a realistic value for the planar, metallic separator type of stack.

Channel geometry

To calculate velocities and heat transfer, the dimensions of the anode and cathode channels given in table 5.1 have been used. The velocities in the channels have been calculated by assuming an effective area (table 5.1), which is defined as the ratio of the area of the channels (i.e. available to the gas flow) to the total cross section of the anode and cathode layer respectively.

Cell resistance

The effective cell resistance which has been selected for these calculations is 1 Ω cm^2 for MCFC cells and 0.75 Ω cm^2 for the SOFC. The values for the cell resistance are estimated from the data on cell and stack performance available in public literature (see **Appendix 4**). The cell resistance characterises the performance of a fuel cell. It determines the cell voltage which can be achieved at a specific current density (see below).

Table 5.1: Specification of the geometry (= dimensions and material characteristics) of the cell for the calculation series with the detailed model

name[1]	mcoe	mcne	mcni	scoe	scni
fuel cell	MCFC	MCFC	MCFC	SOFC	SOFC
reforming	external	external	internal	external	internal
flow pattern	co-flow	counter-flow	counter-flow	co-flow	counter-flow
cell area A	1 x 1 m^2	1 x 1 m^2	1 x 1 m^2	0.25x 0.25 m^2	0.25x 0.25 m^2
cell resistance R[1]	1 Ω cm^2	1 Ω cm^2	1 Ω cm^2	0.75 Ω cm^2	0.75 Ω cm^2
anode channels	1.5 x 2 mm^2	1.5 x 2 mm^2	1.5 x 2 mm^2	1.5 x 2 mm^2	1.5 x 2 mm^2
effective area anode	80%	80%	80%	80%	80%
cathode channels	3 x 2 mm^2	3 x 2 mm^2	3 x 2 mm^2	3 x 2 mm^2	3 x 2 mm^2
effective area cath.	90%	90%	90%	90%	90%

[1] The specified value of the cell resistance is the value at average cell temperature, i.e. 650 °C for the MCFC cell and 925 °C for the SOFC

5.2.2 Design conditions

The performance of the fuel cell is not only determined by its 'design' (the geometrical data), but also by the way it is operated. These design conditions (inlet concentrations and temperatures, operating pressure, etc.) are discussed below. Table 5.2 summarizes the design conditions which have been used for the calculations in this chapter.

Table 5.2: Specification of the design(= operating) conditions for the calculation series with the detailed model (corresponding to cases specified in table 5.1)

name	mcoe	mcne	mcni	scoe	scni
	MCFC-ER	MCFC-ER	MCFC-IR	SOFC-ER	SOFC-IR
anode gas (NG = natural gas)	reformed NG	reformed NG	NG + steam (S/C=3)	reformed NG	NG + steam + anode rec.
cathode gas	air/CO_2	air/CO_2	air / CO_2	air	air
inlet temperature	600 °C	600 °C	600 °C	850 °C	850 °C
T_{max} electrolyte	700 °C	700 °C	700 °C	1010 °C [1]	1010 °C [1]
operating pressure	1 bar	1 bar	1 bar	1 bar	1 bar
fuel[2] utilisation U_F	75%	75%	80%	85%	70%[3]
cell voltage	775 mV	775 mV	775 mV	675 mV	675 mV

[1] Calculated for the reference system (scoe) assuming an outlet temperature of 1000 °C (see text)
[2] Only fuel utilisation specified, oxygen and CO_2 utilisation are calculated
[3] Fuel utilisation per passage based on an overall fuel utilisation of 85% (see text)

Inlet concentrations anode

For the external reforming fuel cell model calculations (mcoe, mcne and scoe) the anode gas composition corresponds to reformed natural gas. The compositions for this reformate have been determined using the reformer model in the system calculations (**Section 7.3**). For the internal reforming cells, the anode gas consists of a mixture of natural gas with steam. For the MCFC, is natural gas is mixed with steam to obtain a steam/carbon ratio of 3. In the case of the SOFC it is necessary to limit the rate of the reforming reaction at the inlet of the cell in order to limit the temperature gradients in the fuel cell. In the calculations for the internal reforming SOFC fuel cell systems (**Section 8.5**), part of the anode off-gas is recycled to the anode inlet. This recycle flow strongly reduces the reforming rate. For the calculations with the fuel cell model for the internal reforming SOFC case, the typical inlet concentrations for this situations have been used.

Inlet concentrations cathode

In the fuel cell calculations, only the influence of the local O_2 and CO_2 partial pressures on the cell resistance have been taken account, because insufficient data are available to make a reliable assessment of the influence on the local distribution. For the design calculations with the fuel cell model air and air + CO_2 have been considered as cathode gas for SOFC and MCFC respectively. Due to the low oxidant utilisations in these calculations, the range of values of the partial pressures is limited in all calculations.

In- and outlet temperatures

Cell degradation in the MCFC, the decrease in performance of the cell over time, depends strongly on the maximum temperature which occurs in the fuel cell (see [Saito, 1991], [Freni, 1997-b]). For the SOFC, although the correlation with degradation is not as strong, mechanical strength of the ceramic components is a factor which will limit the maximum temperature which should occur in the cell. The maximum temperature which occurs in the fuel cell depends mainly on two parameters: the cathode gas flow at the inlet of the fuel cell and the inlet temperature. The cathode gas is used to cool the cell. The mass flow cathode gas therefore depends on the amount of heat which has to be removed from the fuel cell stack. And because more heat can be removed from the fuel cell stack if the temperature increase over the fuel cell stack is larger, the cathode gas flow also depends on the temperature difference between the in- and outlet flows (ΔT).

This leads to an interesting trade-off. Because the fuel cell operates more efficiently at higher temperature (see **Appendix 5**) the inlet temperature should not be to low. But the temperature difference (ΔT) over the stack should be as large as possible, to minimise the amount of cathode gas required to cool the fuel cell stack (and thereby minimise the duty of the compressor required to pressurise the cathode gas flow). The selection of the inlet temperature is therefore mainly a trade-off between the fuel cell efficiency (high inlet temperature=high efficiency), and the cost and auxiliary power requirements of the system (lowest cost and power consumption at a low inlet temperature). Other aspects can be relevant as well, for example the fact that thermal stresses in an SOFC may become unacceptable if the ΔT becomes too large. For the MCFC the inlet temperatures (anode and cathode gas) are mainly determined by the cell resistance which becomes too high if the temperature decreases very rapidly at temperatures below 600 °C. Therefore this value was used for the inlet temperature in the MCFC calculations. For the SOFC the temperature difference over the stack (rather than the absolute value of the inlet temperature) is important. The assumed outlet temperature of 1000 °C and 150 K temperature difference correspond to a 850 °C inlet temperature (see table 5.2).

Temperature approach

The outlet temperature is mainly limited by the allowable temperature of the hardware, which is determined by the rate of degradation and thermal stresses. But the temperature difference between the outlet temperature and the maximum temperature depends on the operating conditions. The temperature difference between the (cathode) outlet flow and the maximum temperature is indicated as the "temperature approach" .This will turn out to be an important parameter for the simplified model in the next chapter. A small temperature approach is preferred. If the temperature approach is small, a relatively large ΔT of the gas flows can be achieved for a given maximum temperature in the fuel cell hardware. On the other hand, a larger temperature approach means that at the same maximum temperature in the cell, a larger air flow is required to cool the cell. Both temperatures, outlet temperature and maximum hardware temperature are calculated by the detailed model[j]. If the outlet temperature is used as a constant input parameter (i.e. an outlet temperature of 1000 °C is assumed for all SOFC calculations), the maximum hardware temperature will be different in each calculations. To be able to make a 'fair' comparison between different stack configurations, the detailed model uses the maximum temperature in the fuel cell as the input parameter and the temperature at the outlet is calculated. For the MCFC this value has been set to 700 °C. For the SOFC a maximum hardware temperature of 1010 °C is assumed[k].

Fuel utilisation

Not all the fuel which is supplied to the fuel cell is converted in the fuel cell. Depending on the system design and the fuel cell design, 75% to 90% of the fuel is converted in the fuel cell. The remaining fuel in the anode off-gas is burned to produce heat. In the external reforming MCFC, for example, the anode off-gas is used to supply heat to the reformer. The fuel utilisation in the MCFC external reforming system should not be to high, or insufficient heat will be supplied to the reformer. In this case it is the reformer which determines the fuel utilisation rather than the fuel cell. As a result, in the external reforming MCFC base case the fuel utilisation is limited to 75 % (see **Section 7.3.3**). In the external reforming SOFC system the fuel utilisation is higher (85%) because the heat which is generated in the fuel cell (at 1000 °C) can be used more effectively in the reformer. The internal reforming MCFC system does not require a reformer and therefore a higher value of the fuel utilisation (80%) is possible. Here the fuel utilisation is limited by the material properties of the anode. In the internal reforming SOFC system the situation is again different. A large part of the anode gas is recycled to limit the rate of the reforming reaction at the cell inlet[l]. Although the overall fuel utilisation is the same as the overall fuel utilisation for the external reforming SOFC system (85 %), the utilisation per passage is only 70 %. Correspondingly this value has been used for the fuel cell calculations.

Cell voltage

The values of the cell voltage for both types of fuel cells is a compromise between efficiency and power density. The calculated power density at 775 volt for the specified cell resistance

---

[j] the maximum hardware temperature in the model corresponds to the maximum electrolyte temperature: see **Chapter 4**

[k] The temperature approach in the reference calculation (external reforming) is 10 K.

[l] By recycling part of the anode off-gas the fuel the reactants partial pressures become lower and the product partial pressure become higher, enabling a better control of the reforming reaction at the anode inlet

corresponds to 1.3 kW/m^2. This should be compared to for example the 1.8 kW/m^2 target which NEDO has set [Morita,1995]. For the SOFC the target power densities are higher, in the range of 3-5 kW/m^2. Therefore the selected cell voltage is considerably lower for the SOFC than for the MCFC. Nonetheless, the selected value of the cell voltage (675 mV) leads to a power density of 1.6 kW/m^2 for the SOFC.

5.3 EXTERNAL REFORMING FUEL CELLS

5.3.1 Co-flow external reforming MCFC (*mcoe*)

Figures 5.3 - 5.7 summarise the calculation results for the base case external reforming MCFC cell (mcoe). In all of these graphs, the local properties have been plotted against the distance from the inlet. Unless indicated otherwise, this refers to the anode inlet. The parameter (x) has been made dimensionless by dividing it by the length of the cell (L).

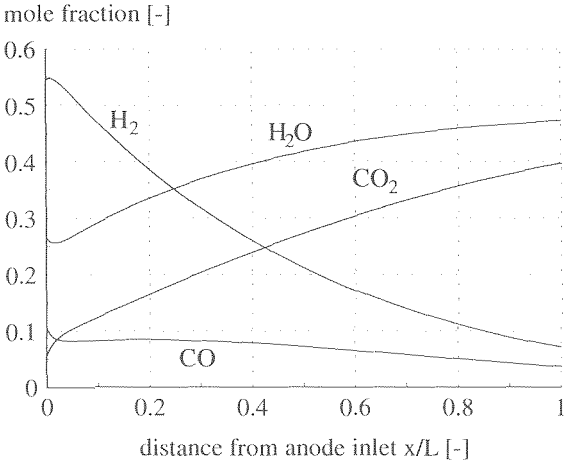

Figure 5.3: Calculated mole fractions at the anode for the base case ER-MCFC (mcoe)

Figure 5.3 represents the mole fractions at the anode. In the external reforming fuel cell system, a reformer supplies gas to the anode. The concentrations at the anode outlet have been determined assuming an equilibrium temperature of 800 °C and a steam/carbon ratio equal to 3. This results in a H_2 concentration at the inlet of 55% and 25% H_2O. The remainder of the gas consists of CO_2, CO and small concentrations of N_2 and CH_4 (not shown in the graph). The concentration profile for hydrogen is determined by the two anode reactions which are included in the model for the external reforming fuel cell:

$$H_2 + CO_3^{=} \rightarrow H_2O + CO_2 + 2\,e^- \quad (\textit{electrochemical reaction})$$

$$CO + H_2O \rightarrow H_2 + CO_2 \quad (\textit{shift reaction})$$

Initially the hydrogen concentration increases slightly due to the shift reaction, but this reaction plays a role only in a small inlet zone near the anode inlet. The electrochemical reaction determines the further concentration of hydrogen, which decrease gradually to the

outlet concentration (7%). The concentration CO decreases as a result of the shift reaction: as hydrogen is removed by the electrochemical reaction, the shift reaction will 'compensate' for the decreasing hydrogen concentration by consuming CO and producing hydrogen. The concentration of the products in the electrochemical reaction (H_2O and CO_2) evidently will increase from in- to outlet. At the outlet the concentration of the two reaction products (i.e. $H_2O + CO_2$) is almost 90%. The ratio between the CO at the anode inlet and the CO_2 at the anode outlet shows that the high CO_2 concentration at the outlet is due mainly to the transport of CO_2 through the electrolyte in the form of $CO_3^=$.
The electrochemical and chemical reactions determine the change in concentrations along the cell. They also determine the power and heat which is generated in the fuel cell. In figure 5.4 the local power density and the heat generated per m^2 cell area are shown. Because the cell voltage is constant over the cell, the power density and current density are proportional. The average power density is 1.3 kW/m^2, locally the value varies from 1.75 kW/m^2 at the inlet to 0.8 kW/m^2 at the outlet of the cell. The power to heat ratio (P/Q) in the external reforming MCFC is relatively high, almost 1.5. This is the result of high cell voltage which has been selected for this calculation. Furthermore, as can be seen in figure 5.4, the local heat flux (kW/m^2) is approximately proportional to the power production, except at the inlet zone ($x/L<0.1$).

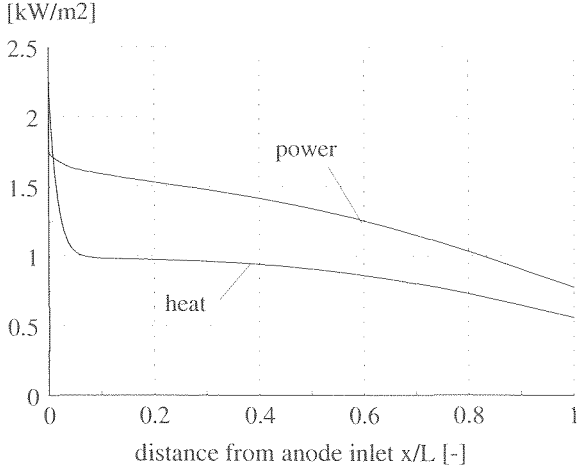

Figure 5.4: Power and heat generated in the fuel cell for the base case ER-MCFC calculation (mcoe)

The local power density is determined by the two mechanisms illustrated in figure 5.5: the local voltage difference and the local cell resistance. The voltage difference ΔV is the difference between the local Nernst voltage and the actual cell voltage. The latter is constant over the cell. The Nernst voltage (equation 4.2 and 4.3) depends on the concentrations of the reactants. In particular as a result of the decrease in hydrogen concentration, the Nernst voltage decreases from 1.07 V at the inlet of the cell to 0.85 V at the outlet. The voltage difference decreases much sharper. The value at the outlet corresponds to 25% of the value at the inlet. As figure 5.4 shows, the power density is distributed more uniformly than the cell voltage (the value of the power density at the outlet is approximately 50% of the value at the inlet). Evidently, the drop in the voltage difference is partially compensated by a simultaneous decrease of the cell resistance (see **Section 4.3.1**)

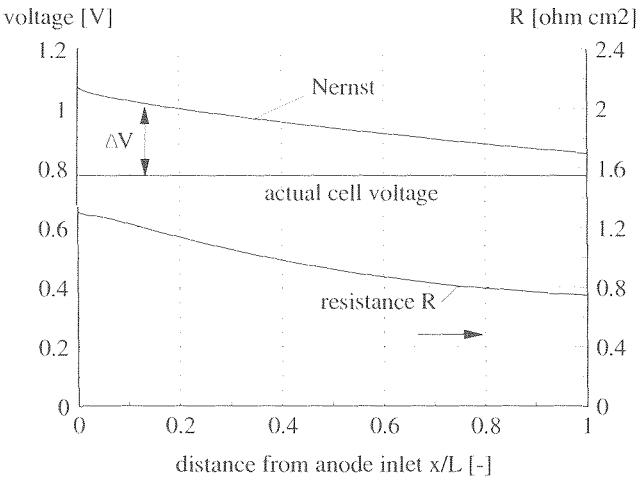

Figure 5.5: Local Nernst voltage and cell resistance and the cell voltage (calculation mcoe: base case ER-MCFC)

Figure 5.5 shows that the cell resistance varies from 1.3 ohm·cm^2 at the inlet to 0.75 ohm·cm^2. The decrease in cell resistance is due to the increase in temperature from in- to outlet. The calculated temperature distribution in the fuel cell is shown in figure 5.6. The main starting points for the calculation of the temperature (see **Section 4.3.3**) include the assumption of a constant temperature in a cross section of the hardware of the cell (electrolyte, separator plate). Besides the electrolyte temperature, the local temperature of the anode flow and the cathode flow are calculated. As indicated in table 5.1 co-flow is assumed. Therefore the temperature of both gasses at x/L=0 are equal to the specified inlet temperatures (600 °C). The heat which is generated in the electrolyte is transferred to the process flows. As a result, the temperature of the electrolyte will be higher than the temperature of the process flows. For the cathode flow this is evident in figure 5.6: the average temperature difference is approximately 10 K. The temperature difference between the anode and the electrolyte is much smaller and in figure 5.6 the curves for the electrolyte and anode temperature are hard to distinguish: the average temperature difference is 0.5 K. The difference between the temperature distribution in the anode and cathode channels is due to two separate phenomena. The first is the difference in flow: the mole flow cathode gas is considerably larger than the anode flow. Correspondingly, the heat capacity of the cathode flow (in [kJ/K]) is 15 times as large as the heat capacity of the anode flow. Therefore, considerably less heat is required to heat the anode gas than the cathode gas. The second difference is the difference in thermal conductivity. The thermal conductivity of each flow is determined by the thermal conductivities of the components which are present in the anode and cathode flow (H_2, H_2O, CO_2, O_2, etc.). The thermal conductivities of the pure components are roughly equal, with exception of thermal conductivity of hydrogen, which has a value an order of magnitude higher than the other thermal conductivities. As a result, the anode gas, which is rich in hydrogen, has a much higher thermal conductivity than the cathode gas.

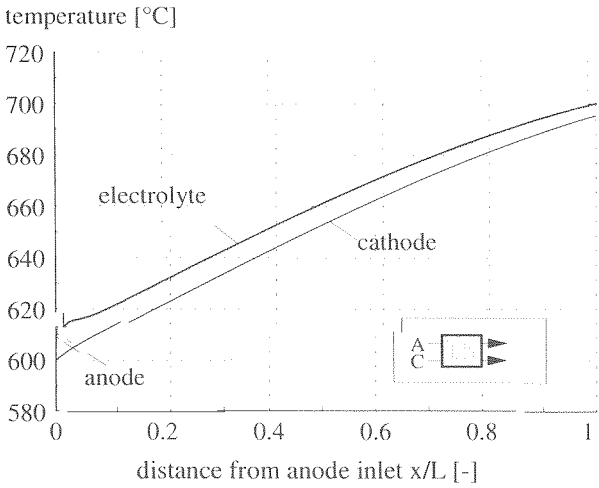

Figure 5.6: Temperature distribution for the base case ER-MCFC calculation (mcoe)

The maximum temperature in the cell hardware is 700 °C (this has been specified as input for the calculation). The corresponding outlet temperature of the cathode gas calculated by the model is 695 °C. The temperature difference between the cathode and electrolyte near the inlet of the cell is approximately 15 K and decreases to 5 K at the outlet of the cell. The maximum (electrolyte) temperature in the cell occurs at the outlet of the cell. The 5 K temperature difference at the outlet therefore corresponds to the temperature approach which was defined in **Section 5.2.2**.

The temperature difference between the cathode gas and the electrolyte depends on the amount of heat which is transferred ($q \sim \alpha \Delta T$). The decrease in temperature difference from approximately 15 to 5 K therefore corresponds to a decrease in heat flux between inlet and outlet. Figure 5.4 shows that high heat flux occurs near the inlet and the heat flux decreases gradually along the cell. To clarify the form of the heat flux curve, the heat 'sources' will be considered. The heat is produced in the shift reaction and in the electrochemical reaction. In the inlet zone, the rate of the shift reaction is high because the inlet anode gas is out of equilibrium with respect to the shift reaction[m]. This leads to a high heat flux near the inlet of the cell. At x/L=0.05 however, the shift reaction is in equilibrium and the contribution of the shift reaction to the heat production becomes small as shown in figure 5.7.

The heat is mainly generated as a result of the electrochemical reaction. As indicated in figure 5.7 the heat in this reaction can be split into two parts: the reversible part and the polarisation heat[n]. The equations for calculating reversible and polarisation heat were discussed in **Section 4.4.4**. The reversible part of the heat of the electrochemical reaction is the heat which is generated if the reaction occurs reversibly, i.e. without polarisation losses. In that case the ratio between the power and heat is determined fully by the Nernst voltage

---

[m] The anode gas composition is determined by the high temperature at which the shift and reforming approach equilibrium in the reformer.

[n] Again no distinction is made between voltages losses as a result of ohmic losses, activation polarisation, etc.

(equation 4.3). If the Nernst voltage is high, the power to heat ratio is high. If the Nernst voltage decreases, the ratio becomes less advantageous: less power and more heat are produced. The resulting distribution of the reversible heat shown in figure 5.7 is the sum of two effects. On one hand, the electrochemical reaction produces more heat (and less power) toward the outlet of the cell. At the same time the rate of the electrochemical reaction decreases considerably (the rate of the electrochemical reaction is proportional to the power density in figure 5.4). As a result, the heat in the reversible electrochemical reaction is more or less evenly distributed over the cell.
The polarisation heat is the result of the voltage losses and can be represented by the conventional i^2R or $(\Delta V)^2/R$ term. The distribution of the polarisation heat is determined mainly by the distribution of the voltage loss ΔV and the cell resistance R which are shown in figure 5.5. Although the effect is slightly weakened by decrease of R, the cell resistance, the uneven distribution of the polarisation heat is determined mainly by the decrease of the voltage loss ΔV from in- to outlet.

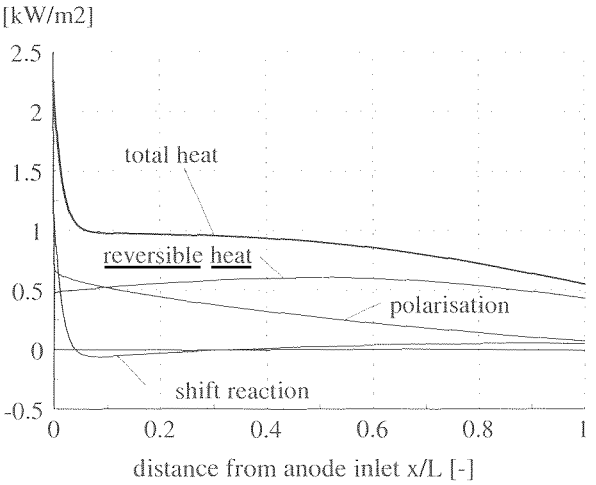

Figure 5.7: Calculated heat flux from the electrolyte to the process flows for the ER-MCFC (mcoe)

5.3.2 Counter-flow external reforming MCFC (*mcne*)

For external reforming cells co-flow is assumed, but for internal reforming cells the counter-flow configuration is considered. This makes the comparison of external and internal reforming more complicated. It is simpler if the internal reforming configuration can be compared with an counter-flow external reforming configuration. Therefore a counter-flow external reforming MCFC configuration has been modelled as well.
The main difference between the co- and counter-flow fuel cell is the temperature distribution. In the counter-flow configuration the cold cathode gas enters fuel cell opposite to the anode. The parameter x/L has been defined as the dimensionless distance to the anode inlet. Therefore in the counter-flow configuration the anode gas enters the fuel cell at x/L=0 and the cathode gas at x/L=1.

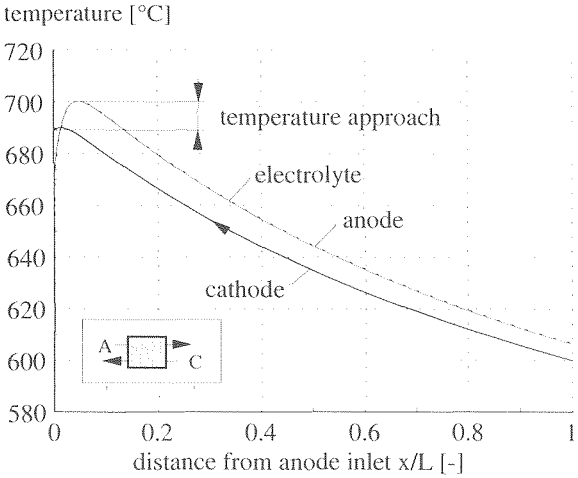

Figure 5.8: Temperature distribution in the counter-flow external reforming MCFC (mcne)

In figure 5.8 the three calculated local temperatures (anode, cathode and electrolyte) are plotted against x/L. As indicated in the previous section, the cathode flow has much higher heat capacity [kJ/K] than the anode (10 ... 15 times as high). Therefore, as can be seen in figure 5.8, the cathode flow determines the temperature profile. The cathode gas is supplied to cell at 600 °C at x/L=1 and heats up gradually. The electrolyte temperature lies approximately 10 K above the cathode temperature. Near the cathode outlet (x/L=0.05) the electrolyte temperature drops sharply due to the cold anode gas which is supplied to the stack at x/L=0. The temperature of the cathode gas, as a result, does not increase strongly and even drops slightly near the outlet. In the figure the temperature approach is indicated. For a given maximum temperature, a small temperature approach will allow a higher outlet temperature. The temperature approach in the counter-flow configuration is larger than for the co-flow configuration (11 K vs. 5 K). The air flow required to remove one kW of heat from the cell is proportional to the temperature increase of the air flow over the cell. In figure 5.10 the temperature increase is shown for both cases. Consequently, more air is required to remove the same amount of heat in the counter-flow cell (ΔT=89 K) than in the co-flow cell (ΔT=95 K).

In all MCFC calculations the cell voltage is the same (775 mV). A better performance, as a result of a higher Nernst voltage or a lower cell resistance, will therefore lead to a higher the power density and the current density. The calculated average power density for the counter-flow cell lies higher (+3%) than the corresponding value for the co-flow configuration. It is not clear on forehand how this better performance of the counter-flow cell can be explained. Both the Nernst voltage and the cell resistance are shown in figure 5.9. For comparison, the values previously calculated for the co-flow cell are shown as well. In the counter-flow configuration the difference in Nernst voltage between the inlet and outlet (1.05→0.90 V) is not as large as in the case of co-flow (1.07→0.85 V). In the co-flow configuration the Nernst voltage decreases toward the outlet because the reactant concentrations decrease and because the temperature increases. The decrease of the Nernst voltage as a result of the increase in temperature from 600 to 700 °C is approximately 0.03 V. The remainder of the change in Nernst voltage over the cell is due to the change in concentrations. Because the temperature

and concentration effects in the counter-flow configuration work against each other, the Nernst voltage in the counter-flow cell, is more evenly distributed. However, the average value of the Nernst voltage is approximately the same in both cases.

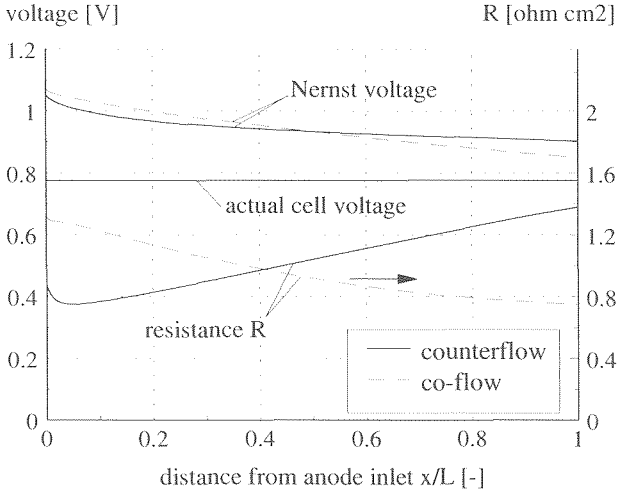

Figure 5.9: Comparison of the Nernst voltage and resistance for co- and counter-flow (mcoe/ mcne)

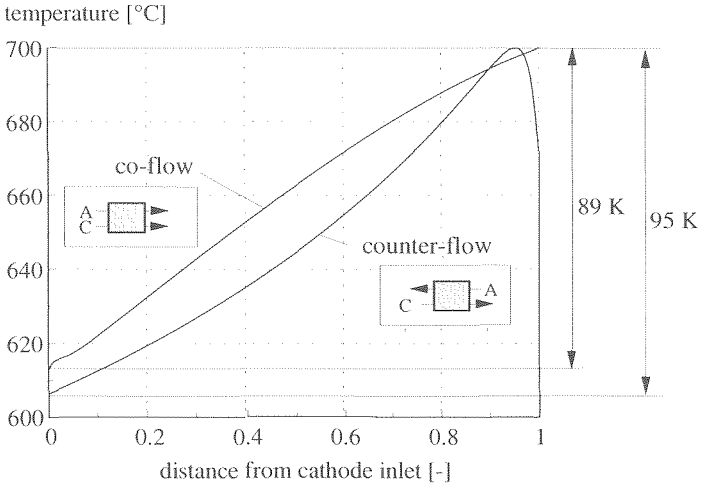

Figure 5.10: Comparison of the electrolyte temperature for co- and counter-flow (mcoe,mcne)

The local cell resistance only depends on the temperature. To clarify the influence of the temperature on the average value of the resistance, the electrolyte temperature curves for the co- and counter-flow cells are shown in figure 5.10. The curve for the cell resistance by definition is the mirrored image of the curve for the electrolyte temperature (high T_e = low R). As a result, the cell resistance for the counter-flow cell is low at the (anode) inlet and high

at the outlet. The average temperature in the counter-flow cell however appears to be lower. This average temperature can be calculated from:

$$\overline{T} = \int_0^1 T \frac{dx}{L} \qquad (5.1)$$

The average temperature calculated in this manner for the co- and for the counter-flow configuration correspond to 659 °C and 655 °C respectively. Because the cell resistance is mainly determined by the temperature, one would expect the average cell resistance to be lower and the current density to be higher for the co-flow cell. However, the performance (the average power density and current density) of the co-flow cell is lower. Figure 5.11 shows the calculated current density curves for both cells. In the counter-flow cell the average current density equals 1.72 kA/m^2 while the current density for the co-flow cell is 1.67 kA/m^2, corresponding to power densities of 1.33 and 1.29 kW/m^2 respectively. The difference in both cases is the 3% better performance of the counter-flow cell discussed earlier. Evidently the higher current density for the counter-flow cell is due not due to the difference in average values of the parameters but to differences in distribution of the parameters which determine the performance (current density, cell resistance). Figure 5.11 shows the importance of the high current density in the anode inlet zone (=cathode outlet zone) of the configuration. In this area of the fuel cell, the temperature is high, which leads to a low cell resistance, while the hydrogen concentration is high. In the co-flow configuration the high temperatures occur near the anode outlet, while the highest current density occurs near the anode inlet zone. In other words, the better performance of the fuel cell in counter-flow operation is due to the fact that a considerable hydrogen conversion is achieved in that area where the efficiency is highest, i.e. at high temperature and therefore low cell resistance. This effect is illustrated differently in figure 5.12. The better performance of the counter-flow fuel cell is due to the fact that a larger part of the fuel is converted at the hot end of the fuel

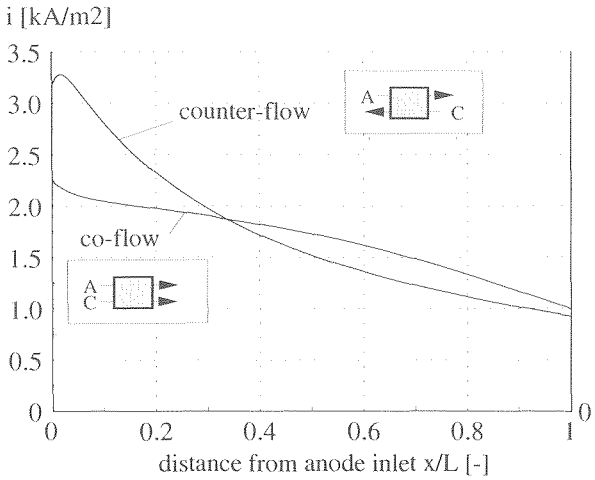

Figure 5.11: Comparison of the current density distribution for the co-flow and counter-flow configuration (ER-MCFC: mcoe and mcne)

cell. Therefore the amount of fuel converted in the hottest part of the fuel cell has been calculated. The maximum electrolyte temperature in the fuel cell is 700 °C, therefore the fraction of fuel which is converted at a higher temperature is zero. In the graph in figure 5.12, the cumulative conversion above a certain temperature is given. In other words each bar indicates the fraction of fuel which is converted above the indicated temperature[o]. In the counter-flow stack 19% of the fuel is converted at a temperature higher than 690 °C and 29% is converted at a temperature above 680 °C, etc. The data for the corresponding temperatures in the co-flow cell are 13% (690-700 °C), 25% (680-700 °C), etc. Because 600 °C is the minimum temperature in the fuel cell, in both case 100% of the fuel is converted above this temperature. In the co-flow only 13% of the fuel is converted at T>680 °C (vs. 19% for the counter-flow cell). As the graph illustrates, this trend continues and as result on average the fuel is converted at a higher temperature in the counter-flow cell.

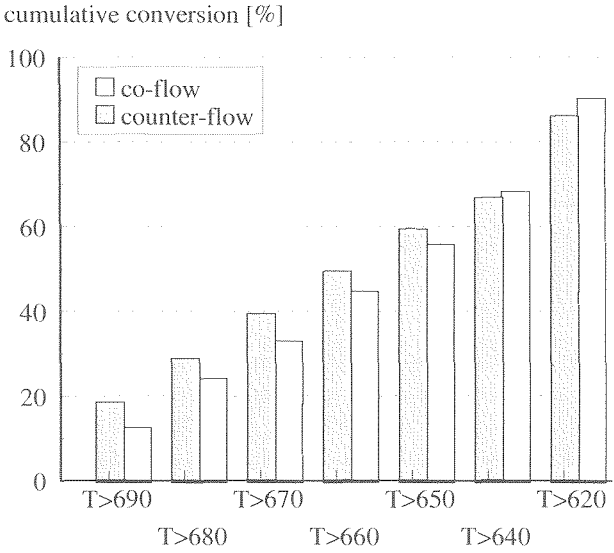

Figure 5.12: Conversion of the fuel in the electrochemical reaction: the length of a bar represents the fraction of the fuel converted at a temperature higher than T.

To characterise the performance of the fuel cell, it would be useful to be able to define an average cell resistance. But as the above shows, the cell resistance at average cell temperature is not a good indicator. The 'average' cell resistance (defined by $R(T_{av})$) will be higher for the co-flow cell with a higher the average temperature (659 °C vs. 655 °C for the counter-flow cell) although the performance is poorer. Instead, the effective cell resistance is introduced. This property is defined by:

$$R_{eff} = \frac{A}{I} \int_0^L (V_{rev} - V) \frac{dx}{L}$$

[o] This diagram is created by calculating the total fuel conversion in all subcells which have an electrolyte temperature $T_e > T$ for T = 600, 610, etc.

Where I is the total current of the stack (i.e. the 'performance'), R_{eff} a constant cell resistance and the integral is the average voltage drop over the stack. The effective cell resistance calculated using this equation is 0.989 ohm cm^2 for the co-flow cell and 0.973 ohm cm^2 for the counter-flow cell.
The cell resistance is an explicit function of the temperature. In other words, it is not only possible to determine what the resistance will be at a certain temperature. It is also possible to determine what the (effective) temperature corresponds to a specific value of the cell resistance. Based on the effective resistance, a corresponding effective temperature for the fuel cell can be defined. The effective temperature is defined as the temperature at which the cell resistance is equal to the effective resistance:

$$R_{eff} = R(T_{eff})$$

For the co- and counter-flow configuration an effective temperature of 652 °C and 654 °C is calculated respectively by the above method. This already shows that a small change in the effective temperature (2 K) can have a substantial influence on the effective resistance (3%). The effective temperature can be used to explain the influence of the temperature distribution on the performance of the cell. As such it will be shown to be an important parameter for the simplified fuel cell model in **Chapter 6**.

5.3.3 Co-flow external reforming SOFC *(scoe)*

The calculation results for the external reforming SOFC cell are summarised in figures 5.13 - 5.17. In figure 5.13 the mole fractions for the most important components at the anode are shown (N_2 for example is not shown because the mole flow N_2 does not change along the cell. Again the inlet concentration corresponds to reformate (reformed natural gas, S/C-ratio is 3). Because of the high steam to carbon ratio, the anode gas at the inlet consists mainly of H_2 and H_2O. The gas at the outlet (x/L=1) consists mainly of H_2O, although some CO_2 is produced as well through the shift reaction. The CO_2 concentration is the largest difference between the concentration profiles in the MCFC and the SOFC. In the MCFC the reaction products of the electrochemical reaction are both H_2O and CO_2 (see the corresponding graph for the MCFC in figure 5.3). In the SOFC, the only reaction product of the electrochemical reaction is water:

$$H_2 + O^{=} \rightarrow H_2O + 2\,e^{-}$$

The ratio between CO and H_2 is determined by the equilibrium of the shift reaction. In the external reforming systems, the anode gas is produced in the reformer at an equilibrium temperature of 800 °C (see **Section 7.3.1**). At a low temperature CO will be consumed in the shift reaction to produce H_2. At a high temperature the equilibrium shifts toward higher CO concentrations. In the SOFC the operating temperature at the inlet is higher than the reformer temperature. Therefore initially hydrogen is consumed in the anode inlet zone (x/L<0.05) and CO is produced. As hydrogen is consumed in the electrochemical reaction, the shift reaction reverses to produce hydrogen and CO_2 further from the inlet zone.

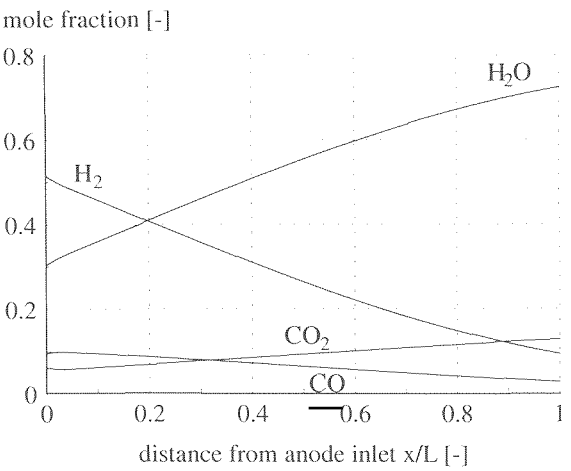

Figure 5.13: Calculated mole fractions at the anode for the external reforming SOFC cell (scoe)

The (small) effect of the shift reaction is evident in figure 5.14, which shows the heat flux from the electrolyte to the process flows. The shift reaction initially uses a small amount of heat. Downstream of the inlet zone, the reaction reverses and hydrogen is produced through the shift reaction and the reaction becomes exothermic instead of endothermic. However, as figure 5.14 shows, the role of the shift reaction in the heat balance is evidently small. The heat generated by the electrochemical reaction, again separated in the reversible heat and the polarisation, is dominant. As in the case of the external reforming MCFC, the reversible heat is produced evenly over the cell and the polarisation losses decrease strongly from in- to outlet.

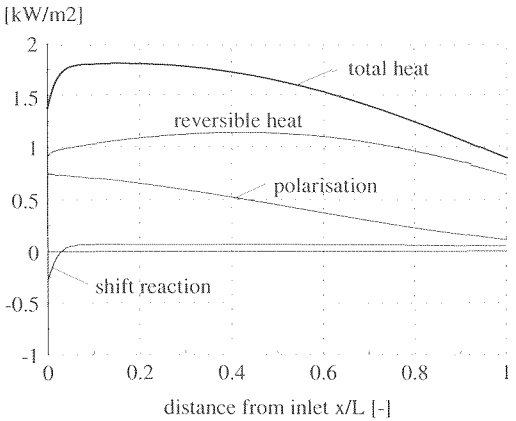

Figure 5.14 Calculated heat flux from electrolyte to process gas for the ER-SOFC cell (scoe)

The calculated temperature distribution is shown in figure 5.15. The anode and cathode gas enter the fuel cell at 850 °C. The anode gas temperature closely matches the electrolyte temperature within 2 K. The maximum temperature in the cell is 1010 °C (as specified). The model calculates an outlet temperature for the cathode gas of 1003 °C, which corresponds to a temperature approach of 7 K

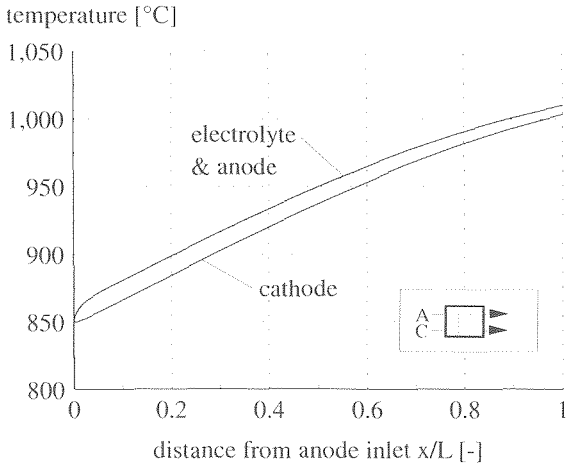

Figure 5.15 Temperature distribution for the external reforming co-flow SOFC calculation (scoe)

The electrical performance of the cell is again determined by the two curves shown in figure 5.16: the local Nernst voltage and the cell resistance. For comparison figure 5.16 also shows the corresponding curves for the external reforming MCFC. The Nernst voltage lies substantially lower for the SOFC than for the MCFC. The difference can be explained mainly by the higher operating temperature for the SOFC. If the temperature increases from 650 °C to 925 °C (the average operating temperatures for the two cells), the Nernst voltage decreases by 80 mV. The difference between the Nernst voltage calculated for the SOFC and for the MCFC with the fuel cell model is slightly higher. This is due to differences in concentrations, eg. as a result of the shift equilibrium and to the different partial pressures relative to the Nernst voltage (compare equations 4.2 and 4.3). But the voltage difference (ΔV = Nernst voltage - actual voltage) in the SOFC configuration corresponds well to the voltage difference in the MCFC.
Even though the driving force (ΔV) is approximately the same, the power density in the SOFC is considerably higher. This difference in power density is due to the lower cell resistance in the SOFC. Figure 5.16 shows the cell resistance for both SOFC and the MCFC. Both curves show a similar decrease in resistance towards the outlet of the cell as a result of the higher temperature, but the average value of the cell resistance in the SOFC cell is substantially lower.

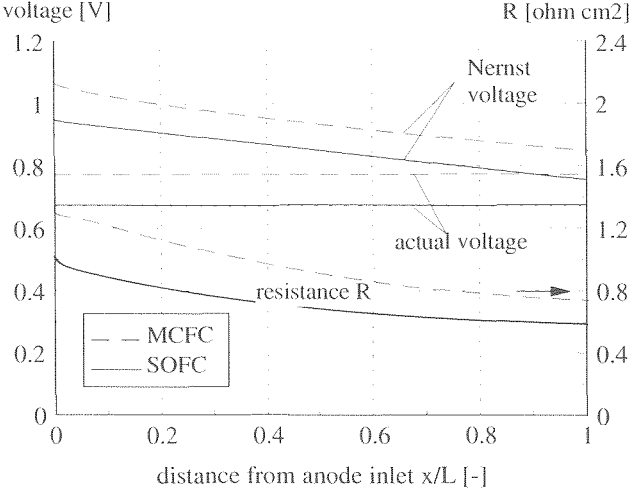

Figure 5.16: Local Nernst voltage and cell resistance and the cell voltage for the external reforming co-flow configurations SOFC and MCFC (calc's scoe and mcoe)

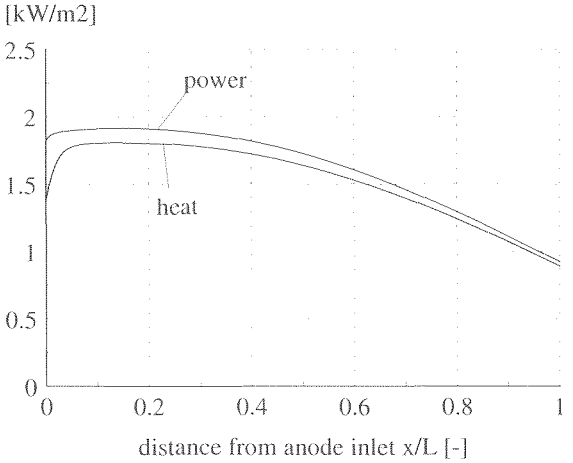

Figure 5.17: Calculated local power density and heat flux for the ER-SOFC configuration (scoe)

Figure 5.17 shows the local power density and heat flux for the external reforming SOFC. This figure can be compared to the corresponding diagram for the external reforming MCFC in figure 5.4. In the MCFC fuel cell the shift reaction is out-of-equilibrium at the inlet of the fuel cell. This effect is smaller in the SOFC cell because of the smaller difference in temperature between the fuel cell inlet and the reformer. The most important differences between the MCFC and SOFC system is the difference in the ratio between power and heat. In the MCFC system approximately 40% more power than heat is produced (power/heat ratio

of 1.4) . As figure 5.17 shows, the ratio in the SOFC is close to unity (1.05). The difference is not due to the polarisation heat: as previously noted, the cell resistance in the SOFC is lower. In the SOFC the reversible heat is considerably higher than in the MCFC. This effect (which can be also seen by comparing figures 5.7 and 5.14) is due to the higher operating temperature of the SOFC stack. A higher heat production has a pronounced effect on the system design, as will be shown in **Part III**. Cooling the cell stack requires even larger gas flows for the SOFC stack than for the MCFC due to the higher reversible heat production.

5.4 INTERNAL REFORMING FUEL CELLS

5.4.1 Counter-flow internal reforming MCFC (*mcni*)

For the calculation of the internal reforming cell the reforming reaction has been modelled using data and the equations discussed in **Chapter 4**. The fuel cell is of the direct internal reforming type, i.e. the reforming reaction takes place on the catalyst which is placed in the anode channels. Although the model includes the possibility to model a graded catalyst distribution [Ohtsuki, 1992], for the calculation in this thesis a uniform distribution of the reforming catalyst is used. For all other input parameters, the same values are used as for the external reforming cells (tables 5.1 & 5.2).

The calculated concentrations at the anode are shown in figure 5.18. The mixture which is supplied to the anode consists mainly of H_2O and CH_4. Some hydrogen is present in the gas (2%) as a result of the assumption that higher hydrogen carbons are pre-reformed before the fuel cell. The concentrations correspond to a low steam/carbon ratio (S/C) of 1.6. The hydrogen concentration is determined by the balance between production in the reforming reaction and the consumption in the electrochemical reaction. The hydrogen concentration increases initially more hydrogen is produced in the reforming reaction than is consumed in the electrochemical reaction. At x/L=0.095 the hydrogen concentration reaches the maximum value (32%). From that point, the hydrogen consumption exceeds the hydrogen production and the concentration decreases gradually.

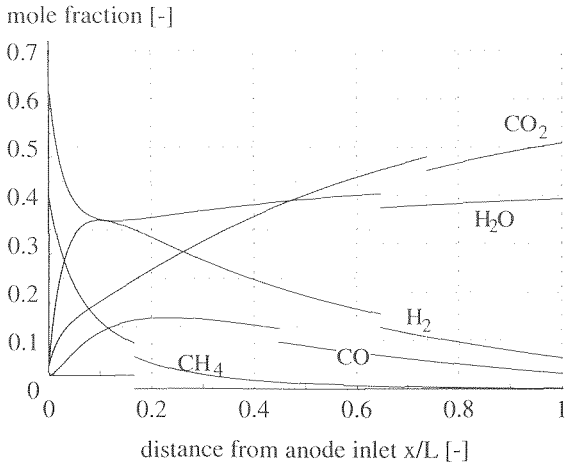

Figure 5.18: Calculated mole fractions at the anode for the internal reforming MCFC (mcni)

The rate of the reforming reaction is determined mainly by two factors: the (electrolyte) temperature, which determines the kinetics of the reaction, and the reactant concentrations, which determine the driving force for the reaction ($\Delta_r g$). The temperature distribution is shown in figure 5.19. At the inlet of the anode the anode flow consists nearly completely of H_2O and CH_4, the reactants in the reforming reaction. Although the rate of the reforming reaction is high at the inlet zone, the rate is limited by the relatively low temperature in the inlet zone. As the anode gas flows through the anode, the reactant concentrations (CH_4 and H_2O) decrease and the product concentrations (H_2 and CO) increase. This leads to a rapid decrease of the driving force for the reforming reaction. However, the simultaneous increase in the temperature improves the reaction kinetics. As a result, the reforming rate decreases very smoothly. At x/L=0.2 the maximum temperature occurs in the electrolyte. The concentration CH_4 at that point is reduced to 5% and decreases gradually. At the outlet the concentration CH_4 is very low (0.2%). This corresponds to experimental data (e.g. [Murahashi, 1994]).

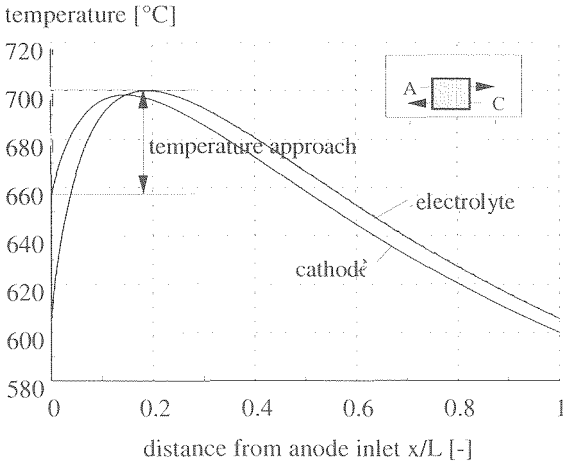

Figure 5.19: Temperature distribution for the base case IR-MCFC calculation (mcni)

The temperature profile shown in figure 5.19 shows the cathode gas enters the fuel cell at 600 °C at x/L=1 in counter-flow with the anode gas. The cathode gas increases in temperature as a result of the local heat flux from the electrolyte. The temperature reaches a maximum temperature at x/L=0.14, where the net heat flux becomes zero. Between x/L=0.14 and x/L=0 the cathode gas cools down: the reforming process cools the electrolyte and heat is transferred from the cathode gas tot the electrolyte. Therefore the temperature of the cathode gas between x/L=0.14 and the cathode gas outlet (x/L=0) decreased considerably. The temperatures have been calculated again using a maximum temperature in the electrolyte equal to 700 °C. For this maximum electrolyte temperature, the cathode gas reaches a maximum temperature of 698 °C and subsequently cools down to 656 °C. The large temperature approach of 44 K which results, is due to the cooling effect of the reforming reaction in the inlet zone. Again the consequences for the system design are important. The cell is cooled by transferring heat to the process flows. The amount of air which is required to remove 1 kW of heat from the stack depends on the temperature difference over the stack. In the case of the internal reforming cell the amount of air required per kW of heat generated is

almost twice as large as in the case of external reforming because of the smaller ΔT over the stack. This effect is reenforced by the net temperature increase over the stack of the anode gas. Although this flow is much smaller than the cathode flow and therefore contributes less to the cooling, the anode flow in the internal reforming cell is cooled down almost to inlet temperature. As a result, the contribution of the anode gas cooling the cell becomes minimal. All heat is removed by the cathode gas flow or used in the reforming reaction.
The heat balance of the internal reforming cell is more complicated than for the external reforming cell. Figure 5.20 shows the calculated heat which is considered to be generated in the electrolyte and transferred to the process gases. Heat is generated in both in the electrochemical reaction and in the shift reaction. Heat is consumed in the reforming reaction. The amount of heat consumed in the reforming reaction corresponds to ⅔ or the heat produced by the electrochemical reaction in cell. The net heat production of the cell is therefore approximately ⅓ of the net heat produced in the external reforming cell. Despite the smaller ΔT is over the stack for the internal reforming system, the amount of air required to cool the stack (in the calculated cases) is lower for internal reforming than for external reforming (This will be discussed in more detail in **part III**). As figure 5.20 shows, the reforming reaction occurs primarily in the inlet zone (x/L=0.2) and the heat generated in the electrochemical reaction is released more or less evenly over the cell (although, evidently, the heat flux is larger near the inlet than near the outlet). The result is a negative heat flow in the inlet zone: the transport of heat in the inlet zone is from the process gas to the electrolyte. The 'break-even' point lies at x/L=0.14. Further from the inlet the heat produced in the electrochemical reaction is larger than the heat used by the reforming reaction.

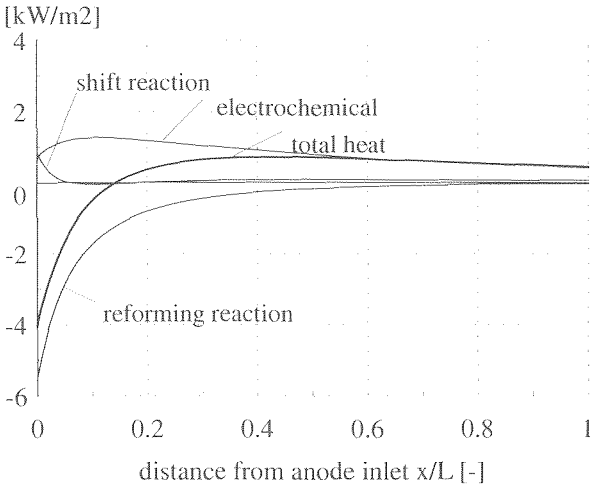

Figure 5.20: Heat generated in the (electro-)chemical reactions in the IR-MCFC (mcni)

The electrical performance of the fuel cell depends on the Nernst voltage and the cell resistance. The curves for these parameters are shown in figure 5.21. At the inlet, the concentration H_2 is low. Correspondingly the Nernst voltage is only 0.94 V (compared to 1.05 V for the external reforming counter-flow cell). The Nernst voltage initially increases as a result of the increasing H_2 concentration and subsequently decreases slowly to the outlet value 0.89 V. Compared again to the external reforming system, the Nernst voltage is slightly

lower over the whole cell because of the lower hydrogen concentration. In the first part of the cell this is due to the fact that the hydrogen is released gradually. The outlet concentration is lower due to the higher fuel utilisation in the internal reforming cell (80% vs. 75%). The current density for the internal reforming cell is shown in figure 5.22. The curve corresponds closely to the curve for external reforming (counter-flow), except for the inlet zone, where the hydrogen concentrations differ considerably. The lower Nernst voltage in the cell is compensated largely by the lower cell resistance (figure 5.21).

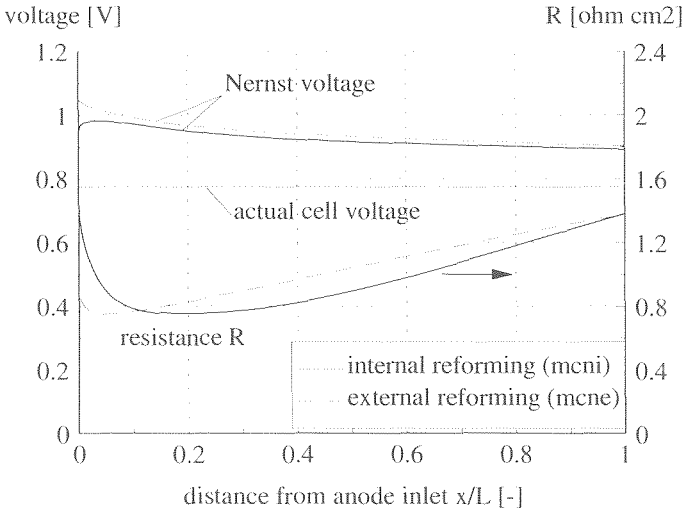

Figure 5.21: Local Nernst voltage and cell resistance and the cell voltage (IR-MCFC)

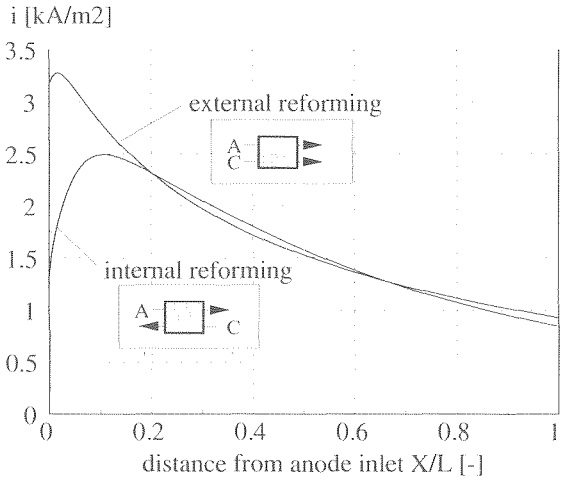

Figure 5.22: Current density for the counter-flow external reforming MCFC (mcne) and internal reforming MCFC (mcni)

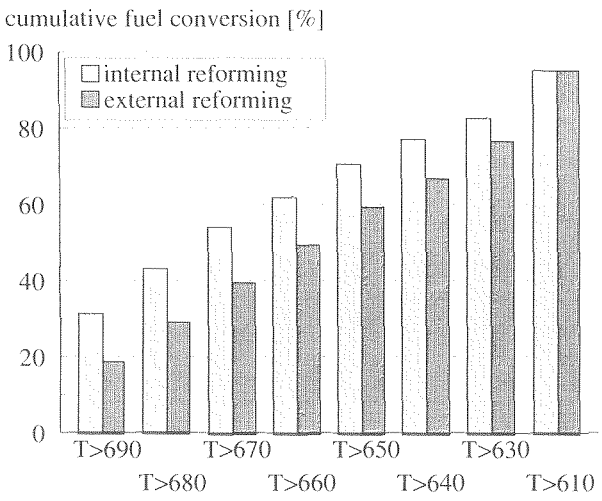

Figure 5.23: Cumulative temperature distribution of the fuel conversion for the internal and the external reforming MCFC (calculations mcne and mcni)

Figure 5.23 represents the percentage fuel which is converted above a given temperature. In **Section 5.3.2** this figure was used to compare the two external reforming configurations (figure 5.12). In this case the external reforming fuel cell and internal reforming fuel cell are compared. The first bar from the left indicates that more than 30% of the fuel is converted in the internal reforming fuel cell at an electrolyte temperature above 690 °C. In the external reforming cell the corresponding value is only 19%. Therefore the average temperature at which the fuel is converted is higher in the internal reforming cell. Again this can be quantified by calculating the effective resistance defined in Section 5.4. For the internal reforming cell the effective resistance equals 0.929 ohm cm^2. This value lies considerably lower than the value calculated for the external reforming cell, which equals 0.973 ohm cm^2. It lies more than 7% lower than the cell resistance at average cell temperature (650 °C => 1 ohm cm^2). The corresponding effective temperature (defined by $R^{eff} = R(T^{eff})$) for the internal reforming system equals 661 °C. Again the fact that a large part of the fuel is converted in the hottest part of the fuel cell leads to a much better performance than expected.

5.4.2 Counter-flow internal reforming SOFC *(scni)*

The last base-case calculation is calculation of the internal reforming SOFC. With respect to the reforming reaction two phenomena are relevant. Firstly the operating temperature of the SOFC is high enough to achieve almost complete conversion of methane based on equilibrium for the reforming reaction even at the inlet composition. Secondly, it is not possible to adjust the amount of catalyst in the anode channel, as can be done in the MCFC, where the catalyst is added separately. In the case of the SOFC the catalyst for the reforming reaction is the electrode material itself. Due to these phenomena, the problem in the SOFC is to limit the rate of reforming reaction. If the rate becomes too high, the temperature gradients in the fuel cell become too large which may lead to degradation or break-down of the cells. In the calculations in this thesis, two methods to

reduce the temperature gradients have been applied: recycling part of the anode off-gas and pre-reforming (see **Section 8.5**). Both anode gas recycling and pre-reforming increase the hydrogen concentration and decrease the CH_4 concentration and therefore reduce the $\Delta_r G$ for the reaction. The inlet concentration of the anode gas is based on the system calculations in **part III**. As figure 5.24 shows, the anode gas at inlet contains approximately 20% H_2 and 10% CH_4.

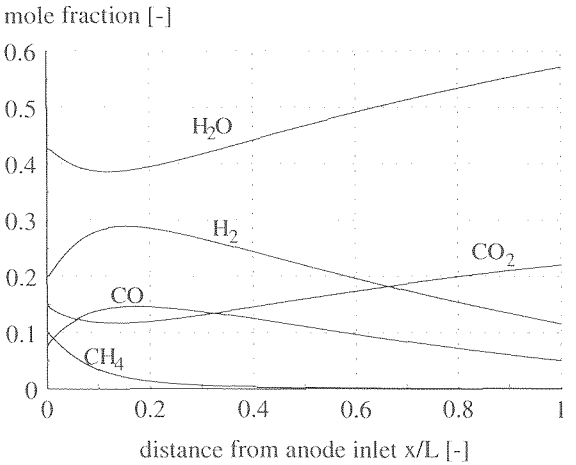

Figure 5.24: Calculated mole fractions at the anode for the internal reforming SOFC (scni)

The methane is almost fully converted at x/L=0.3. The hydrogen concentration reaches the maximum value at x/L=0.15 and subsequently decreases. The concentration H_2 is relatively high (12%) at the outlet. The calculation is based on a low utilisation (70%) per passage. However, the total fuel utilisation is the same as in the case of the external reforming SOFC (85%) because a large part of the hydrogen and CO at the outlet is recycled to the inlet by the anode off-gas recycle. The difference between the external and internal reforming cases lies in the amount of steam which is mixed with the natural gas. The anode off-gas recycle also supplies steam to the inlet of the fuel cell. To achieve the same steam/carbon ratio at the inlet of the fuel cell less steam is required.
The temperature profile for the internal reforming SOFC is shown in figure 5.25. The heat generated in the electrochemical and the chemical reactions is shown in figure 5.26. The main characteristics of the graph correspond to those of the corresponding graph for the internal reforming MCFC, except for the absolute values of the temperatures. The cathode and anode gas are supplied at opposite sides at 850 °C. The cathode gas, which is supplied at x/L=1, is heated to 1005 °C, which is little below the maximum temperature of 1010 °C which has been specified. The temperature approach is determined by the strong cooling effect of the reforming reaction near the inlet. Figure 5.26 also shows the highly uneven heat generation in the fuel cell as a result of the internal reforming reaction. Notwithstanding the low concentration CH_4 in the inlet gas, the cathode gas is cooled down to 959 °C (ΔT_{app}=51 K). Therefore the ΔT over the cell is reduced by approximately ⅓

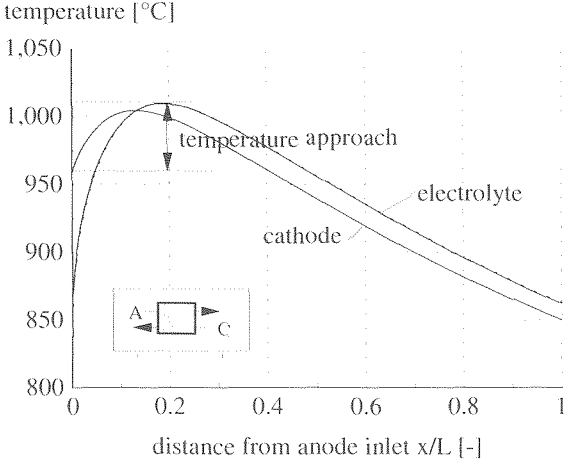

Figure 5.25: Temperature distribution for the base case IR-SOFC calculation (scni)

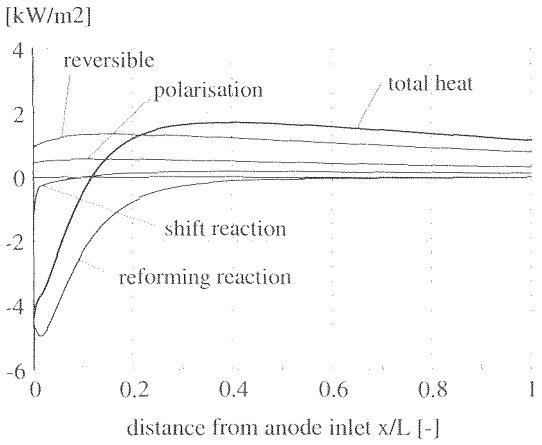

Figure 5.26: Heat generated in the (electro-)chemical reactions in the IR-SOFC calculation (scni)

The curves for the Nernst voltage and cell resistance are shown in figure 5.27. In contrast to the previous cases, the curve for the Nernst voltage is very even in the internal reforming SOFC. The small difference between the Nernst voltage at in- and outlet is due to the use of an anode off-gas recycle. The inlet concentrations are relatively low due to the 'dilution' of the anode gas with recycled gas. Secondly, the temperature and the hydrogen concentration profiles are similar in form. Therefore, in the inlet zone and near the outlet, the lower temperature (V_{rev} ↑) compensates the low hydrogen concentration (V_{rev} ↓), while the high temperature limits the Nernst voltage where high hydrogen concentrations occur around x/L=0.2.

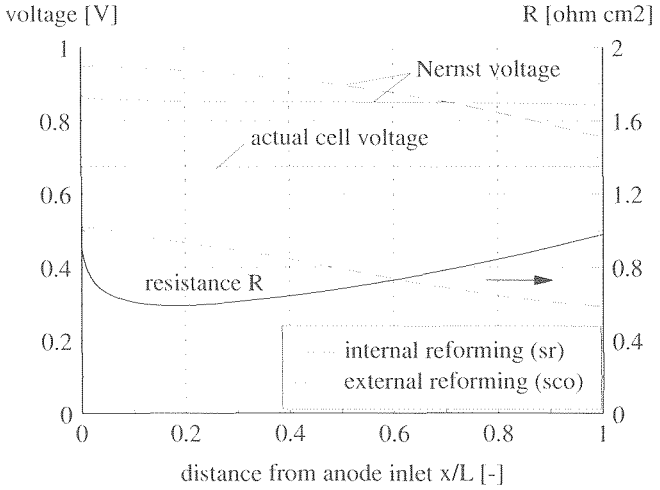

Figure 5.27: Nernst voltage and cell resistance for the IR-SOFC calculation (scni)

As shown before, if high hydrogen concentrations coincide with low local resistance (i.e. high temperature), the fuel is converted at a relatively high temperature. In other words, the effective resistance in that case is low. The calculated value for the effective cell resistance is 0.71 ohm cm^2, which is substantially lower than the value at 925 °C (average of in-and outlet temperature) which is 0.75 ohm cm^2 (specified). Correspondingly the effective temperature is high as well: 940 °C.

CHAPTER 6
DEVELOPMENT OF A SIMPLIFIED FUEL CELL MODEL FOR SYSTEM CALCULATIONS

6.1 INTRODUCTION

A fuel cell system consists of different types of components, such as heat exchangers, compressors and pumps, reactors, etc. To calculate the thermodynamic performance of the complete system all mass and energy flows to and from the components in the system are determined. This calculation includes solving the mass and energy balances for each of the components in the system. For each of the components in the system a model is required to calculate the energy flows (heat, power) and conditions of the process flows (mass flows, temperatures, pressures and compositions) in and out of the component. Standard models for many unit operations are available in the type of flow sheeting software which is used to calculate the performance of energy conversion system. In the flow sheeting program used for this thesis, CYCLE-TEMPO, a simple fuel cell model has been added. This model assumes a constant temperature for the processes in the fuel cell. Although this greatly simplifies the calculations in the model and reduces the calculation times and convergence to levels required for flow sheeting calculations, it is not evident whether this is an acceptable simplification. In this chapter the isothermal model is compared with the detailed model discussed in the previous chapters. Based on this comparison of the results for both models improvements of the simple isothermal model are suggested.
The performance of the fuel cell stack at design conditions can be predicted relatively well. The main parameters which determine the performance, e.g. the cell voltage, fuel utilisation and temperature difference over the fuel cell stack, can be found in literature. For the prediction of the performance at design conditions a simple model suffices, which basically calculates the power generated and the efficiency of the fuel cell stack from the cell voltage and the mass flows from the mass and energy balances over the cell. However, for system calculations which aim at optimisation of the system, the model should not only predict the performance at design conditions, but also predict the performance well at other conditions. Most important: the behaviour predicted at other conditions (off-design) should be consistent with the values calculated for design conditions. This requires a more detailed model. Because the detailed fuel cell (e.g. the model developed in **Chapter 4**) is much too complex to use in the system calculations, a two-step approach is used. First the results for the detailed model at off-design conditions are used to 'validate' and improve the isothermal model and subsequently the improved isothermal model is used in the system calculations in part III.

The correlations for the isothermal model are developed in **Section 6.2**. Subsequently, the off-design behaviour of the different fuel cell types (MCFC/SOFC, internal/external reforming) which has to be modelled with the isothermal model is considered. The basis of comparison between the isothermal and the detailed model is discussed in **Section 6.3**. The off-design behaviour calculated with the detailed model of external reforming fuel cells is discussed **Section 6.4** and for internal reforming fuel cells in **Section 6.5**. Finally in **Section 6.6** the isothermal and detailed model are compared.

6.2.1 Considerations leading to the development of an isothermal model

Local variables: detailed model
The detailed model (**Chapter 4**) uses correlations which describe the process at a local level in the fuel cell. The Nernst voltage and cell resistance are treated as place dependent variables and used to calculate the local current density in a cross section. Equally heat transfer and chemical reactions are modelled on subcell level in the fuel cell. The results of these calculations are temperature and concentration profiles along the fuel cell. The complexity of the model is due to the interdependence of the chemical and electrochemical reactions and the heat generation and transfer, which determine the concentration and temperature profiles respectively. As a result, solving the detailed model requires an iterative procedure as discussed in **Section 4.5**.

Global variables: lumped model
It is possible to model the fuel cell without calculating the concentration and temperature profiles. Because only mass and energy flows have to be solved, the simplest model calculates mass and energy balances on basis of global variables: fuel utilisation, specified ΔT's over the fuel cell stack, chemical equilibrium at the outlet, etc. However, any fuel cell model will require calculation of the cell voltage to be able to calculate the amount of heat and power generated. Else no energy balances can be solved. But, instead of using an extensive model for the processes in the cell, average values can be used. For example in a very simple model the local values of the Nernst voltage and cell resistance are substituted by an average values for the cell. A model in which the process within the fuel cell is described by using average values is indicated as a lumped model. The main weakness of a lumped model is the correlation which is used for the determination of an average value of the Nernst voltage. In the lumped model only the inlet and outlet conditions of the anode and cathode flow are known. Correspondingly, only the Nernst voltage for the inlet conditions and for the outlet conditions can be determined. However, as the calculations in the previous chapter show, the Nernst voltage, expressed as a function of the location along the fuel cell, is a strongly non-linear function as a result of the changes in composition. Consequently, a correlation for the Nernst voltage based only on in- and outlet conditions will have limited accuracy, particularly with respect to the off-design behaviour. This reduces the applicability of such a lumped model for system calculations.

Concentrations place dependent, temperature lumped: isothermal model
Evidently for the system calculations a model has to be selected which does not require the time consuming iterative process for calculation of compositions and temperatures which is characteristic for the detailed model. On the other hand, the model should be able to calculate the effective value of the Nernst voltage in a more sophisticated manner than the lumped model. These requirements have led to the development of a the model which is used in the system calculations in part III 'System studies'. This model is indicated as the isothermal model.
In the isothermal fuel cell model the local processes are modelled, but the model is simplified by assuming all processes in the cell occur at a specific temperature in the fuel cell: the isothermal temperature T_{iso}. As a default value the average of in and outlet temperature can be used for the isothermal temperature. It will be shown however in this chapter that a more advanced choice of isothermal temperature can significantly improve the isothermal model.

Using a single temperature in the fuel cell model simplifies the calculation process, because it is not necessary to model heat transfer. However, the main advantage is that the calculations of the global parameters from the local values is simplified. As a result of the constant temperature, the need for iterations within the fuel cell model is eliminated.
Although the influence of the temperature distribution on the Nernst voltage is not taken into account in the isothermal model, the influence of the concentrations is. This is based on the assumption that the uneven distribution of the Nernst voltage is caused primarily by the concentration profiles and to a lesser extent by the temperature distribution. This approach will be validated by the comparison of the isothermal and the detailed model results over a wide range of off-design conditions (see **Section 6.6**).

6.2.2 Correlations for the isothermal fuel cell model

6.2.2.1 Electrical submodel

The basis for the isothermal model is the equation for the local current density. As in the detailed model, the local current density in the isothermal model is linearized by using the cell resistance R:

$$i = \frac{V_{rev} - V}{R} \tag{6.1}$$

The values for V_{rev} and R are temperature dependent. In the isothermal model the values are determined using the isothermal temperature $T_{iso.}$ The total current for a subcell (see **Section 4.3.1**) depends on the local current density and the area of the subcell dA:

$$dI = i\,dA \tag{6.2}$$

In **Section 4.3.4** the reaction coordinate for the electrochemical reaction (ε_e) has been defined as the number of moles hydrogen converted in this reaction over a period Δt. Using the reaction coordinate, the current for the subcell can be calculated from the Faraday Law as well (see equation 4.20):

$$dI = z\,F\,d\varepsilon_e \tag{6.3}$$

Combining the equations (6.1), (6.2) and (6.3) leads to the following general correlation for the subcell based on the quasi-ohmic relationship between i and V:

$$z\,F\,d\varepsilon_e = \frac{V_{rev} - V}{R}\,dA \tag{6.4}$$

The reaction coordinate ε_e has the dimension [moles/s]. The value of the reaction coordinate at the outlet of the fuel cell (anode) is equal to the total number of moles of hydrogen converted in the fuel cell. The hydrogen which is converted in the fuel cell, is supplied to the fuel cell either directly as hydrogen or indirectly in the form of another fuel component (CO, CH_4, etc.) which can be converted to hydrogen. The total number of moles H_2, direct and indirect, which can potentially be converted in the electrochemical reaction is indicated as the (hydrogen) equivalent flow (**Section 4.3.2**). If the anode gas contains H_2, CO and CH_4 as fuel components, then the maximum value that the reaction coordinate can obtain (when all fuel is converted) equals:

$$\varepsilon_e^{max} = \varphi_a \left(x_{H_2}^{o} + x_{CO}^{o} + 4\,x_{CH_4}^{o} \right)$$

where φ_a is the total mole flow anode gas and x_i^0 are the inlet concentrations. With the fuel utilisation, the fraction of the fuel actually converted, the total current is equal to:

$$I = z F \varepsilon_e^{max} U_F \tag{6.5}$$

The reaction coordinate ε_e (which has the dimension [moles/s]) can be made dimensionless by dividing the reaction coordinate by the total number of moles hydrogen supplied to the fuel cell. The dimensionless reaction coordinate is defined as:

$$d\lambda = \frac{d\varepsilon_e}{\varepsilon_e^{max}} \tag{6.6}$$

Substituting the expression for $d\varepsilon$ in equation (6.4) gives:

$$dA = z F \varepsilon_e^{max} R^{\square} \frac{d\lambda}{V_{rev}(\lambda) - V}$$

Both sides of the equation are integrated over the fuel cell. The dimensionless reaction coordinate changes from 0 at the inlet of the cell to U_F at the outlet. Because only V_{rev} depends on the dimensionless reaction coordinate λ, the other parameters can be placed outside of the integral:

$$\int_0^A dA = z F \varepsilon_e^{max} R^{\square} \int_0^{U_F} \frac{d\lambda}{V_{rev}(\lambda) - V}$$

Which can be rearranged to:

$$\frac{A}{z F \varepsilon_e^{max}} = R^{\square} \int_0^{U_F} \frac{d\lambda}{V_{rev}(\lambda) - V} \tag{6.7}$$

The denominator depends only on the fuel flow which is supplied to the fuel cell. Using equation (6.5) this expression can be replaced by I/U_F. Rewriting this equation gives the following expression:

$$\frac{I}{A} = \frac{U_F}{R^{\square} \int_0^{U_F} \frac{d\lambda}{E - V}} \tag{6.8}$$

Equation (6.8) is the required correlation between the parameters I, A and V for the isothermal model. To evaluate the integral in equation (6.8), which is done numerically in the isothermal fuel cell model, the Nernst voltage must be determined as a function of the dimensionless reaction coordinate λ. The Nernst voltage depends on the partial pressures and consequently on the concentrations at anode and cathode. These concentrations are calculated by the thermodynamic submodel.

6.2.2.2 Thermodynamic submodel

The thermodynamic submodel only calculates the concentration profiles in the anode and cathode channels and not, as in the detailed model, both temperature and concentration profiles. At the cathode, the concentrations are determined only by the amount of O_2 (and

CO_2 in the MCFC) which has been used for the electrochemical reaction. The calculation of the cathode flow composition is the same as in the detailed model (**Section 4.4.1**) where the composition is calculated from the reaction coordinate for the electrochemical reaction (ε_e). The reaction coordinate is directly linked to λ by (equation 6.6), which makes it possible to determine the partial pressures at the cathode as a function of λ, as required for solving the integral equation (6.8).
At the anode, chemical reactions will play a role as well. In the detailed model, the rate of reaction is calculated either by assuming equilibrium or by using a kinetic rate of reaction. The local equilibrium composition will depend on the amount of hydrogen which has been consumed by the electrochemical reaction and on pressure and temperature, which are constant in the isothermal model. Therefore, if chemical equilibrium is assumed, the composition and the partial pressures at the anode depend only on λ and E in equation (6.8) depends on λ only. The cell current is found by integrating over λ. Including the reaction rate in the model will make the model much more complicated. To keep the model simple the chemical reactions in the fuel cell model are calculated assuming chemical equilibrium. Again this assumption will be validated in **Section 6.6**.
As in the detailed model two reactions are taken into account in the isothermal model: the shift reaction and the reforming reaction. The concentrations are calculated assuming the shift reaction in equilibrium (external reforming cells) or both shift and reforming reaction in equilibrium (internal reforming). In the latter case the method developed in **Section 4.4.3** has been used to calculate the simultaneous equilibrium for both reactions.

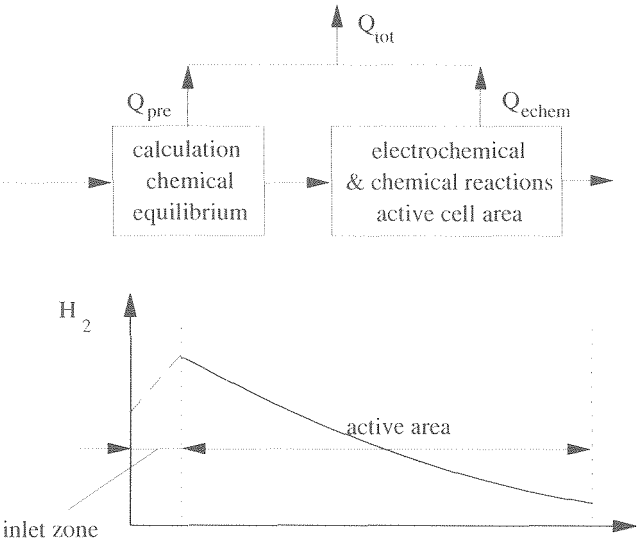

Figure 6.2: Separate calculation of the chemical equilibrium at the anode inlet in the isothermal model

In the external reforming SOFC the anode gas at the inlet will not be far from equilibrium, because the difference between the temperature at which equilibrium for the shift reaction is achieved in the reformer and the inlet temperature of the SOFC is small (50-100 K). Due to the high temperature both reactions can be considered as equilibrium reactions. In the MCFC the temperature difference between the outlet of the reformer (800-850 °C) is larger and

therefore the assumption that the composition is in equilibrium is not acceptable on forehand. In the external reforming MCFC the reforming reaction is slow because no catalyst is present for the reaction. In this case only the shift reaction is considered. Because the influence of the shift reaction on the Nernst voltage is small, modelling the composition based on equilibrium (for the shift reaction only) seems acceptable.
For internal reforming cells (both SOFC and MCFC), the equilibrium model is less obvious. The anode gas which enters the fuel cell is (in general) far from equilibrium and consequently the equilibrium composition as function of λ is discontinuous at the inlet (λ=0). Therefore, for internal reforming cells, the chemical equilibrium of the inlet composition is calculated first. The fuel cell model, as illustrated in figure 6.2, consists of a separate inlet zone for the reforming reaction and an active area in which the electrochemical reaction occurs. The first step, where the reforming reaction reaches equilibrium (for λ=0), can be considered as a pre-reforming zone. The heat in the first step is calculated separately and indicated as the pre-reforming heat (Q_{pre}). Subsequently the equilibrium composition of the anode gas as a function of λ is used to calculate the cell current I from integral (6.8). Although this procedure differs from the process in an actual internal reforming cell, the calculated performance will be shown to agree quite well (**Section 6.6**).

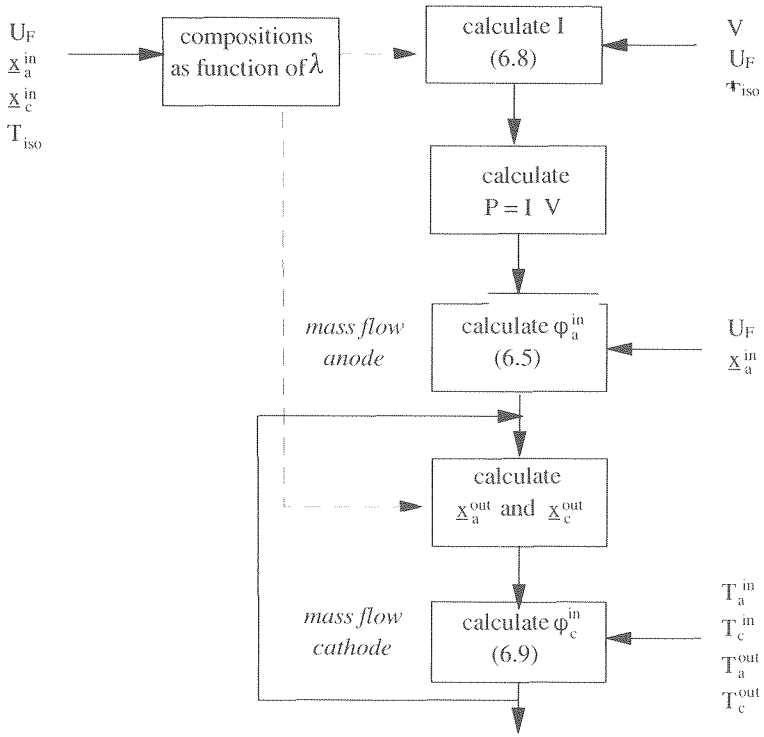

figure 6.3: Overview of the calculation procedure for the isothermal model

By solving the integral in equation (6.8), the cell current I is calculated. The cell power P can be calculated from P=I·V. Once the power P has been calculated, the energy balance over the fuel cell is used to calculate the cathode flow:

$$\varphi_a^{in} h_a(T_a^{in}, \underline{x}_a^{in}) + \varphi_c^{in} h_c(T_c^{in}, \underline{x}_c^{in}) - \varphi_a^{out} h_a^{out}(T_a^{out}, \underline{x}_a^{out}) - \varphi_c^{out} h_c^{out}(T_c^{out}, \underline{x}_c^{out})$$

$$= P_e - Q_{loss} \qquad (6.9)$$

6.2.3 Overview of the input and output parameters for the isothermal model

In figure 6.3 the calculation procedure for the isothermal model is summarised. The compositions as a function of the dimensionless reaction coordinate are calculated to obtain the cell current using equation 6.8. The calculated compositions depend on the values at the inlet (x_a^{in} and x_c^{in}) and on the fraction of hydrogen which reacts in the cell or the fuel utilisation (U_F). Furthermore, depending on the type of cell which is modelled, the equilibrium of the shift and/or the reforming reaction is included and therefore the average temperature (T_{iso}) is an input parameter for the calculation of the composition.
The composition as a function of the reaction coordinate is used to calculate the cell current I by integrating equation (6.8) and several parameters linked directly to the cell current (power P_e, the anode gas flow at the inlet φ_a^{in}) and to calculate the outlet compositions ($\lambda=U_F$). Finally solving the energy balance (6.9) the cathode gas flow can be calculated. This requires an iterative procedure because the flow at the cathode inlet which is calculated from the energy balance depends on the calculated composition at the cathode outlet (x_c^{out}), while the composition at the cathode outlet depends on flow on the inlet. Therefore these calculations are repeated a number of times to obtain the required accuracy. The overview of input and output for the isothermal model is shown in figure 6.4.

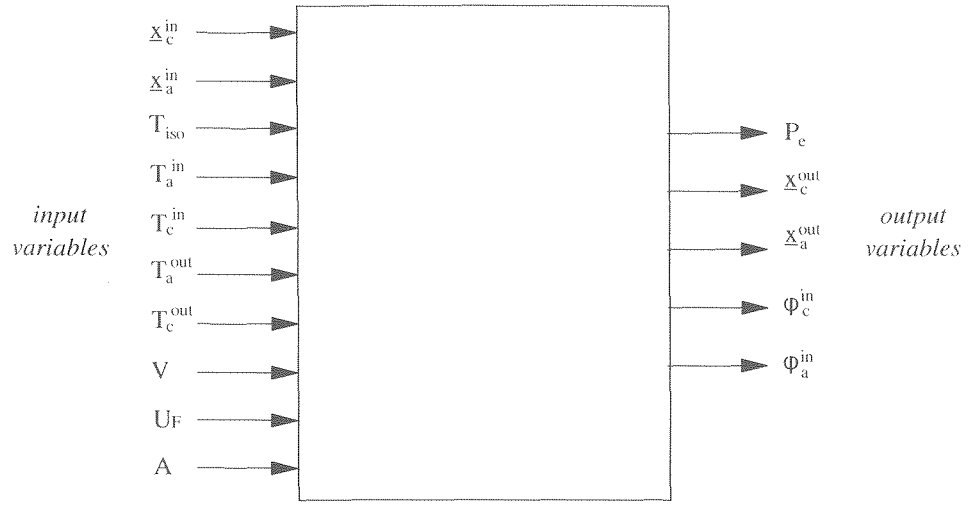

Figure 6.4: Overview of input and output parameters for the isothermal fuel cell model

If this figure is compared to the corresponding scheme for the detailed model, the difference is that in the detailed model outlet temperatures and the effective (average) temperature are calculated in the model by specifying the inlet temperatures and maximum material temperature. In the isothermal model all temperatures have to be specified. For off-design conditions the following effects are therefore not taken into account in the isothermal model.

- The outlet temperatures may vary at off-design conditions, due to differences in the temperature approach (see **Section 5.2**). In the isothermal model the outlet temperatures are constant.
- The average or effective temperature may depend on the off-design conditions as well. The isothermal temperature, which represents the average temperature in the isothermal model, is constant as well.

Whether this affects the calculation results substantially will be investigated in the following sections.

6.3 OFF-DESIGN CALCULATIONS WITH THE DETAILED FUEL CELL MODEL

6.3.1 Input and output parameters characterising the off-design behaviour

In this section the off-design behaviour of the different types of fuel cells will be characterised using the detailed fuel cell model. The first issue is: which parameters will be considered? The description of the integrated detailed model (**Section 4.6**) shows that many parameters are directly linked. For example: given the fuel flow, the fuel utilisation and cell current cannot be varied independently. Therefore, it is not possible to specify both values as input parameters. Neither is it useful to compare the detailed and the isothermal model using both variables: comparing the fuel utilisation or the cell current will suffice.

Output parameters

The most important parameters which are calculated by the fuel cell model are of course the electrical power generated by the fuel cell and the amount of heat generated in the fuel cell. As will be shown below, the differences in calculation between a detailed and the isothermal model result in different values for the calculated power (P) and heat (Q). It is sufficient to compare the models on these two variables. Instead of using the calculated heat Q, which is not an explicit variable, the mass flow of the cathode gas will be used to compare both models in **Section 6.6**. The cathode gas flow is a measure of the amount of heat which is generated, because the cathode flow is used to cool the stack.

Calculated power

In both fuel cell models the fuel utilisation and the cell voltage, which are used to calculate the generated power, are input parameters. The average current density, which is the remaining unknown parameter required to calculate the power generated is calculated im a different manner than in the detailed model. In the detailed model this calculation requires the iterative procedure described in **Section 4.5** in order to calculate both the temperature distribution and the reaction coordinates over the fuel cell. In the isothermal model only the reaction coordinates need to be determined, because the processes in the fuel cell are considered to occur at an average cell temperature. If the value for the power generated calculated in both models correspond, all other 'electrical variables' (fuel utilisation U_F, cell current I, amount of hydrogen reacted in the electrochemical reaction, etc.) will correspond as well.

Calculated mass flow of the cathode gas

As shown in **Section 4.5** the mass flow cathode gas is calculated from the energy balance over the stack. The amount of heat which is generated in the electrochemical and chemical reactions is removed from the fuel cell by the cathode gas. The calculated mass flow depends on:

- The temperature difference between in- and outlet for the cathode gas;
- The heat which is generated in the fuel cell.

Differences between the calculation results between the detailed fuel cell model and the isothermal model can result either because the model uses a different temperature difference over the stack or because the calculated heat is not the same in both models. By comparing the calculated mass flow for the cathode gas, the effect of using different values for both variables can be checked.

The analysis therefore shows, that the generated power and the mass flow cathode gas are the parameters for which the calculated value in the isothermal model should correspond to the value calculated in the detailed model.

Input parameters

The second issue which has to be addressed is, which parameters should be varied to characterise the off-design performance. Again, a large number of parameters in the fuel cell models is linked. Therefore they cannot be varied independently. For example if the cell voltage is an input variable, the mass flow fuel and the fuel utilisation cannot be both specified at the same time. In **part III** different configurations are compared. The focus in the system calculations is on the different possible configurations for a given fuel cell design. Therefore in the calculations which are used to compare the fuel cell models, the parameters which characterise the fuel cell design have not been varied. Constant values have been used for:

- the inlet temperatures for the stack;
- maximum electrolyte temperature;
- the cell resistance R°;
- the cell area A.

In both models the concentrations of the process flows (anode, cathode) at the inlet are specified. The Nernst voltage is calculated as a function of the conversion in both detailed and isothermal model. Therefore the variations in inlet composition are within the limited range encountered in the system calculations (**part III**) and are not investigated in detail. The influence of the outlet composition at the anode is larger than the influence of the inlet composition (see **Chapter 5**) and is taken into account through variations in the fuel utilisation. Given that the above parameters are fixed, only three main input variables for the fuel cell models remain (see figure 4.16 / figure 6.4):

- the fuel utilisation U_F
- the cell voltage V
- pressure P

The pressure has not been varied in the off-design calculations. The reason is that the fuel utilisation and cell voltage are expected to have a larger impact on the local conditions and will therefore have a larger impact on the difference between detailed and isothermal model. However, it would be of interest to consider the influence of the pressure in future work. In the current work, the off-design conditions are defined by cell voltage V, the fuel utilisation U_F. In order to compare the results of the fuel cell models (detailed and isothermal) at off-design conditions, calculations have been carried out for a range of values for V and U_F.

The values calculated for the power and the mass flow of the cathode gas with the isothermal model and the detailed model will be compared. In the calculations in this section the off-design behaviour of the fuel cell is considered using the detailed model. Two additional parameters are considered in this section, because they can clarify the difference between the detailed and the isothermal model. The difference between both models is the calculation of the temperature distribution in the detailed model. The temperature distribution is used to determine two parameters which are essential for the calculation of the generated power and the cathode gas mass flow.

- The temperature distribution determines at what average temperature the electrochemical reaction takes place. The temperature at which the electrochemical reaction takes place is important because the cell resistance is strongly temperature dependant: a higher average temperature for the process leads to a higher current density at a given cell voltage. The average temperature of the electrochemical reaction in the detailed model is indicated as the effective temperature (see **Section 5.3**). As will be shown the effective temperature will change at off-conditions. This causes a difference between the isothermal and detailed model with regard to the calculation of the electrical power generated.
- The second variable which depends on the temperature distribution is the temperature approach, defined in **Section 5.2** as the difference between the outlet temperature and the maximum (electrolyte) temperature in the cell. In the isothermal model the outlet temperature is not calculated but specified as an input parameter. This is the main difference between the values calculated with the isothermal and the detailed model.

Therefore both the effective temperature and the temperature approach will be considered. In **part III** four series of calculations are carried out corresponding to the different types of fuel cell stacks modelled:

- SOFC external reforming;
- SOFC internal reforming;
- MCFC external reforming;
- MCFC internal reforming

In the following sections the off-design behaviour for these 4 types of fuel cell stacks will be discussed based on the calculations with the detailed model.

6.4 PERFORMANCE AT OFF-DESIGN FOR EXTERNAL REFORMING CELLS

6.4.1 Generated power and heat at off-design conditions

To analyse the performance at off-design, the output of the fuel cell stack at different values of the cell voltage and the fuel utilisation is evaluated. The cell voltage and the fuel utilisation are specified (input) and the values for other parameters (inlet flows, outlet temperatures, generated power P, generated heat Q) are calculated (output). In particular these last two parameters, P and Q, characterise the 'performance' of the fuel cell. The electrical power can be calculated directly from cell voltage and cell current ($P=I \cdot V$). The heat which is generated in the fuel cell is not defined as clearly as the generated power. As the fuel cell is operated adiabatically, there is no direct heat flow from the fuel cell to the surroundings or to another process flow: the heat generated in the (electro-)chemical reactions used to increase the temperature of the process flows. The value of Q which is calculated corresponds to the heat

transferred from the electrolyte to the process flows[p] (see **Section 4.4**).
The generated power P and the generated heat Q at off-design conditions for the external reforming MCFC (co-flow) are shown in figure 6.5. For the external reforming MCFC the cell voltage has been varied from 0.725 V to 0.8 V at a constant fuel utilisation (0.80) and the fuel utilisation has been varied from 0.7 to 0.85 at constant cell voltage (design value 0.775 V). Note that the objective is to verify that the results of the detailed and the isothermal model correspond for the off-design conditions encountered in the system calculations in **part III**. The range of conditions, for example cell voltages, is therefore limited compared to an actual part-load model. The range of cell voltages and fuel utilisations in the off-design calculations is selected to encompass at least to the ranges encountered in the system calculations.

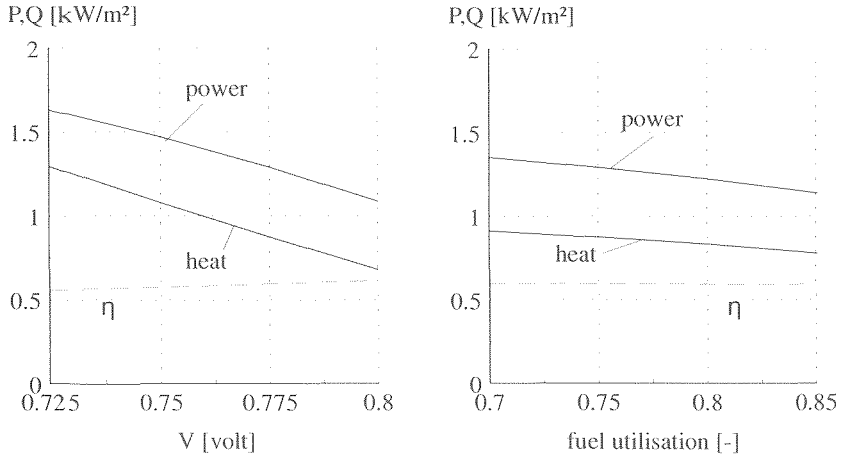

Figure 6.5: Performance of the external reforming MCFC at off-design conditions

If the fuel cell is operated at a higher cell voltage, less power will be generated: in this case the fuel cell operates at part load. If the cell voltage is lower, the current density is higher and more than nominal power will be generated. Evidently the fuel flow will be more or less proportional to the power generated (P) and the cathode gas flow, which cools the cell, more or less proportional to the heat generated (Q). The calculated mass flows for both anode and cathode are shown in figure 6.6
The heat which is generated in the fuel cell follows the same pattern as the generated power as it also depends mainly on the current density. Therefore decreasing the cell voltage also leads to higher heat production in the fuel cell. The graph on the left in figure 6.5 shows the change in both the power density and the heat (also per cell area) if the cell voltage varies in the indicated range. If the cell voltage varies from 0.725 V to 0.8 V, the calculated power decrease from 1.3 kW/m^2 to 0.67 kW/m^2 over that range. The power density is therefore very sensitive to the cell voltage.

---

[p] In terms of the fuel cell system, this heat corresponds to the difference between the heat which is recovered by cooling down the process flows at the outlet of the fuel cell to environment temperature and the heat required to preheat the process flow from this temperature to the inlet temperature

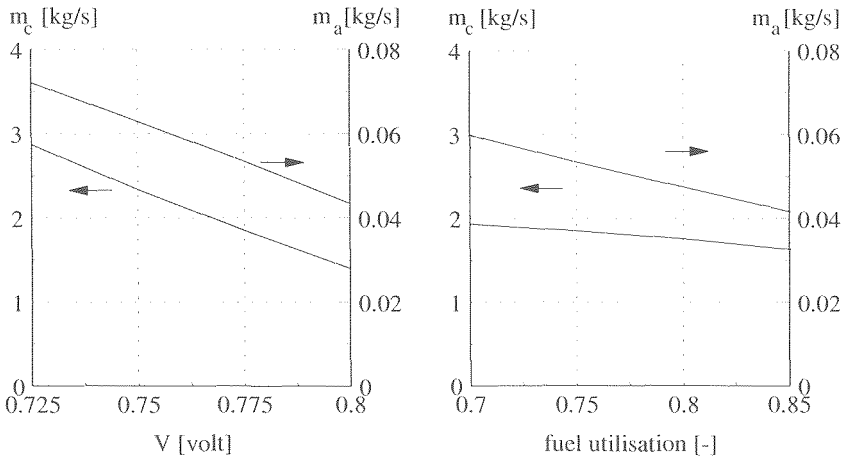

Figure 6.6: Calculated mass flows for the external reforming MCFC at off-design conditions

The graph on the right hand side in figure 6.5 shows the influence of the second off-design variable, the fuel utilisation, on the power and heat which are generated. The fuel utilisation is varied at a constant cell voltage (0.775 V). If the fuel cell is operated at a high fuel utilisation the average hydrogen concentrations are lower, which leads to a lower average Nernst voltage (V_{rev}) in the fuel cell ($U\uparrow \Rightarrow x_{H2}\downarrow \Rightarrow V_{rev}\downarrow$). Consequently the driving force for the electrochemical reaction, the voltage loss ΔV ($=V_{rev}-V$) and the as a result the amount of power generated in the fuel cell become smaller if the fuel utilisation increases. The effect of the utilisation on the generated power is not as large as the effect of the cell voltage.
The (electrical) efficiency of the fuel cell can be defined in different ways. The output of the fuel cell is the electrical power, the input of the fuel cell may vary depending on the definition of the efficiency The chemical energy which is converted in the fuel cell is converted either into heat or into electrical power. The energy balance for the fuel cell, taking into account the conventions with respect to the sign of the energy flow (see **Section 2.2**), equals:

$$Q = P + \Delta H$$

If the efficiency is based on the energy input to the system, the efficiency becomes:

$$\eta = \frac{P}{\Delta H} \tag{6.10}$$

If the calculation is based on the energy obtained by converting the fuel in the fuel cell, the fuel utilisation should be taken into account and the efficiency can be defined as:

$$\eta = \frac{P}{\Delta H} U_F \tag{6.11}$$

Which efficiency definition is 'correct' depends strongly on the integration of the fuel cell into the system as it depends on the way in which the heat and remaining chemical energy are utilised in the system. As in this chapter the focus is on the fuel cell itself, the first definition will be used. To show that this efficiency depends only on the already calculated parameters P and Q, we can rewrite equation (6.10) to:

$$\eta = \frac{P}{P + |Q|} \qquad (6.12)$$

The calculated fuel cell efficiencies are shown in figure 6.5 as well. Operating the fuel cell at higher cell voltage, decreases both the amount of power and the amount of heat which is generated in the er-MCFC, but not proportionally. Consequently, the efficiency, or the ratio P/(P+Q), increases with the cell voltage. This is a fundamental characteristic of the fuel cell as well: the efficiency increases with the cell voltage, i.e. a larger part of the chemical energy is converted into power at part load (**Section 4.3**). The graph on the right in figure 6.5 shows that the ratio (P/P+|Q|) is not affected the fuel utilisation and that the change in efficiency at off-design conditions is therefore entirely determined by the cell voltage.
Figure 6.7 shows the current density distribution of the fuel cell for different values of the cell voltage. The initial increase of the current density is caused by the assumption that the shift reaction is not in equilibrium at the inlet. As the reaction reaches equilibrium (H_2 is formed to achieve equilibrium) the current density peaks. At a larger distance from the inlet the reactant concentrations at both anode and cathode become poorer (the stack is of the co-flow type) and the current density decreases to the outlet value. As indicated, if the cell voltage is higher, the difference between the Nernst voltage and the cell voltage, which is the driving force for the electrochemical reaction, is lower. Consequently the current density is lower at higher cell voltage as well.
Figure 6.8 shows the current density for different values of the fuel utilisation. The average current (the area under the current density curve) decreases if the fuel utilisation increases, again as a result of the lower driving force (V_{rev} - V) for the electrochemical reaction. In contrast to the previous figure, however, this is not due to a change in cell voltage (V), but because the Nernst voltage (V_{rev}) is lower at higher fuel utilisation. As figure 6.8 shows, the current density near the inlet (x/L=0) is independent of the fuel utilisation. At the outlet the hydrogen concentration and therefore the Nernst voltage will decrease at higher fuel utilisation. Consequently the local current density near the outlet decreases as well.

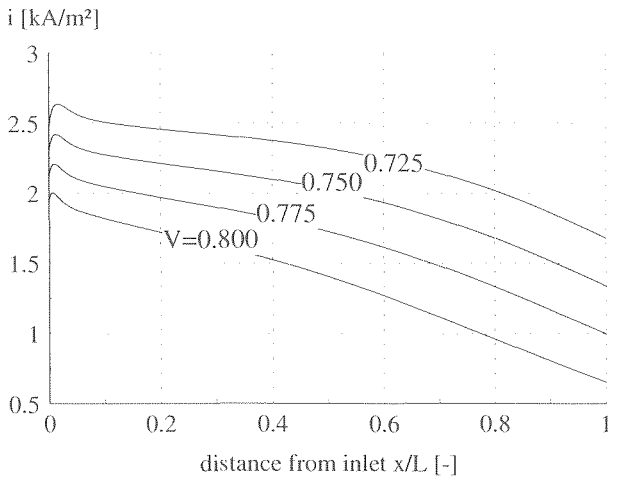

Figure 6.7: Calculated current density distribution for different values of the cell voltage for the co-flow external reforming MCFC

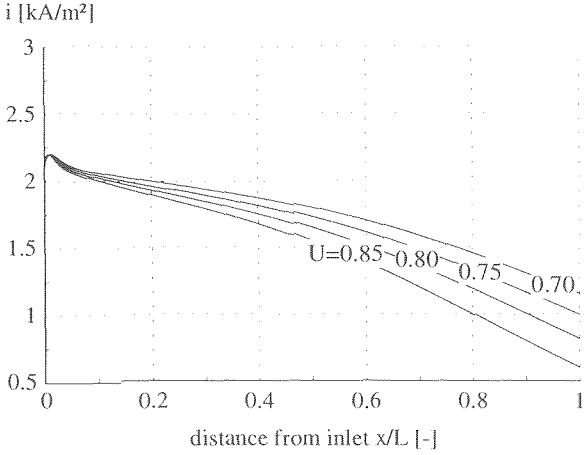

Figure 6.8: Calculated current density distribution for different values of the fuel utilisation for the co-flow external reforming MCFC

6.4.2 Cathode outlet temperature and effective temperature at off-design conditions

Two other important parameters with respect to the off-design behaviour of the fuel cell are shown in figure 6.9. In these two graphs the effect of cell voltage and utilisation on two temperatures is shown. These temperatures are relevant in particular because they play an important role in the comparison of the detailed and the isothermal model. These temperatures are the effective temperature (which determines the average cell resistance) and the temperature approach (difference between the maximum temperature in the stack and the temperature at outlet of the cathode). Again the graph on the left shows the change in these temperature if the cell voltage is varied at a constant fuel utilisation and the graph on the right shows how the temperatures depend on the utilisation at a constant cell voltage.

outlet temperature

Instead of the outlet temperature, the maximum temperature has been specified (700 °C) for the MCFC calculations with the detailed model (see **Section 5.2.2**). The outlet temperature is determined by the temperature approach, which is calculated from the heat transfer correlations. The outlet temperature is important in the system calculation because it influences the amount of cathode gas which is required to cool the cell. The outlet temperature changes from 691 °C to 697 °C if the cell voltage increases from 0.725 to 0.8 V, which corresponds to a change in temperature approach from 9 K to 3 K (=700-T). The sensitivity of the temperature approach for the fuel utilisation is smaller, in figure 6.9 the temperature approach changes from 5 K to 3 K. The difference between the electrolyte temperature and the cathode flow at the outlet, is due to the heat flux. The general equation for heat transfer from the electrolyte to the cathode is:

$$\frac{Q_c}{\Delta A} = \alpha_c \cdot (T_e - T_c) \qquad (6.13)$$

The temperature approach is the difference between the maximum electrolyte temperature and the outlet temperature of the cathode gas. In the co-flow cell this temperature occurs at the

outlet (x/L≈1) of the fuel cell (see **Section 5.3**). Therefore the temperature approach (i.e. the temperature difference at the outlet of the fuel cell) is determined by the current density at the outlet of the fuel cell. The average current density decreases, both with increasing cell voltage (figure 6.7) and with increasing fuel utilisation (figure 6.8). But if fuel utilisation increases, the current density decreases primarily near the outlet in the second case, which has the largest impact on the temperature approach. Therefore the influence of the fuel utilisation on the temperature approach is larger than the decrease in (average) current density indicates.

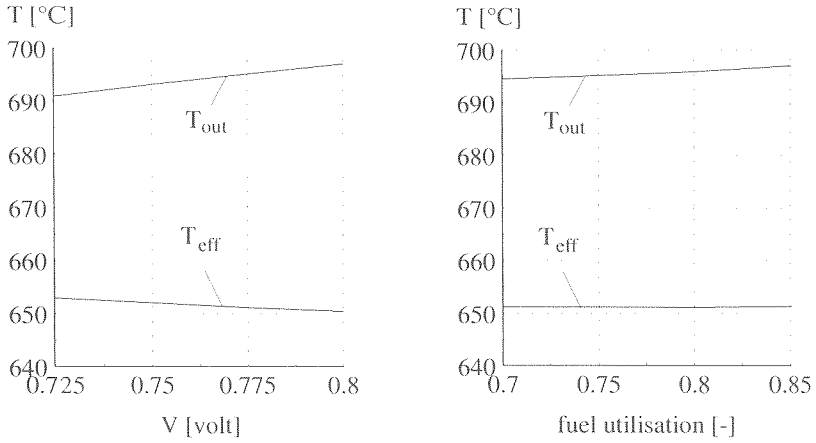

Figure 6.9: The effective temperature (T_{eff}) and the outlet temperature of the cathode gas (T_{out}) at off-design conditions for the MCFC external reforming

effective temperature

The cell resistance is determined to a large extent by the temperature in the cell. A relatively small increase in temperature in the electrolyte can increase the current density substantially. For the complete cell this effect has been quantified by the introduction of the effective temperature in **Section 5.3**. If the effective temperature is high, the apparent cell resistance is low and vice versa. As shown, the effective temperature depends on the combination of the temperature distribution and the current density distribution. It is advantageous if the temperature is high in that part of the fuel cell where the current density is high as well. The effective temperature will be high (low apparent resistance). If the high temperature zone coincides with low current densities, a lower effective temperature will result.

Small changes in effective temperature will lead to noticeable changes in the efficiency of the cell. In figure 6.9 the effective temperature at off-design conditions is given. If the cell voltage increases the effective temperature decreases slightly. If the fuel utilisation increases, the influence on the effective temperature is negligible. Because of the large impact of the effective temperature, explaining these differences will help understand the differences between the detailed model and the isothermal model in the following sections.

In figures 6.10 and 6.11 the temperature profiles are shown for two different values of the cell voltage and two different values of the fuel utilisation. To explain the changes in T_{eff} at off-design the temperature profiles are not sufficient. Fro

of the fuel utilisation either. To explain the changes in effective temperature at off-design, both the current densities (figures 6.7 and 6.8) and the temperature distribution are relevant. In the co-flow configuration the temperature increases more or less linearly and high temperatures occur near the outlet zone (x/L≈1). The current density is high near the inlet zone

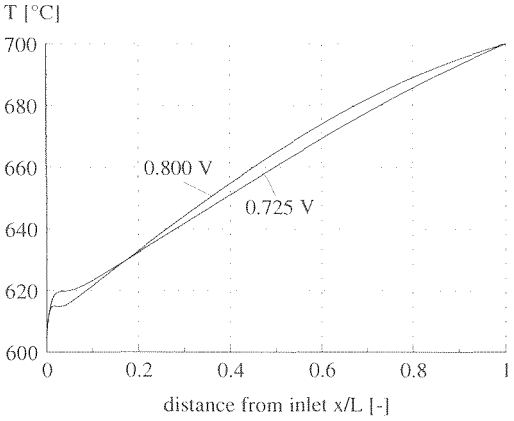

Figure 6.10: Calculated temperature profile of the electrolyte for two values of the cell voltage for the external reforming MCFC (@ U_F=0.8)

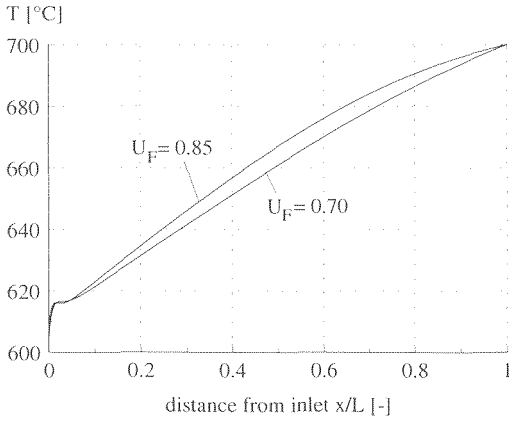

Figure 6.11: Calculated temperature profile of the electrolyte for two values of the fuel utilisation for the external reforming MCFC (@ V=0.775)

The influence of the cell voltage on the temperature in figure 6.10 shows a higher average temperature in the cell at a higher cell voltage. However, there are two effects which off-set this higher temperature. The average temperature in the first part of the cell (x/L<0.5) is approximately the same. The average temperature is higher mainly in the second part of the fuel cell (x/L>0.5) where the current density is relatively low. Secondly the current density profile at higher cell voltage becomes more unevenly distributed. For the co-flow stack, with the high temperature near the outlet of the cell, this leads to a decrease of the effective temperature.

At a higher fuel utilisation the current density decreases. But as figure 6.8 shows, this decrease occurs mainly in the second (cold) part of the cell (x/L<0.5). In the hot part of the cell (x/L>0.5) the change in current density is only small. On average, the conversion takes place at a lower temperature as a result of this effect. In the case of an increase in fuel utilisation, the increasingly uneven distribution of the current density is compensated by the increase in average temperature (figure 6.11) and the net result is a constant effective temperature.
Figures 6.12 and 6.13 show the main calculation results for the external reforming SOFC. These graphs should be compared to the corresponding graphs for the external reforming MCFC (figure 6.5 and 6.9, respectively). Comparison reveals that the absolute values (of P, Q, T_{out}, etc) are different, but the trends are similar. Evidently the same phenomena determine the off-design behaviour for both types of external reforming cells.

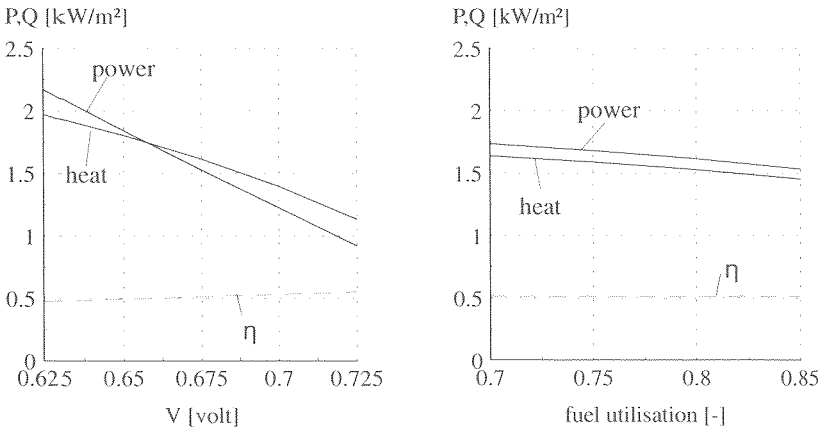

Figure 6.12: Performance of the external reforming SOFC at off-design conditions

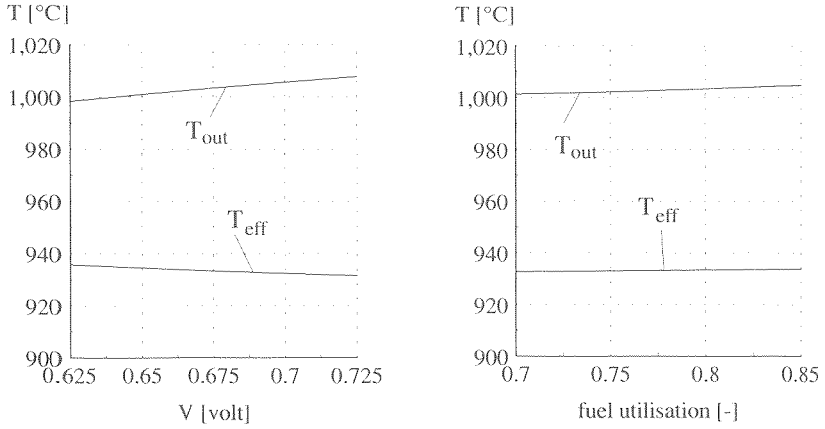

Figure 6.13: The effective temperature (T_{eff}) and the outlet temperature of the cathode gas (T_{out}) at off-design conditions for the external reforming SOFC

6.5 OFF-DESIGN PERFORMANCE FOR THE INTERNAL REFORMING CELLS

6.5.1 Generated power and heat at off-design conditions

The calculated performance for the internal reforming MCFC at off-design conditions is summarised in figure 6.15. Again the performance of the stack operating at different values of the cell voltage and fuel utilisation is evaluated. For the calculations these parameters are varied for a specific stack design (area, R, T_{max}, inlet temperature) and the corresponding values for other parameters (inlet flows, generated power P, generated heat Q, outlet temperatures) are calculated.
The main difference between the graphs for the internal reforming MCFC in figure 6.15 and the corresponding graphs for the external reforming MCFC in figure 6.5 is the difference in the net amount of heat Q which is generated in both cases. In an external reforming cell, the net heat production of the cell is approximately equal to the heat which is generated in the electrochemical reaction. In the internal reforming cell heat is also used for the reforming reaction. The net heat (which is shown in figure 6.15) is equal to the heat which is generated in the electrochemical reaction (indicated in the figure as 'heat produced') minus the heat which is used in the reforming reaction.

$$Q_{net} = Q_{ec} - Q_{ref} \qquad (6.14)$$

If the fuel cell stack is operated at a higher cell voltage the driving force (ΔV) decreases. The fuel cell operates at part load, the generated power P decreases and the heat generated in the electrochemical reaction decreases as well (see **Section 6.4.1**). Operating the stack at a higher cell voltage also corresponds to a lower fuel flow to the stack. Because the amount of heat consumed in the reforming reaction changes more or less proportionally to the fuel flow, the net heat changes approximately proportional to the power generated as well.
If the fuel cell is operated at a higher fuel utilisation the driving force for the electrochemical reaction decreases as well (see **Section 5.4**). Consequently the power and the heat generated

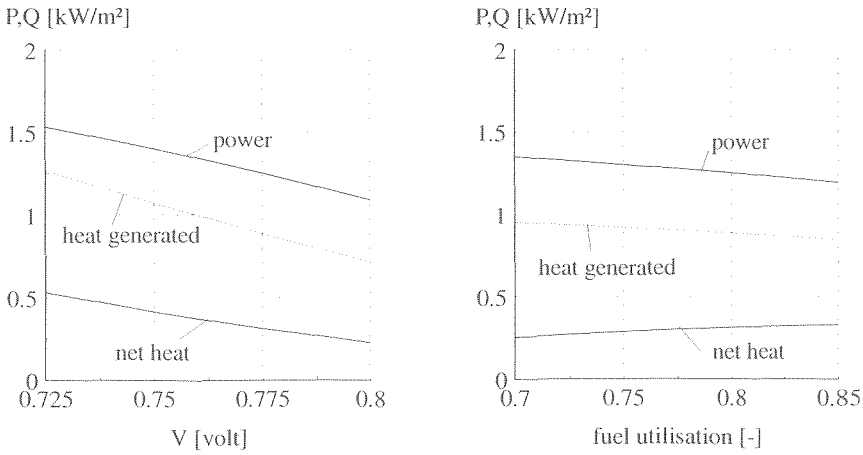

Figure 6.15: Performance (generated power + heat) of the internal reforming MCFC at off-design conditions

in the electrochemical reaction will both decrease. However, as can be seen in figure 6.15, the net heat which is produced increases. This can be explained as follows. The amount of heat which is generated in the electrochemical reaction is approximately proportional to the amount of fuel which is converted in the fuel cell. On the other hand, virtually all methane which is supplied to the fuel cell is reformed and the heat required for this conversion therefore depends only on the amount of fuel supplied to the fuel cell. The fuel utilisation is the ratio between the amount of fuel converted in the fuel cell and the fuel supplied to the cell. Operating at a higher fuel utilisation therefore leads to a higher amount of the heat generated in the electrochemical reaction compared to the heat which is used for the reforming reaction. In other words, if the fuel utilisation is high, the cooling effect of the reforming reaction becomes less important.
For the internal reforming system the fuel cell efficiency can be defined as in equation (6.12) where Q is the net heat produced in the fuel cell. However, if this definition is used in the internal reforming fuel cell, a higher efficiency is calculated for the fuel cell if more heat is used in the reforming reaction. More relevant to the performance of the fuel cell is the definition of the efficiency as the ratio between P and the energy converted in the electrochemical reaction:

$$\eta = \frac{P}{P + |Q_{ec}|} \tag{6.15}$$

Both the efficiency based on the net heat (equation 6.12) and the efficiency based on the heat produced in the electrochemical reaction (equation 6.15) are shown in figure 6.15.

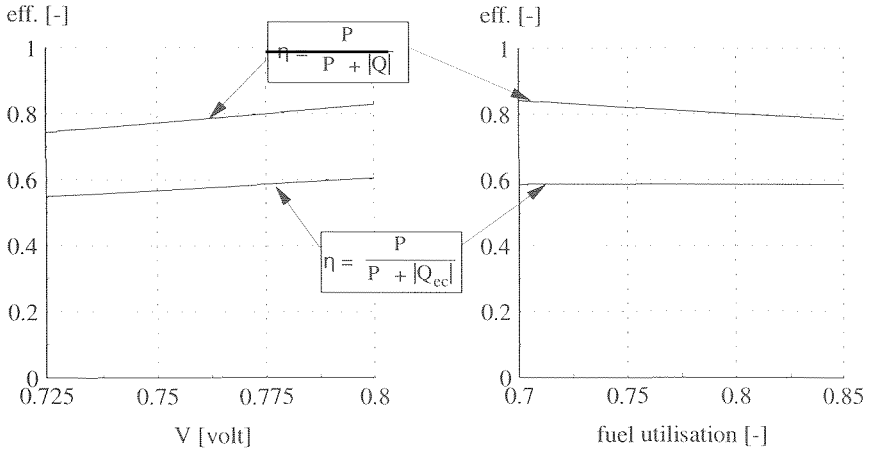

Figure 6.16: Efficiencies of the internal reforming MCFC at off-design conditions

The changes in efficiency at off-design conditions, using the definition based on Q_{ec}, correspond to the changes in efficiency calculated for the external reforming fuel cell:

- The efficiency as a function of the cell voltage increases with the voltage, in accordance with fuel cell theory (**Section 4.3.1**);
- The efficiency is again independent of the fuel utilisation.

6.3.2 Cathode outlet temperature and effective temperature at off-design conditions

Figure 6.17 shows the effect of the off-design conditions on the outlet temperature and on the effective temperature. The effective temperature changes little, both if the cell voltage is varied at constant utilisation and if the fuel utilisation is varied at constant voltage. The cathode outlet temperature, however, depends strongly on the off-design conditions. The temperature at the cathode outlet decreases if the cell voltage increases and increases with the fuel utilisation.

outlet temperature

The temperature profile of the electrolyte for the internal reforming cell is determined by the cathode gas (**Section 5.4.1**). The cathode gas is in counter-flow with the anode gas and is supplied to the cell at x/L=1. Initially the cathode gas heats up as a result of the heat generated in the electrochemical reaction and is subsequently cooled by the reforming reaction, which occurs mainly in the inlet zone of the anode (0<x/L<0.2). The cooling effect of the reforming reaction at the anode inlet is stronger if the fraction of the methane which reacts in the inlet zone is higher and if the ratio between the heat required for the reforming reaction is and the heat which is generated is higher.

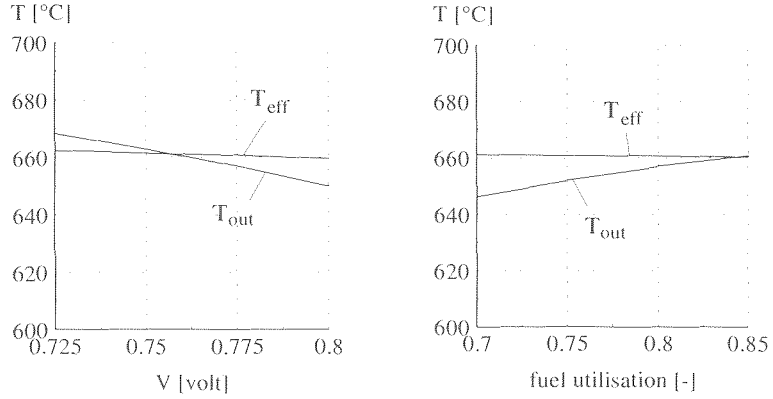

Figure 6.17: The effective temperature (T_{eff}) and the outlet temperature of the cathode gas (T_{out}) at off-design conditions for the internal reforming MCFC

If the voltage increases, the stronger cooling effect of the reforming reaction leads to the decrease of the outlet temperature shown in figure 6.17. Both effects indicated above enhance the cooling effect of the reforming reaction.

- Due to the higher efficiency of the electrochemical reaction at higher voltage, less heat is produced in the electrochemical reaction and ratio between the heat consumed by the reforming reaction and the generated heat increases.
- At part load (higher cell voltage) the fuel flow decreases and the relative rate of reaction for the reforming reaction increases (figure 6.18). The conversion of methane seems considerably faster at the higher cell voltage. The mole fraction CH_4 at x/L=0.2 corresponds to 20% of the inlet concentration at 0.725 V, while the fraction of CH_4 which has not been converted at 0.800 V is closer to 10% of the inlet concentration. The difference is due to the change in the fuel flow, which can be seen in figure 6.19. If the voltage increases from 0.725 to 0.800 V the anode flow decreases by 35%.

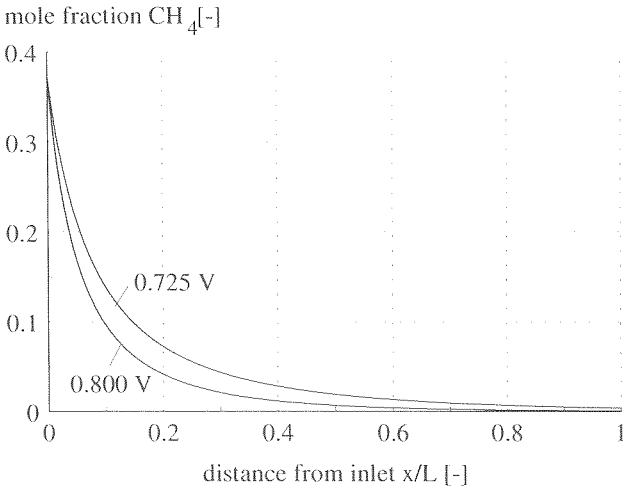

Figure 6.18: Mole fraction CH_4 in the fuel cell for two different values of the cell voltage (MCFC-ir)

The graph also shows the mass flow at the cathode, which is determined by the cooling requirements for the fuel cell. The amount of heat which is generated in the cell ("net heat" in figure 6.15) decreases strongly (-60% at 0.800 V compared to the value at 0.725 V). The mass flow of the cathode gas required to cool the cell decreases as well, but not as much (only to -40% for a corresponding decrease of the cell voltage). This is due to the smaller temperature difference over the stack at higher cell voltage. The temperature effect ($V\uparrow \Rightarrow \Delta T\uparrow \Rightarrow \varphi_c\downarrow$) reduces the effect of the higher heat production ($V\uparrow \Rightarrow Q\uparrow \Rightarrow \varphi_c\downarrow$)

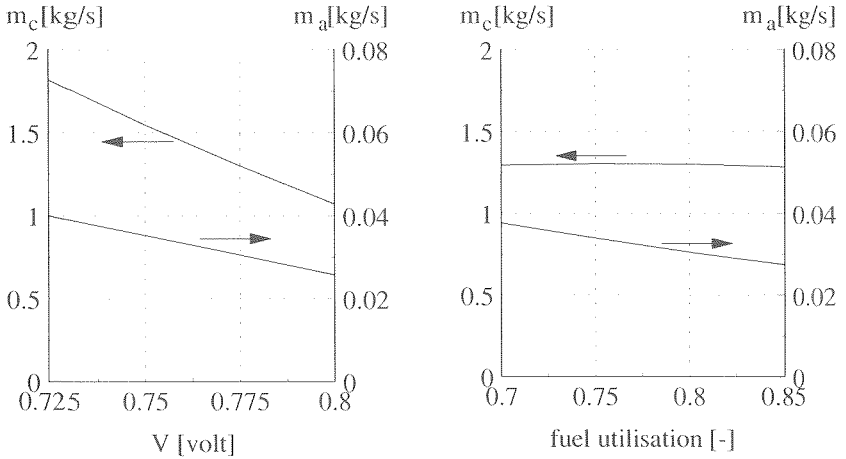

Figure 6.19: Mass flows cathode (m_c) and anode (m_a) gas at off-design conditions for the internal reforming fuel cell (MCFC)

The temperature at the outlet increases with higher fuel utilisation, as shown in figure 6.17. As indicated, at high utilisation less heat is required by the reforming reaction compared to the heat which is generated in the electrochemical reaction. Consequently the temperature approach is smaller at high utilisation. As a result, the calculated temperature approach decreases from 55 K at a fuel utilisation of 0.7 to 40 K at 0.85. In this case the effect of ΔT and Q on the mass flow of the cathode gas m_c almost cancel out, as figure 6.19 shows.

effective temperature

The calculated effective temperature decreases slightly with the cell voltage (figure 6.17) and is almost constant if the fuel utilisation is varied. As in the case of the external reforming cell, two factors play a role in the effective temperature: the temperature profile and the current density distribution in the cell.

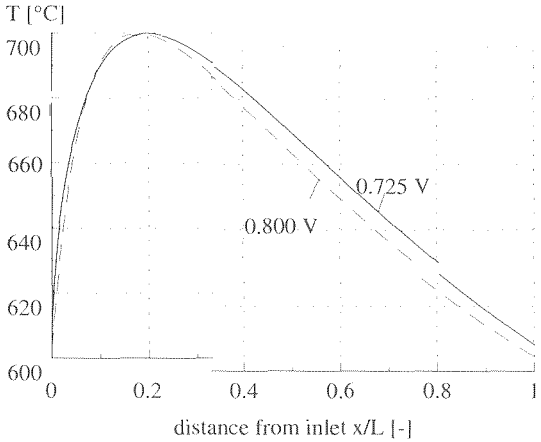

Figure 6.20: Calculated temperature profile of the electrolyte for two values of the cell voltage for the internal reforming MCFC

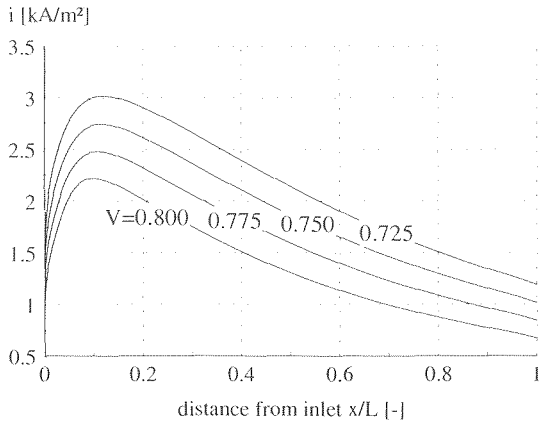

Figure 6.21: Calculated current density distribution for different values of the cell voltage for the internal reforming MCFC

Figures 6.20 and 6.21 show the influence of the cell voltage on, respectively, the temperature in the fuel cell and the current density. The average temperature in the fuel cell is evidently lower at higher cell voltage. However, this does not result in a substantially lower effective temperature. This is due to the changes which occur simultaneously in the current distribution. Just as in the case of the external reforming cell, the current density becomes more unevenly distributed if the cell voltage increase (see Section 6.4.1). At high cell voltage the current density near the outlet decreases more than the maximum current density (at x/L≈0.1). As a result, a larger fraction of the fuel is converted in the high temperature zone at higher cell voltage. Therefore, despite the decrease of the average temperature, the effective temperature does not decrease.
Figures 6.22 and 6.23 show the temperature in the fuel cell and the current density distribution for different values of the fuel utilisation. If the fuel utilisation changes, the average temperature changes little, although the location where the maximum temperature

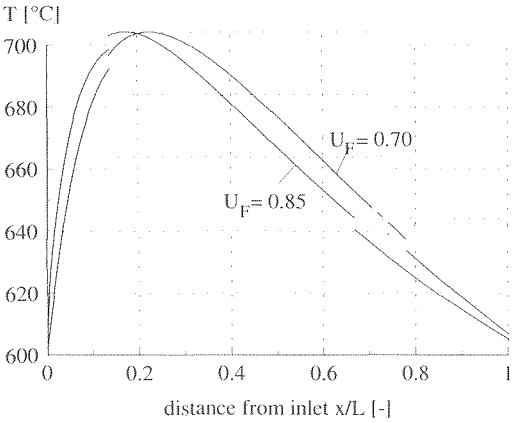

Figure 6.22: Calculated temperature profile of the electrolyte for two values of the fuel utilisation for the internal reforming MCFC

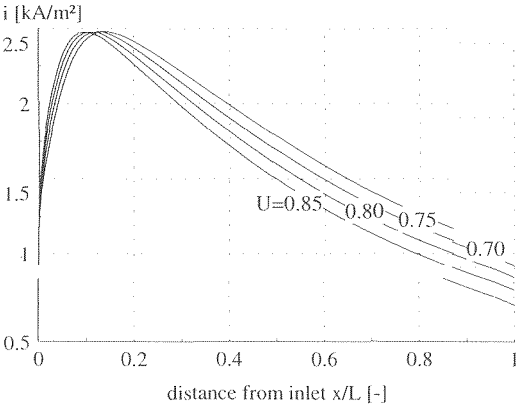

Figure 6.23: Calculated current density distribution for different values of the fuel utilisation for the internal reforming MCFC

occurs shifts toward the inlet at higher fuel utilisation. Because the form of the current density distribution changes approximately in the same manner as the temperature profile, the average temperature at which the fuel is converted is not altered. This corresponds well to the calculated values of the effective temperature shown in figure 6.17.

Off-design results for the SOFC

The off-design results for the internal reforming SOFC are summarised in figures 6.24 and 6.25. The main difference between the internal reforming MCFC and internal reforming SOFC is the influence of the off-design conditions on the effective temperature. The other calculation for the SOFC agree with the previously discussed results for the MCFC.

In the case of the MCFC if the cell voltage or fuel utilisation changes, the change in average temperature is compensated by the changes in the distribution of the current density and the temperature profiles. As a result, the change in effective temperature at off-design conditions is limited (see figure 6.17).

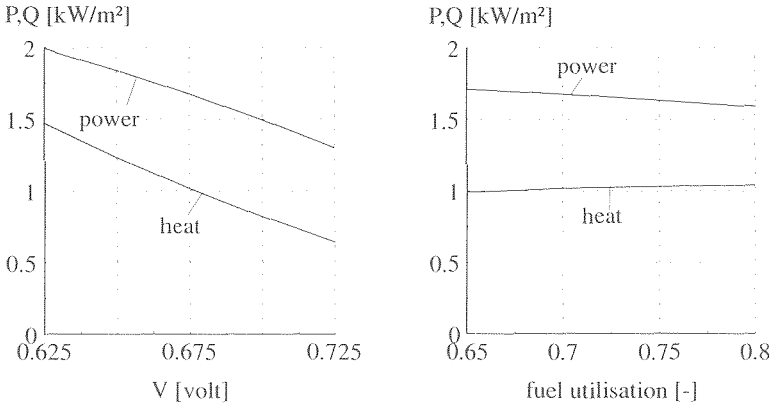

Figure 6.24: Performance of the internal reforming SOFC at off-design conditions

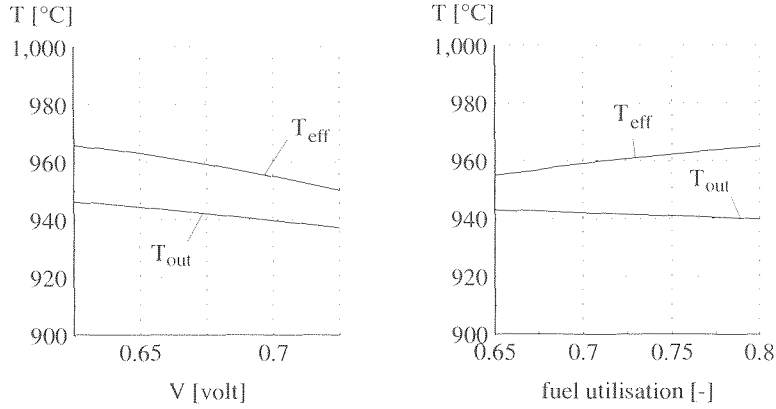

Figure 6.25: The effective temperature (T_{eff}) and the outlet temperature of the cathode gas (T_{out}) of the internal reforming SOFC at off-design conditions

However, in the case of the internal reforming SOFC, a high anode recycle is assumed (**Section 8.4**) and the influence of the current distribution is much smaller. Due to the almost constant Nernst voltage in the SOFC (figure 5.25), the current density is much more evenly distributed at design conditions. Consequently the effective temperature is mainly determined by the average temperature.
The influence of the off-design conditions on the average temperature is the same for the SOFC as for the MCFC (see figures 6.20 and 6.22). At higher cell voltage the average temperature becomes lower. As a result, the effective temperature decreases as the voltage increases as well. If the fuel utilisation increases, the average temperature does not change, but the maximum temperature occurs closer to the anode inlet. The effective temperature increases because this leads to a closer 'match' between the current density and temperature profile and hence to a higher average temperature of conversion.
The effect of the cell voltage and the fuel utilisation on the outlet temperature, also shown in figure 6.25, is the same as for the MCFC : V↑ ⇒ T_{out} ↓ and U↑ ⇒ T_{out} ↑.

6.6 COMPARISON OF THE ISOTHERMAL AND DETAILED MODEL

In this section the calculation results for the isothermal fuel cell model are compared to the results of the detailed model. The objective is to determine how the assumption of a constant temperature in the model affects the calculation results of the model. Evidently this is not an actual validation of the isothermal model, because this requires measured data. The comparison of both models, however, can be used to determine whether or not the approximations in the isothermal model are acceptable. As discussed in **Section 6.3.1**, the detailed and isothermal model are compared on basis of the values calculated for the generated power and the mass flow of the cathode gas.
The reason to use an off-design model is to be able to compare the results of two different system calculations for the same system. This requires that the calculated performance in one system calculation is consistent with the performance in the other calculation. The off-design model has to predict what the performance will be under certain conditions (off-design), given the performance under other conditions (design conditions). The task of an off-design model is therefore primarily to extrapolate the performance at design conditions to the off-design conditions.
Therefore a three-step approach has been used, both for the comparison of the isothermal and the detailed model, and in the system calculations in part III:

- First the performance at design conditions is determined using the detailed model;
- Subsequently the parameters of the isothermal model are adjusted in such a manner that the performance at design conditions corresponds to the performance calculated with the detailed model (fitting);
- Finally the off-design model is used to calculate the performance at off-design conditions.

The two parameters which are compared, are the power and the cathode flow. By changing the isothermal temperature, the value of the power calculated with the isothermal model can be matched to the detailed model. The advantage of this approach is, that the isothermal temperature can be interpreted as the equivalent of the effective temperature introduced in the previous section. The isothermal model also uses the outlet temperature which has been calculated by the detailed model. This is sufficient to match the cathode flow with the cathode flow calculated in the detailed model.

6.6.2 Comparison of the isothermal and the detailed model for external reforming cells

The performance at off-design condition for the external reforming fuel cells (MCFC and SOFC) have been calculated with the detailed model (**Section 6.4**). In this section these calculation results will be compared to those calculated with the isothermal model which was developed in **Section 6.2**. Figures 6.26 and 6.27 show the performance for the detailed model and the isothermal model at off-design for the MCFC and the SOFC respectively. The upper graph shows the influence of the cell voltage at constant utilisation, the graph below shows the influence of the fuel utilisation.
As determined in the previous section, the performance of the fuel cell is characterised by the power P and the mass flow of the cathode gas. If the cell voltage increases the fuel cell operates at part load. Therefore both the power which is generated and the cathode gas flow

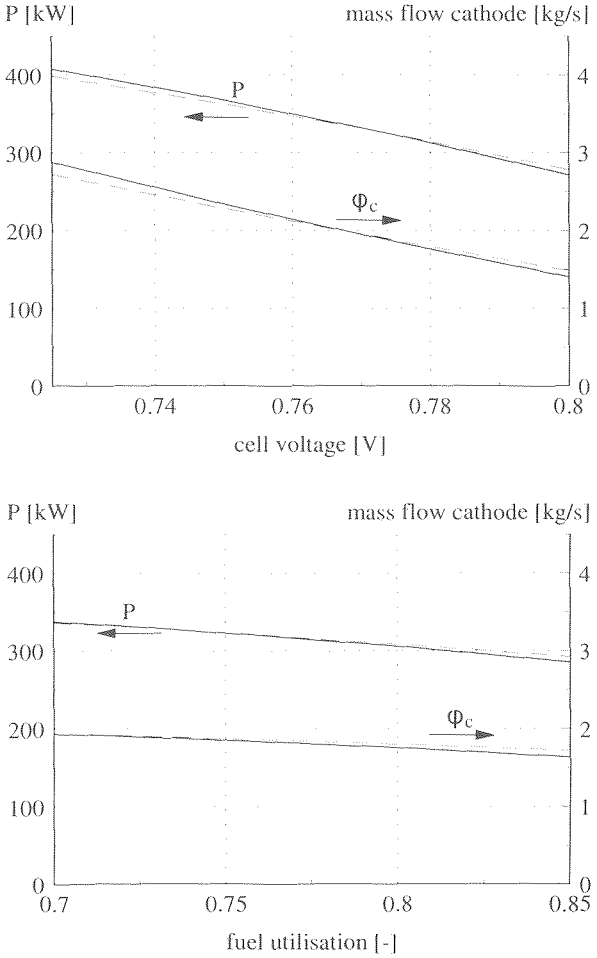

Figure 6.26: Comparison of the power and cathode gas flow calculated with the detailed (—) nd the isothermal (--) model ER-MCFC stack at off-design conditions

which is required to cool the stack decrease. The value for the power which is calculated by the isothermal model at design conditions corresponds reasonably well to the power calculated with the detailed model (**Section 6.4.1**). At lower cell voltage the value calculated with the isothermal model is too low, while at higher cell voltage the value calculated with the isothermal model is too optimistic.
The corresponding diagram for the influence of the fuel utilisation on the performance, shows that the generated power decreases with the fuel utilisation. As the off-design calculations with the detailed model showed, the low power at a high value of the fuel utilisation is due to a lower average hydrogen concentration and consequently a lower value of the Nernst voltage. The isothermal model is too optimistic at high values of the utilisation. However, the difference between the calculated values for the power is much larger if the cell voltage varies than if the value of the fuel utilisation changes.

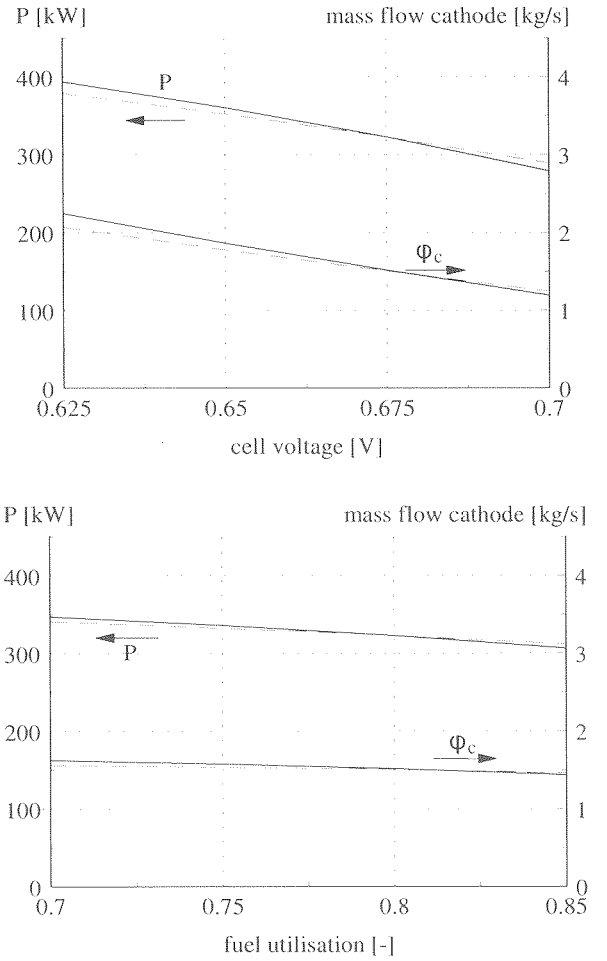

Figure 6.27: Comparison of the power and mass flow of the cathode gas calculated with the detailed (—) and the isothermal (--) model for the ER-SOFC stack at off design

The mass flow of the cathode gas in both models differs for two reasons. The first is that the temperature difference ΔT over the stack varies in the detailed model and is constant in the isothermal model. The second reason is the different value for the amount of heat generated in the fuel cell which is used in both models. For a given cell voltage, the amount of heat which is generated is proportional to the power. If both model calculate different values of the power, as shown in figure 6.26 and 6.27, the value of the heat is different as well. The main difference between the value of the cathode flow calculated with the detailed model and with the isothermal model is due to the different power calculated. Therefore, to improve the model with respect to the calculation of the cathode flow, the priority is to achieve a better agreement between the values of the power calculated in both models.

6.6.3 Improved isothermal model for the external reforming fuel cell

At higher cell voltage the fuel cell operates at part load because the driving force for the electrochemical reaction (V_{rev} - V) decreases. A second effect of the change in voltage is a change in the effective temperature due to the lower average temperature of the electrolyte (**Section 6.4.2**). Part of this effect is cancelled out by the increasingly uneven current density distribution at higher cell voltage.
Clearly the effective temperature is not taken into account in the isothermal model. As figures 6.26 and 6.27 indicate, the value of the power calculated with the isothermal model is too high at higher cell voltage. A possible explanation for the difference is the use of a constant temperature in the isothermal model. Therefore to improve the isothermal model, the influence of the effective temperature should be taken into account. The lower effective temperature is due to the lower heat production at higher cell voltage which results in a lower temperature difference between the cathode and the electrolyte. Assuming all heat Q is removed from the cell by the cathode gas, than the temperature difference can be calculated from the average heat transfer coefficient α and the cell area A:

$$\Delta T_{c-e} = \frac{Q}{\alpha A} \tag{6.15}$$

A starting-point for the development of the off-design model is that the power generated at design conditions is the same in the detailed model and in the isothermal model (Section 6.4.1). This is achieved by adapting the temperature which is used in the isothermal model. For all the off-design calculations with the isothermal model for which the results are shown in figure 6.26 and 6.27 the temperature T_{iso} is equal to the value determined for the design conditions (T^{o}_{iso}). Using the expression for the temperature difference between cathode and electrolyte, an estimate for the isothermal temperature at off-design conditions is:

$$T_{iso} = T^{o}_{iso} + \frac{Q^{o} - Q}{\alpha A} \tag{6.16}$$

where Q^{o} is the heat generated at design conditions. The effective temperature is not the only temperature which changes at off-design conditions. Another important variable is the outlet temperature because the ΔT over the stack and consequently the cathode gas flow required to cool the stack depend on this parameter. The temperature approach (T_{max} - T_{out}) depends on the heat flow as well.

Again using the average temperature difference between electrolyte and cathode, the temperature approach at off-design conditions is estimated from the temperature approach at design conditions ΔT^{o}_{app}:

$$\Delta T_{app} = \Delta T^{o}_{app} \cdot \frac{Q}{Q^{o}} \tag{6.17}$$

This equation assumes a more or less proportional change of the temperature difference between the electrolyte and the cathode at off-design conditions. However, if the fuel utilisation increases, the current density distribution becomes much more uneven and consequently the change in the temperature difference between electrolyte and cathode is not constant over the cell (Section 6.4.2). If the fuel utilisation increases, the current density at the outlet will decrease stronger than the average current density. If the fuel utilisation approaches unity, the current density will approach zero near the outlet.
Consequently the heat flow and the resulting temperature difference between the electrolyte and cathode flow will approach zero as well. To include this effect in the isothermal model, the temperature approach is calculated using the fuel utilisation U and the fuel utilisation at design conditions U^{o}:

$$\Delta T_{app} = \Delta T^{o}_{app} \frac{Q}{Q^{o}} \left(\frac{1-U}{1-U^{o}} \right) \tag{6.18}$$

This equation has been used to estimate the temperature approach for the "improved isothermal model".
In figure 6.28 the outlet temperature which is calculated using the detailed model is compared to the value used in the "improved isothermal model" (estimated from equation 6.18) for the MCFC cell.

- If the cell voltage is varied, the calculated value of the outlet temperature in the detailed model varies stronger than predicted by equation (6.18). Evidently, the change in ΔT_{e-c} at the outlet is not proportional to the average temperature difference between electrolyte and cathode. This agrees with the change in current density distribution which was calculated (figure 6.9) which is larger than average at the outlet. Nonetheless, the assumption is considerably more accurate than the assumption of a constant temperature used in the previous section.
- If the fuel utilisation is varied, the value of the outlet temperature calculated with equation (6.18) corresponds better with the value from the detailed model.

In figure 6.28 the effective temperature which is calculated for the detailed model is also compared to the temperature used in the improved isothermal model, calculated using equation (6.16). The figure shows that in each case (both if the cell voltage and the fuel utilisation changes) the trend is predicted correctly.

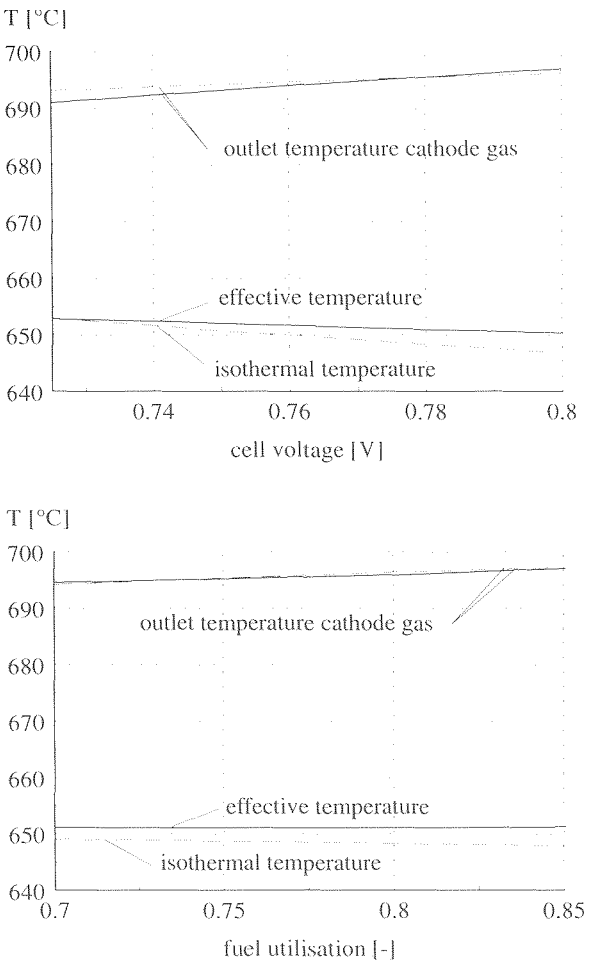

Figure 6.28: The outlet temperature used in the detailed (—) and isothermal (--) model and effective temperature and isothermal temperature for the MCFC-er at off design

The relevant comparison is the comparison of the power calculated using the detailed model and with power calculated using the isothermal model and corresponding isothermal models. These results are compared in figure 6.29 for the external reforming MCFC and in figure 6.30 for the external reforming SOFC.
The graphs show that for the MCFC external reforming cell the results of the improved model correspond very well to those of the detailed model. Both the calculation results at different values of the cell voltage and at different values of the fuel utilisation correspond better with the detailed model than the previous calculations using constant temperatures (figure 6.26).

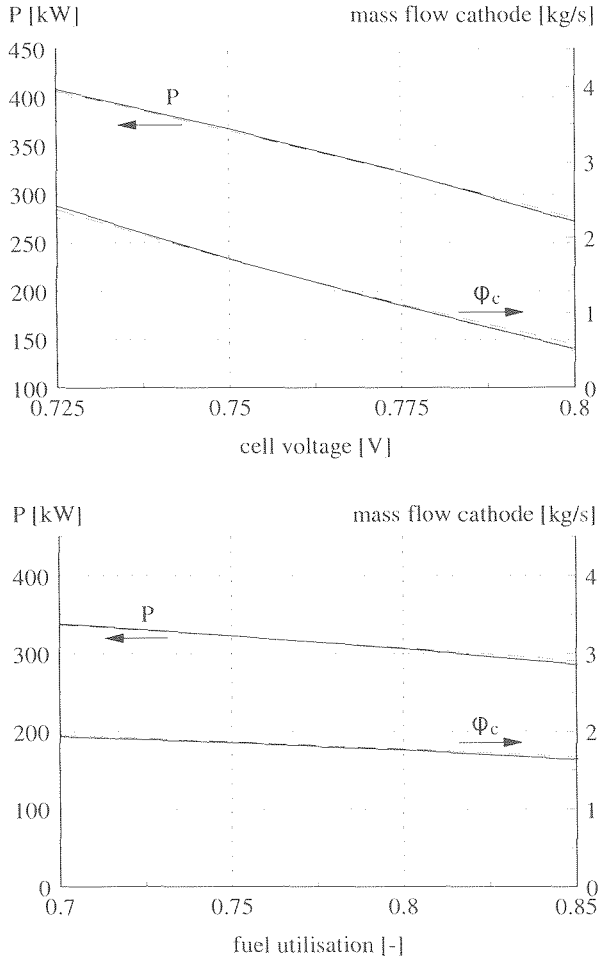

Figure 6.29: Comparison of performance calculated with the detailed (—) and the improved isothermal (--) model for the ER-MCFC stack at off-design conditions

The same is true for the external reforming SOFC. However, for the SOFC the difference between the improved and the detailed model is larger than for the MCFC. Evidently the influence of the temperature and current density distribution is larger in the case of the SOFC. A possible explanation for the difference between the calculation results for both types of fuel cells is the higher average current density in the SOFC.
Because the correspondence for both types is considerably better than the basic isothermal model in the previous section, the calculations for the external reforming fuel cells in the system calculations have been carried out using the improved isothermal model, i.e. using equation (6.16) to calculate the isothermal temperature and (6.18) to calculate the temperature approach.

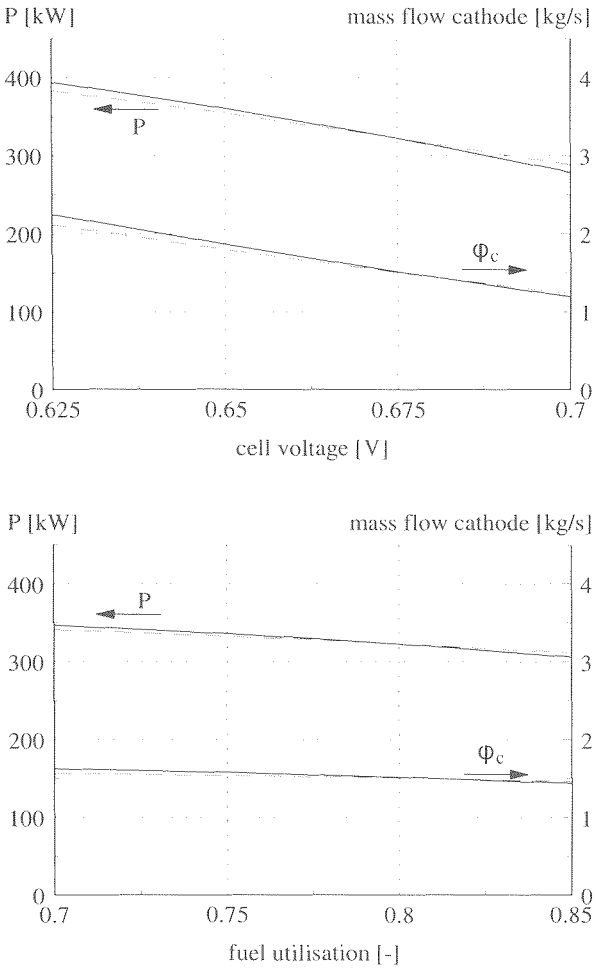

figure 6.30: Comparison of the performance calculated with the detailed (—) and the improved isothermal (--) model for the ER-SOFC stack at off-design conditions

6.6.4 Comparison of the isothermal and the detailed model for internal reforming

The isothermal model for internal reforming is based on the assumption that the reforming reaction achieves equilibrium rapidly near the anode inlet. Consequently the model first calculates the equilibrium for the reforming reaction and subsequently the chemical and electrochemical reactions are calculated along the active cell area (**Section 6.2.2**). This approach is based on the low current density in the first part of the fuel cell, due to the low temperature in this region of the cell. Figures 6.31 and 6.32 show the calculation results for both the detailed model and the isothermal model for the internal reforming MCFC and the internal reforming SOFC respectively.

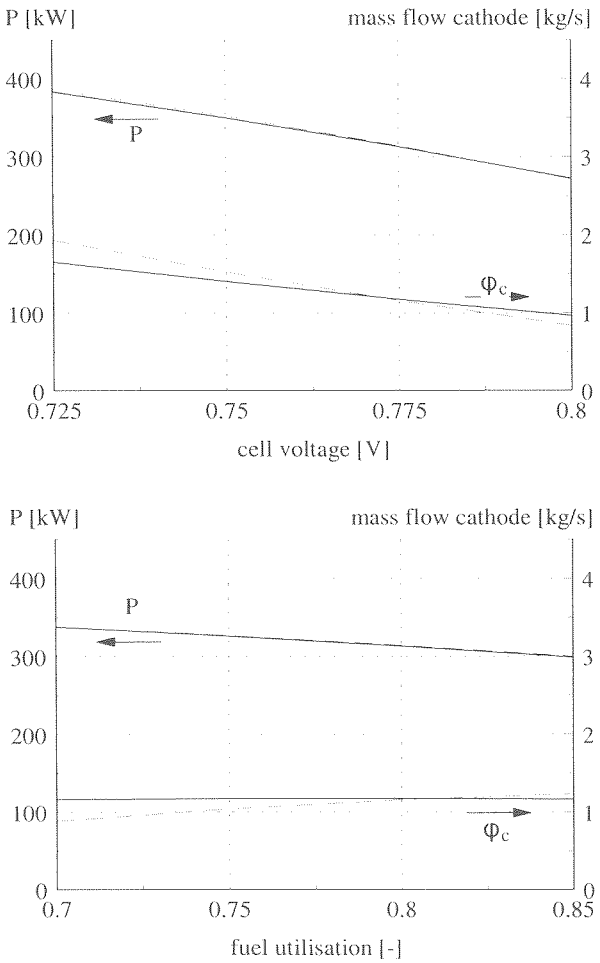

figure 6.31: Comparison of the performance calculated with the detailed (—) and isothermal (--) model for the internal reforming MCFC at off-design conditions

Calculated power P

In both cases the power calculated with the isothermal model corresponds remarkably well with the detailed model. The starting-points for the calculation of the MCFC and SOFC are very different. The MCFC case is calculated with steam/natural gas as anode gas, while the SOFC is calculated assuming a high anode off-gas recycle which results in a relatively high hydrogen concentration at the inlet and a low fuel utilisation per pass. This influences the process in the inlet zone in particular, which is the zone in which the isothermal model, which assumes sequential reforming and electrochemical reaction, differs strongly from the detailed model, in which both reactions occur simultaneously. None the less, the results of the isothermal model compare well with the isothermal model, both for the MCFC (figure 6.31) and for the SOFC calculations (figure 6.32).

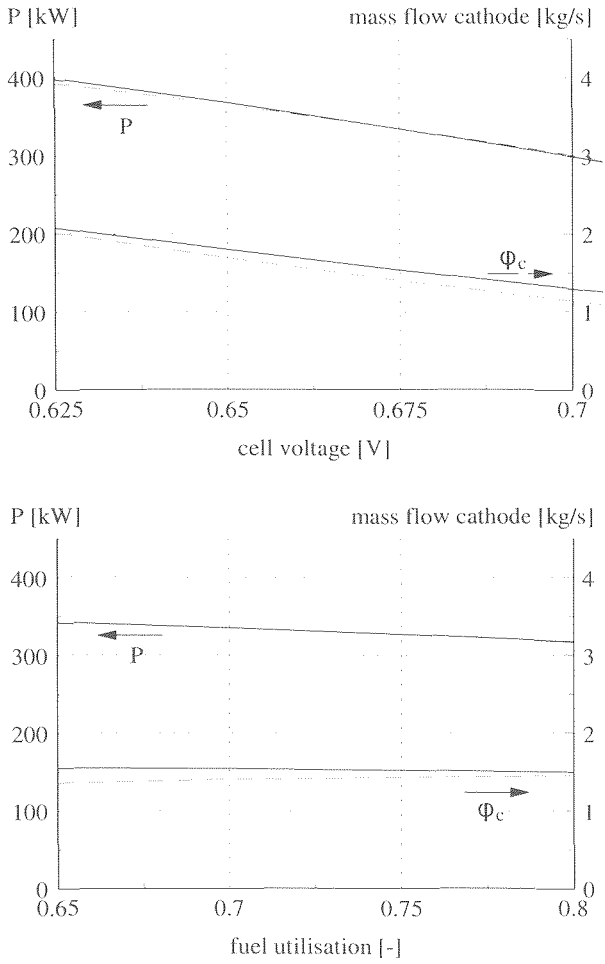

Figure 6.32: Comparison of the performance calculated with the detailed (—) and isothermal (--) model for the internal reforming SOFC at off-design conditions

Calculated cathode flow φ_c

The main difference between the detailed and the isothermal model for the internal reforming fuel cell is the value of the mass flow of the cathode gas which is calculated. In the isothermal model the outlet temperature of the cathode gas is constant at off-design conditions. However, the off-design calculations in **Section 6.5** show that the outlet temperature calculated with the detailed model changes considerably. As a result, the amount of cathode gas required for each kW of heat which has to be removed from the cell is not calculated correctly. Figures 6.31 and 6.32 shows that cathode gas flow calculated with the isothermal model differs significantly from value calculated with the detailed model, both for changing values of the cell voltage as for the different values of the fuel utilisation.

In the SOFC there is another reason why the value of the cathode gas flow calculated with the

isothermal model differs from the value calculated in the detailed model. In the detailed model, the H_2/CO ratio at the outlet corresponds to the shift equilibrium at the outlet temperature. In the isothermal model, equilibrium is determined at the isothermal temperature. In most cases, this will only have minor impact on the heat balance of the cell, because of the low concentrations H_2 and CO at the outlet. However, the SOFC calculations are base on a low fuel utilisation and a high anode off-gas recycle, which leads to much higher concentrations at the outlet. Consequently the different H_2/CO ratio in the case of the internal reforming SOFC leads to a difference between both models with respect to the calculated cathode gas flow, even at design conditions (figure 6.32).

6.6.5 Improved isothermal model for the internal reforming fuel cell

Evidently in the case of the internal reforming cell, the difference between the isothermal and the detailed model is not due to differences in the calculated power as for the external reforming cells: the calculated values for the power correspond much better than the calculated values of the mass flow of the cathode gas. Therefore, the issue is to improve the isothermal model for the internal reforming cell by improving the estimate for the outlet temperature.

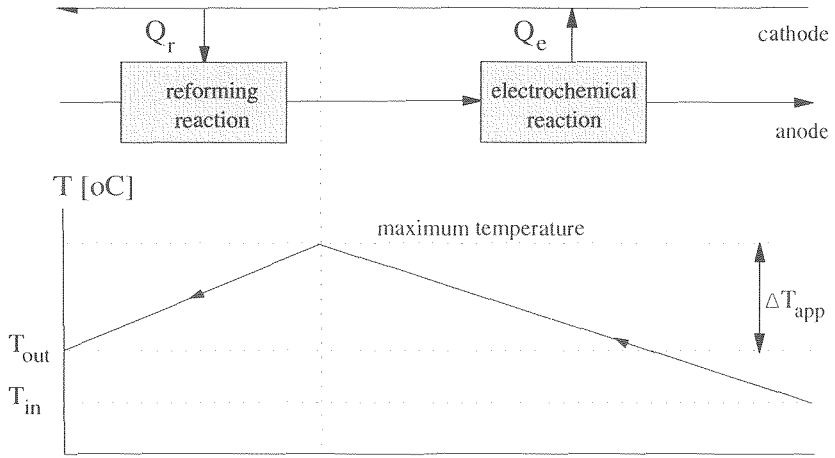

Figure 6.33: Schematic representation of the temperature profile of the cathode gas in an internal reforming fuel cell

The outlet temperature is determined by the two heat flows in the fuel cell (**Section 5.4**). The cathode gas flows in counter-flow with the anode gas. First the temperature of the cathode gas increases due to the heat which is generated in the electrochemical reaction. As the cathode gas approaches the cathode outlet, the gas is cooled down by the reforming reaction. This process is shown schematically in figure 6.33. The cathode outlet temperature in the simplified process will depend on the ratio between the heat which is required for the reforming reaction (Q_r) and the heat generated in the electrochemical reaction (Q_e), which is denoted by α:

$$\alpha = \frac{Q_r}{Q_c} \tag{6.19}$$

If α is equal to zero, no cooling occurs near the cathode gas outlet, if the value of α approaches unity, the outlet temperature is equal to the inlet temperature (in the simplified model). To estimate the temperature approach, the following equation has been used:

$$\Delta T_{app} = \Delta T^{o}_{app} \left(\frac{\alpha}{\alpha^{o}}\right) \tag{A}$$

where again the superscript 'o' indicates the values at design conditions.

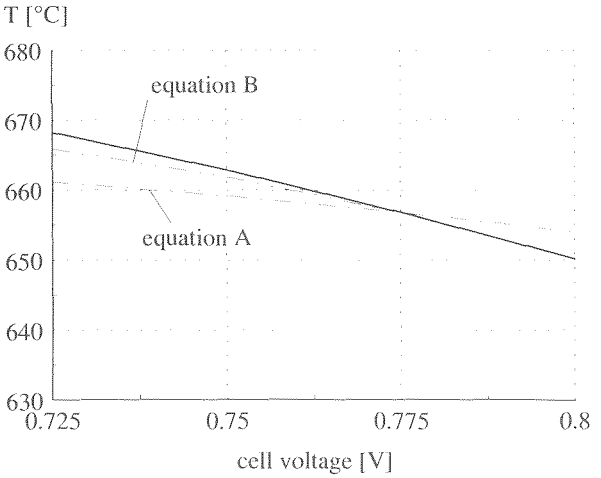

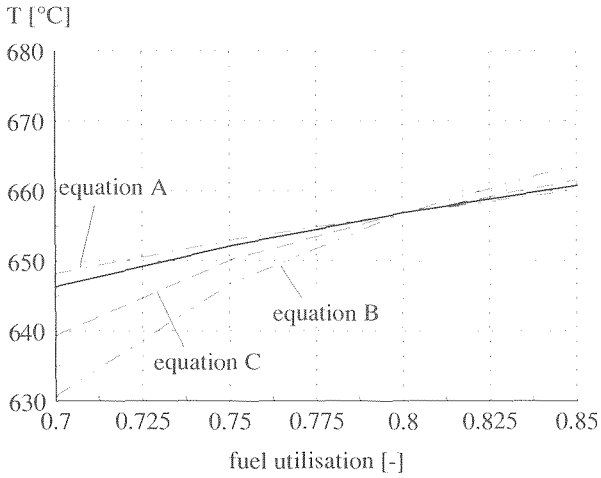

Figure 6.34: Comparison of the outlet temperature calculated in the detailed model and the estimates calculated with different equation (A, B and C) for the IR-MCFC at off design

This approach (figure 6.34, curve **A**) corresponds well with the outlet temperature calculated with the detailed model if the fuel utilisation is varied. However, if the value of the cell voltage changes, the calculated values differ substantially. A better result is achieved if in the denominator in equation (6.19) not the heat in the electrochemical reaction, but the net heat (Q_e - Q_r) is used, i.e.:

$$\beta = \frac{Q_r}{Q_e - Q_r} \tag{6.20}$$

and:

$$\Delta T_{app} = \Delta T^{o}_{app} \left(\frac{\beta}{\beta^o}\right) \tag{B}$$

In this case (figure 6.34, curve **B**) , the difference in calculated temperature between the detailed and the isothermal model is smaller for varying cell voltage. However, in particular for low utilisation curve **B** deviates strongly from the temperature approach calculated with the detailed model.
The estimate for the outlet temperature can be improved by including the fuel utilisation. This does not influence the estimate at varying cell voltage (= constant utilisation), which is satisfactory, but can improve the large deviation at low fuel utilisation. The improved estimate assumes the temperature approach is proportional to the ratio of the fuel utilisation (U_F) and the fuel utilisation at design conditions (U^o_F):

$$\Delta T_{app} = \Delta T^{o}_{app} \left(\frac{\beta}{\beta^o}\right) \left(\frac{U_F}{U^o_F}\right) \tag{C}$$

All previous corrections on ΔT_{app} of T_{eff} were based on analysis of the calculation results of the detailed model. The correction (**C**) is simply found by fitting the results of the isothermal model to the results of the detailed model. However, because the isothermal models for both the SOFC and MCFC improve by using the correlations, they have been used in the system calculations. Model **C** has been selected because it gives reasonable results for both types of fuel cells (although not shown here, the there is a difference less than 2K difference between the models for the SOFC). The temperature difference between the models is highest for the MCFC model at low fuel utilisation.

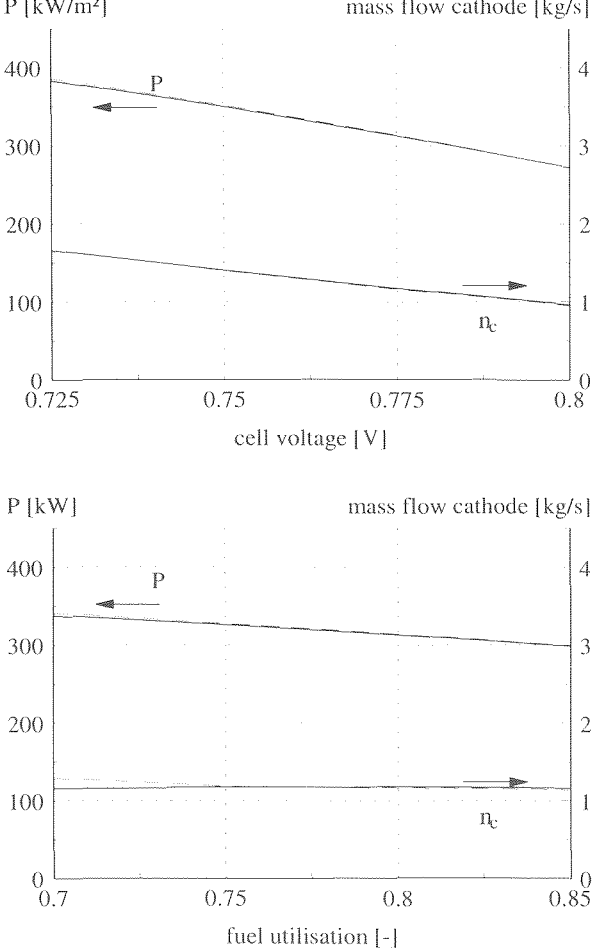

Figure 6.35: Comparison of the power and mass flow of the cathode gas calculated with the detailed and the improved isothermal model (C) for the IR-MCFC stack at off-design conditions

The calculation results for the improved isothermal model using equation (**C**) are shown in figures 6.35 (MCFC) and 6.36 (SOFC). The results for the improved model correspond well to the detailed model on al but two points. The value of the mass flow of the cathode gas calculated with the isothermal model for the SOFC is structurally lower than the value calculated with the detailed model. This, as was indicated earlier, is due to different temperatures used to calculated the shift reaction equilibrium at the outlet. Furthermore, for the MCFC, the limited accuracy of the estimation of the temperature approach in the isothermal model at low fuel utilisation, leads to different value of the cathode gas flow in both models.

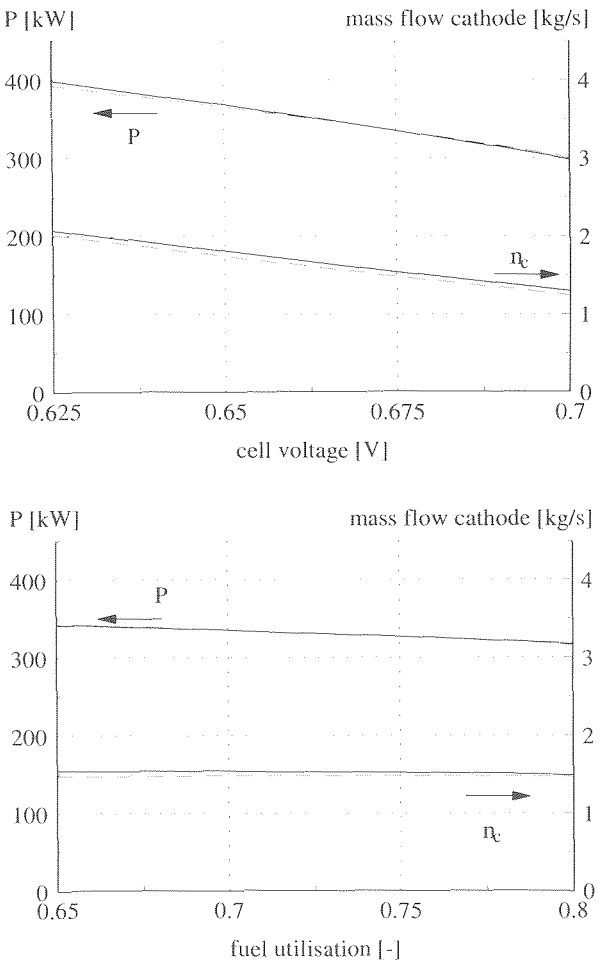

Figure 6.36: *Comparison of the power and mass flow of the cathode gas calculated with the detailed and the improved isothermal model for the IR-SOFC stack at off-design conditions*

DISCUSSION II
'FUEL CELL MODEL'

A 1-dimensional model for the fuel cell is developed in **Chapter 4**. The model calculates the current density (distribution) along the fuel cell. If the current distribution is known, all other relevant 'electrical' parameters (e.g. power generated by the fuel cell) can be simply calculated. Other phenomena which are included in the model are the calculation of heat transfer in the hardware and from the cells hardware to the process flow and calculation of the rate of the chemical reactions occurring in the fuel cell. By introducing reaction coordinates for the (electro-)chemical reactions, the composition can be described using only 3 variables (i.e. the number of reaction occurring in the fuel cell). The temperature in a cross-section is determined by three temperatures: the temperatures of the process flows (anode and cathode gas) and the temperature of the hardware in the cross-section. The three parameters fully characterise the 'state' in a cross-section. The full concentration and temperature profiles are calculated by the model. The most important output parameters for the system calculation in **part III** are the compositions and temperatures at the outlet of the fuel cell (cathode and anode).

In **Chapter 5** the detailed fuel cell model developed in the previous chapter has been used to calculate several fuel cell configurations and types: MCFC and SOFC, co- and counter-flow, external and internal reforming. The objective is to understand which characteristic parameters have a large influence on the fuel cell performance. This knowledge can be used to simplify the fuel cell model for system calculations in **Chapter 6**. Specifically two essential parameters are identified which characterise the temperature distribution in the fuel cell:

- the temperature approach;
- the effective temperature.

The temperature approach is the difference between the maximum temperature in the fuel cell (which is a fixed value) and the outlet temperature of the cathode flow. Because the fuel cell is cooled by the cathode flow, the outlet temperature of the cathode flow determines how much heat can be removed from the fuel cell. The calculations show that, if a maximum temperature is assumed for the hardware, the outlet temperature depends on the operating characteristics (e.g. fuel utilisation, cell voltage). For co-flow external reforming fuel cell this temperature difference is only small (5-10 K). For internal reforming fuel cells and counter-flow configurations the temperature approach becomes much larger (e.g. 50 K). Because the value of the temperature approach depends on many factors (e.g. current density distribution, heat transfer, fuel utilisation), this is an important parameter to consider in the simplified model

The performance of the fuel cell improves with temperature. The cell resistance becomes much lower at higher temperatures. But the calculations also show that the performance of the cell is not characterised by the temperature profile in itself. The interaction between the temperature distribution and(mainly) the H_2 concentration is shown to determine the performance. If the concentration hydrogen is high in the cold part of the cell, the performance of the cell will be lower than if the high concentrations coincide with the high temperature (even though the average value of H_2 concentration and temperature may be the same in both cases). To quantify the effect on the average cell resistance in the cell, the effective temperature is introduced. Relatively small changes in the effective temperature

have a considerable effect on the fuel cell performance. The effective temperature is shown to be higher in the counter-flow than in the co-flow configurations. Furthermore internal reforming fuel cells have a higher effective temperature than external reforming fuel cells. The temperature approach and the effective temperature are essential parameters because both have a large impact on the system calculations. The temperature approach determines how much air is needed to cool the cell stack. The effective temperature is a measure for the performance of the fuel cell stack.

In **Chapter 6** a simplified model of the fuel cell is developed for the system calculations. The main simplification in the model is that the processes in the fuel cell (electrochemical and chemical reactions) are calculated at a constant temperature. Therefore the simplified model (or isothermal model), does not require iterative procedures to solve for the temperature and current density distributions.
The main requirement for the simplified model is that it predicts the behaviour at off-design conditions, i.e. at other conditions than the design point. In this study the off-design conditions considered are varying values of the cell voltage (i.e. part-load conditions) and varying values of the fuel utilisation, as these are the most important parameters in the system studies (**part III**). The detailed fuel cell model is used to predict the performance at design-conditions. Subsequently the simplified model (or off-design model) should predict the behaviour at off-design conditions starting from the performance specified for the design conditions. In other words, the fuel cell model extrapolates from the design point.
Using the detailed model, the performance of the fuel cell at different off-design conditions (different values of cell voltage and fuel utilisation) is studied. The main output variables which are considered are the electrical power output of the fuel cell and the mass flow oxidant, because these parameters strongly determine the system efficiency (as will be shown in **part III**).
The analysis of the detailed model in **Chapter 5** showed two temperatures in the fuel cell model to be critical parameters: the temperature approach and the effective temperature. It is shown that using simple correlations for these temperatures, based on the physical phenomena in the cell, the performance predicted with the simplified off-design model, corresponds well with the performance predicted using the detailed model.

PART III:

"System Analysis"

INTRODUCTION III
SYSTEMS ANALYSIS

The objective of this thesis is to identify and clarify the mechanisms which determine the efficiency of high temperature fuel cell systems. As indicated in the introduction, the choice has been made to analyse a limited number of configurations in detail instead of covering a wide range of applications superficially. Therefore the scope of the systems calculations has been limited to one specific application. The following starting points were selected for this system in **Chapter 1**:

- 1 MW electrical power;
- combined heat and power (CHP);
- heat exported as process steam (180 °C/10 bar);
- natural gas fuelled.

Two high-temperature fuel cell system types are analysed: the SOFC and the MCFC system. The objective is not an extensive search for the optimum configuration: the aim is to improve understanding of the factors which are relevant for the efficiency of the system. Therefore configurations have not been selected for analysis primarily because of the high efficiency.
In **Chapter 7** two base case systems are discussed: an SOFC system and an MCFC system. The calculated energy efficiencies and energy flows in the system and into and out of the system are evaluated. Subsequently the exergy losses in the system are discussed. The exergy analysis makes use of the method of distinguishing different types of exergy losses and graphical methods developed in **part I**: "Exergy Analysis". To calculate the exergy losses in the fuel cell stack, the detailed models for the external reforming SOFC stack and the external reforming MCFC stack developed in **part II**: "Fuel Cell Modelling" are used.
In **Chapter 8** several SOFC configurations are analysed. For the system calculations the fuel cell is modelled using the simplified model developed in **part II**. The analysis in **Chapter 7** demonstrates the importance of losses as a result of heat transfer. First the influence of using a cathode recycle on the SOFC system as a method of reducing the amount of heat which is transferred in the air preheaters is evaluated and compared to the base case SOFC system in **Chapter 7**. Subsequently the effectiveness of pressurizing the system to reduce heat transfer losses is discussed and the influence of the fuel utilisation is analysed.
An effective way to reduce the amount of heat transferred in the system is the use of internal reforming. A reference internal reforming system is discussed and again the influence of the pressure on the performance of the system and the losses in the system is evaluated. Finally the amount of pre-reforming, which is shown to influences the performance of the pressurised system considerably, is investigated separately.
Chapter 9 discusses the results of the calculations for a number of MCFC systems. Again the starting point is the large exergy losses as a result of heat transfer in the base case external reforming system. First a number of options to decrease this loss by increasing the net power generated by the expander and compressor combination (CEC) are reviewed. Several ways of increasing the mass flows through the expander are considered: preheating the air, steam injection and the use of a direct anode gas recycle. Subsequently the influence of the pressure on the efficiencies and losses is analysed. For the MCFC systems internal reforming is an attractive option as well. An internal reforming configurations of the system therefore analysed as well. Finally the influence of the fuel utilisation on the internal reforming MCFC system is evaluated.

PART III: SYSTEM ANALYSIS

CHAPTER 7
ANALYSIS OF SOFC AND MCFC BASE CASE SYSTEMS

7.1 INTRODUCTION

The use of fuel cells is considered for a wide range of applications which differ in scale, in type of fuel which is used, etc. To enable detailed analysis the choice has been made to limit analysis to one single power output. As stated in the introduction, the focus of this thesis is on 1 MW_e natural gas fuelled CHP systems. The choice for natural gas as a fuel in these calculations is based on the consideration that the first systems are operating on natural gas because it requires minimal gas clean-up. The selection of combined heat and power (CHP) as application for the unit is a logical consequence of the relatively small scale of the system compared to centralised power systems. The heat which can be made available in the high temperature fuel cell systems is suited for industrial CHP application. The calculations are therefore based on heat production in the form of intermediate pressure (10 bar) steam. In this chapter two reference configurations are analysed: the base case SOFC system and the base case MCFC system. In the next chapters several configurations for each type of fuel cell will be compared (SOFC configurations in **Chapter 8**, MCFC in **Chapter 9**).

In **Section 7.2** the general starting points for the system calculations are discussed. For both the SOFC and the MCFC base case systems the flow sheet and the main calculations result are presented in **Section 7.3**. In **Section 7.4** the exergy losses in both systems are analysed. This analysis is based on the classification of exergy losses according to the methodology developed in **part I**. Based on this analysis, two types of exergy losses are considered in more detail. In **Section 7.5** the exergy losses as a result of heat transfer are discussed. The losses in the fuel conversion steps are treated in **Section 7.6**

7.2 STARTING POINTS FOR THE SYSTEM CALCULATIONS

7.2.1 General starting points

The compositions and conditions of the process flows into and out of the system which have been used in the calculations are summarised in table 7.1. For the exergy analysis the environment proposed by [Baehr, 1978] has been selected (see **Section 2.5**). This environment definition is based on an environment temperature of 25 °C. Because the temperature which is used for all gasses (natural gas, air) which are supplied to the system (natural gas, air) is 15 °C, the environment definition for the exergy calculation has been corrected for this temperature [Meijer, 1993]. The resulting environment definition is shown in table 7.1 For natural gas the table shows the composition of Dutch Slochteren gas. The natural gas and air compositions are the standard compositions used in CYCLE-TEMPO.

Table 7.1: Definition of composition and standard conditions of the environment and of the process flows to the system used in the system calculations

mole fractions [-]	environment	air	natural gas	process steam	condensate	cooling water
N_2	76.78	77.29	14.32			
O_2	20.60	20.75	0.01			
H_2O	1.68	1.01		100	100	100
Ar	0.91	0.92				
CO_2	0.03	0.03	0.89			
CH_4			81.29			
C_2H_6			2.87			
C_3H_8			0.38			
C_4H_{10}			0.15			
C_5H_{12}			0.04			
C_6H_{14}			0.05			
pressure [bar]	1.013	1.013	5.0	10	10	1.013
temperature [°C]	15.0	15.0	15.0	180	25	12.0

7.2.2 Input data for the fuel cell

In **part II** fuel cell models were developed for use in the system calculations. First a detailed model is developed. To simplify the calculations an isothermal model is used for the off-design calculations. Comparing the results of the detailed and simplified model showed a the results of the isothermal model correspond reasonably well to the results of the detailed model. If two non-isothermal effects are included in the isothermal model, the predicted values correspond very well with the detailed model. Use is made of correlations for the effective temperature and the outlet temperature for the fuel cell stack. For the calculations in this chapter the detailed model is used to simulate the performance at design conditions (e.g. the cell voltage) as well as generate the necessary values for the parameters in the isothermal model. The isothermal model is used for off-design calculations in **Chapters 8** and **9**. The main input parameters for the detailed fuel cell model are given in table 7.2.

7.2.3 Input data for other components

Heat exchangers

For a heat exchanger in most of the system calculations carried out for this study, one or more of the in- and outlet temperatures and the pressure drops for the process flows are specified. Specifying the temperatures generally determines the driving temperature difference for heat transfer. A large driving temperature difference between the process flows will lead to a compact and low cost heat exchanger design, but will also lead to larger (exergy) losses. If U is the average heat transfer coefficient ($W/m^2 K$), ΔT_{log} the logarithmic temperature difference and A the effective area of a heat exchanger, the heat which is transferred in the heat exchanger can be calculated from:

$$Q = U A \Delta T_{log}$$

For a given heat duty Q, increasing ΔT_{log} will reduce the required area. On the other hand, increasing the heat exchanger area enables the transfer of Q at a lower (logarithmic) temperature difference. The pressure losses in a heat exchanger depend strongly on the design

of the heat exchanger: for a wide range of specified values of the pressure drop, a heat exchanger can be designed. According to a CEC-study on SOFC systems 'any pressure loss is attainable at a cost' [Dicks, 1990]. An increase of the allowable pressure drop on the other hand leads to an increase of the heat transfer coefficients and therefore to a more compact heat exchanger design. In the mentioned study the pressure drop was found to be proportional roughly to $1/A^3$ where A is the heat exchanger area.
The most economic temperature difference and pressure drop depends on numerous factors of which many can only be quantified in a later stage of design. For the system calculations in this study for the minimal temperature difference values of 100 K to 200 K for gas/gas heat exchangers and a 25 K temperature difference for gas/fluid heat exchangers are used, depending on the temperature level, type of process flow, etc. For gas flows pressure losses between 0.5% and 2% of the inlet pressure have been specified for the heat exchangers, again depending on the temperature level, heat duty, media, etc. For liquid flows (water) higher pressure drops ($\leq$ 5%) are used because of the much lower compression power required for these flows. Table 7.3 gives an overview of the default input data for heat exchangers and other components in the system calculations.

Rotating equipment
For the calculation of the performance of compressors and other rotating equipment, the isentropic efficiency of the compressor, the electrical efficiency of the motor (if the compressor is driven by an electrical drive) and the combined mechanical efficiency for both drive and compressor are taken into account. The efficiency of compressors is, once again, the result of an optimisation of the investment vs. efficiency. Use can be made of correlations for compressor efficiency as a function of size, for example [Coulson]. As these correlation usually concern chemical plants, which have a much lower life time than power plants, the estimated efficiencies will be too low. Furthermore, for the 1 MW systems modelled in this work, the volume flows are relatively small and are generally outside the validity range of such correlations.
For clarity in this thesis a fixed value of 75% is used for the isentropic efficiencies for the main rotating equipment: air compressors and expanders. The efficiency of other compressors and pumps have been estimated starting from this figure and taking into account differences in flow, pressure ratios and operating temperature). The electrical and mechanical efficiency of compressor and drive have been determined using a correlation between the electrical power and the product of mechanical and electrical efficiency [CYCLE, 1995].

Reformer
For external reforming systems the reformer is a crucial component because of the high degree of integration of the reformer with the rest of the system. Most importantly, the reformer in a fuel cell system uses anode off-gas to produce the heat for the reforming reaction. A high heat flux from the flue gas to the reformer bed is necessary for a compact design of the reformer. To obtain a high flux a high temperature in the combustor of the reformer is required. For the calculations a minimum temperature of 1200 °C in the reformer is used.
Another important parameter concerning the fuel processing subsystem is the steam to carbon ratio or S/C-ratio of the reformer feed (natural gas + steam). The S/C-ratio is the number of moles steam to the number of moles carbon in the natural gas. To convert all hydrocarbon in the natural gas the S/C-ratio must be at least 1. However, in general the S/C-ratio is considerably higher to prevent carbon deposition in the reformer and in the fuel cell. Based on the absolute necessity to prevent carbon deposition, the S/C ratios which are used will be

in the range from 2.5 to 4. In the current work an S/C-ratio of 3 is used to determine the required steam flow for the reformer.

Table 7.2: Input parameters for the fuel cell model

SOFC	cell voltage	V	output fuel cell model (**part II**)
	electrical power	P	1042 kW_{DC} / 1000 kW_{AC}
	cell resistance @ 925 °C	R	0.75 Ω cm^2
	total cell area (at 1.4 kW/m^2)	A	700 m^2
	inlet temperature	T_i	850 °C
	outlet temperature [a]	T_o	1000 °C
	fuel utilisation	U_F	85%
	pressure loss [% of inlet pressure]	Δp	anode 5% cathode 5%
MCFC	cell voltage	V	output fuel cell model (**part II**)
	electrical power	P	1042 kW_{DC} / 1000 kW_{AC}
	cell resistance @ 650 °C [b]	R	1.0 Ω cm^2
	total cell area (at 1.25 kW/m^2)	A	750 m^2
	inlet temperature	T_i	600 °C
	outlet temperature [a]	T_o	700 °C
	fuel utilisation [c]	U_F	≤80%
	pressure loss [% of inlet pressure]	Δp	anode 5% cathode 5%

[a] For off-design conditions the outlet temperature is calculated (see **part II**)

[b] Influence of temperature and partial pressures at off-design conditions taken into account

[c] U_F is determined in the MCFC system by the minimum heating value required by the reformer.

Table 7.3: Main input parameters for some other components in the system calculations

heat exchanger	pressure drop	gas flow:	0.5% .. 2% of inlet pressure
		liquid flow:	≤5% of inlet pressure
	min. temperature difference hot/cold streams	gas/liquid	25 K
		gas/gas:	100 ... 200 K
main rotating equipment	isentropic efficiency	75%	
	mechanical + electrical	correlation as function of electrical power	
DC/AC - conv	efficiency [Beishon, 1992]	96%	
reformer	inlet temperature flue gas	1200 °C	
	temperature approach	50 K	
	S/C-ratio	3 mole/mole	

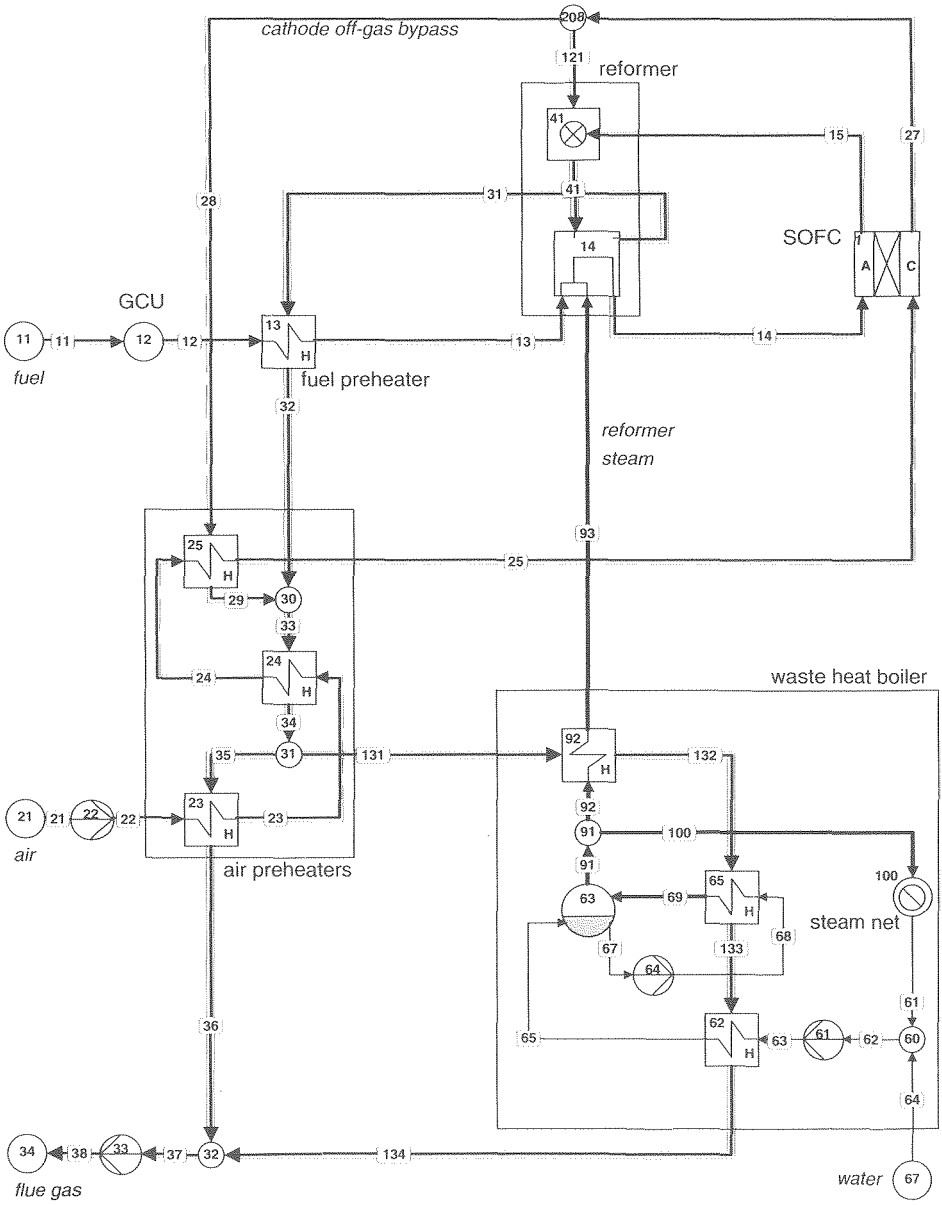

Figure 7.1: Process flow diagram for the base case configuration external reforming SOFC system

7.3 BASE CASE SYSTEMS

7.3.1 Description of the SOFC system

The base case SOFC system operates at atmospheric pressure, eliminating the need for an expander/compressor combination[a]. The process flow diagram is shown in figure 7.1. Natural gas is supplied to the system (stream 11) and preheated to 400 °C in the fuel preheater (app. 13). Steam is produced in the waste heat boiler (whb) and preheated to 400 °C in the superheater (app. 92). In the reformer (app. 14) the fuel and steam are mixed and supplied to the reformer bed. The reformed fuel leaves the reformer at a temperature of 850 °C. An equilibrium temperature of 800 °C is assumed corresponding to almost complete conversion of the methane (>99%).
The fuel utilisation in the fuel cell is 85%. Therefore the gas at the anode outlet still contains approximately 15% of the H_2 and CO supplied to the anode. The anode off-gas leaves the stack at 1010 °C and is supplied to the combustor.
The air (stream 21)which enters the system at 15 °C is preheated to 850 °C in three air preheaters and is supplied to the fuel cell. The specified inlet and outlet temperatures result in a temperature difference over the cathode side of the stack of 150 K (1000-850 °C). The mass flow through the fuel cell is calculated from the energy balance of the fuel cells. The temperature of the flue gasses which are used to supply heat to the reformer must be at least 1200 °C. The amount of oxygen in the cathode off-gas is several times the amount required to convert the fuel components (H_2, CO) in the anode off-gas. Therefore it is not necessary to supply all cathode off-gas to the combustor as this limits the combustion temperature by diluting the flue gas. To achieve the required temperature used in the combustor only part of the air (stream 121) is used in the combustor (app. 41) and part (stream 28) is bypassed to the high temperature air preheater (app. 25).
The flue gas from the combustor supplies heat to the reforming process. After the fuel preheater the flue gas is mixed with the bypassed cathode gas which has been used to preheat air in the high temperature air preheater. Both flows have approximately the same temperature to minimise the exergy losses.
After passing through the medium temperature air preheater (app. 24) the flue gas is split into a stream to the low temperature air preheater (app. 23) and a stream to the waste heat boiler. In the economizer (app. 62) and the evaporator (app. 65) saturated steam of 180 °C is produced. Part of this steam is can be used as process steam and is delivered to the steam net (app. 100). The larger part (approximately 3/4) is superheated to 400 °C (app. 92) and supplied to the reformer as reformer steam.

7.3.2 Calculation results for the SOFC system

The flow sheeting program Cycle Tempo has been used to calculate the mass and energy flows for the SOFC configuration in figure 7.1. Table 7.4 summarises the energy in- and outputs and efficiencies. The AC power generated by the fuel cell in the external reforming SOFC system is specified (1000 kW) and the detailed fuel cell model has been used to calculate the cell voltage. For the calculation both the total cell area (700 m^2) and the cell resistance (0.75 ohm cm^2) have been specified (see table 7.2). The specified area corresponds

---

[a] In **Chapter 8** the effect of pressurization of the SOFC system will be analysed.

to a power density is equal to 1.49 kW/m^2. Using these input data the cell voltage calculated with the detailed model is equal to 0.677 volt at a current density of 2198 A/m^2.

Table 7.4: Calculated energy flows and efficiencies for the base case SOFC system

	component name	no.[a]	energy flow [kW]	totals [kW]	% of input
input to system	fuel supply	11		1884.4	100.0
gross power	fuel cell	1		1000.0	53.1
aux. power consumption	flue gas compressor	33	47.3		
	feed pump	61	0.4		
	circulation pump	64	0.8		
	air compressor	22	102.4		
	total auxiliary		-	150.8	8.0
net power				849.2	45.1
delivered heat	steam net	100		140.5	7.5
total				989.7	52.6

[a] numbers refer to the apparatus in the flowsheet (figure 7.1)

The **gross electrical efficiency** is for the fuel cell system is defined as the ratio between the power generated in the fuel cell after conversion from DC tot AC power and the energy supplied to the system with the fuel (natural gas):

$$\eta_g = \frac{P_{AC}}{\varphi_{NG}\, LHV_{NG}} \tag{7.1}$$

For the SOFC base case the lower heating value of the fuel supplied to the system is equivalent to 1884.4 kW and the gross electrical efficiency equals 53.1% (table 7.4). To calculate the **net electrical efficiency** the auxiliary power has to be taken into account as well:

$$\eta_{el} = \frac{P_{AC} - P_{aux}}{\varphi_{NG}\, LHV_{NG}} = \frac{P_{net}}{\varphi_{NG}\, LHV_{NG}} \tag{7.2}$$

In the SOFC system auxiliary power is consumed mainly in the air compressor (app. 22) and the flue gas compressor (app. 33). The total calculated auxiliary power equals totals 150.8 kW. The net electrical efficiency as a result is significantly lower, namely 45.1 %. Both electrical power and heat are produced by the fuel cell system. This is taken into account in the definition of the **total efficiency:**

$$\eta_{tot} = \frac{P_{net} + Q_{steam}}{\varphi_{NG}\, LHV_{NG}} \tag{7.3}$$

The total efficiency is equal to 52.6%, indicating that the amount of heat produced in the fuel cell system is limited. Even though in the fuel cell more than 900 kW of heat is generated in the electrochemical reactions, the heat which is delivered by the system in the form of 10 bar process steam is only 140.1 kW. This corresponds to 7.5 % of the energy in the fuel input.

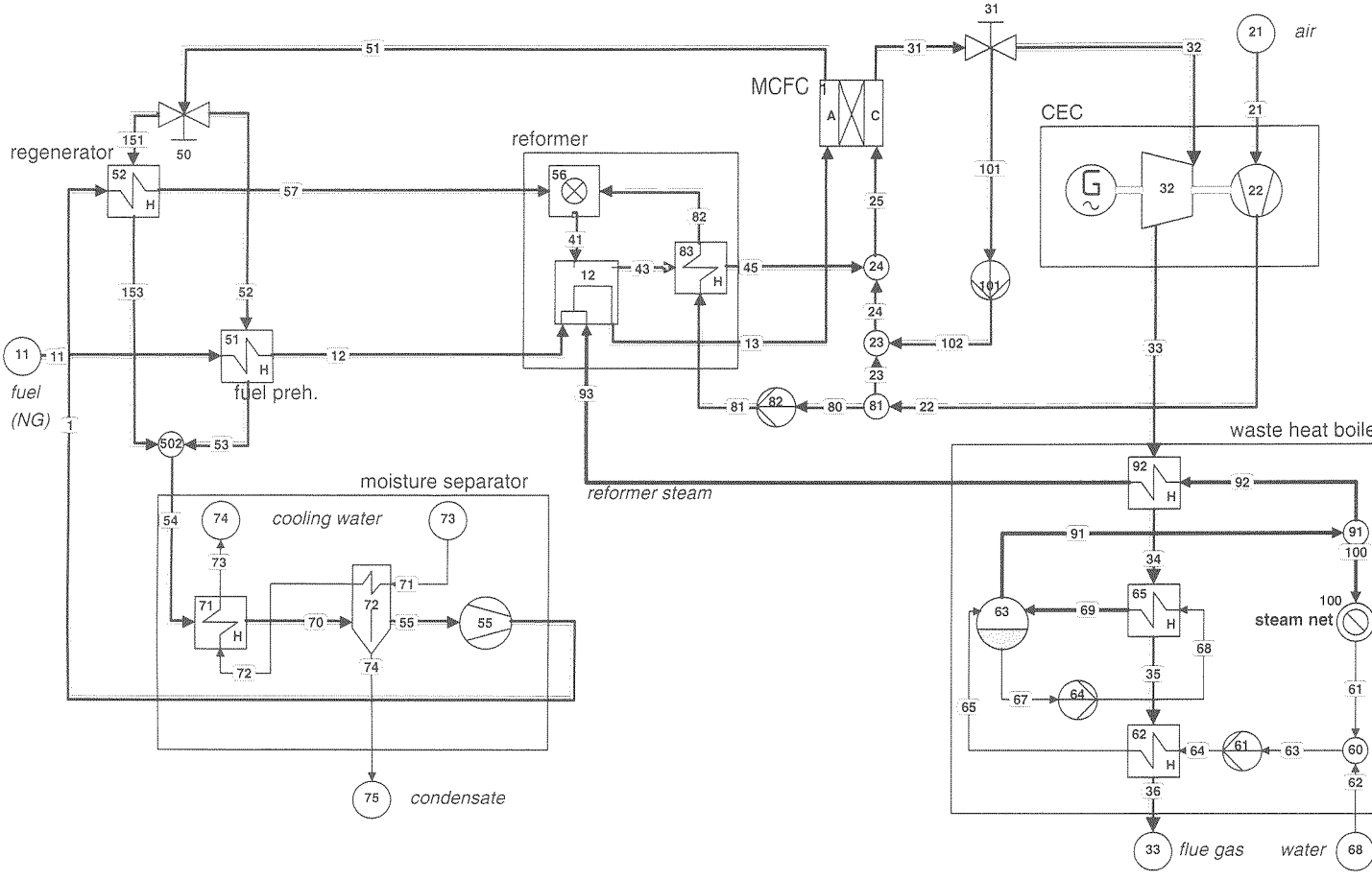

Figure 7.2: Process flow diagram for the base case configuration of the external reforming MCFC system

7.3.3 Description of the MCFC system

The flow sheet for the MCFC system is shown in figure 7.2. The operating pressure for the fuel cell for this calculation is 4 bar. Natural gas is assumed to be available at the system inlet at sufficient pressure (5 bar). The fuel is preheated to 400 °C in the fuel preheater (app. 51) and is mixed with steam. The molar steam to carbon ratio (S/C-ratio) is set to 3 [mole/mole] which is regarded high enough to prevent carbon deposition in the reformer and the fuel cell. The reformer in the simulation is represented by three components: the reforming reactor (app.12), the combustor and the air preheater (app. 83). In the reforming reactor (app. 12) the methane and higher hydrocarbons react with steam to CO and H_2. The composition of the product gas (i.e. reformed natural gas) at the outlet of the reformer is calculated by assuming an equilibrium temperature for the reforming reaction equal to 800 °C. Because of the higher pressure at which the reformer operates compared to the reference SOFC system, the methane conversion is lower (97%). Part of the heat which is present in the gas at the exit of the reforming bed (where the temperature is equal to 850 °C), is recovered within the reformer (for a description of the reformer model see **Appendix 3**). As a result of the heat exchange within the reformer, the outlet temperature of the product gas is from the reformer is 600 °C. This corresponds to the inlet temperature for the fuel cell stack. The fuel cell (app. 1) delivers 1000 kW AC power (taking into account a DC/AC conversion efficiency of 96%). To achieve sufficient the required combustion temperature in the reformer (1200 °C), the heating value of the anode off-gas must be high enough. The heating value depends on the fuel utilisation: as the fuel utilisation of the fuel cell increases the concentration H_2 and CO in the anode off-gas decreases and a lower heating value results. Therefore the value of the fuel utilisation is calculated to satisfy the required temperature in the reformer.

Table 7.5 Calculated energy flows and for the base case MCFC system

	component name	no.	energy flow [kW]	totals [kW]	% of input
input to system	fuel supply	11		1966.3	100.0
gross power	fuel cell	1	1000.0		50.9
	compressor	22	350.4		
	expander	32	299.2		
	net CEC	32-22	51.2		2.6
				1051.2	53.5
aux. power consumption	anode gas rec. compressor	33	13.9		
	feed pump	61	0.4		
	circulation pump	64	0.2		
	comb. air compressor	82	4.4		
	cath. gas rec. compressor	101	97.3		
	total auxiliary		-	116.1	5.9
net power				935.1	47.6
delivered heat	steam net	100		154.8	7.9
total				1089.8	55.6

The fresh air is pressurised in the air compressor (app. 22). The air is mixed with recycled cathode gas. As a result of the 16 K temperature increase in the recycle blower (app. 101) the temperature of at the outlet of the blower is higher than the temperature of the cathode off-gas (700 °C). The "recycle ratio" α is defined as the ratio between the recycle flow (stream 101) and the cathode off-gas flow (stream 31). The air is partially preheated by the recycle flow. The recycle ratio is calculated to satisfy the required inlet temperature for the fuel cell (600 °C). In the MCFC CO_2 is required by the cathode reaction. The CO_2 is provided to the cathode by mixing the air with combusted anode off-gas.
The anode off-gas (stream 51) exits the fuel cell at 700 °C and is first cooled to remove water from the gas. Removing water from the flow increases the heating value of the gas and makes it easier to achieve the required combustion temperature in the reformer. As a second advantage this increases the CO_2 concentration of the flue gas (stream 45) which is mixed with the cathode gas. The heat released when the anode off-gas is cooled, is recovered in the fuel preheater (app. 51) and the anode gas regenerator (app. 52). The remainder of the heat which has to be removed, is transferred to the cooling water in the cooler (app. 71) and the moisture separator (app. 72). The amount of water which is separated, is calculated by assuming the partial pressure of water to correspond to the outlet temperature of the separator. For this outlet temperature a value of 80 °C is used, which corresponds to a water content of the anode off-gas at the outlet of 12.5%.
The anode gas is then reheated and supplied to the reformer combustor. The combustion air (stream 81) is separated from the air flow after the compressor. The combustion air blower (app. 82) therefore only serves to overcome the pressure losses in the combustor and reformer. The combustion air is preheated to 400 °C in the combustion air preheater.
The cathode off-gas which is not recycled (stream 32) is used to produce power in the flue gas expander (app. 32). The flue gas is subsequently supplied to the waste heat boiler which produces process steam (10 bar / 180 °C) and superheated reformer steam (400 °C).

7.3.4 Calculation results for the MCFC system

In addition to the 1000 kW net fuel cell power, in the MCFC system the expander produces electrical power. The total power produced by the expander is not a good measure for the increase of the system performance: the largest part of the energy which is obtained in the expander is used by the compressor. Therefore the combination of both components is treated as a unit and indicated as the expander/compressor combination (**CEC**). The CEC operates as the combination of compressor and expander in a gas turbine. The net duty of the CEC is equal to the expander power minus the compressor power:

$$P_{CEC} = P_{exp} - P_{comp}$$

The gross electrical efficiency for the system operating at higher pressure is based on the power delivered by fuel cell and the net duty of the CEC:

$$\eta_g = \frac{P_{AC} + P_{CEC}}{\varphi_{NG}\, LHV_{NG}} \qquad (7.1b)$$

In the base case MCFC system the expander the power delivered by the expander is equal to 350.4 kW and the power required by the air compressor 299.2 kW. The calculated net duty for the CEC therefore corresponds to 51.2 kW. Based on the lower heating value (LHV) the energy supplied to the system with the fuel is equal to 1966.3 kW, resulting in a gross

efficiency of 53.5% (table 7.5). The net efficiency for the pressurised system is equal to:

$$\eta_{el} = \frac{P_{AC} + P_{CEC} - P_{aux}}{\varphi_{NG}\, LHV_{NG}} \qquad (7.2b)$$

The auxiliary power in this case does not include the duty of the air compressor. In the base case MCFC system the remaining pumps and compressors in the system consume a total of 116.1 kW. The main auxiliary is the duty of the cathode recycle blower (98.8 kW). The net efficiency of the MCFC system equals 47.6%.
In the waste heat boiler 154.8 kW_{th} is delivered to the process steam net. The total efficiency, which is defined as the sum of the net electrical power and the heat divided by the fuel input, equals 55.6%.
Essential data which are calculated for the fuel cell are the cell voltage and the fuel and oxidant utilisation. For these calculations of the AC power (1000 kW), the cell resistance (1 ohm cm^2) and the cell area (750 cells of 1 m^2) are specified and the cell voltage is calculated using the detailed model (**Chapter 4**). The calculated cell voltage is 720 mV at 1750 A/m^2. The value of the fuel utilisation achieve the required reformer flue gas inlet temperature of 1200 °C is 76.9% .
At the cathode side the O_2 and CO_2 utilisation are determined by the oxidant flow. In the fuel cell 817 kW is converted in to heat. To remove this heat from the cell at the 100 K temperature difference between inlet and outlet of the cathode, 6.7 kg/s oxidant is required: approximately 30 times the mass flow fuel. The corresponding utilisations (per passage) for O_2 and CO_2 are respectively 13.5% and 41.7%. The low utilisation for O_2 shows that the mass flow oxidant is determined by the heat flow and not by the required moles of reactant (i.e the stoichiometry)

7.4 ENERGY AND EXERGY ANALYSIS OF THE BASE CASE SYSTEMS

7.4.1 Introduction

In the previous section the efficiencies of the two base case systems were calculated. In both systems, the SOFC and the MCFC system, the amount of energy in the fuel converted to electrical power corresponds to less than half of the lower heating value (LHV) of the fuel supplied to the system (45.1 % and 47.7 % respectively) and less than 10% of the energy is recovered in the form of process steam in the waste heat boiler. To improve the electrical and thermal efficiency of the systems, it is essential to understand what factors limit these efficiencies. In the following paragraphs the losses in both base case systems will be analysed in detail.
In table 7.6 the energy and exergy efficiencies are summarised. The exergy value of the natural gas is 4% higher than the lower heating value (LHV). As a result, all efficiencies based on the exergy input to the system will be lower than the corresponding energy efficiencies. The total exergetic efficiency of the base case SOFC system equals 45.8 %. The largest difference between the energy and the exergy efficiency lies in the value for the heat. In terms of energy this represents 7.5 % of the fuel input and in terms of exergy the heat corresponds to 2.4 % of the exergy input to the system. As a result the total exergy efficiency is considerably lower than the energy efficiency (45.8 % vs. 52.5 % respectively). For the MCFC system table 7.6 shows comparable results.

Table 7.6: Calculated energy and exergy flows and efficiencies for the base case external reforming SOFC system (se) and MCFC system (me)

	SOFC (se)				MCFC (me)			
	Energy		Exergy		Energy		Exergy	
	[kW]	[%]	[kW]	[%]	[kW]	[%]	[kW]	[%]
fuel supply	1884.4	100.0	1954.2	100.0	1966.3	100.0	2039.0	100.0
gross power	1000.0	53.1	1000.0	51.2	1051.2	53.5	1051.2	51.6
net electrical	849.2	45.1	829.1	43.5	935.1	47.6	935.1	45.9
generated heat	140.5	7.5	46.3	2.4	154.8	7.9	47.4	2.3
total	969.6	52.5	875.4	45.8	1089.8	55.6	982.5	48.2

7.4.2 Analysis of the energy flows in the fuel cell system

For the calculation of the efficiencies only the energy flows over the boundary of the system are considered: the fuel which is supplied to the system, the electricity required for the pumps and compressor, the electricity which is generated by the system in the fuel cell and by the expanders, the steam which is produced by the system, etc. To analysis which factors limit the efficiency of the system, the energy flows occurring within the system are relevant as well.

Sankey diagram for the SOFC system
The calculated energy flows within the SOFC system are shown in figure 7.3 in an energy flow or Sankey diagram. The energy flows are based on the higher heating value (HHV)[b]. As shown in the diagram, the fuel flow represents 2088 kW (HHV). The energy of the syngas flow leaving the reformer is much larger (3321 kW) due to the increase in the thermal energy as a result of the increase in temperature from 20 to 800 °C and to the increase of the chemical energy in the reforming reaction. Furthermore substantial energy is supplied to the process in the form of reforming steam (458 kW). The air which is supplied to the system represents a small amount of energy[c]. A large amount of energy is supplied to this process flow as the air is preheated from 20 to 800 °C (4535 kW). The energy which is used to heat the air is supplied to this flow mainly by the hot cathode off-gas which bypasses the combustor (4245 kW) and part of the heat from the flue gas after the reformer.
Fuel and air are supplied to the fuel cell where 1000 kW of electrical power (AC) is generated. Taking into account the auxiliary power of the system (171 kW) the resulting net electricity production is only 829 kW.

---

[b] if the gas phase is considered as the reference state for water/steam, which is the case for the calculation of the lower heating value (LHV), energy must be supplied to water in the liquid phase in order to achieve the standard (=zero) state. Therefore liquid water will have a negative value of the energy if the LHV is used.

[c] the energy of the air flow is positive, even at environment conditions because it contains water vapour. Using the HHV as reference, the condensation heat of the water vapour is taken into account

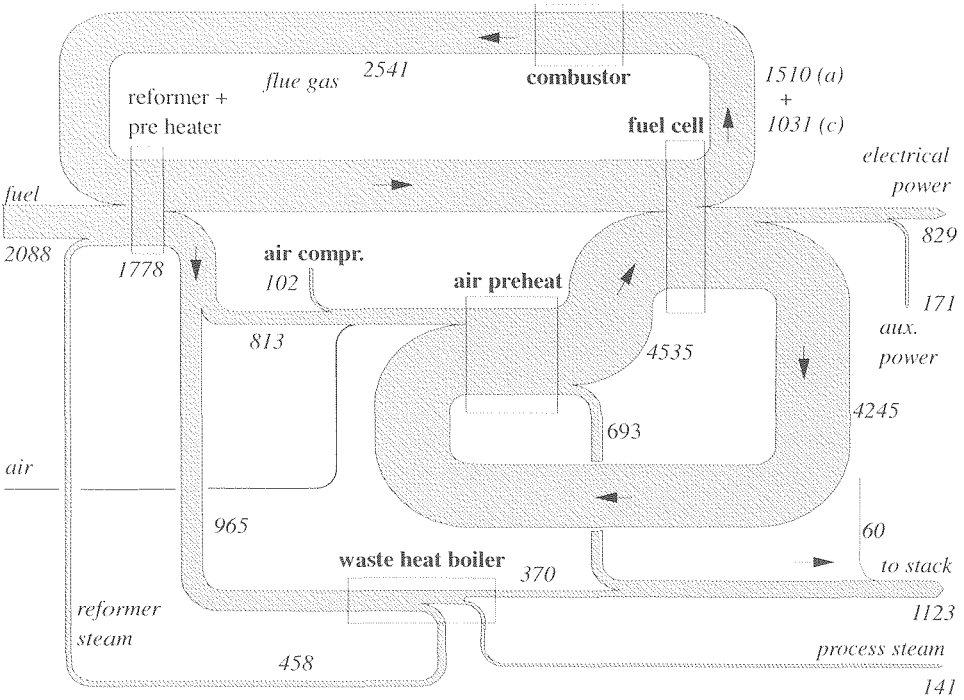

Figure 7.3: Sankey diagram for the external reforming SOFC system (se) based on the higher heating value: (energy flows in kW)

The energy flow of the anode off-gas (1031 kW) consists of the thermal energy and the chemical energy (400 kW) of the flow. This flow is mixed with part of the cathode off-gas (1510 kW). The total energy (i.e. thermal and chemical) is converted fully into thermal energy in the combustor (2541 kW). This heat is (partly)used in several steps. First heat is supplied to the reformer (775 kW). Subsequently part or the heat in the flue gas flow is used in the air preheaters (813). The remainder of the heat (965 kW) is supplied to the waste heat boiler where the largest part (458 kW) of this heat is used to produce the reformer steam and process steam (141 kW). The flue gas and the bypassed cathode off-gas exit the system through the flue gas stack, where a substantial part of the energy supplied to the system is lost (1123 kW).

The Sankey diagram illustrates an important point for this system: the extremely large energy flows in the system. The energy supplied to the fuel cell (thermal and chemical) with the anode and cathode flow totals 7847 kW. Therefore only 12.7% of the energy supplied to the fuel cell is converted into electrical power (on AC-basis). The system evidently requires large energy flows to be recycled. The diagram shows two main recycle loops.

- The upper loop represents the energy of the anode gas and part of the cathode gas which is used mainly to increase the energy of the fuel flow. The flow is used to transfer heat to the reformer, to the air preheaters and the waste heat boilers. But although the largest part of the energy is recovered, the efficiency of heat recovery is low for the air preheater and in waste heat boiler.
- The largest energy recycle is the heat which is supplied to the incoming fresh air by cooling the cathode off-gas bypass flow (stream 28). The energy which is used to preheat

the air is more than twice the amount of energy supplied tot the system with the fuel. The large energy recycle is partly due to the high temperature to which the oxidant must be preheated, but the main cause of the large amount of heat necessary to preheat the oxidant lies in large flow of air. In the fuel cell stack, not only 1041 kW of electrical power is generated but 912 kW of heat is released as well. The air flow (5 kg/s) required to remove this heat at the given temperature difference over the stack is approximately 25 times the mass flow fuel. This results in an oxidant utilisation as low as 13.5%, i.e. a mass flow air nearly ten times higher than required on basis of the O_2 requirements at the cathode.

.

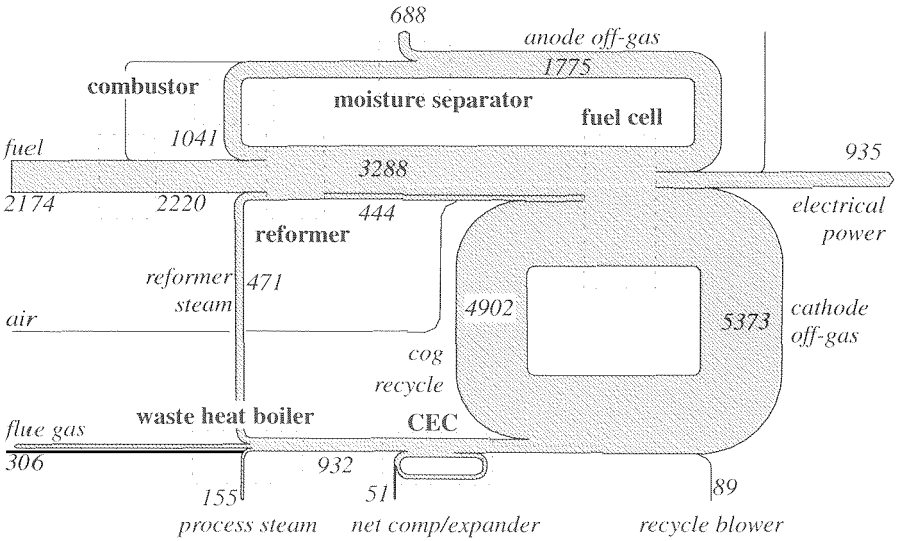

Figure 7.4: Sankey diagram for the external reforming MCFC system (me) based on the higher heating value: (energy flows in kW)

Sankey diagram for the MCFC system

The corresponding diagram for the MCFC system is shown in figure 7.4. In the MCFC system the fuel supplied to the system has a higher heating value of 2174 kW and is used to produce 935 kW of AC power in the fuel cell, 51 kW in the CEC (compressor/expander combination) and 155 kW of process steam.

There are two mayor differences between the energy flow diagrams for the SOFC (figure 7.3) and for the MCFC system (figure 7.4). The first is that the recycle of energy to the combustor is much smaller. In the SOFC system the energy flow to the combustor consists of both the (chemical + thermal) energy in the anode off-gas and the cathode off-gas. In the MCFC system only the chemical energy of the anode off-gas is used in the combustor. The cathode off-gas is not used in the combustor. Instead fresh air is supplied to the combustor of the reformer: Supplying cathode off-gas to the combustor would require a separate high temperature blower for this flow (because the flue gas from this combustor is used to supply CO_2 to the fuel cell. Furthermore, in removing water from the anode off-gas recycle is cooled to partially remove water vapour from this flow. As a result, a substantial amount of the thermal energy in this flow is removed as well. Consequently, the amount of heat recycled to the reformer is much smaller.

The second difference is also due to the moisture separator in the anode off-gas recycle. In the SOFC system nearly all energy which is lost, is removed from the system by the flue gas stack. In the MCFC system approximately ⅓ of the energy is removed through the flue gas stack and ⅔ is removed by the cooling water in the anode off-gas recycle.
In both systems however, the recycle flows are large compared to the energy which is produced. The high recycle of energy in both systems is likely to cause of significant losses. But the energy analysis only shows the energy which is rejected from the system: in the SOFC through the flue gas stack and in the MCFC system through moisture separator and flue gas stack. How the recycles contribute to these losses is not evident. One way to make the losses in the system visible, is the calculation of the exergy flows and losses.

7.4.3 Exergy losses in the components

Exergy losses in the SOFC system
The calculated exergy efficiency of the SOFC system is 44.8 % (see table 7.6). Therefore more than half of the exergy which is supplied to the system with the fuel is lost in the process. Table 7.7 shows the losses in the main components of the system in order of decreasing exergy loss.

Table 7.7: Calculated exergy losses in the components of the external reforming SOFC system (numbers refer to the apparatus in figure 7.1)[1]

no.	app.	exergy loss	no.	app.	exergy loss
				(continued)	
23	air preheater 1	179.2	1-a	DC/AC-converter	41.6
14	reformer	116.9	25	air preheater 3	41.0
34	flue gas stack	104.0	22	air compressor	30.1
24	air preheater 2	101.2	13	fuel preheater	17.9
41	anode gas comb.	100.3	62	economiser (whb)	17.6
1	fuel cell (SOFC)	95.5	33	fg-compressor	12.4
65	evaporator (whb)	66.8	92	superheater (whb)	11.4
30	flue gas mixer	44.0			

[1] Only components with exergy losses >10 kW are shown in this table

The total losses equal 1080 kW. The highest exergy losses occur in the first air preheater (179.4 kW), which is 10% of the exergy input to the system. In the next five components in the table the exergy losses are comparable (each corresponding to 5-6% of the exergy input to the system). These components include the three components in which the fuel is converted: the fuel cell, the reformer and the combustor. Considerable losses also occur in several heat exchangers and the flue gas stack.

Exergy losses in the MCFC system
The fuel which is supplied to the base case MCFC system represents an exergy flow equal to 2049 kW. Taking into account the net power output of the system (934 kW) and the exergy of the process steam which is supplied to the steam net (47.1 kW), the total exergy losses of the system therefore equal 1068 kW. Table 7.8 gives an overview of the most important

exergy losses in the components of the system. In the fuel cell stack the exergy loss is 111.6 kW, which corresponds to 5.4 % of the exergy supplied to the system with the fuel. This excludes the exergy loss in the DC/AC-converter which is equal to 41.7 kW. To evaluate whether this represents a high exergy loss, it is necessary to convert the absolute value of exergy loss to a relative value. This can be done by comparing the exergy loss to the energy conversion process in which it occurs. For example, for the combustor and the fuel cell, which serve to convert chemical energy into another form of energy, the amount of chemical energy converted is the comparison. Likewise for heat exchanging apparatus the transferred heat and for rotating equipment the electrical power consumed or generated is listed. In table 7.8 the exergy losses and the figure characterising the energy conversion process is shown for each step.

Table 7.8: Calculated total exergy losses and exergy losses per type in the components of the base case external reforming MCFC system (me)

no.	name	characteristic parameter	energy flow [kW]	exergy loss [kW]	% of exergy input
56	anode gas combustor	chemical energy	565.2	126.4	6.2
1	fuel cell	chemical energy	1858.0	111.6	5.4
72	moisture separator	transferred heat	438.3	103.9	5.1
71	anode gas cooler	transferred heat	224.3	90.9	4.5
23	cath. gas mixer		-	87.8	4.3
12	reformer	transferred heat	598.9	81.1	4.0
65	evaporator	transferred heat	417.5	69.0	3.4
22	cath.air.compressor	electrical power	301.4	66.0	3.2
24	anode gas mixer		-	58.2	2.6
32	expander	electrical power	351.7	47.4	2.3
5	regenerator	transferred heat	299.8	36.8	1.8
101	cath. gas compressor	electrical power	97.1	14.6	0.7
92	superheater	transferred heat	73.3	13.9	0.7
51	fuel preheater	transferred heat	47.6	12.6	0.6

The chemical energy is converted into heat and electricity in the fuel cell and in the combustor. In the fuel cell 1858 kW of chemical energy is converted vs. 565 kW in the combustor, which corresponds to 77 % fuel utilisation in the fuel cell and 23 % of the fuel combusted. Comparing the exergy loss in the fuel cell (111.6 kW) and the combustor (126.4 kW) shows that the latter are nonetheless higher than the losses in the fuel cell. This illustrates the very efficient process in the fuel cell compared to combustion.
The exergy losses in the anode gas cooler and the moisture separator, which serve to remove water from the anode gas, are high. This is due to the fact that the amount of heat which is dissipated with the cooling water is very large and more importantly of a temperature level considerably above environment temperature. Considerable losses also occur when the fresh air is mixed with the recycled cathode-off gas (87.8 kW) and anode off-gas (53.6 kW) and in the rotating equipment, for example the expander (47.5 kW) and the cathode air compressor (66.4). Although the system has a relatively small number of heat exchangers as a result of the direct cathode gas recycle, exergy losses in heat exchangers as for example the evaporator (68.7 kW) and the regenerator (37.4 kW) are considerable.

7.4.4 Detailed exergy analysis of the SOFC system

Exergy losses in subsystems

Although tables 7.7 and 7.8 contains most of the relevant data (the table only shows the losses >10kW) the information is not very easily accessible. One way to improve this is to group the components into subsystems. For the purpose of analysis the external reforming SOFC system is split into 6 subsystems:

- In the **fuel conditioning** step the natural gas is preheated in the fuel preheater, mixed with steam and reformed;
- The most important step in the fuel conversion takes place in the **fuel cell** where the H_2 and CO react electrochemically, generating heat and electrical power;
- The remaining combustible components in the anode off-gas react in the **combustor**;
- The **air preheat** subsystem contains the air preheaters and the air compressor;
- The **waste heat boiler** is the subsystem which produces steam from the heat in the flue gasses and consists of several heat exchangers, pumps and a steam drum;
- Finally the **flue gas stack** is the part of the system where the flue gas flows from the waste heat boiler and the oxidant preheat are mixed and transported from the system by the flue gas compressor.

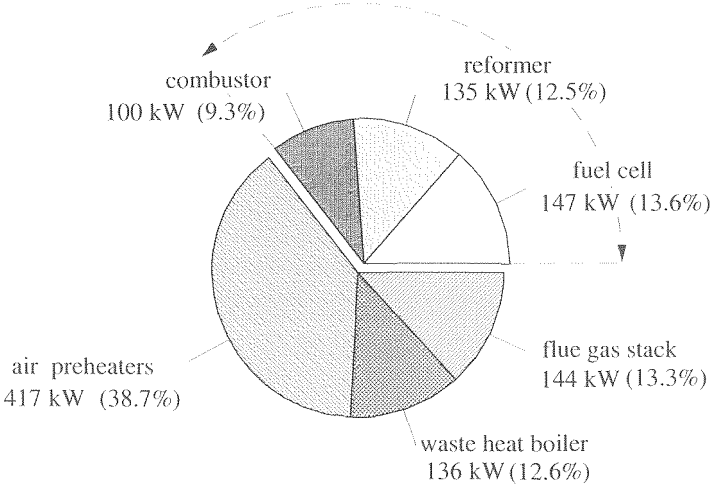

Figure 7.5: Calculated exergy losses classified according to the subsystem for the external reforming SOFC system (se)

In Figure 7.5 the exergy losses for each of these subsystems are shown. The system can be considered as a combination of 2 process steps [de Groot, 1993]:

- In the first process step the chemical energy of the fuel is converted into power and heat in a series of (electro-)chemical reactions;
- In the second system, the heat in the flue gasses is recovered to produce steam and preheat the incoming air and fuel flows.

Using figure 7.5 the exergy losses in these two processes can be compared. The losses in first process step, the fuel conversion process consisting of the combustor, the reformer and the fuel cell, amount to approximately ⅓ of the total losses. The remaining ⅔ of the losses occur in the air preheating system, in the waste heat boiler and in the flue gas stack. Nearly 40% of

the losses occur in the air preheating subsystem. This is clearly related to the large amount of energy which is recycled from the cathode off-gas to the incoming air which is shown in figure 7.3. This illustrates the relatively high efficiency of the chemical and electrochemical conversion process. Where in the conventional thermal power plant the combustion process itself is responsible for considerable exergy losses [Baehr, 1978], the exergy losses in the actual conversion of chemical energy in the fuel cell systems are relatively low.

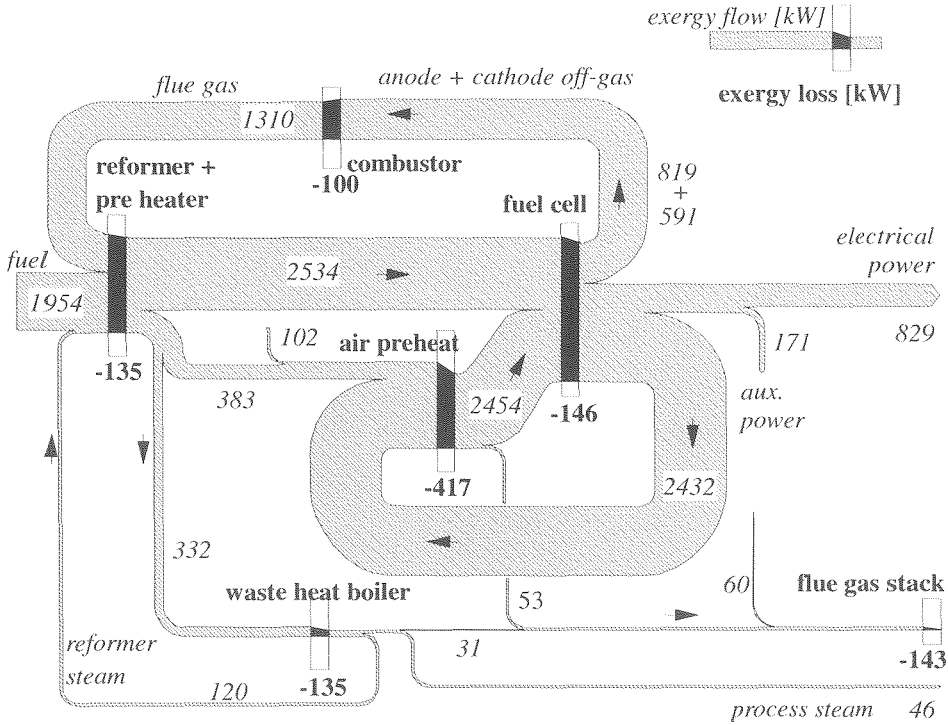

Figure 7.6: Grassman or exergy flow diagram for the base case SOFC system (se)

The exergy flows

Another way of representing the exergy losses in the system is by making use of the exergy flow diagram sometimes indicated as the 'Grassman' diagram. In this diagram, which is shown in figure 7.6 for the external reforming SOFC system, the exergy flows between the subsystems of the system are represented just as the energy flows in the Sankey diagram. In the Sankey diagram the first law of thermodynamics ensures that the energy in the flows to the subsystem are equal to the energy flows exiting that subsystem. In the case of exergy flows, this is not true: as a result of exergy losses the sum of the exergy flows leaving the subsystem is smaller than the sum of the incoming flows. In the exergy flow diagram this loss is represented by the decreasing width of the exergy flows (represented by the black polygons). The exergy losses correspond to the exergy losses of the subsystems in figure 7.6. The form of the exergy flow diagram is more or less the same as that of the Sankey diagram. The fuel input and the electrical power output are approximately the same in both diagrams. But there

are a number of differences[d]. For example, the energy which is recycled to the cathode corresponds the 4245 kW (figure 7.3) while the exergy value is 2432 kW, even though the temperature at the inlet of the fuel cell is very high (850 °C). The flows to and from the waste heat boiler are clearly much smaller in the exergy flow diagram than in the Sankey diagram. In terms of energy for example, the stack losses are 1123 kW, more than half of the energy input to the system. In terms of exergy this loss is only 143 kW.
The diagram therefore clearly shows that the effort in increasing the exergy efficiency of the system should not focus on recovering more heat from the flue gasses, for example by cooling the flue gas further. The maximum (theoretical) increase of the exergy recovery which can be achieved in this way is 86.1 kW, i.e. the thermal exergy of the flue gasses (see table 7.10). Another difference between the Sankey and the exergy flow diagram is that the exergy flow diagram also visualises the losses in the recycles. It confirms the link between the large (energy) recycles and losses occurring in the system.

Table 7.9: Calculated total exergy losses and exergy losses per type in the components of the base case external reforming SOFC system

no.	app.	total	heat transfer	friction	mixing	chemical	electrical
23	air preheater 1	179.2	166.3	12.9	-	-	-
14	reformer	116.9	71.6	5.4	14.3	25.6	-
34	flue gas stack	104.0	86.1	-	18.0	-	-
24	air preheater 2	101.2	85.8	15.4	-	-	-
41	anode gas comb.	100.3	-	1.0	63.4	35.9	-
1	fuel cell (SOFC)	95.5	18.0	9.8	-	-	67.7
65	evaporator (whb)	66.8	60.1	6.7	-	-	-
30	flue gas mixer	44.0	0.1	-	43.9	-	-
1-a	DC/AC-converter	41.6	-	-	-	-	41.6
25	air preheater 3	41.0	34.6	6.4	-	-	-
22	air compressor	30.1	-	30.1	-	-	-
13	fuel preheater	17.9	15.7	2.3	-	-	-
62	economiser (whb)	17.6	16.3	1.3	-	-	-
33	fg-compressor	12.4	-	12.4	-	-	-
92	superheater (whb)	11.4	9.3	2.2	-	-	-

Analysis of the types of exergy losses in the fuel cell system
In **Chapter 3** a classification of 5 types of exergy losses has been developed. The exergy losses in the fuel cell system can be attributed to the following processes:
- Heat transfer;
- Friction;
- Isothermal mixing with (different compositions);
- Chemical reactions;
- Electrical charge transfer.

For the components in the external reforming SOFC system the contribution of each of the causes to the total exergy losses have been calculated (table 7.9). To assess the importance of

[d] the scale is different for both diagrams to make the exergy losses in the exergy flow diagram visible

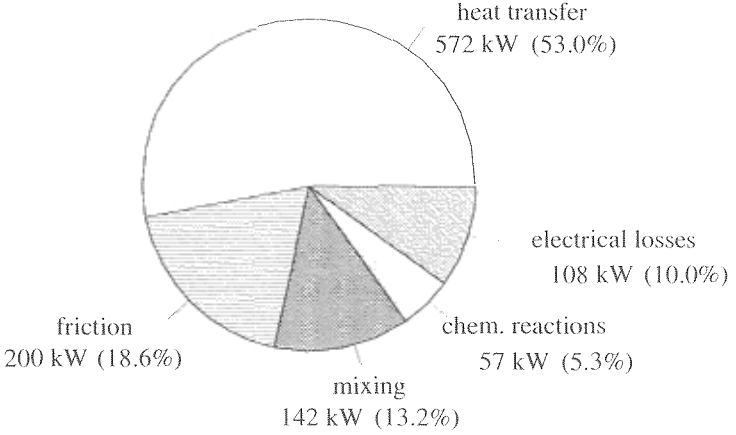

Figure 7.7: Calculated exergy losses per cause in the external reforming SOFC system and their contribution to the total exergy loss

each of these causes for the exergy losses of the total system, the total contributions are shown in figure 7.7. The importance of heat transfer losses is evident: more than half of the exergy losses result from heat transfer. These losses will be analysed in more detail in the **Section 7.5**. The losses in the fuel conversion, i.e. the chemical and electrical losses have a relatively low contribution. Chemical losses in the external reforming SOFC system cause only 5.3% of the losses, the electrical losses in fuel cell and DC/AC-converter account for 10% of the loss. From figure 7.7 the first priorities can be set for analysis and optimisation of the fuel cell system. The losses in the fuel conversion process (exergy losses as a result of chemical reactions and electrical charge transfer) are relatively small. It is not evident how the mixing losses can be reduced and the same is true for the friction losses which occur distributed over the whole system. The first priority is therefore to reduce the losses as a result of heat transfer.

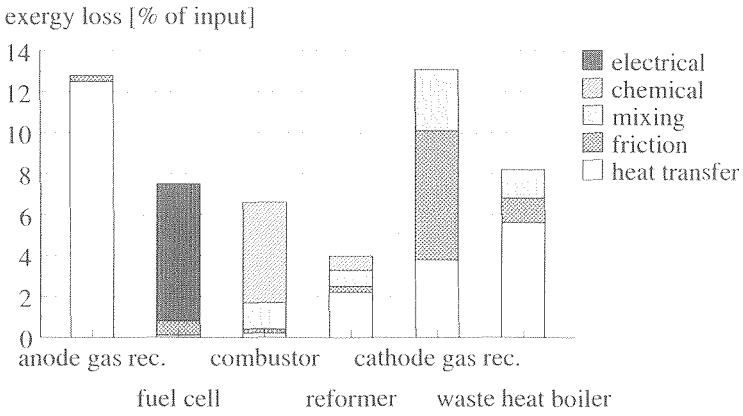

Figure 7.8: Exergy losses in the base case external reforming MCFC system (me) classified according to the cause of the loss and the subsystem

Table 7.10: Calculated total exergy losses and exergy losses per type in the components of the base case external reforming MCFC system

app.	name	total	heat transfer	friction	mixing	chemical	charge transfer
56	anode off-gas combustor	124.6	-	1.1	24.9	98.6	-
1	fuel cell (MCFC)	111.6	2.8	14.3	-	-	94.6
72	moist. separator	103.9	103.9	-	-	-	-
71	anode gas comp.	92.5	92.5	-	-	-	-
23	cgr. mixer	87.3	73.2	-	14.1	-	-
12	reformer	80.8	46.9	5.8	15.0	13.2	-
65	evaporator	68.6	66.2	2.4	-	-	-
22	cathode air comp.	65.9	-	65.9	-	-	-
24	agr. mixer	53.0	2.4	-	50.6	-	-
33	fg-stack	50.2	-	-	-	-	-
32	expander	47.2	-	47.2	-	-	-
11	DC/AC converter	41.7	-	-	-	-	41.7
52	regenerator	37.3	36.3	1.0	-	-	-
62	economiser	19.2	16.7	2.5	-	-	-
101	cgr. compressor	14.6	-	14.6	-	-	-
92	superheater	13.9	10.6	3.3	-	-	-
51	fuel preheater	12.7	12.6	0.1	-	-	-

7.4.5 Detailed exergy analysis of the MCFC system

The contributions of the different types of exergy losses has been calculated for all components in the external reforming MCFC system as well. The results are shown in table 7.10.The components in the MCFC system have also been grouped into subsystems. Figure 7.8 shows the total exergy losses in the subsystems taking into account the different types of exergy losses defined in **Section 3.2**.

- The **fuel cell**, because of its importance has been defined as a separate subsystem. In the fuel cell electrical losses are the main cause of exergy losses. In the graph the losses as a result of the conversion from DC to AC have been included as well. The total 'electrical' exergy loss corresponds to 6.7 % of the exergy input to the system of which one third occurs in the DC/AC-converter and the remainder in the electrochemical process in the fuel cell.
- The **reformer** is defined as a separate subsystem as well. For the reformer 4 types of exergy losses appear in figure 7.8. The role of heat transfer in the reformer is evident. Friction losses occur as well, partly as a result of the relatively high pressure drops in this component (specifically the expansion of the steam from 10 bar to 5 bar). The loss as a result of mixing (steam + natural gas) is the second largest cause of exergy losses: it exceeds the losses as a result of the chemical reaction.
- The **combustor** subsystem includes the combustion air preheater and compressor. The losses as a result of chemical reactions are predominant in the combustor. However, the process of (isothermally) mixing air and fuel leads to an exergy loss which is approximately a quarter of total losses in the combustor.

- The **anode off-gas recycle** (aog) consists of the heat exchangers to cool and reheat the gas and the compressor which is necessary to overcome the pressure losses in this subsystem. The exergy losses in the anode gas recycle subsystem are particularly large (corresponding to 12.8 % of the exergy input to the system). In this subsystem the exergy loss is almost entirely cause by heat transfer from the anode off-gas to the cooling water.
- In the **cathode off-gas recycle** (cog) subsystem the air is mixed with the recycled anode and cathode gas. The losses in the expansion and compression of respectively the flue gas and air are strongly related to the cathode gas recycle and are therefore included in this subsystem. The losses in the cathode gas recycle are of most interest. Nearly half of the losses in this subsystem (48%) are caused by friction. These losses occur mainly in the expander (31) and the air compressor (22). The two other causes of exergy losses in the subsystem are heat transfer and mixing of air with recycled anode gas and recycled cathode gas.
- Finally the **waste heat boiler** (whb) is the subsystem where part of the waste heat in the flue gas is used to produce process steam and steam for the reformer.

In figure 7.9 the contribution of each of the five causes of exergy losses is shown for the system as a whole. The losses as a result of heat transfer are responsible for almost half of the total losses. The other 4 causes of exergy losses are responsible for approximately equal contributions to the total exergy loss.

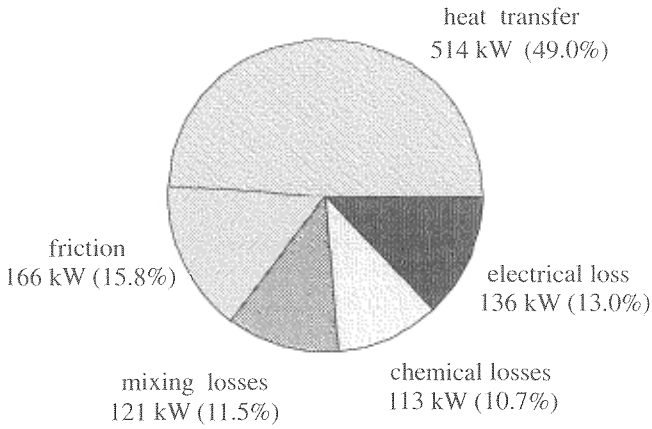

Figure 7.9: Calculated exergy losses for the base case MCFC system per cause

7.5 ANALYSIS OF HEAT TRANSFER IN THE FUEL CELL SYSTEM

Both the exergy analysis of the SOFC system and of the MCFC system in the previous sections showed the large contribution of heat transfer to the exergy losses. Therefore in this section these losses are studied in more detail.

7.5.1 Heat transfer in the SOFC system

The heat which is transferred in the fuel cell system is heat which is generated in the fuel cell and in the combustor. The heat is used in the reformer to enable the reforming process and in the fuel and air preheaters to preheat the fuel and air flow. Finally in the waste heat boiler heat

is recovered from the flue gas and used to produce steam. As shown by the Sankey diagram for the SOFC system, the heat which is recovered from the flue gas exceeds the amount of heat which is generated in the fuel cell stack and the combustor: for the largest part of the heat which is recovered from the flue gas has first been supplied to the process flow by preheating the flows. This was shown to lead to a large recycle of heat.

The heat transfer in the SOFC system is visualised in the diagram in figure 7.10. In this Q,T-diagram the temperature at which the heat is transferred is shown on the y-axis. On the x-axis the amount of heat which is transferred is shown. In the case of the SOFC system, heat is exchanged in the heat exchangers but also in the reformer and as a result of mixing flows with different temperatures. The mixing process can be considered as heat transfer in a ideal co-flow heat exchanger ($\Delta T=0$).

In the first 3 components in the diagram (30, 13, 14) the secondary or cooled fluid is the flue gas between the outlet of the combustor and the inlet of second air preheater (see the process flow diagram in figure 7.1). In reversed order with respect to the fuel flow (i.e. in counter current) the flue gas passes through the reformer (app. 14) where the flow is cooled down to 800 °C. The primary or heated medium is the process gas in the reformer bed containing the catalyst. The linear temperature profile indicated in figure 7.10 is an approximation. However model calculations (see **Appendix 3**) show that this approximation is reasonable. After the reformer the flue gas is cooled further in the fuel preheater (app. 13) and mixed (app. 30) with the bypassed cathode off-gas flow.

The next three components in the Q,T-diagram are the air preheaters (app. 23, 24 and 25). The primary fluid is the incoming air flow which gives an almost linear temperature profile. The secondary fluid is different for each heat exchanger (see the process flow diagram in figure 7.1). The other components in the Q,T-diagram show the heat transfer as a result of mixing the two flue gas flows (app. 32) and in the heat transfer in the waste heat boiler: the economiser (app. 62), the evaporator (app. 65) and the superheater (app. 92).

The exergy analysis in the previous section led to the conclusion that heat transfer causes the largest part of the losses. The Q,T-diagram gives a good indication of the cause of the size of this loss. The total amount of heat transferred in these components is almost 6 MW or 6 times the electrical power generated in the system. The largest part of the heat (approximately ¾) is transferred in the air preheaters.

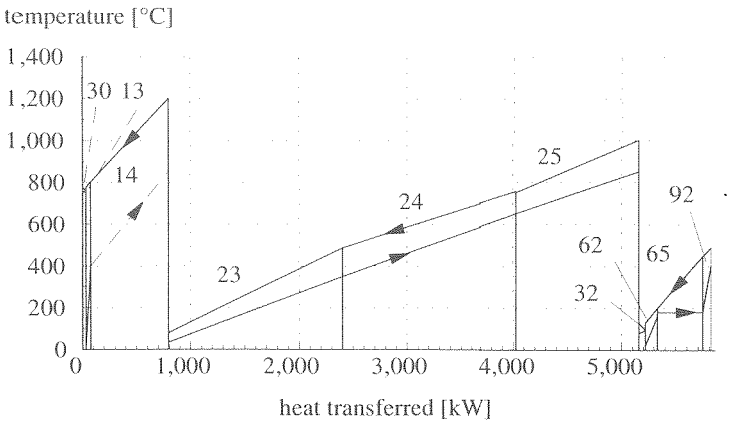

Figure 7.10: Q,T-diagram for the base case SOFC system (numbers refer to the apparatus numbers in the process flow diagram in figure 7.1)

the value diagram

The temperature differences between hot and cold process flow can be estimated from the Q,T-diagram (e.g. figure 7.10). For example, the temperature difference at which the heat is transferred in the SOFC system in the reformer is high and smaller in the air preheaters. The temperature difference determines the exergy losses as a result of heat transfer, because it is the driving force for the process. However, the temperature difference is not the only factor. The exergy losses also depend on the average temperature of heat transfer. To estimate the exergy losses the value diagram (see **Section 3.5**) can be used. In this diagram the Carnot factor ($1-T_o/T$) is plotted against the transferred heat.

As was shown in **Section 3.5.1**, the areas enclosed by the curves for the cold (primary) and hot (secondary) flow correspond to the exergy losses as a result of heat transfer. The components have been arranged in the same manner in the Q,T-diagram and in the value diagram (figure 7.11).

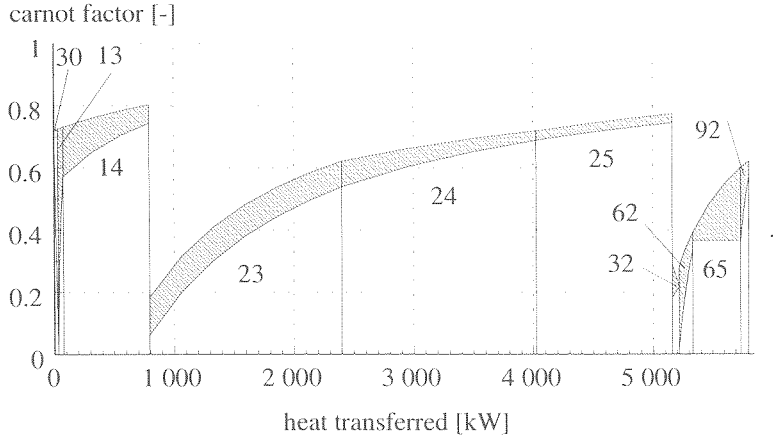

Figure 7.11: Value diagram (f,Q) for the base case SOFC system (se)

Comparing the two diagrams, the influence of the average temperature of heat transfer is clear. At high temperature, for example in the reformer (app. 14) and in the high temperature air preheater (app. 25) the exergy losses are smaller than expected based on the ΔT. On the other hand, the losses in the low temperature air preheater (app.23) are much larger. The value diagram evidently gives more information about the exergy losses than the Q,T-diagram.

the pinch diagram

In the pinch diagram, developed by Linnhof [1987], the heat transferred is analysed for a system or a subsystem as a whole. In the Q,T-diagram the temperature curves for each separate component are shown for the hot and the cold process flow. But in a pinch diagram these separate trajectories are combined into two curves: one for all the process flows which supply heat (hot composite curve) and one from all the process flows which absorb heat (cold composite curve). The diagram therefore shows how much heat is available at which temperature. The pinch diagram for the external reforming SOFC system is shown in figure 7.12. The cold composite curve represents the air and fuel which are preheated, the steam production in the waste heat boiler and the heat which is used in the reformer.

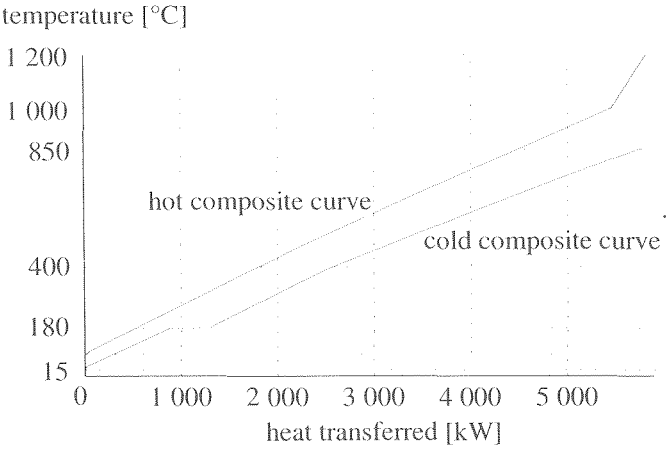

Figure 7.12: Pinch diagram for the base case SOFC system (including steam production and reformer)

The cold composite curve shows how much heat is required and at what temperature. Following the cold composite curve, the slope is (approximately) constant from 15 °C to 180 °C. 180 °C is the evaporation temperature in the waste heat boiler. Therefore the slope becomes zero at this temperature (dT/dQ = 0). The constant slope resumes when all evaporation heat has been supplied. At 400 °C the slope decreases: this is the inlet temperature for the reformer. The slope between 180 °C and 400 °C corresponds to pre-heating air, fuel en steam. Above 400 °C heat is used in the reforming reaction as well and continues up to 850 °C the temperature to which the process flows to the fuel cell have to be preheated. The hot composite curve indicates how much heat is available. In the case of the SOFC reference system, this curve consists of 2 stretches. From 1200 °C to 1000 °C the cooling fluid is the flue gas from the combustor. Below 1000 °C much more heat is available because the curve includes the cathode off-gas.
In the analysis of high temperature fuel cell systems, the pinch diagram can be used to determine how much heat is theoretically required or available at a high temperature[f]. This is done by matching the required heat with the available heat represented by the cold and hot composite curves in the diagram. The amount of heat available or required is determined by the pinch point. This is the point where the temperature difference between the hot curve and the cold curve is minimal. If heat is available at a high temperature, the hot composite curve can be shifted to the left until the temperature difference at the pinch point corresponds to a given minimum. If heat is required to match the cooling and the heated flows, the hot curve has to be shifted to the right to achieve the pre-set pinch.
In figure 7.13 the amount of heat which could be recovered at high temperature is determined using a pinch of 0 K. To estimate the amount of heat which is available or required, only those flows should be include which are inherent to the process in the given configuration. In the SOFC system these are the flows which have to be preheated and the flue gas which has to be cooled to stack temperature. This does not include the production of steam for external use in

[f] in this thesis only one aspect of pinch technology is used. An overview of pinch technology can be found in literature

the fuel cell system. Therefore heat required for preheating the water and evaporating this steam has not been included in the cold composite curve. The heat required for producing steam for the reformer has been included, because this is inherent to the process.
Figure 7.13 shows that the pinch occurs at the lowest temperature (80 °C), i.e. a the flue gas stack temperature. If the pinch is 0 K, the diagram shows the amount of heat which could theoretically be removed from the system to be approximately 400 kW. This 400 kW is only a small part of the total amount of heat which is transferred in the system. However, if it is compared to the fuel input to the system or to the electricity production, 400 kW is considerable.

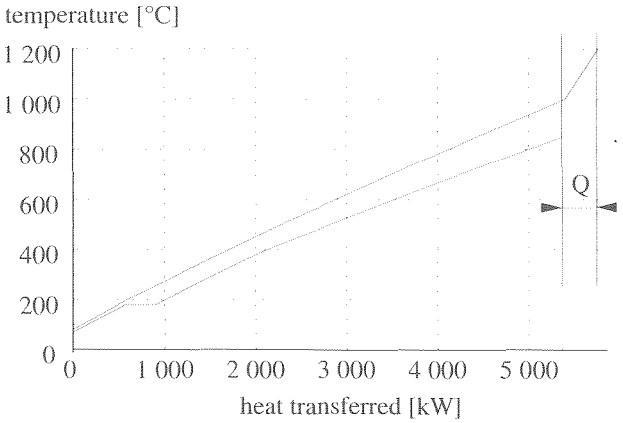

Figure 7.13: Pinch diagram for the base case SOFC system (excluding steam production)

The pinch diagram with 0 K pinch represents the situation where the given hot and cold flows in the system are ideally matched. To determine the exergy losses in this case, which represent the minimal exergy losses as a result of heat transfer possible by adapting the heat exchanger network, the pinch diagram can be translated to a pinch-value diagram by using the Carnot factor ($1-T_0/T$) on the y-axis instead of T.

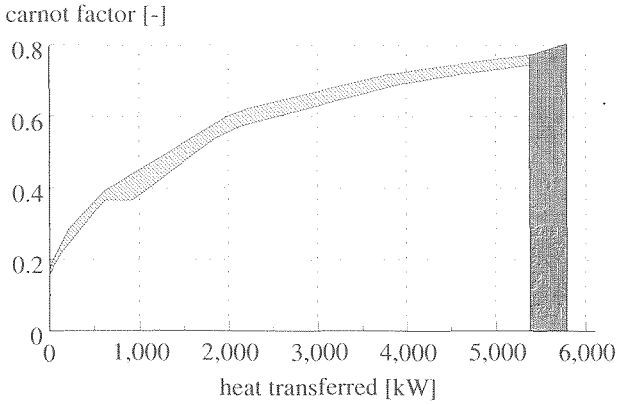

Figure 7.14: Pinch-value diagram for the base case SOFC system (excluding steam production)

The result for the SOFC system is shown in figure 7.14. The hatched area represents the exergy loss if the cold and hot flows in the system are ideally matched. To achieve this optimal match, an amount of heat will have to be extracted from the system at the highest possible temperature. The exergy of this heat is represented by the shaded area in figure 7.15. If Q = 400 kW and the Carnot factor 0.78 (estimated from the pinch-value diagram) the exergy of the heat is equal to 310 kW. This is more than half of the total exergy losses as a result of heat transfer (572 kW). This represents the upper limit for the exergy losses which could be prevented by recovering the heat at high temperature:

- Even if heat could be recovered at a high temperature, it will be recovered with a limited exergy efficiency;
- Secondly the 400 kW is based on a 0 K pinch. As can be seen in figure 7.11 the temperature differences at which heat is transferred are already small in the area below the pinch. Reducing the temperature difference at which the heat is transferred will substantially increase the heat exchanger area required.

7.5.2 Heat transfer in the MCFC system

Heat transfer is responsible for almost half of the total exergy losses in the MCFC system. Figure 7.15 shows the Q,T-diagram for the external reforming MCFC system. In the anode off-gas recycle heat transfer takes place in respectively the moisture separator (71), the anode off-gas cooler (app. 72), the regenerator (app. 52) and the fuel preheater (app. 51).

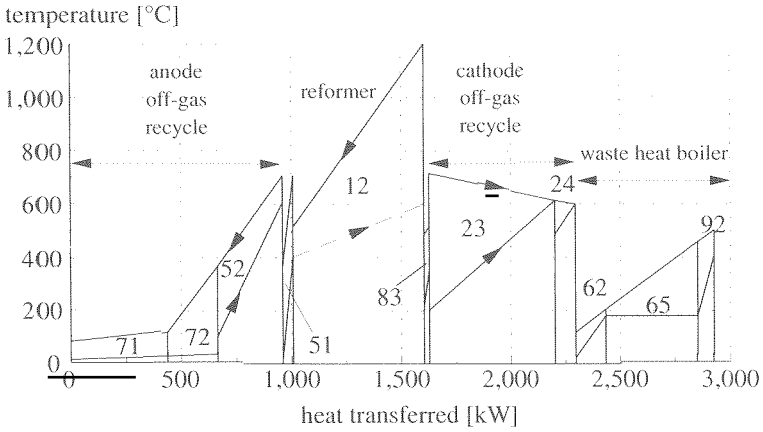

Figure 7.15: Q,T-diagram for the base case external reforming MCFC system

For the reformer again a linear profile has been used as an approximation (see **Appendix 3**). The temperature increase of the fresh air is primarily achieved by mixing the air with the recycled cathode off-gas (see the process flow diagram in figure 7.2). In the Q,T-diagram in figure 7.15 the mixing process (in apparatus 23 and 24) is represented by ideal co-flow heat exchange. The temperature of the air before mixing is 202 °C as a result of the compression from 1 to 4 bar. The temperature of the recycled cathode off-gas is 716 °C due to a 16 K temperature increase in the recycle blower (outlet temperature fuel cell = 700 °C). After mixing air and recycled cathode off-gas the temperature is 613 °C. Further mixing of this flow with the flue gas from the reformer (508 °C) leads to the required inlet temperature for the fuel

cell (600 °C). The cathode off-gas which is not recycled is used to produce power in the expander (app.32). As a result of the expansion the temperature decreases from 700 °C to 500 °C, the temperature at which the flue gas is supplied to the waste heat boiler. In the waste heat boiler the flue gas is further cooled down to 110 °C. The heat is used to produce process and reforming steam at 10 bar and 180 °C.
The corresponding value diagram for the MCFC system is shown in figure 7.16. The exergy losses for heat transfer at low temperature are much larger than the exergy losses if the same amount of heat is transferred at the same temperature difference but at a higher average temperature.

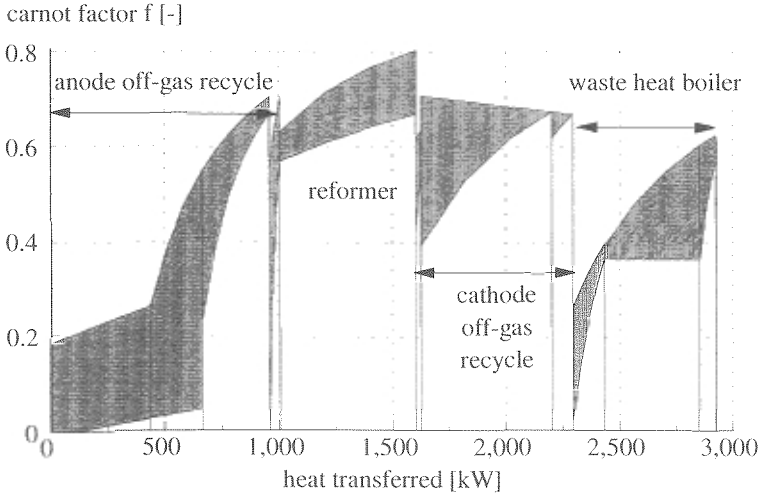

Figure 7.16: Value diagram for the external reforming MCFC system

Therefore the losses in the moisture separator and the anode off-gas cooler in the anode off-gas recycle are high even though the temperature difference is low. On the other hand the exergy losses resulting from heat transfer in the reformer, due to the high temperature at which the heat is transferred are relatively low. Comparison of the Q,T-diagram to the value diagram shows the benefit of using the value diagram to evaluate losses as a result of heat transfer.

7.6 EXERGY LOSSES IN THE FUEL CONVERSION

7.6.1 Chemical energy conversion

The purpose of a fuel cell system is to convert the chemical energy in the fuel into power (and heat). This process, the fuel conversion, in the external reforming fuel cell system consists of three consecutive steps:

- Chemical reaction of natural gas and steam in the reformer to a hydrogen rich syngas;
- Electrochemical conversion of the chemical energy in the syngas into power and heat in the fuel cell;
- Combustion of the remaining fuel components in the anode off-gas in the combustor.

In the SOFC system the exergy losses in the 3 components in which the chemical reactions take place (reformer, fuel cell and combustor) constitute roughly one third of the total losses.

In the MCFC system the contribution of these components to the exergy losses is comparable. In figure 7.17 a Sankey diagram is shown for fuel conversion process in the MCFC system. The chemical energy and thermal energy flows have been separated to represent the conversion of chemical energy into heat and power. A similar diagram can be drawn for the SOFC system. The chemical energy supplied to the system with the natural gas is equal to 1971 kW. In the reformer the chemical energy of the fuel is increased as a result of the reforming reaction. 753 kW of heat is supplied to the reformer from the flue gas of which 453 kW is used to increase the chemical energy (LHV) of the fuel from 1971 kW to 2424 kW for the reformed gas and 300 kW is used to increase the thermal energy of the fuel flow.

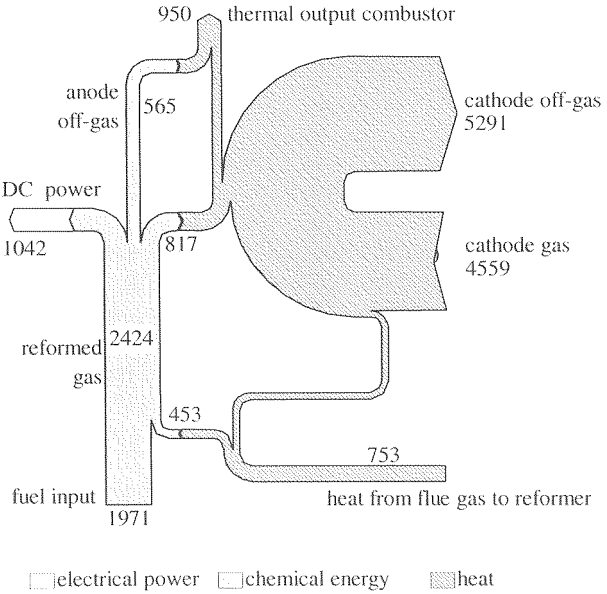

Figure 7.17: Sankey diagram for the fuel conversion with separated chemical and thermal energy [kW HHV] flows

Of the 2424 kW chemical energy which is supplied to the fuel cell 1859 kW is converted: 1042 kW is converted into DC-power and 817 kW into heat. In the combustor the remaining chemical energy (565 kW) is converted into heat. The heat released in the fuel cell is used to increase the temperature of the process flows, mainly the cathode flow. The figure shows the huge amount of heat which is transported through the fuel cell with the cathode flow.
The purpose of the 3 components, reformer, fuel cell and combustor, is to convert the chemical energy. Therefore it is logical to relate the size of the exergy losses in the 3 components to the chemical energy converted. In the given example the chemical energy converted in reformer, fuel cell and combustor is 453 kW, 1859 kW and 565 kW respectively. Using these as a reference the exergy loss in the fuel cell is approximately 8% of the converted chemical energy while the exergy loss in the reformer and the combustor amounts to resp. 18% and 22% of the chemical energy converted In the following sections the exergy losses for each of these components will be investigated in detail to clarify the differences in 'conversion efficiency'.

7.6.2. Losses in the fuel cell

In the fuel cell stack four types of losses occur:
- Heat transfer;
- Friction;
- Chemical reactions;
- Electrical losses.

In **Section 3.3** a method has been developed to calculate the contribution of each of these process to the total exergy loss.

Losses in the SOFC stack

Using this method the separate contributions were calculated for the SOFC stack (cf. table 7.9). The total exergy loss in the fuel cell stack amounts to 95.5 kW.

- The calculated losses in the chemical reactions are negligible in the external reforming fuel cell stacks. The two chemical reactions which are relevant are the reforming and shift reactions. The losses in the reforming reaction are small because the concentration methane in the anode gas is low. The shift reaction is almost reversible because the reaction is very fast.
- Heat is transferred from the electrode/electrolyte where the heat is generated to the process flows. In **Section 5.3.3** the calculation results from the detailed fuel cell model for the external reforming SOFC were reported. A very small temperature difference is calculated between the hardware and the anode flow as a result of the high H_2 content of the anode gas (and corresponding high thermal conductivity) and the relatively small flow. Between the electrolyte and the cathode flow the temperature differences are larger, but still limited to an average 10 K temperature difference. Consequently losses as a result of heat transfer in the fuel cell are very small (<2 kW). The higher value which is given for these losses in table 7.9 includes the heat losses from the fuel cell stack for which an estimated value of 2 % of the electrical power of the fuel cell has been used.
- Friction losses, mainly due to the use of the cathode flow to cool the cell, contribute a further 10 kW to the exergy losses.
- The largest part of the exergy losses however are the electrical losses or losses as a result of charge transfer. In the fuel cell stack polarisation and ohmic losses leads to an exergy loss of 67.7 kW which is more than 70 % of the total exergy loss in the fuel cell stack.

Figure 7.18 shows the f,H-diagram of the process in the fuel cell stack. The Carnot factor f is defined as a generalized exergy/energy ratio in **Chapter 3**. Characteristic is that the areas in this figure correspond to exergy flows or losses. In the diagram in figure 7.18 the upper curve is the Carnot factor for the process flow. As shown in **Section 3.5** the Carnot factor can be calculated by:

$$f_p = 1 - T_0 \frac{dS}{dH}$$

The area between the x-axis and the curve (f_p) is equal to the change in exergy of the anode and cathode gas flow over the fuel cell. The exergy is recovered both in the form of heat and in the form of electrical power. The Carnot factor for the power indicates which part of the heating value in the fuel is converted into power:

$$f_{el} = \frac{dP_e}{dH}$$

Because this is proportional to the cell voltage (see **Section 4. 4**) this value does not change as the reaction proceeds. The second area in figure 7.18 (f_Q) corresponds to the exergy of the heat which is generated:

$$f_Q = (1 - \frac{T_o}{T})$$

The hatched area corresponds to the total exergy loss. Finally the sum of the three areas is the decrease of the exergy of the process flows (anode + cathode), i.e. the 'converted' exergy. The An important fact that can be seen from the f,H-diagram is that the exergy loss (the hatched area in figure 4.18), compared to the 'converted' exergy, is relatively small (approximately 5%). Furthermore the diagram shows that the high efficiency of the fuel cell is not due to the high efficiency of the direct conversion of chemical energy in to electrical power alone. From the figure the exergy efficiency of the direct conversion to electrical power can be seen to be slightly higher than 50%. But the main reason that the efficiency of the fuel cell is that the heat which is generated in the fuel cell stack is of high temperature and consequently has a high exergy value as well

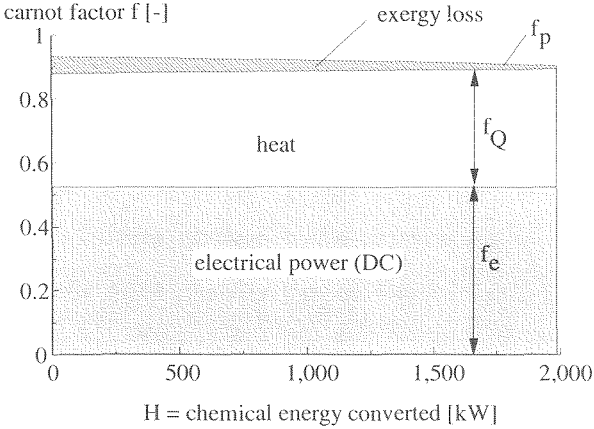

Figure 7.18: f,H-diagram for the external reforming SOFC in which the areas correspond to the exergy losses, the exergy of the chemical energy converted into heat and the exergy of the produced electrical power

Losses in the MCFC stack

In the MCFC exergy losses occur as result of the same driving forces as the in the SOFC: heat transfer from the electrolyte to the anode and cathode flow, friction losses in both flows, chemical reactions and polarisation. The total exergy loss in the fuel cell stack in the external reforming MCFC system are equal to 111.6 kW (table 7.8). The losses as a result of chemical reactions, heat transfer and polarisation were again determined using the detailed fuel cell model.

- Heat transfer in the fuel cell stack contributes only 2.6 kW to the exergy losses.
- The exergy losses as a result of chemical reactions are again negligible.
- Losses as a result of friction are 50% higher than for the SOFC (14.3 kW vs. 10 kW). The temperature difference ΔT over the stack is higher for the SOFC (100 K for the MCFC, 150 K for the SOFC). As a result the flow of cathode gas required to cool the stack is

higher and consequently losses as a result of friction are higher.

- Again the exergy losses as a result of electrical charge transfer (polarisation and ohmic losses) are by far the most important cause of exergy loss and leads to an exergy loss equal to 94.5 kW.

The f,H-diagram for the MCFC system is shown in figure 7.19. The two (almost) rectangular areas correspond to the exergy of the electrical power and heat which is generated, the hatched area to the exergy loss. In general the f,H-diagram for the MCFC and the SOFC stack (figure 7.19) are very similar. It is interesting to note some differences.

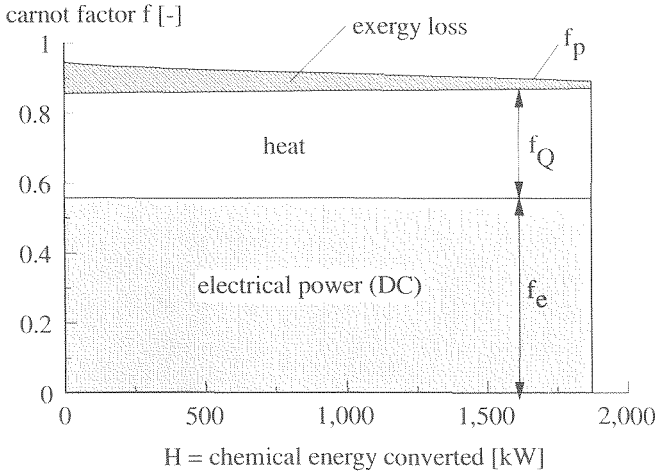

Figure 7.19: *f,H-diagram for the external reforming MCFC representing the exergy losses and the exergy of the produced heat and electrical power*

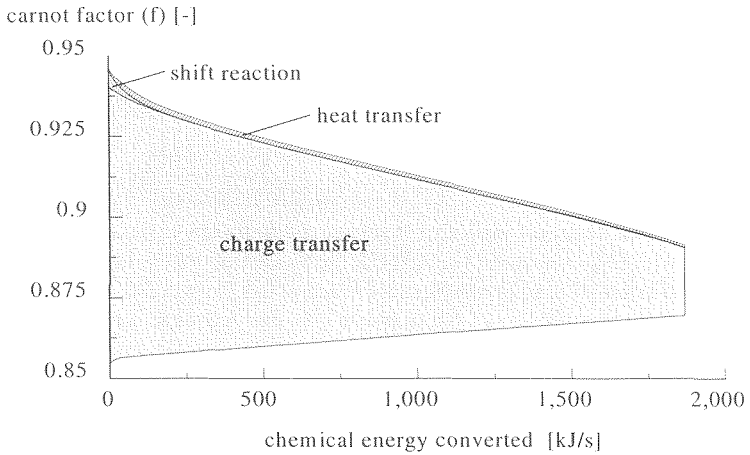

Figure 7.20: Representation of the exergy losses in the f,H-diagram for the external reforming MCFC (detail of figure 7.19)

The direct conversion of chemical energy into electrical power is slightly higher in the MCFC due to the higher cell voltage. The exergy value of the heat is different as well. The most important factor is the operating temperature. In the SOFC stack the heat is released at approximately 925 °C, while the average temperature at which the heat is generated in the MCFC is 650 °C. The lower exergy value of the heat as is apparent comparing both f,H-diagrams.
The exergy losses in the MCFC stack exceed the losses in the SOFC stack. There are two reasons for this higher loss. The first is the lower temperature and consequently the lower value of the heat which is produced in the electrochemical reaction. For all conversion processes in the fuel cell the exergy loss is proportional to T_o/T, which can be considered as the factor which indicates how much 'lost work' is recovered (see **Section 3.2**). Due to this effect the same polarisation or chemical reaction will lead to larger losses at the lower average temperature of the MCFC than in the SOFC. The largest difference between MCFC and SOFC is the size of the polarisation losses. Even though a larger cell voltage is assumed for the MCFC stack, the increase in the cell voltage is not as large as the increase of the driving force for the electrochemical reaction, the Nernst voltage. The net effect of the lower temperature in the MCFC is therefore a higher voltage drop and correspondingly higher exergy losses as a result of polarisation at lower temperature. In figure 4.20 the exergy losses in the MCFC are shown in detail in the f,H-diagram. The losses shown in this diagram are the losses as a result of charge transfer and the small contribution of exergy losses as a result of chemical reactions and heat transfer.
The decrease of the exergy losses from inlet to outlet has three causes. The first cause is that the rate of the electrochemical reaction decreases as the fuel and oxidant become (to some extent) depleted towards the outlet of the cell thus decreasing the driving force (i.e. the Nernst voltage). Secondly the polarisation resistance and Nernst voltage depend strongly on the temperature which increases toward the outlet. This leads to a decrease of the exergy losses as a result of electrical charge transfer. Finally the higher temperature at the outlet of the cell also leads to a lower exergy loss because the heat developed as a result of polarisation has a higher exergy content due to the higher temperature (the loss factor T_o/T). The graph shows that the efficiency of the processes is higher near the outlet than near the inlet.

7.6.3. Losses in the reformer

In the reformer methane and higher hydrocarbons are converted into a CO and H_2 rich mixture by steam reforming. The equilibrium temperature at the end of the catalyst bed in the reformer, in order to achieve a sufficiently high conversion of methane, has to be approximately 800 °C. A 50 K temperature approach is used to take into account the kinetics of the steam reforming. The temperature at the outlet of the reformer bed is therefore equal to 850 °C. This corresponds to the inlet temperature of the anode flow to the fuel cell stack in the SOFC system calculation. Therefore if the product gas is supplied to the fuel cell directly, i.e. at the temperature at which it leaves the reformer bed, no further heat exchangers are required between the reformer outlet and the anode inlet in the SOFC system. Furthermore in the SOFC system the temperature difference between the flue gas flow and the product gas is very large. Therefore for the SOFC system a simple single-pass reformer is most suited. This is the type of reformer most like the conventional reformer for hydrogen production [Pietrogrande]. The process in the reformer bed for the MCFC system is the same as for the SOFC system, with an inlet temperature of 400 °C and an outlet temperature of 850 °C. In the MCFC system, however, the inlet temperature of the anode off-gas is much lower (600 °C). Secondly the temperature difference between product flow and flue gas is smaller because of lower

operating temperature of the fuel cell. In the reformer for the MCFC system part of the thermal energy of the product gas is recovered in counter-flow with the reformer bed. In the calculation the outlet temperature of product gas from the reformer is the same as the inlet temperature for the fuel cell to minimise the use of (high temperature) heat exchangers. This type of reformer, in which part of the heat from the product gas is recovered, is similar to the type of reformer developed for fuel cell applications (PAFC, MCFC) ([Laursen, 1994],[Togari, 1990], [Uematsu, 1994]). For the two types of (external reforming) fuel cell system, two separate types of reformers are therefore uses. The models for both types of reformers are described in **Appendix 3**.

Exergy losses in the reformer have different causes:

- Heat transfer;
- Friction;
- Mixing;
- Chemical reactions.

In **Section 3.3** a method is developed to calculate the contributions of each of these types of exergy losses separately. It is shown that it is possible in some cases to separate the exergy losses by 'sequential modelling', i.e. by considering processes to occur one after another. For the reformer the losses resulting from the friction (pressure losses) and the losses as a result of mixing steam and natural gas can be separated from the total exergy losses by sequential modelling. The situation is different for the losses as a result of heat transfer and chemical reactions. To separate these losses it is necessary to know the concentration and temperature profiles. However, a black box model for the reformer is used in the system calculation. To calculate the exergy losses as a result of heat transfer and as a result of chemical reactions therefore a separate, more detailed, model was used. This model is described in **Appendix 3.** Using the results from the calculations with the detailed model, the separate contributions of heat transfer and chemical reactions to the exergy losses are calculated.

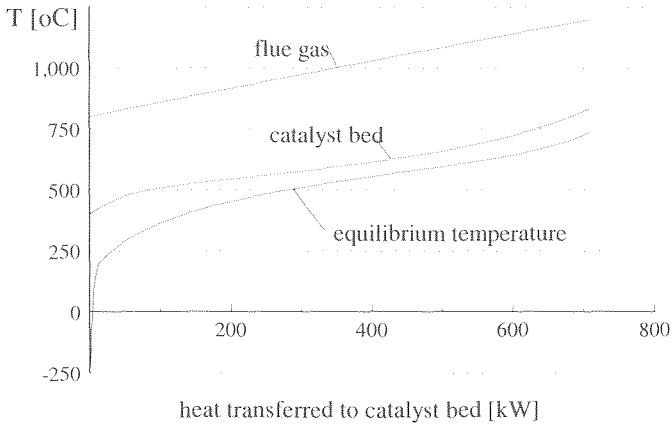

Figure 7.23: Calculated temperature profiles including the equilibrium temperature for the reformer in the base case SOFC system (see appendix 1)

Losses in the once-through reformer (SOFC system)

In the SOFC system the heat required for the reforming reaction is obtained by cooling the flue gas from the combustor. The temperature of the flue gas at the outlet of the combustor is 1200 °C. Product side the steam and natural gas are supplied at 400 °C and leave the reformer

at 850 °C. Based on the specified temperatures and the calculated mass flows a temperature of the flue gas at the outlet of the reformer of 802 °C is calculated. The large driving temperature difference between catalyst bed and flue gas (approximately. 400 K), confirms the selection of the simple single pass reformer. The temperature profiles calculated with the detailed model are shown in figure 7.23.
The calculated concentrations have been used to calculated the equilibrium temperature (see **Section 3.4.4**) for the reforming reaction is also shown in the diagram. The difference between the equilibrium temperature and the actual bed temperature is indicated as the temperature approach and is a measure for the exergy losses. The equilibrium temperature can therefore be used to get a first estimate of the exergy losses in the reforming reaction. The exergy loss in the chemical reaction can be estimated from the temperature approach by assuming that the heat capacity of reactants and products is equal. In that case the exergy loss is equal to the exergy loss calculated with the general equation for exergy loss as a result of heat transfer (equation 3.1) with the ΔT equal to the temperature approach and Q equal to the heat of reaction. This is a reasonable approach if the temperature approach is not very large and enables us to estimate the ratio between heat transfer losses and losses as a result of chemical reactions directly from the Q,T-diagram.
The exergy losses estimated on basis of the Q,T-diagram using the equilibrium temperature coincide reasonably well with the calculated values for the exergy losses for the SOFC reformer. This can be seen in the f,H-diagram (figure 7.24). In this diagram the exergy losses as a result of heat transfer and the reforming reaction correspond to the area enclosed by the curves f_b, f_p And f_f. The curves and areas have been calculated with the equations derived in **Section 3.5.1** are shown. The upper curve is the exergy/energy ratio f for the heat transferred to the catalyst bed. If T_{fg} is the flue gas temperature, the Carnot factor for the heat from the flue gas is equal to:

$$f_{fg} = 1 - \frac{T_o}{T_{fg}}$$

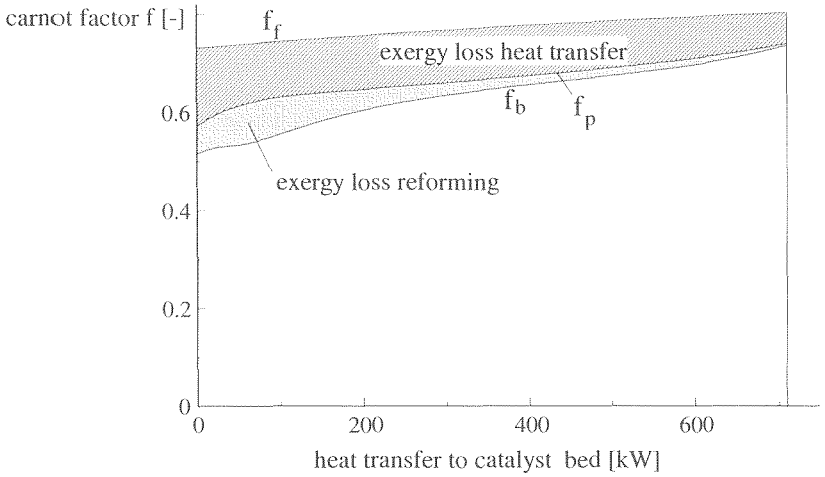

Figure 7.24 f,H-diagram for the reformer in the base case SOFC system distinguishing the losses as a result of heat transfer and as a result of the reforming reaction

The lower curve is the Carnot factor for the product flow f_p. This ratio is calculated from the enthalpy and entropy for the product flow in the catalyst bed:

$$f_p = 1 - T_o \frac{dS}{dQ}$$

where dS is the entropy increase of the product flow and dQ=dH is the heat transferred to the product flow. The area below this curve is the increase of the exergy of the product flow. If the lower curve (f_p) represents the increase in exergy of the product flow and upper curve (f_{fg}) the corresponding decrease of the exergy of the flue gas flow, then the area between the two curves is equal to the total exergy loss This total loss can be considered as having two causes:

- The heat which is used to drive the process is obtained at a temperature higher than the actual process ($T_f > T_b$), which leads to exergy losses as a result of heat transfer;
- The reforming reaction is irreversible, leading to exergy losses as a result of chemical reactions.

To distinguish these two types of losses in the diagram, a second curve has been drawn which represents the Carnot factor of the heat that is absorbed by the process flow in the catalyst bed *at the bed temperature* T_b:

$$f_b = 1 - \frac{T_o}{T_b}$$

The area under this curve is the exergy of the heat absorbed by the bed. Consequently the area between this curve f_b and the upper curve for f_{fg} is equal to the exergy loss as a result of heat transfer from the flue gas to the catalyst bed. The area between the lower curve (f_{prod}) and the middle curve (f_b) is equal to the exergy loss as a result of the reforming reaction.
Evidently the losses in the chemical reaction are much lower than the losses resulting from heat transfer (25.6 and 71.6 kW respectively, cf. table 7.9). The f,H-diagram for the reformer clearly shows that the exergy losses as a result of chemical reaction occur mainly in the beginning of the process where the driving force for the chemical reaction is large, while the reaction is nearly at equilibrium in the last part of the reformer bed, leading to much smaller losses. Moreover, as the temperature increases the kinetics of the reaction become much faster and the losses as a result of the chemical reaction decrease rapidly. The exergy losses as a result of heat transfer are high during the whole process. At the outlet of the catalyst bed the temperature of the flue gas is high (1200 °C). But the temperature difference between flue gas and catalyst bed is also high (see figure 7.23). Near the inlet the temperature difference between the flue gas and the catalyst bed is somewhat lower, but the absolute temperature is lower as well. Therefore the exergy losses as a result of heat transfer are almost constant over the reformer.

Losses in the recuperative reformer (MCFC system)

In the MCFC is that exergy losses occur as result of heat transfer from occur as a result of heat transfer to the bed from both the flue gas and from the return flow (see **Appendix 3** for a description of the recuperative reformer). The total exergy loss for the reformer is 80.6 kW corresponding to 4.0 % of the exergy input to the system. This is substantially lower than the losses in the SOFC reformer. The losses that occur when steam and fuel are mixed are 15.6 kW and the losses as a result of friction are 6.0 kW. These losses are approximately equal to the corresponding losses in the SOFC reformer. Therefore the difference between the two

types of reformers lies in the losses as a result of heat transfer and chemical reactions. In the MCFC reformer the losses as a result of heat transfer are 46.7 kW and the losses in the reforming reaction are 15.0 kW. It is interesting to note that although the sum of these losses decreases strongly, the ratio between both types of losses is approximately 75:25 in both cases.

To calculate these exergy losses as a result of heat transfer and as a result of the chemical reactions separately, again use has been made of the reformer model described in the appendix. The calculated temperature profiles are shown in figure 7.25. The temperature profile (T vs. Q) for the catalyst bed is shown twice. The first part of the graph represents the heat transfer from the return flow which is cooled from 850 °C (the outlet temperature of the catalyst bed) to 515 °C (pipe 43, table 7.9). The heat is supplied in counter-flow to the catalyst bed in which the temperature increases from 400 °C at the inlet to 850 °C at the outlet. Again the equilibrium temperature has been calculated and plotted as well. The second part of the graph represents the heat transfer from the flue gas to the same catalyst bed. Evidently the larger part of the heat supplied to the catalyst bed comes from the flue gas.

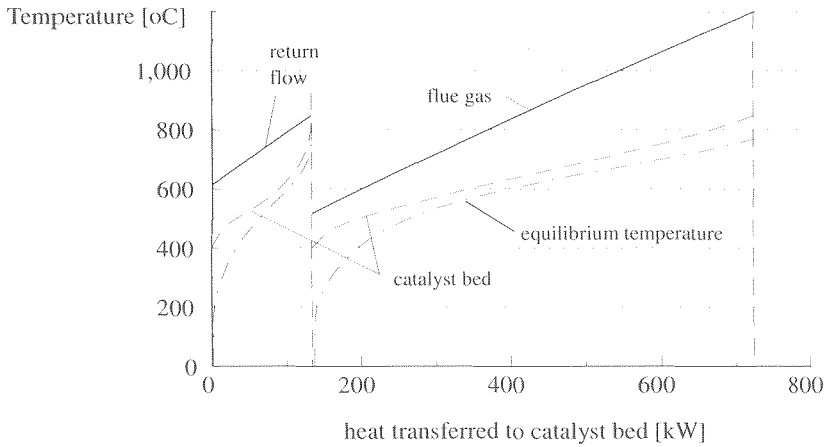

*Figure 7.25: Calculated temperature profiles including the equilibrium temperature for the reformer in the base case MCFC system (see **Appendix 3**)*

The f,H-diagram can again be used to compare the losses as a result of heat transfer and chemical reactions. In this case, the bed receives heat from two sources, the flue gas and the return flow. Correspondingly two exergy/energy ratios are calculated for the heat which is supplied. If T_{rf} is the return flow temperature, the exergy/energy ratio for the heat from the return flow is equal to:

$$f_{rf} = 1 - \frac{T_o}{T_{rf}}$$

If β is the ratio between the heat from the flue gas to the bed and the heat from the return flow to the bed, then the effective exergy / energy ratio for the energy flows f_c is equal to:

$$f_c = \beta f_{fg} + (1 - \beta) f_{rf}$$

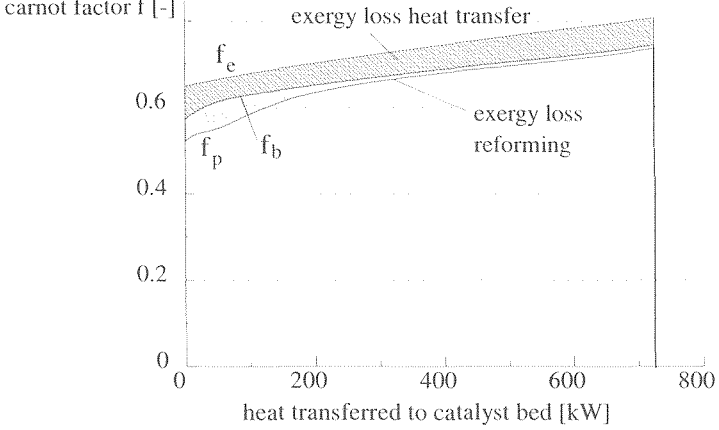

Figure 7.26 f,H-diagram for the reformer in the base case MCFC system distinguishing the losses as a result of heat transfer and as a result of the reforming reaction

Using this value for f_e which is a weighted average of the flue gas and return flow Carnot factor, the f,H-diagram shown in figure 7.26 results. The exergy losses as a result of the chemical reactions in the reformer show the same pattern as in the once-through reformer. At the inlet of the bed the rate of reaction is low. As the temperature increases, the rate of reaction increases as well. Due to the large driving force (the temperature approach), the exergy losses in the chemical reaction are large. The equilibrium temperature approaches the actual bed temperature very quickly (figure 7.25) and as a result the losses in the chemical reaction become small. Heat transfer losses are again distributed relatively evenly in figure 7.26

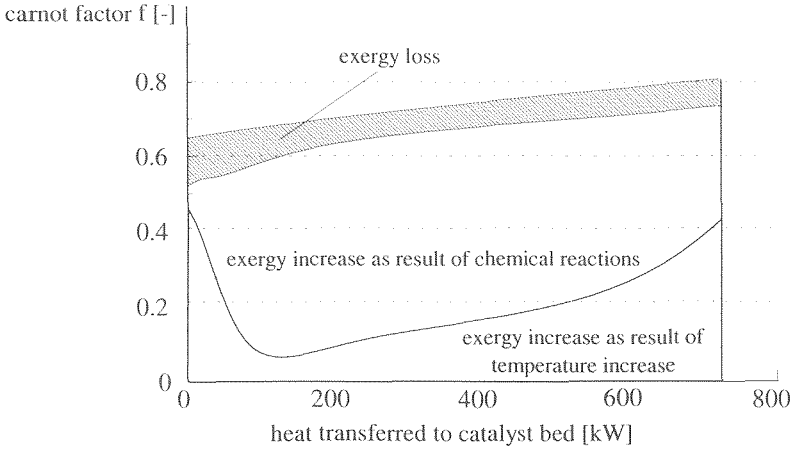

Figure 7.27 f,H-diagram for the reformer in the base case SOFC system the total exergy losses and the exergy increase of the process flow

shown. Initially the rate of reaction is low and all heat supplied to the catalyst bed is used to heat the process flow. As the temperature increases the reaction rate increases very quickly and the larger part of the exergy increase is due to the chemical reactions.

7.6.4. Losses in the combustor

In the combustor losses occur as a result of the combustion reaction, friction and mixing of oxidant and fuel. The combustion process was modelled as described in **Section 3.3** using a sequential model to separate friction, mixing and chemical exergy losses. The result is shown in figure 7.28.

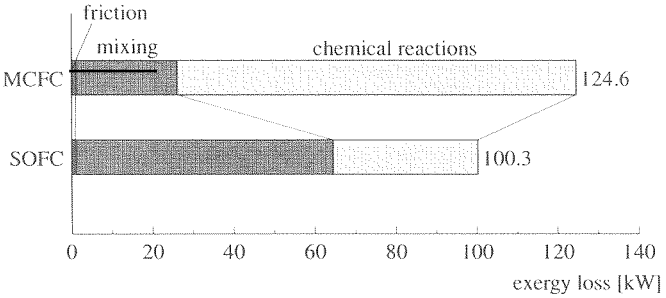

Figure 7.28: Exergy losses per type in the combustor for the two base case systems

The chemical reactions appear to be the most important cause of exergy losses in the combustor in the MCFC system. Surprisingly, the exergy losses as a result of the chemical reaction are much smaller in the combustor of the SOFC system, where the losses as a result of mixing are dominant.
In the combustor in the MCFC system the exergy losses due to the chemical reaction in the combustion process are 98.6 kW on a total of 124.6 kW. Mixing losses constitute the larger part of the remaining losses 24.9 kW while friction losses are responsible for only a small fraction of the losses (1.1 kW). In the SOFC system the total exergy losses are 100.3 kW of which 63.4 kW are due to isothermal mixing, 35.9 kW due to the chemical reactions and the remaining 1.1 kW as a result of friction.
The difference in losses as a result of mixing between the two calculations (SOFC and MCFC), lies in the oxidant stoichiometry. For both combustors a temperature at the outlet has been specified (1200 °C). In the MCFC system the fuel utilisation is calculated from this temperature: if the combustor outlet temperature is too low, more anode off-gas has to be burned in the combustor and consequently a lower conversion in the fuel cell is selected. The amount of air to the combustor is calculated from the prescribed air stoichiometry of 1.1. In the SOFC system cathode off-gas is used which has a temperature of 1000 °C. Therefore to achieve the required temperature only an 200 K temperature increase in the combustor is necessary. The fuel flow is now fixed and the air flow (i.e. the stoichiometry) is calculated from the outlet temperature, which results in a much higher oxidant stoichiometry equal to 8. The mixing losses in the SOFC system are therefore much higher simply because the oxidant flow is several times as large as in the case of the MCFC system.
The difference between exergy loss in the chemical reaction in the SOFC and the MCFC system has several causes. The exergy loss in the chemical reaction can be considered as the

result of the difference in equilibrium temperature (for the given composition and pressure) and actual temperature of the process flow (**Section 3.4.3**). For the SOFC system these two temperatures are shown. To construct this graph, the reaction has been considered to occur in a premixed flow and the temperature of the flow has been calculated assuming an adiabatic process[g]. The inlet flow consists of a mixture of anode and cathode off-gas or air. As a result of the reactions in the preceding fuel cell, the reactant flows have been 'diluted'. The dilution of the reactants leads to a smaller driving force. The driving force can be expressed as the exergy change of reaction (see **Section 2.3.2**). For hydrogen for example this is given by (see equation 2.38):

$$\Delta e_r = \Delta e_r^{o} + RT_o \ln \frac{p_{O_2} p_{H_2}}{p_{H_2O}}$$

The second term represents the influence of the partial pressures on the exergy of reaction. Evidently as the reactant concentrations decrease, the same is true for the driving force (Δe_r)[h]. This trend is apparent in figure 7.29. Note however that even at the start of this curve the reactants partial pressures correspond to the fuel cell outlet and therefore the largest part of the fuel has already been converted.

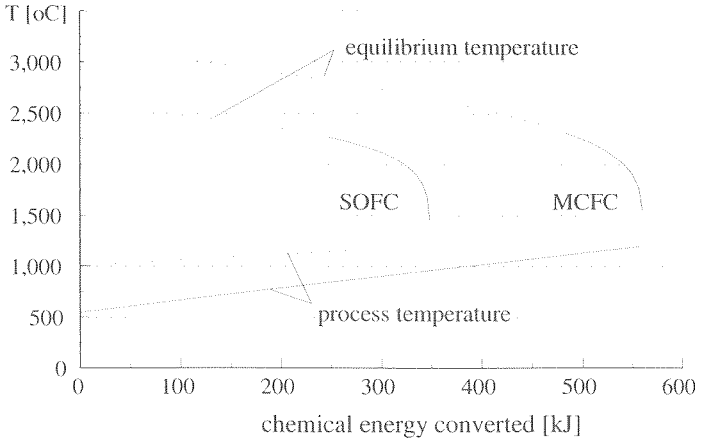

Figure 7.29: Equilibrium and process temperature assuming premixed and adiabatic combustion for the combustor in the SOFC and in the MCFC system

For the MCFC the fuel utilisation in the fuel cell stack is lower and consequently the partial pressures of the reactants (H_2, CO) are higher. As shown in figure 7.29 the equilibrium temperature is higher in the combustor in the MCFC system.
The exergy losses are determined by the actual process temperature as well as the equilibrium temperature. Where a low equilibrium temperature is advantageous with regard to the exergy losses, a high process temperature leads to low exergy losses. The low losses in the chemical reactions in the combustor in the SOFC system are due to the low reactant partial pressures

---

[g] the equilibrium temperature in the range >2500 °C is represented by a dotted line as the data used for calculation of the reaction entropy and enthalpy are accurate only below this temperature

[h] the analogy with the fuel cell, where the Nernst voltage decreases as the reaction proceeds, is clear.

(low equilibrium temperature) because of the high fuel utilisation in SOFC. The high 'pre-heat' temperature of 1000 °C (i.e. a high process temperature) is advantageous as well. Combined this results in a very efficient combustion reaction.

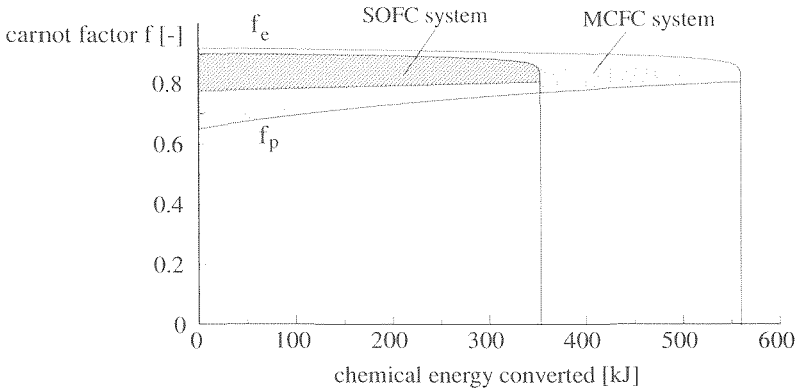

Figure 7.30: f,H-diagram for the combustor in the SOFC and in the MCFC system assuming premixed and adiabatic combustion

The temperature (of the fuel/oxidant mixture) at the inlet of the combustor in the MCFC system is 550 °C, i.e. much lower than the corresponding temperature in the SOFC system. Combined with the higher equilibrium temperature this leads to the substantially higher exergy losses as a result of chemical reaction shown in the f,H-diagram in figure 7.30.

CHAPTER 8
ANALYSIS OF SOFC CONFIGURATIONS

8.1 INTRODUCTION

Analysis of the SOFC configuration in the previous chapter demonstrated the importance of reducing the exergy losses as a result of heat transfer in order to increase the efficiency of the system. It also showed that, given the configuration used in the reference calculation, the amount of heat which has to be transferred is very large. This is the main reason for the large contribution of exergy losses as a result of heat transfer. Priority in optimising the fuel cell system therefore lies in reducing the amount of heat which is transferred. The main reason for the high losses as a result of heat transfer is the cell cooling concept. Given the limited allowable temperature increase of the process flows between the inlet and outlet of the stack, the mass flow air is dictated directly by the amount of heat which has to be removed from the stack. Given the temperatures used in the reference calculation, the amount of heat which has to be supplied to the air to preheat the flow to the inlet temperature of the fuel cell stack is 5 to 6 times the amount of heat that can be removed from the stack by the air flow. In other words, 5 to 6 times more heat is transferred in preheating the "coolant" than in the actual cooling process. In this chapter options for reducing the exergy losses in the SOFC system as a result of heat transfer are considered. The efficiency and losses are calculated and analysed for different configurations.

Section 8.2 evaluates the effect of using a recycle for the cathode off-gas on the heat transfer and performance of the system. Although this increases the amount of power which could potentially be recovered in the system, all this energy is converted into low temperature heat. In **Section 8.3** the pressurised system is considered in which part of this heat can be converted into electrical power. Instead of utilising the heat more effectively, it is also possible to decrease the amount of heat which is generated in the fuel cell. To achieve this the fuel utilisation can be increased. This approach is used in **Section 8.4**. Another option to reduce the heat generation in the fuel cell is the use of internal reforming. The internal reforming system is analysed in **Section 8.5**. The combination of pressure and internal reforming is considered in **Section 8.6**.

8.2 SOFC SYSTEMS USING A CATHODE OFF-GAS RECYCLE

8.2.1 Description of system and calculations

The most effective solution is to recycle part of the cathode gas. This was suggested for MCFC systems by ERC in an early systems study for EPRI [Patel,1983]. An extensive systems study for the EU [Dicks, etal., 1990], demonstrated this to be very effective for SOFC systems as well. The principle of a cathode off-gas recycle is two-fold. Firstly, the cell is now only partially cooled by the fresh air flow: part of the cooling is provided by the cathode recycle flow which has been cooled down from the fuel cell stack outlet temperature to the inlet temperature. As a result, the amount of air which has to be preheated is strongly reduced. The second benefit of a cathode off-gas recycle is that part of the preheating can be

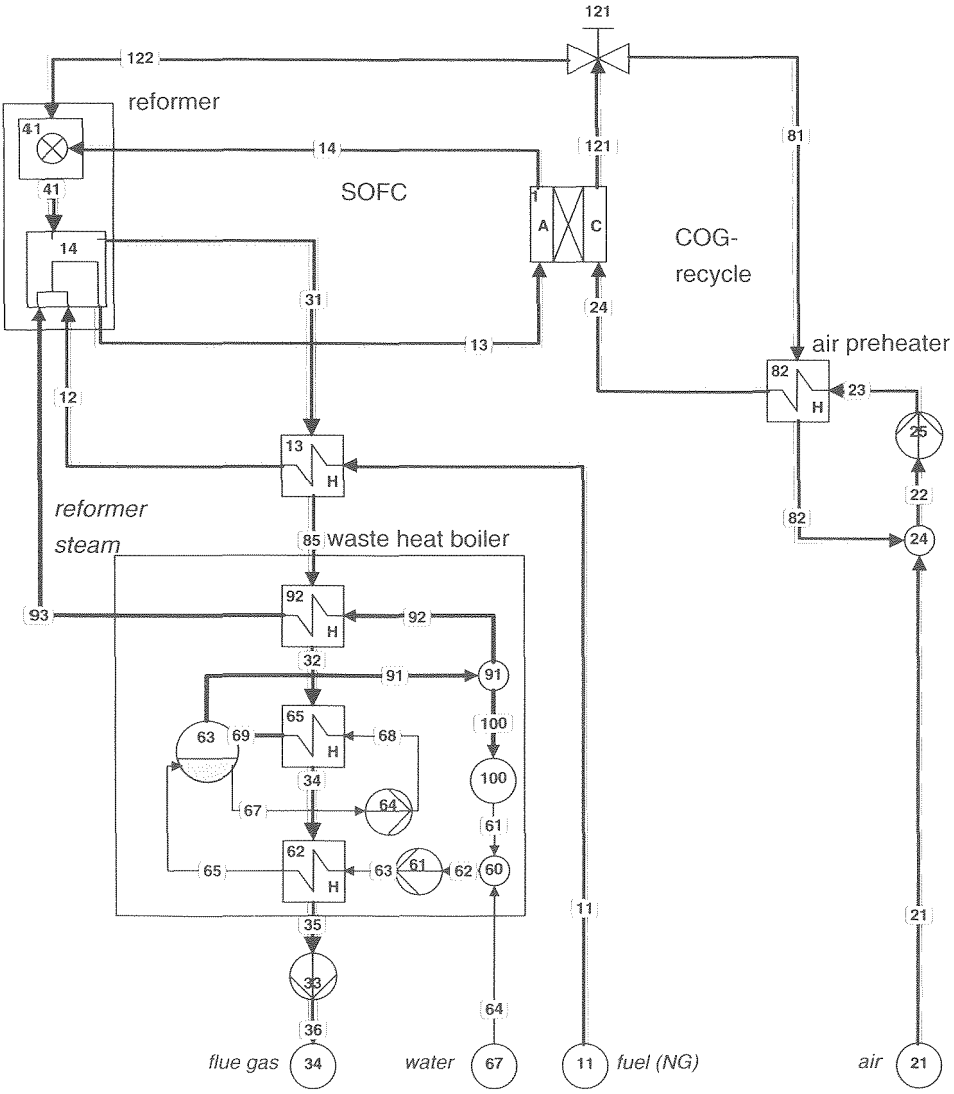

Figure 8.1: Process flow diagram for the ER-SOFC system with cathode off-gas recycle (sr1)

achieved simply by mixing the hot recycle flow with the cold air. This reduces the heat exchanger area which is required considerably. Depending on the temperature at which the recycle blower operates, different types of recycle systems are possible. **Appendix 10** gives an overview of some of these options. All recycle options considered here are is based on an inlet temperature of the recycle blower of 450 °C. Therefore the hot cathode off-gas has to be cooled to this temperature prior to the recycle blower.

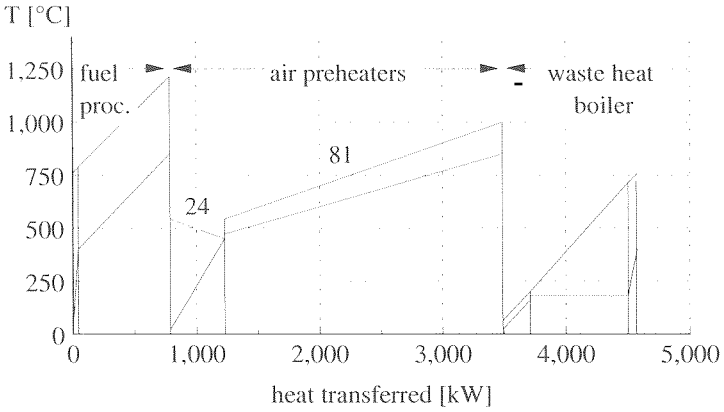

Figure 8.2: Q,T-diagram for the SOFC system with cathode gas recycle

The most basic recycle configuration is shown in figure 8.1. In this configuration part of the cathode off-gas (cog) recycle (stream 81) is cooled and is mixed with the incoming air (stream 21). The mixed flow passes through the recycle blower. To achieve the required inlet temperature of 450 °C for the recycle blower (app. 25), the recycle flow has to be cooled down from 1000 °C to 543 °C prior to mixing with the fresh air. As can be seen in the Q,T-diagram for this configuration in figure 8.2, the temperature difference between the hot and cold flow in the air preheater in the system with recycle (app. 81) is much lower than in the base case system. Although the benefit is of course that exergy losses are small, transferring the heat with a the small temperature difference will require a large and costly heat exchanger. Air preheater (81) is critical as it transfers a large amount of heat (Q) at a small (logarithmic) temperature difference $\Delta T_{log.}$ The heat exchanger area depends on the overall heat transfer coefficient U, the transferred heat Q and the logarithmic temperature difference ΔT_{log} following the equation:

$$A = \frac{Q}{U \, \Delta T_{log}} \qquad (8.1)$$

The cathode gas must be preheated to 850 °C and the cathode off-gas flow has a temperature equal to the outlet temperature of the fuel cell stack (1000 °C). The temperature difference at the hot side of heat exchanger (81) is therefore fully determined by the fuel cell conditions (150 K). Because only part of the cathode off-gas is recycled, the recycle is a smaller flow than the cathode gas flow to the fuel cell. The smaller heat capacity of the recycle flow compared to the cathode gas results in a temperature difference at the cold end of the heat exchanger of approximately 100 K. This leads to a large heat exchanger. Therefore other configurations have been considered as well. Increasing the operating temperature of the recycle blower and increasing the temperature difference over the fuel cell stack will increase the average temperature difference in the air preheater, but this require different technologies for the blower and fuel cell respectively. Two other configurations have been considered in which the temperature difference in the heat exchanger becomes larger. One option (sr1, figure 8.3) is to extract heat from the recycle flow by using the cathode off-gas. As shown in **Appendix 11**, extracting heat from the recycle leads to a higher recycle ratio and consequently to the required larger temperature difference. In configuration sr2 this has been achieved by using heat from the cathode off-gas recycle to preheat the fuel and steam as well

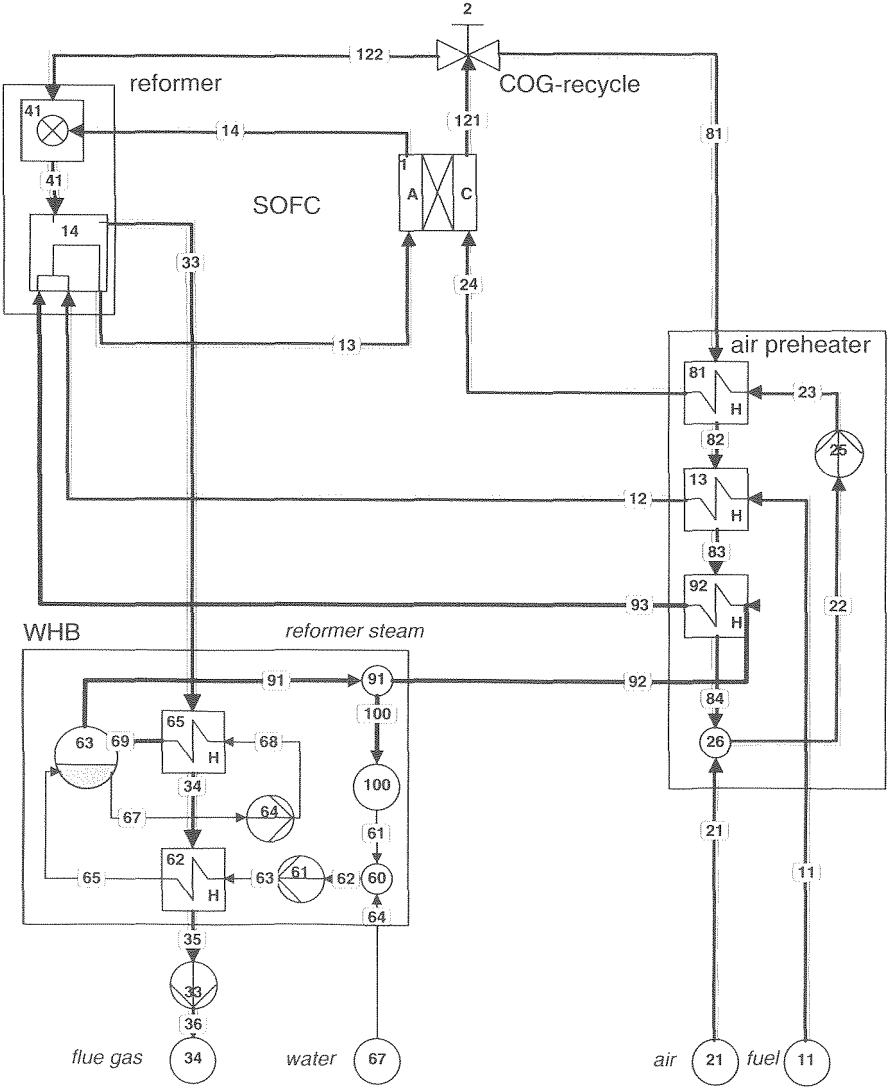

Figure 8.3: Process flow diagram for the ER-SOFC system with cooled cathode off-gas recycle (sr2)

as the incoming air In the other configuration (sr3, figure 8.4) all the cathode off-gas is supplied to the preheater, making the mass flows on both sides of the air preheater approximately equal. To prevent that the temperature in the combustor becomes too low, the cathode off-gas flow to the combustor is not cooled down completely. The air preheater is split in two heat exchangers. The heat capacities on both sides of the heat exchanger are now approximately equal leading to a constant temperature difference between both flows in heat

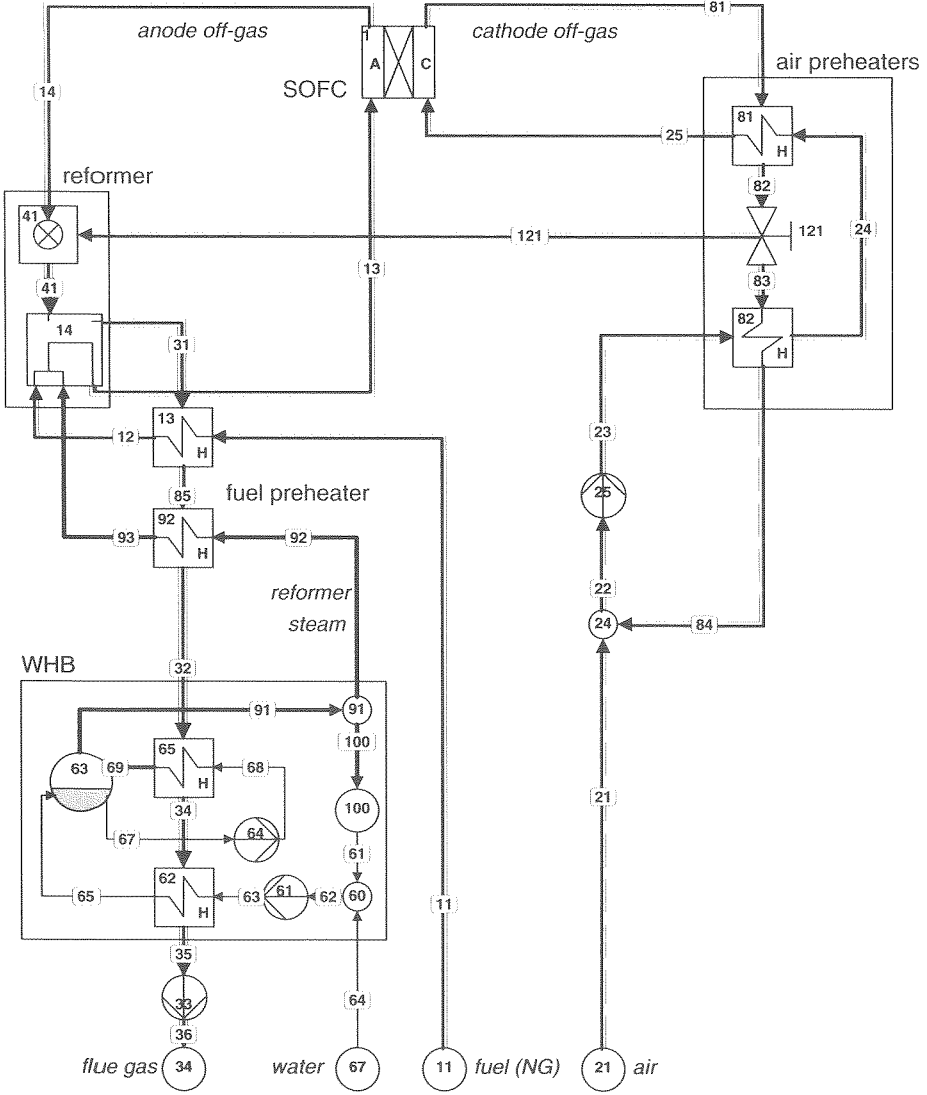

Figure 8.4: Process flow diagram for the SOFC external reforming system with cathode off-gas split in the recycle (sr3)

exchanger 81, as can be seen in the Q,T-diagram (figure 8.5). In heat exchanger 81 the cathode off-gas is cooled down to 850 °C. Subsequently the cathode off-gas is split into a flow to the combustor and a flow to the second air preheater (82). To achieve the required combustion temperature, the value selected for the intermediate temperature is 850 °C. As the Q,T-diagram for this system shows (figure 8.5), the temperature difference at the cold end of the preheaters (app. 81 and 82) is larger than in configuration sr1 (cf. figure 8.2).

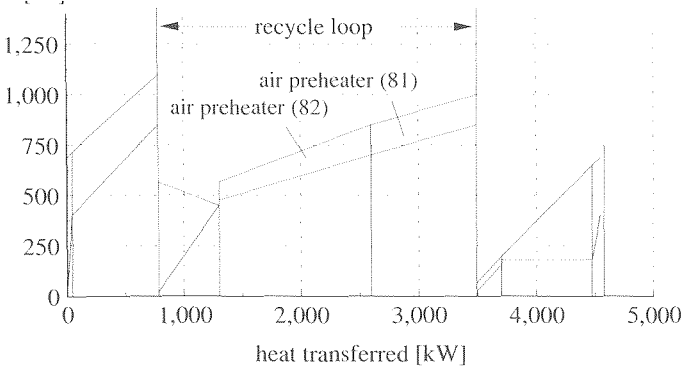

Figure 8.5: Q,T-diagram for calculation sr3 (recycle and integrated air preheater)

Using equation (8.1) the total heat exchanger area[i] required has been estimated for the three systems with recycle (sr1, sr2, sr3) relative to the base case calculation (se). The result is shown in figure 8.6. The heat exchanger area required for the configuration with recycle is almost 50 % lower than for the reference configuration. But further reduction of the heat exchanger area is possible by rearranging the heat exchangers in the system (e.g. in configuration sr3).

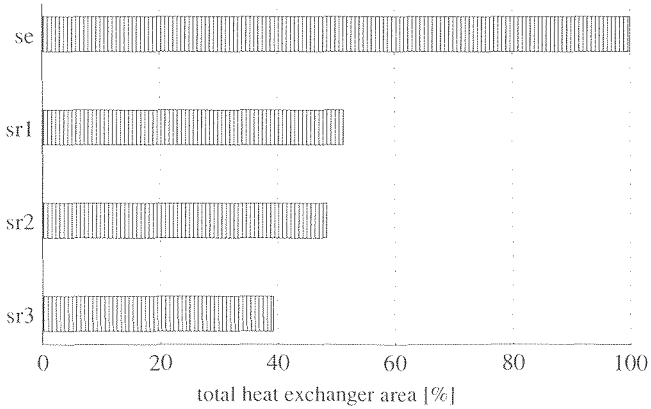

Figure 8.6: Estimated total required heat exchanger area for the different configurations (relative to the base case se) calculated using equation (8.1). Heat transfer coefficients based on [Klapp, 1980].

8.2.2 Energy analysis

Figure 8.7 shows the net and gross electrical efficiency and total efficiency for the four configurations. The specific definitions of each efficiency (gross vs. net, electrical vs. total) are given in **Section 7.3**. The graph clearly shows the difference between the reference

[i] heat exchanger area in the reformer is not included in the estimate

The total efficiency in the systems with recycle is substantially higher. On the other hand the electrical efficiency is lower in all configurations with a cathode off-gas recycle. The gross electrical efficiencies for these systems are between 1.2 and 1.9 %pt lower than the base case while the difference in net electrical efficiencies ranges from 2.0 to 4.2%pt. The differences between the calculated efficiency for the configurations with recycle (sr1, sr2 and sr3) are small. The key parameter in explaining the differences between the configurations in figure 8.7 is the recycle ratio.

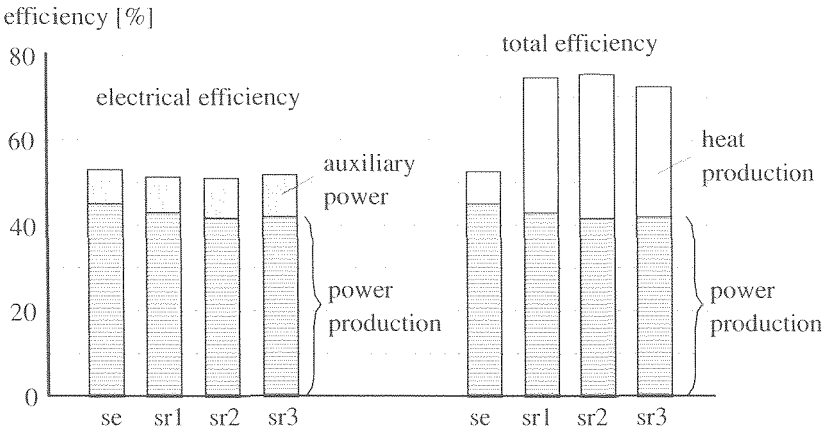

Figure 8.7: Calculated efficiencies for the system without recycle (se) and different arrangements of the heat exchangers in the cathode off-gas recycle loop (sr1...sr3)

The recycle ratio α (see **Appendix 11**) is defined as the ratio between the recycle flow (stream 121 in figure 8.1) and the cathode off-gas flow (stream 81). In the basic configuration with recycle (sr1) α is equal to 83%, i.e. only 17% of the cathode off-gas is fed to the combustor. Only 15% of the gas fed to the cathode is fresh air. However, the oxygen utilisation per passage[j] is only 18%. The resulting overall utilisation is equal to 58 %. The high recycle ratio does however lead to a much lower average oxygen concentration. The low oxygen utilisation in the reference case leads to an average concentration which is only little below the concentration in the fresh air (19.8% vs. 20.8% in the fresh air). At a recycle rate of 83% the average concentration drops considerably to 10.9 %. This leads to a smaller reversible or Nernst voltage in the system with recycle. The calculated cell voltage consequently decreases from 677 mV in the reference system (se) to 656 mV for the system with recycle (sr1).
Recycling cathode off-gas primarily influences the air flow. If cathode off-gas is recycled, the cell is cooled partially by recycle cathode off-gas and consequently the fresh air flow is reduced. As a result the flue gas flow is lower too. The corresponding smaller flue gas stack losses explain the a higher total efficiency in the systems with recycle. For the configuration without recycle (se) the mass flow cathode gas which cools the fuel cell is equal to

[j] The oxidant utilisation per passage is calculated by comparing φ_{O2} in the cathode inlet (stream 24 in figure 8.1) to φ_{O2} in the cathode outlet (stream 121)). The overall utilisation compares total φ_{O2} supplied to the fuel cell (stream 21) to discharge of the cathode off-gas recycle (stream 122).

0.171 kg/s. The cathode off-gas is mixed with the combusted anode off-gas. Therefore the flue gas flow is slightly higher (0.181 kg/s). The cathode flow in the system with recycle is higher than in the reference case due to the use of the recycle (0.180 kg/s in sr1 vs. 0.171 kg/s in the reference system). But the flue gas flow is much lower (0.045 kg/s in sr1). The lower electrical efficiency shown in figure 8.7 for the systems with recycle is due to two factors:

- The gross efficiency depends on the cell voltage, which is lower for the systems with recycle due to the lower average oxygen concentration at the cathode of the fuel cell stack. The difference in gross efficiency between the different configurations with recycle are small (from 51.2 to 51.9 %);
- The blower in the case of the reference system operates at environment temperature. If a recycle is used, the blower operates at higher temperature (450 °C) and therefore the duty is much larger than for similar pressure ratios at low temperature[k]. The net efficiencies for the systems with recycle vary more than the gross efficiency, because of the larger differences in auxiliary power. The highest net electrical efficiency is found for configuration sr1 (43.0 %) and the lowest for sr2 (41.7 %), while the net efficiency of the reference system is 45.1 %.

The differences in efficiency between the configurations with cathode off-gas recycle (sr1, sr2 and sr3) are relatively small and are determined mainly by the recycle ratio α. The recycle ratio in the system with heat extraction from the recycle (sr2) increases only slightly from 83 % to 85%. The limited increase is due to the fact that the amount of heat which is transferred to the fuel (app. 13) and the steam (app. 92) is relatively small as can be seen in the Q,T-diagram (figure 8.2) compared to the heat transferred in the air preheater. If the cathode off-gas is first cooled down before splitting the flow (calculations sr3), more heat remains in the recycle flow and therefore the recycle ratio decreases (**Appendix 11**). For sr3 α equals 79%.

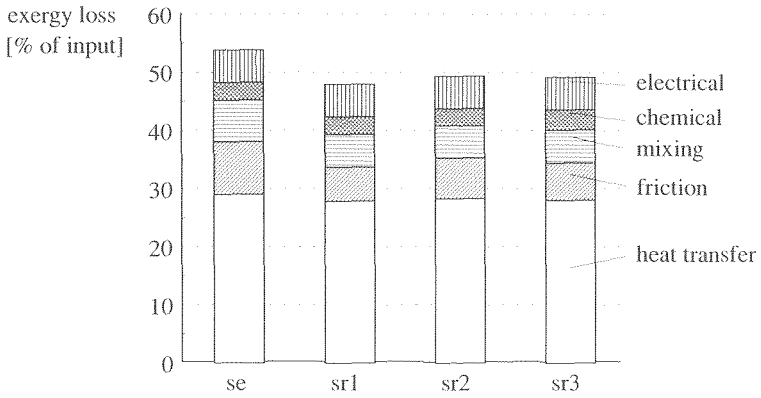

Figure 8.8: Calculated exergy losses per type of exergy loss for the system with (se) and without recycle (sr1...sr3)

[k] The pressure increase of the fresh air delivered by the recycle blower in the 4 calculated case. Although the compressor duty will be lower using a separate fresh air compressor, the potential reduction in auxiliary power is limited due to the low ratio fresh air / recycle flow

8.2.3 Exergy analysis

Figure 8.8 shows the exergy losses in the 4 configurations. Using the approach developed in **part I** a distinction is again made between the different types of losses. The losses are expressed as fraction of the exergy input. The figure shows considerably lower exergy losses for the systems with recycle (sr1 ... sr3). The exergy losses in figure 8.8 also include the losses flue gas stack losses and other energy flows to the environment. Therefore the sum of the exergy loss + exergy efficiency is equal 100%.The lower exergy losses shown in figure 8.8 for the systems with recycle correspond to an increase of exergy efficiency (relative to the base case se) ranging from 4.5 % for sr2 to 5.9 % for sr1.
Figure 8.8 shows that differences in exergy losses between the different configurations are determined by the differences in losses as a result of heat transfer and the losses as a result of friction. The contribution of the other causes is approximately the same for all 4 configurations. The exergy losses as a result of heat transfer are lower for the systems with cathode gas recycle. However, the influence is very limited, in particular compared with the amount of heat produced in the system (compare the total efficiency in figure 8.7).
For further analysis the exergy losses for the subsystems (again expressed as a fraction of the exergy input to the system) are shown in figure 8.9 for the reference calculation (se) and the basic configuration with recycle (sr1). In the fuel cell, the combustor and the fuel conditioning subsystem including the reformer (the components where the fuel is converted) the exergy losses are not or hardly influenced by the cathode recycle. The differences occur the air preheater/cathode off-gas recycle and the waste heat boiler (including the flue gas stack). The losses in the air preheater subsystem are more than 10 % lower in the system with recycle. However, the lower losses in the air preheaters are partially off-set by higher losses in the waste heat boiler.

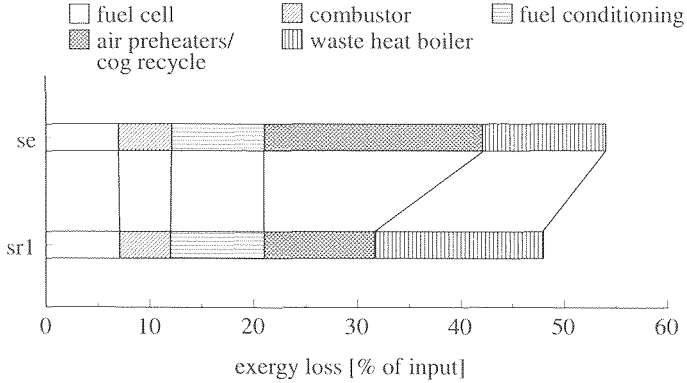

Figure 8.9: Comparison of the exergy losses per subsystem for the base case (se) and a system with recycle (sr1)

In figure 8.10 exergy losses as a result of heat transfer for both systems can be compared in more detail. In the value diagram the area enclosed between the two curves is equal to the exergy losses as a result of heat transfer (see **Section 7.5.1**). In this diagram the external losses (for example the sensible and latent heat in the flue gas) are not included. The losses in the high temperature heat exchangers are small in both cases (se and sr1) due to the high temperature at which the heat is transferred. Large losses occur in the low temperature air

preheater in the system without recycle (se). In the system with recycle (sr1), preheating the fresh air occurs with relatively high losses as well. This is due to the highly irreversible process of mixing the high temperature recycle and the cold air. However, due to the recycle, the amount of air which has to be preheated is much smaller. As a result, the exergy loss in the mixing process is approximately half of the loss in the first air preheater in system without recycle (sr1). In the medium and high temperature air preheaters, the average temperature difference in the system with recycle is much smaller than in the reference system. But because the exergy losses as a result of heat transfer are already relatively small at high temperature, this does not affect the total exergy losses as a result of heat transfer considerably.

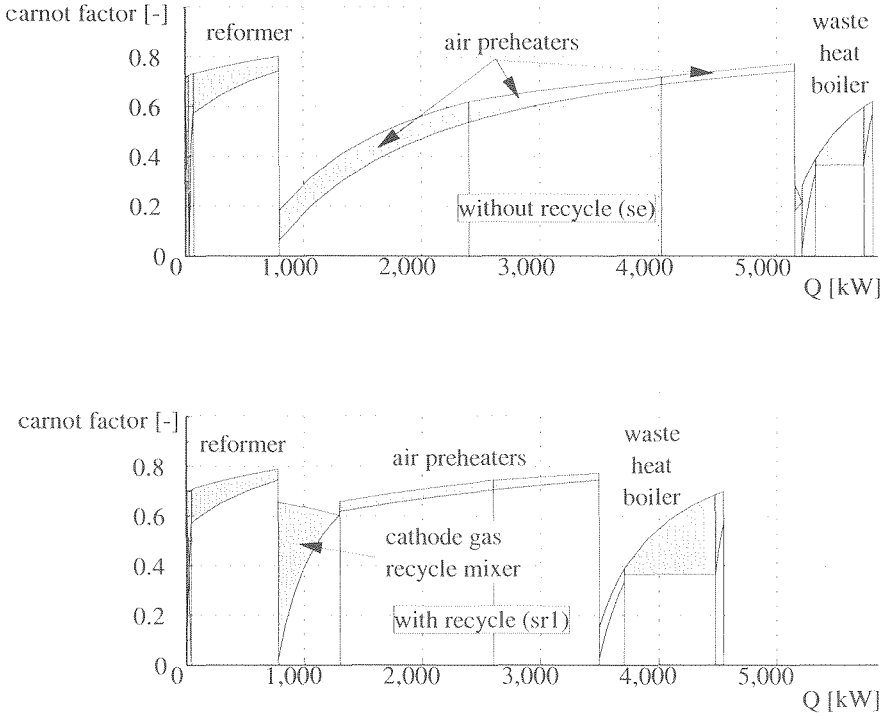

Figure 8.10: Comparison of exergy losses as a result of heat transfer for the base case (se) and a system with recycle (sr1) using the value diagrams

By comparing the two diagrams another important fact can be learned. The more efficient heat transfer in the cathode off-gas recycle subsystem in sr1 results in a higher temperature of the flue gas. The flue gas is therefore supplied to the waste heat boiler with a higher temperature (= high exergy value). In the waste heat boiler the heat is still used to produce intermediate pressure steam which has a limited exergy value (f=0.36). Consequently, the losses in the waste heat boiler are higher if a cathode off-gas recycle is used.
In **Section 7.5** the pinch-value diagram was used to estimate the exergy of the heat which could be extracted from the system at a high temperature. The pinch-method determines how much heat can be recovered at high temperature taking into account the heat required to

preheat the process flows. By using combining this with the value diagram, the exergy of this heat is shown. Figure 8.11 shows the pinch-value diagram for the SOFC system with cathode gas recycle (sr1). The lower curve (cold composite curve), which represents the flows which absorb heat, is dominated by the heat which is supplied to the cathode gas in the cathode off-gas recycle (470 °C → 850 °C). Correspondingly the upper curve, which represents the flows which supply the heat, is dominated by the cooling of the cathode off-gas from 1000 °C at the outlet off the fuel cell to the inlet temperature of the recycle compressor (450 °C). The shaded area on the right again corresponds to the exergy of the heat which could be recovered at high temperature.
The corresponding diagram for the reference system is shown in figure 8.14. If all the surplus heat which is available in the system is converted into power without exergy losses (theoretically), a potential increase of the power produced by 330 kW was estimated for the base case (se). In the system with recycle (sr1) the exergy of the surplus heat, i.e. the area indicated in figure 8.11, is 540 kW, that is even higher. Lower losses as a result of heat transfer occur in the system with recycle because less heat is transferred. But the corresponding decrease in exergy losses in preheating the air does not lead to a strong increase in exergy efficiency, because no use is made of the exergy in the flue gas, except to produce steam at 180°C. To improve the exergy efficiency of the system it is therefore not enough to locate the losses as a result of heat transfer. It is also necessary to determine how the heat which is/becomes available can be used. The analysis shows that exergy of the heat which could potentially be recovered at high temperature is higher for the systems with recycle. A configuration which makes better use of the available heat will be considered in the next section.

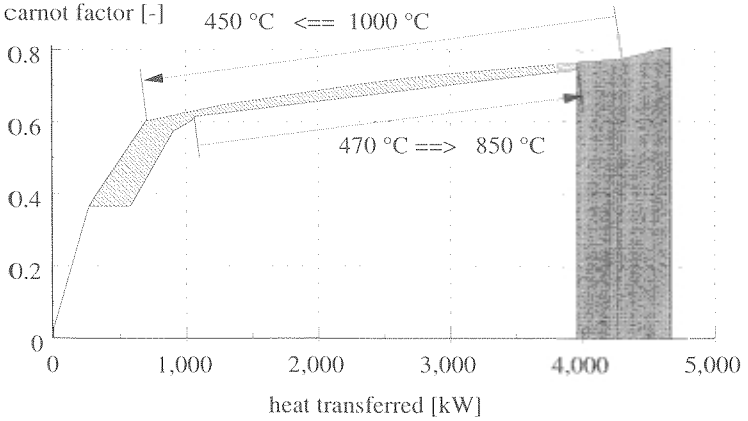

Figure 8.11: Pinch-value diagram for a SOFC configuration with cathode gas recycle

8.3 INFLUENCE OF THE OPERATING PRESSURE

8.3.1 Description of the system and calculations

The analysis of the reference system indicates that to increase the efficiency of the SOFC system, it is important to reduce the exergy losses as a result of heat transfer. However, comparison of the systems with and without recycle shows, that to achieve this, it is

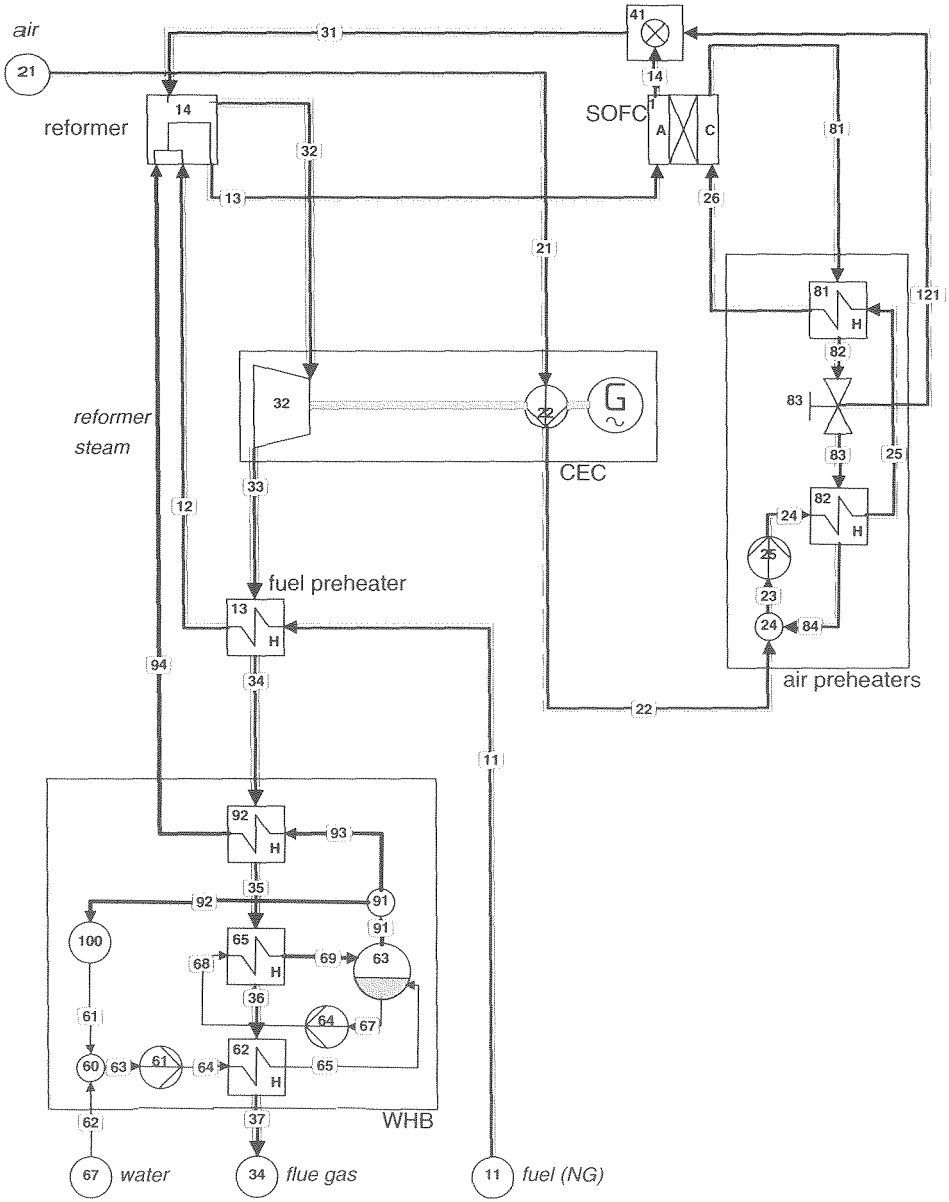

Figure 8.12: Process flow diagram for the pressurised external reforming SOFC system (sep)

important to utilise the heat which is available for something else than the production of intermediate pressure steam. One way to achieve this is by pressurising the system. If the fuel cell operates under pressure, the heat which is generated in the fuel cell can be partially converted into power in an expander. To assess the potential of pressurisation, calculations have been carried out for a system operating at 6 bar[l].

The process flow diagram of the system is shown in figure 8.12. The configuration is based on configuration sr3 (split air preheater in the cathode off-gas recycle) in the previous section. An air compressor and a flue gas expander have been added to the scheme. The air is pressurised in the air compressor (app. 22). For the calculation, compressor and expander are considered to operate on a single-shaft, as they would in many gas turbine designs. Both components are assumed to operate at an isentropic efficiency of 75 %. After compression the air is mixed with the cathode off-gas recycle (stream 84), preheated in the air preheaters (app. 81 and 82) and supplied to the fuel cell at 6 bar[m]. After the fuel cell, the cathode off-gas passes through air preheater (81) and is subsequently split into two parts. The part of the cathode off-gas which is not recycled, is mixed with the anode off-gas in the combustor. The heat in the flue gas is used in the reformer (app. 14), the expander (app. 32), the fuel preheater (app. 13) and the waste heat boiler respectively.

The power delivered by the expander increases with the inlet temperature. By placing the expander after the reformer, the duty of the expander is lower than if the flue gas is expanded before the reformer. However, by expanding the flue gas after the reformer it is easier to achieve the required temperature difference between flue gas and catalyst bed. This configuration is also preferable because it allows integration of combustor and reformer and limits the pressure difference between flue gas and catalyst bed. The pressure losses used in the calculations vary proportionally to the operating pressure. This assumption is based on the fact that the pressure loss ratio ($\Delta p/p$), rather than the absolute value of the pressure loss, determines the auxiliary power required to overcome the pressure loss.

8.3.2 Energy analysis

In figure 8.13 the calculated efficiencies for the atmospheric system (sr3) and the system operating at 6 bar (sep) are shown. There are two large differences in efficiency between the atmospheric and the pressurised system. Firstly, the calculated electrical efficiency for the external reforming SOFC system is considerably higher for the system operating at higher pressure. Secondly heat production in the pressurised system is much lower. The second effect is so strong, that a substantially lower total efficiency (heat +power) results (see figure 8.13).

Electrical efficiency

The net electrical efficiency is 40.5 % for the atmospheric and 51.7% for the pressurised system. The large increase in efficiency is due to three factors:

1. The efficiency of the fuel cell increases. Expressed as a fraction of the fuel input to the system, the fuel cell efficiency increases from 51.9 % to 56.1 %. This is due to the higher Nernst voltage (see **Section 4.3.1**) at higher pressure resulting in a substantially higher cell voltage: 662 mV (atm.) and 715 mV (at 6 bar) respectively. The higher cell voltage directly leads to a higher efficiency of the fuel cell.
2. Part of the heat in the pressurised system is used to generate power in the

---

[l] the "operating pressure" is equal to the pressure at the inlet of the fuel cell

[m] the influence of the pressure is considered in other sections, see **Section 8.6, 9.6**.

compressor/expander combination (CEC). The net power production of the compressor/expander combination equals 5.1 % of the energy supplied to the system with the fuel. The gross system efficiency increases correspondingly.

3. The amount of heat which is generated in the fuel cell depends on the efficiency of the fuel cell. If the efficiency is higher, less heat is generated. Therefore, the amount of heat generated in the pressurised stack is lower than in the atmospheric stack. In the calculated cases, the heat which is generated in the stack is 1025 kW for the atmospheric and 871 kW for the pressurised system. Consequently less cathode gas is required to cool the cell in the pressurised system. The reduced duty of the recycle blower in the pressurised system contributes to another 1.9 % increase in the electrical efficiency of the system.

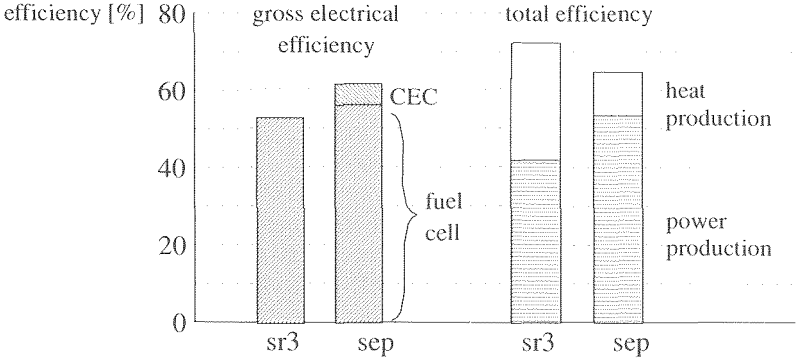

Figure 8.13: Comparison of the efficiencies for the atmospheric (sr3) and pressurised external (sep) reforming SOFC system

Total efficiency

The amount of heat which is produced in the pressurised system is much lower than in the atmospheric case. In the atmospheric system all heat is used to produce steam. In the pressurised system part of the heat is used to produce power in the CEC (compressor/expander combination). Therefore a lower production of heat is expected in the pressurised system. However, the heat produced in the pressurised system corresponds is only one third of the corresponding value for the atmospheric system (30.4% vs. 11.6% of the fuel input). Extraction of heat to produce power by the CEC alone cannot explain the considerable decrease in heat production of the system shown in figure 8.13.

In figure 8.14 the Q,T-diagrams for both the atmospheric and the pressurised system are shown. Indicated in the diagram is the decrease in temperature of the flue gas over the waste heat boiler. Evidently the temperature drop of the flue gas in the waste heat boiler is much larger in the atmospheric system than in the pressurised system, both as a result of the lower inlet temperature (outlet temperature reformer / expander) and the higher outlet temperature of the flue gas (flue gas stack temperature). The difference in inlet temperature between the atmospheric and the pressurised system is due to the expander. The expander extracts part of the heat from the flue gas flow. As a result, the temperature of the flue gas at the inlet of the waste heat boiler decreases from 735 °C for the atmospheric system (sr3) to 496 °C for the pressurised system (sep).

The higher temperature of the flue gas at the outlet of waste heat boiler is mainly due to a higher recycle ratio α in the pressurised system. To estimate the cathode off-gas recycle ratio α the following equation was derived in **Section 8.1**:

$$\alpha \approx \frac{T_{cat} - T_{air}}{T_{cog} - T_{air}}$$

The relevant temperatures are the temperature of the fresh air (T_{air}), the temperature at the inlet of the cathode (T_{cat}) and the temperature of the cathode off-gas at the cathode outlet (T_{cog}). α is calculated as the ratio between the temperature increase required for the fresh air ($T_{cat} - T_{air}$) and the temperature difference between the recycle flow and the fresh air prior to mixing ($T_{cog} - T_{air}$) . The temperature of the fresh air (T_{air}) in the atmospheric system is equal to the ambient temperature (see figure 8.14). In the pressurised system, however, the air is 'preheated' by the compressor. If T_{air} in the equation for α becomes larger, the ratio between the temperature differences is lower and a lower value for α is found.
Given the pressure ratio (6) and an isentropic efficiency of the compressor (75 %), the calculated temperature at the outlet of the compressor is 271 °C. Due to the increase in the temperature at which the air is supplied to the cathode off-gas recycle, the recycle ratio α decreases from 80% in the atmospheric system to 70 % in the system operating at 6 bar. The effect of 'preheating' the air on the recycle ratio can be understood by considering the energy

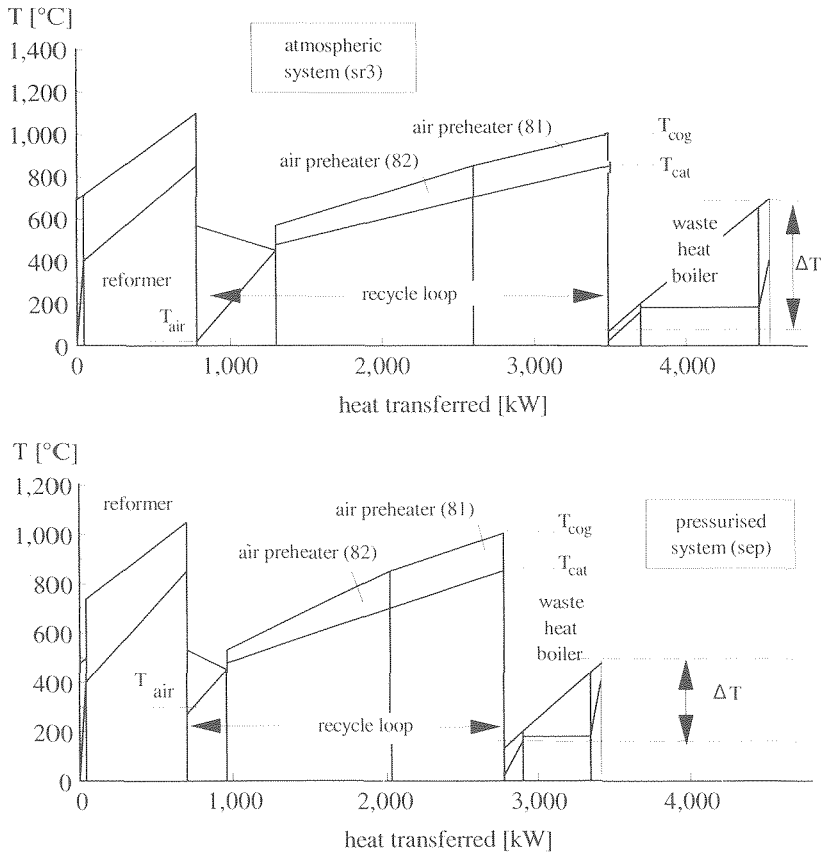

Figure 8.14: Comparison of the Q,T-diagrams of the atmospheric (sr3) and pressurised external reforming SOFC system

balance of the recycle loop. All heat generated in the fuel cell is removed from the recycle by the cathode off-gas flow to the combustor. This flow becomes larger as less gas is recycled. Therefore if less gas is recycled, less heat is removed from the recycle. In the pressurised system heat is supplied to the cathode off-gas recycle not only by the fuel cell but also by the compressor. To restore the heat balance of the recycle loop, more heat has to be removed from the recycle. This is achieved by reducing the recycle ratio, i.e. supplying more fresh air and removing more (hot) cathode off-gas from the recycle.
The flue gas temperature after the waste heat boiler (i.e. the flue gas stack temperature) is influenced by the amount of air which is supplied to the system: if more air is supplied to the system, the flue gas flow becomes larger. Compared to the atmospheric system, the air/fuel ratio [kg/kg] in the pressurised system 27% higher due to the lower recycle rate α. In the pinch diagrams in figure 8.15 the higher flue gas flow in the pressurised system results in a smaller slope of the flue gas curve.
A second reason for the higher flue gas stack temperature is the lower heat demand at low temperature in the pressurised system. In the atmospheric system, the cold curve at temperature below 400 °C consists of the superimposed curves for the steam production and for air pre-heating[n]. Below 180 °C, the evaporation temperature for the 10 bar steam, the heat is mainly used for air preheating. Consequently the hot curve (flue gas) and cold curve (mainly air) have approximately the same slope. In the pressurised system, the air is 'preheated' to 271 °C by the compressor. Below the pinch temperature of 180 °C, the amount of heat which is recovered is small. Consequently below 180 °C, the temperature of the steam in the waste heat boiler, only a small part of the heat in the flue gasses is used.

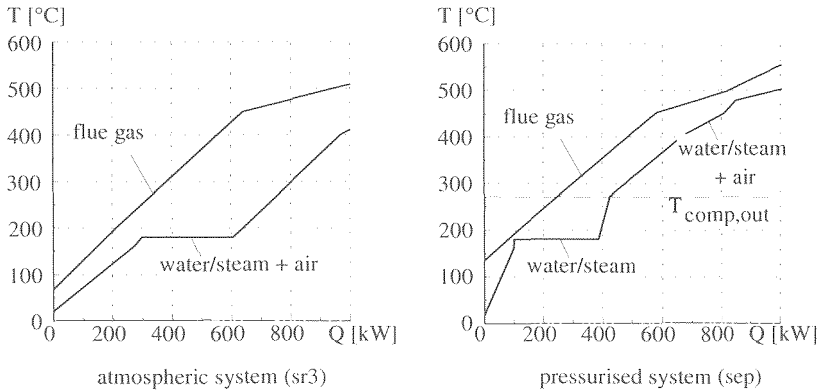

Figure 8.15: Pinch diagrams for the atmospheric (sr3) and pressurised external reforming SOFC system (only lower part of composite curves shown)

Process steam and reformer steam
The temperature decrease of the flue gas in the waste heat boiler (and therefore the amount of heat transferred) is larger in the atmospheric system than in the pressurised system. As shown above, this is due to:
- Heat extraction by the expander;
- A lower recycle rate in the cathode recycle;

[n] In the system heat transfer to the incoming air takes place by mixing the hot and cold flows, but both for the pinch diagrams both heating and cooling curves have been included in the respective composite curves.

- The lower amount of heat required for air preheating.

The Q,T-diagram in figure 8.14 shows that the amount of heat transferred in the waste heat boiler in the pressurised system is approximately half of the heat transferred in the atmospheric system. However, even a stronger decrease of the heat production in the system is found by comparing the efficiencies in figure 8.13. The difference can be explained by considering the energy balances for the total system and for the waste heat boiler (figure 8.16).

The first two bars in figure 8.16 represent the total energy supplied to the system with the fuel[o]. This energy is converted into electricity or into heat in the fuel cell system. The heat is partly recovered in the form of process steam, while the remainder is lost, mainly through the flue gas stack. The first two bars confirm the large difference in the production of process heat in the waste heat boiler: the pressurised system produces approximately ⅓ of the process steam produced in the atmospheric system. The apparent efficiency of heat recovery can be defined as:

$$\text{heat recovery efficiency} = \frac{\text{heat produced by the system}}{\text{heat generated in the system}}$$

In the atmospheric system the heat recovery efficiency is approximately 50% (half of the heat produced is recovered in the form of process steam). The apparent efficiency of heat recovery in the pressurised system, based on the total energy balance for the system, drops to approximately 20% in figure 8.16.

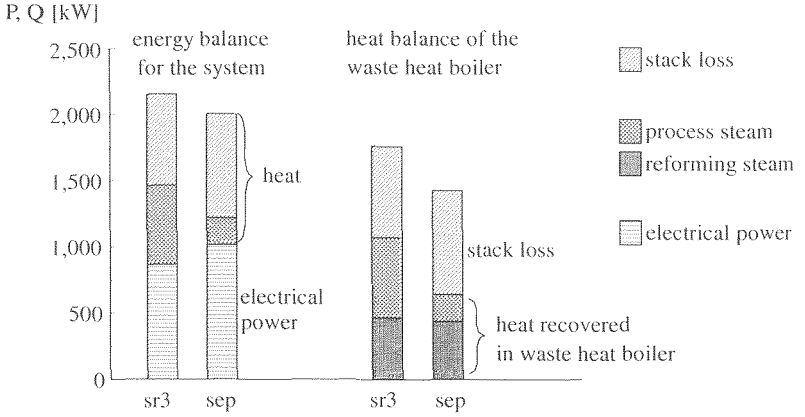

Figure 8.16: Energy balances for the total system and for the waste heat boiler for the atmospheric (atm.) and the pressurised system (p=6)

This sharp decrease in apparent efficiency of heat recovery can be explained by considering the second set of bars, which represent the heat balance of the waste heat boiler. The total length represents the heat supplied to the waste heat boiler by the flue gas. Part of the heat is lost as flue gas stack loss, while the remaining part is recovered, either as process steam or as reformer steam. Evidently the amount of heat produced by the system (= process steam) and

[o] Due tot the higher fuel cell efficiency of the pressurized stack, the total energy in figure 8.16 is lower for the pressurized system: the power generated by the fuel cell is the same in all calculations (1 MW)

the heat losses appear both in the energy balance of the whole system (the first set of bars) and the energy balance for the waste heat boiler (the second set of bars). However, the heat required for the reformer steam appears in the energy balance of the waste heat boiler only. Because this heat is recycled, this heat does not appear in the total energy balance. The amount of heat required for producing the reforming steam is approximately the same in the atmospheric and the pressurised system. As a result, the amount of process steam decreases much stronger than the total amount of heat transferred to the waste heat boiler. In other words, the efficiency of heat recovery does not drop as sharply as the energy balance for the total system (the first to bars in figure 8.16) suggest.
The analysis in the section shows that the explanation of a relatively simple change in performance of the system (the lower heat production in the pressurised system) already requires an extensive analysis. The relative sharp decrease in thermal efficiency of the system is influenced by the cathode off-gas recycle ratio, heat extraction in the expander, the pre-heating effect of compressor and the changing ratio between reformer steam and steam production.

8.3.3 Exergy analysis

In figure 8.17 the exergy losses for the atmospheric and the pressurised system are shown. The exergy losses are classified according to the type of loss identified in **Section 3.2**. The total losses are significantly smaller for the pressurised system. As can be seen in the figure, this can be attributed almost fully to the lower losses as a result of heat transfer. The other categories, with the exception of the friction losses, are not notably influenced. The friction losses increase as a result of the larger friction losses in the rotating equipment in the pressurised system.

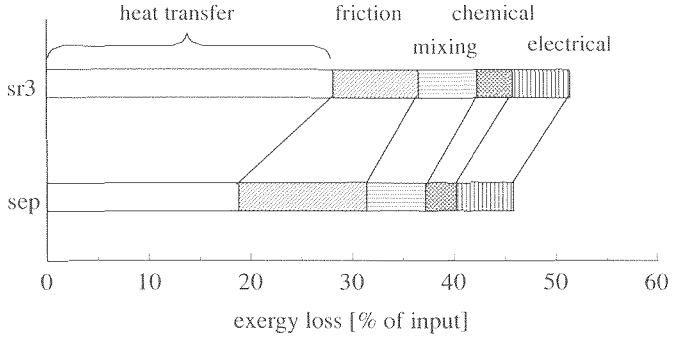

Figure 8.17: Exergy losses per type for the atmospheric (sr3) and pressurised system (sep)

The heat transfer losses, as shown in **Section 3.2**, depend on two factors: the average temperature of heat transfer and the temperature difference at which the heat is transferred. To decrease exergy losses as a result of heat transfer, temperature difference at which the heat is transferred should be minimised. Comparing the value diagrams for both pressurised and atmospheric systems (figure 8.18) shows that the two points in the system where the strongest reduction of the exergy losses occurs are the air/cathode off-gas recycle mixer and the evaporator. The effect of pressurisation is a strong reduction of the heat transfer losses (-10.4%pt).
The penalty for the higher operating pressure is higher losses as a result of friction

(+3.9 %pt). Comparing gain and penalty, a further increase in pressure seems effective. However, closer analysis of the value diagram for the atmospheric and the pressurised system (figure 8.18) leads to a different conclusion.

The major heat transfer losses occur in 4 components, the reformer, the cathode off-gas recycle mixer, the air preheaters and the waste heat boiler.

- The losses in the reformer are mainly influenced by the amount of fuel which has to be reformed. In order to limit the heat exchanger area the temperature difference can not be reduced considerably without resulting in a strong increase of the cost of the reformer;
- The losses in the recycle as a result of mixing the cathode off-gas and the fresh air are large at atmospheric operation. However, these losses are already so strongly reduced (from 123 kW to 21 kW) by operating the system at 6 bar that further reduction of the losses will be much smaller;
- In the air preheaters the same limit is reached with regard to the temperature difference and required heat exchanger area. If the pressure is increased further a different layout of the heat exchangers is required (see **Section 8.2**) to limit heat exchanger costs.
- Therefore increasing the operating pressure can only reduce the losses as a result of heat transfer in the waste heat boiler. The losses as a result of heat transfer in the waste heat boiler are 274 kW in the atmospheric system and in the pressurised system 172 kW.

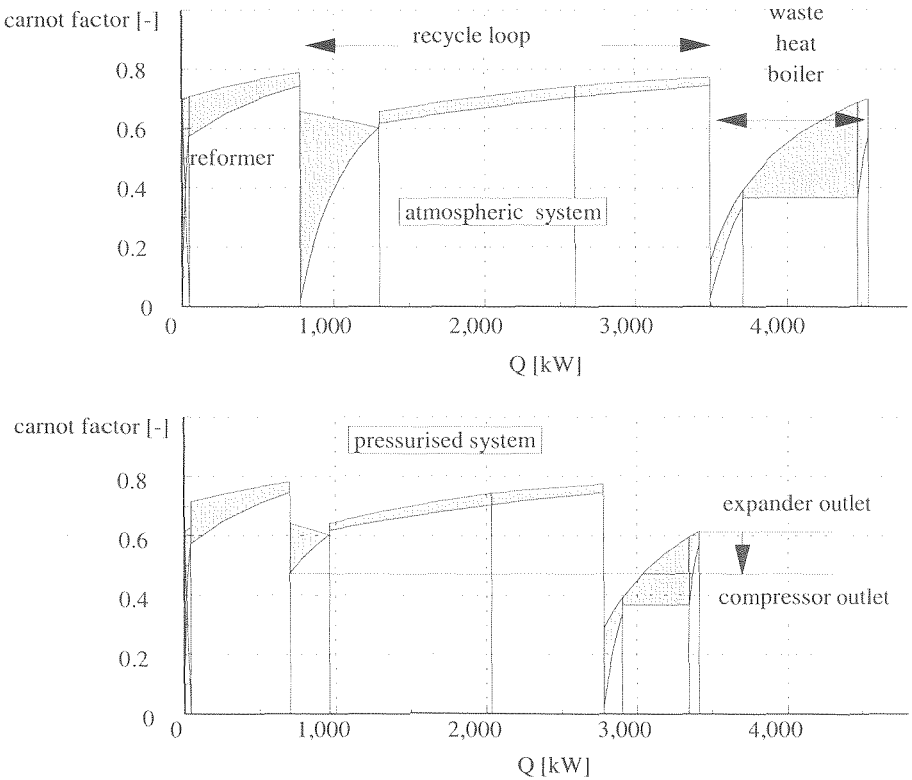

Figure 8.18: Comparison of the value diagram for the atmospheric and the pressurised system

Even though the losses are still substantial in the waste heat boiler, only a small fraction of these exergy losses could be converted into work by increasing the operating pressure. The operating principle of a gas turbine is the difference in temperature between compression and expansion. Therefore, the outlet temperature of the compressor must always be higher than the outlet temperature of the expander (otherwise the last stage of the expansion occurs at a lower temperature than the last stage of the compression). As can be seen in the value diagram, the largest part of the exergy losses in the waste heat boiler as a result of heat transfer, however, occur below the compressor outlet temperature. These losses can not be reduced by increasing the operating pressure. Not indicated in the value diagram are the losses in the flue gas stack, which constitute approximately nearly half of the exergy loss as a result of heat transfer in the waste heat boiler (82 kW). As these exergy losses occur at a temperature substantially lower than the compressor outlet temperature, the part of the losses which could be decreased by increasing the operating pressure, is even smaller than the value diagram for the pressurised system in figure 8.18 suggests. Furthermore the amount of heat generated in the fuel cell will also be lower at higher operating pressure, reducing the potential heat recovery in the CEC even further. Given the low efficiency of the compression/expansion process a further increase in operating pressure can only lead to a very limited increase in electrical efficiency (as will be shown **Sections 8.6** and **9.6**)

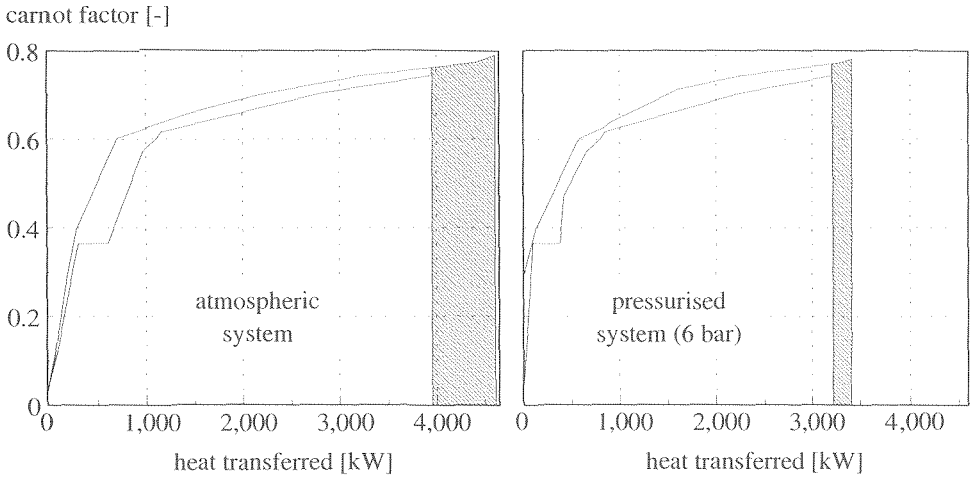

Figure 8.19: Comparison of the pinch-value diagram for the atmospheric (sr3) and the pressurised system (sep)

The results are confirmed by the analysis based on the pinch-value diagram (see **Section 7.5**). In the pinch-value diagrams in figure 8.19 again the shaded area represents how much exergy could be recovered by extracting heat. Again the exergy is determined by determinining both the amount of heat which could be extracted from the system and the highest temperature at which it could be made available in the system, taking into account the need to preheat air, fuel and produce steam for the reforming process. The exergy of the heat which could potentially be converted into electrical power in the atmospheric system according to figure 8.19 is roughly 480 kW. The corresponding amount for the pressurised system is much lower: approximately 160 kW.

Influence of the efficiency of rotating equipment

The amount of electrical power which is produced by the CEC in the pressurised system is 99 kW, i.e. much smaller than the difference in potential (480-160=320 kW). Evidently the CEC does not convert the available heat very efficiently into electrical power. This is due to the low efficiency of the rotating equipment.

For the calculations an isentropic efficiency of the main rotating equipment (air compressors, recycle blower, expander) of 75 % has been assumed. Components with higher efficiencies are available, although the cost will be higher. To assess the influence of the efficiency of the rotating equipment, calculations have been carried out for different values of the efficiency for the air compressor and expander: 80%, 85% and 90%. Figure 8.20 shows the effect of the efficiency of the rotating equipment on the system efficiency. Most important is the increase in net electrical efficiency from 53.6 % to 61.6 %. The increase in system efficiency is proportional to the isentropic efficiency: between 75 % and 90 % every 5 %pt increase in efficiency of the rotating equipment, leads to an increase of 2.7 %pt increase of the net electrical efficiency of the system. If an isentropic efficiency of 90% is assumed for the components of the CEC, the power produced by the CEC becomes 244 kW. This corresponds well with the maximum of 320 kW estimated for the system from the pinch-value diagram (which corresponds to a CEC operating reversibly, i.e. with 100% isentropic efficiency).

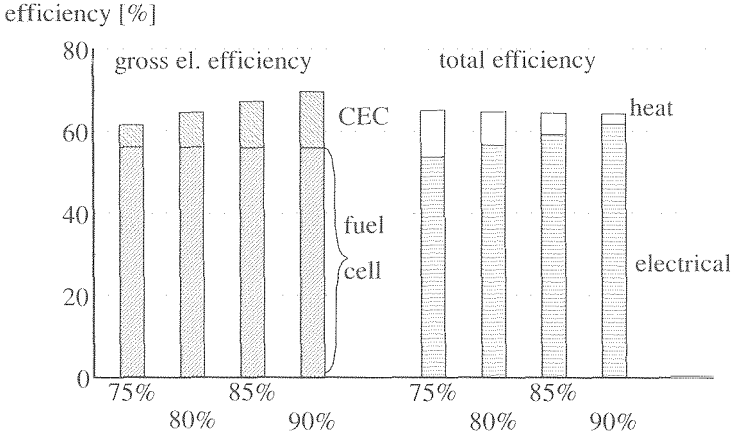

Figure 8.20: Gross electrical and total efficiency for the fuel cell system for different values of the isentropic efficiency for the compressor and expander (reference calculation = 75%)

Figure 8.21 shows the exergy losses for different values of the rotating equipment efficiency. The total exergy losses can be seen to decrease substantially. As before, a distintion is made between the different types of the exergy losses. The losses of heat transfer decrease slightly because less heat is produced in the system if the rotating component become more efficient. But only the losses as a result of friction are influenced significantly by the efficiency. The losses consist of the friction losses caused by pressure losses in the pipes and components and the losses in the two components of the CEC. The first type of friction losses are independent of the compressor and expander efficiency, while the losses in the CEC evidently do depend on the efficiencies. The two types of friction losses are shown separately in figure 8.21. The figure confirms that the exergy losses as a result of pressure losses are almost independent of

the efficiency of the CEC. The friction losses in the CEC clearly decreases with increasing isentropic efficiency. These losses are approximately proportional to 1-η, where η is the isentropic efficiency of the rotating equipment. The calculation of the exergy losses as a result of friction therefore predicts the influence of the isentropic efficiency of the rotating equipment well.
The energy and exergy analysis in this section shows, that pressurising the system reduces the losses as a result of heat transfer considerably, both because the expander utilises high temperature heat and because the fuel cell operates more efficiently. However, the efficiency of the rotating equipment limits the effectivity of the heat utilisation. As a result, the decrease in exergy losses as a result of heat transfer is partly 'compensated' by the increase in exergy losses as a result of friction. The exergy analysis predicts a small increase in efficiency if the system is operated at higher pressure and also clearly shows the influence of the isentropic efficiencies of the compressor and expander. Furthermore the energy analysis also shows the flue gas stack losses increase strongly because recycle ratio becomes smaller when the system is pressurised.

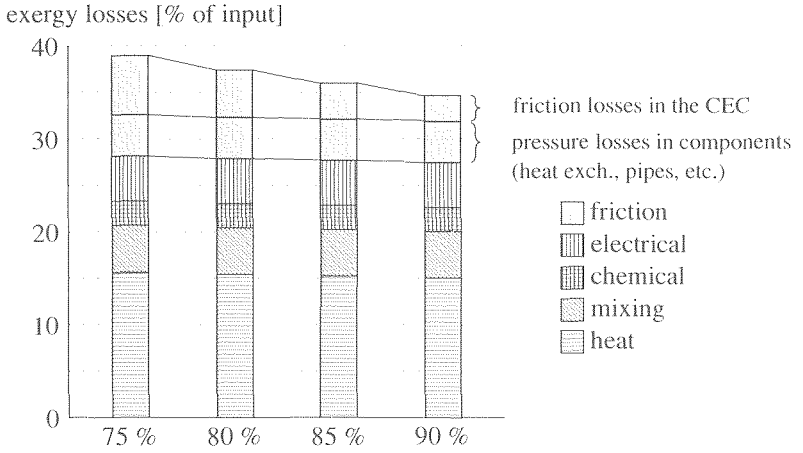

Figure 8.21: Exergy losses per type of loss for different values of the isentropic efficiency for the CEC

8.4 INFLUENCE OF THE FUEL UTILISATION

8.4.1 Description of system and calculations

The main cause of exergy losses in the external reforming SOFC system is heat transfer. One approach which aims at reducing these losses, is to make use of the high temperature heat which is available in the system. By operating the system under pressure part of the heat which is generated in the system is recovered. As shown in the preceding section, the heat is not recovered very effectively. Another approach is to reduce losses as a result of heat transfer by reducing the amount of heat generated in the fuel cell system. In the combustor chemical energy is converted fully into heat. In the fuel cell chemical energy is converted into both heat and electrical power. In order to minimise the total amount of heat which is generated in the system, the fuel utilisation in the fuel cell should be high to minimise heat production. For both systems discussed in the preceding section, the atmospheric system (sr3)

and the pressurised system (sep), the performance has been calculated using different values of the fuel utilisation. For the atmospheric system the fuel utilisation was varied from 77.5% to 87.5%. The performance of the pressurised system was calculated was for values from 77.5% to 85% (for higher values of the utilisation to little high temperature heat is available to preheat all the air/cathode gas).

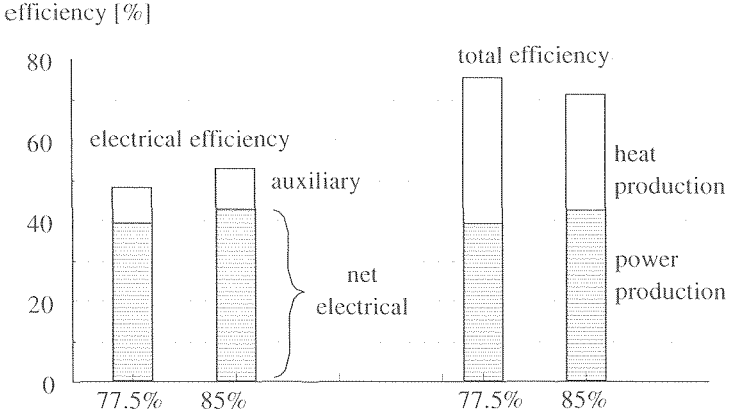

Figure 8.22: System efficiencies for the atmospheric system (sr3) at two values of the fuel utilisation (U_f=77.5% and U_f=87.5%).

8.4.2 Energy analysis

atmospheric system

In figure 8.22 the system efficiencies are shown for two values of the fuel utilisation. The first two bars represent the electrical efficiencies. The total length of the bar corresponds to the gross efficiency: generated power as a fraction of the fuel energy input. The 'fuel cell efficiency' is defined as the ratio between the power generated in the fuel cell and the fuel supplied to the system[p]. At 77.5% utilisation, the fuel cell efficiency is equal to 48.2% . This increases to 53.0% at 87.5 % fuel utilisation. The 'electrochemical efficiency' of the fuel cell is the ratio between the power generated by the fuel cell and the energy which is converted in the fuel cell. This value indicates how efficient the electrochemical process occurs within the fuel cell. If the electrochemical efficiency remains constant, the fuel cell efficiency (P_{fc}/LHV_{in}) is proportional to the fuel utilisation. Assuming a constant electrochemical efficiency, the fuel cell efficiency would be 54.4% at 87.5% fuel utilisation. The difference between the actual (53.0%) and predicted (54.4%) fuel cell efficiency, shows that the electrochemical efficiency becomes lower at higher fuel utilisation. The cell voltage, which is a measure for the electrochemical efficiency (**Section 4.3.1**), drops from 674 mV at 77.5 % to 657 mV at 87.5 %. As discussed in **Section 6.4**, the decrease of the cell voltage is due to the lower reversible voltage or Nernst voltage at higher utilisations. If the fuel utilisation is higher, a larger part of the energy supplied to the system is converted in the fuel cell. On the other hand the conversion in the fuel cell becomes less efficient at higher values of the fuel utilisation. Within the range of fuel utilisations considered here, the net result of increasing

[p] In the atmospheric system this corresponds to the gross efficiency (see **Section 7.3** for the definition of efficiencies)

the fuel utilisation is positive: the gross electrical efficiency increases. If the fuel utilisation increases from 77.5 to 87.5%, this corresponds to a 13% increase of the fuel utilisation and leads to a 2.5% decrease of the cell voltage.
However, there is also an increase of the auxiliary power requirements at higher fuel utilisation. As a result, the increase in net electrical efficiency of the system is limitted. The calculated efficiency increases from 39.3% to 42.8% (+2.5%pt). This increase in net efficiency is considerably lower than the increase in the gross efficiency (+4.8%pt). At high fuel utilisation the larger amount of heat is generated in the fuel cell. Consequently a higher mass flow cathode gas is required to cool the cell. The corresponding higher duty for the air and the recycle blower limits the increase in net efficiency. The increases in net efficiency corresponds to approximately one third of the increase which would result if the electrochemical efficiency and auxiliary power would remain constant.
The fuel which is not converted into electrical power in the fuel cell is converted into heat. It seems efficient to convert as much fuel as possible in the fuel cell stack. Assuming an approximately constant efficiency of heat recovery (heat produced/heat generated: see **Section 8.3**), maximising electricity production in the fuel cell also leads to a higher total efficiency (electricity + heat). However, figure 8.22 indicates that the total efficiency is considerably lower at high fuel utilisations. The reason for the lower total efficiency lies in the cathode flow which is required to cool the stack.
Assuming an constant voltage, the amount of heat which has to be removed from the stack is proportional the amount of fuel converted in the fuel cell (i.e. not the amount of fuel supplied to the fuel cell). At a high fuel utilisation a larger fraction of the fuel is converted in the fuel cell. Therefore, for a given input of fuel to the system, the cathode flow is proportional to the fuel utilisation. If the effect of the lower cell voltage is taken into account, the required cathode flow increases more than proportional with the fuel utilisation.
The combustor uses both the anode off-gas and the cathode off-gas. The air/fuel ratio in the combustor is therefore determined directly by the air/fuel ratio of the fuel cell (cathode inlet/anode inlet). The higher cathode gas flow at higher fuel utilisation results in a higher air/fuel ratio for the combustor as well. At 77.5% fuel utilisation the amount of oxygen in the cathode off-gas is slightly less than 2 times the amount required to combust the anode off-gas. At 87.5 % fuel utilisation the stochiometry increases to 2.6. The resulting larger flue gas stack losses, is the main reason for the lower total efficiency of the system shown in figure 8.22.

pressurised system
In the pressurised system, the efficiency is not only determined by the performance of the fuel cell, but also by the performance of the compressor-expander combination (CEC). If the fuel utilisation increases from 77.5 % to 85 %, the fuel cell efficiency increases from 52.2 % to 56.1 % (figure 8.23). However, the increase in fuel utilisation simultaneously reduces the amount of heat generated in the combustor. As a result, the duty of the CEC is lower at high utilisation. As a fraction of the fuel input, the CEC contribution decreases from 7.4 % to 5.5 % for the same change in fuel utilisation. The increase in the gross electrical efficiency is therefore 2.1%pt: half of what is gained in the fuel cell is lost in the CEC. The auxiliary power is determined by the cathode recycle blower. Due to the increase of the cathode flow as a result of the higher cooling requirements (which were found for the atmospheric system as well), the increase in net electrical efficiency is even smaller: 1.1 %pt.

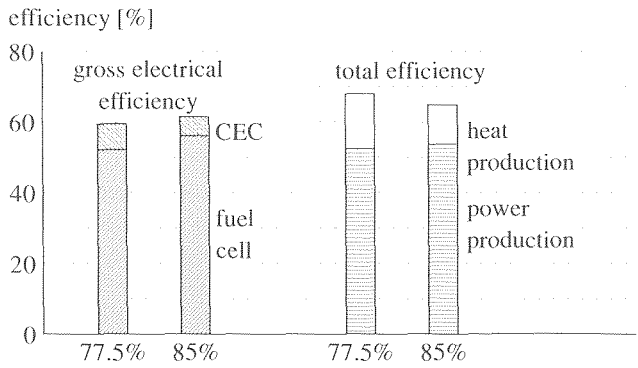

Figure 8.23: System efficiencies for the pressurised system (sep) at two values of the fuel utilisation (U_F=77.5% and U_F=85%).

Comparison of these results to the corresponding data for the atmospheric system, confirms that the efficiency increases less in the pressurised system. The increase in fuel cell efficiency in the pressurised system corresponds closely to the increase of the fuel cell efficiency in the atmospheric system: if the fuel utilisation increases from 77.5% to 85%, this leads to an increase in the efficiency of +3.7 %pt for the atmospheric and +3.9 %pt for the pressurised system. However, in the pressurised system the CEC duty at higher fuel utilisation is lower and the increase in gross efficiency is much smaller for the pressurised system (+2.1 %pt) than for the atmospheric system (+3.7 %pt). If the auxiliary power consumption is taken into account, the difference is even larger. The increase of the net electrical efficiency is +2.6 %pt vs. 1.1 %pt for atmospheric and the pressurised system respectively.

8.4.3 Exergy analysis

In figure 8.24 the exergy losses in the atmospheric system (sr3) per subsystem are shown for the same two values of the fuel utilisation: 77.5% and 87.5 %. The exergy losses increase with utilisation in the fuel cell and in the cathode off-gas recycle. Lower losses at a higher fuel utilisation occur in the other subsystems, but mainly in the waste heat boiler.

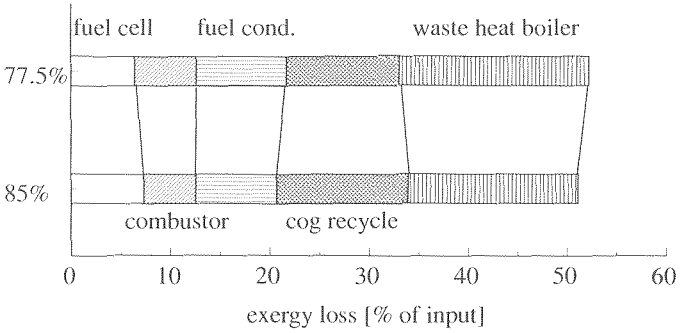

Figure 8.24: Comparison of the exergy losses per subsystem for the atmospheric system (sr3) at two values of the fuel utilisation

In the **fuel cell** the increase in exergy losses is due to two factors.

- More fuel is converted in the fuel cell at higher fuel utilisation;.
- To achieve the same power density at the lower Nernst voltage (lower average hydrogen concentration at the anode) the cell voltage will be lower. A lower cell voltage results in a lower electrochemical efficiency.

In the **combustor**, less fuel is converted at higher fuel utilisation and the exergy losses are lower. Exergy losses in the combustor are mainly caused by the chemical reactions and as a result of mixing air and fuel. If the fuel utilisation increases from 77.5 to 87.5 % the chemical losses in the combustor decrease as a result of the lower conversion in the combustor: from 3.0% to 1.8%. The losses as a result of mixing are determined primarily by the cathode off-gas flow. As shown, air/fuel ratio increases strongly with the fuel utilisation. As a result the mixing losses increase from 3.2% (at U_F=77.5) to 3.4% (at U_F=87.5 %). Note that the sum of the exergy losses in fuel cell and combustor (figure 8.24) is hardly affected by a change in utilisation.

In the **fuel conditioning** subsystem the exergy losses decrease at higher fuel utilisation according to figure 8.24. The lower heating value of the anode off-gas at higher fuel utilisation, results in a lower temperature at the outlet of the combustor. As a result the temperature difference at which the heat is transferred in the reformer is lower. This can be seen by comparing the losses in the reformer in the value-diagrams in figure 8.25.

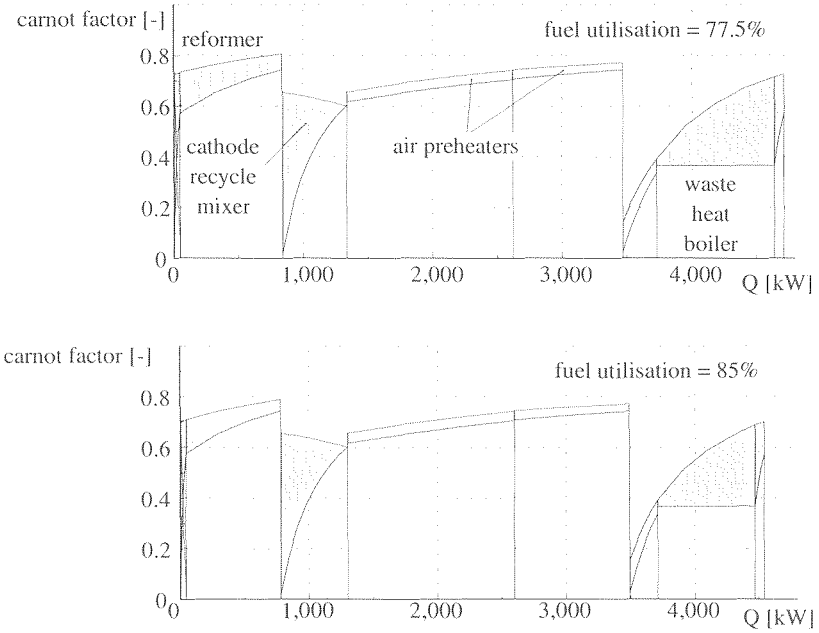

Figure 8.25: Comparison of exergy losses as a result of heat transfer in the atmospheric system (sr3) for two values of the fuel utilisation

The exergy losses in the **cathode off-gas recycle** increase according to figure 8.24. The exergy losses as a result of heat transfer in the cathode off-gas recycle increases as a fraction of the fuel input (figure 8.24) although the absolute value of the exergy losses is

approximately equal[q] (see the value diagram in figure 8.25). The reason the absolute losses are not effected by the lower fuel flow is that the cathode flow (and therefore the losses in the cathode off-gas recycle) is mainly determined by the power generated in the fuel cell (which remains constant).

Finally in the **waste heat boiler** the losses are smaller at high fuel utilisation. Again, as for the fuel conditioning subsystem, this is due to the lower combustion temperature (i.e. lower flue gas temperature), but mainly because less heat is transferred in the waste heat boiler. Figure 8.26 shows the exergy losses per type at two values of the fuel utilisation. Evidently the exergy losses as a result of heat transfer as a whole decrease with fuel utilisation. The reduction of the exergy losses which is achieved however is limited. The losses downstream of the combustor decrease, as expected. However the decrease of these losses in the rest of the system is largely cancelled out by the increase of the exergy losses as a result of heat transfer in the cathode off-gas recycle. These losses are relatively higher at high utilisation due to the larger amount of heat generated in the fuel cell stack.

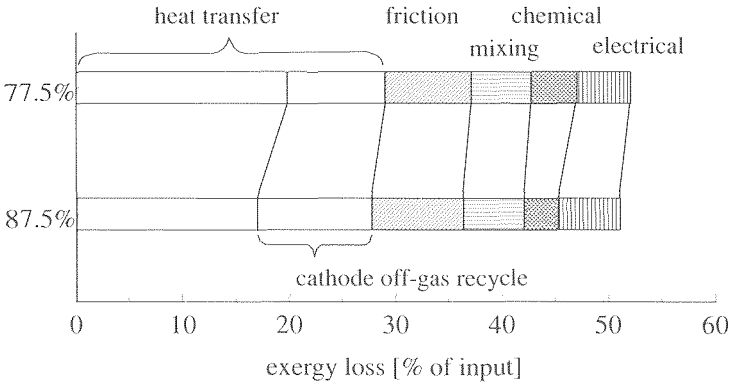

Figure 8.26: Comparison of the exergy losses per type of loss for the atmospheric system (sr3) at two values of the fuel utilisation

pressurised system

The atmospheric system is expected to benefit most from reducing the heat production by increasing the fuel utilisation. In the previous section (**8.2**) the pinch-value diagram for the atmospheric system and for the pressurised system were compared (see figure 8.19). The amount of exergy of the heat which could potentially recovered is much smaller in the pressurised system than in the atmospheric system. Furthermore figure 8.19 already showed the strong reduction in exergy losses as a result of heat transfer in the pressurised system. These two factors indicate that reducing the amount of heat which is generated will be more effective in the atmospheric system than in the pressurised system to produce electrical power.

In the atmospheric system, increasing the fuel utilisation, leads to a limited increase in exergy efficiency. As figure 8.27 shows, if the fuel utilisation increases from 77.5% to 85% the exergy efficiency increases less than 1%pt (from 49.3% to 50.2%). For the pressurised system the exergy efficiency decreases. For the corresponding increase of fuel utilisation the

[q] The electrical power (1 MW) for the fuel cell is the same in all calculations. This leads to a lower fuel input in the calculations at higher fuel utilisation

exergy efficiency decreases from 55.6 to 55.3%. This is again an unexpected result, as it indicates that if more fuel is converted in the fuel cell (a highly efficient component) the exergy efficiency of the total system decreases. In figure 8.28 the exergy losses in the atmospheric and pressurised system are compared. The changes in exergy losses in the first three subsystems in the graph (fuel cell, combustor and fuel conditioning) are similar for both the atmospheric and the pressurised system. Both in the atmospheric and in the pressurised system, an increase in fuel utilisation leads to:

- Higher losses in the fuel cell as a result of the larger amount of fuel converted in the fuel cell and the lower cell voltage;
- Lower losses in the combustor due to the lower fraction of fuel converted in this component;
- Lower losses in the reformer (fuel conditioning subsystem) due to the lower temperature of the flue gas entering the reformer due to the lower heating value of the anode off-gas.

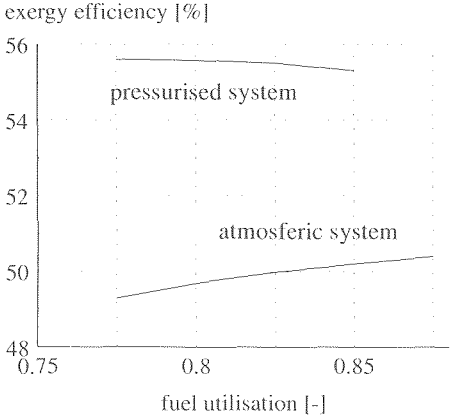

Figure 8.27: Exergy efficiency for the atmospheric (sr3) and the pressurised system(sep) as a function of the fuel utilisation

Differences between the atmospheric and the pressurised system occur in the exergy losses in the last three subsystems: the cathode off-gas recycle, the waste heat boiler and (in the pressurised system) in the CEC. In the system operating at atmospheric condition the losses in the cathode off-gas recycle subsystem increase due to the higher amount of heat which is generated in the fuel cell stack. In the waste heat boiler the losses are lower due to the higher fraction of fuel that is converted directly into electrical energy in the fuel cell stack, resulting in a lower amount of heat supplied to the waste heat boiler.
In the pressurised system the same effects occurs. However, due to the higher pressure the heat generated in the fuel cell stack is already lower and correspondingly the role of the recycle is of less importance. Consequently the increase of losses in the cathode off-gas recycle system is smaller as well. Similarly the effect of utilisation on the losses in the waste heat boiler is weaker as well for the pressurised system. Because the CEC uses part of the heat to produce power in the pressurised system, the losses in the waste heat boiler are already lower. Furthermore the decrease of the electrical power generated in the CEC partially compensates the lower heat production in the system. As a result, the exergy losses in the waste heat boiler are less sensitive to the fuel utilisation at higher pressure.

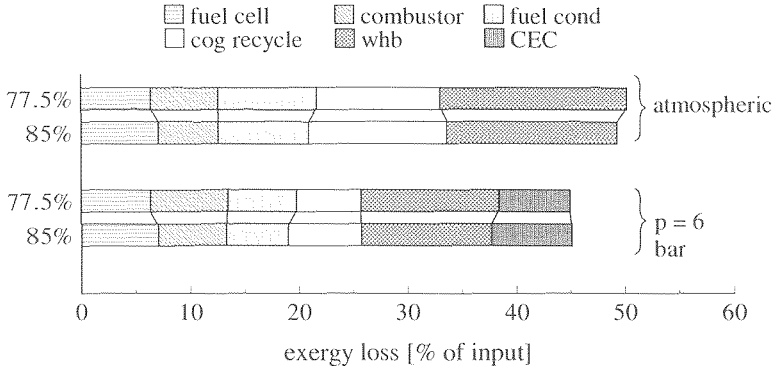

Figure 8.28: Influence of the fuel utilisation on the exergy losses in the subsystems in the atmospheric (sr3) and in the pressurised system (sep)

The main reason why the exergy losses increase with fuel utilisation in the system operating at elevated pressure is the increase in losses in the CEC. In figure 8.29 the specific power (power/mass flow) and the specific exergy losses (exergy loss/mass flow) of the compressor and expander are shown as a function of the utilisation. The specific exergy losses in both components are constant. However, the specific power of the expander, which depends on the temperature at which the expander operates, decreases. As the fuel utilisation increases from 77.5 % to 85 %, the average temperature in the expander (the average of in and outlet temperature) decreases from 687 °C to 615 °C. This is due to the higher air/fuel ratio in the combustor. The efficiency of the CEC depends on the difference in average temperature of compression and expansion. Because the average temperature in the compressor does not change the difference becomes smaller and the efficiency of the heat recovery by the CEC decreases strongly at higher utilisation.
The net effect of increasing the fuel utilisation in both the atmospheric and the pressurised system is limited. Although the conversion process is more efficient in the fuel cell than combustor (see **Section 7.6**), increasing the fuel utilisation does not improve the exergy

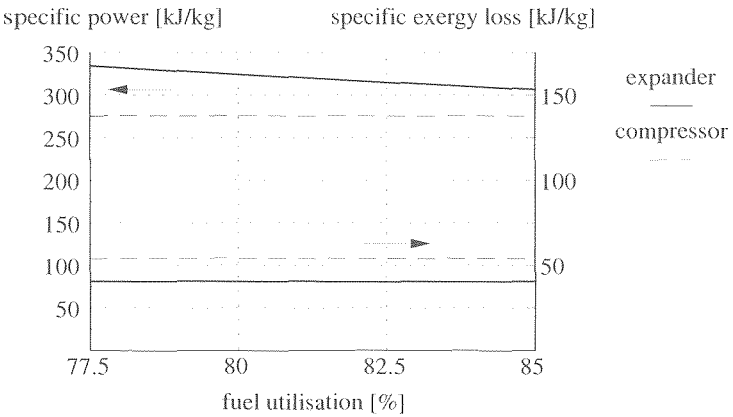

Figure 8.29: Comparison of the influence of the fuel utilisation on the specific power and specific exergy losses for the expander and the compressor

efficiency of the system considerably. This is partly due to the lower electrochemical efficiency of the fuel cell at higher fuel utilisation. Note that the sum of the exergy losses in fuel cell and combustor (in figure 8.24) is hardly affected by a change in utilisation. Correspondingly, as shown for the atmospheric system in figure 8.26, the sum of electrical (i.e. electrochemical) and chemical losses is almost unchanged.
On the other hand, losses in the system, for example the flue gas stack losses and the exergy losses as a result of heat transfer in the cathode off-gas recycle (figure 8.26) increase because more heat has to be removed from the fuel cell and a larger cathode gas flow therefore is required. In the pressurised system the exergy losses in the CEC even increase because of the lower combustion temperature. Although in principle the electrochemical reaction is thermodynamically more advantageous than the combustion reaction (primary effect), the analysis shows that a change in fuel utilisation there are a number of "secondary effects", which lead to an increase in other losses.

8.5 ANALYSIS OF AN INTERNAL REFORMING SYSTEM

8.5.1 Description of the system and calculations

The exergy losses as a result of heat transfer are dominant in the fuel cell system. The main reason is the method of cooling the cell. Air, which is preheated to a very high temperature, is used to remove the heat which is generated in the electrochemical reaction from the cell. The most efficient manner in which the heat generation in the fuel cell can be reduced, is to integrate the reforming reaction in the fuel cell. The endothermal reforming reaction, in which methane is converted into hydrogen, uses a significant part of the heat generated in the cell, strongly reducing the amount of heat which has to be removed from the cell. To analyse the influence of internal reforming on the performance and losses in the SOFC system, a configuration based on an internal reforming SOFC stack has been modelled. The cell voltage and other relevant parameters for the internal reforming SOFC cell have been determined using the detailed model (see **Section 5.4**) using the input compositions from the system calculation.
The flow sheet for the (direct) internal reforming system is shown in figure 8.30. In order to decrease the rate of the reforming reaction, in particular at the inlet of the fuel cell, the fuel supplied to the fuel cell has a relatively low concentration CH_4 and high concentrations H_2 and CO. This is achieved in two ways: the fuel is pre-reformed and part of the anode off-gas is recycled. As a result of both pre-reforming and recycle, the methane concentration at the inlet of the anode is 10% and the hydrogen concentration 25%. This inlet composition has been used for the calculations with the detailed fuel cell model (see **part II**).
The anode off-gas recycle does not only serve to increase the concentrations H_2 and CO at the inlet of the fuel cell, but is used to supply heat to the adiabatic pre-reformer. Natural gas is mixed with steam and anode off-gas prior to the pre-reformer. To prevent carbon deposition, more steam is mixed with the fuel than required for the reforming reaction. For the calculations, a steam/carbon ration of 3 at the inlet of the fuel cell is used. Due to the high concentration H_2O in the anode off-gas, only part of the H_2O required has to be supplied by the waste heat boiler in the form of steam. The anode off-gas recycle flow is determined by the temperature which is required at the pre-reformer outlet. To achieve sufficient conversion of methane an equilibrium temperature of 450 °C has been used. As a conservative estimate, the same temperature approach used in the external reformer is used (50 K), which leads to an outlet temperature of the pre-reformer of 500 °C.

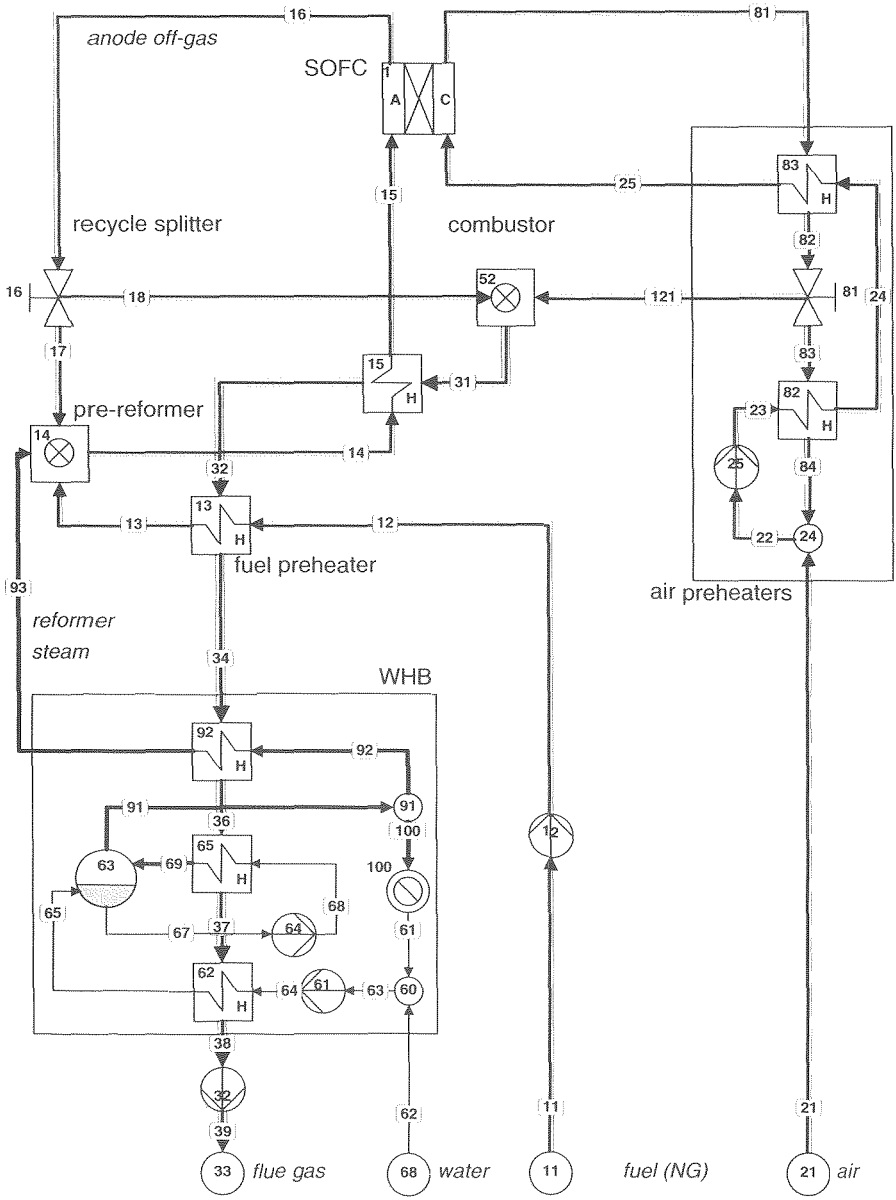

Figure 8.30: Process flow diagram for the base case internal reforming SOFC system

The fuel utilisation is determined by the need to maintain a sufficiently reducing atmosphere (i.e. a high enough H_2/H_2O ratio) in the anode to prevent oxidation of the anode material. For a system with anode off-gas recycle, it is not the fuel utilisation per pass which determines the H_2/H_2O ratio, but the overall utilisation. For the system calculations, an overall fuel utilisation of 85 % is specified and the utilisation per pass is calculated.
The cathode recycle layout for the internal reforming system (si) is the same as in the external reforming system (sr3). The part of the cathode off-gas which is not recycled is mixed with the anode off-gas which is not recycled and supplied to the combustor. The flue gas is used to preheat the anode gas and to produce steam in the waste heat boiler.

8.5.2 Energy analysis

In figure 8.31 the energy efficiency for the internal reforming system is compared to the efficiency for the external reforming system with cathode gas recycle (calculation sr3, **Section 8.2**). The fuel cell efficiency is slightly higher due to the higher cell voltage (51.9 % for ER vs. 52.1 % for IR). The auxiliary power is lower in the case of internal reforming. This leads to an increase in the net electrical efficiency from 42% for the external reforming system to 43.7% for the internal reforming system. The lower auxiliary power in the internal reforming system is to be expected: in the case of internal reforming the cooling requirements of the cell are much lower. However, the decrease in the auxiliary power consumption is not as strong as the decrease in heat generated in the fuel cell.

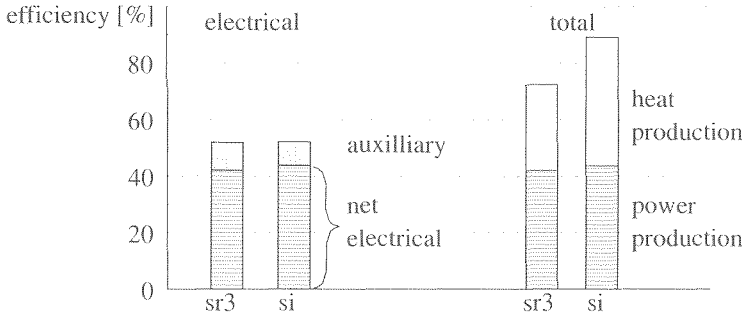

Figure 8.31: Efficiencies for an external reforming (sr3) and an internal reforming SOFC system (si)

To explain this effect, the heat balances for the external and internal reforming fuel cell stack are compared in figure 8.32. The upper bar of the two sets of bars represent the heat generation, while the lower of the two represents the heat consumption or heat sinks. The heat is generated as a result of irreversible losses ($i \cdot \Delta V$), and as a result of reversible heat term of the electrochemical reaction ($T\Delta S$). In both cases the amount of heat generated is almost the same, even if the cell voltage in the internal reforming system is higher. The higher cell voltage for the internal reforming case is caused by the higher effective temperature for the internal reforming cell (see **Section 5.4**). The higher effective temperature indicates a more advantageous combination of the concentration and temperature profile over the stack. The voltage gain is not as high as the calculations with the detailed model in **Section 5.4** indicated, due to the lower oxygen content of the cathode gas. The higher cell voltage leads lower ohmic losses in the internal reforming stack, as can be seen in figure 8.32.

But the reversible heat generated (TΔS) is higher because the reactant concentrations at anode and cathode are lower.

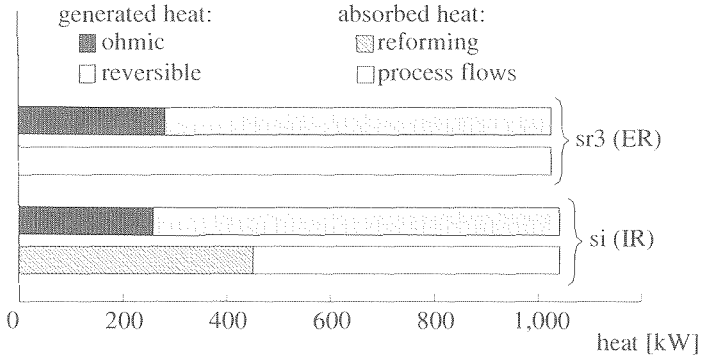

Figure 8.32: Heat balances for the fuel cell for the external (sr3) and the internal reforming SOFC (si)

The essential difference between the two stacks however lies in the way which the heat which is generated in the stack is removed. In the external reforming stack, all heat is absorbed by the process gasses, in particular of course the cathode gas. In the internal reforming stack approximately 40% of the heat is absorbed by the reforming reaction, leading to a corresponding decrease of the amount of heat left to be absorbed by the process flows.
The mass flow cathode gas required to cool the stack, however, does not decrease as strongly. The mass flow at the cathode inlet is only 11% lower in the internal reforming case than in the external reforming case. This due to the lower temperature at the outlet of the fuel cell stack. As the calculations in **Section 5.4** indicated, for a given maximum temperature in the fuel cell stack, the outlet temperature of the cathode gas is much lower for external reforming than for internal reforming. The outlet temperature in the external reforming stack is equal to 1000 °C. For the same maximum temperature the outlet temperature of the internal reforming stack becomes 950 °C. This results in a temperature difference over the fuel cell stack of 150 K in the external reforming and 100 K in the internal reforming system. Hence the amount of air required to remove the same amount of heat in the internal reforming stack is one third higher and therefore the mass flow is not 40 % but only 11 % lower. The auxiliary power, which consists mainly of the power required by the recycle compressor decreases correspondingly, from 9.9 % for the external reforming system to 8.4 % in the internal reforming system.
On the other hand the fresh air flow (stream 21 in figure 8.30) is reduced by more than 30% relative to the external reforming case. The fresh air flow does not only depend on the mass flow required to cool the cell, but on the recycle rate as well. As shown by equation 8.3, the recycle rate α depends on the temperatures of the fresh air and at the inlet of the recycle blower (which are unaltered) and on the outlet temperature of the fuel cell. Due to this effect the recycle rate in the internal reforming system (α=0.85) is higher than for the external reforming system (α=0.79). As a result, the amount of fresh air required is much lower in the internal reforming system. The flue gas flow and consequently the heat loss through the flue gas stack are also much lower. This results in the much higher total efficiency for the internal reforming system (72.4 % for ER vs. 89.2 % for IR).

8.5.3 Exergy analysis

In figure 8.33 the processes which cause the exergy losses for the external reforming and the internal reforming are compared. Evidently the greatest difference lies in the much lower losses as a result of heat transfer in the internal reforming system. This is due mainly to the fact that no heat is transferred from the process gas to the reformer bed. In the external reforming system the exergy loss as a result of heat transfer in the reformer is equal to 3.0 % of the exergy input to the system. The difference in exergy losses as a result of heat transfer between the external and the internal reforming system is 4.2 %pt. Therefore the elimination of the reformer explains the largest part of the difference. The rest is mainly caused by the lower air flow in the internal reforming system.

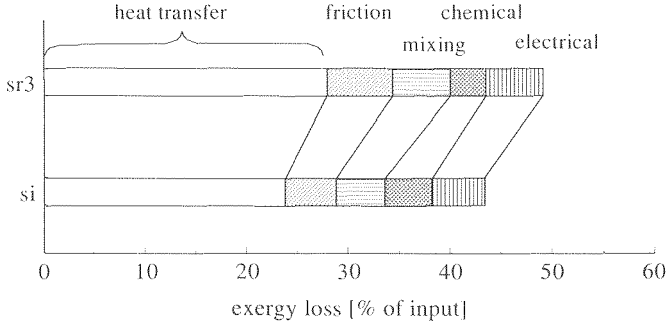

Figure 8.33: Comparison of the exergy losses per type of loss in the external reforming (sr3) and internal reforming SOFC system (si)

For most other causes the exergy losses in the internal reforming configuration are lower than in the external reforming configuration (figure 8.33). Both losses as a result of mixing (-0.9 %pt) and friction (-1.4 %pt) are closely related to the air and flue gas flow and correspondingly are lower in the case of internal reforming.
The electrical losses are lower (-0.3 %pt) as a result of the higher cell voltage which in turn is due to the higher effective temperature in the fuel cell stack. The only losses which are higher for internal reforming are the losses as a result of chemical reactions. As shown in **Section 3.4**, a high temperature for the (endothermal) reforming reaction leads to higher exergy losses. If the reforming reaction occurs in the fuel cell, the process takes place at a higher average temperature (≈900 °C) than if it occurs in the external reformer (400 °C to 850 °C). Consequently the exergy losses are higher in the internal reforming system. The exergy losses as a result of the reforming reaction in the external reformer correspond to 1.3% of the exergy input to the system and in the internal reforming configuration the exergy losses as a result of the reforming reaction are 2.2%.
The Q,T-diagram for the internal reforming system is shown in figure 8.34. As can be seen by comparing the Q,T-diagram to the corresponding diagram for the external reforming system (figure 8.5), the temperature difference at which the heat is transferred in the cathode gas recycle (air preheaters 82 and 83) is smaller. This is due to the fact that the temperature difference between the in- and outlet of the cathode gas is only 100 K in the internal reforming configuration compared to 150 K in the external reforming system. Figure 8.34 also shows the high temperature at which the flue gas is supplied to the waste heat boiler. This leads to an increase in exergy losses as a result of heat transfer in the waste heat boiler in

the internal reforming configuration compared to the external reforming system. The value diagram in figure 8.35 shows this effect.
Figure 8.36 shows the exergy losses classified according to the subsystem in which the losses occur. Differences in exergy losses between the external and the internal reforming system occur in every subsystem. The losses in the **fuel cell** are higher for internal reforming fuel

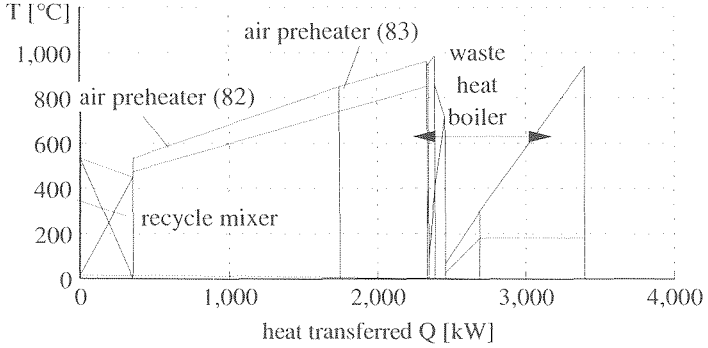

Figure 8.34: Q,T-diagram for the internal reforming SOFC system (si)

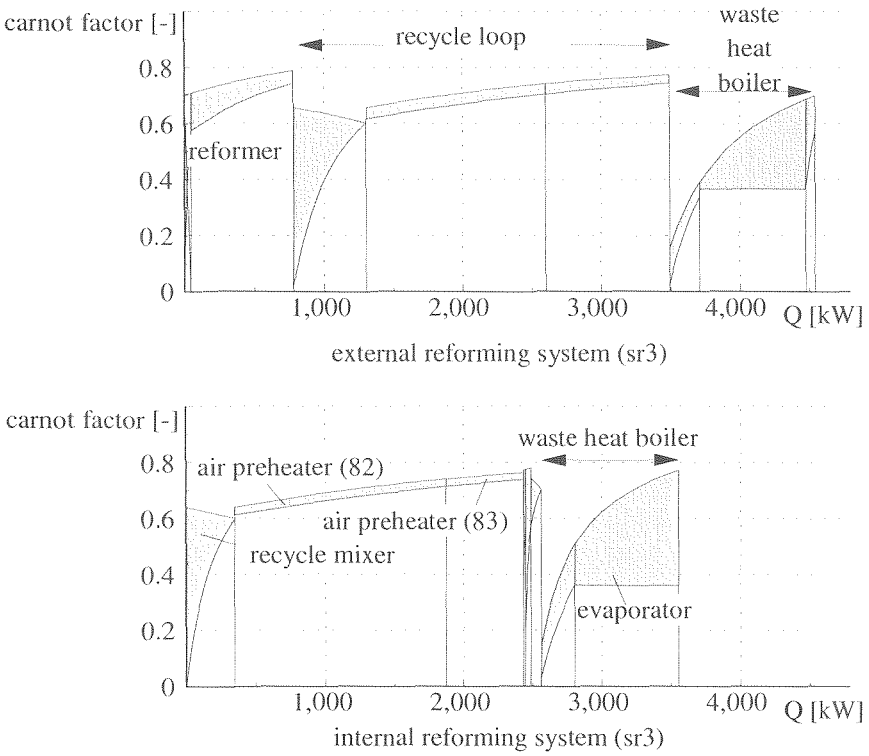

Figure 8.35: Value diagram for the external reforming (sr3) and internal reforming SOFC system (si)

cell stack (+2.0 %pt). The main reason is simply that the losses include the exergy losses in the reforming reaction. The exergy losses in the fuel cell have been calculated using the detailed fuel cell model. The results are shown in the f,H-diagram for the fuel cell in figure 8.37.The diagram shows that the reforming reaction occurs mainly near the inlet and achieves equilibrium (i.e. negligible exergy losses) rather quickly. The electrical losses are more evenly distributed and smaller than in the external reforming fuel cell. This is again due to the influence of the effective temperature (**Section 5.4**) and the resulting higher cell voltage.

The amount of heat which is transferred from the electrolyte to the process flow and vice versa is larger than in the external reforming cell: the cathode gas is first heated to the maximum temperature and subsequently cooled to supply heat to the reforming reaction (**Section 5.4**). The effect on the exergy losses however is minimal, both because of the relatively small ΔT and the high temperature at which the heat is transferred. Using an anode recycle increases anode gas flow by 40% compared to the external reforming system. The higher mass flow leads to higher exergy losses as a result of friction in the fuel cell. These losses are not shown in the f,H-diagram (see **Section 3.5**).

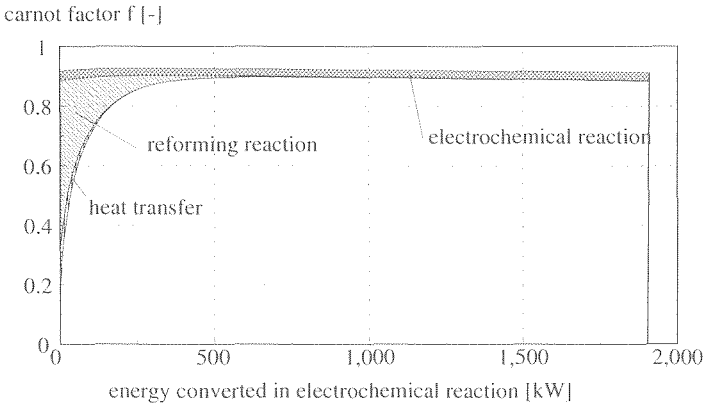

Figure 8.36: f,H-diagram for fuel cell in the internal reforming SOFC system (sip)

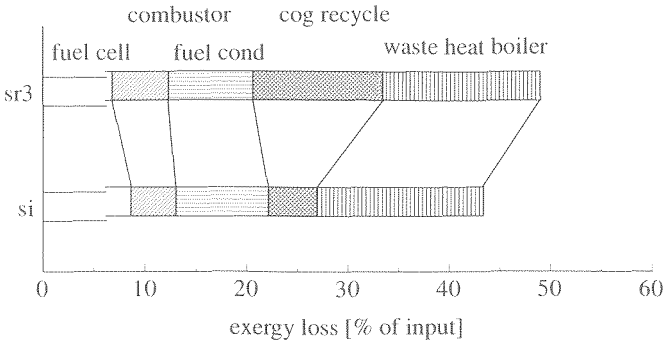

Figure 8.37: Comparison of exergy losses per subsystem in the external reforming (sr3) and internal reforming SOFC system (si)

Other losses which are higher or lower for the internal reforming system are:

- The losses in the **combustor** are lower in the case of internal reforming (-1.1 %pt). The losses as a result of mixing are far lower (decreasing from 3.3 % to 1.9 % of the exergy input to the system). The lower losses are due to the much lower air/fuel ratio in the internal reforming system compared to the external reforming system (15 vs 22 kg/kg) and the lower water content of the anode off-gas (only a small amount of reforming steam is used). The chemical reaction losses in the combustor are slightly smaller for the IR system due to the higher fuel utilisation (less fuel converted in the combustor);
- In the **fuel conditioning** subsystem the losses are evidently much smaller in the internal reforming system, because the reforming reaction and associated losses do not occur in this subsystem but in the fuel cell stack;
- The exergy losses in the **cathode off-gas recycle** subsystem are substantially lower for the internal reforming system. This is fully attributable to the lower air flow resulting from the lower cooling requirements;
- The high losses in the **waste heat boiler** can be considered a result of the high exergy efficiency of all preceding process steps. As a consequence the temperature of the flue gas flow which is supplied to the waste heat boiler is very high. But the waste heat boiler still produces process steam of a relatively low exergy value, the losses in this subsystem are large (see figure 8.35).

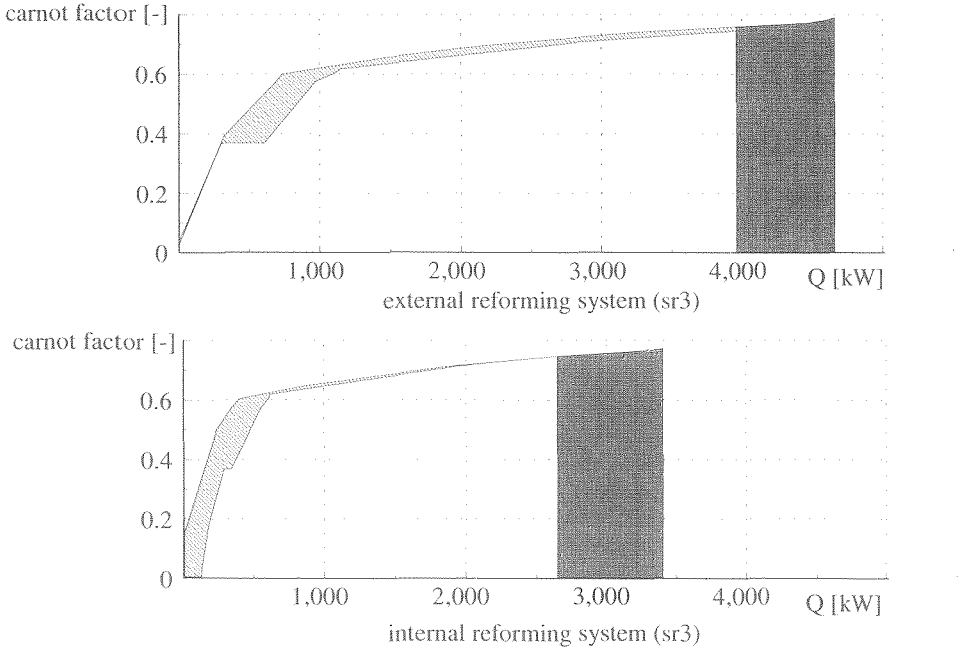

Figure 8.38: Pinch-value diagram for the external and the internal reforming SOFC system

The exergy efficiency of the internal reforming system is 56.3%, which is 5.6%pt higher than the efficiency of the corresponding external reforming system (sr3). This is mainly due to the lower losses in the cathode off-gas recycle. However, higher exergy losses occur in the waste heat boiler. The exergy losses are partly reduced and partly relocated (from the cathode off-gas recycle to the waste heat boiler). As a result, the exergy efficiency does not increase as

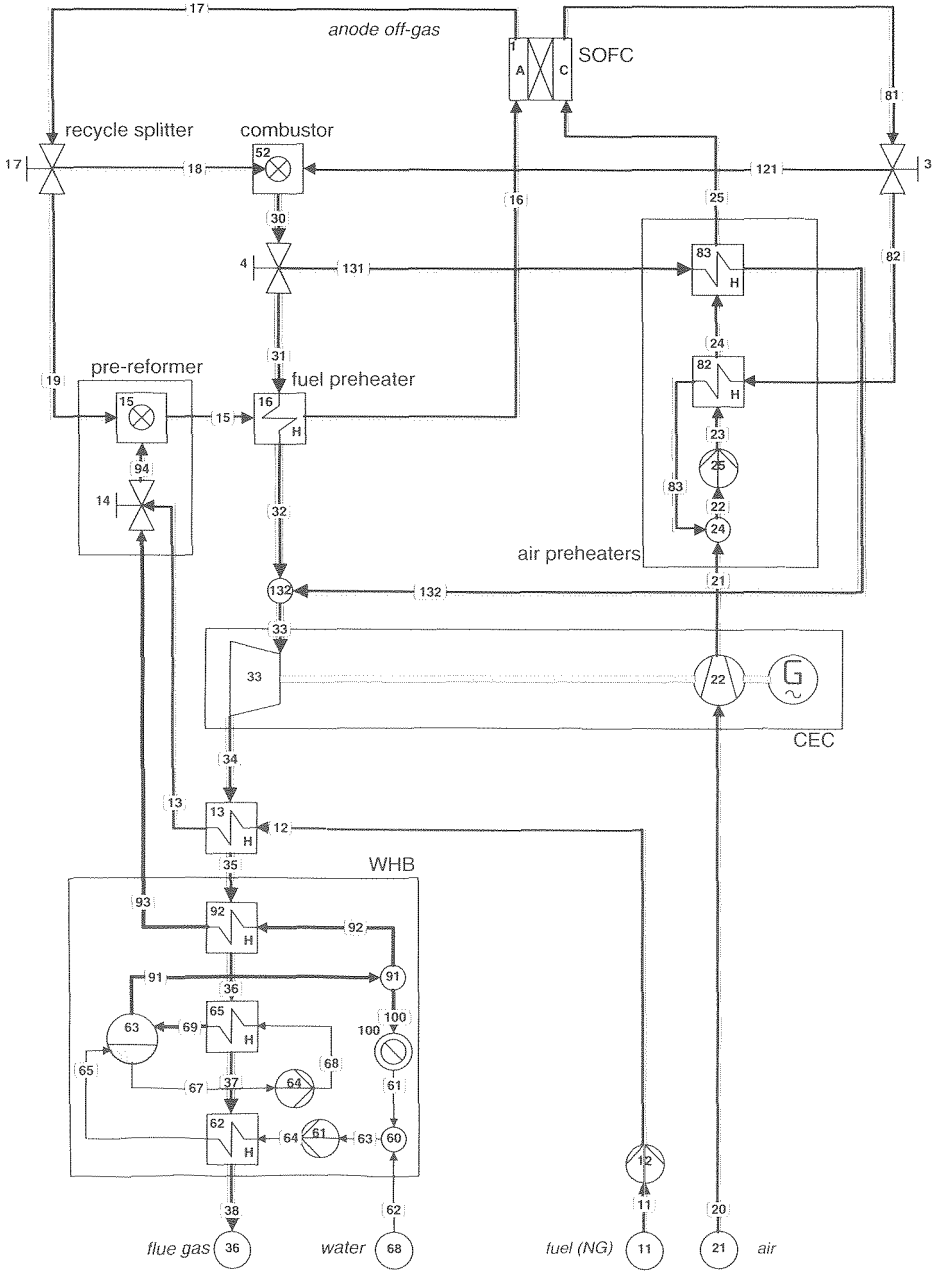

Figure 8.39: Flow sheet for the pressurised internal reforming SOFC system

much as expected. On the other hand, it should be easier to reduce the losses if they occur in the waste heat boiler. This is confirmed by the pinch-value diagram in figure 8.40. If the corresponding diagrams for the external reforming system (sr3) and the internal reforming system are compared, the heat which can be recovered at high temperature is slightly higher for the internal reforming system. Taking into account the higher exergy efficiency of the internal reforming system, this indicates that the internal reforming system will have a higher efficiency than the external reforming as well if the heat is utilised effectively. However, this is not the case in the system considered in this section.

8.6 INFLUENCE OF PRESSURE ON THE INTERNAL REFORMING SYSTEM

8.6.1 Description of the pressurised internal reforming system

Even though internal reforming limits the amount of heat which has to be removed from the fuel cell, it does not change the net amount of heat which is generated in the system. As a result, as analysis of the reference internal reforming system shows, heat transfer losses are still considerable in the internal reforming system. One way in which part of the heat in the fuel cell system can be used to produce power, is by operating the system under pressure and using an expander. Therefore calculations have been carried out for a pressurised configuration of the internal reforming SOFC system as well. The pressure has been varied from 2 to 8 bar.
Figure 8.39 shows the flow sheet for the pressurised internal reforming system. There are two main differences between the atmospheric and the pressurised system. The first is of course the addition of a compressor (app. 22) and an expander (app. 33). For both components again a 75% isentropic efficiency and a single shaft were assumed. The second difference between the two systems is a different arrangement of the heat exchangers. In the pressurised internal reforming system, figure 8.39, the final step in preheating the cathode gas is achieved using hot flue gas instead of cathode off-gas. This is necessary because using the cathode off-gas for preheating the cathode gas leads to very small temperature difference (at higher pressure even to cross-over), due to the influence of the pressure on the mass flows and temperatures in the cathode off-gas recycle. The anode gas, which is preheated from the outlet temperature of the pre-reformer to the required anode inlet temperature, is heated using heat from the flue gas after the combustor as well. To maximise the power output, the expander should operate at the highest possible temperature. In the internal reforming system, the expander is therefore placed between the final preheaters (app. 17 and app. 83) and the waste heat boiler

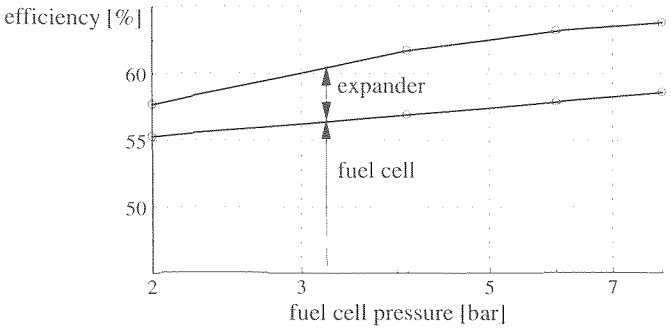

Figure 8.40: Gross efficiency of the internal reforming system as function of pressure

8.6.2 Energy analysis

Figure 8.40 shows the calculated gross efficiency for the internal reforming system as function of the pressure. The gross efficiency is the sum of the power generated by the fuel cell and by the compressor/expander combination (CEC) as a fraction of the fuel input. The power generated in the fuel cell increaseses approximately logarithmic with pressure. This is due to the log (p) term in the Nernst equation (equation 4.3). The increase in fuel cell power corresponds to approximately 1.6%pt if the pressure increases by a factor 2.
The power generated in the compressor/expander combination (CEC) increases from 2.4% of the energy input to the system at 2 bar to 4.8% at 4 bar. Further gain in CEC power is minimal and the calculated net power generated by the CEC even decreases with pressure above 6 bar.

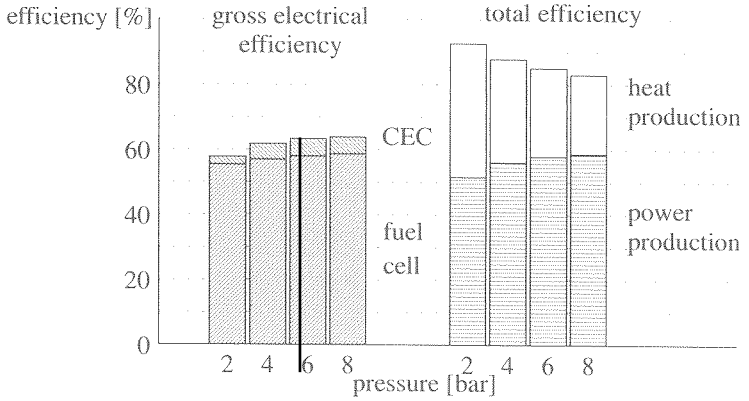

Figure 8.41: Net electrical efficiency and total efficiency of the internal reforming system for different values of the pressure

Even though the efficiency increase of the CEC may be marginal above 4 bar, the gross efficiency of the system increases considerably due to the higher power generated by the fuel cell. At 2 bar the gross efficiency is equal to 55.3 %, increasing to 58.6% at 8 bar.
Figure 8.41 shows the net electrical output of the system and the total output (heat + electrical) as a function of system pressure. The net electrical efficiency increases even stronger than the gross efficiency due to a decrease of auxiliary power at higher pressure. This decrease of auxiliary power, more specifically the recycle blower, is the result of the lower amount of heat which has to be removed from the fuel cell stack at higher pressure. The decrease in auxiliary power is considerable. Figure 8.42 can be used to explain why this is the case.
The upper bar of the two sets of bars in this figure represent the heat generation, while the lower of the two represents the heat consumption (or "heat sinks"). The heat is generated as a result of irreversible losses ($i \cdot \Delta V$), and as a result of reversible heat term of the electrochemical reaction ($T\Delta S$). At higher pressure the Nernst voltage becomes higher. Therefore the reversible heat becomes smaller (see **Section 4.4.4**). At constant power density, the higher voltage also leads to a lower current density and therefore the irreversible heat decreases as well.

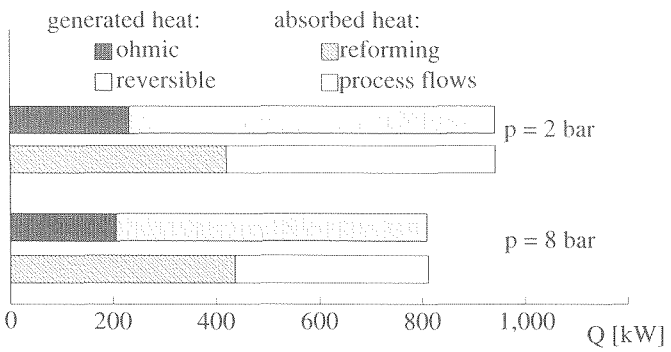

Figure 8.42: Heat balances for the fuel cell stack in the internal reforming SOFC system at 2 and 8 bar

The heat which is generated is partly absorbed by the reforming reaction. As figure 8.42 shows, the amount of heat absorbed by the reforming reaction is slightly higher at 8 bar than at 2 bar system pressure. The higher amount of cooling supplied by the reforming reaction combined with the lower amount of heat which is generated at higher pressure, leads to a strong reduction (-30 %) in amount of heat which has to be removed from the fuel cell stack by the process flows. As for the system with external reforming, a lower total efficiency is calculated at higher pressure (see figure 8.41). This decrease in total efficiency is due to the higher flue gas stack losses at elevated pressure. The higher losses are due to both the higher temperature and the higher flue gas flow (as will be shown).

The air flow to the system is determined by two effects:

- A lower air flow is expected on bases of the calculated reduction of the mass flow cathode gas required to cool the cell, which decreases from 4.4 kg/s to 3.4 kg/s.
- The cathode off-gas recycle α is determined by the temperature of cathode off-gas, the temperature of the cathode gas at the inlet of the stack and the temperature of the air which is mixed with the recycle flow. The temperature of the air is determined by the pressure ratio of the air compressor and leads to a lower recycle rate at higher pressure. The calculated recycle rate at 2 bar is 78 % and decreases to 72 % at 8 bar.

The net result is that the mass flow air which is required is equal at 2 bar and at 8 bar operating pressure. At the same time, the fuel flow decreases from 0.048 kg/s at 2 bar to 0.045 kg/s at 8 bar. This leads to an increase of the air/fuel ratio results. The increase of the air/fuel ratio in the internal reforming case is +7 % for a pressure increase from 2 to 8 bar, whereas a much stronger effect of the pressure on the air/fuel ratio was found for the external reforming system (28 % if the pressure increases from 1 to 6 bar). The moderate increase of the air/fuel ratio in the internal reforming system is due to the approximately constant cooling effect of the reforming reaction (see figure 8.42).

As indicated, the second reason for the higher flue gas stack losses is an increase in the temperature of the flue gas stack. The reason for the higher temperature with which the flue gas leaves the flue gas stack is the same as in the pressurised external reforming system (see **Section 8.3**). At 2 bar more heat is required below 200 °C than in the system at 8 bar. If the pressure is 2 bar the compressor outlet temperature is <100 °C. At 8 bar the outlet temperature of the compressor increases to 312 °C and consequently no heat is required to preheat the air. Therefore in the system operating at 8 bar the flue gas can only be used below

180 °C (temperature of the steam) by preheat and evaporating water in the waste heat boiler and preheat the natural gas. Because the heat required for this purpose is only small, the flue gas is cooled to 101 °C instead of 60 °C (2 bar).

8.6.3 Exergy analysis

Exergy losses per subsystem
The calculated exergy losses in the different subsystems of the internal reforming configuration are compared in figure 8.43 for two values of the pressure: 2 bar and 8 bar. The total exergy losses decrease from 37.3 % at 2 bar to 35.7 % at 8 bar.
The exergy losses in the **fuel cell stack** are smaller at higher pressure, which is due in part to the higher Nernst voltage. However, it turns out that a more significant effect is the reduced exergy loss in the internal reforming reaction. This will be discussed in more detail further on.
The losses in the **combustor** are higher at high pressure. This is the direct result of the higher A/F ratio. In the combustor losses occur as a result of mixing, chemical reactions and friction. The higher air flow causes an increase of all three types of losses, although the increase in friction losses is very small. The mixing losses increase from 2.1 % to 2.4 % of the exergy input to the system.
The main losses in the **cathode off-gas recycle** subsystem are the exergy losses as a result of heat transfer, which correspond to $^4/_5$ of the losses in this subsystem.

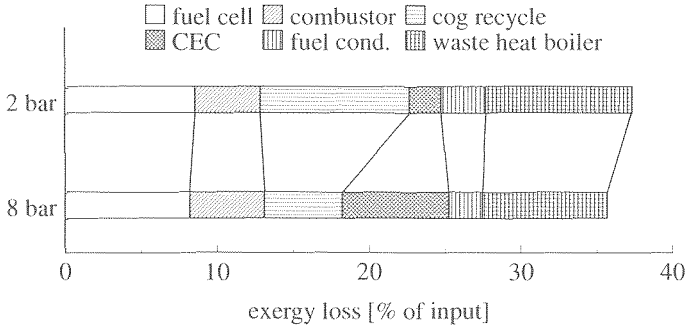

Figure 8.43: Exergy losses per subsystem for the internal reforming SOFC system at 2 bar / 8 bar

To understand the exergy losses in the cathode off-gas recycle, the value diagram is used (figure 8.44). As can be seen from the value diagram there are two reasons why the losses in the cathode off-gas recycle are lower at higher pressure:

- The largest losses as a result of heat transfer in the cathode gas recycle at 2 bar operating pressure occur when the incoming cold air is mixed with hot cathode off-gas. In the system operating at 8 bar, the compression ratio for the air compressor is 4 times as large and consequently the temperature of the air at the outlet of the compressor is much higher. In a sense, the compressor eliminates the need to preheat from 20 to 200 °C. As a result transferring heat at low temperatures, which is disadvantageous from the point of view of exergy efficiency, is avoided;
- The reduced cooling requirements for the fuel cell lead to lower amount of heat which has to be transferred in the cathode gas recycle and subsequently to lower exergy losses.

The losses in the **compressor/expander combination CEC** increase considerably. The increase in these losses, caused by friction, is even larger than the decrease of the losses in the cathode off-gas recycle subsystem. At 8 bar the both the power consumed by the compressor and the power generated by the expander is considerably higher than at 2 bar. But the net power delivered by the CEC, i.e. the difference between the delivered power (expander) and required power (compressor), is lower. This is due to the decreasing efficiency of the CEC as the difference between the average temperature of compression and expansion becomes smaller. The effect is illustrated in figure 8.45. In this figure the length of the bars represents how much the exergy change of the process flows through the compressor and expander decreases. The exergy change in the process is equal to the sum of actual the net duty of the CEC and the exergy losses (see **Chapter 2**). This value reflect s how large the duty in the CEC would be if the process would be reversible. The exergy losses indicate how the CEC duty could increase if rotating equipment with a higher efficiency were to be used. As figure 8.45 shows, the ratio between losses and duty becomes more disadvantageous at higher pressure. Two conclusions can be drawn. The first is that the system efficiency can be improved considerably by improving the efficiency of the rotating components. This has been shown for the external reforming pressurised system in **Section 8.3**. Secondly, the figure also shows that the optimal pressure will depend on the efficiency of the rotating components. The duty of the CEC does not increase further if the pressure increases from 6 to 8 bar. The graph shows that this is due to the higher losses. If the efficiency of the rotating equipment increases the duty becomes larger and the losses smaller. In that case the step from 6 to 8 bar may lead to a significant increase of CEC power.

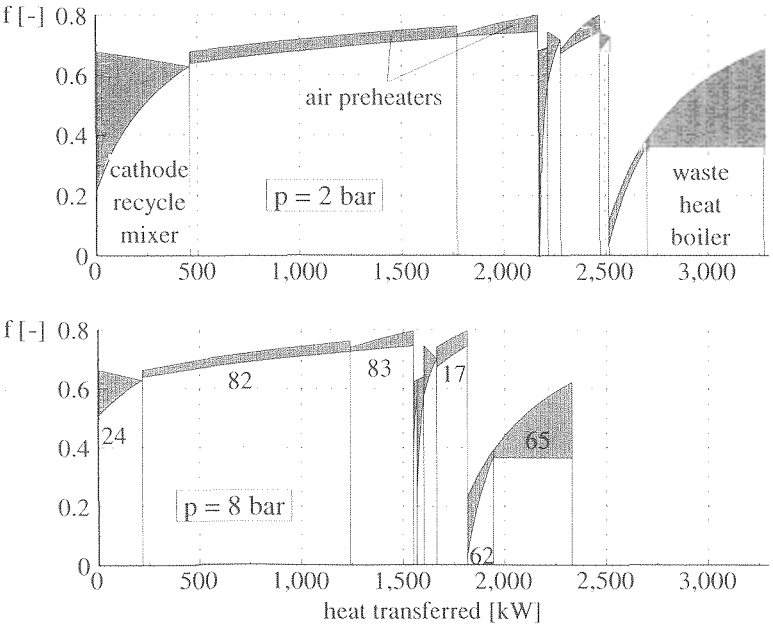

Figure 8.44: Value diagrams for the internal reforming SOFC system at 2 bar and at 8 bar

The losses in the **fuel conditioning** subsystem are substantially lower at higher pressure. Losses are reduced in all main components. In the fuel preheater the losses are lower because of the lower temperature of the flue gas at the outlet of the expander. But lower losses in the pre-reformer are the main reason for the decreased losses at higher pressure (see below). Finally, the value diagram shows (figure 8.44) the large losses which occur in the **waste heat boiler**. All heat transferred in the waste heat boiler occurs very inefficiently and therefore the lower production of steam at 8 bar automatically reduces exergy losses as a result of heat transfer.

Exergy losses per type

Figure 8.46 shows the calculated exergy losses for two values of the pressure (2 bar and 8 bar) according to the cause of the loss. Evidently a strong reduction of the exergy losses as a result of heat transfer occurs if the system pressure increases. Simultaneously the losses as a result of friction increase. On the given pressure range (2 → 8 bar) the decrease of heat transfer losses is larger than the increase in losses as a result of friction. This is the most important reason for the lower total exergy losses at 8 bar than for 2 bar.

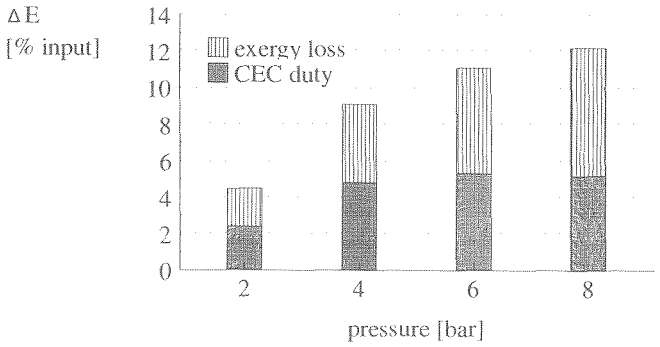

Figure 8.45: Exergy loss and duty of the CEC as a function of operating pressure

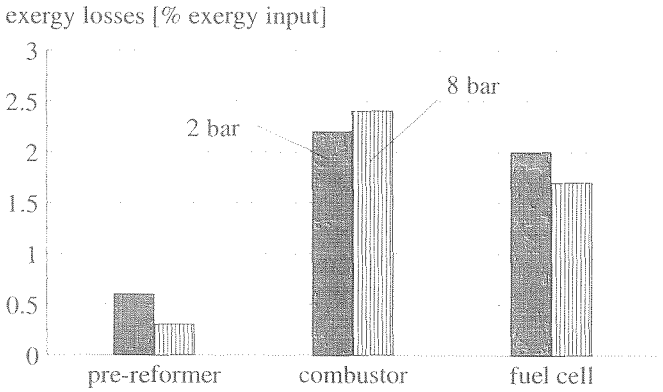

Figure 8.48: Exergy losses as a result of chemical reactions in the internal reforming fuel cell system

In figure 8.47 the sum of the exergy losses as a result of heat transfer and friction in the internal reforming system is shown as a function of pressure. As can be seen in this graph, if the pressure increases from 2 to 4 bar, the sum of both types of losses decreases. However, for a increase of pressure from 4 to 6 bar, the increase in the losses as a result of friction is almost as large as the decrease in heat transfer losses. Further increase in pressure leads to higher exergy losses as a result of heat transfer and friction. The optimum pressure for this configuration (given the efficiency of rotating equipment, fuel cell performance, etc.) is 6 bar. A second effect occurs, which influences the total exergy losses in the system as well, although to a lesser extent. This is the decrease of the chemical reaction losses at higher pressure. The calculated losses as a result of chemical reactions in the internal reforming configuration decrease with pressure. At 2 bar the losses as a result of chemical reactions amount to 4.7% of the exergy input to the system and at 8 bar the corresponding value is 4.4 % of the exergy input (figure 8.46). In figure 8.49 the components in which the chemical reactions occur and the size of these specific losses are indicated. Chemical reactions occur in three components of the system: the pre-reformer, the combustor and the fuel cell. An increase of the exergy losses as a result of chemical reactions can be noted in the combustor, while a decrease of the exergy losses occurs in the pre-reformer and the fuel cell. The higher losses in the combustor are due to the increase in A/F ratio. As a result of the higher A/F ratio, the combustion temperature is lower and consequently the losses in the chemical reaction increase. In the pre-reformer the losses decrease from 0.6 % to 0.3 %, in the fuel cell

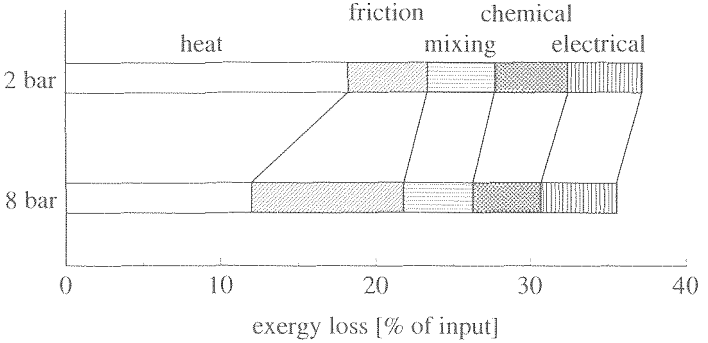

Figure 8.46: Exergy losses per type in the IR-SOFC system at two different operating pressures

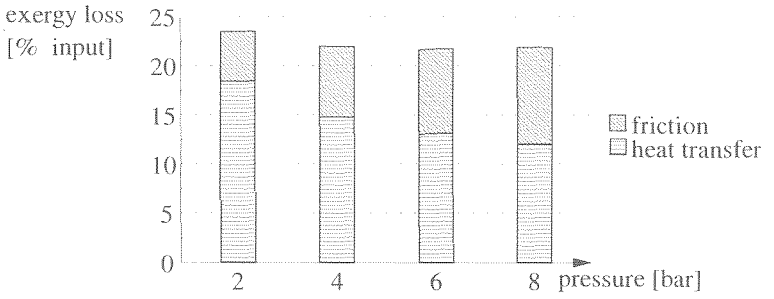

Figure 8.47: Losses as a result of friction and heat transfer as a function of the operating pressure

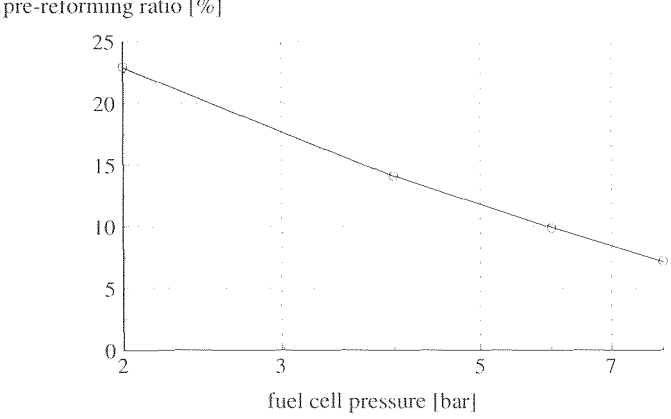

Figure 8.49: Pre-reforming ratio as function of pressure for the internal reforming SOFC system

the losses as a result of chemical reactions decrease from 2.0 to 1.7 %
The lower losses in the pre-reformer are due to a different methane conversion in the pre-reformer at 2 bar and at 8 bar. The fraction of the methane which is converted in pre-reformer can be indicated as the pre-reforming ratio. The pre-reforming ratio is determined by the equilibrium composition at the outlet of the pre-reformer of the methane reforming reaction (see **Section 8.4**):

$$CH_4 + H_2O \leftrightharpoons 3\,H_2 + CO$$

Due to the higher number of moles on the right-hand side of the reaction, higher pressure will reduce the conversion of methane. In figure 8.49 the pre-reforming ratio is given as a function of pressure. At 2 bar operating pressure 23% of the methane is converted in the pre-reformer and at 8 bar this ratio has decreased to 7%. Conversely the amount of methane converted in the fuel cell increases from 77 % to 93 % (full conversion of methane is achieved in the fuel cell stack). Although the conversion increases, the exergy losses as a result of the reforming reaction in the fuel cell decrease. Again the effect of pressure on the reforming reaction is responsible. At higher pressure the reforming reaction is closer to equilibrium in the fuel cell. In other words, the equilibrium temperature (see **Chapter 3**) is closer to the actual temperature.
These analysis in this section shows a large increase in electrical efficiency if the system is operated at higher pressure (at 4 bar the efficiency is more than 12 %pt higher than the efficiency of the atmospheric system). This is an even larger increase in efficiency than the external reforming system. The effect of pressurisation is the same as in the system with external reforming (an increase in electrical efficiency of the fuel cell, more power delivered by the CEC and less power required for the recycle blower). Differences between the effects of pressurisation in the internal and external reforming system are found as well:

- In the internal reforming system, part of the natural gas is reformed in the pre-reformer. Because less methane is pre-reformed at higher pressure, the cooling effect of the reforming reaction is stronger at higher pressure;
- The influence of the pressure on the efficiency of the fuel cell is stronger than in the external reforming case.

CHAPTER 9
ANALYSIS OF MCFC CONFIGURATIONS

9.1 INTRODUCTION

Exergy analysis of the base case MCFC system in **Chapter 7**, clearly shows the importance of the heat transfer losses. Half of the exergy losses in the base case MCFC system are due to heat transfer (see **Section 7.4**). The main reason for the large loss lies in the large amount of high temperature heat which is generated in the system, i.e. in the fuel cell and in the combustor. Part of this heat is utilised within the system. Another part of the heat is used to produce intermediate pressure steam at 180 °C in the waste heat boiler. Producing the steam, or removing the heat from the system through the cooling water or flue gas stack occurs at a temperature much lower than the temperature at which the heat is generated (>600..1200 °C). This leads to large exergy losses.
There are two obvious methods to reduce these losses:

a. Recovering heat at a higher temperature than the process steam temperature
   The two components which utilise high temperature heat in the MCFC system are the reformer and in the expander. The amount of heat which is used in the reformer can not be influenced (it is determined by the fuel flow). Therefore increasing the amount of heat (of high temperature) which is used in the expander seems the most favourable option to decrease the 'heat surplus' in the MCFC system. In the first part of this chapter several ways of increasing the power generated by the compressor/expander combination (CEC) are evaluated.
b. Reducing the amount of heat which is transferred in the system.
   In the fuel cell system a substantial amount of heat is transferred in the reformer and in the cathode off-gas recycle to preheat the cathode gas. By using an internal reforming fuel cell stack, heat transfer to the reformer is eliminated and heat transfer to cathode gas is strongly reduced. Internal reforming is the therefore a very effective method for reducing the amount of heat which is transferred in the system.

Reducing the (exergy) losses as a result of heat transfer is the main focus of this chapter. In **Section 9.2** recovering heat in the anode off-gas recycle is considered as a way to reduce the losses. **Section 9.3** discusses the effect of preheating the air before the cathode off-gas recycle. Direct recycling of anode off-gas is considered in **Section 9.4**. The benefits of increasing the duty of the expander by use of steam injection are evaluated in **Section 9.5**. Increasing the pressure ratio over the expander is another way of recovering more energy with the expander. **Section 9.6** discusses the influence of the pressure. The second part of the chapter is devoted to the analysis of two internal reforming configuration. **Section 9.7** analyses a base case system and **Section 9.8** analyses the influence of the fuel utilisation on the performance of and the losses in the internal reforming system

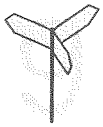

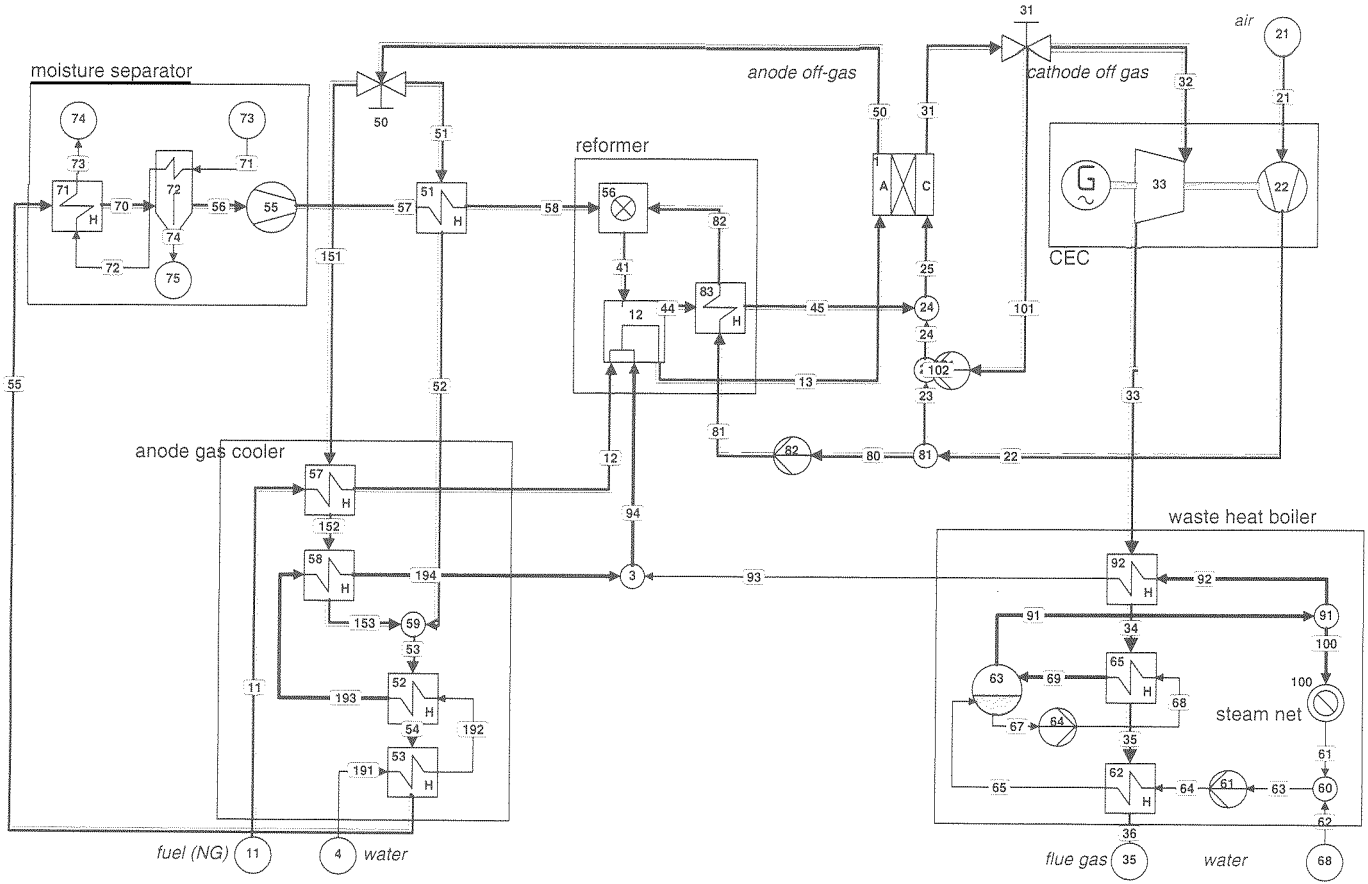

Figure 9.1: Process flow diagram for the external reforming MCFC system with steam production in the anode off-gas recycle (me1)

9.2 SYSTEM WITH HEAT RECOVERY IN THE ANODE OFF-GAS RECYCLE

9.2.1 Description of the system and calculations

In **Chapter 7** the exergy losses as a result of heat transfer in the MCFC system have been determined. The value diagram for the base case system (figure 7.16) shows that large exergy losses occur in the anode gas recycle. The anode off-gas is cooled down to remove a large part of the water and then reheated before it is used in the reformer. Based on the large exergy losses in the process of cooling and reheating the anode off-gas, found in the analysis of the base case system, an improved system is considered in this section. In the improved system part of the heat which is released by cooling down the anode off-gas, is used to produce process steam. In all other aspects, the system corresponds to the base case system discussed in **Chapter 7**. The flow sheet for the system with heat recovery in the anode off-gas recycle (me1) is shown in figure 9.1. In the anode recycle loop, the anode off-gas flow is split into two parallel flows: one flow to provide heat to the anode off-gas which is reheated in the generator and one flow which is used for preheating the fuel (app. 57) and superheating the reformer steam (app. 58). The mass flows have been calculated in such a manner that the temperature of both flows are the same at the outlet of respectively the superheater and the regenerator. The mixed flow passes through the evaporator (app. 52) and the preheater (app. 53). The pressure of the reformer steam is not 10 bar, as in the waste heat boiler, but 5 bar. This allows further cooling of the anode off-gas as the saturation temperature of the steam in the evaporator decreases to 147 °C (vs. 180 °C in the waste heat boiler). The amount of heat in the anode off-gas is not sufficient to generate all the required reforming steam, the remainder of the reforming steam must be generated in the waste heat boiler.

9.2.2 Energy analysis

In figure 9.2 the efficiencies for the base case external reforming MCFC system and for the system with the improved anode off-gas recycle are shown. All values, except the heat production and the total efficiency, are the same in both systems. By making use of part of the heat of the cooling anode off-gas to generate steam in the recycle, a smaller fraction of the steam produced in the waste heat boiler is used in the reformer and more steam can be exported. This results in an increase or the heat production from 7.9% to 19.1% of the energy input to the system. Correspondingly the total efficiency increases from 55.6% to 66.7%.

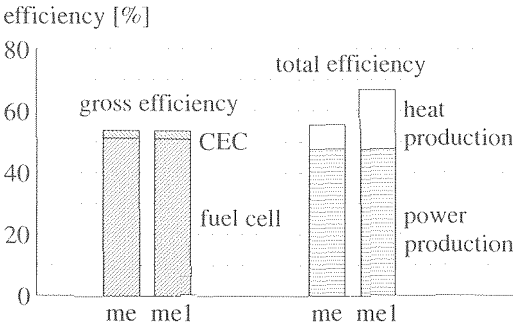

Figure 9.2: Comparison of the efficiencies of the base case system (me) and the system with heat recovery in the anode off-gas recycle (me1)

Figure 9.3 shows the two composite curves for the system. The cold curve clearly shows the two separate pressures at which steam is generated in the reference system: 5 bar/150 °C in the anode gas recycle loop and 10 bar/180 °C in the waste heat boiler. Furthermore heat is required for preheating the process flows (15 °C → 600 °C) and for the reforming process (400 °C → 800 °C). The small slope (dQ/dT) in the temperature range from 400 °C to 600 °C indicates that most heat is required in this temperature range. The hot curve starts at 1200 °C, which is the outlet temperature for the combustor. The heat which is generated in the fuel cell is released mainly in the cathode gas recycle, i.e. between 700 °C and 600 °C, with additional heat generated between 700 °C and 715 °C by the recycle blower.

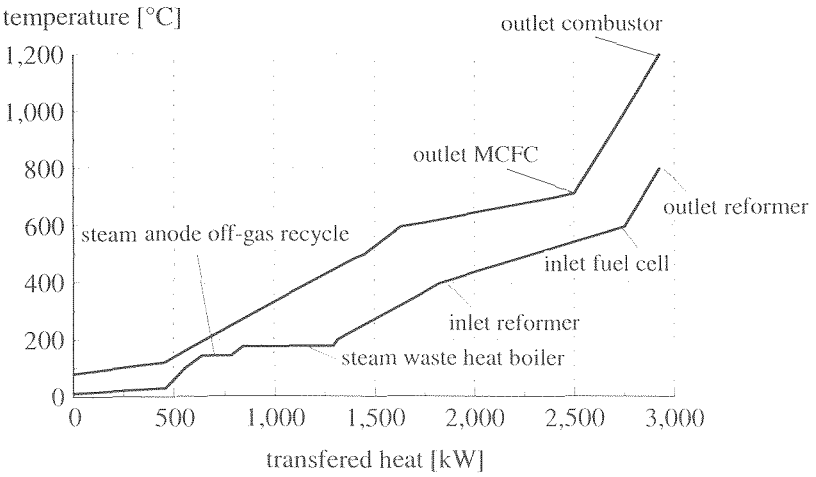

Figure 9.3: Cold and hot composite curves for the system with heat recovery in the anode off-gas recycle (me1)

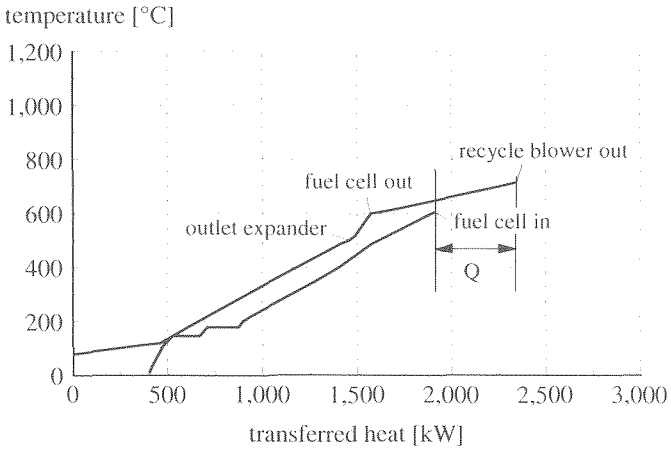

Figure 9.4: Pinch diagram for the reference system excluding the heat to the cooling water and the process steam and the heat transferred in the reformer

In the pinch diagram in figure 9.3 all heat flows in the system are included. However, to determine how much heat could be recovered at high temperature, not all heat flows are relevant for the pinch analysis. Only the heat used to generate the reformer steam in the waste heat boiler should be taken into account. The heat which is used to produce process steam can potentially be used in other ways (at higher temperature). The heat which is transferred to the cooling water does not have to be taken into account, as this heat is not required for the process in the fuel cell system. Finally the heat which is exchanged in the reformer is not included. Because of the assumption that the reformer (bed) requires a flue gas inlet temperature of 1200 °C, the flue gas in all configurations considered in this thesis will first pass through the reformer. Therefore, for the analysis only the heat in the flue gas after the reformer is relevant. The pinch diagram excluding the heat to the cooling water, the heat used to produce process steam and the heat transferred in the reformer is shown in figure 9.4. The diagram indicates the amount of heat which potentially could be recovered at a higher temperature. Compared to the base case system, this amount increases by approximately 50%. To see how this relates to the efficiency of the system, the exergy of the heat has to be taken into account.

9.2.3 Exergy analysis

The exergy losses in the system are shown in figure 9.5. In comparison with the exergy losses in the base case system (figure 7.8) only the losses in the anode off-gas (aog) recycle are lower. Heat transfer losses however remain dominant.

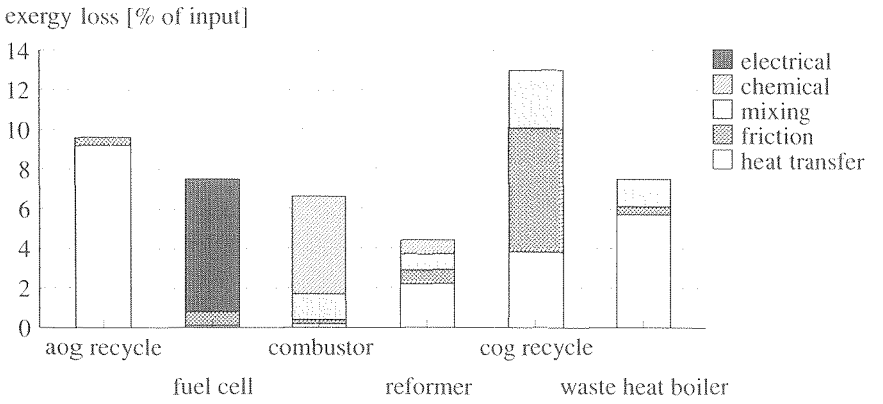

Figure 9.5: Exergy losses in the system with improved anode off-gas recycle (me1) for each subsystem and type of exergy loss

In the system with improved recycle, part of the heat in the anode off-gas is used for producing steam, leading to the higher total efficiency shown in figure 9.2. However, because the heat is produced at much higher temperature, the heat is not utilised with a high exergy efficiency. To examine the potential use of this heat the pinch-diagram in figure 9.4 can be used. If the temperature on the Y-axis in this diagram is replaced by the Carnot factor of the heat, the exergy of this heat is visualised. This diagram is shown for both the base case system (**Chapter 7**) and the system with heat recovery in the anode off-gas recycle in figure 9.6. The hatched area on the right indicates represents the exergy of the heat which can

be recovered at high temperature. In the system with improved anode off-gas (aog) recycle this is approximately equal to 300 kW. This corresponds to 15 % of the exergy supplied to the system with the fuel and is also substantially higher than in the base case system. The graph therefore shows that decreasing the losses as a result of heat transfer can therefore substantially increase the exergy efficiency of the system. It is however essential to utilise the heat which is (or becomes) available. Using the heat to produce steam at 180 °C (corresponding to a Carnot factor f_Q=0.34) limits the efficiency of the total process. As the pinch-value diagram in figure 9.6 shows, the efficiency with which the heat can be recovered is at best not more than approximately 50% if the heat is used to produce steam (assuming the system produced 10 bar steam). The actual improvement in exergy efficiency of the system (from 48.1% for the base case system to 51.4% for the improved system) corresponds well with this analysis.

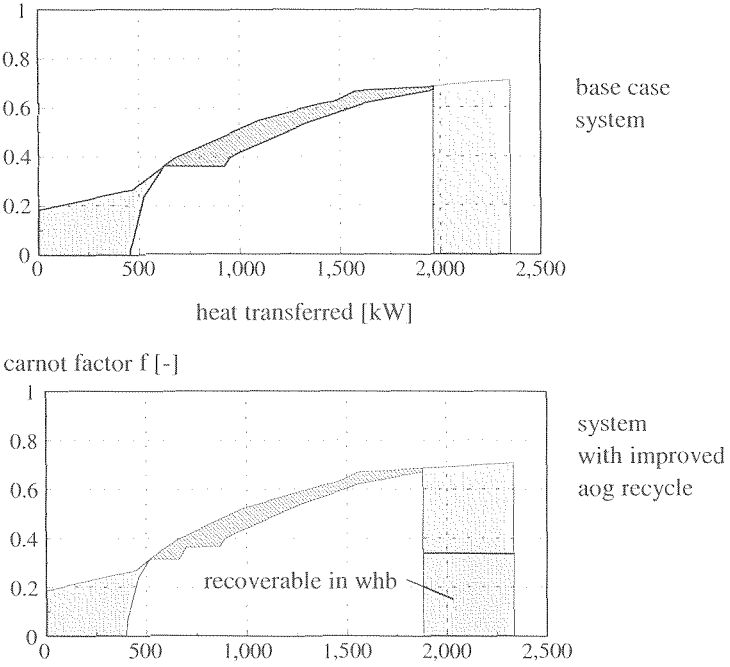

Figure 9.6 Pinch-value diagram for the ER-MCFC system with improved anode off-gas (aog) recycle

9.3 USING AIR PREHEATING TO REDUCE HEAT TRANSFER LOSSES

9.3.1 Description of the system and calculations

Using high temperature heat to produce process steam inevitably leads to exergy losses. To increase the efficiency of the system, it is better to use the heat to produce electricity in the CEC (compressor/ expander combination). One way in which the net power generated in the CEC can be increased is by increasing the mass flow which passes through the compressor

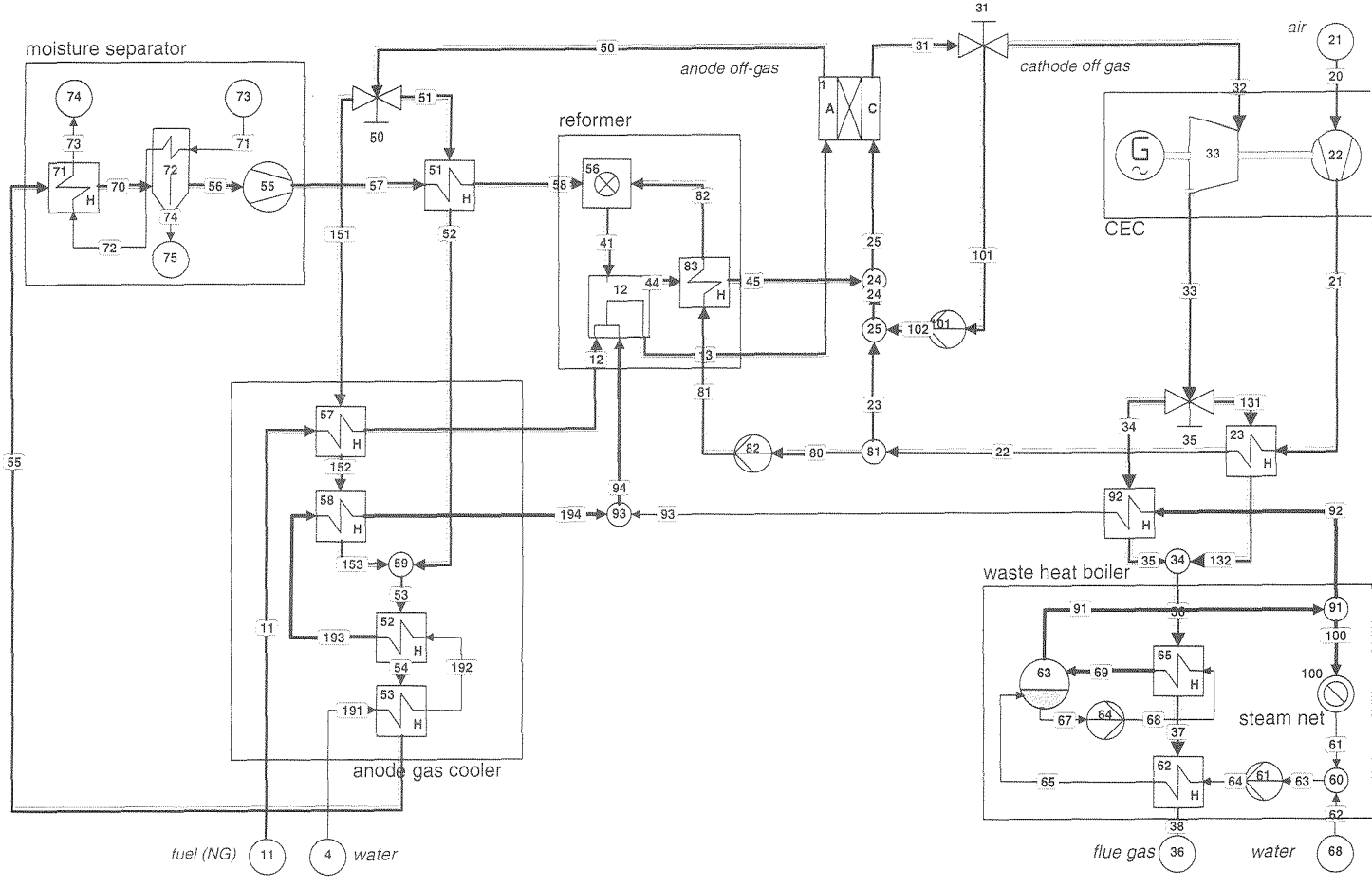

Figure 9.7: Process flow diagram for the external reforming MCFC system with air preheater before the cathode off-gas recycle (me1)

and the expander. This can be achieved by preheating the air which is supplied to the cathode off-gas recycle loop. The calculations for the pressurised systems in chapter 8, showed that temperature of the air has a considerable influence on the mass flow through the CEC. In this section the effect of preheating on the duty of the CEC and on the efficiency and the losses of the total system will be considered.

The mass flow through the expander is a mixture of two flows. The first flow is the flue gas from the combustion of the anode off-gas. The second flow is the air flow. These flows are mixed before the fuel cell in which a fraction of the O_2 is removed from the flow. The air flow exceeds the fuel flow by an order of magnitude (see **Section 7.3**). The flow through the CEC (i.e. the compressor and expander) is therefore mainly determined by the amount of fresh air supplied to the system.

The flow through the cathode side of the fuel cell is determined primarily by the amount of heat which must be removed to cool the stack. In the reference system (figure 9.1) the air is preheated by mixing the cold air with recycled hot cathode off-gas. To this end 75% of the cathode gas is recycled. As a consequence the fresh air flow, and therefore also the flow through the CEC, is approximately 4 times as small as it would be without recycling cathode off-gas. One method to increase the flow through the expander is therefore to reduce the recycle ratio.

Analysis of the recycle ratio in the SOFC system (**Section 8.2**) showed that the recycle ratio is determined by the energy balance of the cathode off-gas recycle loop. The energy balance is determined by the temperatures of the flows which are supplied to and exit from the recycle loop. The relevant temperatures in the recycle loop correspond to in- and outlet of the fuel cell stack and can therefore not be chosen freely. But the temperature at which the fresh air is supplied to the recycle loop can be varied by preheating the air. If the air is preheated before it is mixed with cathode off-gas, the amount of cathode off-gas that must be recycled to achieve the required inlet temperature for the fuel cell will decrease.

The flow sheet for the system with air preheating is shown in figure 9.7 and corresponds to the reference system, but for the addition of an air preheater. The temperature at the outlet of the air compressor (app. 22) is equal to 204 °C as a result of adiabatic compression. This temperature is further increased to 300 °C in the air preheater (app. 23) and subsequently mixed with the hot cathode off-gas and the combusted anode off-gas to reach the required inlet temperature of 700 °C. The flue gas flow at the outlet of the expander (T=500 °C) is split into two flows[r]. The first is used to superheat the reformer steam and the second flow is used to preheat the air.

9.3.2 Energy analysis

The efficiencies for the calculations me1 (reference system) and me2, the system with air preheater are shown in figure 9.8. The first two bars in the graph represent the gross electrical efficiency for both the calculations[s]. The compressor/expander duty increases from 2.6 % to 3.5 % of the fuel input on LHV basis. In spite of the larger contribution of the compressor/expander to the generated power, the gross efficiency is slightly lower for the system with air preheating me2 (53.4%) compared to 53.5 % for the reference system me1. This is due to the lower power generated by the fuel cell. Expressed as a fraction of the

---

[r] If heat exchangers 23 and 92 are placed in series, temperature cross-over occurs in the downstream heat exchanger

[s] The gross power output for the system is defined as the power generated in the fuel cell stack (AC-power) plus the net power delivered by the compressor/expander combination (CEC).

energy input to the system, the electrical power generated in the fuel cell decreases from 50.9 % to 49.9 % (figure 9.8). As will be shown below, the difference in performance is due to the influence of reactant concentrations in the recycle loop (O_2 and CO_2).

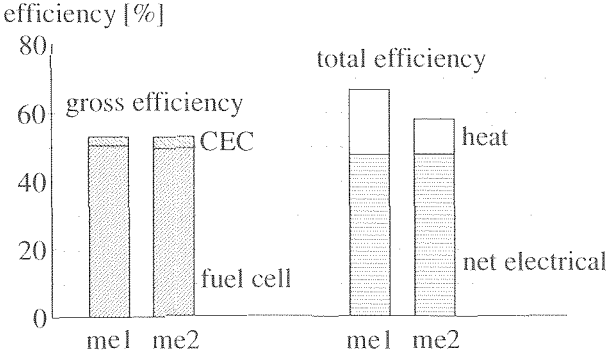

Figure 9.8: Calculated efficiencies for the reference system (me1) and the system with air preheater (me2)

The auxiliary power required is determined mainly by the cathode off-gas recycle blower (app. 101). The lower recycle ratio in the second configuration (me2) leads to a slightly lower auxiliary power requirement. The influence on the net efficiency is very small (47.6% for the reference system vs. 47.8% for the system with air preheater). The amount of steam that is produced in the waste heat boiler is lower in the system with air preheater. This results in a substantially lower total efficiency (net electrical power + heat) of 58.2 % vs. 66.7 % for the reference system. To explain these results first the effect of the recycle on the reactant concentration on the cathode side will be discussed. Subsequently the exergy losses will be analysed.

Influence of the recycle ratio on the reactant concentration

The cell voltage, and consequently the efficiency of the fuel cell, depend on the reactant concentrations at both anode and cathode. Firstly the Nernst voltage depends on the reactant concentrations (**Section 4.3**). More importantly (at least with respect to these calculations), the reactant concentrations influence the cell resistance. In **Appendix 4** a correlation is selected for the cell resistance which assumes the cell resistance to be proportional to:

$$R \sim \log (1 + p_{O_2}^{½} \cdot p_{CO_2})$$

The different values of the fuel cell efficiency (50.9 % for the reference system and 49.9 % for the system with air preheat) can be explained for ⅓ as a result of the difference in the Nernst voltage in both cases. The remaining part (⅔) of the change in fuel cell efficiency is due to difference in cell resistance as a result of changes in reactant concentrations at the cathode side for both calculations. For the reference system the calculated concentration CO_2 at the inlet of the fuel cell equals 7.8 % and the O_2 concentration 12.0 %. For the system with air preheating the CO_2 concentration decreases to 6.4 % and the O_2 concentration increases to 14.7 %. The lower CO_2 concentration for the second calculation has a larger influence and leads to a lower value of the cell voltage for the system with air preheat (706 mV) than for the reference system (720 mV). This is mainly due to the lower calculated resistance in the latter case (1.00 ohm cm^2 and 1.02 ohm cm^2 respectively)

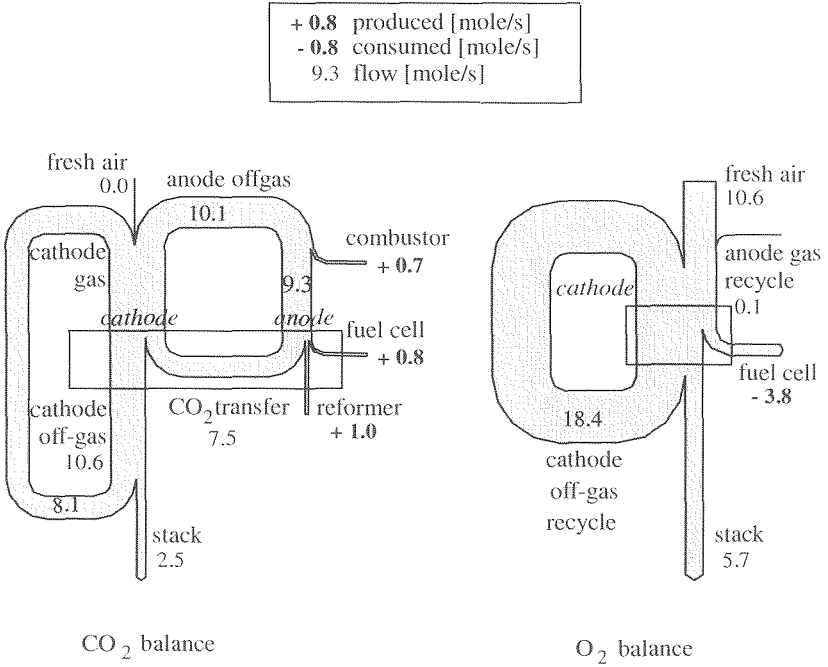

Figure 9.9: Mole balances for CO_2 and O_2 for the reference external reforming MCFC system (me1)

To understand why the CO_2 concentration is lower than for the reference system and how the concentrations of the reactants can be increased, mole balances (in mole/s) have been determined for these two components for the reference system. The flows of the components can be seen in figure 9.9.

To supply CO_2 to the cathode, the fresh air (which contains virtually no CO_2) is mixed with recycled anode off-gas and cathode off-gas. The total mole flow CO_2 at the inlet of the cathode is 18.2 mole/s. The anode off-gas recycle contains 10.1 mole CO_2/s (figure 9.9). The CO_2 in the anode off-gas originates from four different sources.

- The largest part of the CO_2 (7.5 mole/s) is transferred from the cathode side to the anode flow in the fuel cell. This is the CO_2 which is transported through the electrolyte in the form of $CO_3^{=}$ ions;
- In the reformer methane is converted into H_2 and CO in the reforming reaction and subsequently part of the CO is oxidised into CO_2 in shift reaction. This produces 1.0 mole CO_2/s;
- In the fuel cell hydrogen is consumed and consequently CO is converted into H_2 in the shift reaction producing 0.8 mole/s CO_2;
- Finally the combustion of CO in the anode off-gas combustor leads to an additional production of 0.8 mole/s.

The largest source of CO_2 at in the cathode gas is CO_2 which is recycled from the cathode outlet (8.1 mole/s).

The fresh air flow supplies O_2 to the system. More than ⅓ of the oxygen supplied to the fuel cell comes directly from the fresh air. The remainder of the O_2 comes from the cathode off-gas recycle. O_2 is only supplied in negligible quantity from the anode side: the flue gas from

the anode gas combustor contains 0.6 % O_2.
The differences between CO_2 and O_2 balance are clear. The flow O_2 in the air supplied to the system equals 10.6 mole/s. This is considerably higher than the CO_2 production (total 2.5 mole/s) and subsequently it is much easier to achieve higher concentrations O_2 at the in- and outlet of the cathode. The difference is also that the air flow supplies the O_2 to the cell, while the CO_2 supplied to the cell comes from different sources and relies strongly on the recycles. Furthermore the ratio between the CO_2 produced in the system (reformer + anode + combustor=2.5 mole/s) and the CO_2 required to enable the electrochemical reaction (7.5 mole/s) is not favourable.
One of the main parameters which determines the CO_2 concentration is the recycle ratio. If less cathode off-gas is recycled, the fresh air flow becomes larger. Consequently, a low cathode off-gas recycle ratio leads to a low CO_2 concentration at the cathode. The effect of the recycle on the O_2 is the opposite. Lowering the recycle will lead to a higher flow of fresh air and as a result to a higher input of O_2 to the system. The net result of preheating the air is a lower recycle ratio. The system with air preheater therefore has both a lower CO_2 and a higher O_2 concentration at the cathode. Because the cell resistance is more sensitive to the CO_2 (mainly because this reactant is available in lower concentrations) the cell voltage decreases from 720 mV in the reference system (me1) to 706 mV in the system with air preheater (me2).

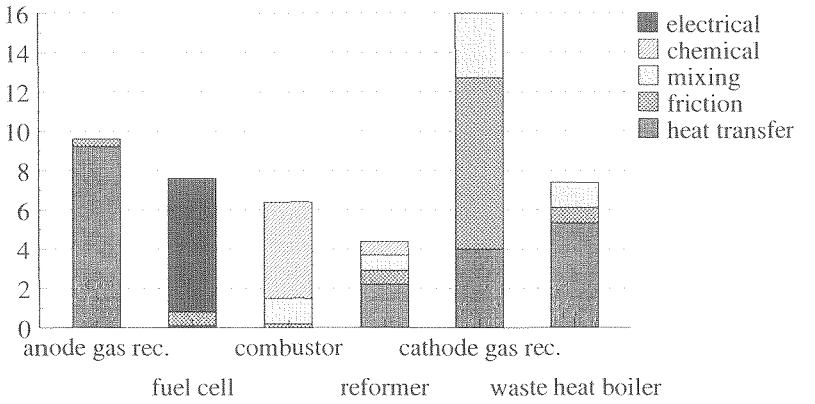

Figure 9.10: Exergy losses in the subsystems classified according to the cause of the exergy loss for the system with air preheater (me2)

9.3.3 Exergy analysis

In figure 9.10 the contributions to the exergy losses for the system with air preheat are shown for each subsystem and for each separate cause and in figure 9.11 the exergy losses for the different causes are compared for the reference system (me1) and the system with air preheater (me2). The losses as a result of mixing, chemical reactions and the electrical losses are approximately the same in both cases. The slight increase of electrical losses is due to a small increase of the polarisation, due to the decrease of reactant concentration at the cathode side. The difference in exergy losses in both systems is mainly due to a higher loss as a result of friction and a lower loss as a result of heat transfer in the case with air preheating.

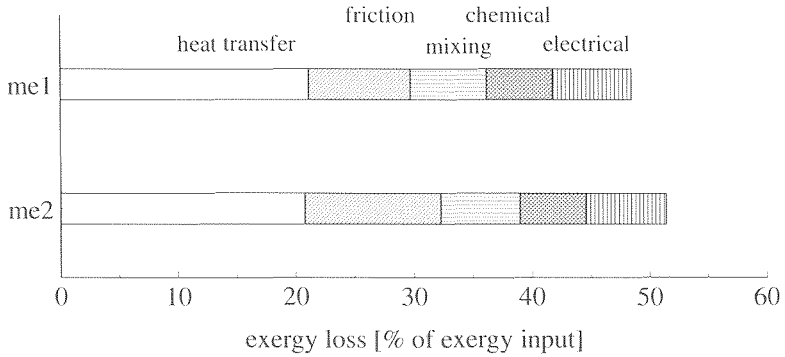

Figure 9.11: Comparison of the contributions of the causes of exergy losses to the total for the reference system and the system with air preheater

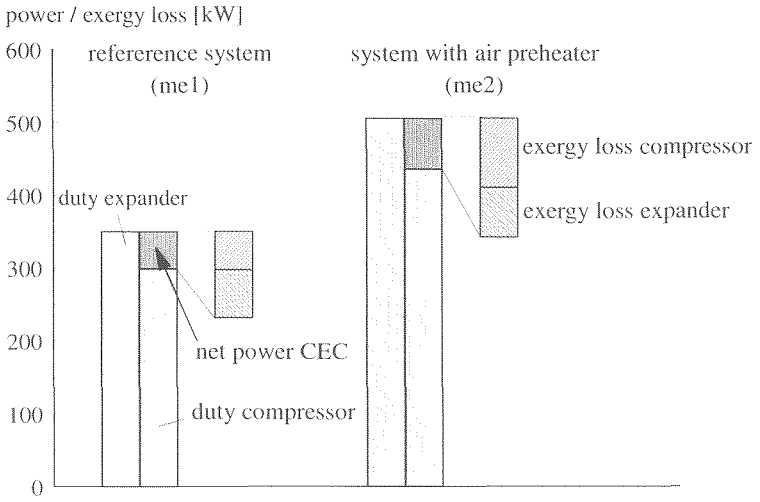

Figure 9.12: Comparison of the net power delivered by the compressor/expander combination and the exergy losses in its components

friction

If the air is preheated, the losses as a result of friction increase from 8.6 % to 11.4 % of the exergy input to the system. This is due to the increase of the exergy losses in the expander and the compressor. The expander generates 505.9 kW and the compressor consumes 436.3 kW. The difference is the net generated power and equal to 69.6 kW. For the compressor the exergy loss equals 22 % of the power input to the compressor, for the expander the exergy loss equals 13 % of the generated power. However, if the exergy losses in the compression/expansion process are compared to the net power generated by the expander and the compressor, the result is different. This is shown in figure 9.12 where the net power and exergy losses for the CEC are compared. In the reference system the net power

generated is equal to 51.1 kW and the losses total 112.6 kW, i.e. more than twice as large as the net power generated.
For the system with air preheater, both the flows through the compressor and expander are higher than in the reference system. Comparing both cases it can be seen that if the air is preheated the net power generated in the expander/compressor combination increases with 18.5 kW but the exergy losses increase with 40.9 kW. This indicates a relatively low 'efficiency' of the compression/expansion process.

heat transfer
The losses as a result of heat transfer are expected to decrease if the air is preheated based on two considerations. As shown in **Section 7.5** the main reason for the high losses as a result of heat transfer in the reference system is the high temperature of the available heat. If the air is preheated, the flow through the expander increases and therefore more heat is used to produce power in the expander. The surplus of high temperature heat therefore decreases. Secondly the highest losses as a result of heat transfer in the reference system occur when the fresh air is mixed with the hot cathode off-gas recycle flow due to the high temperature difference between both flows. Preheating the air flow decreases the temperature difference and the therefore the exergy losses as a result of heat transfer.
The decrease of the exergy losses as a result of heat transfer if the air is preheated is much smaller than expected on basis of these considerations. Why the decrease of the exergy losses

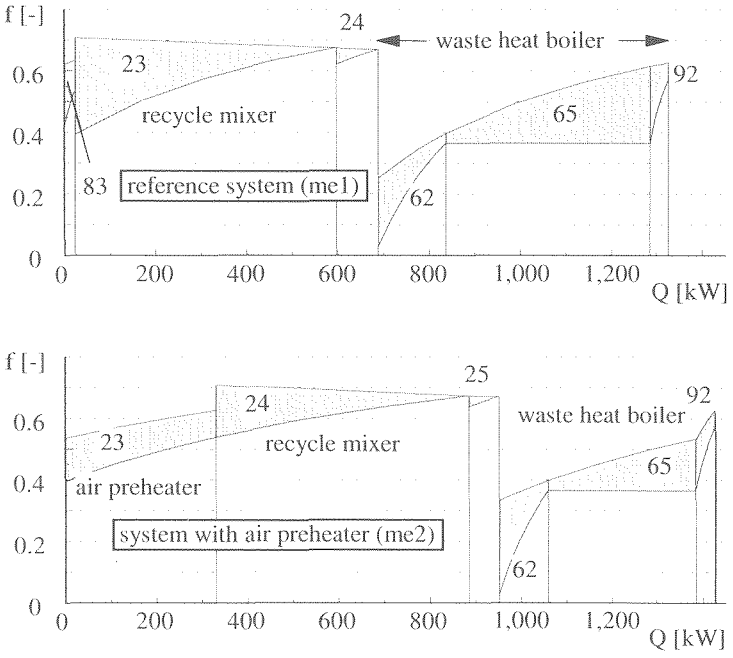

Figure 9.13: Value diagrams for the reference ER-MCFC system(me1) and the system with air preheating (me2) (only waste heat boiler and cog recycle shown)

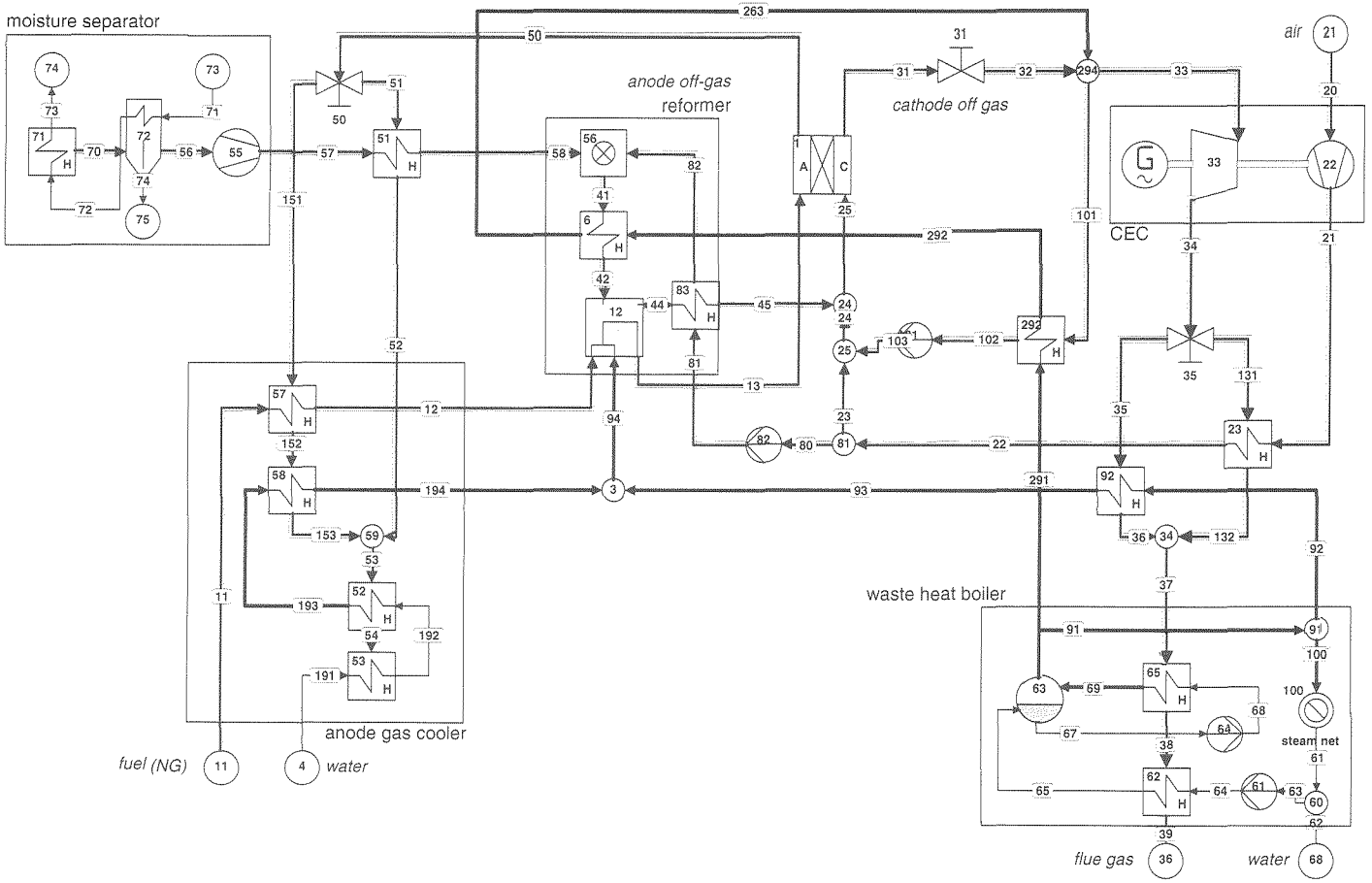

Figure 9.14: Process flow diagram for the external reforming MCFC system with steam injection before the expander (me3)

is smaller than expected can be seen by comparing the value diagrams for the reference system and the system with air preheating in figure 9.13. The diagram shows that the temperature difference between the media is smaller in the case of air preheating, resulting in smaller losses per kW of heat transferred. But this effect is nearly completely cancelled out by the increase of the amount of heat which is transferred. The heat which is supplied to the air in the reference system (including the combustion air preheater) is equal to 596 kW. If the air is preheated, the amount of heat which is used to heat the air increases to 886 kW. There are two reasons for this increase. Firstly the amount of fresh air which has to be preheated increases because of the lower recycle rate. Secondly a larger flow of air is necessary to cool the cell because more heat is generated in the fuel cell stack. The net result of preheating the air is a reduction of the exergy losses as a result of heat transfer. The decrease however is only small due to the increase in the amount of heat which must be transferred.
Again the analysis in this section shows how changing one single aspect of the system (in this case adding an air preheater), results in a series of changes (reactant concentrations, recycle ratios, etc.). Understanding the difference between the configurations requires understand the different mechanisms.

9.4 EXTERNAL REFORMING SYSTEM WITH STEAM INJECTION

9.4.1. Description of the system and calculations

In the system analysed in the previous section, the duty of the expander was increased by increasing the flow through the expander. This was achieved by reducing the recycle ratio by preheating the air. However, the increase in efficiency obtained by the resulting increase in the flow of fresh air to the cathode gas recycle loop and corresponding flue gas flow through the expander is very limited. This is mainly due to higher compression losses and the reduced efficiency of the fuel cell. Therefore another method of increasing the flow through the expander has been investigated.
The losses which occur when a fluid is compressed are much larger if the fluid is in the gas phase then when it is in the liquid phase. If steam is injected in the gas flow before the expander, the duty of this component will increase. The heat which is available in the system is used to evaporate the water and is partly converted into power in the expander. However, because the steam is pressurised in the form of liquid water, the pressure increase is achieved efficiently. Furthermore, because the water is injected downstream of the fuel cell, the reactant concentration is not influenced. Therefore the two causes of additional losses in the system with air preheating are eliminated.
The flow sheet for this configuration (me3) is shown in figure 9.14. The water is compressed and evaporated in the waste heat boiler. No steam is exported in this configuration because all the steam is injected before the expander and the steam pressure is determined by the pressure at the inlet of the reformer. Therefore the steam pressure in the waste heat boiler in this configuration is lower (4.5 bar) than in the previous configurations where 10 bar process steam is produced . The steam which is used in the reformer is superheated to 400 °C in the reformer steam superheater (app. 92). The remainder of the steam is heated to 650 °C against the recycled cathode off-gas in the cathode gas recycle loop (app. 292). To prevent a temperature decrease at the expander inlet as a result of the steam injection the steam is further heated to 700 °C against the combustor exit flow. The air in this configuration is preheated to 300 °C before mixing the air with recycled cathode off-gas to compensate for the heat which is used to superheat the steam in the cathode recycle loop.

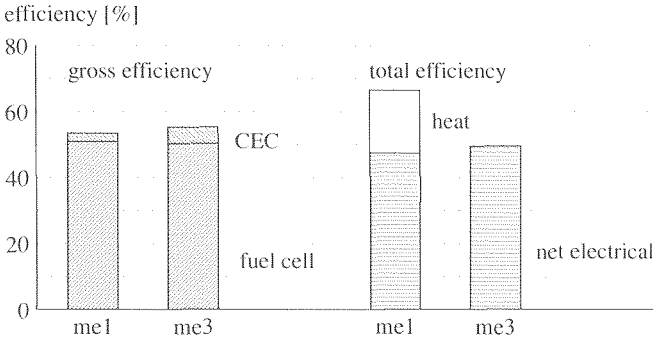

Figure 9.15: Comparison of the efficiencies for reference system (me1) and the system with steam injection (me3)

9.4.2 Energy analysis

In figure 9.15 the calculated efficiencies for the system with steam injection are compared to the efficiencies calculated for the reference system. The gross efficiency of the system increases from 53.5 % to 55.4 %. This is due to the increase of the power generated by the expander from 350 kW for the reference system to 411 kW for the system with steam injection. This leads to an increase in gross efficiency of 2.5 %pt.
To achieve the required inlet temperature at the reformer of 1200 °C, the utilisation is lower than in the reference system as a result of the heat which is used to heat the steam to 700 °C. As a result, the fuel cell efficiency (based on the fuel input to the system) therefore decreases by 0.6 % leaving a net increase of the gross system efficiency of 1.9 %pt.
The total efficiency falls sharply from 66.8 % to 49.5 %. The net electrical efficiency increases from 47.6 to 49.5 %. As no steam is exported in the system with steam injection, the total efficiency is equal to the net electrical efficiency.

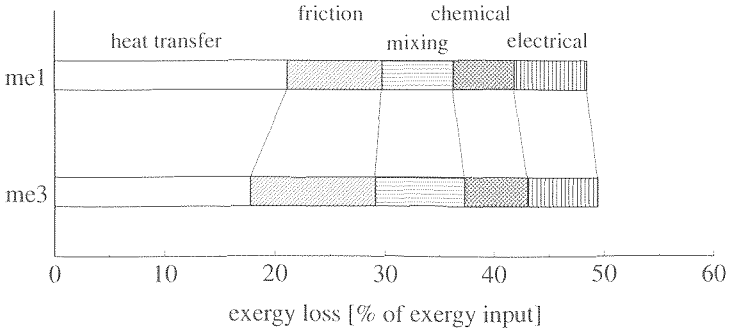

Figure 9.16: Exergy losses in the reference system(me1) and in the system with steam injection (me3)

9.4.3 Exergy analysis

For the reference system an exergy efficiency of 51.4 % was calculated. For the system with steam injection the calculated exergy efficiency is 47.6 %. Correspondingly the total exergy losses in the reference system correspond to 48.6 % and in the system with steam injection to 52.4 % of the exergy input to the system. The increase of the exergy losses with 3.8 %pt compared to the reference system indicates that the heat is used more efficiently to produce the process steam (i.e. the reference system) than to produce power in the expander by injecting the steam in the flue gas.
Figure 9.16 shows the contributions of the different causes of exergy losses for both systems. The decrease of the exergy losses as a result of heat transfer is evident. This is achieved by producing steam of a higher quality and subsequently utilising the available heat more efficiently. However, the figure also shows that injecting the steam in the flue gas, increases the losses as a result of (isothermal) mixing and as a result of friction.
The increase of the exergy losses occurs in two subsystems: the cathode gas recycle loop and the waste heat boiler. In the other subsystems the exergy losses are approximately the same for both cases. The losses according to cause in the two relevant subsystems for the reference system and the system with steam injection are shown in figure 9.17.

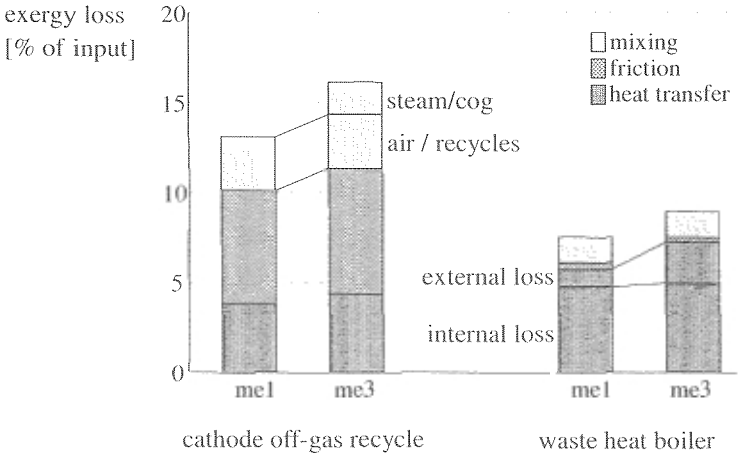

Figure 9.17: Comparison of the exergy losses in the subsystems cathode gas recycle and waste heat boiler

cathode off-gas recycle
The losses in the cathode gas recycle are due to heat transfer, friction and mixing. The loss as a result of heat transfer in the cathode gas recycle increases from 3.8 % (as a fraction of the total exergy input of the system) for the reference system to 4.4 % for the system with steam injection. In the value diagram in figure 9.18 the exergy losses as a result of heat transfer in the cathode gas recycle and the waste heat boiler are shown for the system with steam injection. The losses in the cathode gas recycle are the losses as a result of preheating the air (app. 23, 24 and 25) and superheating the steam which is mixed with the flue gas (app. 292 and 293). The large temperature difference in the steam superheater (292) results in high exergy losses in this component compared to the other components in the cathode gas recycle.

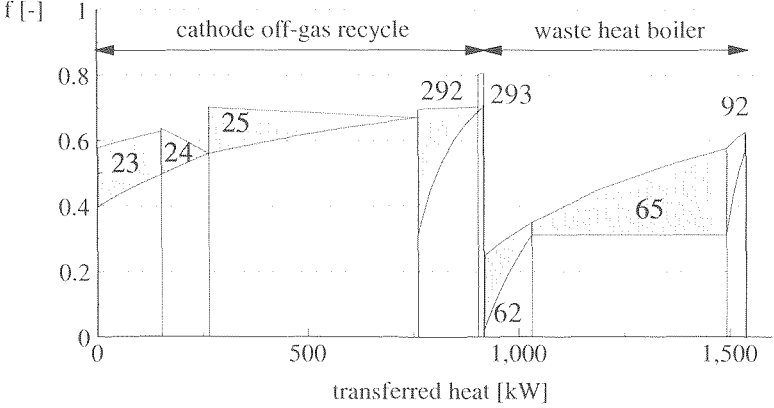

Figure 9.18: Value diagram for the cathode gas recycle loop and the waste heat boiler for the system with steam injection (me3)

As can be seen from figure 9.17, the exergy loss as a result of friction is the most important cause of losses in the cathode off-gas recycle loop, which includes the expander and compressor, The exergy loss as a result of friction is 0.8 %pt higher than in the reference system. This is due to the increase of the mass flow through the expander. The mixing loss is 1.8 %pt higher as a result of mixing of steam and cathode off-gas ('steam/cog' in figure 9.17) before the expander. This large increase is due to the decrease of the partial pressure of the steam. The steam is supplied at 3.9 bar. This corresponds to a saturation temperature of 143 °C and therefore the evaporation heat which, to generate the steam, must be supplied minimally at 143 °C. After the mixing process the partial pressure of the steam in the gas mixture is 0.72 bar corresponding to a saturation temperature of 90 °C. Therefore the heat which was supplied to the steam at a temperature higher than 143 °C can be recovered at a temperature which lies below 90 °C.

waste heat boiler

In the waste heat boiler the exergy loss increases from 7.5 % of the exergy input to the system to 8.9 %. This is caused by the increased exergy loss as a result of heat transfer. The exergy losses as a result of heat transfer can be split into two forms of exergy loss:

- Internal exergy losses as a result of heat transfer occur when heat is transferred from one fluid to another within the system. These losses can be shown in the value diagram.
- External losses as a result of heat transfer occur when the flue gas is discharged from the system. The flue gas still contains a certain amount of thermal energy at a temperature which is higher than the environment temperature.

The internal and external losses have been indicated separately in figure 9.17.

In the reference system the steam pressure is 10 bar. In the system with steam injection no steam is exported so the pressure of the steam in the waste heat boiler used in this calculation is determined by the pressure at the inlet of the expander. This results in a pressure of 4.5 bar in the evaporator and a corresponding evaporation temperature of 145 °C. Therefore the heat in the waste heat boiler is absorbed by the water/steam flow at a lower average temperature. The average temperature at which the heat is transferred from the flue gas is lower due to the fact that the flue gas is first cooled in the air preheater. The net result is an increase of the internal exergy losses as a result of heat transfer of 0.2 %.

The largest part of the increase of the losses as a result of heat transfer is due to the external losses which for the reference system equal 1.0 % of the exergy input and for the system with steam injection 2.3 %. This is due to the high water content of the flue gasses in the second case (18.6 % vs. 7.4 % for the reference system). Although the temperature at which the condensation heat could be recovered is low, the amount of heat is very large. The losses which result from discharging the water in the flue gas in the gas phase for the system with steam injection are equal to 2.1 %

The analysis shows that injecting steam is not an effective method of increasing the electrical efficiency of the system. The increase in efficiency is limited and the losses as a result of steam injection (mixing steam with cathode off-gas, flue gas losses, etc.) are substantial.

9.5 MCFC SYSTEM WITH DIRECT RECYCLE OF ANODE OFF-GAS

9.5.1 Description of the system and calculations

In the reference system water is removed from the anode gas recycle for several reasons:

- Firstly, if the water is not removed from the anode off-gas, the adiabatic combustion temperature will be lower. To achieve the same temperature at the outlet of the combustor, the heating value of the fuel will have to be increased by lowering the fuel utilisation in the fuel cell (see **Section 7.3**).
- Water can be considered as an inert species in the cathode recycle loop. Therefore, the reactant concentrations (O_2 and CO_2) at the cathode are higher if water is removed. Higher reactant concentrations lead to higher system efficiency (see **Section 9.3**)

The analysis in the previous section has shown that the presence of a considerable amount of water in the flue gas at the inlet of the expander increases the power generated by the compressor/expander combination (CEC) significantly. In the previous section the high water content in the flue gas flow through the expander was achieved by injecting steam in the flue gas, which was shown to result in large exergy losses. These losses are due mainly to the mixing process of steam and cathode off-gas and as a result of the large stack losses. In this section an alternative method of increasing the moisture content of the flue gas flow through the expander will be considered. Instead of injecting steam in the flue gas, the combusted anode off-gas is recycled directly, i.e. without separating water from the gas flow in the anode recycle loop.

The system with direct anode off-gas recycle is shown in figure 9.19. The anode off-gas (stream 51) is supplied directly the combustor of the reformer. The fuel utilisation in the fuel cell is determined by the required temperature of the flue gas at the outlet of this combustor. For these calculations a minimum combustion temperature of 1200 °C is assumed (see **Section 7.2**). The combustion temperature is strongly influenced by the ratio between the combustible components (H_2, CO) and inert components (N_2, Ar, CO_2 and H_2O). The inert components limit the combustion temperature as (a considerable) part of the heat of reaction is used to heat these components. The anode off-gas is a low caloric fuel. Therefore, whether or not part of the water is removed from the anode off-gas will largely influence the combustion temperature.

In the reference system, the fuel utilisation is equal to 76.1 %. This results in a mole fraction combustible components (H_2 + CO) in the anode off-gas at the outlet of the fuel cell equal to 9%. By removing the largest part of the water from the anode off-gas, the fraction combustible components increases to 15%. If this flow is combusted, the temperature at the outlet of the combustor is equal to 1200 °C. In the system with direct anode gas recycle, the water in the anode off-gas is not removed. To compensate for the increase in the number of

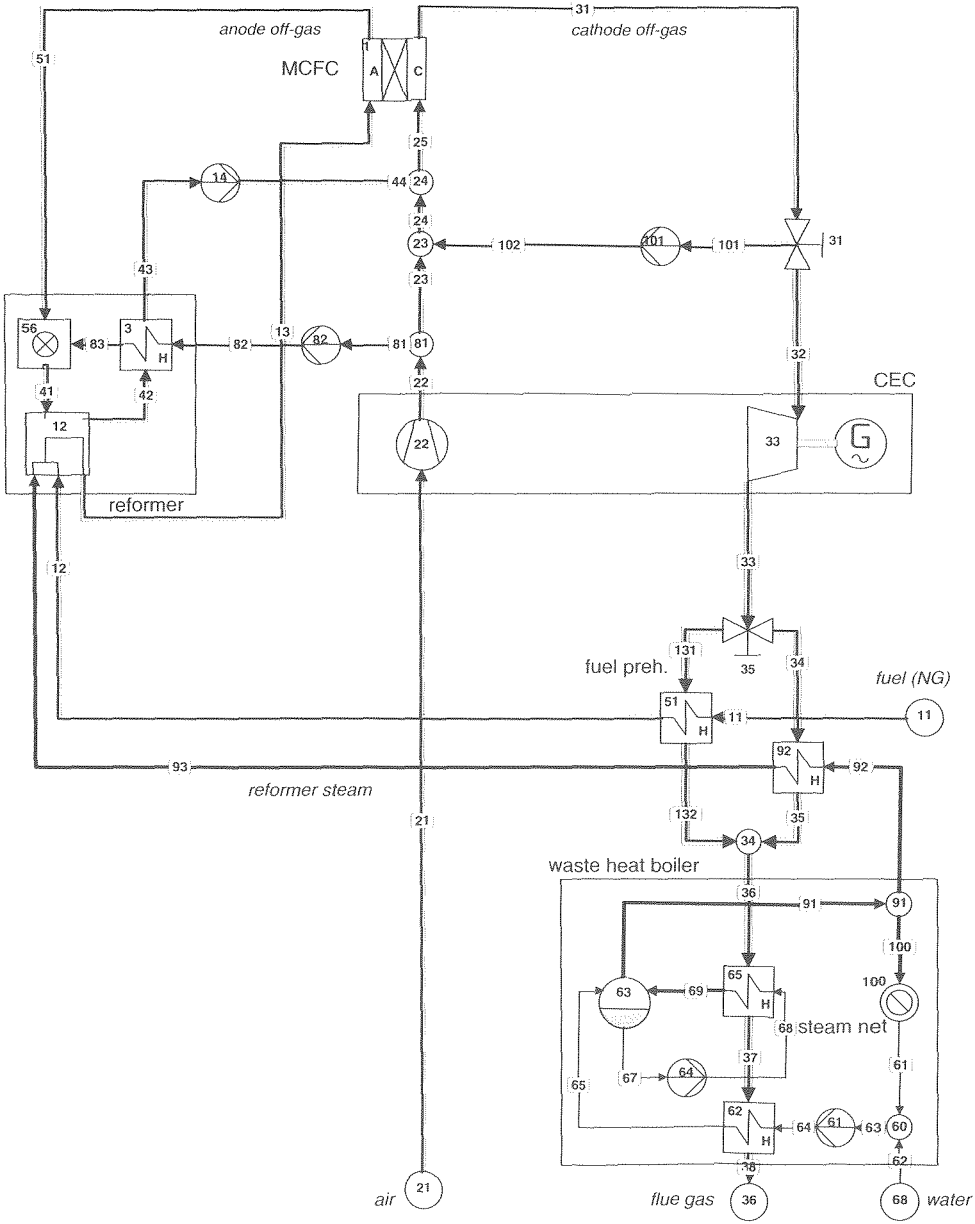

Figure 9.19: Flow sheet for the external reforming MCFC system with direct anode off-gas recycle (me4)

moles inert species in the anode off-gas, the fuel utilisation in the fuel cell must decrease from 76.1 % to 71.3 % to achieve the same combustion temperature. As in the reference system, the flue gas after the reformer is mixed with cathode gas to supply CO_2 to the fuel cell. The cathode side of the flow sheet is the same as in the reference system. The only difference is that all steam is generated in the waste heat boiler and none in the anode off-gas recycle.

9.5.2 Energy analysis

The calculated efficiencies for the reference system and for the system with direct anode off-gas recycle are shown in figure 9.20. The gross efficiency is approximately the same for both systems: 53.5 % for the reference system and 53.3 % for the system with direct anode off-gas recycle. However, in the case of the reference system, the contribution of the expander to the generated power is small: the net power of the compressor/expander combination corresponds to 2.6 % of the energy input to the system (LHV). If anode off-gas is recycled directly, this increases to 6.5 %. Simultaneously the power delivered by fuel cell decreases from 50.9 % of the energy input to the system for the reference system to 46.8 % for the system with direct recycle.
The auxiliary power requirements are higher in the system with direct recycle. The anode gas recycle blower in the system with direct recycle (app. 14) operates at a higher temperature than in the reference system. Furthermore, because the water is not removed from the anode off-gas, the flow through the recycle blower is larger. Consequently the power required by the compressor is substantially higher, leading to an electrical efficiency of the system with direct recycle of 46.8 % compared to 47.6 % for the reference system.
Equal fractions of the energy input to the system are discharged from the system as useful heat in the form of process steam. In both cases the amount of heat generated by the system corresponds to 19.1 % of the energy input to the system.

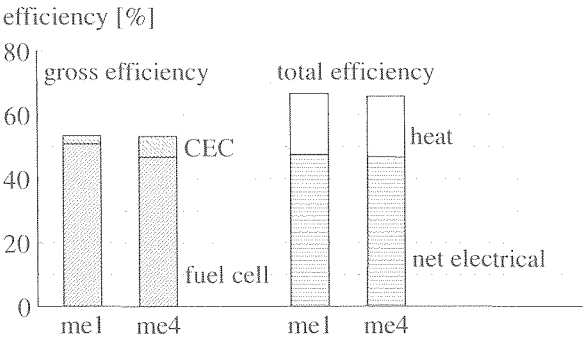

Figure 9.20: Comparison of the efficiencies for the reference system (me1) and the system with direct anode off-gas recycle (me4)

Power generated in the fuel cell stack
Compared to the reference system, the power generated in the fuel cell stack is considerably lower. In the reference system 50.9 % of the energy input to the system is converted directly into (AC) electrical power. For the system with direct anode off-gas recycle this decreases to 46.8 %. Approximately half of the decrease in power generated by the fuel cell in the second

case is due to the lower fuel utilisation. The remainder of the difference is caused by the lower reactant concentrations at the cathode in the system with direct recycle. The concentration CO_2 at the inlet of the cathode in the reference system is equal to 7.9 %. In the system with direct recycle this concentration is considerably lower: 6.6 %. There are several reasons for the difference in CO_2 concentration.

- The most important reason is the CO_2 concentration in the flue gas which is supplied to the cathode gas recycle loop. In the reference system, the flue gas from the anode off-gas combustor consists largely of CO_2 (53.5 %). Because no water is removed in the system with direct anode gas recycle, the concentration CO_2 in the flue gas in this case is much lower (32.9 %).
- Another factor which influences the CO_2 concentration is the energy balance of the cathode off-gas recycle. The gas which is supplied to the cathode is a mixture of three flows: the anode off-gas recycle, the cathode off-gas recycle and the fresh air. The total flow is determined by the amount of heat which is generated in the fuel cell, while the ratio between the fresh air and the recycle flows is determined by the energy balance over the recycle loop. If more fresh air is supplied to the cathode, the CO_2 concentration at the cathode will decrease (see **Section 9.3**). In the system with direct recycle, both the flow and the temperature at which the combusted anode off-gas is supplied to the cathode gas recycle loop are higher than in the reference case. Consequently less cathode off-gas is therefore needed to achieve the required inlet temperature for the fuel cell stack and more fresh air is supplied.

On the other hand, the lower fuel utilisation leads to a decrease of the amount of heat generated in the fuel cell stack and consequently to a decrease of the total amount of cathode gas necessary to cool the cell. This reduces the fresh air flow without affecting the recycle ratio in the cathode off-gas recycle and therefore increases the CO_2 concentrations at the cathode.

The net result of the changes in mass flows and concentrations in the flows in the cathode recycle loop, is a decrease of the CO_2 concentration indicated above, while the O_2 concentration is the same in both configurations. The lower effective reactant concentration leads to an increase of the polarisation resistance and a decrease of the Nernst voltage (see **Section 9.3**) . Compared to the reference system, the changes in composition lead to a decrease of the cell voltage from 0.720 for the reference system to 0.707 volt for the system with direct anode off-gas recycle.

Power generated in the expander

The net power delivered by the compressor/expander combination in the reference system equals 51.1 kW. For the system with direct anode off-gas recycle the net power increases to 139.6 kW. The most important cause for this increase is the increase of the mass flow through the expander as a result of the larger anode off-gas recycle flow. The water, which in the system with direct recycle is not removed from the anode off-gas and contributes to the generated power in the expander. A second cause of the increased net power generated by the expander/compressor combination is the lower recycle ratio in the cathode recycle loop (see above) which leads to an increase of the mass flow air supplied to the cathode gas recycle loop. The increase of the air flow results in an increase of the net compressor/expander power of approximately 15 kW[1]. The remainder of the increase (74 kW) is due to the larger flow of anode off-gas which passes through the expander.

---

[1] this estimate is based on the ratio of the flow through the air compressor and the net power for the reference system

Figure 9.20 shows that the gross electrical efficiency is approximately the same for the reference system and for the system with direct recycle. The CEC delivers more power and the fuel cell less in the latter system. The net electrical efficiency for the system with direct anode off-gas recycle however is 0.9 % lower. This is due to the higher duty of the anode gas recycle blower. The increase is due partly because of the larger flow through the compressor and the higher operating temperature.

9.5.3 Exergy analysis

The objective of recycling the anode off-gas directly (instead of removing the water from the anode off-gas) is to increase the amount of heat which is converted into power in the expander. In this way part of the high temperature heat which is available in the system is used to produce power instead of relatively low quality heat. Consequently the exergy losses as a result of heat transfer should be lower than to the corresponding losses in the reference system. This is confirmed by figure 9.21, which shows the exergy losses for both systems grouped according to type of exergy loss. At the same time direct recycle leads to an increase of the exergy losses as a result of friction and as a result of mixing. The net result is that the exergy losses are higher in the system with direct recycle.

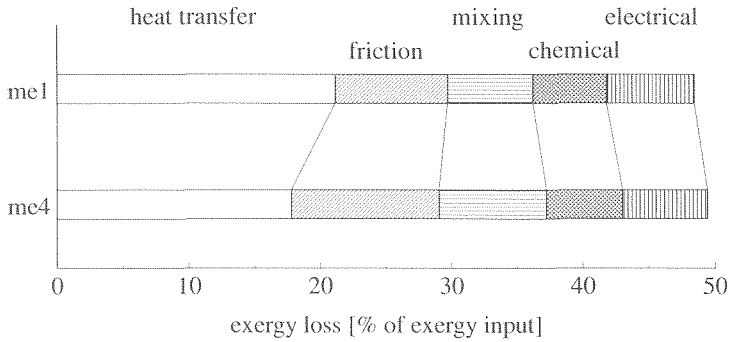

Figure 9.21: Causes of exergy losses in the reference system (me1) and the system with direct anode off-gas recycle (me4)

The increase of the exergy losses as a result of friction is due to the higher flows through the air compressor, the expander and the anode recycle blower, which were discussed in the previous section. The increase of the exergy loss as a result of mixing can be attributed to the mixing of anode off-gas with the cathode recycle flow (in app. 24 in figure 9.19). In **Section 9.4** it was shown that the process of mixing steam and a gas mixture leads to considerable losses. The losses are due to the difference in partial pressure of the H_2O before and after mixing. In the system with direct recycle it is not a pure steam flow which is mixed with a gas mixture. Instead a H_2O rich and a H_2O poor mixture are mixed. The difference in partial pressure before and after mixing is smaller in this case and therefore the exergy loss smaller. However, due to both the increase of the water content and the mole flow of the recycled anode off-gas, the exergy loss as a result of mixing in the cathode gas recycle loop increases substantially from 6.2% in the reference system to 8.3 % for the system with direct recycle.

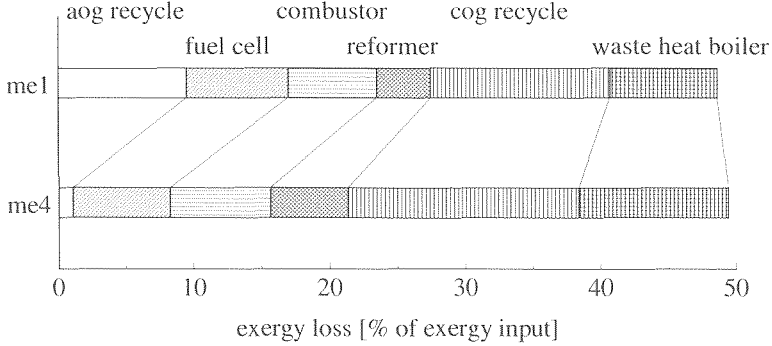

Figure 9.22: Exergy losses in the subsystems for the reference system and the system with direct recycle

The exergy losses in the **anode off-gas recycle** loop evidently are much smaller in the system with direct recycle than for the reference system (figure 9.22). The large exergy losses in this subsystem for the reference system are caused by the cooling and reheating of the anode off-gas flow which is omitted in the system with direct recycle.
The increase of the exergy losses in the **reformer** is due to the increased temperature difference at which the heat is transferred. In the reference system the flue gas, which at the inlet of the reformer has a temperature of 1200 °C, is cooled down to 516 °C. In the system with direct recycle the inlet temperature is the same. However, the flue gas flow is much larger because no water has been removed from the anode off-gas, resulting in a much higher temperature of the flue gas at the outlet of the reformer (752 °C). The exergy losses as a result of heat transfer in the reformer therefore increase.
The exergy loss in the **combustor** subsystem increases by 0.9 %. The combustor subsystem includes the air preheat (app. 83 in 9.19), in which the exergy loss increases because of the higher temperature of the flue gas at the outlet of the reformer. The remainder of the increase is caused by the higher losses as a result of mixing (because of the higher H_2O content of the anode off-gas).
The increase of the losses in the **cathode off-gas recycle** loop is entirely due to the increase of the friction losses and the mixing losses. Friction losses increase as a result of the larger anode off-gas and air flow. Losses as a result of mixing are higher as a result of the higher water content of the anode off-gas flow.
Finally the exergy losses in the **waste heat boiler** show the largest increase: + 3.5 %. The increase is entirely due to the losses as a result of heat transfer. As was done in **Section 9.3**, these losses can be split into the internal and the external losses. In the reference system part of the reformer steam is generated in the anode gas recycle loop. In the system with direct recycle all reformer steam is generated in the waste heat boiler. This causes an increase of the internal losses by 1.5 %. The external losses increase by 2.0 % due to the high concentration H_2O in the flue gas.
Analysis of the system with direct anode off-gas recycle shows that the change in performance of the system is due to a number of secondary effects. The method of detailed exergy analysis makes it possible to determine which changes occur by analysing where losses change and which type of losses are influenced by the change in the flow sheet design.

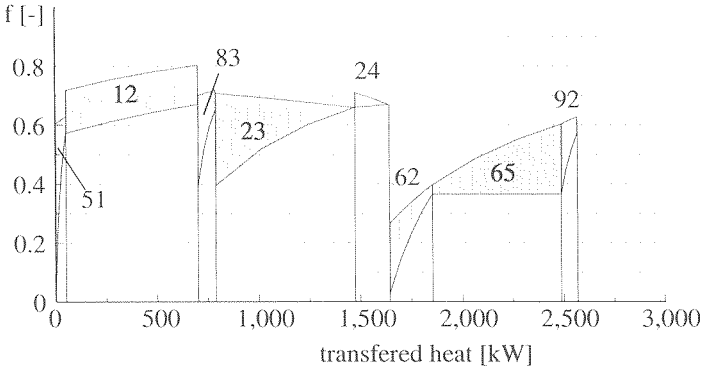

Figure 9.23: Value diagram for the system with direct anode recycle (me4)

9.6 INFLUENCE OF THE PRESSURE ON THE EXTERNAL REFORMING SYSTEM

9.6.1 Description of the system and calculations

As the analysis shows, a surplus of high temperature heat is available in the system. Increasing the flow through the expander has been de objective of the different system configurations evaluated in the previous sections. This is one way to increase the amount of heat utilised in the expander. Another way of increasing the amount of heat used in the expander is to increase the pressure ratio over the expander.
To investigate the influence of the pressure on the performance and losses in the system, calculations have been carried out for the reference system (figure 9.1, **Section 9.2**) using different operating pressures for the fuel cell (p = 2, 3, 4, 5 and 6 bar). For these calculations the input data (specified temperatures, compressor efficiencies, etc.) are the same as for the reference system with two exceptions.

- Firstly the pressure losses which are specified for the components in the system have been modified. The exergy losses and lost work (see **Section 6.4**) do not depend on the pressure loss Δp but on the ratio between the pressure loss and the absolute pressure. At a higher pressure therefore a higher pressure loss is acceptable. For these calculations the pressure losses in the main components have been regarded as a fraction of the absolute pressure.
- Secondly the temperature of the anode off-gas at the outlet of the moisture separator in the anode gas recycle was altered as the system pressure changes. In the moisture separator (app. 72 in figure 9.1) the anode off-gas is cooled to condense part of the water. The partial pressure of the water in the off-gas at the outlet of the separator is equal to the saturation pressure of water/steam at the outlet temperature. For the reference system this equilibrium assumptions leads to a calculated moisture content of 12.5% in the anode off-gas at the outlet of the separator. If the system pressure increases, a constant temperature at the outlet of the separator (i.e. a constant partial pressure of the water in the anode off-gas) results in a lower water concentration. As the moisture content of the anode gas strongly influences the fuel cell efficiency (**Section 9.5**), the moisture content was kept constant for all values of the operating pressure. This leads to a higher temperature at the outlet of the anode gas cooler / moisture separator at higher operating pressure (figure 9.24).

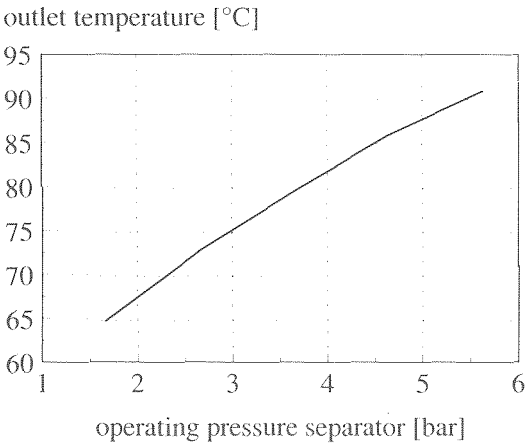

Figure 9.24: Outlet temperature of the separator varied as a function of total pressure to achieve a constant moisture content at the outlet

9.6.2 Energy analysis

Figure 9.25 shows the power generated by the fuel cell stack and the compressor/expander combination (CEC) as a function of the operating pressure. Expressed as a fraction of the energy input to the system, the power generated by the fuel cell stack increases from 47.2 % to 52.1 %, an increases with 4.9 %pt, if the system pressure is raised from 2 to 6 bar. Half of this increase (2.4 %pt) is achieved by increasing the pressure from 2 to 3 bar. A similar gain in fuel cell efficiency results if the pressure increases from 3 to 6 bar.
The increase in fuel cell efficiency is due to the lower cell resistance at higher reactant partial pressures. As a result of the pressure increase the cell resistance decreases from 1.11 ohm·cm^2 at 2 bar to 0.94 ohm·cm^2 at 6 bar. Correspondingly an increase in cell voltage results. The voltage gain if the pressure is increased from 2 to 4 bar is more than 50 mV (from 0.669 V at 2 bar to 0.720 V at 4 bar). The voltage increases another 20 mV if the pressure increases further to 6 bar.

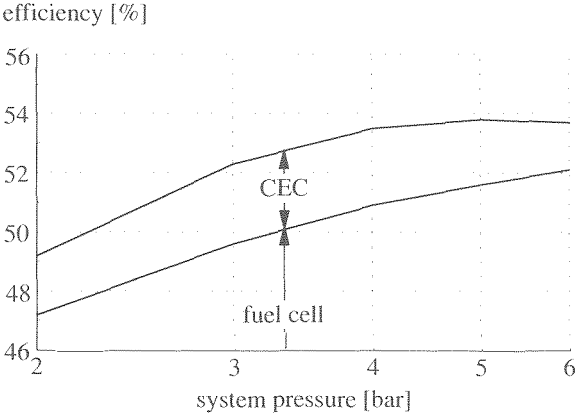

Figure 9.25: Calculated gross efficiency for the reference system with separate contributions of the CEC and the fuel cell as a function of operating pressure

The power generated by the CEC increases initially if the pressure is increased from 2 to 3 bar. Again expressed as a fraction of the energy input to the system, the CEC output increases from 2.0 % to 2.7 %. Further pressurisation does not lead to an increase but to a decrease of the net power. For the pressure increase from 3 to 4 bar the decrease is slight, but further pressurisation reduces the power produced by the CEC substantially to 1.6 % at 6 bar. The gross electrical efficiency (fuel cell + CEC) increases from 49.2% at 2 bar to 53.7% at 6 bar.

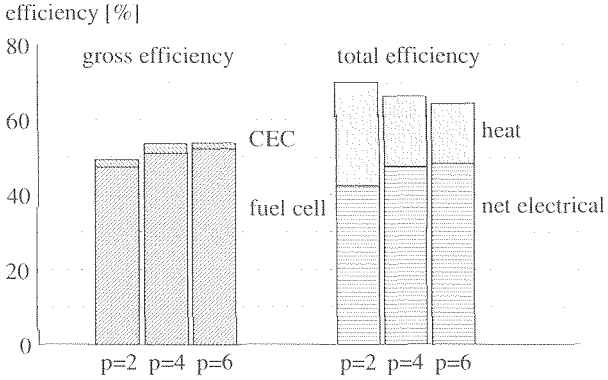

Figure 9.26: Net electrical efficiency and total efficiency as a function of pressure for the reference system

The auxiliary power demand decreases from 6.9 % of the fuel input at 2 bar to 5.4 % at 6 bar. The difference between the net and the gross electrical power output for the system decreases slightly with pressure. The lower auxiliary power demand is due to the fact that less heat is generated in the fuel cell at higher pressure and therefore less cathode gas is necessary to remove the heat from the stack. As a result, the duty of the recycle blower is lower. The gain in net system efficiency is therefore somewhat higher than the gain in gross efficiency (from 42.3% at 2 bar to 48.2% at 6 bar).

The amount of heat which the system produces in the form of process steam, decreases with pressure. This is to be expected. At high pressure more heat is converted into work in the expander and consequently the amount of steam which can be generated in the waste heat boiler decreases. But if the fraction of heat which is recovered remains constant, the total efficiency will increase with pressure. However, as can be seen in figure 9.26 as well, the total efficiency of the system decreases considerably: from 70.2 % at 2 bar to 64.5 % at 6 bar. A much smaller fraction of the heat produced in the system is utilised at higher pressure. The lower heat recovery is due to the same mechanism which was found in the analysis of the SOFC system operating at higher pressure: the temperature increase of the air in the compressor (see **section 8.3**). The temperature increase has two effects:

- More heat is supplied to the cathode off-gas recycle. As a result, the recycle ratio for the cathode off-gas recycle becomes smaller, which leads to an increase of the air/fuel ratio by 17.5% and a similar increase in the flue gas flow and corresponding losses;
- The process flow which requires most heat to preheat is the air flow. If the air temperature of the air increases to 100-200 °C, less heat is required below this temperature for preheating. Consequently the amount of heat recovered from the flue gas is lower and the temperature at which the flue gas is discharged to the flue gas stack becomes higher, leading to higher stack losses.

9.6.3 Exergy losses

In figure 9.27 the calculated exergy losses for each type of loss for the system operating at 2, 4 and 6 bar are shown. At 2 bar the exergy losses amount to 50.6% of the exergy input to the system. Increasing the system pressure leads to a decrease of the exergy losses: at 4 bar the exergy losses decrease to 48.4% of the exergy input. Further increase of the system pressure leads to a (small) increase in exergy losses.
The advantage of increasing the system pressure is two-fold. Firstly the fuel cell operates more efficiently at higher pressure. The influence of the pressure on the efficiency is due to both the lower cell resistance and the higher Nernst voltage. Combined they lead to the increase of the cell voltage indicated above. The higher fuel cell efficiency is also visible in the lower exergy losses as a result of polarisation and resistance (electrical losses) in figure 9.27. The decrease in exergy losses as a result of polarisation and resistance in the fuel cell if the pressure increases from 2 to 6 bar corresponds to 1.1%pt of the exergy input to the system. The electrical losses decrease substantially if the pressure increases from 2 to 4 bar and only marginally for further pressurisation.

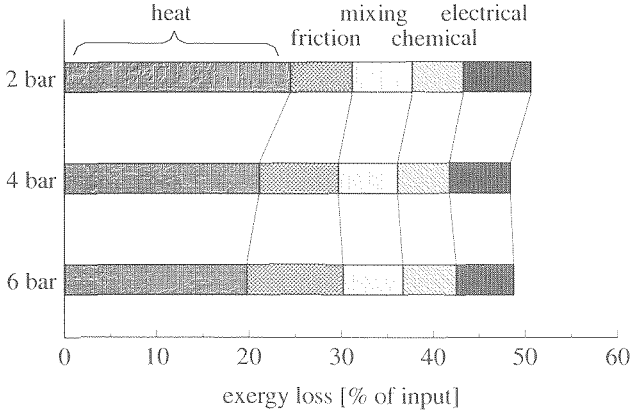

Figure 9.27: Exergy losses for the reference system at different values of the operating pressure

The main positive effect which is expected from increasing the system pressure is the larger amount of heat which is converted in the expander. By using this heat in the expander, a reduction of the losses as a result of heat transfer can be achieved. As can be seen from figure 9.27, the effect of a pressure increase on the exergy losses as a result of heat transfer is considerable. These losses decrease from 24.6% at 2 bar to 19.8% at 6 bar: a decrease of almost 5% (of the exergy input to the system).
Even though the exergy losses as a result of heat transfer and the electrical losses decrease considerably at higher pressure, the decrease of the total exergy losses was seen to be relatively small. The limited gain in exergy efficiency is caused by the sharp increase of friction losses at higher pressure. From 6.5 % at 2 bar the exergy losses as a result of friction increase to 10.9 % at 6 bar. As a result the sum of the exergy losses as a result of heat transfer and as a result of friction is not very sensitive to the operating pressure. For a pressure increase from 2 to 4 bar the sum of the losses as a result of heat transfer and friction decreases

slightly, but if the pressure is increased further the increase of the friction losses exceeds the decrease of the losses as a result of heat transfer.

friction losses

The friction losses occur mainly in the CEC. As the pressure ratio increases, the exergy losses increase as well. However, as indicated the duty of the CEC is at its maximum at 3 bar and decreases as the pressure becomes higher. Evidently the efficiency of the CEC becomes poorer at high pressure. For both compressor and expander the isentropic efficiency is equal to 75% in these calculations. It is interesting to know, how the efficiency will improve if the efficiency of the rotating equipment increases. There are two approaches possible. The first approach is to consider the lost work as the potential improvement. The second is to look at the exergy losses in the process. The difference between these approaches will be discussed. The expander operating at an isentropic efficiency η_{isen} delivers power P. If the process were reversible, the expander would deliver P_{rev}. To calculate the actual power P from the power of the ideal process the isentropic efficiency is used:

$$P = \eta_{isen} \cdot P_{rev}$$

The difference ΔP between P and P_{rev} is the 'lost power' of the expander. The exergy loss in the actual process is not equal to the lost power. Less power is generated in the expander if the process is irreversible but instead heat is generated. If the process in the expander occurs at high temperature (as is the case in the expander in the MCFC system), this heat represents a considerable amount of exergy. Therefore, the lost power is larger than the actual exergy loss. If the actual outlet temperature is T_{out} and the temperature at the outlet of the reversible expansion process would be T_{rev}, then the exergy loss is approximately equal to (see **Section 3.2**):

$$\Delta E_L \approx \frac{T_o}{T_{exp}} \Delta P$$

The equations for the compression process are similar. In this case the lost work is the increase of the work which has to be supplied to the compressor. Again the exergy loss is smaller than the lost work.

In figure 9.28 the reversible process has been determined on basis of both exergy losses and lost work. In the MCFC system the heat after the expander is used in the waste heat boiler to produce steam. If the efficiency of the expander increases, more power is produced in the CEC and consequently less steam is produced in the waste heat boiler. The exergy loss takes this into account. However, as has been shown before, the heat is used in the system with a low efficiency. It is not realistic to assume the heat produced in the expander will be used with 100% exergy efficiency. Therefore the two curves represent the two extremes. One approach assumes that the exergy of the heat produced as a result of the irreversible expansion or compression is used fully (exergy loss method), the other that or that the exergy of the heat is not used at all (lost work method). The latter method gives a more optimistic estimate of the potential of the improvement of the efficiency of the rotating equipment, the first method will tend to underestimate the performance improvement. The actual increase in efficiency will be between the two estimates.

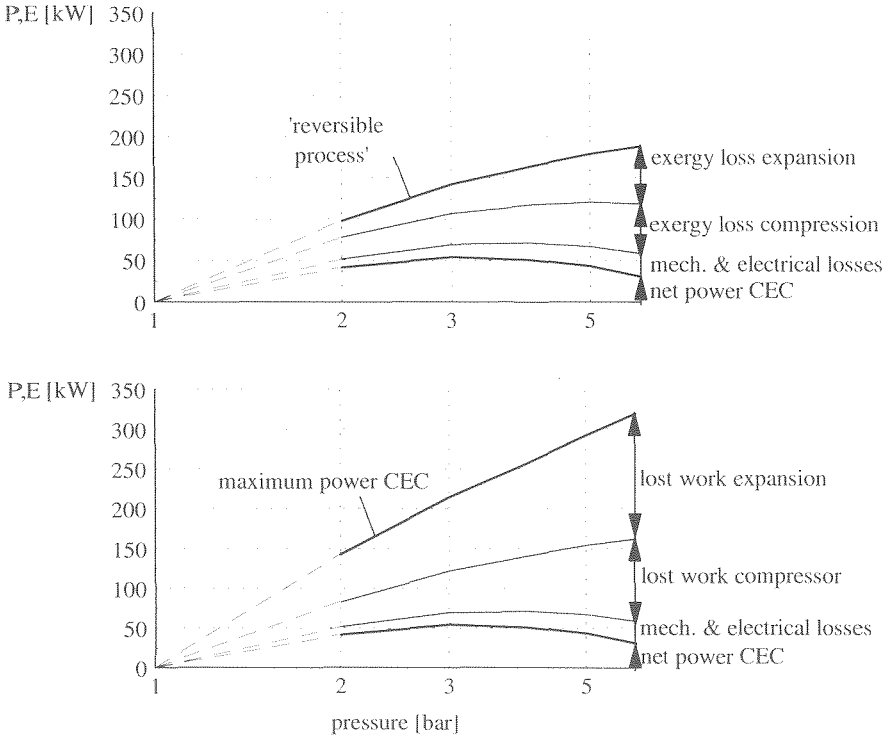

Figure 9.28: Estimating the influence of the isentropic efficiency on the increase in exergy production by system based on the exergy losses (above) or lost work (below)

heat transfer losses

In figure 9.29 the value diagrams for both operating pressures (2 and 6 bar) are shown. The following observation can be made based on the comparison of these diagrams:

- The losses as a result of heat transfer in the anode gas cooler / moisture separator become more important at higher pressure. The losses in the moisture separator increase mainly because of the higher condensation temperature of the water in the anode off-gas. The condensation heat is therefore removed at a higher temperature and correspondingly with larger exergy losses at higher pressure. On the other hand, because of the higher efficiency of the fuel cell system, the fuel flow is smaller and the amount of heat removed from the anode off-gas in the moisture separator is smaller as well;
- The losses as a result of heat transfer in the reformer are almost equal in both cases. Because the temperatures remain almost unchanged, the exergy losses depend only on the amount of fuel converted;
- The losses in the cathode off-gas recycle are reduced strongly. This partly is due to the higher temperature at which the air is mixed with the recycled cathode off-gas because of the temperature increase in the compressor. The second reason is, that less heat is transferred to the air. This is due to the lower heat generation in the fuel cell stack, which leads to a 20% lower cathode flow if the pressure increases from 2 to 6 bar;

- The losses in the waste heat boiler are strongly reduced because of the lower temperature of the flue gas at the inlet of the waste heat boiler (i.e. the outlet of the expander) and the lower amount of heat transferred in the waste heat boiler. This more than compensates the higher flue gas temperature at the outlet of the waste heat boiler;

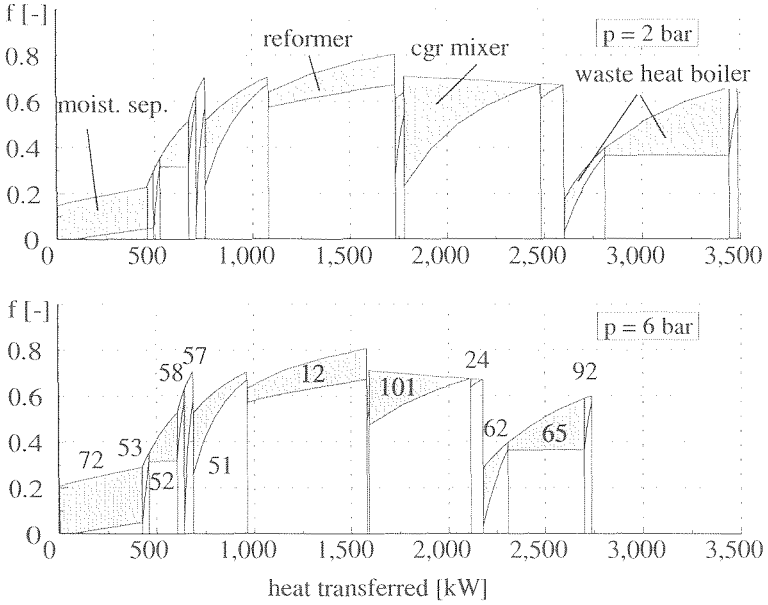

Figure 9.29: Value diagram for the external reforming system (me1) at a different values (2 bar vs. 6 bar) of the operating pressure (numbers refer to app. numbers in the flow sheet in figure 9.1)

The positive effect of pressurisation relies on making use of high temperature heat which is available in the system. To estimate how much of this heat is available in the system use has been made of the pinch-value diagram. Figure 9.30 shows the pinch-value diagrams for the system at an operating pressure of 2 bar and 6 bar respectively. The shaded area on the right hand side represents the exergy of the heat which could be recovered at high temperature. At 2 bar the potential is approximately 450 kW (=0.7 x 650) and at 6 bar the area corresponds to an estimated 270 kW (=0.7 x 380). Part of the reduction is due to the fact that heat is utilised to produce electrical power (even though, as indicated, this does not occur very efficiently). The reduction of the potential is also due to the fact that in the fuel cell less heat is produced. Also indicated is the Carnot factor of the steam produced in the waste heat boiler (0.36). If this is compared to the Carnot factor of the heat which is released in the fuel cell, it shows that even for full recovery of this heat in the form of process steam, the exergy of the steam will be less than 50% of the exergy available in the heat. The pinch diagram shows that 70% to 80% of the actual exergy of the steam generated in the waste heat boiler heat is actually recovered. This corresponds to an efficiency of heat recovery (exergy based) for the system of 35% to 40%.

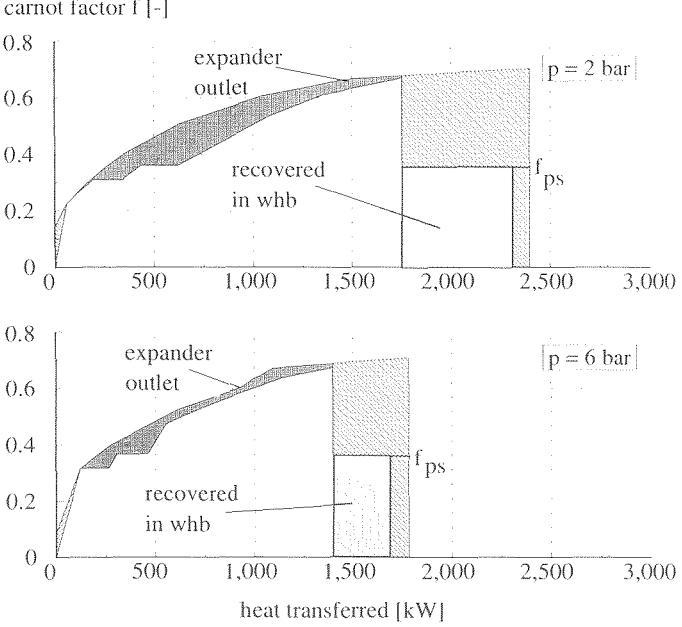

Figure 9.30: Pinch-value diagram for the external reforming MCFC system (me1) at low pressure (2 bar: top) and high pressure (6 bar: bottom)

The analysis in this section again shows the large influence of the operating pressure on the system performance, despite the low (exergy) efficiency of the compressor/expander combination. The two methods used to assess the influence of the rotating equipment ("lost work" and "exergy" analysis) both show that the losses in the CEC cycle are considerably larger than the power production in the CEC.

9.7 ANALYSIS OF AN INTERNAL REFORMING SYSTEM

9.7.1 Description of the system and calculations

The exergy analysis in the previous sections has shown the importance of heat transfer as a cause of (exergy) losses in the fuel cell system. Approximately one third to half of the exergy losses which occur in the MCFC system result from heat transfer. These large losses as a result of heat transfer are caused by two effects:

- Firstly heat is generated in the fuel cell stack at a high temperature (600 - 700 °C). To limit losses in heat transfer, this heat must be used at a comparable level. However, is was shown in the previous sections that the demand for heat of this temperature (given the starting points with regard to scale, etc) are limited. In the foregoing calculations only a relatively small part of the heat is converted into work in the compressor/expander combination (CEC). The net power generated in this process is limited due to the relatively low efficiency of this process at the given pressure ratios and temperatures. The remainder of the heat is mainly used to produce intermediate pressure steam at 180 °C.
- The second reason for the high losses as a result of heat transfer is that the heat is removed

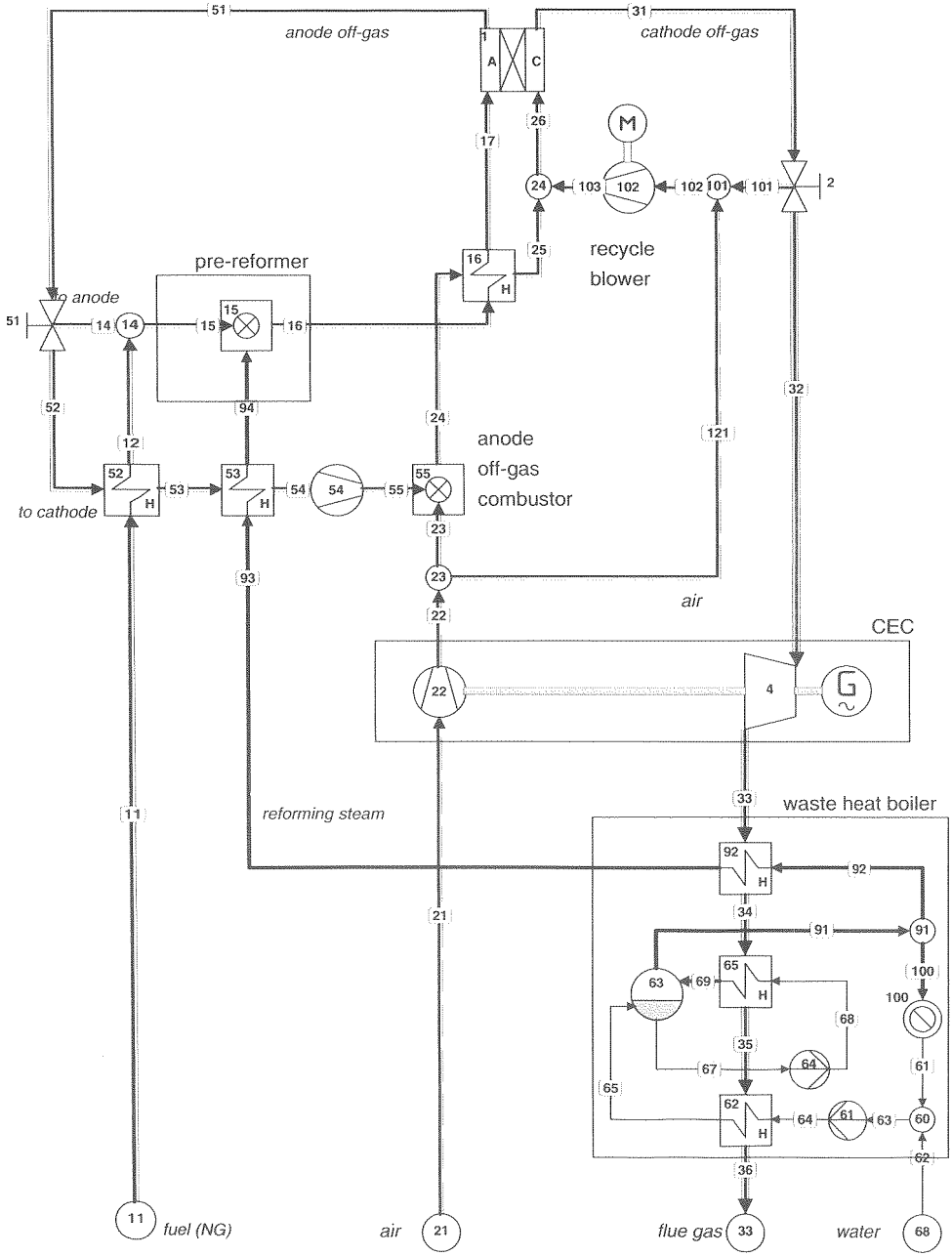

Figure 9.31: Process flow sheet for the internal reforming MCFC system (mi)

from the fuel cell stack by the cathode flow. Due to the large amount of heat which has to be removed, this cathode flow has to be large. As the exergy analysis showed, this leads to high exergy losses as a result of heat transfer, mainly in the cathode gas recycle.

An important option to reduce the amount of heat generated in the fuel cell stack, and therefore the exergy losses as a result of heat transfer, is application of internal reforming. In the internal reforming stack the methane in the fuel is converted with steam into hydrogen in the stack and part of the heat which is generated in the electrochemical reaction is used in the endothermal methane reforming reaction. As a result the cooling requirement of the stack is strongly reduced. Application of internal reforming MCFC stacks greatly simplifies the system design by eliminating the need for an external reformer.

The flow sheet for the internal reforming system is shown in figure 9.31. The fuel (natural gas) is heated to 400 °C in the fuel preheater (app. 52) and mixed with steam which has been heated to the same temperature in the superheater (app. 53). Higher hydrocarbons have a greater tendency to deposit carbon through cracking than methane. To prevent carbon deposition in the fuel cell stack, the fuel passes through an adiabatic pre-reformer (app. 15). After the pre-reformer the fuel is further heated to 600 °C, the required anode inlet temperature for the fuel cell in the fuel preheater (app. 16).

In the pre-reformer higher hydrocarbons are converted into H_2 and CO. Based on the chemical equilibrium, higher hydrocarbons can be reformed at lower temperature than methane. In the temperature range from 350 °C to 450 °C almost full conversion of higher hydrocarbons is obtained, while only a fraction methane is converted. The heat which is required for the pre-reforming reactions is supplied by recirculating part of the hot anode off-gas to the fuel/steam mixture. The gas enters the pre-reformer at 430 °C and as a result of the endothermal reaction cools down to 400 °C. The composition at the outlet of the pre-reformer is calculated assuming chemical equilibrium and a 50 K temperature approach. Steam is mixed with the fuel to achieve a specific steam/carbon ratio at the inlet of the fuel cell. The amount of steam is calculated by assuming the same S/C ratio at the inlet of the fuel cell as in the calculations for the external reforming systems (see **Section 7.3**).

The cell voltage and other relevant parameters for the (direct) internal reforming MCFC stack have been determined using the extensive model (see **Section 5.4**). The following starting points have been used:

- The outlet temperature of the cathode off-gas equals 680 °C. The outlet temperature for the anode is calculated by the model. Because the fuel cell calculations are based on a model for a counter-flow fuel cell the outlet temperature of the anode off-gas which leaves the fuel cell stack is low (610 °C).
- The fuel utilisation in this calculation is equal to 80%. The fuel utilisation determines how much H_2 and CO are present in the anode off-gas. In the case of the external reforming system the fuel utilisation is limited because the temperature at the outlet of the combustor must be high enough (1200 °C) to achieve the required heat transfer from flue gas to the reforming reaction. In the base case ER-MCFC calculation this limited the fuel utilisation to 76.9 %. In the internal reforming system a higher fuel utilisation is possible because the external reformer is eliminated. But, because at a high fuel utilisation the risk of oxidation of the anode catalyst occurs, the value used for the internal reforming stack is not much higher than in the external reforming case.

The reactions at the cathode require O_2 and CO_2. O_2 is provided to the cathode with the fresh air (stream 21), CO_2 is provided to the cathode by combusting anode off-gas and mixing the flue gas (stream 24) with the air. The fresh air flow is split into two flows after the air compressor. One part is supplied to the combustor (app. 55) where the air is used to combust the anode off-gas. The largest part of the air flow bypasses the combustor. This is necessary

to achieve a sufficient high temperature in the combustor to oxidise the fuel components completely. The temperature at the outlet of the combustor is 940 °C. To achieve the required inlet temperature at the fuel cell stack (600 °C), 60 % of the hot cathode off-gas (stream 31) is

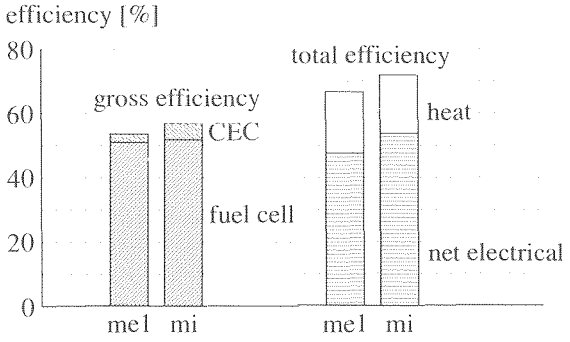

Figure 9.32: Comparison of the efficiencies for the external reforming MCFC system (me1) and the internal reforming MCFC system (mi)

recycled. The cathode off-gas which is not recycled is used in the expander (app. 32) to generate power and in the waste heat boiler to produce 180 °C/10 bar process and reforming steam.

9.7.2. Energy analysis

The heating value of the fuel which is supplied to the system is equal to 1945 kW (LHV). The fuel cell generates 1000 kW AC power and an additional 98 kW electrical power is generated by the compressor/expander combination (CEC). The calculated efficiency of the fuel cell does not differ much from the value calculated for the external reforming system. The efficiencies are compared in figure 9.32. The electrical power (AC) which is generated in the fuel cell stack corresponds to 51.4% of the energy input to the system in the internal reforming system and 50.9 % in the external reforming system. The difference is small because of two opposite effects. On one hand the cell voltage is lower in the internal reforming case: 700 mV for the IR-MCFC system compared to 720 mV for the reference ER-MCFC system. However, the lower cell voltage of the internal reforming stack is compensated by the higher fuel utilisation.
The CEC delivers considerably more power in the case of internal reforming because no water is removed from the anode off-gas increasing the mass flow through the expander (see **Section 9.5**). In the internal reforming system the net power delivered by the CEC equals 4.1% of the energy input to the system, while the corresponding value for the external reforming system is only 2.6%.
The gross efficiency of the system (fuel cell + CEC), is equal to 56.5 % and the net efficiency 53.6 %. Auxiliary power is mainly consumed by the recycle blowers for the cathode recycle loop (app. 102) and for the anode recycle loop (app. 54). The difference in net electrical efficiency between the external and the internal reforming system is 6.0 %, i.e. much higher than the difference in gross efficiency. This is due to the much lower auxiliary power in the latter case. Less power is used by the blowers because of the lower cooling requirements of the internal reforming type of stack. As a result of the internal reforming reaction the net heat

generated in the fuel cell stack is about half the value in the case of external reforming (807 kW vs. 412 kW).
Slightly more than half of the heat transferred to the water/steam in the waste heat boiler is heat is used to generate steam for the reforming process. The remainder of the heat is exported in the form of process steam. The exported steam represents 30.4% of the energy input, making the total efficiency, i.e. the efficiency of combined heat and power generation, equal to 71.8 %.

9.7.3 Exergy analysis

As in the previous calculations, the exergy losses have been calculated for all components and streams. Furthermore, for all components the different contributions (heat transfer, friction, etc.) were determined using the method developed in **Chapter 3**.

Exergy losses in the fuel cell stack
The most interesting component with respect to the exergy analysis is the fuel cell stack, because of the many different processes which occur in this component. In the fuel cell stack the following causes of exergy losses contribute to the total exergy loss:
- Polarisation and ohmic resistance in the electrolyte and electrodes (electrical losses);
- Chemical reactions, i.e. the shift and reforming reactions;
- Heat transfer;
- Friction losses resulting in a pressure drop of the gas flows.

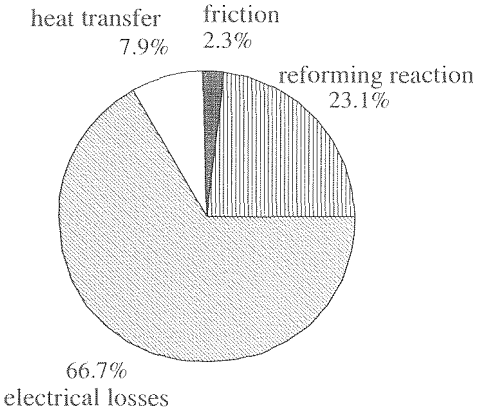

Figure 9.33: Distribution of the exergy losses in the fuel cell for the separate causes of exergy losses (total exergy loss is 126.5 kW)

To separate the contributions as a result of heat transfer, chemical reactions and electrical losses, the temperature and concentration profiles calculated with the detailed fuel cell model were used. Using the calculated values for temperatures and composition the different contributions to the total exergy loss in the fuel cell stack can be calculated (see **Section 3.3**). The total exergy loss in the fuel cell stack is 126.5 kW, which corresponds to 8.3% of the exergy input to the system. Figure 9.33 shows the contributions of the different causes.

A - Polarisation or electrical losses

The most important cause of exergy losses (84.4 kW) are the electrical losses, i.e. the losses as a result of polarisation in the electrochemical reaction. Polarisation causes two thirds of the total exergy loss in the fuel cell. To assess the importance of this loss, it can be compared to the energy which is converted in the fuel cell which equals 1909 kW. The ratio between the losses and the chemical energy converted indicates the high efficiency of the electrochemical reaction in the fuel cell.

If the exergy losses as a result of polarisation in the internal reforming fuel cell stack are compared to the corresponding losses calculated for the external reforming fuel cell, lower losses are expected in the external reforming stack:

- The amount of chemical energy which is converted is higher in the internal reforming because of the higher fuel utilisation. Correspondingly, the losses are expected to be higher as well;
- Furthermore the calculated cell voltage is lower in the case of internal reforming, indicating a lower efficiency of the electrochemical reaction.

Instead, lower polarisation losses are calculated for the fuel cell stack in the internal reforming stack (84.4 kW) than for the external reforming cell (94.5 kW). The reason that the exergy losses are smaller in the internal reforming system lies in the lower average H_2 concentration at the anode in this case. In the external reforming system the fuel is reformed almost fully (equilibrium temperature 800 °C) prior to entering the fuel cell. Therefore the concentration hydrogen in the anode gas is high at the inlet of the fuel cell stack. The combination of a high driving force for the electrochemical reaction (the Nernst voltage) and a high cell resistance at the inlet of the external reforming fuel cell leads to high losses. On the other hand in the internal reforming stack the hydrogen concentration is initially much lower because, as the calculations with the fuel cell model showed, the reforming reaction at the inlet of the cell is rate limiting. This leads to a much lower average hydrogen concentration in the internal reforming stack and therefore a lower Nernst voltage. Consequently exergy losses in the electrochemical reaction are lower. This is the same effect described here was found in **Chapter 5** to lead to a higher effective temperature for internal reforming than in external reforming fuel cells.

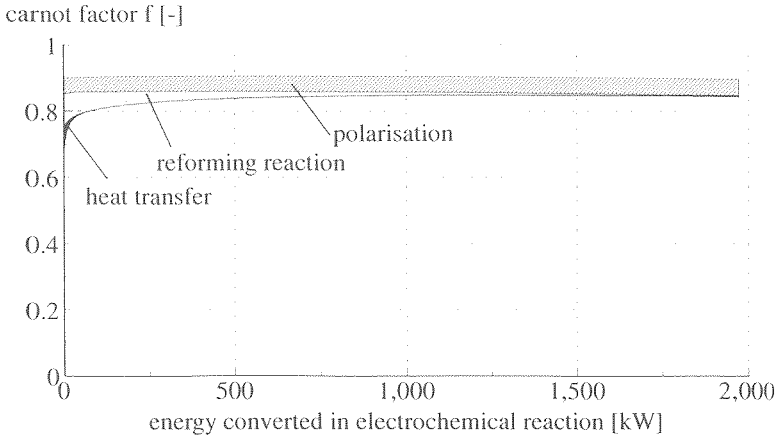

Figure 9.34: f,H-diagram for the internal reforming MCFC stack

B - Reforming reaction

The exergy losses as a result of the reforming reaction can be interpreted as a result of the difference between the actual process temperature (600 ... 700 °C) and the equilibrium temperature. The fuel which is supplied to the anode, has been brought to chemical equilibrium in the pre-reformer. Consequently the equilibrium temperature is equal to the 400 °C at the inlet of the fuel cell. As methane is converted the equilibrium temperature approaches the actual process temperature. If the heat for the reforming reaction (450 kW) is supplied at the average cell temperature (650 °C), the exergy of the heat supplied to the reforming reaction is equal to 168 kW. The equilibrium temperature at the inlet is equal to the pre-reformer temperature (400 °C). At the anode outlet the equilibrium temperature is approximately 600 °C (see **Section 5.5**). If 500 °C is used as an average value for the equilibrium temperature, the increase in the exergy as a result of the reforming reaction corresponds to 140 kW. The exergy losses in the chemical reaction estimated in this manner (28 kW) correspond well to the calculated value (29.2 kW). This shows the equilibrium temperature to be a useful tool in interpreting exergy losses in chemical (equilibrium) reactions.

C - Other losses

Heat transfer and friction are the remaining causes of exergy losses. The friction losses are reduced by 50 % compared to the losses in the external reforming case due to the lower flow at the cathode. Heat is transferred within the cell at relatively small temperature differences. Correspondingly the exergy losses as a result of heat transfer in the fuel cell stack are only small (1.8 % of the total loss in the fuel cell stack). The distribution of the exergy losses as a result of heat transfer, polarisation and the reforming reaction in the fuel cell stack are shown in the f,H-diagram in figure 9.34. The polarisation losses are roughly proportional to the rate of the electrochemical reaction. The even distribution of the losses in figure 9.34 indicates that the efficiency of the electrochemical reaction does not vary widely from in- to outlet.

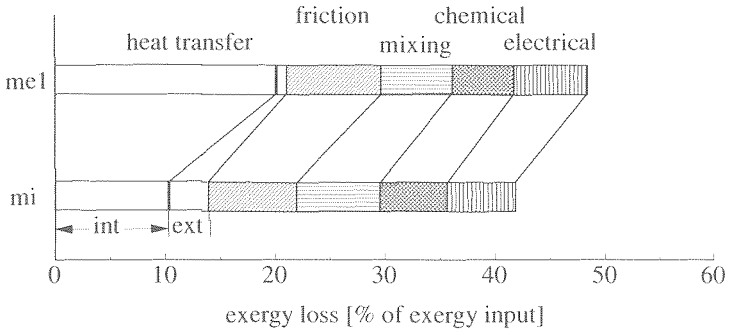

Figure 9.35: Comparison of the contributions for each of the separate causes of exergy losses the reference system (me1) and the internal reforming system (mi)

The other losses are not uniformly distributed but occur mainly near the anode inlet. However, the reason for the uneven distribution is different in both cases.

- The reforming reaction takes place mainly near the inlet (see **Section 5.5**) and correspondingly the losses occur mainly in this region.
- Heat transfer is distributed more evenly, but the exergy losses are concentrated near the

inlet because the temperature difference is between cathode and anode is large in this region (see the calculated temperature profiles in figure 5.18, **Section 5.4**)

Exergy losses in the subsystems

The total exergy efficiency of the internal reforming system equals 57.5 %. The other 42.5 % is equal to the total exergy losses in the system. Figure 9.35 shows how the losses for the total system are distributed over the different causes for the external reforming system (me1) and the internal reforming system (mi).

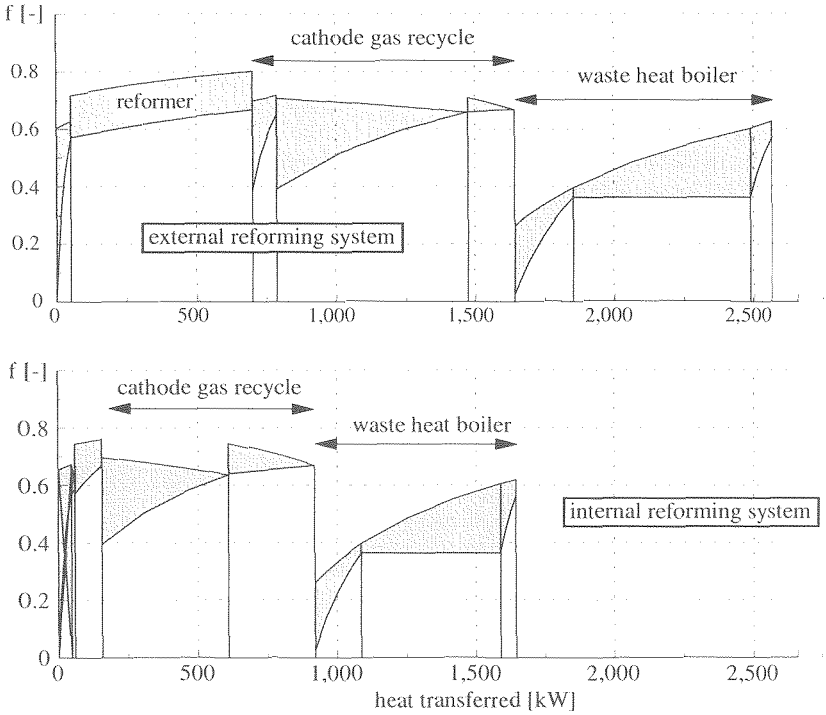

Figure 9.36: Comparison of the value diagram for the external reforming (me4) and the internal reforming system with direct anode off-gas recycle (mi)

A - Heat transfer losses

The losses as a result of heat transfer are much lower for the internal reforming system than for the external reforming system. This is due to two changes in the process design. The first is the use of internal reforming and elimination of the external reformer. The second change is that the internal reforming system uses a direct anode off-gas recycle and in the external reforming system the anode off-gas is cooled to remove water from this flow. The analysis in **Section 9.5** showed, that exergy losses as a result of heat transfer are high if the anode off-gas is cooled. To compare the influence of internal vs. external reforming on the exergy losses as a result of heat transfer, the systems with direct recycle for both internal and external reforming are compared (figure 9.36) The diagram shows that the exergy losses are much lower in the internal reforming system because:

- The reformer is eliminated. The losses as a result of heat transfer in the internal reforming fuel cell are not included in this diagram, but were shown to be negligible;
- The amount of heat transferred in the cathode gas recycle is much lower. This is due to the lower flow of cathode gas required to cool the fuel cell. However, this effect is only limited: due to the lower recycle ratio in the internal reforming system, the fresh air flow decreases less than the cathode gas flow.
- Substantial reduction of the exergy losses is achieved in the waste heat boiler. Because of the higher electrical efficiency of the system (+6%) less heat is transferred in the waste heat boiler.

The exergy losses as a result of heat transfer can be split into the external losses (i.e. the 'flue gas stack losses') and the internal losses (i.e. losses in the heat exchangers in the system). The internal heat losses occur mainly in the waste heat boiler and the cathode gas recycle and are visible in the value diagram. The external losses are large because of the high water content of the flue gas (20%) and the relatively high temperature (120 °C) due to the direct recycle of anode off-gas in the internal reforming system (see **Section 9.5**). In the internal reforming system, the total losses as a result of heat transfer correspond to 14.0% of the exergy input to the system. The internal losses equal 10.2% and the external reforming losses are equal to 3.8%. This shows that the analysis of heat transfer losses should not be limited to the internal losses.

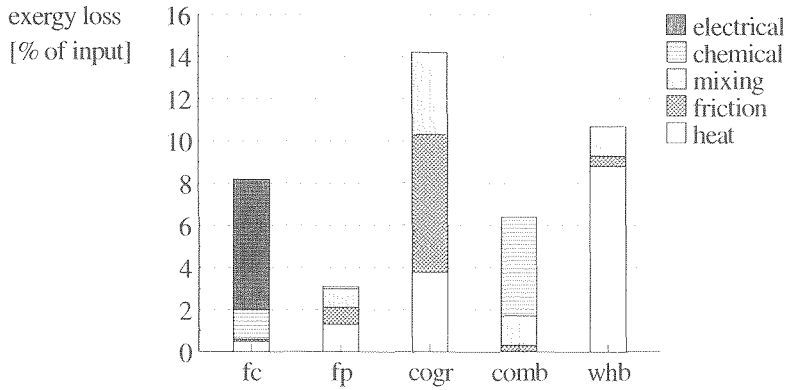

Figure 9.37: Exergy losses per type in the subsystems of the internal reforming system

B - Other losses

- Losses as a result of friction occur in all subsystems due to the pressure drops over the components and pipes. Figure 9.37 gives a detailed view of the exergy losses in the internal reforming system. The diagram shows that friction losses occur in each of the subsystems. The main losses however occur in the compressor and expander (i.e the cathode off-gas recycle subsystem).
- Losses as a result of mixing occur in nearly all subsystems as well: the cathode gas recycle, the waste heat boiler, the combustor and the pre-reformer (figure 9.37). It was shown previously that the main reason for the mixing loss is the decrease in partial pressure of H_2O when steam or a water-rich gas is mixed with a flow which contains little or no water vapour. As a result of such a mixing process the partial pressure of the water vapour decreases sharply and the temperature at which the latent heat can be recovered drops. This is evidently the case in this configuration as well. The highest loss occurs when

the air in the cathode recycle is mixed with the highly humid combustion off-gas. In the mixing process the condensation temperature of the vapour in the mixture drops from 115 to 91°C.

- Chemical reactions take place in the pre-reformer, the fuel cell and the combustor. The losses in the pre-reformer are small and are mainly the result of mixing and (to a lesser extent) heat transfer (i.e. the mixing of two flows with different temperatures). The chemical reaction in the pre-reformer contributes only for a minimal part to the total loss (0.1 % of the exergy input to the system). The exergy losses as a result of the reforming reaction in the fuel cell stack have been discussed previously: the calculated loss of 29.2 kW corresponds 1.4% of the exergy input. The largest losses as a result of chemical reactions occur in the combustor. The losses in the combustion reaction are substantial: 4.7% of the exergy input to the system.
- The electrical losses (126 kW) includes the losses as a result of polarisation and ohmic losses in the fuel cell. Another cause of electrical losses is the conversion of DC to AC power. Based on a conversion efficiency of 96 % the calculated loss equal 41.7 kW. The relatively high losses in the AC/DC-converter are caused by the fact that no heat is recovered from the converter, while the losses in the fuel cell stack are recovered as high temperature heat. The total electrical losses correspond to 6.2% of the exergy input to the system

The analysis in this section shows a considerably higher (electrical) efficiency for the internal reforming fuel cell. A higher fuel utilisation and lower auxiliary power are the main effects. The exergy losses decrease primarily because less heat is transferred in the system.

9.8 INFLUENCE OF THE FUEL UTILISATION ON THE INTERNAL REFORMING SYSTEM

9.8.1 Description of the system and calculations

Natural gas is converted in three steps in the fuel cell system: (1) the fuel is reformed, (2) electrochemically reacted in the fuel cell and (3) the remaining fuel components react in the combustor. The exergy losses in these processes can be visualized using a f,H-diagram. In this diagram (see **Section 3.5**) the x-axis corresponds to the energy of the conversion and the y-axis corresponds to the Carnot factor or the ratio between exergy and energy conversion (f). The exergy losses in the conversion can be shown as areas in the diagram. In figure 9.38 the f,H-diagram for the fuel conversion processes in the reference internal reforming MCFC system (mi) is shown[u]. The losses in the fuel cell were discussed in **Section 9.7** and are caused by heat transfer, polarisation and the reforming reaction. In the combustor the losses are due to the chemical reaction between air and the anode off-gas.
What can be read clearly in the f,H-diagram is the difference in efficiency between the conversion in the fuel cell system and the combustor. The exergy of the (chemical) energy which is converted corresponds to the total area enclosed by the highest curve. The exergy losses are indicated in the figure: the losses as a result of the reforming reaction and polarisation in the fuel cell and the loss in the combustion reaction in the combustor. The remaining area is the exergy which is "generated" in the fuel cell stack and the combustor. If areas representing the exergy of the energy which is generated in both components are

[u] The f,H-diagram does not show the losses as a result of mixing and friction as no characteristic energy transfer is associated with these losses

compared to the losses, the losses in the fuel cell amount to approximately 10% and in the combustor 25% of the exergy conversion (estimated from the diagram). In other words, the fuel cell operates at an efficiency approximately 90% and the combustor at 75%. However, this does not reflect the actual impact of the two components on the exergy losses in the system. In the case of the process in the fuel cell stack approximately ⅔ of the exergy which is produced in the electrochemical reaction is produced in the form of DC power (the area indicated with 'P' in the f,H-diagram). The electrical power is converted into AC-electrical power with a high efficiency (both exergy and energy) of 96 % in the DC/AC-converter. The area which represents the exergy of the heat which is generated in the fuel cell and the combustor is the area in the f,H-diagram indicated with Q. This heat is used with a much lower exergy efficiency.

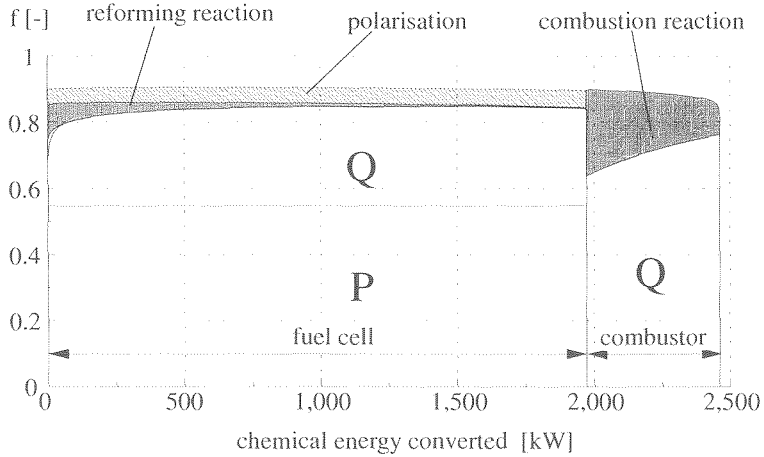

Figure 9.38: f,H-diagram for the fuel conversion process in the reference internal reforming MCFC system (mi)

To estimate the efficiency with which the heat is converted, it should be considered to what end the heat is used. The heat which is produced in the fuel cell and in the combustor is used to generate process steam ($E_{Q,PS}$= 114.5 kW) and to produce work in the expander/compressor combination (P_{CEC}=97.4 kW). The amount exergy (E_Q) in the heat produced in the fuel cell and combustor can be determined by estimating the average value for f for the exergy production from figure 9.38. The exergy of the heat which is generated in both components is approximately equal to 840 kW. Based on these data, it is possible to estimate roughly the efficiency with which the heat generated in fuel cell and combustor are converted:

$$\eta \approx \frac{P_{CEC} + E_{Q,ps}}{E_Q} \times 100\ \% = 24\ \%$$

If the difference in efficiency with which the heat is further processed (24%) and the efficiency with which the electrical power generated in the fuel cell is utilised (96%) and the ratio between heat and power production (1:2) is taken into account, the efficiency of the

process in the fuel cell is approximately 65 %[v]. Using the same method for the calculation of the efficiency of the combustor results in an effective efficiency of 18% (=0.75· 0.24). This illustrates the importance of converting as much of the chemical energy in the fuel directly into electrical power, i.e. increase the fuel utilisation in the fuel cell. The parameter which determines how much energy is converted in the fuel cell and how much in the combustor is the fuel utilisation. In order to assess how the performance of the system depends on fuel utilisation, the utilisation has been varied from U=77.5% to U=85%.

9.8.2 Energy analysis

If the fuel utilisation in the internal reforming MCFC system increases from 77.5% to 85%, the electrical efficiency of the system increases from 53.0% to 55.5%. The efficiencies for both cases are compared in figure 9.39. The main reason for this efficiency increase is the higher fuel cell efficiency. At high utilisation a larger fraction of the energy input to the system (in the fuel) is converted into electrical energy in the fuel cell stack. The fuel cell efficiency, defined as the ratio of electrical power produced in the fuel cell stack to the total energy input to the fuel cell system, increases from 50.4% to 53.9%.
The electrochemical efficiency of the fuel cell[w] determines the ratio between the heat produced in the fuel cell and the power. If the electrochemical efficiency remains constant as the fuel utilisation

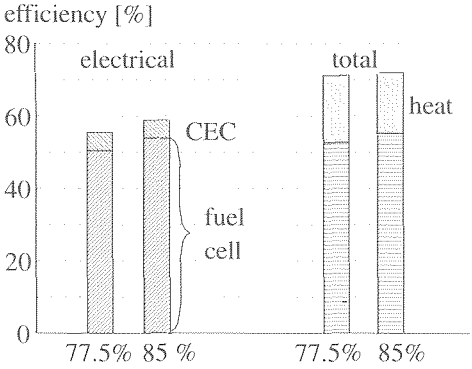

Figure 9.39: Comparison of the calculated efficiencies for the internal reforming MCFC system at 77.5% and 85% fuel utilisation

increases, the fuel cell efficiency (P_{FC}/LHV_{in}) is proportional to the fuel utilisation U. The calculations show that the fuel cell efficiency increases less than the fuel utilisation. Figure 9.40 compares the calculated values of the fuel cell efficiency (✱) and the values estimated assuming proportionality of the efficiency with U (the line U/U_0). Evidently the P/Q ratio is not constant: at higher fuel utilisation relatively more heat and less power is generated in the fuel cell stack.
The Nernst voltage decreases at higher fuel utilisation because of the lower average reactant

---

[v] the exergy efficiency of the fuel cell equals 90%, ⅔ of the chemical energy converted into electrical DC power which is converted into AC power with 96% efficiency and ⅓ heat which converted with 24% efficiency gives a total efficiency of ⅔·0.90·0.96 + ⅓·0.90·0.24 = 65%

[w] this is the P/Q ratio which was used in chapter 5 to indicate the efficiency with which fuel is actually converted in the fuel cell

concentration (H_2) at the anode. If the Nernst voltage decreases a larger part of the chemical energy is converted into heat in the reversible reaction (TΔS becomes larger). The decrease of the Nernst voltage also leads to a lower cell voltage and consequently to higher ohmic or polarisation losses. In figure 9.41 the heat balance for the fuel cell stack is shown for two values of the fuel utilisation: 77.5% and 85%. The diagram shows an increase of both ohmic and reversible heat.

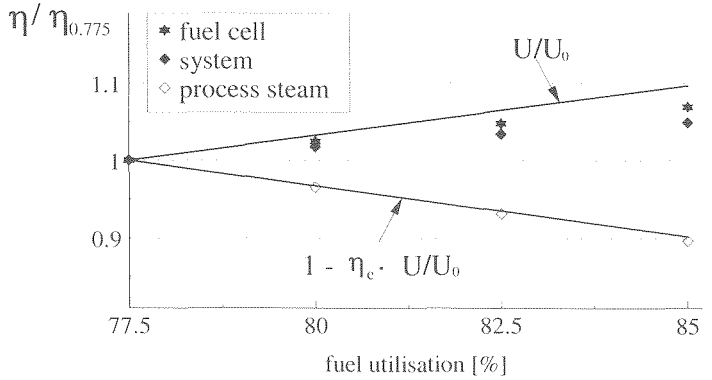

Figure 9.40: Comparison of actual calculated values of fuel cell and system electrical efficiency and heat production with simple predictions

If the fuel utilisation increases from 77.5% to 85%, the calculated value of the cell voltage decreases from 0.706 V to 0.687 V. This is due both to lower concentrations at the anode as to lower CO_2 concentrations at the cathode. The lower CO_2 concentration at the cathode leads to an increase of the polarisation by 0.5%.
The increase in electrical efficiency of the system is not as large as the increase in fuel cell efficiency: the net electrical efficiency increases +2.5%pt and the fuel cell efficiency

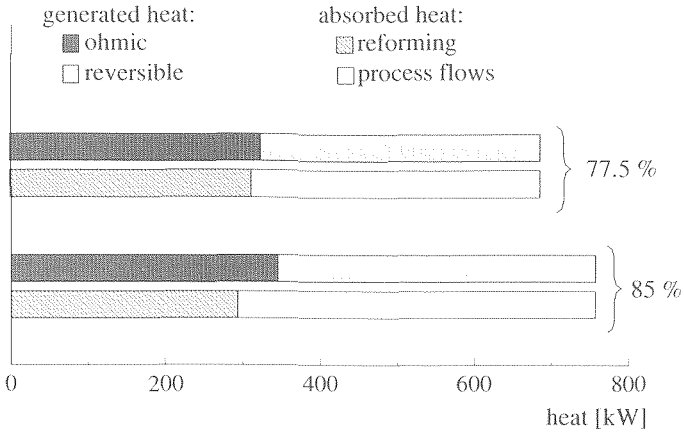

Figure 9.41: Heat balances for the fuel cell stack (IR-MCFC) for different values of the fuel utilisation (77.5% and 85%)

+3.5%pt. The net efficiency of the system is indicated in figure 9.40 as well (◆). The difference between net and fuel cell efficiency is due to the higher amount of heat generated in the fuel cell stack at higher fuel utilisation. As the cell is cooled by the cathode flow, more results in a larger flow of cathode gas required to cool the cell. However, this is not only the reason why more heat has to be removed from the fuel cell by the process flows. The largest effect is a decrease of the ratio between the heat generated by the electrochemical reaction and the heat consumed by the reforming reaction. This effect can be seen in the heat balances for the fuel cell stack in figure 9.41. The cooling effect of the reforming reaction depends only on the amount of methane supplied to the fuel cell. Because the fuel flow decreases at higher fuel utilisation (the power generated by the fuel cell stack is 1 MW in all calculations), so does the cooling effect. But because more heat is generated in the fuel cell, the amount of heat which has to be removed by the process flows increases strongly. If the utilisation is increased from 77.5% to 85.0% the oxidant flow which is required to cool the cell increase from 4.0 to 4.9 kg/s, an increase of almost +25%. Consequently the power requirements of the recycle blower increase. A net increase of the auxiliary power consumption from 2.6% to 3.3% results

The amount of heat which is produced by the system in the form of process steam depends on the fuel utilisation as well. The amount of heat generated in the combustor will decrease with the fuel utilisation. However, while less heat is generated in the combustor at higher fuel utilisation, more will be produced in the fuel cell. The heat generated in the fuel cell depends on U, the fraction of the fuel converted in the fuel cell. If η_e is the electrochemical efficiency, $(1-\eta_e)$ is the fraction of the chemical energy converted in the fuel cell, which is converted into heat. The heat generated in the combustor depends on the fraction not converted in the fuel cell (1-U).the total amount of heat generated in the two components combined is proportional to $1-U/U_0 * \eta_e$. In figure 9.40 the line $\mathbf{1-U\ U_0 * \eta_e}$ is shown assuming an efficiency of 67% for the fuel cell[x]. The calculated values compare well to the prediction.

9.8.3 Exergy analysis

The exergy losses were calculated for different values of the fuel utilisation as well.
Figure 9.42 shows the calculated exergy losses for each type of loss for two values of the fuel utilisation (77.5% and 85%). The main change occurs in the electrical losses and the losses as a result of chemical reactions.

A - Losses as a result of the chemical and electrochemical conversions

The exergy losses as a result of chemical reactions decreases with 1.7% if the fuel utilisation increases from 77.5% to 85%. At the same time the exergy losses as a result of polarisation in the fuel cell ('electrical' in figure 9.42) increase with 0.8%. This is the logical result of the increase in fuel utilisation. Increasing the fuel utilisation means that more energy is converted in the electrochemical reaction and less energy is converted in the combustion reaction. Correspondingly losses in the electrochemical reaction increase and losses decrease in the chemical reactions.

The amount of energy which is converted in the combustor decreases substantially. The exergy loss decreases almost proportionally. The small difference is caused by the slightly lower combustion temperature at higher fuel utilisation which leads to marginally higher losses per kW converted.

---

[x] The higher heating value of the anode gas is 2206 kW and the higher heating value of the anode off-gas is equal to 548 kW. Because P=1000 kW, P/Q is approximately 2: ⅔ of the energy is converted into electrical power and ⅓ into heat.

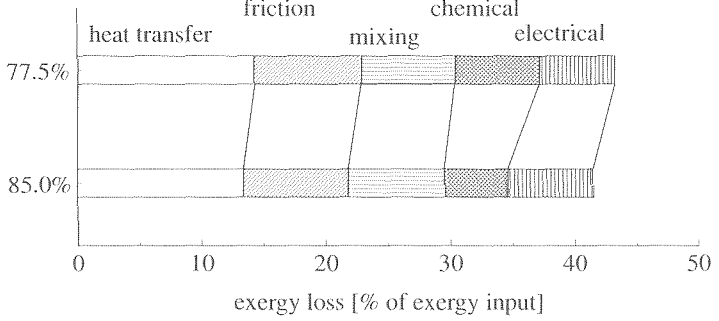

Figure 9.42: Exergy losses per type of loss in the reference internal reforming MCFC system (mi) for two values of the fuel utilisation

In the case of the fuel cell the change in exergy loss does not follow the change in energy converted as closely. Increasing the fuel utilisation from 77.5% to 85% leads to an increase of the electrical power generated by 6% but the exergy losses increase by 14% (from 6.0 to 6.8% of the fuel input to the system). This difference is due to the decrease in efficiency in the fuel cell (lower cell voltage). As a result, the power generated increases less than proportional to the amount of fuel converted in the cell and the losses increase more than proportional.

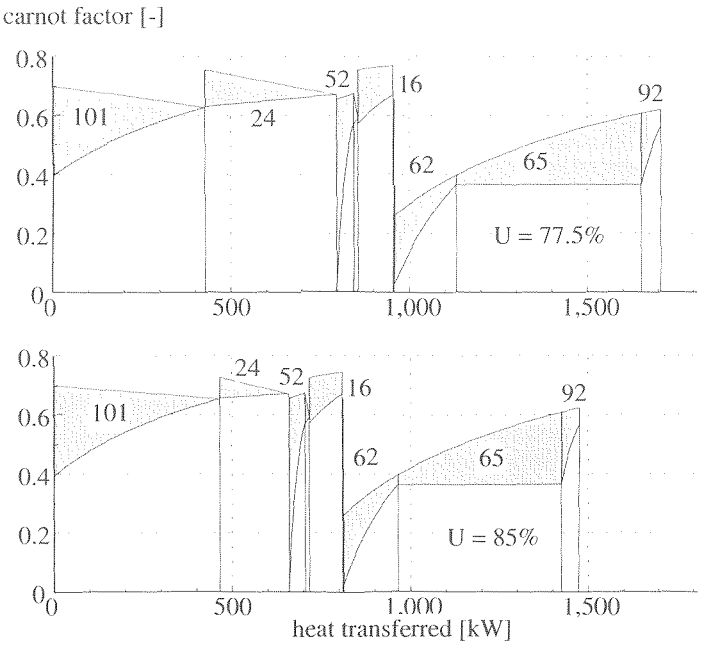

Figure 9.43: Value diagram for the reference internal reforming MCFC system (mi) for two values of the fuel utilisation

The net effect of increasing the fuel utilisation is positive: the increase in losses in the electrochemical reaction is smaller than the decrease in the losses in the chemical reaction. This is because of the higher exergy efficiency of the reaction in the fuel cell compared to the combustor. Therefore, even though the fuel cell efficiency decreases, the effect of increasing the fuel utilisation is an increase of efficiency.

B - Other losses

The fuel utilisation does not only influence the chemical and electrochemical reactions. It also influences the cathode off-gas recycle. The recycle ratio of the cathode off-gas was shown to be an important parameter in several of the previous analyses. This parameter is determined by the energy balance of the cathode off-gas recycle. This is influenced by the fuel utilisation in the MCFC system because the heat which is generated in the combustor is supplied to the cathode side with the anode off-gas. Therefore an in increase in fuel utilisation leads to a higher recycle. Although this affects the mass flows considerably (the air and flue gas flow decrease, the recycle flows increase) the net effect on the exergy losses as a result of friction is minimal (-0.1%). But the effect on the exergy losses as a result of heat transfer is more important. If the fuel utilisation increases from 77.5% to 85%, the exergy losses as a result of heat transfer decrease from 14.3% of the exergy to 13.4%. Figure 9.43 shows the value diagram for both cases. Heat transfer occurs mainly in the cathode gas recycle (app. 101 & 24) and in the waste heat boiler (62, 65 and 92). The losses decrease strongly in app. 24, because less heat is transferred and the temperature difference is smaller. Figure 9.44 illustrates that it is useful to separate different types of losses. Although the exergy losses in app. 24 are still considerable, reducing the exergy losses by decreasing the temperature difference between the mixed flows, will only reduce the exergy losses as a result of heat transfer. But the detailed exergy analysis shows that the largest part of the losses is not caused by the temperature difference, but by the difference in composition.

The losses decrease in both subsystems mainly because less heat is transferred. The value diagram in figure 5.43 shows the influence of the recycle ratio as well. As the recycle ratio increases, more heat is supplied to the fresh air by mixing flow with recycled cathode off-gas (apparatus 101 in figure 9.31). But the amount of heat supplied to the cathode gas by mixing the gas with recycled anode off-gas (apparatus 24) decreases. It is interesting to compare the change in exergy losses as a result of heat transfer with the total exergy losses in these two components of the system (app. 24 and 101). The losses as a result of heat transfer in app. 24 decrease at higher fuel utilisation because:

- Less heat is 'transferred' in the cathode off-gas recycle;
- A larger fraction of the heat transferred in the cathode off-gas recycle is transferred in app. 101 and less in app. 24;
- The temperature at which the hot flue gas is supplied to app. 24 is lower

As a result, the exergy loss as a result of heat transfer in app. 24 decreases very strongly (-70%). It is interesting to see that the total losses in this component decrease only 20%. This is illustrated in figure 9.44 which shows the exergy losses for the mixing of the fresh air with the cathode off-gas in app. 101 and with anode off-gas in app. 24. Although the losses as a result of heat transfer decrease very strongly in app.24, the same is not true for the losses as a result of mixing, which even increase slightly. By considering the different types of losses, it is evident that example by reducing the temperature difference between hot and cold flow, will not lead to a substantial further reduction of exergy losses because the exergy losses as a result of heat transfer are already small. This shows the value of the method of considering the different types of losses separately.

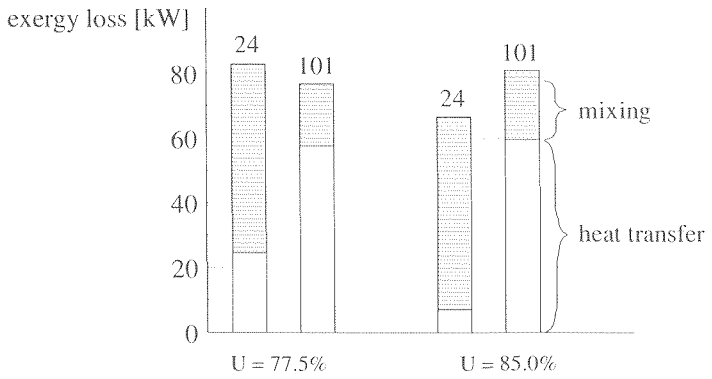

Figure 9.44: Exergy losses as a result of heat transfer and mixing in the reference internal reforming MCFC system for two values of the fuel utilisation

The analysis in this section shows that the (exergy) efficiency of fuel cell is much higher than the efficiency of the combustor. If the fuel utilisation increases, more fuel is converted in the fuel cell and less in the combustor. The efficiency of the total system therefore increases. A number of secondary effects reduce the effectivity of increasing the fuel utilisation. The electrochemical efficiency of the fuel cell decreases and the cathode flow required to cool the cell increases. Nevertheless the electrical efficiency increases by 2.5% if the fuel utilisation increases from 77.5% to 85.0%. The lower recycle ratio plays an important role in achieving this increase in efficiency.

DISCUSSION III
SYSTEM ANALYSIS

In **Chapter 7** the calculation results for the two base case systems, an external reforming SOFC system and an external reforming MCFC system, are discussed. The method of detailed exergy analysis developed in **part I**, which distinguishes different causes of exergy losses, has been used to clarify the main mechanisms of exergy losses in the fuel cell systems. The most important conclusion is that heat transfer is the dominant cause of exergy losses. In both the SOFC and the MCFC base case system, exergy losses as a result of heat transfer are responsible for half of the exergy losses. One of the most important reasons for the large losses as a result of heat transfer are the large recycle flows. For example, the amount of heat which is recycled from the outlet to the inlet of the fuel cell to preheat the cathode gas is 4-5 times as large as the electrical power generated in the fuel cell (both in the SOFC and in the MCFC system). By representing the energy flows in both systems in Sankey diagrams, the impact of these recycles on the efficiency of the system becomes evident.
The value diagram and the pinch-value diagram are used in **Chapter 7** to assess the exergy losses as a result of heat transfer in detail. In the SOFC system the largest part of these losses occur in the air preheaters and in the MCFC system the losses arise mainly in the cathode off-gas recycle (where 'cold' air is mixed with cathode off-gas) and in the anode off-gas recycle.
It is important to realise that the fuel cell not only generates electrical power. The heat which is generated in the fuel cell represents a substantial part of the total exergy (power+heat) 'generated'. In the SOFC the exergy of heat and power are approximately equal. The calculations show a slightly higher power-to-heat ratio for the MCFC.
This heat generated in the fuel cell is generally much larger in quantity and quality than the heat required in the system (e.g. for steam production or preheating the anode and cathode gas). There is therefore a 'heat surplus' in the system. Using the pinch diagram, the amount of heat which could be recovered at high temperature can be assessed. Combining this diagram with the value diagram, allows estimating how much exergy is lost because the available and required heat do not match. In this way a potential improvement of the (exergy) efficiency of the system can be estimated.
Although the losses as a result of heat transfer are dominant in the system, the key components in the fuel cell system are the components in which the fuel is converted: the fuel cell, the reformer and the combustor. The losses in these components have been analysed in detail. The f,H-diagrams discussed in **Chapter 7** facilitate a better understanding of the conversion process. The diagram for the fuel cell, for example, shows how important the generated heat in the fuel cell is for the (system) efficiency. Comparing the diagram for the MCFC to the diagram for the SOFC, also clearly shows how the lower operating temperature influences the electrochemical process. Another example is the analysis of the losses in the combustion process, which shows two different mechanisms are dominant in the combustion process in the SOFC and the MCFC system. Although the analysis shows clearly that optimising the efficiency of the system should focus on reducing the exergy losses as a result of heat transfer, it is necessary have a good understanding of the processes in these "fuel conversion" components. The exergy losses in these components are small, but changes in the process within these components have large consequences for the system performance (as calculations in the later chapters show).

Based on the exergy analysis of the base case SOFC system, a number of different system configurations is evaluated in **Chapter 8**. The focus is on reducing losses as a result of heat transfer in the system.

The effect of using a cathode off-gas recycle to reduce the amount of heat transferred in the air preheaters is investigated in **Section 8.2**. Less (fresh) air is required if a cathode off-gas recycle is used. The primary effect is therefore that the lower flue gas stack losses and lower amount of heat required to preheat the air lead to a higher thermal efficiency than for the base case system without a recycle. The electrical efficiency of the system becomes slightly lower, mainly due to a lower oxygen concentration in the cathode gas and the higher operating temperature of the blower. Exergy analysis shows that the exergy losses as a result of heat transfer shift from the air pre-heaters to the waste heat boiler. This is not trivial, as further analysis indicates. Using the pinch-value diagram, the amount of heat which could be extracted from the system at high temperature can be determined. In the system with recycle the exergy of this heat, i.e. the maximum power which could be produced using this heat, is almost twice as large as in the system without recycle. This shows that, although the performance of the system is not much better than the performance of the system without recycle, it is a better starting point for further optimisation.

The electrical efficiency improves spectacularly by operating the system with recycle at higher pressure. **Section 8.3** shows this is due to three factors:

- The net power production by the compressor/expander combination (CEC);
- A better performance of the fuel cell;
- A lower duty of the recycle blower.

Surprisingly the total efficiency of the system decreases with pressure. This is due mainly to the lower recycle ratio. As is evident in most calculations in **part III** of this thesis, the intended or primary effect (in this case converting part of the available heat into power by pressurising the system) is in many cases partly off-set by other effects, which will be indicated as the secondary effect (in this case the lower recycle ratio). Exergy analysis is particularly helpful in identifying the secondary effects.

The operating pressure used in the calculations for the pressurised system is 4 bar. Given the large increase in efficiency (+11 %pt) which is achieved by increasing the pressure from 1 to 4 bar, a further increase in operating pressure seems to be attractive. However, the exergy analysis shows this is not the case. This analysis is based again on the heat which can potentially be recovered at high temperature as estimated using the pinch-value diagram. As shown in **Section 8.2**, the potential in the atmospheric system with recycle is very large (480 kW). However, in the pressurised system, the potential is already reduced to 160 kW. Two conclusion can be derived from these data:

- The largest part of the potential has been used in the pressurised system, limiting the improvement of performance which can be achieved by increasing the pressure further (this is also confirmed by the calculations in **Section 8.6**);
- The efficiency with which the compressor/expander combination (CEC) utilises the heat is low: the 320 kW which could potentially be converted into power (i.e. 480 kW - 160 kW), result in a net power production of the CEC of 99 kW.

This last point is confirmed by repeating the system calculations for the pressurised system for different values of the efficiency of the rotating component in the CEC. These calculations show that the power generated by the CEC increase strongly with rotating component efficiency. For example, increasing the efficiency of compressor and expander from 75% to 90% leads to a further increase in efficiency of 8 %pt. The calculations also

confirm the method using the pinch-value diagram. The estimated improvement potential given above (320 kW) is a good estimate for the power which could be produced using at ideal CEC (i.e. with 100% isentropic efficiency of the rotating components).

The exergy efficiency of a fuel cell is much higher than the efficiency of the combustor. It is therefore to be expected that the efficiency of the system will increase if a larger part of the fuel is converted in the fuel cell (and less in the combustor). The influence of the fuel utilisation is calculated for two external reforming SOFC systems (**Section 8.4**): an atmospheric and the pressurised configuration. Based on the efficiency of the fuel cell an increase in electrical efficiency of 6.2 %pt can be expected. Again the primary effect (converting more fuel in the efficient fuel cell) is off-set by a number of secondary effects:

- Decrease of the fuel cell efficiency;
- Higher cathode gas flow to cool the cell;
- Lower efficiency of the expander (in the pressurised system).

As a result of the secondary effects, the actual calculated increase of the (exergy) efficiency is not more than 2.5%pt in the atmospheric system. The efficiency of the system operating under pressure even decreases slightly if the fuel utilisation increases. Again the exergy analysis shows exactly how the change in a single parameter (the fuel utilisation in the fuel cell) affects all subsystems, for example:

- Losses in the cathode off-gas recycle increase at higher fuel utilisation as a result of the larger mass flows through the system;
- In the combustor the losses as a result of chemical reactions are lower (less fuel is converted), but the mixing losses increase because of the higher air/fuel ratio;
- Losses in the expander increase as a result of the lower inlet temperature.

The analysis shows that a detailed accounting of the exergy losses (distinguishing different types of losses) in the system helps identifying and understanding these primary and secondary effects.

In an internal reforming SOFC, the fuel cell is partially cooled by the reforming reaction and much less air or cathode gas is required to cool the cell. Therefore it is a possibility to reduce heat transfer in the system. The calculated efficiencies for the system with internal reforming are compared to the efficiencies calculated for the corresponding external reforming configuration (**Section 8.5**). The net electrical efficiency is higher for the internal reforming system than for the external reforming system due to the lower duty for the cathode off-gas recycle flow. But the effect is not very strong (=1.7%pt). Again secondary effects plays an important role in this system.

- The amount of heat which has to be generated is 40% lower in the internal reforming fuel cell, but the temperature difference over the cell is much smaller as well. Using the detailed fuel cell model (see **Section 5.4**) the outlet temperatures are calculated for the internal reforming SOFC (950 °C) and the external reforming SOFC (1000 °C). The difference in outlet temperature means that more gas is required to remove the same amount of heat and the net effect of internal reforming is a cathode gas flow which is not 40% but only 10% lower than in the external reforming system.
- Another (secondary) effect is the influence of the temperature difference over the stack (i.e. the temperature difference between inlet and outlet of the cathode gas) on the energy balance of the recycle. As the analysis shows, the lower temperature at the outlet flow of the stack leads to a much higher cathode off-gas recycle ratio. As a result of this higher recycle ratio total efficiency is almost 17%pt higher for this configuration.

Comparison of the exergy losses in the internal reforming system with the exergy losses in

the external reforming configuration is again useful because it enables differentiating between the different effects the change in process design has. The exergy analysis shows that the losses as a result of the reforming reactions are higher than in the external reforming system because the reforming reaction occurs at a higher temperature. It shows the improved performance of the fuel cell because of the higher effective temperature. It also shows that the decrease of losses as a result of heat transfer in the system is mainly due to the lower air and cathode off-gas flows. Again the pinch-value diagram is useful in assessing how much of the exergy of the heat available in the system (used mainly to produce steam in the waste heat boiler) could be recovered. Interestingly, the analysis shows that the potential is slightly higher than in the external reforming system with recycle (even though the efficiency of the system is already higher).

This result is confirmed by the calculations in **Section 8.6**. These calculations shows that by increasing the pressure from 1 to 4 bar in the internal reforming system, the electrical efficiency of the system increases by more than 12 %pt. This is an even larger increase in efficiency than the external reforming system, corroborating the assessment of the improvement potential for the internal reforming system. Basically the same effects of pressurisation are found as for the system with external reforming (an increase in electrical efficiency of the fuel cell, more power delivered by the CEC and less power required for the recycle blower). Differences between the effects of pressurisation in the internal and external reforming system are found as well:

- In the internal reforming system, part of the natural gas is reformed in the pre-reformer. Because less methane is pre-reformed at higher pressure, the cooling effect of the reforming reaction is stronger at higher pressure;
- The influence of the pressure on the efficiency of the fuel cell is stronger than in the external reforming case.

Analysis of the base case MCFC system in **Chapter 7** showed the losses as a result of heat transfer are dominant in this system as well. In **Chapter 9** different MCFC system configurations are evaluated. Different configurations of the external reforming system are analysed to evaluate the effect of changes in the process scheme. In each case the objective is to make better use of the heat which is available in the system. First a number of external reforming MCFC systems are considered.

One way in which these losses can be reduced in the base case MCFC system is by using heat from the anode gas recycle to produce steam for the reforming process (**Section 9.2**). This improves the total efficiency by 11%pt. The pinch value diagram, is used to determine how much heat can (theoretically) be extracted at a high temperature by optimising the heat exchanger network and the highest possible temperature at which it can be extracted. The exergy of this heat corresponds to 300 kW ($\approx$15% of the energy input to the system) Analysis also shows that by optimising the heat exchanger network half of this exergy (=150 kW) can be recovered in the form of process steam (theoretically, i.e. at 0 K pinch). This is only little higher than the exergy of the process stream actually recovered in the reference system. This illustrates that to improve the exergy efficiency changes, in the process design are necessary which go beyond increasing the heat recovery in the waste heat boiler. Either less heat should be generated or better use should be made of the heat which is generated (i.e. the heat should be used at a higher temperature).

Adding an air-preheater to reduce exergy losses in the cathode gas recycle is considered in **Section 9.3**. The difference in performance between the reference system and the system with air preheater is mainly determined by the lower cathode off-gas recycle ratio in the latter case. The decrease of both electrical and total efficiency, is due to several secondary effects, including a larger air and flue gas flow, a lower cell voltage and larger losses in the compressor and expander. The analysis of the exergy losses shows that the smaller temperature difference at which the heat in the system is transferred is off-set by a larger amount of heat transferred.

Another option to reduce the heat surplus, a configuration with injection of steam in the gas flow before the expander, is discussed in **Section 9.4**. Instead of producing (low quality) steam from the heat which is generated in the system, by injecting the steam before the expander, the heat can be used to produce additional electrical power. However, the calculations show that the amount of electrical power which is produced is rather limited. Although the electrical efficiency increases, the overall exergy efficiency decreases. Large exergy loss occur in the process of mixing steam and cathode off-gas. The loss can be interpreted as the decrease of the partial pressure of the steam which results in a lower temperature at which the evaporation heat can be recovered after the mixing process. The high water content of flue gasses, even though the temperature at which the heat could be recovered is low, leads to considerable exergy losses in the flue gas stack. Because in both cases the exergy losses are directly due to the injection of steam, adding steam to the gas flow before the expander is shown to be an inefficient process.

A different approach to reduce the heat surplus is to eliminate the water separator in the anode off-gas recycle (**Section 9.5**). In that case the flow through the expander increases. Again the performance of the fuel cell system is determined by primary and secondary effects. The power generated by the compressor/expander combination (CEC) increases, as expected. The main secondary effect of the direct recycle is the lower fuel cell efficiency. The resulting loss completely off-sets the increase in expander power. The exergy analysis shows that the change in a single subsystem (the anode off-gas recycle) affects losses in many other subsystems. By comparing the exergy losses in both systems, the changes in each of the subsystems become apparent. In the reference system, condensing water in the anode off-gas recycle leads to large losses. In the system with direct recycle, higher losses occur when anode off-gas is mixed with air. The higher water content of the flue gas leads to higher flue gas stack losses. Although heat transfer losses are favourably influenced by increasing the expander power, the lower fuel utilisation in the fuel cell and the corresponding higher fraction of fuel which is combusted also lead to a shift in exergy losses as a result of heat transfer within the system. Exergy analysis again is useful, because it reveals how all these changes in the system relate to the change in process design: recycling anode off-gas directly instead of removing the water from anode off-gas.

Pressurising the system is shown to be an effective way to reduce the high temperature heat surplus in the MCFC system as well as in the SOFC system. To evaluate the influence of pressure on the external reforming MCFC system, calculations were carried out for the reference system at pressures ranging from 2 to 6 bar. The electrical efficiency increases strongly with pressure. Total efficiency decreases with pressure. As in the SOFC system, this is due to a lower cathode off-gas recycle ratio and a higher flue gas stack temperature. The exergy analysis shows that the main result of pressurisation is a reduction of the losses as a result of heat transfer, but an increase in the losses as a result of friction (in the compressor

and expander). The optimum pressure for the system (with respect to exergy efficiency) is a trade-off between heat transfer and friction losses. For the reference system the analysis shows that the optimum pressure is 5 bar. The main factor limiting improvement in system efficiency at higher pressure is the low efficiency of the CEC. The net duty of the CEC is the difference between the (much larger) duties of the compressor and expander. As a result, the net efficiency of the CEC is very sensitive to the isentropic efficiency of both components. Two methods are considered for estimating the potential improvement of the system efficiency if more efficient rotating components are used. The first method is the "lost work" approach, which calculates how the performance of the CEC improves. The second method uses the exergy losses. This approach does not only take into account the improvement of the CEC performance, but also the influence of the changing isentropic efficiencies on the rest of the system. However, this method assumes that heat generated in the expander and compressor is used in the system with high (exergy) efficiency. The actual potential lies between the values given by the two methods.

To reduce the amount of heat in the system, internal reforming is an effective method. An MCFC configuration with internal reforming is assessed in **Section 9.7**. Compared to the reference (external reforming) system, the gross efficiency (fuel cell and CEC) is considerably higher in the internal reforming system. The efficiency increase in the MCFC system is also much more pronounced than in the SOFC system. The positive effect that internal reforming has on the CO_2 recycle, seems to play an role.

To analyse the effect of the fuel utilisation on the performance of the internal reforming system, calculations have been carried out for different values of the fuel utilisation (**Section 9.8**). The efficiency of the system increases, even if the electrochemical efficiency decreases. Another secondary effect of the change in fuel utilisation is influence on the heat balance of the internal reforming fuel cell. At high fuel utilisation the cooling effect of the reforming reaction becomes less pronounced. Consequently at higher fuel utilisation, a considerably higher cathode flow is required to cool the cell. The exergy analysis shows a more efficient conversion of the fuel. The direct losses in this conversion are the losses as a result of chemical reactions and the electrical losses. The calculation shows that the sum of these losses decreases. A second effect is that less heat is produced in fuel cell and combustor combined, resulting in lower losses as a result of heat transfer in the system. But even if the amount of heat which is generated becomes smaller at higher fuel utilisation, the duty of the CEC, which converts part of this heat into power, does not decrease significantly. As a result, the higher utilisation is more effective in this configuration than for example in the SOFC configuration analysed in **Chapter 8**.

It is dangerous to try to draw general conclusions with respect to the different systems which have been considered (external/internal reforming and MCFC/SOFC) based on the system analysis in this thesis. Comparing different types of systems requires making the analysis on basis of more or less optimised systems and a methodical assessment of sensitivity of the system performance to key parameters as cell resistance, in- and outlet temperatures, etc. No such approach has been attempted in this thesis. However, based on the exergy analysis a number of observation on the fundamental differences between the different types of systems can be made.

- The exergy losses in the fuel cell are small. Nonetheless, the analysis still offers some interesting insights. For example, the exergy analysis shows that in the SOFC almost half of the exergy the fuel cell 'generates' is in the form of heat. For the MCFC this ratio is

closer to ⅔ (power) and ⅓ (heat). Pressurising the system (or in general utilising the heat well) is therefore more beneficial in the SOFC system than in the MCFC system.

- Comparison of the results for these four systems shows that the exergy losses as a result of the reforming reaction are determined mainly by the average temperature at which the (endothermal) reaction occurs. The highest losses occur in IR-SOFC system, where the reforming reaction occurs largely at high temperature (>850 °C). The external reforming systems have the lower (average) temperature of reaction and correspondingly the exergy losses in the reforming reaction are lower. Interestingly, the exergy losses in the electrochemical reaction are lowest in the internal reforming systems. This is explained by the higher effective temperature (see **Chapter 5**) and the lower hydrogen concentration in the feed.
- The exergy losses as a result of heat transfer are much lower in the internal reforming system than in the external reforming system. This is due to elimination of the reformer and the resulting direct heat transfer from electrochemical reaction to the reforming reaction. But the smaller cathode gas flow required to cool the cell, resulting in lower flows in the cathode off-gas recycle and the waste heat boiler also contribute to lower losses.
- In both systems even simple changes in parameters (e.g. fuel utilisation in the fuel cell) can lead to a series of (primary and secondary) effects. But the MCFC system is more sensitive to changes than the SOFC system. The main reason seems to be the required transport of CO_2 to the cathode inlet, which leads to an additional recycle loop.

How does exergy analysis help in optimising the fuel cell system? On a general level, it is offcourse necessary to understand the relative importance of the different aspects of the total process. For example understanding the fundamental importance of heat transfer in the system, or having a feeling for the influence of the efficiencies of fuel conversion in fuel cell and combustor. But there is also a more direct way in which exergy analysis contributes to optimisation. As the analysis shows, optimising the fuel cell system is not straight forward. Optimisation is more than identifying the exergy losses in the system and redesigning the process to reduce the losses. Comparison of the different configurations clearly indicates that the effect of even simple changes in process design or changes in process parameters generally is not simple. A distinction is therefore made in this thesis between the intended or primary effect of a change in process design and the (unintended) secondary effects. As shown, it is the secondary effects which make optimisation difficult. Because the calculated efficiencies are often the cumulative result of a number of different effects, it is difficult to identify what changes occur by considering only the energy inputs and outputs. But by determining the exergy losses and comparing the exergy losses in different configurations, it is possible to determine where the changes in the system occur and to quantify them. The method of separating exergy losses into different types of losses, as introduced in this thesis, is a particularly powerful method. Firstly because it makes it possible to detect changes in the process which are more difficult to recognize by considering the total exergy losses. Secondly, by identifying the cause of the losses, it is easier to trace the underlying changes in the process which cause the exergy losses. Understanding how changes in one part of the system affect the system as a whole is the key to optimising the system. Detailed exergy analysis offers a systematic approach to identifying these changes.

CHAPTER 10
CONCLUSIONS

Exergy losses in high temperature fuel cell systems can be attributed to different types of processes: heat transfer, mass flow (friction), chemical reactions, mixing and charge transfer (**Chapter 3**).

Analysis shows heat transfer can cause as much as half of the total exergy losses in the fuel cell system (**Chapter 7**). It is further shown that these losses are mainly due to the large heat flows which are transferred in the system in order to preheat and reform the inlet flows for the fuel cell. Reducing the losses as a result of heat transfer is essential for optimising the system (**Chapters 8, 9**).

For any chemical reaction for which the reaction exergy is smaller than reaction enthalpy, an equilibrium temperature can be determined. If an equilibrium temperature exist, the exergy loss in the chemical reaction can be interpreted in analogy with the exergy losses as a result of heat transfer, considering the difference between the actual process temperature and the equilibrium temperature as the driving force (**Chapter 3**).

The exergy losses associated directly with the fuel conversion (exergy losses as a result of the chemical and electrochemical reactions) are smaller than the losses as a result of heat transfer. This illustrates the relatively high efficiency of the electrochemical conversion. On the other hand, small changes in the process in the fuel cell are shown to have large impact on the exergy losses elsewhere in the system (**Chapters 8, 9**).

For the system analysis, a detailed fuel cell model is used which calculates heat transfer, temperatures of process flows and hardware, equilibrium and kinetically determined chemical reactions and local current densities along the cell in a 1-dimensional model. By describing the chemical and electrochemical reactions using reaction coordinates, the model can determine temperatures, mass flows, heat fluxes and compositions along the fuel cell using only 6 independent parameters (**Chapter 4**).

The main parameter influencing the efficiency of the fuel cell is the temperature at which the electrochemical reactions occur. Analysis of the calculation results of the detailed model shows that the combination of temperature and current density distribution is important. This leads to the definition of the 'effective temperature' as a measure for the average temperature at which the electrochemical reaction takes place (**Chapter 5**).

A much simpler model, based on an isothermal approach, is used to calculate the performance at off-design conditions. Comparison of the isothermal model with the detailed model shows good agreement over a wide range of conditions, by incorporating equations for the effective temperature and the outlet temperature of the fuel cell in the isothermal model (**Chapter 6**).

The extensive analysis of a limited number of high temperature fuel cell configurations shows that understanding the difference in performance between two configuration is often determined by a large number of different effects. The distinction between primary and secondary effects of process design changes is therefore introduced (**Chapters 8, 9**).

The analysis illustrates that the recycles in the system, both of mass and energy, make optimisation of these systems difficult. The secondary effects often partially off-set the primary or intended effect (**Chapters 8, 9**).

In many cases changes in process design result in changes in composition at the inlet of the fuel cell. A fuel cell model which takes into account the influence of such changes in composition is therefore required for real optimisation (**Chapters 5, 8, 9**).

In the fuel cell chemical energy is converted into heat and power. Exergy analysis shows that the exergy of the heat can be almost as large as the exergy of the electrical power which the cell generates. As a result, considerably higher efficiencies (10-15%pt) can be achieved by operating the fuel cell systems at higher pressure, using a compressor and expander to produce power and utilising the high temperature heat which is available in the system (**Chapters 8, 9**).

The method of detailed exergy analysis developed in this thesis helps identifying and understanding the primary and secondary results of a change in process design (**Chapters 8, 9**).

REFERENCES

Achenbach, E. (1993) *Three-dimensional and time-dependent simulation of a planar solid oxide fuel cell stack:* In: Proceedings of the 3rd Grove Symposium, Journal of Power Souces, vol. 49, no. 3, p. 333

Aguiar, P.; Chadwick, D. & Kershenbaum, L. (2002) *Modelling of an indirect internal reforming solid oxide fuel cell,* Chemical Engineering Science 57, p. 1665

Ahrendts, J. (1980) *Reference states,* Energy 5, pp. 667.

Akers, W.W., Camp, D.P., (1955) *Kinetics of the Methane-steam reaction*, A.I.Ch.E. Journal, vol.1, no. 4

Alefeld, G. (1988) *Exergy and the Second Law of Thermodynamics,* Brennst. -Waerme-Kraft 40/11, pp. 458-464.

Arakawa, M; Watanabe, K & Yamazaki, Y. (2003) *A Thermal Stress Analysis of Tubular Flat Plate Type SOFCs with Parallel Gas Paths*, In: Proc. of the 2002 Fuel Cell Seminar, Nov 18-Nov 21, Palm Springs, Ca, 285.

Baba, Y.; Ogiwara, T.; Yakabe, H. & Matsuzaki, Y. (2002) *Development of Anode-Supported SOFC with High Energy Conversion Efficiency at Reduced Temperature*, In: Proc. of the 2002 Fuel Cell Seminar, Nov 18-Nov 21, Palm Springs, Ca, p.340.

Baehr, H. D. (1978) *Thermodynamik,* Springer Verlag, Berlin

Baehr, H. D. (1979) *Exergy of fuels,* Brennst. -Wärme-Kraft 31/7, pp. 292-295.

Baehr, H. D.; Diederichsen, C. (1988) *Calculation equations for enthalpy and entropy of the components of air and combustion gases,* Brennst. -Wärme-Kraft 40/1/2, pp. 30-33.

Bagger, C.; Hendriksen, P. V. & Mogensen, M. (1996) *Technical problems to be solved before the solid oxide fuel cell will be commercialized,* In Proc. of the 1996 Fuel Cell Seminar, 17-20 Nov, Kissimmee, FL, USA, pp. 44-47.

Barringer, E. A.; Kneidel, K. E.; Morris, T. A.; Cable, T. L.; Elongovan, S. & Olenick, J. (2002) *AMPS, the SOFCo Planar Solid Oxide Fuel Cell*, In: Proc. of the 2002 Fuel Cell Seminar, Nov 18-Nov 21, Palm Springs, Ca, p.299.

Bauer, B., (1989) *Thermodynamic evaluation of chemical reactions* (in German), Chem. Ing. Tech, 61/11, p. 870-878

Beie, H.J., Blum, L., Drenkhahn, W., Greiner, H., Schichl (1998) *Development of Planar SOFC at Siemens - Status and prospects*, European solid oxide fuel cell forum, 2-5 June, Nantes, France

Beishon, D. S.; Taylor, M. R. (1994) *A system study for a 200kWe combined heat and power package*, Energy Technology Support Unit, Harwell (United Kingdom), ETSU/FCR-008 C2- F/01/00012/00/00.

Benjamin, T.G., Camara, E.H., (1980) *Handbook of Fuel Cell Performance*, IGT, DOE-Contract No. EC-77-C-03-1545

Bessette, N. F.; Wepfer, W. J. (1994) *Thermodynamic Performance of Solid Oxide Fuel Cells*, In: Proc. of the 1994 Fuel Cell Seminar, Nov 28-Dec 1, San Diego, Ca, p.148.

Bessette, N. F.; Wepfer, W. J. (1996) *Prediction of on-design and off-design performance for a solid oxide fuel cell power module,* Energy Conversion and Mngmt 37/3, pp. 281-293.

Bonds, T.L., Dawes, M.H.,Roberts, R., Schnacke, A.W., (1978) *Molten Carbonate Fuel Cell Power Plant System Evaluation, interim report june - 1979*, EPRI 1097,Palo Alto, Ca.

Bosio, B.; Arato, E. & Costa, P. (2003) *Concentration polarisation in heterogeneous electrochemical reactions: a consistent kinetic evaluation and its application to molten carbonate fuel cells,* Journal of Power Sources 115, pp. 189-193.

Bossel, U., (1992a) *Performance potentials for prominent SOFC configurations*, In Proc. of the 1992 Fuel Cell Seminar, Nov. 29-Dec. 2, Tucson, Az, USA, p. 261

Bossel, U., (1992b) *Facts and Figures - Final report on SOFC data*, International Energy Agency Programme of R,D&D on advanced fuel cells, Annex II, Swiss Federal Office of Energy, Berne, April 1992

Braun, R. J.; Gaggioli, R. A. & Dunbar, W. R. (1996) *Improvements of a molten carbonate fuel cell power plant via exergy analysis*, In Proc. of the ASME Advanced Energy Systems Division. AES-Volume 36, ASME New York, NY, pp. 321-331.

Brown, C. R.; etal.. (1994) *Current Status of the IMHEX Power Plant Demonstrations*, In: Proc. of the 1994 Fuel Cell Seminar, Nov 28-Dec 1, San Diego, Ca, p.454.

Buchkremer, H. P.; Stoever, D. & Diekmann, U. (1996) *Realisation of an anode supported planar SOFC system,* In Proc. of the 1996 Fuel Cell Seminar, 17-20 Nov, Kissimmee, FL, USA, pp. 175-178.

Campanari, S. (2003a) *Carbon dioxide separation from high temperature fuel cell power plants,* Journal of Power Sources 112, pp. 273-289.

Campanari, S. (2003b) *Thermodynamic model and parametric analysis of a tubular SOFC module,* Journal of Power Sources 92, pp. 26-34.

Cao, G.; Yoshiba, F.; Kouda, E. & Watanabe, T. (1995) *Modeling and simulation of internal temperature conditions in Molten Carbonate Fuel Cell*, pp. 103-114.

Chick, L. A., etal., (2002) *Experimentally-Calibrated, Spreadsheet-Based SOFC Unit-Cell Performance Model*, In: Proc. of the 2002 Fuel Cell Seminar, Nov 18-Nov 21, Palm Springs, Ca, p.383.

Cobben, O. (1994) *A reformer model for Cycle Tempo*, Delft Technical University, EV-1759.

Dahl, I., (1990) *SOFC Reforming chemistry*, In: Proceedings of the IEA Workshop on Modelling and Evaluation of Advanced SOFC, June 24-29

Daubert,T.E. (1986) *Chemical Engineering Thermodynamics*, 5th ed., McGraw-Hill, 1986

de Groot, A., Woudstra, N. (1993) *Exergy analysis of a Fuel Cell System*, Journal of the Institute of Energy, Vol. 68, p. 39

de Groot, A. (1998) *The role of recycle loops in the optimisation of high temperature fuel cell systems*, In: Proc. of the 1998 Fuel Cell Seminar, Nov 16-Nov 19, Palm Springs, Ca, p. 198.

Dekker, N. J. J. (1994) *Development and Validation of a MCFC Stack Model*, Fuel Cell Seminar, 28 Nov - 1 Dec 1994, San Diego, Ca, USA, 156.

Dicks, A., Carpenter, R.J., Erdle, E., Lander, D.F., Lilley, P.D., Melman, A.G., Woudstra, N., (1990) *Solid oxide fuel cell systems study,* CEC contract EN 3E-0165-NL,

Ding, J.; Patel, P. S.; Farooque, M. & Maru, H. C. (1997) *A Computer Model for Direct Carbonate Fuel Cells*, Energy Research Corp., Danbury, CT (United States), DOE/MC/31184-97/C0775

Doshi, R.; Roubort, J. & Krumpelt, M. (1996) *Characterization of ceria-based SOFCs*, Argonne National Lab., IL Fuel Cell Seminar, 17-20 Nov, Kissimmee, FL, USA, ANL/CMT/CP-89672

Drenckhahn, W.; Lezuo, A. & Reiter, K. (1991) *Technical and economic aspects of the use of fuel cells in cogeneration plants (in German),* VGB Kraftwerkstechnik 71/4, pp. 332-335.

Drenkhahn, W., (1993) *Do we need new materials development for SOFC plants,* In:5th IEA Workshop, SOFC Materials, Process Engineering and Electrochemistry, 2-4 March, Jullich, Germany

Dunbar, W. R.; Lior, N. & Gaggioli, R. A. (1990) *Exergetic advantages of fuel cell systems,* In A future for energy. Proceedings of the Florence World Energy Research Symposium, 28 May-1 Jun 1990, pp. 359-370.

Elongovan, S.; Khandkar, A.; Hartvigsen, J.; Rowley, D. & Tharp, M. (1998) *Recent Progress in SOFCo's Planar SOFC Development,* In: Proc. of the 2002 Fuel Cell Seminar, Nov 18-Nov 21, Palm Springs, Ca, p.465.

Farooque, M., etal. (1992) *Direct carbonate fuel cell development,* In 1994 Fuel Cell Seminar, San Diego, Ca, USA, p. 234.

Freni, S.; Giordano, N. & Cavallaro, S. (1990) *Temperature influence on the MCFC life time,* In Proc. of the 1990 Fuel Cell Seminar, Nov. 25-28, Phoenix, Az, USA, p. 191

Freni, S.; Aquino, M.; Giordano, N. & Cavallaro, S. (1992) *Mass and energy balances in a molten-carbonate fuel cell with internal reforming,* Journal of Power Sources 39/2, pp. 203-214.

Freni, S.; Maggio, G. & Passalacqua, E. (1997a) *Modeling of porous membranes for molten carbonate fuel cells,* Materials Chemistry and Physics 48/3, pp. 199-206.

Freni, S.; Passalacqua, E. & Barone, F. (1997b) *The influence of low operating temperature on molten carbonate fuel cells decay processes,* International Journal of Energy Research 21/12, pp. 1061-1070.

Gaggioli, R.A., Petit, P.J. (1977) *Use of Second Law First,* Chemtech, p.476-506.

Gerwen, R. J. F.; Veer, J. H. C. van der (1998) *A Condition Monitoring Model for a 100kW SOFC Unit,* In: Proc. of the 1998 Fuel Cell Seminar, Nov 16-Nov 19, Palm Springs, Ca, p.76.

Gordon, S., McBride, B.J. (1977) *Computer program for the calculation of complex chemical equilibria,* NASA Lewis Research Center

Han, J., etal. (2002) *Polarization study in MCFC by single-cell with reference electrode,* In: Proc. of the 2002 Fuel Cell Seminar, Nov 18-Nov 21, Palm Springs, Ca, p. 475

Hassmann, K. (2001) *SOFC power plants, the Siemens-Westinghouse approach,* Fuel Cells 1/1, pp. 78-84.

Haynes, C.; Wepfer, W. J. (1996) *High pressure operation of tubular solid oxide fuel cells and their intergration with gas turbines,* In 1996 Fuel Cell Seminar, 17-20 Nov, Kissimmee, FL, USA, pp. 111-114.

Haynes, C. (1998) *Reconsideration of Air/Fuel Ratios for Thermal Management of Tubular Solid Oxide Fuel Cell Stacks,* In: Proc. of the 1998 Fuel Cell Seminar, Nov 16-Nov 19, Palm Springs, Ca, p.406.

Haynes, C.; Rooker, W. (2002) *Thermal Management of Planar SOFCs Via Design Optimization,* In: Proc. of the 2002 Fuel Cell Seminar, Nov 18-21, Palm Springs, Ca, p.538.

He, W., Chen, Q., (1994) *Three-dimensional simulation of a Molten Carbonate Fuel Cell Stack,* Delft University of Technology, report EV-1774

Hinseveld, M., (1989) *Heat and Mass Transfer in a high temperaterature solid-oxide fuel cell,* Univestity of Twente, The Netherlands

Hirshenhoffer,J.H., Stauffer, D.B., Engleman,R.R.,Klett,M.G., (1998) *Fuel Cell Handbook, 4th ed.*, DOE/FETC-99/1076

Hosaka, M.; Morita, T.; Matsuyama, T. & Otsubo, M. (1996) , *Status of MCFC stack technology at IHI,* In Proc. of the Fuel Cell Seminar, 17-20 Nov, Kissimmee, FL, USA, pp. 284-287.

Iio, M.; Komoda, M. & Esaki, Y. (1998) *Performance of MCFC on Plant Gas Condition*, In: Proc. of the 1998 Fuel Cell Seminar, Nov 16-Nov 19, Palm Springs, Ca, p.158.

Ishida, M., Zheng, D., Akehata, T. (1986) *Evaluation of a chemical-looping combustion power-generation system by graphic analysis*, Energy, Vol.12, p. 147-154

Ishida, M., Suziki, T., Yamamoto, M. (1998) *Loops and thermodynamics*, Proceeding of the ASME advanced energy systems division, ASME1998

Itoh, H., Mori, M., Mori, N., Abe, T. (1994) *Production cost estimate of solid oxide fuel cells*, J. of Power Sources, vol. 49, p.315-332

Ivers-Tiffee, E.; Wersing, W. & Reichelt, B. (1990) , *Multilayer electrodes for planar SOFC,* In 1990 Fuel Cell Seminar,, Washington, DC (USA), pp. 137-140.

Kakihara, T.; Morita, T.; Suzuki, A. & Yamamasu, Y. (1994) *Development of a 100kW MCFC Stack and its Components*, 1994 Fuel Cell Seminar, Nov 28-Dec 1, San Diego, Ca, p. 450.

Kang, B-S; Lee, C-G; Seo, H-K; Lim, H-C; Ahn, K-S & Yoo, Y-S (2002) *100 kW MCFC System Development in Korea*, In: Proc. of the 2002 Fuel Cell Seminar, Nov 18-Nov 21, Palm Springs, Ca, pp. 481-484.

Karoliusen, H., Nisancioglyu. H., Solheim, A., Odegard, R. (1993) *Numerical simulation of a SOFC utilizing methane*, In:5th IEA Workshop, SOFC Materials, Process Engineering and Electrochemistry, 2-4 March, Jullich, Germany

Kato, T.; Negishi, A.; Nagata, S. & Nozaki, K. (1998) *Solid Oxide Fuel Cell Using Ceria Electrolyte for Transportation*, In: Proc. of the 1998 Fuel Cell Seminar, Nov 16-Nov 19, Palm Springs, Ca, p.59.

Kawashima, T.; Yasuda, I.; Matsuzaki, Y.; Ogasawara, K. & Hishinuma, M. (1994) *kW-Class Planar Type Solid Oxide Fuel Cell Development at Tokyo Gas*, In: Proc. of the 1994 Fuel Cell Seminar, Nov 28-Dec 1, San Diego, CA

Kinoshita, N. (1996) , *MCFC power plant with CO[sub 2] separation,* In Proc. of the Fuel Cell Seminar, 17-20 Nov, Kissimmee, FL, USA, pp. 351-354.

Kivisaari, T. (1994) *Studies of MCFC Power Plants*, In: Proc. of the 1994 Fuel Cell Seminar, Nov 28-Dec 1, San Diego, CA

Klapp, E. (1980) *Apparat und Anlagetechnik*, ISBN 3-540-009452-0, Springe-Verlag, Berlin, 1980

Klenke, J.W., (1978) *Heat and Work in Thermodynamics* (in German), Brenn. Waerme Kraft, 30/2

Koda, Eiichi (1993) *The conceptual design of MCFC power plants (LNG fueled, external reforming)*, In Proc. of the 3rd Int. Symposium on Carbonate Fuel Cell Technology, eds. D. Shores, etal., Electrochemical Society, Inc., Pennington, NJ (United States), pp. 75-88.

Koga, M.; Kamata, T.; Kawakami, S. & Tanigawa, K. (1992) *Development of pressed separator for molten carbonate fuel cell,* IHI Engineering Review 25/4, pp. 117-124.

Koh, J. H.; Seo, H.-K.; Yoo, Y.-S. & Lim, H.-C. (2002) *Considerations of numerical simulation parameters and heat transfer models for a Molten Carbonate Fuel Cell stack,* Chemical Engineering Journal 87, pp. 367-379.

Koh, J. H.; Seo, H. K.; Lee, C. G.; Yoo, Y. S. & Lim, H. C. (2003) *Pressure and flow distribution in internal gas manifolds of a fuel-cell stack,* Journal of Power Sources 115, pp. 54-65.

Koh, J. H.; Seo, H. K. & Lim, H. C. (2001) *Consideration of Numerical Simulation Parameters and Heat Transfer Models for a Molten Carbonate Fuel Cell Stack,* Chemical Engineering Journal 87, pp. 367-379.

Kortbeek, P.J., Ottervanger, R.G. (1998) *Developing advanced DIR-MCFC co-generation for clean and competitive power*, In: Proc. of the 1998 Fuel Cell Seminar, Nov 16-Nov 19, Palm Springs, Ca, p.9.

Kotas, T. J. (1980) *Exergy criteria of performance for thermal plant,* Int. J. Heat Fluid Flow 2/4, pp. 147-163.

Kotas, T. J. (1986) *Exergy method of thermal and chemical plant analysis,* Chem. Eng. Res. Des. 64/3, pp. 212-229.

Kraaij, G., Rietveld, G., Makkus, R.C. Huijsmans, J.P.P. (1998) *Development of second generation direct internal reforming molten carbonate fuel cell stack technology for congeneration application*, J. Power Sources, Vol. 71, No. 1-2, p. 215

Kraus, P.; Huppmann, G.; Heiming, A. & Aasberg-Petersen, K. (1998) *The Hot Module Compact Carbonate Fuel Cell CoGencration Plant Operational Experience*, In: Proc. of the 1998 Fuel Cell Seminar, Nov 16-Nov 19, Palm Springs, Ca, p.9.

Kreysig, E., (1983) *Advanced Engineering Mathematics,* 5th edition , John Wiley & Sons, 1983

Krist, K. (1994) *Fabrication Costs For Reduced Temperature Solid Oxide Fuel Cells*, In: Proc. of the 1994 Fuel Cell Seminar, Nov 28-Dec 1, San Diego, CA

Krist, K.; Wright, J. D.; Romero, C. & Chen, Tan Ping Bechtel Group Inc. San Francisco CA United States (1996) *Cost projections for planar solid oxide fuel cell systems,* In Proc. of the 1996 Fuel Cell Seminar, 17-20 Nov, Kissimmee, FL, pp. 497-500.

Kunz, H. R.; Bergoli, L. J. & Szymanski, S. T. (1984) *A homogeneous/agglomerate model for molten carbonate fuel cell cathodes*, J. Electrochem. Soc. 131/12, pp. 2815-2821.

Kunz, H. R.; Murphy, L. A. (1985) *The effect of Oxidant composition on the performance of Molten Carbonate Fuel Cells.*

Larminy, J.,Dicks, A., (2000) *Fuel Cells Explained*, John Wiley & Sons, UK

Laursen, C. L.; Christiansen, L. J. & Udengaard, N. R. (1990) *Advances in reforming technology for fuel cell applications,* In Proc. of the 1990 Fuel Cell Seminar, Nov. 25-28, Phoenix, Az, USA, pp. 44-47.

Laursen, C.; Udengaard, N. R. (1994) *Heat Exchange Reformers Development and Application*, In: Proc. of the 1994 Fuel Cell Seminar, Nov 28-Dec 1, San Diego, CA

Lee, A.L., (1987) *Internal reforming development for Solid Oxide Fuel Cells* - IGT final report for DOE, Chicago (Ill.), Feb. 1987

Lee, C.; Nakano, H.; Nishina, T.; Uchida, I.; Izaki, Y. & Kuroe, S. (1996a) *Transient response analysis on an 100cm[sup 2] class molten carbonate fuel cell,* Denki Kagaku Oyobi Kogyo Butsuri Kagaku (Electrochemistry and Industrial Physical Chemistry) 64/6, pp. 486-490

Lee, K. S.; Kim, H., Hong, S. A., Lim, H. C. (1996b) *Prediction of temperature profile in MCFC stack,* In Proc. of the Fuel Cell Seminar, 17-20 Nov, Kissimmee, FL, USA, pp. 434-437.

Lee, C.-G.; Kang, B.-S.; Seo, H.-K. & Lim, H.-C. (2003) *Effect of gas-phase transport in molten carbonate fuel cell*, Journal of Electroanalytical Chemistry 540, pp. 169-188.

Le Goff, P.; Rivero, R.; de Oliveira, S. Jr & Cachot, T. (1990) *Application of the enthalapy-Carnot Factor diagram to the exergy analysis of distillation processes,* In Proceedings of the winter annual meeting,, ASME, New York, NY, pp. 21-28.

Le Goff, P.; Cachot, T. & Rivero, R. (1996) *Exergy analysis of distillation processes,* Chemical Engineering and Technology 19/6, pp. 478-485.

Lim, T-H; Han, J.; Yoon, S.-P.; Nam, S.-Y.; Hong, S.-H. & Hwang, G. C. (2002) *Polarization Study in MCFC by a Single Cell with Reference Electrode*, In: Proc. of the 2002 Fuel Cell Seminar, Nov 18-Nov 21, Palm Springs, Ca, p. 475.

Lukas, M. D.; Lee, K. Y. & Ghezel-Ayagh, H. (2002) *Modeling and cycling control of carbonate fuel cell power plants,* Control Engineering Practice.

Lundberg, W. L. (1989) *cogeneration-system of natural gas-fueled Solid-oxide fuel-cell systems*, Westinghouse Electric Corp., Pittsburgh, PA (USA). Advanced Energy Conversion Dept., p. 119.

Ma, Z.; Jeter, S. M. & Abdel-Khalik, S. I. (2003) *Modeling the tranport processes within multichannel molten carbonate fuel cells,* International Journal of Hydrogen Energy 28, pp. 85-97.

Machielse, L. A. H. (1991) *Simple model for the estimation of isothermal fuel cell performance*, Netherlands Energy Research Foundation (ECN), Petten (Netherlands), ECN-RX-91-071

Makkus, R.C., Weewer, R., Hemmes, K., de Wit, J.H.W. (1988) *Fundamental research on MCFC electrode materials, part I: the cathode*, In: Proc. of the 1988 Fuel Cell Seminar, Oct. 23-26, Ca, Usa, p. 335

Marcenaro, B. (2002) *Moving MCFC to the Market: The Ansaldo Case*, In: Proc. of the 2002 Fuel Cell Seminar, Nov 18-Nov 21, Palm Springs, Ca, p.449.

Marianowski, L. G.; Ong, E. T.; Petri, R. J. & Remick, R. J. (1991) *Development of internal manifold heat exchanger (IMHEX™) molten carbonate fuel cell stacks*, Institute of Gas Technology, Chicago, IL (United States), CONF-9108177-1.

Maru, H, etal. (1992) *Development of direct carbonate fuel cell stacks*, In Proc. of the 1992 Fuel Cell Seminar, Nov. 29-Dec. 2, Tucson, Az, USA, p. 481.

Massardo, A. F.; Lubelli, F. (2000) *Internal reforming solid oxide fuel cell-gas turbine combined cycles (IRSOFC-GT): Part A -- Cell model and cycle thermodynamic analysis,* Journal of Engineering for Gas Turbines and Power 122/1, pp. 27-35.

Masuda, Y.; Kasai, H.; Suzuki, A. & Hosaka, M. (1998) *Evaluation and Analysis of High Performance MCFC*, In: Proc. of the 1998 Fuel Cell Seminar, Nov 16-Nov 19, Palm Springs, Ca, p.53.

Mathur, A.; Bali, S.; Balakrishnan, M.; Perumal, R. & Batra, V. S. (1999) *Demonstration of coal gas run molten carbonate fuel cell concept,* International Journal of Energy Research 23/13, pp. 1177-1185.

Matsumura, M.; Hirai, C. (1998) *Deterioration mechanism of direct internal reforming catalyst,* Journal of Chemical Engineering of Japan 31/5, pp. 734-760.

Melhus, O.; Ratkje, S. K. (1995) *Simulations of Diffusion Controled Reaction on the micro-m scale in single, flat solid oxide fuel cells`*.

Meijer, M. G. (1993a) *Calculation of exergy values (in Dutch)*, Delft Technical University, EV-1692.

Meijer, M. G. (1993b) *Study of the performance of a 250 kW Molten Carbonate Fuel Cell system (in Dutch)*, Delft Technical University, EV-1763.

Mitteldorf, J.; Wilemski, G. (1984) *Film thickness and distribution of electrolyte in porous fuel cell components*, J. Electrochem. Soc. 131/8, pp. 1784-1788.

Mogensen, M.; Kindl, B. & Malmgren-Hansen, B. (1990) *On the prospects of operating an SOFC on dry natural gas*, In Proc. of the 1990 Fuel Cell Seminar, Nov. 25-28, Phoenix, Az, USA, p. 195.

Mogensen, M.; Bagger, C. & Knudsen, P. (1994) *SOFC R&D at RISO*, In: Proc. of the 1994 Fuel Cell Seminar, Nov 28-Dec 1, San Diego, Ca, pp. 543.

Morita, Y.; Moriya, N. & Hayasaka, M. (1992) *Hybrid combustor and heat exchange reformer for MCFC power generation system*, In Proc. of the 1992 Fuel Cell Seminar, Nov. 29-Dec. 2, Tucson, Az, USA, p. 481.

Morita, H.; Moriya, N.; Hayasaka, M. & Horie, T. (1994) *Demonstration Test Of A 1MW Heat Exchange Reformer And Hybrid Combustor For Fuel Cell Applications*, In: Proc. of the 1994 Fuel Cell Seminar, Nov 28-Dec 1, San Diego, CA,. pp. 112.

Morita, H., etal. (1995) *Performance and life of MCFC at high current density - view of correlation between operating condition and cell performance*, Yokosuka Res. Report No W.93022.

Morita, Y.; Horie, T.; Ogawa, M. & Mizumoto, Y. (1996) *Demonstration test of a reformer employing thermal radiation media for multi-megawatt fuel cell applications*, In Proc. of the 1996 Fuel Cell Seminar, 17-20 Nov, Kissimmee, FL, USA, pp. 722-725.

Morita, H., etal. (2003) *Performance analysis of molten carbonate fuel cel using a Li/Na electrolyte*, Journal of Power Sources 112, pp. 509-518.

Mugikura, Y., etal. (1998) *Performance and life of 10-kW molten-carbonate fuel cell stack using Li/K and Li/ Na carbonates as the electrolyte*, Journal of Power Sources 75/1, pp. 108-115.

Munsch, M.; Mohr, T. & Futterer, E. (1990) *Exergy analysis and assessment of process plants with flow-sheeting systems*, Chem. -Ing. -Tech. 62/12, pp. 995-1002.

Murahashi, T.; Sasaki, A. (1994) *Development of Internal Reforming Molten Carbonate Fuel Cell*, In: Proc. of the 1994 Fuel Cell Seminar, Nov 28-Dec 1, San Diego, Ca, USA, p. 230.

Namba, S. (1993) *Development of MCFC Plant Simulation Technology*

Norrick, D.; Barringer, E.; Kantak, M.; Sanders, D. & Watson, G. (2002) *10 kW SOFC Power System Commercialization*, In: Proc. of the 2002 Fuel Cell Seminar, Nov 18-Nov 21, Palm Springs, Ca, p.960.

Odegard, R. (1994) *Statoil's SOFC Program*, In: Proc. of the 1994 Fuel Cell Seminar, Nov 28-Dec 1, San Diego, Ca, pp. 658.

Ohtsuki, J., etal. (1992) *Development of indirect internal reforming molten carbonate fuel cell*, In Proc. of the 1992 Fuel Cell Seminar, Nov. 29-Dec. 2, Tucson, Az, USA, In 1992 Fuel Cell Seminar, Tucson, Az, USA, pp. 481-484.

Oishi, N.; Rudkin, R.; Brandon, N. P.; Lewis, G.; McColm, T. & Steele, B. (2002) *Operation at 500-600°C of Stainless Steel Supported IT-SOFC*, In: Proc. of the 2002 Fuel Cell Seminar, Nov 18-Nov 21, Palm Springs, Ca, p.878.

Okada, T.; Ide, H.; Miyazaki, M.; Tanaka, T.; Narita, S. & Ohtsuki, J. (1990) , *Study of temperature control in indirect internal reforming MCFC stack,* In Proc. of the 25th IECEC, eds. P. A. Nelson, etal., AIChE, New York, NY (USA), pp. 207-212.

Ong, E. T.; Remick, R. J., Sishtla, C. I. (1996) *Endurance testing With Li/Na electrolyte*, Institute of Gas Technology, Des Plaines, IL, DOE/MC/30133-97/C0781

Parsons, J., Randall, S., (1992) *Experimental determination of Kinatic Rate Data for SOFC Anodes*, In Final Report on SOFC Micromodelling, IEA Programme on R,D&D of advanced Fuel Cells, Berne, Switzerland, 1992

Patel, P., (1983) *Assessment of a 6500-BTU/kWh Heat Rate Dispersed Generator*, EPRI EM-3307, Palo Alto, Ca.

Pietrogrande, P., Bezzeccheri, M., (1993) *Fuel Processing*, In: Fuel Cell Systems, ed. Blomen, L.J.M.J., Mugerwa, M.N., Plenum Press, New York

Pigeaud, A.; Wilemski, G.; Rigos, D. & Chamberlin, R. (1986) *Modeling of electrolyte migration in the molten carbonate fuel cell stack,* In Proc. of the 1986 Fuel Cell Seminar, Oct. 26-29, Tucson, Az, USA, p.211-214.

Pigeaud, A.; Helbe, J. J. & Senior, C. L. (1994) *Trace Contaminant Effects and Emissions with Integrated Coal Gasification and Cleanup* ., In: Proc. of the 1994 Fuel Cell Seminar, Nov 28-Dec 1, San Diego, Ca, pp. 539.

Rant, Z., (1956) *Exergie, ein neues Wort fur "technischeArbeitsfähigkeit*, Forsch. Ing.-Wes. 22, S. 36/37

Ray, E. R. (1994) *Westinghouse SOFC Technology Status Update*, In: Proc. of the 1994 Fuel Cell Seminar, Nov 28-Dec 1, San Diego, Ca, pp. 670.

Recknagle, K. P.; Williford, R. E.; Chick, L. A.; Rector, D. R. & Khaleel, M. A. (2002) *Thermal Management of Planar SOFCs Via Design Optimization,* In: Proc. of the 2002 Fuel Cell Seminar, Nov 18-Nov 21, 542.

Recknagle, K. P.; Williford, R. E.; Chick, L. A.; Rector, D. R. & Khaleel, M. A. (2003) *Three-dimensional thermo-fluid electrochemical modeling of planar SOFC stacks,* Journal of Power Sources 113, pp. 109-114.

Reid, R.C., Prausnitz, J.M., (1987) *The properties of Gases and Liquids,* 4th ed., McGraw Hill, New York

Riekert, L. (1981) *Regarding the reference point of the exergy of chemically reactive systems,* Brennst. -Waerme-Kraft 33/7/8, pp. 334-335.

Rietveld, G.; Nammersma, P.; Ouweltjes, P. & Drutten, G. van (2002) *Solid Oxide Fuel Cell Development at ECN and Production at InDEC,* In: Proc. of the 2002 Fuel Cell Seminar, Nov 18-Nov 21, Palm Springs, Ca, p.887.

Rögener, H., (1988) *Energy conversion, a thermodynamic analysis (in Geman)*,Brennst. - Waerme-Kraft 40/1 pp. 34-37.

Romero, C. A.; Wright, J. D. (1996) *Value and manufacturing costs of planar solid oxide fuel cell stacks*. TDA Research, Inc., Wheat Ridge, GRI-5087-260-1543.

Rosen, M. A. (1990) *Comparison based on energy and exergy analyses of the potential cogeneration efficiencies for fuel cells and other electricity generation devices,* International Journal of Hydrogen Energy 15/4, pp. 267-274.

Saito, T.; Itoh, Y.; Nishioka, M. & Miyake, Y. (1991) *Effect of operating temperature on the performance of molten-carbonate fuel cells,* Journal of Power Sources 36, pp. 69-77.

Selman, J. R., Herbin, R. , Flueck, M. & Gruber, R. (1990a) *2-D and 3-D Modelling at the Stack level*, In: proc of the Int. Energy Agency (IEA), Workshop 'Modeling and Evaluation of Advanced SOFC, Swiss Federal Office of Energy, June 24-29, 1990

Selman, J.R., Nishina, T., Lin, Y.P., Tryk, D.B., Yeager, E.B. (1990b) *Electrolyte chemistry and wetting effects on MCFC cathode kinetics and performance*, In: Proc. of the 1990 Fuel Cell Seminar, Nov. 25-28, Phoenix, Az, USA, p. 214

Selman, J.R., (2000) *Fuel Cell Modeling- Status and overview*, NETL, Morgantown, WV, USA, April 18, 2000

Simner, S. P., etal. (2002) *Development of Cathode Materials for Low Temperature SOFCs*, In: Proc. of the 2002 Fuel Cell Seminar, Nov 18-Nov 21, Palm Springs, Ca, p.344.

Singhal, S. C. (1998) *Advances in Solid Oxide Fuel Cell Technology*, In: Proc. of the 1998 Fuel Cell Seminar, Nov 16-Nov 19, Palm Springs, Ca, p.266.

Sishtla, C.; Vasil, D.; Platon, R., Ong, E. T. (1994) *Effect of Pressure on Performance and Endurance of a Molten Carbonate Fuel Cell*, 1994 Fuel Cell Seminar, Nov 28-Dec 1, San Diego, 400.

Smith, J. M., van Ness, H. C. (2003) *Introduction to Chemical Engineering Thermodynamics*, 5th ed, McGraw-Hill Chemical Engineering Series.

Snowdon, C.B., etal., (1991) *Conceptual design study of a planar solid oxide fuel cell co-generation system*, ETSU Report, ETSU/FCR/004

Standaert, F.; Hemmes, K. & Woudstra, N. (1996) *Analytical fuel cell modeling*, Journal of Power Sources 63/2, pp. 221-234.

Standaert, F.; Hemmes, K. & Woudstra, N. (2001) *Nernst loss in fuel cells and fuel cell designs in dead-end mode.*

Steele, B.C.H., (1993) *Oxygen transport and exchange in oxide ceramics*, In: Proceedings of the 3rd Grove Symposium, Journal of Power Souces, vol. 49, no. 3, pp. 333-349

Szargut, J.; Morris, D. R. & Steward, F. R. (1988) *Cumulative exergy consumption and cumulative degree of perfection*, In Energy analysis of thermal, chemical, and metallurgical processes, Electronic Conventions Inc., Los Angeles, Ca, pp. 171-191.

Takashima, S. (1993) *MCFC Stack Modeling and Testing at Hitachi.*

Takeda, Y.; Kanno, R.; Tomida, Y. & Yamamoto, O. (1997) *Cathodic Polarisation Phenomena of Perovskite Oxide Electrodes with Stabilised Zirconia*, J. Electrochem. Soc. 134/11, pp. 2656-2661.

Tanaka, K.; Wen, C. & Yamada, K. (2000) *Design and evaluation of combined cycle system with solid oxide fuel cell and gas turbine*, Fuel 79/12, pp. 1493-1507.

Tanimoto, K.; Yanagida, M.; Kojima, T.; Tamiya, Y.; Matsumoto, H. & Miyazaki, Y. (1998) *Long-term operation of small-sized single molten carbonate fuel cells*, Journal of Power Sources 72/1, pp. 77-82.

Thijssen, J. H. J.; Fulton, C.; Stringfellow, R. & Sriramulu, S. (2002) *Structural Limitations in the Scale-Up of Planar Anode Supported Solid Oxide Fuel Cell (SOFC) Stacks*, In: Proc. of the 2002 Fuel Cell Seminar, Nov 18-Nov 21, Palm Springs, Ca, p.894.

Togari, O. (1990) *Hybrid combustion of MCFC anode exhaust gas for heat exchange steam reformer*, In Proc. of the 1990 Fuel Cell Seminar, Nov. 25-28, Phoenix, Az, USA, p. 199

Uchiyama, Y.; Segawa, T. (1990) *Subsequent Results of a 1 MW class pilot Plant development.*

Uematsu, H.; Hasegawa, T. & Okano, T. (1994) *Demonstration of Fuel Processing Unit for MCFC Power Generation System*, In: Proc. of the 1994 Fuel Cell Seminar, Nov 28-Dec 1, San Diego, Ca, pp 268.

Van herle, J.; Marechal, F.; Leuenberger, S. & Favrat, D. (2003) *Energy balance model of a SOFC cogenerator operated with biogas,* Journal of Power Sources 118, pp. 375-383.

Vetter, K.J., (1967) *Electrochemical Kinetics*, Academic Press, New York, NY.

van Heuveln, F.H., Huijsmans, J.P.P., (1993) *Long term stability for solid oxide fuel cells - products and systems evaluation*, In:5th IEA Workshop, SOFC Materials, Process Engineering and Electrochemistry, 2-4 March, Jullich, Germany

van Lier, J. J. C.(1978) *Use of the term 'Exergy' for the evaluation of the energy transformation in electricity and/or heat generation,* Brennst. -Waerme-Kraft 30/12, pp. 475-484.

van Lier, J. J. C.(1992a) *Thermodynamic insight in process calculations* (in Dutch), *Part 1* Mechanische Technologie 2/5, pp. 18-22 & *Part 2,* Mechanische Technologie 2/8, p. 40

Watanabe, T. (1992a) *Development of molten carbonate fuel cell stack performance analysis model (part 1)*, Central Research Inst. of Electric Power Industry, Tokyo (Japan), CRIEPI-W-90028.

Watanabe, T.; Mugikura, Y.; Izaki, Y.; Koda, E.; Kinoshita, H. & Abe, T. (1992b) *Modeling analysis on molten carbonate fuel cells and stacks*, In Proc. of the 27th intersociety energy conversion engineering conference,Warrendale, PA (United States), p.3.

Watanabe, T.; Mugikura, Y.; Yoshikawa, M.; Morita, H.; Kawase, M.; Yoshiba, F., Asano, K. (2002) *High Performance and Long Life MCFC Development for Wide Application,* In: Proc. of the 2002 Fuel Cell Seminar, Nov 18-Nov 21

Wilemski, G.; Ghezel-Ayagh, H. G.; Patel, P. S. & Maru, H. C. (1985a) *Modeling of internal reforming direct fuel cell,* In Proc. of the 1985 Fuel Cell Seminar, May 19-22, Tucson, AZ, USA, p. 1.

Wilemski, G., Wolf, T. L. (1985b) *The role of heat transfer in molten carbonate fuel cell performance*, American Institute of Chemical Engineers, New York, NY.

Wilemski, G. (1986) *Modeling of H_2S effects on the performance of molten carbonate fuel cells,* In Proc. of the 1986 Fuel Cell Seminar, Oct. 26-29, Tucson, Az, USA, p. 177.

Williams, M. C.; Berry, D. A. (1990) *Overview of the DOE-funded fuel cell contaminants R&D program,* In Proc. o/t 1990 Fuel Cell Seminar, Nov. 25-28, Phoenix, Az, USA, p.306

Wolf, T. L.; Wilemski, G. (1983) *Molten carbonate fuel cell performance model,* J. Electrochem. Soc. 130/1, pp. 48-55.

Yamamoto, M., Ishida, M. (1997) *Graphical analysis of microscopic energy transformation schemes*, Journal of Chem. Eng. of Japan, vol 30, no. 5

Yuh, C. Y.; Selman, J.R. (1984a) *Porous Electrode Modeling of the Molten Carbonate Fuel Cell Electrode - A status report*

Yuh, C. Y.; Selman, J. R. (1984b) *Polarization of the molten carbonate fuel cell anode and cathode*, J. Electrochem. Soc. 131/9, pp. 2062-2069.

Yuh, C. Y.; Selman, J. R. (1991) *The polarization of molten carbonate fuel cell electrodes. 1 Analysis of steady-state polarization data,* Journal of the Electrochemical Society 138/12, pp. 3642-3648.

Yuh, C.; Johnsen, R.; Doyon, J. & Allen, J. (1996) *High power density carbonate fuel cell,* In Proc. of the 1996 Fuel Cell Seminar, 17-20 Nov, Kissimmee, FL, pp. 386-389.

APPENDICES

TABLE OF CONTENTS

APPENDIX 1
CORRELATIONS USED FOR THE CALCULATION OF THERMODYNAMIC PROPERTIES

The calculations with the fuel cell model in **Part II** and the system calculations in **Part III** require calculations of thermodynamic properties. The correlations used for the calculations in this thesis are summarised in this appendix. The enthalpy h_i is the enthalpy of the pure species at temperature T. For the fuel cell model the thermodynamical properties have been calculated using the JANAF tables. These tables give the coefficient for the correlations:[Gordon & McBride]:

$$h_i = a_1 + \frac{a_2}{2} T^2 + \frac{a_3}{3} T^3 + \frac{a_4}{4} T^4 + \frac{a_5}{5} T^5 \qquad \text{(A1-1)}$$

A similar correlation can be used to calculate the entropy of the pure species:

$$s_i = a_1 + a_2 \ln(T) + \frac{a_3}{2} T^2 + \frac{a_4}{3} T^3 + \frac{a_5}{4} T^4 + R \ln\left(\frac{p_i}{p_o}\right) \qquad \text{(A1-2)}$$

Note that the enthalpy of the pure species h_i, because of the ideal gas assumption, depends only on the temperature, while the entropy of the pure species s_i depends on temperature and on the partial pressure at which the species occurs in the mixture. Other thermodynamic properties for the pure species (heat capacity c_p, Gibbs energy g, etc.) can be derived from these two correlations. For the calculation of the properties of water and steam in the system calculations (**Chapters 7-9**) use has been made of the "Properties of Water and Steam in SI-Units" [Schmidt & Grigul] based on "The 1967 IFC formulation for Industrial Use". The enthalpy of a mixture and other thermodynamic properties (S, G, exergy) have been calculated assuming ideal gas behaviour.
The dynamic viscosity η_i for component i is calculated from the critical properties (T_c and p_c) and molar mass M_i using [Reid & Prausnitz, 1987]. The viscosity of a gas mixture is calculated from the conductivity of the components [Cobben, 1994] using Wilke's relation:

$$\eta_{mixture} = \sum_{i=1}^{m} \frac{x_i \eta_i}{\sum_{i=1}^{m} x_i \varphi_{i,j}} \qquad \text{(A1-3)}$$

where η_i are the viscosity of the component i and the $\varphi_{i,j}$'s are calculated using the relation suggested by Zipper and Herning [Reid & Prausnitz, 1987] from the molar masses M_i of the components:

$$\varphi_{i,j} = \left(\frac{M_j}{M_i}\right)^{1/2}$$

Heat conductivity is calculated using 3rd order polynomials from the same reference. The heat conductivity of the mixture is calculated from:

$$\lambda_{mixture} = \sum_{i=1}^{m} \frac{x_i \lambda_i}{\sum_{i=1}^{m} x_i A_{i,j}} \qquad \text{(A1-4)}$$

with:

$$A_{i,j} = \left(\frac{[1 + (\eta_i/\eta_j)^{1/2} (M_j/M_i)^{1/4}]}{[M_i/M_j]^{1/2}} \right)^{1/2}$$

APPENDIX 2
CALCULATION METHOD FOR THE CHEMICAL EXERGY OF A PROCESS FLOW

In this appendix the method for calculating the chemical exergy of a flow, described in general terms in **Section 2.5**, is described in greater detail using a calculation example. By definition the exergy of the environment components at the partial pressure at which they are present in the environment is equal to zero. In the given example for simplicity the environment definition is limited to 4 components: CO_2, O_2, H_2O and N_2. For the mole fraction of the components which define the environment (further indicated as the 'environment components') table 2.2 (**Section 2.5**) is used[a]:

$$\underline{y}_o = \begin{bmatrix} y_{CO_2} \\ y_{o,H_2O} \\ y_{o,N_2} \\ y_{o,O_2} \end{bmatrix} = \begin{bmatrix} 0.0003 \\ 0.0312 \\ 0.7553 \\ 0.2030 \end{bmatrix} \qquad \text{(A2-1)}$$

The process flow in this example is an equimolar mixture of CH_4 and N_2. The composition of the process flow is characterised by the vector:

$$\underline{y}_s = \begin{bmatrix} y_{CH_4} \\ y_{s,N_2} \end{bmatrix} = \begin{bmatrix} 0.5 \\ 0.5 \end{bmatrix} \qquad \text{(A2-2)}$$

Step 1: De-mixing

The first step is to calculate the exergy of the pure environment components at reference pressure $p_o = 1$ atm. The vector with the exergy of the environment components at 1 atm is e^o_o, were the subscript o indicates the environment components and the superscript o indicates that the partial pressure equals the reference pressure. The exergy of an environment component at 1 atm is equal to the work required to compress the component from the partial pressure in the environment to 1 atm. This can be calculated with:

$$e^o_{o,i} = -RT_o \ln \frac{p_{o,i}}{p_o}$$

where $p_{o,i}$ is the partial pressure of component i in the environment. For CO_2 table 2.2 specifies a mole fraction of 0.0003, which is used to calculate the exergy of CO_2 at 1 atm:

$$e^o_{o,CO_2} = -RT_o \ln \frac{p_{o,CO_2}}{p_o} = -RT_o \ln y_{o,CO_2} = 19.4 \qquad \text{[kJ/mole]}$$

The general expression using vector algebra is:

$$\underline{e}_o = RT_o \ln \underline{y}_o \qquad \text{(A2-3)}$$

---

[a] Ar is not included separately in this example: the fraction Ar is added to the N_2 fraction in table 2.2

where the notation a=ln (y) indicates the vector with elements a(i)=ln(y(i)). The exergy of the environment components at 1 bar is calculated using the concentrations in (A2-1). For the four environment components the exergy at standard pressure is given by:

$$\underline{e}^{o}_{o} = \begin{bmatrix} e^{o}_{o,CO_2} \\ e^{o}_{o,H_2O} \\ e^{o}_{o,N_2} \\ e^{o}_{o,O_2} \end{bmatrix} = \begin{bmatrix} 19.4 \\ 8.3 \\ 0.7 \\ 3.8 \end{bmatrix} \quad [kJ/mole]$$

Step 2: Dissociation

From the exergy of these components, the exergy of the elements (e^{o}_{el}) in molecular form (i.e. C, H_2, N_2 and O_2) at reference pressure can be calculated. However, for the derivation of the appropriate equations, the starting point is calculating the exergy of the environment components at 1 bar from the exergy of the elements at 1 bar (i.e. the reverse calculation). The exergy of the elements given by:

$$\underline{e}^{o}_{el} = \begin{bmatrix} e_C \\ e_{H_2} \\ e_{N_2} \\ e_{O_2} \end{bmatrix}$$

The exergy of an environment component, for example CO_2, can be determined from the formation reaction for CO_2 (i.e. the formation from the elements), in this case:

$$C + O_2 \rightarrow CO_2$$

The exergy balance for the formation reaction is

$$e^{o}_{o,CO_2} = e^{o}_{el,C} + e^{o}_{el,O_2} + \Delta_f e^{o}_{CO_2}$$

where $\Delta_f e^{o}_{CO2}$ indicates the exergy change as a result of the CO_2 formation reaction and the superscript o indicates that all reactants are at a reference pressure. At environment temperature ($T=T_o$) the exergy change in a chemical reaction ($\Delta h - T_o \Delta s$) is equal to the change in Gibbs energy ($\Delta h - T\Delta s$). Therefore the exergy change in this step is equal to the Gibbs energy of formation at reference conditions:

$$\Delta_f e = \Delta_f g^{o}$$

The calculation of the 4 values of $e^{o}_{el,k}$ (k=C, O_2, H_2 and N_2) uses the 4 formation reactions:

$C + O_2 \rightarrow CO_2$

$H_2 + \frac{1}{2} O_2 \rightarrow H_2O$

$N_2 \rightarrow N_2$

$O_2 \rightarrow O_2$

The last two 'formation reactions' indicate that the elements are already present in the environment definition. Corresponding to the 4 reactions given above, the 4 exergy balances for the formation reactions of the environment components form a set of equations:

$$
\begin{aligned}
e^{o}_{o,CO_2} &= e^{o}_{el,C} + e^{o}_{el,O_2} + \Delta_f e^{o}_{CO_2} \\
e^{o}_{o,H_2O} &= e^{o}_{el,H_2} + \tfrac{1}{2} e^{o}_{el,O_2} + \Delta_f e^{o}_{H_2O} \\
e^{o}_{o,O_2} &= e^{o}_{el,O_2} + \Delta_f e^{o}_{O_2} \\
e^{o}_{o,N_2} &= e^{o}_{el,N_2} + \Delta_f e^{o}_{N_2}
\end{aligned}
\qquad \text{(A2-4)}
$$

This set of equations can be solved to calculate the values for the exergies of the pure components $e^{o}_{o,j}$ (j=CO_2, O_2, H_2O and N_2). A general method to solve this set of equations makes use of a matrix F_o which contains the stoichiometric coefficients for the formation reactions of the environment components. The stoichiometric coefficients (see **Section 2.3.1**) indicate in what ratios a component is formed from the elements. For example the formation reaction of CO_2 involves 1 molecule C and 1 molecule O_2. The stoichiometric coefficients for this formation reaction are therefore:

$$\nu_{C,CO_2} = 1 \quad \nu_{H_2,CO_2} = 0 \quad \nu_{N_2,CO_2} = 0 \quad \nu_{O_2,CO_2} = 1$$

Using the stoichiometric coefficients for this and the other formation reactions, the formation matrix for the environment components F_o can be constructed for the 4 reactions :

$$
F_o = \begin{bmatrix} \nu_{C,CO_2} & \nu_{H_2,CO_2} & \nu_{N_2,CO_2} & \nu_{O_2,CO_2} \\ \nu_{C,H_2O} & \nu_{H_2,H_2O} & \nu_{N_2,H_2O} & \nu_{O_2,H_2O} \\ \nu_{C,N_2} & \nu_{H_2,N_2} & \nu_{N_2,N_2} & \nu_{O_2,N_2} \\ \nu_{C,O_2} & \nu_{H_2,O_2} & \nu_{N_2,O_2} & \nu_{O_2,O_2} \end{bmatrix} = \begin{bmatrix} 1 & 0 & 0 & 1 \\ 0 & 1 & 0 & 0.5 \\ 0 & 0 & 1 & 0 \\ 0 & 0 & 0 & 1 \end{bmatrix}
$$

$\Delta g^{o}_{f,o}$ is the vector which contains the Gibbs energy of formation of the environment components, which have been calculated using the JANAF tables (**Appendix 1**):

$$
\Delta \underline{g}^{o}_{f,o} = \begin{bmatrix} \Delta g^{o}_{CO_2} \\ \Delta g^{o}_{H_2O} \\ \Delta g^{o}_{N_2} \\ \Delta g^{o}_{O_2} \end{bmatrix} = \begin{bmatrix} -394.3 \\ -229.0 \\ 0 \\ 0 \end{bmatrix} \quad \text{[kJ/mole]}
$$

Using the formation matrix and the Gibbs energy of formation vector, the set of equations in (A2-4) can be written as:

$$\underline{e}^{o}_{o} = F_o \, \underline{e}^{o}_{el} + \Delta_f \underline{g}^{o}_{o}$$

In this set the exergy of the environment components at reference conditions (e^{o}_{o}) is known and the exergy of the elements ($e^{o}_{o,el}$) is the unknown.

Using basic matrix algebra [e.g. Kreysig] the system can be solved. First the inverse of matrix F_o is calculated:

$$F_o^{-1} = \begin{bmatrix} 1 & 0 & 0 & -1 \\ 0 & 1 & 0 & -0.5 \\ 0 & 0 & 1 & 0 \\ 0 & 0 & 0 & 1 \end{bmatrix} \qquad \text{(A2-5)}$$

Subsequently the exergy of the elements at reference condition can be calculated from:

$$\underline{e}^o_{el} = F_o^{-1} [\underline{e}^o_o - \Delta_f \underline{g}^o_o] \qquad \text{(A2-6)}$$

Using the values for the exergy of the elements at reference conditions calculated above, the exergy of the elements at reference conditions becomes:

$$\underline{e}^o_{el} = \begin{bmatrix} e^o_C \\ e^o_{H_2} \\ e^o_{N_2} \\ e^o_{O_2} \end{bmatrix} = \begin{bmatrix} 409.9 \\ 235.4 \\ 0.7 \\ 3.8 \end{bmatrix} \quad \text{[kJ/mole]}$$

Step 3: Formation

To calculate the exergy of a system component at reference conditions, again the formation reactions are used. In the given example, only two components occur in the system: CH_4 and N_2 and the corresponding formation reactions are:

$$2H_2 + C \rightleftarrows CH_4$$

$$N_2 \rightleftarrows N_2$$

The exergy of the pure system components at reference conditions is calculated from the exergy balance, again replacing the exergy of reaction by the Gibbs energy of formation at reference conditions. For the formation reaction of methane, for example:

$$e^o_{CH_4} = e^o_C + 2\, e^o_{H_2} + \Delta_f g^o_{CH_4} \qquad \text{(A2-7)}$$

A second formation matrix can be defined for the system components. For the given example with only two system component, the formation matrix F_s which contains the stoichiometric coefficients for the formation reaction of the system component, becomes:

$$F_s = \begin{bmatrix} \nu_{C,CH_4} & \nu_{H_2,CH_4} & \nu_{N_2,CH_4} & \nu_{O_2,CH_4} \\ \nu_{C,N_2} & \nu_{H_2,N_2} & \nu_{N_2,N_2} & \nu_{O_2,N_2} \end{bmatrix} = \begin{bmatrix} 1 & 2 & 0 & 0 \\ 0 & 0 & 1 & 0 \end{bmatrix}$$

Using the vector containing the Gibbs energy of formation at standard conditions for the system components ($\Delta_f g^o_s$), the exergy of the system components at reference conditions can be calculated from:

$$\underline{e}^o_s = F_s \underline{e}^o_{el} + \Delta_f \underline{g}^o_s \qquad \text{(A2-8)}$$

Using the exergy of the elements at reference conditions calculated above, the exergy of the system components at reference conditions becomes:

$$\underline{e}^o_s = \begin{bmatrix} e^o_{C,CH_4} \\ e^o_{C,N_2} \end{bmatrix} = \begin{bmatrix} 829.2 \\ 0.7 \end{bmatrix} \quad \text{[kJ/mole]}$$

In the last step the exergy of the pure system components (i.e. at 1 atm) is used to calculate the exergy of the components at the partial pressure at which the components are in the system. For example for CH_4 the partial pressure in the given example is 0.5 bar and the exergy of CH_4 at this pressure is calculated (as in equation A2-3) from:

$$e_{CH_4} = e^o_{CH_4} + RT_o \ln x_{CH_4} = 829.2 - 1.7 = 827.5$$

The concentration vector for the system components is:

$$\underline{x}_o = \begin{bmatrix} x_{s,CH_4} \\ x_{s,N_2} \end{bmatrix} = \begin{bmatrix} 0.5 \\ 0.5 \end{bmatrix}$$

The total chemical exergy of the mixture is equal to:

$$E^{CH} = \underline{x}_s^T \left[\underline{e}_s + RT_o \ln \underline{x}_s \right]$$

For the mixture of 50 mole% CH_4 and 50 mole% N_2 given as an example at the beginning of the section, the exergy becomes:

$$E^{CH} = 827.5 \cdot 0.5 + (-1.0) \cdot 0.5 = 413.3 \quad \text{[kJ/mole]}$$

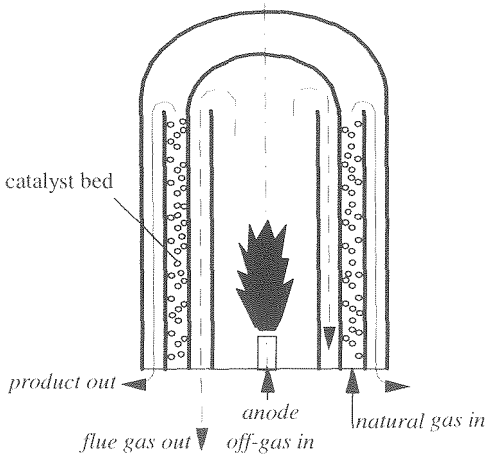

Figure A3.1: Regenerative type reformer for fuel cell applications (see [Pietrogrande, 1993])

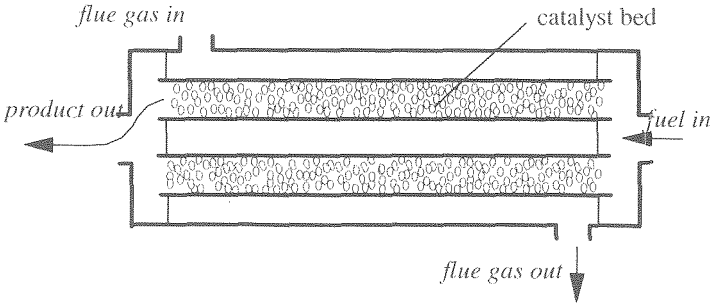

Figure A3.2: Once-through type reformer modeled for the SOFC system

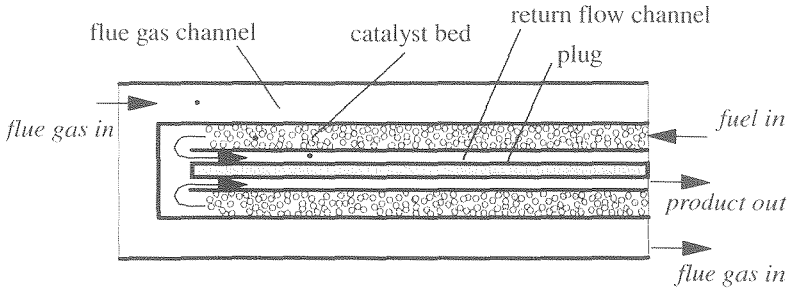

Figure A3.3: Regenerative type reformer modelled for the MCFC system

APPENDIX 3.
MODELLING THE REFORMER FOR THE CALCULATION OF THE EXERGY LOSSES

For the system calculations in **Part III** a black-box model, which calculates the product gas composition assuming chemical equilibrium at a specified equilibrium temperature, is sufficient. But for the calculation of the separate contribution of the heat transfer and chemical reactions to the exergy losses, this type of model does not supply the required information (see **Section 3.3**). The calculation of exergy losses requires the temperature and concentration profiles as input. Therefore, the reformer has been modelled separately in MATLAB to generate these profiles. In this appendix starting points for the detailed model for the reformer are discussed.

The modelled systems are fuelled with natural gas, which must be converted to H_2 in the endothermal steam reforming reaction. Reforming is a well developed technology in the chemical industry, for example for the production of methanol and ammonia. However, there are a number of essential differences between the reformers used in chemical industry and the reformers which are required in fuel cell systems. In industrial reforming processes, part of the heat contained in the flue gasses at the outlet of the reformer is used to generate process steam. In high temperature fuel cell systems a surplus of heat and/or steam is generally available. Therefore heat recovery of the heat in the flue gasses within the reforming process must be maximized in the fuel cell reformer. This leads to other reformer designs in which the main mode of heat transfer is convection. In industrial reformers an important part of the heat is transferred by radiation. Furthermore the combustor in the reformer in a fuel cell system has must be able to operate on low caloric anode off-gas (see **part III**).

These differences have led to the development of specific reformers for fuel cell applications. Figure A3.1 shows a reformer developed for fuel cell applications by IFC. In this design the product in the catalyst bed and the hot flue gasses flow counter current. Additional heat is transferred to the catalyst bed by cooling the product gas which leaves the catalyst bed. This type of reformer is indicated as a regenerative type reformer, because heat is recovered from the hot product gas and used in the reforming process. Other specific reformers for fuel cell systems have been developed by KTI [Pietrogrande, 1993], Chiyoda [Morita, 1996], Haldor Topsoe [Laursen, 1994] and Hitachi [Uematsu, 1994]. IHI has developed a flat plate type reformer for fuel cell applications [Morishima, 1990].

To investigate the exergy losses in the reformer, two different types of reformers have been modelled. In the SOFC system no internal heat recovery is necessary in the reformer. In this system, the anode gas (i.e. the product gas of the reformer) is supplied to the fuel cell at 850 °C. This temperature corresponds to the temperature of the product gas at the outlet of the catalyst bed. Therefore it is unnecessary to cool the product gas to recover heat from this flow. For the SOFC system a simple once-through type of reformer has been modelled (see figure A3.2). The necessary thermodynamic data based on the results of the system calculations (see **part III, chapter 7**). The inlet of the fuel (400 °C), the temperature at the outlet of the combustor (1200 °C) of the flue gas and the composition of the gas supplied to the reformer combustor are the most important results of the system calculation used in the reformer model.

The reformer for the MCFC system is of a different type. For the MCFC system the inlet temperature of the anode is 650 °C. Therefore the efficiency of the system in this case is higher if part of the heat in the gas at the outlet of the catalyst bed to recovered in the reformer. The principle of this type of reformer is shown in figure A3.3. The gas flowing

through the catalyst bed is heated by the flue gas flowing around the pipe containing the catalyst and by the hot product gas which cooled down as it flows back through the inner tube. To achieve sufficient heat transfer from the return flow the use of a plug in the inner pipe is assumed. The diameter of this plug is selected to achieve realistic gas velocities. Appropriate equations for heat transfer and rate of reaction were selected from literature and are discussed elsewhere [Cobben, 1994]. The main assumptions used in the reformer model are:

- Thermodynamic properties (e.g. H, S, c_P) are calculated assuming ideal gas. Correlation for other properties (viscosity, thermal conductivity) are given in **Appendix 1**;
- The reformer model assumes plug flow for both product and flue gas. Bulk temperatures are used in heat transfer and reaction rate calculations;
- Heat transfer is by convection only (no radiation or conductive heat transfer taken into account). The flue gas inlet temperature used in the model is calculated assuming adiabatic combustion of anode off-gas;
- The shift reaction is considered to be very fast (equilibrium), while the rate of the reforming reaction is determined by a kinetic equation of the form:

$$k = k_0 \cdot (p_{CH_4})^m \cdot e^{-\frac{E_a}{RT}}$$

With all equations for heat transfer and rate of chemical reactions given and the in and outlet temperatures for the reformer determined in the system calculations, the 'design geometry' of the reformer must be adapted to achieve this value. The 'geometry' of the reformer in the model consists of a the following variables:

- diameters of the subsequent pipes (flue gas channel, catalyst bed, return flow channel, plug);
- length of the pipes;
- number of pipes;

Taking into account other boundary conditions (for example the velocities which have to be within reasonable ranges) a design could be fixed for each type of reformer which compared reasonably with the dimensions and temperature profiles of the reformers for which data could be found in literature. The calculation results (e.g. those temperature profiles) are discussed in **Chapter 7**.

APPENDIX 4.
CORRELATIONS FOR THE CELL RESISTANCE

A4.1 CALCULATION OF THE CELL VOLTAGE IN THE SOFC MODEL

A4.1.1 Background: SOFC types

There is a large number of references in public literature which discuss equations for the calculation of the voltage losses in an SOFC model. However, in many cases the calculations are reported in general terms only. Few authors discuss the equations and parameters in sufficient detail to enable using their correlations for modelling. Selecting the appropriate data and equations to be used in a fuel cell model is further complicated by the fact that the correlations discussed in literature are often contradictory. Different authors make very different assumptions with regard to the effects which are included in the model and the effects which are neglected. The lack of a widely accepted set of correlations is partly due to the lack of understanding of the fundamental processes at the electrode/electrolyte interface. For example Divisek [1994] indicates that the mechanism which determines the cathode polarisation will change with temperature, while different partial oxygen pressures or different fabrication methods will influence the rate determining mechanism as well. Takeda [1987] showed a similar change of rate determining step for different materials in the cathode. However, the main reason for the large variation in type of correlation used in the different models lies is due to the development of different types of fuel cells. Different types of losses become dominant in each type. Basically a distinction can be made between three types of SOFC:

- Anode supported;
- Electrolyte supported;
- Cathode supported.

Electrolyte supported cell

Originally, focus of development was on the electrolyte supported cell. In this type of cell the electrolyte is manufactured in a first step and subsequently electrodes are applied to both sides to form the PEN-element. To make a good PEN layer requires porous electrodes but a dense and gas-tight electrolyte. In the 1960's a thick (0.5 mm) electrolyte was used [Hirschenhofer, 1998]. This limits application of the SOFC to high temperatures. Only at temperatures as high as 1000 °C the ionic conductivity of the electrolyte becomes sufficient to achieve a satisfactory performance of the fuel cell. Development of better fabrication technologies lead to the use of considerably thinner electrolytes (100-200 μm). Even though losses in the electrolyte decrease considerably when using a thin electrolyte, in the electrolyte supported SOFC the ohmic losses in the electrolyte[b)] are much larger than other types of losses. This is also due to rapid kinetics of all reactions involved at the high temperatures at which the electrolyte supported SOFC is operated. The electrolyte supported cell is used the for example by Sulzer Hexis [Sulzer] and by SOFCo [Barringer, 2002].

---

[b] Although the current in the electrolyte consists of ions and not electrons, the losses are generally referred to as 'ohmic' or 'IR-losses'.

electrode supported cell

The high operating temperature, while it leads to low polarisation, causes large mechanical problems. Sealing, mechanical integrity and low-cost material selection are all much more difficult to achieve at 1000 °C than at 800 °C. Therefore many manufacturers have chosen to develop 'intermediate temperature' concepts, which operate in the 700-800 °C temperature range[c]. However, performance at this temperature becomes much lower if the standard cell is used due to the higher losses in the electrolyte and the large increase of cathode polarisation at this temperature [Krist, 1994]. To limit losses in the electrolyte at this temperature requires a much thinner electrolyte (10-20 µm). Although making a gas-tight electrolyte is feasible using state-of-the-art fabrication technologies, such a thin electrolyte will not be strong enough. Therefore one of the electrodes, anode or cathode, will have to be thick enough to support the electrolyte or a supporting layer (for example metallic) will have to be added. Generally the electrochemical reduction of O_2 is much more difficult than the oxidation of H_2. In other words, polarisation losses at the cathode will generally be much larger than the anode losses. Therefore most manufacturers have opted for the anode supported cell. Developers of this type include Tokyo Gas [Baba, 2002], PNNL [Simner-2002], Global Thermo-electric [Tang-2002]. The cathode supported cell is used by Westinghouse [Ray, 1992]. Although this choice appears to be based mainly on the system design (integrating air pre-heating in the tubular SOFC), the cathode supported cell offers a number of fundamental advantages. According to Rietveld [2002] the main issues are on the anode side (sulphur, oxidation resistance, dry reforming/direct oxidation of methane). An important advantage of cathode supported cells is that they offer more freedom for 'engineering' the anode.

Three types of losses occur in the SOFC:

- Ohmic losses or IR losses as a result of transport of ions in the electrolyte and electrons in electrodes and current collectors;
- Concentration polarisation (η_a), which represents the performance decrease as a result of lower concentrations reactants at the reaction sites. For example concentration gradients related to diffusion in the electrodes might be an important factor.
- Activation polarisation (η_c), which is the performance loss due to the slow kinetics of one or more reaction steps. In the SOFC activation polarisation occurs mainly at the cathode.

The contribution of the different types of losses depends strongly on the type of cell. In high temperature cells the main losses are ohmic, because reactions are very rapid. Activation polarisation becomes much more important at lower temperatures (e.g. 800 °C). Analysis by for example Krist [1994] shows that cathode polarisation becomes dominant at this temperature.

Because the supporting electrode is considerably thicker than the other components, transport of gasses through the electrode is hindered. Typical results for the anode supported cell are reported by Tokyo Gas [Baba, 2002]. Plots of V vs. U show a pronounced decrease of V above 70-80%. This indicates some form of concentration polarisation at the anode. This large concentration polarisation is not found in the electrolyte supported cells. It is therefore essential to determine which type of fuel cell will be modelled, because the phenomena to be include differ per type of cell. Based on the development status the selection of correlation focusses on high temperature SOFC's (both Sulzer and Westinghouse develop this type of fuel cells). For planar stacks the high temperature operation is used in electrolyte supported cells. Therefore this type of cell is considered.

---

[c] The term 'intermediate' suggest that there is also a low temperature development. There is no comparable industrial development of SOFC's with at operating temperature < 700, although some work is being done on SOFC's operating at 500-600 °C [Steele, 1993]

A4.1.2 Overview of correlations used in literature

Many of the detailed models discussed in literature are used analyse to temperature and flow distribution in the fuel cell stack (e.g. [Murashi, 1994], [Dekker, 1994], [Ding, 1997]). Other models are used to determine stresses occurring in the fuel cell (e.g. [Sullivan, 2002], Watanabe, 2002]). Generally these models involve a very large number of calculations and simple correlations are used to calculate the cell voltage. Typically the calculations use a linear approximation for the current density-cell voltage:

$$V = V_{rev} - i \cdot R^{\square} \qquad \text{(A4-1)}$$

A different approach is used by Campanari, who uses a fixed cell voltage and applies linear corrections for the cell voltage as function of temperature, pressure and partial pressures of reactants [Campanari, 2001]. This is an adaptation of the method used by Benjamin, etal. [1980] and expanded by Kinoshita [1992].
More phenomenological approaches are useful. Steele has suggested making a distinction between the ohmic resistance and 'interfacial resistance' [Steel, 1993], where the interfacial resistance (R_{if}) is the resistance associated with all processes at the electrode-electrolyte interface.

$$V = V_{rev} - i \cdot (R^{\square}_{ohm} + R^{\square}_{if})$$

A more advanced method based on this distinction has been used for SOFC modelling by NTT [Watanabe, 2002]. In their model they incorporate a linear correlation for the ohmic losses and a quadratic correlation for the polarisation:

$$V = V_{rev} - i \cdot R^{\square}_{ohm} - i^2 \cdot R^{\square}_{pol}$$

R_{ohm} and R_{pol} depend on the temperature. Watanabe proposes the following relationship between temperature and resistance[d]:

$$R^{\square}_{ohm} = R^{\square}_{ohm,T_0} \cdot e^{(E_e/RT - E_e/RT_0)}$$

and to calculate the polarisation resistance at different temperatures.

$$R^{\square}_{pol} = R^{\square}_{pol,T_0} \cdot e^{(E_c/RT - E_c/RT_0)} \qquad \text{(A4-2)}$$

Values for R_{ohm} and R_{pol} were estimated from the performance of the cell and activation energies (E_e for ionic conductivity of the electrolyte and E_c for the main cathode reaction) were base on data from literature.
Wepfer, etal. [1985] of Georgia Institute of Technology discussed an analytical model of the SOFC taking into account all three types of losses (ohmic, concentration and polarisation). Although this leads to a model with so many parameters that it does not have practical use, it can be used as a starting-point for simplification of the model by taking into account only the most important losses. Later work at this institute showed that for high temperature fuel cells the activation potential is negligible [Haynes, 2000]. For an anode supported cell operating at

---

[d] For processes involving an activation energy, for example (electro-)chemical reactions, the influence of the temperature on the rate of reaction depends on the activation energy E_a [kJ.mol] and can be calculated using:

$$k = k_{T_0} \cdot e^{E_a/RT}$$

800 °C, Haynes uses the following correlation incorporating parameters for both activation and concentration polarisation:

$$V = V_{rev} - iR_{ohm}^{\square} + (a + \ln(i)) + \frac{RT}{4F}\ln\left(1 - \frac{i}{i_{cs}}\right) + \frac{RT}{2F}\ln\left(1 - \frac{i}{i_{as}}\right) + \frac{RT}{2F}\ln\left(1 - \frac{i}{i_{as}}\frac{p_{H_2}}{p_{H_2O}}\right)$$

The last three terms use the limiting current density at the cathode (i_{cs}) and anode (i_{as}) to calculate the concentration losses. The a + ln (i) refers to activation losses. The parameters in this model can be estimated from experimental data. However, the parameters used in this correlation are not reported.
A complete set of equations for the SOFC has been published by KFA Jullich [Achenbach, 1994]. The general equation used to calculate the cell voltage is:

$$V = V_{rev} - i \cdot (R_{ohm}^{\square} + R_a^{\square} + R_c^{\square})$$

The cathode and anode polarisation are calculated using the activation energies:

$$\frac{1}{R_c^{\square}} = \frac{RT}{2F} \cdot \left(\frac{p_{O_2}}{p}\right)^m \cdot k_c \, e^{-E_c/RT} \qquad \text{(A4-3a)}$$

and:

$$\frac{1}{R_a^{\square}} = \frac{RT}{2F} \cdot \left(\frac{p_{H_2}}{p}\right)^m \cdot k_a \, e^{-E_a/RT} \qquad \text{(A4-3b)}$$

The activation energies are estimated from literature data. Estimates for the pre-exponential factors estimated from experimental data in literature are given in the article.
Although other models can be found in literature, the above gives a good impression of the large number of different approaches which are used in SOFC modelling. This divergence in modelling methods is mainly due to the lack of widely applicable and accepted models.

A4.1.3 Selection of a correlation for the cell resistance

To assess which equations could be used in the fuel cell model, the experimental data reported in literature have been used. A large number of experimental i-V curves has been published. However, interpretation of these data is difficult. The reported results generally represent rather arbitrary points in the continuous process of improvement of performance. Furthermore conditions under which the experiments are carried out, if they are fully report at all, in many cases do not correspond to the actual conditions in the fuel cell.
On the other hand some conclusion can be drawn from the experimental data reported in public literature. The most relevant conclusion is that for high temperature operation (>800 °C) the i-V curves are approximately linear. Therefore the approximation using an effective cell resistance is acceptable. Because the cell resistance incorporates ohmic, concentration and activation losses, the cell resistance is a function of temperature, pressure and concentration. The temperature is clearly the most important factor. The main loss in the

fuel cell is the resistance of the electrolyte[e]. According to Bossel [1992-b] the electrolyte conductivity can be represented by:

$$\sigma_e = A\ e^{B/T} \qquad \text{(A4-4)}$$

with A = 28800 [ohm^{-1} m^{-1}] and B = 10300 [K]. If d is the thickness of the electrolyte, the corresponding resistance is:

$$R_e = \frac{d}{\sigma_e}$$

The ionic and electronic conductivity does not depend on partial pressures of the components and is therefore not dependant on total pressure and reactant concentrations. Concentration polarisation 'tails' [f] are found only at very high utilisation [Chick, 2002] and in low temperature, anode supported cells. For the normal operation conditions for the electrolyte supported cell the concentration polarisation does not seem to be an important factor. Therefore the contribution of the activation polarisation, which does depend on the partial pressures, determines whether this effect has to be taken into account. The anode polarisation is only small. Westinghouse for example reports anode polarisation in the range of 7-15 mV. The main contribution will be the cathode activation polarisation.
For the MCFC a large number experimental studies have been carried out to identify which losses occur and distinguish between for example activation polarisation and ohmic losses. For the SOFC this type of work is lacking. In a GRI study [Romero, 1996] the polarisation and ohmic losses are calculated separately as a function of temperature. These calculations show that at 1000 °C polarisation has a small contribution (10-15%) increasing to approximately 30% at 900 °C.
The most useful data come from Siemens-Westinghouse (SWPC), because they have gained much experience with their tubular concept. Siemens-Westinghouse has tested their system at pressures from atmospheric to 15 bar. Reported results (for example in [Hirschenhofer, 1998]) show that the voltage increase $V(p_2)$-$V(p_1)$ is only slightly larger than the change in Nernst voltage as a result of the pressure increase $V_{rev}(p_2)$-$V_{rev}(p_1)$. This confirms the limited influence of the pressure (and partial pressures) on the cell resistance. Therefore the cell resistance is considered to be a function of temperature only.
At 1000 °C and 80% fuel utilisation the Nernst voltage will be approximately 0.9 Volt. Operating current densities are expected to be in the range of 3-5 kA/m^2 for planar type cells. Assuming the operating cell voltages lies in the range of 0.65-0.75 volt, this corresponds to a cell resistance varying from 0.8 ohm·cm^2 down to 0.4 ohm·cm^2.
Based on model calculations and measurements on small single cells it is expected that values of the cell resistance as low as 0.25-3 ohm·cm^2 can be achieved (eg. [Bagger, 1994], [Steele, 1993]). However, the cell performance of actual fuel cell stacks corresponds to much higher values for the cell resistance. This is partly due to the increasing losses as the area per cell increases and corresponding larger in-plane losses. But the electronic losses in the interconnect and contact resistance between cells in a stack appear to be the mayor reasons why stack performance and single cell performance is very different for planar SOFC's. Therefore the cell resistance which is used in this thesis (0.75 ohm·cm^2 @ 925 °C) is in the

---

[e] The illustrate the effect of temperature on the losses in electrolyte: the voltage drop across the electrolyte increases by more than 40% if the temperature decrease from 1000 °C to 900 °C.

[f] The phrase concentration 'tails' was introduced by Chick [2002] to indicate the typical dip in the i-V curve associated with concentration polarisation at high current density

high end of the calculated range. Because the contact resistance and in-plane losses are not considered to be highly temperature dependent, the correlation for the cell resistance is split in a temperature dependent part (IR losses in the electrolyte and polarisation losses) and the lumped 'stacking' losses which are temperature independent:

$$R^{\square} = R_T^{\square} + R_{stack}^{\square}$$

To determine the temperature dependant resistance of the electrolyte the equation supplied by Bossel was used. For the cathode the equation supplied by Achenbach (A4-3a) was used. For the activation energy of the cathode, depending on the material, the activation energy lies in the range of 100 to 200 kJ/mol [Takeda, 1987]. Lower estimates have been used for example by the Gas Research Institute (USA) (105 kJ/mol) [Krist, 1994] and Dornier (D) (70 kJ/mol) [Erdle, 1990]. Because the activation energy for the electrolyte on which the Bossel equation is based is equal to 85 kJ/mol falls well in this range, this value has been adapted for the cathode as well. Using this the cell resistance can be written as:

$$R^{\square} = R_{T_0}^{\square} \cdot e^{(E/RT - E/RT_0)} + R_{stack}^{\square} \qquad (A4.5)$$

with E=85 kJ/mol and T_0 is 925 °C. The ratio R_T/R_{stack} has arbitrarily assumed to equal 1. In figure A4.1 the ratio R_T/R_0 between the calculated cell resistance at temperature T and the cell resistance at reference temperature (925 °C) is compared to single-cell data from literature ([van Heuveln, 1993] and [Drenkhahn, 1993]). The figure also shows the data calculated with the equations from Achenbach [1994]. The data show a reasonable correspondence.

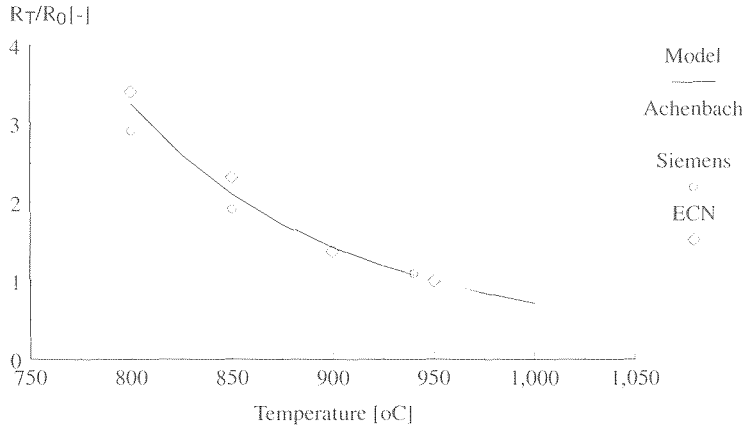

Figure A4.1: Comparison of the temperature dependant part of the cell resistance with single-cell data for the SOFC from literature

The expression used in the SOFC model therefore becomes:

$$R^{\square} = 0.375 \cdot \left(e^{(10300/T - 8.60)} + 1\right)$$

A4.2 CALCULATION OF THE CELL VOLTAGE IN THE MCFC MODEL

A4.2.1 Background: Modelling the porous electrodes

The basic design used by most MCFC stack developers is more or less similar. Although different materials are evaluated, similar techniques and materials are generally used. Therefore developing a model for the calculation of the cell voltage in the MCFC seems simpler. However, the process around the electrolyte/electrode interface in the MCFC is even more complex than in the case of the SOFC. Firstly because of the many reactions occurring simultaneously in the molten carbonate. A large number of different mechanisms and intermediate species have been proposed. Secondly the interaction between the liquid electrolyte and the gas phase in the porous electrode is difficult to model. Although much work has been done to clarify the performance of the MCFC, the situations is similar to the SOFC. No generally applicable and widely accepted models exist for the MCFC to calculate the cell voltage.
Early in the development of the MCFC it was recognised that understanding the processes at the electrode/electrolyte interface is necessary and essential to be able to optimise the fuel cell and emphasis was placed on modelling the processes in the porous electrodes. A significant step was the adaptation of the agglomerate pore model by Yuh and Selman [1984]. This model enabled describing the processes in the porous electrodes. Another mayor step was the development of the PSI model (see [Wolf, 1983], [Wilemski, 1985a], [Willemski, 1985b]).
Losses in the MCFC have been investigated using many different techniques (for example [Makkus, 1990], [Selman 1990b], [Han, 2002], [Lee, 2003]). Typically the interfacial losses in the anode (concentration + polarisation + electronic resistance of the anode) will contribute 10-15% of the total losses. The remainder of the losses is divided over the IR losses in the electrolyte (ionic transport) and the losses in the cathode. The cathode polarisation appears to be larger than the IR losses, in particular at low temperature [Morita, 1998]. But both types of losses have to be taken into account to develop an effective correlation for the cell voltage. The losses in the electrolyte are mainly determined by the temperature. Ionic conductivity improves strongly within the temperature range in which the MCFC operates. For example, IR losses decrease by 30% if the temperature increases from 575 °C to 675 °C. Pressure and gas phase concentrations do not influence the conductivity of the electrolyte. Partial pressures for O_2 and CO_2 however do influence the polarisation losses at the cathode. Therefore the influence of temperature, pressure and reactant concentrations have to be taken into account in the calculation of the cell resistance. Again, selecting an appropriate correlation and parameters is not straight forward. For example, the influence of the temperature on the cell resistance is found to vary with electrolyte composition [Morita, 1998] as well as with the filling degree of the porous electrolyte [Huijsmans, 1998]. The influence of the partial CO_2 pressure (p_{CO2}) turns out to be different at the high CO_2 concentrations in the standard gas used for cell testing (air/CO_2=70/30) than at the much lower concentrations which occur in the actual system.

A4.2.2 Overview of correlations used in literature

Many different types of models can be found in literature. The most simple model to calculate the cell voltage is by using the 'differentials'. For example, the average change in cell voltage with temperature is determined from experimental data. Examples of this approach can be found in Benjamin [1980] and Saito [1991]. In the 4th edition of the Fuel Cell Handbook

[Hirschenhofer, 1998] a complete set of data is given to determine the influence of temperature, pressure and reactant concentrations. Although it makes a practical approach for system modelling, it is not a very accurate method.
An empirical correlation which incorporates the influence of temperature, pressure and the cathode concentrations can be found in [Izaki, 1993]. A 6 kW MCFC stack was used to generate a large number of data sets for different conditions. The data were summarised in an equation for the cell voltage V. A value for V is extrapolated from a known cell voltage at reference conditions V_{ref} using the fuel utilisation U_f, the pressure p and the cathode concentrations x_{O2} and x_{CO2}:

$$V = V_{ref} - 0.17\,(U_F - U_{F,ref}) + 0.85\,{}^{10}\log\left(\frac{p}{p_{ref}}\right) + 0.110\,{}^{10}\log\left(\frac{x_{O2}\cdot x_{CO2}}{(x_{O2}\cdot x_{CO2})_{ref}}\right) \qquad \text{(A4.6)}$$

Ansaldo has used a semi-empirical correlation fitted to data from their own MCFC programme:

$$R^{\square}_{tot} = \frac{A\,e^{B/T}}{p^{\beta}_{O_2}} + c_{IR} + D\,e^{F/T}$$

The values of the coefficients have not been published in the article.
Selman and Lu [1991] have determined correlations for the cathode and anode polarisation based on lab cell measurements. By fitting the experimental results to theory based equations, expressions for cathode and anode polarisation are found. The cathode polarisation is found to depend on the temperature and reactant partial pressures cathode (p_{O2}, p_{CO2}):

$$R^{\square}_{pol,c} = 7.504\cdot 10^{-6}\cdot e^{77.8\cdot 10^3/RT}\cdot \ln\left(p_{O_2}^{0.43}\cdot p_{CO_2,cat}^{0.09}\right) \qquad \text{(A4.7a)}$$

and a similar correlation is developed for the anode polarisation:

$$R^{\square}_{pol,a} = 0.4567\cdot 10^{-7}\cdot e^{109\cdot 10^3/RT}\cdot \ln\left(p_{H_2}^{1.801}\cdot p_{CO_2,an}^{1.48}\cdot p_{CO}^{1.533}\right) \qquad \text{(A4.7a)}$$

Similar type of equations were also developed by the Japanese CRIEPI [Watanabe, 1992]. This extensive modelling analysis has been carried out using experimental data from a small bench-scale test. The correlation for the cell voltage makes use of a parameter indicated as the Nernst loss (ΔV_{ne}). This parameter is included to model the effect of lower cell voltage at higher fuel and oxidant utilisation (i.e. at lower reactant concentrations).

$$V = V_{rev} - \Delta V_{ne} - i\cdot(R^{\square}_{ohm} + R^{\square}_{a} + R^{\square}_{c})$$

Again theoretical expressions have been fitted to obtain equations for the cathode and anode polarisation and the IR-resistance:

$$R^{\square}_{ohm} = 2.71\cdot 10^{-3}\cdot e^{40.9\cdot 10^3/RT} \qquad \text{(A4.8a)}$$

$$R^{\square}_{pol,an} = e^{-19\cdot 10^3/RT}\cdot \ln\left(1.24\cdot p_{H_2}^{2.82}\cdot p_{CO_2,an}^{2.12}\cdot p_{H_2O}^{3.52}\right) \qquad \text{(A4.8b)}$$

$$R^{\square}_{pol,cat} = 10^{-7}\cdot e^{102\cdot 10^3/RT}\cdot \ln\left(365\cdot p_{O_2}^{5.85}\cdot p_{CO_2,cat}^{2.78}\right) \qquad \text{(A4.8c)}$$

Another approach has been adapted by ERC [Ding,1997] . The starting-point for their model development is the equation:

$$V = V_{rev} - \eta_a - \eta_c - \eta_{conc} - i \cdot R_{IR}^{\square}$$

where η_a and η_c are the anode and cathode polarisations (non-linear in the current density i and therefore not expressed as a resistance). Using the Butler-Vollmer equation [Vetter], expressions are developed for η_a and ηc. Concentration polarisation is lumped and expressed using the limiting current densities for anode and cathode as a parameters. By using a number of simplifying assumptions a 14 parameter model is developed. These parameters have been fitted using 400 data sets from the ERC stack technology. The approach leads to a current density-voltage correlation which shows good agreement over a wide range of current densities (0-2 kA/m^2).

The many different approaches reflect the complexity of modelling the losses in the MCFC. The value of any model is limited by the fact that different MCFC stacks and different operating conditions influence the processes at electrolyte/electrode interface to such an extent that different mechanisms become determining. One should be aware of this limitation, which indicates that a very accurate model can only be made for a specific MCFC stack. However, sufficient information is available to construct a model which reflects the general trends and dependencies sufficiently..

Interesting in all the models described above is the role of CO_2. Qualitatively the influence of temperature, pressure and the partial pressure O_2 is clear. An increase in temperature improves the electrolyte conductivity and the rate of reaction for the electrochemical reactions. An increase in pressure and oxygen concentration reduces the losses as a result of cathode polarisation. However, for the CO_2 concentration different effects are found. As shown by the CRIEPI correlations, the CO_2 concentration has a negative effect on the cathode polarisation. This effect has been found as well by Selman and Yuh. Kunz [1984] shows, using the agglomerate pore model, that the effect of CO_2 on cathode polarisation will depend on the oxidant composition, the cathode porosity and thickness and on the electrolyte content of the electrode. The more detailed analysis has shown a negative effect of CO_2 on polarisation (CRIEPI, Yuh & Selman). On the other hand, other references assume a positive effect of a higher CO_2 concentration.More recent work at CRIEPI has focussed specifically on this issue (see [Morita, 2002]). This has lead to the development of a new correlation for the cathode polarisation (expressed as a resistance):

$$R_{pol,cat}^{\square} = A_{c1} \cdot e^{E_{c1}/RT} \cdot p_{O_2}^{-0.75} \cdot p_{CO_2}^{0.5} + A_{c2} \cdot e^{E_{c2}/RT} \cdot p_{CO_2}^{-1.0}$$

In this correlation two mechanisms are described. The first type of polarisation ('C1')corresponds to the earlier CRIEPI correlations ($\sim p_{O2}^{-0.75}\, p_{CO2}^{0.5}$). This type of polarisation is dominant at the standard testing conditions for MCFC with high partial and C_2 polarisation ($\sim p_{CO2}^{-1.0}$). The second term ('C2') corresponds to a different reaction mechanism and leads to a decrease of cathode polarisation with increasing CO_2 concentration. The equations predicts the cell voltage better at high oxidant utilisation (i.e. at lower partial O_2 and CO_2 pressures).

A4.2.3 Selection of a correlation for the cell resistance

The cell resistance which is used in this thesis is an effective cell resistance in which all types of losses grouped into one parameter. However, the local value of this lumped parameter does change with the temperature, the pressure and reaction concentrations. Therefore the following equations is used:

$$R^{\square} = R_0^{\square} C_T C_p C_x \qquad (A4.9)$$

where $R_0^{\square}$ is the cell resistance at standard conditions and the C_M (M = T, p and x) are corrections for respectively temperature, pressure and concentrations.
For the temperature a fitted 2nd order polynomial has been used which is based measured data [Roussar, 1995]. The data were fitted to a more familiar form:

$$R^{\square} = R_0 \cdot e^{(E_a/RT - E_a/RT_0)} \qquad (A4.10)$$

where T_0 is 650 °C and E_a = 39.5 kJ/mole. In figure A4.2 the value of C_T is compared with data from literature. The first two are based on experimental data reported in [Saito, 1991] and [Morita, 1998]. The other two data sets are based on equations cited above (based on [Watanabe, 1991] and [Yuh, 1991]). The data in itself show quite a distribution. With that limitation, the correlation agrees with the data found in literature.

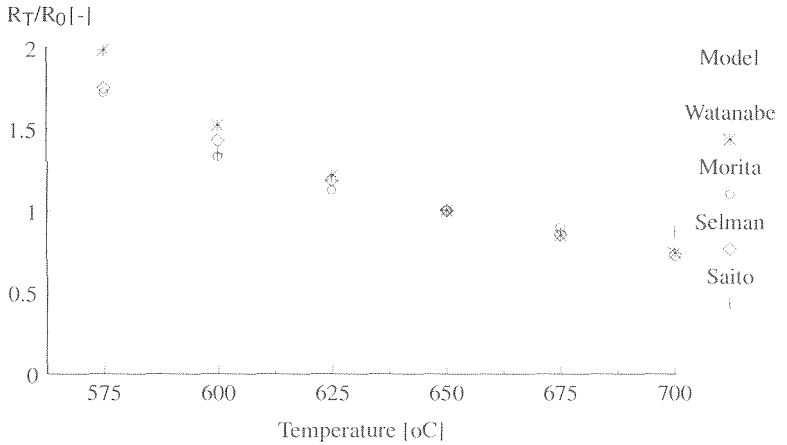

Figure A4.2: Comparison of the temperature dependant part of the cell resistance with single-cell data for the MCFC from literature

The correction factor for the pressure (C_p) is based on the equation:

$$\Delta V = A \cdot \log\left(\frac{p_2}{p_1}\right) \qquad (A4.11)$$

ΔV is the change in cell voltage between two values of the pressure:

$$\Delta V(p_2 \rightarrow p_1) = V(p_2) - V(p_1)$$

and A is a parameter for which values can be found in literature. This is a suitable manner of representing the influence of the pressure, because A (=dV/log dP) is generally constant over a broad range of pressures. Values for A can be found in literature (for example [Benjamin, 1980], [Izaki, 1993], [Hirschenhofer, 1998]) Alternatively, the value for A can be determined easily from published experimental data (eg. [Shistla, 1993]). The values range from 75 to 110 mV. A value of 100 mV was used for the MCFC model.
To calculate C_p from this value requires some work. Using the effective cell resistance, a function of the pressure, the cell voltage can be written as a follows:

$$V = V_{rev}(p) - R^{\square}(p) \cdot i$$

The change in voltage if the operating pressure changes from p_1 to p_2 is therefore equal to:

$$\Delta V(p_2 - p_1) = \Delta V_{rev}(p_2 - p_1) + i \cdot \left(R(p_2) - R(p_1) \right) \qquad \text{(A4.12)}$$

where:

$$\Delta V_{rev} = \frac{RT}{4F} \cdot \ln\left(\frac{p_1}{p_2}\right)$$

At 650 °C the temperature RT/4F equals 46 mV. Introducing the notation:

$$B = \frac{RT}{4F} \cdot \ln(10) \qquad \text{(A4.13)}$$

The expression for the change in reversible voltage can now be written in the same form as the change in the actual cell voltage:

$$\Delta V_{rev} = B \cdot \log\left(\frac{p_1}{p_2}\right) \qquad \text{(A4.14)}$$

Substituting the similar expressions for V (A4.11) and V_{rev} (A4.14) in equation (A4.12) gives:

$$i \cdot \left(R(p_2) - R(p_1) \right) = (A - B) \cdot \log\left(\frac{p_2}{p_1}\right)$$

Rearranging this equation leads to an expression for the pressure dependant resistance:

$$R(p) = R^{0}(1 - a \log p + a \log p^{o}) \qquad \text{(A4.15)}$$

where the parameter a can be calculated from the parameter A in equation (A4.11) and the current density at which parameter A was determined.

$$a = \frac{B - A}{i R_p^{o}}$$

The correction for the pressure C_p can be written as:

$$C_p = \left(1 - a \log \frac{p}{p^{o}}\right) \qquad \text{(A4.16)}$$

Finally the correction factor for the composition has to be determined. Because the anode polarisation is much smaller than the cathode polarisation, only a correction for the cathode side is used. For the cathode composition a correction factor using the concentrations x_{CO2} and x_{O2} can be used, as suggested by Izaki (equation A4.6). However, as the overview of equation from literature shows, the real parameters are the respective partial pressures. It is clear that models presented in literature are not consistent with respect to the influence of the reactant partial pressures at the cathode. However, an important consideration is, that the change in cell voltage as a result of the change in total pressure should be consistent with the change in cell voltage as a result of the changes in partial pressures. Therefore the expression introduced by Benjamin was adapted:

$$\Delta V = C \cdot \log\left(\frac{(p_{O_2}^{1/2} \cdot p_{CO_2})_2}{(p_{O_2}^{1/2} \cdot p_{CO_2})_1} \right) \qquad \text{(A4.17)}$$

It can be shown that the if both (A4.16) and (A4.17) have to be satisfied, the expression for the cell resistance as a function of (partial) pressure becomes:

$$R(p) = R^0 \left(1 - b \log(p_{O_2}^{1/2} \cdot p_{CO_2}) + b \log(p_{O_2}^{1/2} \cdot p_{CO_2})_0 \right) \qquad \text{(A4.18)}$$

with $b = {}^3/_2\, a$. Parameter b has been calculated using A = 100 mV at 1500 A/m^2. For the reference partial pressures the values from the base case MCFC system calculation (see **Chapter 7**) has been used. This leads to the reference value of $p_{O2}{}^{1/2} p_{CO2}$ equal to 0.34. Using equation (A4.10) for the temperature effect and equation (A4.18) to incorporate the influence of the concentration and total pressure, leads to the following expression for the cell resistance:

$$R^{\square} = R_0 \cdot e^{(4750/T - 5.16)} \cdot \left(0.814 - 0.241 \log(p_{O_2}^{1/2} \cdot p_{CO_2}) \right)$$

This expression has been used in the MCFC model.

APPENDIX 5
INFLUENCE OF ASSUMING A UNIFORM TEMPERATURE DISTRIBUTION IN THE CELL HARDWARE

In the model of the cell element which is developed in **Chapter 4**, the hardware of the fuel cell element is assumed to have a uniform temperature distribution. In this appendix this assumption is checked by an approximate calculation of temperature differences within the hardware. The temperature of the process flows in a cross-section in the model is characterized by the two parameters T_a and T_c for the anode and cathode side respectively. Figure A5.1 shows the basic cross section of a high temperature fuel cell. The active elements (electrodes + electrolyte) form a three-layered flat plate indicated as the PEN-layer. The electrical and thermal connect is formed by a corrugated plate which forms the channels for the process flows: anode and cathode flow. The heat in the cell is generated as a result of the electrical currents in the electrolyte and electrodes and as a result of the chemical and electrochemical reaction which take place on the surface in the electrode pores. If the PEN-layer including the pores is considered as one phase (with regard to the heat transport), the assumption can be made that all heat is generated in the PEN-layer.

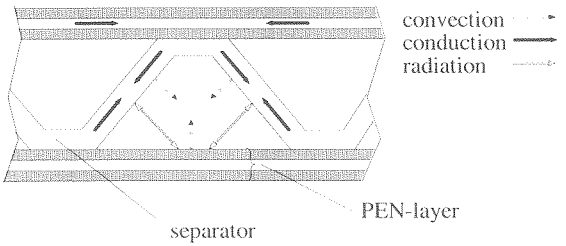

Figure A5-1: Main modes of heat transfer in the cell element

The heat generated in the PEN-layer is discharged from the cell through the process flow, either by transport of heat directly from the PEN-layer to the process flows or through the separator or interconnect. The heat is transported to the surface of the PEN-layer by conduction. Heat transport from the PEN-layer to the separator plate takes place through conduction and radiation while heat transport from the PEN-layer and from the separator to the process flows takes place by convection and by radiation.
If the heat transport from the PEN-layer with temperature T_c to the separator plate with temperature T_s and the heat transport from the separator plate to the process flow (T_{pf}) is considered as a series process, the heat transferred in both steps is equal. U denotes the heat transfer coefficient for the convection and λ the heat conductivity of the separator plate.
If s is half the length of the separator rib (using the symmetry of the fuel cell element), the average path of conduction through the separator is approximately ½ s. If dx is the length of the cell element in the direction of the process flows (perpendicular to the cross-section drawn in figure A5-1), the heat transferred through conduction can be roughly approximated by:

$$q' = \frac{\lambda \cdot dx \cdot d}{½\, s} \cdot (T_c - T_s)$$

The area where the heat transfer from the separator plate to the process flows takes place is equal to dx · s. Therefor the heat transfer from the separator to the process flow can be estimated from:

$$q' = s \cdot dx \cdot U \cdot (T_s - T_{pf})$$

In that case the separator plate temperature is then equal to:

$$T_s = T_e - \frac{(T_s - T_{pf})}{\frac{2 \cdot \lambda \cdot d}{U \cdot s^2} + 1}$$

Using:

$$X_{es} = \frac{1}{\frac{2 \cdot \lambda \cdot d}{U \cdot s^2} + 1}$$

this can be rewritten to:

$$X_{es} = \frac{(T_e - T_s)}{(T_s - T_{pf})}$$

If X_{es} is small, the temperature difference between the separator plate and the PEN-layer (the numerator) is small compared to the temperature difference between hardware and process flows (denominator).

For a MCFC with a metal separator, the following estimates can be used:

λ=25 W/mK	(heat resistant steel at 600 . . 700 °C)
U=300 W/m²K	(based on calculations in **Chapter 5**)
s=0.0015 m	
d=0.0005m	

Using these estimates we find:

$$X_{es} = \frac{1}{\frac{2 \cdot \lambda \cdot d}{U \cdot s^2} + 1} = 0.026 \ll 1$$

Therefore, a relatively small error is introduced if the temperature of the PEN-layer and the separator plate are assumed to be equal. This result can be extended to the SOFC with a ceramic separator: although the conductivity λ of the separator is lower in this case, the thickness d of the ribs will be larger if ceramic material is used to obtain the necessary strength. Based on this result, and the consideration that solid-solid radiation will tend to even out temperature differences between separator and PEN-layer, the model of the fuel cell element uses one temperature to characterize the hardware.

APPENDIX 6
STOICHIOMETRIC MATRICES FOR THE FUEL CELL MODEL

In the fuel cell model, 7 components have been included in the model: H_2, CO, H_2O, CO_2, CH_4, O_2 and N_2. For the anode and cathode the mole flow per component are given by respectively
:

$$\underline{\varphi}_a = \begin{bmatrix} \varphi_{a,H_2} \\ \varphi_{a,CO} \\ \varphi_{a,H_2O} \\ \varphi_{a,CO_2} \\ \varphi_{a,CH_4} \\ \varphi_{a,O_2} \\ \varphi_{a,N_2} \end{bmatrix} \quad \text{and:} \quad \underline{\varphi}_c = \begin{bmatrix} \varphi_{c,H_2} \\ \varphi_{c,CO} \\ \varphi_{c,H_2O} \\ \varphi_{c,CO_2} \\ \varphi_{c,CH_4} \\ \varphi_{c,O_2} \\ \varphi_{c,N_2} \end{bmatrix} \qquad \text{(A6-1)}$$

For the MCFC fuel cell, the reactions occurring at the anode are:

$CO_3^{=} + H_2 \rightarrow CO_2 + H_2O + 2\,e^-$	(electrochemical reaction)
$CH_4 + H_2O \rightarrow 3\,H_2 + CO$	(reforming reaction)
$CO + H_2O \rightarrow H_2 + CO_2$	(shift reaction)

In table A6.1 the stoichiometric coefficients for these reactions are summarised. All other stoichiometric coefficients are zero.

Table A6.1: Reactions in the fuel cell model (MCFC) and corresponding stoichiometric coefficients

name of reaction	subscript	reaction	stoichiometric coefficients	
			anode	cathode
electrochemical reaction	'e'	$O_2 + CO_2(c) + H_2 \rightarrow H_2O + CO_2$ (a)	$\nu_{e,H2} = -1$ $\nu_{e,H2O} = 1$ $\nu_{e,CO2} = 1$	$\nu_{e,O2} = -½$ $\nu_{e,CO2} = 1$
shift reaction	's'	$CO + H_2O \rightarrow H_2 + CO2$	$\nu_{s,H2O} = -1$ $\nu_{s,CO} = -1$ $\nu_{s,H2} = 1$ $\nu_{s,CO2} = 1$	
reforming reaction	'r'	$CH_4 + H_2O \rightarrow 3H_2 + CO$	$\nu_{r,CH4} = -1$ $\nu_{r,H2O} = -1$ $\nu_{r,H2} = 3$ $\nu_{r,CO} = 1$	

Using the components as defined in the composition vector φ_a and the reactions defined in the reaction coordinate vector ε, the stoichiometric matrix can be composed for both anode and cathode. The columns of the matrix correspond to the reactions, the rows with the chemical species. For the MCFC anode the stoichiometric matrix equals:

$$\mathbf{N}_a(\mathrm{MCFC}) = \begin{bmatrix} \nu_{e,H_2} & \nu_{s,H_2} & \nu_{r,H_2} \\ \nu_{e,CO} & \nu_{s,CO} & \nu_{r,CO} \\ \nu_{e,H_2O} & \nu_{s,H_2O} & \nu_{r,H_2O} \\ \nu_{e,CO_2} & \nu_{s,CO_2} & \nu_{r,CO_2} \\ \nu_{e,CH_4} & \nu_{s,CH_4} & \nu_{r,CH_4} \\ \nu_{e,N_2} & \nu_{s,N_2} & \nu_{r,N_2} \end{bmatrix} = \begin{bmatrix} -1 & 1 & 3 \\ 0 & -1 & 1 \\ -1 & -1 & -1 \\ 1 & 1 & 0 \\ 0 & 0 & -1 \\ 0 & 0 & 0 \end{bmatrix} \qquad \text{(A6.2)}$$

For the MCFC cathode only the electrochemical reaction results in changes in composition. The stoichiometric coefficients for the shift and reforming reaction are zero:

$$\mathbf{N}_c(\mathrm{MCFC}) = \begin{bmatrix} \nu_{e,H_2} & \nu_{s,H_2} & \nu_{r,H_2} \\ \nu_{e,CO} & \nu_{s,CO} & \nu_{r,CO} \\ \nu_{e,H_2O} & \nu_{s,H_2O} & \nu_{r,H_2O} \\ \nu_{e,CO_2} & \nu_{s,CO_2} & \nu_{r,CO_2} \\ \nu_{e,CH_4} & \nu_{s,CH_4} & \nu_{r,CH_4} \\ \nu_{e,O_2} & \nu_{s,O_2} & \nu_{r,O_2} \\ \nu_{e,N_2} & \nu_{s,N_2} & \nu_{r,N_2} \end{bmatrix} = \begin{bmatrix} 0 & 0 & 0 \\ 0 & 0 & 0 \\ 0 & 0 & 0 \\ -1 & 0 & 0 \\ 0 & 0 & 0 \\ \tfrac{1}{2} & 0 & 0 \\ 0 & 0 & 0 \end{bmatrix} \qquad \text{(A6-3)}$$

The reaction coordinates indicate the change in composition relative to the inlet compositions. The inlet composition for anode and cathode can therefore be written as:

$$\varphi_a^{in} = \begin{bmatrix} \varphi_{H_2} \\ \varphi_{CO} \\ \varphi_{H_2O} \\ \varphi_{CO_2} \\ \varphi_{CH_4} \\ \varphi_{N_2} \end{bmatrix}_{a,in} \quad \text{and} \quad \varphi_c^{in} = \begin{bmatrix} \varphi_{H_2} \\ \varphi_{CO} \\ \varphi_{H_2O} \\ \varphi_{CO_2} \\ \varphi_{CH_4} \\ \varphi_{N_2} \end{bmatrix}_{c,in} \qquad \text{(A6-4)}$$

APPENDIX 7
CALCULATION OF THE EQUILIBRIUM CHANGE OF REACTION FOR A SINGLE REACTION

General method

The general criterion for (chemical) equilibrium is based on the Gibbs energy G of a mixture. In the fuel cell model, the equilibrium composition is calculated for the outlet of the subcell. The composition at the outlet of the subcell is in chemical equilibrium if the Gibbs energy is minimal:

$$\frac{dG(\varepsilon_k)}{d\varepsilon_k} = 0 \qquad \text{(A7.1)}$$

The first derivative corresponds to the "reaction Gibbs energy" (analogous to the reaction enthalpy and entropy in **Section 2.3.2**). Using the notation for the subcell (**Section 4.4**) the partial pressures as the outlet or the subcell are written as p_i^{j+1}. The temperature at which the equilibrium is calculated is the temperature of the PEN-layer in the subcell (T_e^j). Using the equations (2.25) and (2.32), the reaction Gibbs energy can be written as:

$$\frac{dG(\varepsilon_k)}{d\varepsilon_k} = \sum_{i=1}^{n} \nu_i \left(g_i^o + RT_e^j \ln\left(p_i^{j+1}\right)\right) \qquad \text{(A7.2)}$$

At equilibrium therefore the partial pressures at the outlet of the subcell must fulfill:

$$0 = \sum_{i=1}^{n} \nu_i \left(g_i^o + RT_e^j \ln\left(p_i^{j+1}\right)\right) \qquad \text{(A7.3)}$$

The equilibrium constant K_k for the reaction k, which is defined as [Smith&van Ness]:

$$K_k = e^{\sum \nu_i g_i^o / RT}$$

or:

$$\ln(K_k) = \sum \nu_i g_i^o / RT \qquad \text{(A7.4)}$$

Using the equilibrium constant, equation (A7.4) can be rewritten to the well-known form:

$$K_k = \prod_{i=1}^{n} \left(p_i^{j+1}\right)^{\nu_i} \qquad \text{(A7.5)}$$

This standard formulation of the equilibrium composition for ideal gasses can be rewritten to calculate the change in composition in the subcell of the fuel cell model. The change in composition is represented in the model by the reaction coordinate. Therefore the equilibrium condition will be rewritten to an equation with the reaction coordinate $\Delta\varepsilon_k$ as an explicit parameter.

In **Appendix 9** it is shown that the natural logarithm of the partial pressure for component i at the outlet of the subcell if more than one reaction occurs, can be written as:

$$\ln\left(p_i^{j+1}\right) = \ln\left(\varphi_i^j + \sum_{k=1}^{f} \Delta\varepsilon_k \nu_{i,k}\right) - \ln\left(\varphi^j + \sum_{k=1}^{f} \Delta\varepsilon_k \Delta\nu_k\right) + \ln(p)$$

For a single reaction this simplifies to:

$$\ln(p_i^{j+1}) = \ln(\varphi_i^j + \Delta\varepsilon_k \nu_{i,k}) - \ln(\varphi^j + \Delta\varepsilon_k \Delta\nu_k) + \ln(p) \qquad \text{(A7.6)}$$

If this result is substituted in equation (A7.4), a polynomial of the form:

$$b_0 + b_1\Delta^j\varepsilon_k + b_2(\Delta^j\varepsilon_k)^2 + b_3(\Delta^j\varepsilon_k)^3 + b_4(\Delta^j\varepsilon_k)^4 + \ldots = 0 \qquad \text{(A7.7)}$$

is found. The coefficients b_j depend only on the initial composition φ^j, the pressure p and the equilibrium constant K_k. The number of solutions of equation (A7.7) is larger than one. However, only one solution satisfies the criterion:

$$\min\left(-\frac{n_i}{\nu_i}\right) < \Delta\varepsilon < \max\left(\frac{n_i}{\nu_i}\right) \qquad \text{(A7.8)}$$

Shift reaction

If K_s is the equilibrium constant for the shift reaction at temperature T_e, the equilibrium composition for the shift reaction should satisfy:

$$K_s = \frac{p_{H_2}\, p_{CO_2}}{p_{H_2O}\, p_{CO}} \qquad \text{(A7.9)}$$

For the shift reaction the polynomial from which the reaction coordinate can be calculated is:

$$b_0 + b_1\Delta^j\varepsilon_s + b_2(\Delta^j\varepsilon_s)^2 = 0$$

where: $b_0 = \varphi^j_{H_2}\,\varphi^j_{CO_2} - K_s\,\varphi^j_{H_2O}\,\varphi^j_{CO}$

$b_1 = \varphi^j_{H_2} + \varphi^j_{CO_2} + K_s\,\varphi^j_{H_2O} + \varphi^j_{CO}$

$b_2 = 1 - K_s$

Reforming reaction

Using the equilibrium constant for the reforming reaction K_r, the partial pressures of the components a equilibrium composition for the reforming reaction should satisfy:

$$K_r = \frac{p_{H_2}^3\, p_{CO}}{p_{CH_4}\, p_{H_2O}} \qquad \text{(A7.10)}$$

The partial pressures can be eliminated using the mole flows and the reaction coordinate using equation (4.25). The change of the reaction coordinate for the reforming reaction can be found by solving the polynomial:

$$b_0 + b_1\Delta^j\varepsilon_r + b_2(\Delta^j\varepsilon_r)^2 + b_3(\Delta^j\varepsilon_r)^3 + b_4(\Delta^j\varepsilon_r)^4 = 0 \qquad \text{(A7.11)}$$

where: $b_0 = (\varphi^j_{H_2})^3\,\varphi^j_{CO_2} - \frac{K_r}{P}\,\varphi^j_{CH_4}\,(\varphi^j_{H_2O})^2\,\varphi^j$

$$b_1 = [\varphi^j_{H_2}]^3 + 9[\varphi^j_{H_2}]^2 \varphi^j_{CO_2} + \frac{K_r}{P}\left[\varphi^j_{H_2O}\,\varphi^j_{CH_4}\,\varphi^j + \varphi^j_{H_2O}\,\varphi^j_{CH_4} - \varphi^j\right]$$

$$b_2 = 9[\varphi^j_{H_2}]^2 + 27\varphi^j_{H_2}\varphi^j_{CO_2} - \frac{K_r}{P}\left[\varphi^j_{H_2O}\,\varphi^j_{CH_4} - 4\varphi^j_{H_2O} - 4\varphi^j\right]$$

$$b_3 = 27\varphi^j_{H_2} + \frac{4K_r}{P}\left[\varphi^j_{CH_4} - \varphi^j_{H_2O} - \varphi^j\right]$$

$$b_4 = 27 + \frac{4K_r}{P}$$

Equation (A7.9) can be solved using standard solvers. The correct root can be selected using the stoichiometric coefficients as indicated in equation (A7.8).

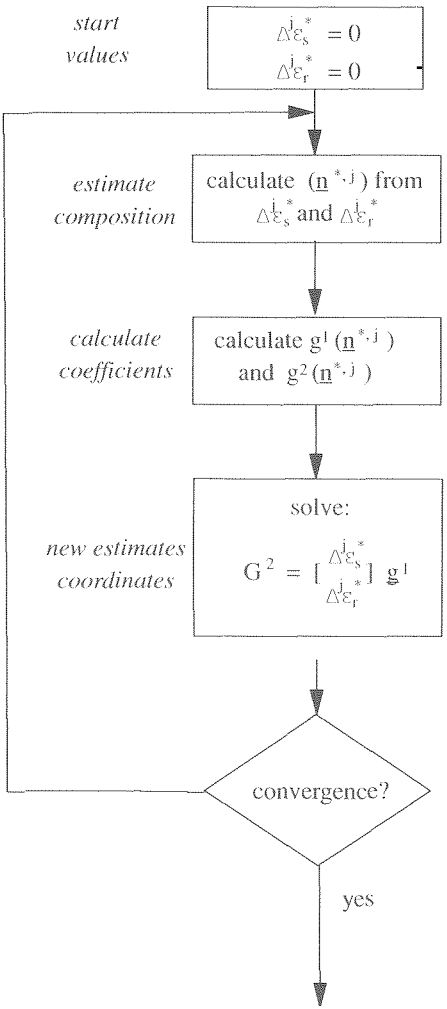

Figure A8-1: Procedure for the calculation of the reaction coordinates for multi-reaction equilibrium

APPENDIX 8
CALCULATION OF THE EQUILIBRIUM CHANGE OF REACTION FOR MULTIPLE REACTIONS

In the fuel cell model in some cases the equilibrium of more than one reaction has to be calculated at the outlet of the fuel cell. In this appendix a new method is developed for the calculation of the chemical equilibria: the linearization method. Just as in the calculation of equilibrium for the single reaction (**Appendix 7**), use is made of the differential $\partial G/\partial \varepsilon_k$ for the reaction k. These differentials are used to define the first derivative g^1 for ℓ different reactions in the fuel cell element:

$$g^1_k = \frac{\partial G(\varepsilon_k)}{\partial \varepsilon_k} \qquad \text{for } k=1..\ell$$

The Gibbs energy of the anode flow at the outlet of the fuel cell element depends on the reaction coordinates ($\Delta\varepsilon_k$ for $k=1..\ell$). The reaction k is in equilibrium at the outlet of the subcell if the Gibbs energy with respect to that reaction is at its minimum. Therefore the criterion for equilibrium of multiple reactions $1..\ell$ is:

$$g^1_k(\Delta^j\varepsilon_k) = 0 \qquad \text{for } k=1..\ell \qquad \text{(A8-1)}$$

In the linearization method the second derivatives of the Gibbs energy to the reaction coordinates are used. The second derivatives represent the change of the equilibrium composition of reaction **k** as a result of the change of the reaction coordinate of reaction **m**. These cross-coefficients therefore reflect the interactions between the different reactions. Including these terms makes the method much faster than the series reactor method (**Section 4.4.3**). The second derivatives are:

$$g^2_{k,m} = \frac{\partial^2 G}{\partial \varepsilon_k \partial \varepsilon_m} \qquad \text{for } k,m=1..\ell \qquad \text{(A8-2)}$$

Using a Taylor series, the value of g^1 at the outlet of the subcell is equal to:

$$g^1_k(\Delta^j\varepsilon_k) = \frac{\partial G(0)}{\partial \varepsilon_k} + \sum_{m=1}^{\ell} \frac{\partial G^2(0)}{\partial \varepsilon_k \varepsilon_m} \Delta\varepsilon_m + \sum_{m=1}^{\ell}\sum_{n=1}^{\ell} \frac{\partial G^2(0)}{\partial \varepsilon_k \varepsilon_m} \Delta\varepsilon_m \Delta\varepsilon_n + \ldots.$$

This equation can be linearize around $\Delta\varepsilon=0$ (inlet subcell), which leads to:

$$g^1_k(\Delta^j\in_k) \approx \frac{\partial G(0)}{\partial \in_k} + \sum_{m=1}^{\ell} \frac{\partial G^2(0)}{\partial \in_k \in_m} \Delta\in_m \qquad \text{(A8-3)}$$

Using the notations g^1 and g^2, the estimates for the reaction coordinates which correspond to chemical equilibrium ($\Delta\varepsilon^*_k$ for $k=1..\ell$) can be determined from the set of ℓ equations:

$$0 = g^1(0) + \sum_{k=1}^{\ell} g^2(0)\,\Delta\varepsilon^*_k \qquad \text{(A8-4)}$$

In **Appendix 9** it is shown, that the values of g^1 and g^2 at the inlet of the subcell can be calculated from:

$$g_k^1(0) = \sum_{i=1}^{n} \nu_{i,k} \left(g_i^o + RT_e \ln(\varphi_i^j) \right) - RT_e \Delta\nu_k \ln(\varphi^j) + RT_e \Delta\nu_k \ln(p) \qquad \text{(A8-5)}$$

and:

$$g_{k,m}^2(0) = RT \sum_{i=1}^{n} \left(\frac{\nu_{i,k} \ \nu_{i,m}}{\varphi_i^j} \right) - RT \frac{\Delta\nu_k \ \Delta\nu_m}{\varphi^j} \qquad \text{(A8-6)}$$

In the fuel cell model the method is used to solve the equilibrium for the shift reaction and for the reforming reaction simultaneously. Again using index 's' for the shift reaction and 'r' for the reforming reaction and introducing the matrix notations the first derivatives are written as:

$$\mathbf{g}^1 = - \begin{bmatrix} g_s^1 \\ g_r^1 \end{bmatrix} \qquad \text{(A8-7)}$$

and the second derivatives are used to define the matrix $\mathbf{G}^2$:

$$\mathbf{G}^2 = \begin{bmatrix} g_{ss}^2 & g_{sr}^2 \\ g_{rs}^2 & g_{rr}^2 \end{bmatrix} \qquad \text{(A8-8)}$$

The system from which the reaction coordinates can be solved is:

$$\begin{bmatrix} g_{ss}^2(0) & g_{sr}^2(0) \\ g_{rs}^2(0) & g_{rr}^2(0) \end{bmatrix} \begin{bmatrix} \Delta^j\varepsilon_s^* \\ \Delta^j\varepsilon_r^* \end{bmatrix} = - \begin{bmatrix} g_s^1(0) \\ g_r^1(0) \end{bmatrix} \qquad \text{(A8-9)}$$

The value calculated with equation (A8-9) is an estimation because this correlation has been obtained by linearization of equation (A8-1). If the subcells are small enough, the estimates for the reaction coordinates for the subcell are sufficiently accurate. In the fuel cell model however an iterative procedure is used to determine the values for $\Delta^j\varepsilon_s$ and $\Delta^j\varepsilon_r$. This is shown in figure A8-1 The estimates for the reaction coordinates ($\Delta\varepsilon_k^*$) are used to estimate the composition at the outlet. Subsequently this composition is used to make a new estimate for the reaction coordinates from equation (A8-9). This procedure is repeated until convergence is achieved.

APPENDIX 9
DERIVATIVES OF THE GIBBS ENERGY G WITH RESPECT TO REACTION COORDINATE ε

In the fuel cell model, the chemical equilibrium is calculated at the outlet of a subcell. If only one chemical reaction occurs in the subcell (single equilibrium), the method for calculating the chemical equilibrium (**Appendix 7**) uses the first derivative ($dG/d\varepsilon_k$). If more than one reaction occurs (multi-equilibria), the method developed in **Appendix 8** uses the first and second derivative ($d^2G/d\varepsilon_k d\varepsilon_j$).
The first derivative corresponds to the "reaction Gibbs energy", analogous to the reaction enthalpy and entropy in **Section 2.3.2**). Using the notation for the subcell (**Section 4.4**) the partial pressures as the outlet or the subcell are written as p_i^{j+1}. The temperature at which the equilibrium is calculated is the temperature of the PEN-layer in the subcell (T_c^j). Using the equations (2.25) and (2.32), the reaction Gibbs energy can be written as:

$$\frac{dG(\varepsilon_k)}{d\varepsilon_k} = \sum_{i=1}^{n} \nu_i \left(g_i^{o} + RT_c^j \ln\left(p_i^{j+1}\right)\right) \qquad \text{(A9.1)}$$

The partial pressure of component i at the anode at the outlet of the subcell, depends on the mole flow of the component φ_i^{j+1} and the total mole flow φ_a^{j+1} at the outlet of the subcell

$$p_i^{j+1} = \frac{\varphi_i^{j+1}}{\varphi^{j+1}} p \qquad \text{(A9.2)}$$

The mole flow for components i at the inlet of the subcell is φ_i^{j+1} and the total flow at the subcell inlet is equal to φ^{j+1}. As a result of the chemical reactions in the subcell, the composition of the flow changes between inlet and outlet of the cell. The partial pressure for component i at the outlet of the subcell is equal to:

$$p_i^{j+1} = \frac{\varphi_i^{j} + \sum_{k=1}^{f} \Delta^j\varepsilon_k \nu_{i,k}}{\varphi^{j} + \sum_{k=1}^{f} \Delta^j\varepsilon_k \Delta\nu_k} p \qquad \text{(A9.3)}$$

The natural logarithm of the partial pressure is therefore equal to:

$$\ln\left(p_i^{j+1}\right) = \ln\left(\varphi_i^{j} + \sum_{k=1}^{f} \Delta\varepsilon_k \nu_{i,k}\right) - \ln\left(\varphi^{j} + \sum_{k=1}^{f} \Delta\varepsilon_k \Delta\nu_k\right) + \ln(p) \qquad \text{(A9.4)}$$

Substituting this expression in equation (A9-1) gives the following equation for the first derivative of the Gibbs energy as a function of the reaction coordinates $\Delta\varepsilon_k$:

$$\frac{dG}{d\varepsilon_k} = \sum_{i=1}^{n} \nu_{i,k} \left(g_i^{o} + RT\ln\left(\varphi_i^{j} + \sum_{k=1}^{f} \Delta^j\varepsilon_k \nu_{i,k}\right)\right) - RT\Delta^j\nu_k \ln\left(\varphi^{j} + \sum_{k=1}^{f} \Delta^j\varepsilon_k \Delta\nu_k\right) + RT\Delta\nu_k \ln(p)$$

Second derivative

To find the second derivative of the Gibbs energy, this expression must be differentiated with respect to $d\varepsilon_m$. Because g_i^o and p do not depend on ε_m, the second derivative becomes:

$$\frac{d^2G}{d\varepsilon_k d\varepsilon_m} = \sum_{i=1}^{n} \nu_{i,k} \left(\frac{d}{d\varepsilon_m} RT \ln \left(\varphi_i^j + \sum_{k=1}^{\ell} \Delta^j \varepsilon_k \nu_{i,k} \right) \right) - \frac{d}{d\varepsilon_m} RT \Delta\nu_k \ln \left(\varphi^j + \sum_{k=1}^{\ell} \Delta^j \varepsilon_k \Delta\nu_k \right)$$

Using the chain rule to differentiate this expression gives:

$$\frac{d^2G}{d\epsilon_k d\epsilon_m} = RT \sum_{i=1}^{n} \left(\frac{\nu_{i,k} \ \nu_{i,m}}{\varphi_i^j + \sum_{k=1}^{\ell} \Delta^j \epsilon_k \nu_{i,k}} \right) - RT \frac{\Delta\nu_k \ \Delta\nu_m}{\varphi^j + \sum_{k=1}^{\ell} \Delta^j \epsilon_k \Delta\nu_k}$$

The following notations are introduced for the first and second derivatives:

$$g_k^1 = \frac{\partial G(\epsilon_k)}{\partial \epsilon_k} \qquad \text{for } k=1..\ell \tag{A9-5}$$

and:

$$g_{j,k}^2 = \frac{\partial^2 G}{\partial \epsilon_k \epsilon_m} \qquad \text{for } k,m=1..\ell \tag{A9-6}$$

To solve the equilibrium at the outlet of the subcell, the value of g^1 and g^2 at the inlet of the subcell are used ($\Delta\varepsilon_k=0$ for $k=1..\ell$). For the first derivative $\Delta\varepsilon_k=0$ leads to:

$$g_k^1(0) = \sum_{i=1}^{n} \nu_{i,k} \left(g_i^o + RT \ln(\varphi_{i,a}^o) \right) - RT \Delta\nu_k \ln(\varphi_a^o) + RT \Delta\nu_k \ln(p)$$

and the second derivative from:

$$g_{k,m}^2(0) = RT \sum_{i=1}^{n} \left(\frac{\nu_{i,k} \ \nu_{i,m}}{\varphi_{i,a}^o} \right) - RT \frac{\Delta\nu_k \ \Delta\nu_m}{\varphi_a^o}$$

APPENDIX 10
OPTIONS FOR USING A CATHODE OFF-GAS RECYCLE

The main issue in the cathode recycle is the temperature at which the compressor operates. The recycle compressor is necessary to overcome the pressure losses in the cathode recycle and in the fuel cell. If the cathode off-gas is recycled directly (figure A10.1), this greatly reduces the required heat exchanger area for pre-heating the oxidant flow as part of the pre-heating occurs as a result of the mixing of (cold) fresh air and (hot) recycled cathode gas. However, the compressor will have to work at a very high temperature (outlet temperature > 1000 °C). This is technically possible, as can be seen from state-of-the-art gas turbine technology but will be very costly and will probably require blade cooling.

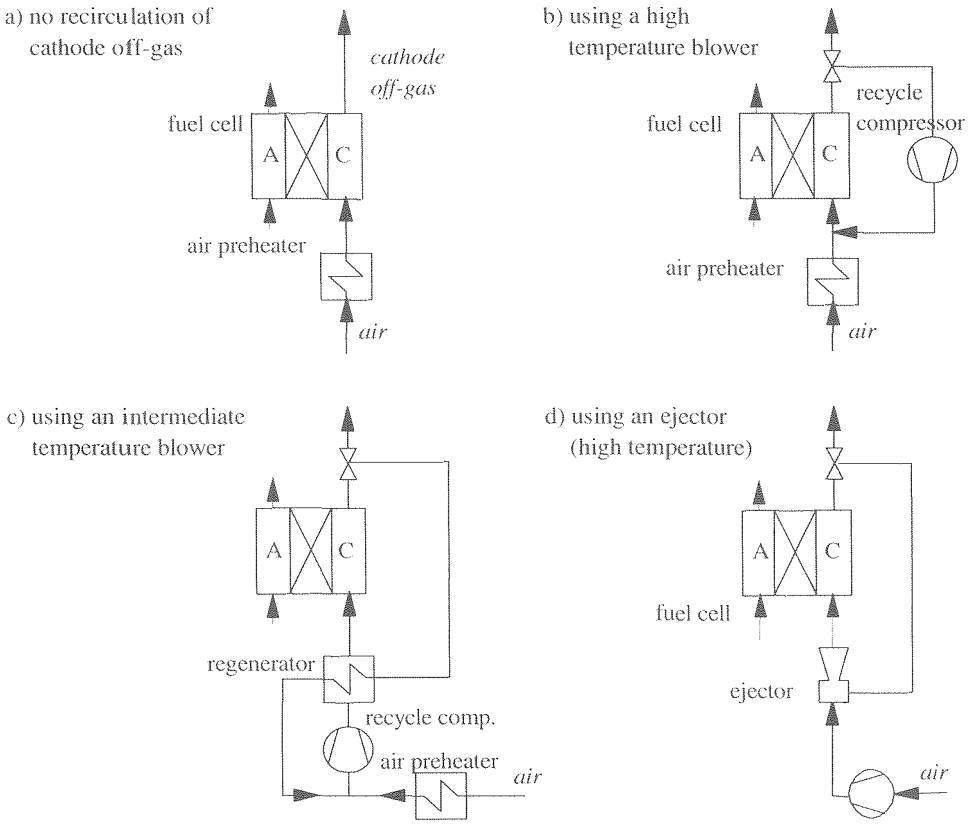

Figure A10-1: Different options to recycle cathode off-gas to the cathode inlet to reduce the air flow

Another possibility is for the cathode recycle compressor to operate at a lower temperature if the cathode gas recycle is cooled down before the recycle compressor (figure A10.1-c). The

MCFC Research Association (J) has developed a high temperature recycle blower which operates at 700 °C and has an efficiency exceeding 75% [Satoh, 1994]. Similar high temperature compressors will be used in other demonstration projects but swill still be very costly. If the gas is cooled down to 400 °C, a fairly standard materials can be used. Although the costs for the compressor will be much smaller, this configuration will require additional heat exchangers working at high temperatures. A penalty is also paid in the form of a higher duty for the compressor to overcome the pressure losses in the large heat exchangers which are required in the cathode recycle.

As an alternative method of increasing the pressure of the recycle flow using ejectors (figure A10.1-d) has been investigated . The efficiency of an injector is defined as the ratio of the kinetic energy of the outlet flow and the high pressure inlet flow [van Dijk, 1971]. Even though the injector has a very low efficiency of approximately 10 .. 20%, system calculations indicated that the application of an injector could increase efficiency, mainly because the compression of the driving medium takes place at a low temperature and the pressure drop in the recycle loop in this case (no heat exchangers are necessary) is low [Achenbach, 1994a]. However, the pressure increase that can be obtained using an ejector is limited and application of an ejector seems feasible only if the pressure drop in the fuel cell stack can be kept very low

APPENDIX 11
CALCULATION OF THE CATHODE OFF-GAS RECYCLE RATIO

The recycle ratio in the cathode off-gas of a fuel cell system is determined by the energy balance of the recycle loop. A simple analysis will show this. The enthalpy of the cathode flow at the inlet of the fuel cell stack [indicated by the subscript "cat"] is the sum of the enthalpy of the fresh air flow ["air"] and the recycle flow ["rec"]:

$$m_{air}\, h_{air} + m_{rec}\, h_{rec} = m_{cat}\, h_{cat} \qquad \text{(A11.1)}$$

The flows are shown in figure A11.1. The recycle ratio is defined as the ratio between the recycle flow and the total cathode off-gas flow:

$$\alpha = \frac{m_{rec}}{m_{cog}}$$

The difference in mass flow between the cathode gas and the cathode off-gas is small, due to the low utilisation of O_2 and the bulk of N_2. Therefore the recycle rate is approximately:

$$\alpha \approx \frac{m_{rec}}{m_{air} + m_{rec}}$$

Assuming a constant c_p value for air and recycled cathode off-gas the enthalpy h for all the flows in figure A11.1 is proportional to the temperature. Using this assumption the energy balance (eq. A11.1) can be rewritten to:

$$m_{air}\, T_{air} + m_{rec}\, T_{cog} \approx (m_{air} + m_{rec})\, T_{cat}$$

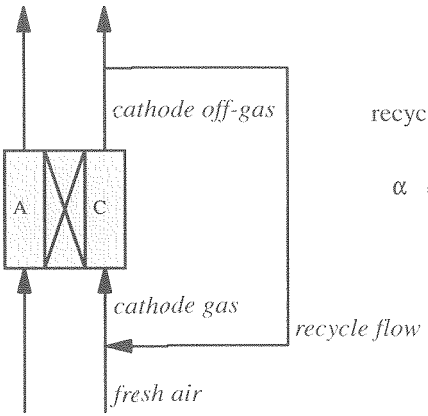

recycle ratio:

$$\alpha = \frac{\text{recycle flow}}{\text{cathode off-gas}}$$

Figure A11.1: Flows in the recycle loop and definition of the recycle ratio

Using the approximation for the recycle rate, this simplifies to:

$$(1 - \alpha)\, T_{air} + \alpha\, T_{cog} \approx T_{cat}$$

Writing α explicitly gives:

$$\alpha \approx \frac{T_{cat} - T_{air}}{T_{cog} - T_{air}} \qquad \text{(A11.2)}$$

The recycle rate is therefore determined by the temperature of the recycled cathode off-gas (cathode off-gas), the required inlet temperature of the fuel cell stack and the temperature at the outlet of the stack. If the temperatures at the in- and outlet of the fuel cell stack are fixed, this leaves only increasing the temperature of the air to the recycle loop as a method to influence the recycle ratio. However, this leads to a decrease of the recycle ratio (see **Section 9.2**), while the interest lies primarily in reducing the amount of air which has to be transferred by further increasing the recycle ratio. One way this can be achieved is by influencing the energy balance of the recycle loop by cooling the recycle flow. If heat Q is extracted from the loop, the temperature decrease in the additional cooler is equal to:

$$\Delta T_{rec} = \frac{Q}{c_p\, m_{rec}}$$

It can be shown similarly to the derivation above, that the recycle rate can be approximated by:

$$\alpha \approx \frac{T_{cat} - T_{air}}{T_{out} - T_{air} - \Delta T_{rec}} \qquad \text{(A11.3)}$$

This equation is valid, if heat is extracted from the recycle loop. An example of a system were the heat is exchanged within the cathode off-gas recycle, is the system shown in **Appendix 10**, figure A10-1c. This does not influence the energy balance in equation (A11.1) and therefore does not affect the recycle rate. Examples of systems where heat is extracted from the recycle are given in **Sections 8.2** and 9.3.

SAMENVATTING

GEAVANCEERDE EXERGIEANALYSE VAN HOGE-TEMPERATUUR BRANDSTOFCELSYSTEMEN

In dit proefschrift wordt het gedrag van hoge-temperatuur brandstofcelsystemen onderzocht, met behulp van een nieuw ontwikkelde exergieanalyse methodiek. Het proefschrift bestaat uit drie delen:

- In het eerste deel wordt een nieuwe exergieanalyse methodiek ontwikkeld. Bij deze methodiek wordt niet alleen naar het totale exergieverlies in een apparaat gekeken, maar wordt onderscheid gemaakt tussen de verschillende oorzaken van exergieverlies;
- Het tweede deel beschrijft de ontwikkeling van een brandstofcelmodel. Een gedetailleerd model wordt gebruikt om na te gaan welke factoren de prestaties van de brandstofcel bepalen. Op basis van deze kennis, is het mogelijk een sterk vereenvoudigd model te ontwikkelen voor gebruik in de systeem berekeningen;
- In het laatste deel wordt de ontwikkelde exergieanalyse methode gebruikt om verschillende brandstofcelsysteem configuraties met elkaar te vergelijken. Het onderzoek richt zich op het begrijpen van de gevolgen van veranderingen in het ontwerp van het systeem. Het gebruik van de nieuwe methodiek wordt geëvalueerd en de voor het systeemrendement meest bepalende factoren geïdentificeerd.

De brandstofcel is een enkele component in een complex systeem. Zoals deze en eerdere studies laten zien, is de systeemintegratie bepalend voor het rendement. De hoge mate van integratie van de verschillende functies van het systeem, noodzakelijk om een hoog rendement te behalen, maakt echter het optimaliseren van het systeem lastig. Het onderzoek richt zich daarom op:

- Het zichtbaar maken op welke wijze de interactie tussen de deelsystemen een eenvoudige optimalisatie bemoeilijkt;
- Nagaan welke rol exergieanalyse kan spelen bij het optimalisatie proces.

Exergieanalyse

De ontwikkelde methodiek onderscheidt in het brandstofcelsysteem 5 drijvende krachten (temperatuurverschil, drukverschil, concentratieverschil, verschil in chemische potentiaal en verschil in elektrische potentiaal). (Exergie)verliezen in het systeem zijn het gevolg van deze drijvende krachten. In het eerste deel worden verschillende manieren om de verliezen per oorzaak te berekenen uitgewerkt. Met name de verliezen als gevolg van warmte-overdracht en chemische reacties zijn van belang in het brandstofcelsysteem. De grafische methoden die in deel I worden ontwikkeld om de exergieverliezen weer te geven, richten zich daarom met name op deze verliezen.

Brandstofcelmodelering

Het gedetailleerde brandstofcelmodel wordt gebruikt om verschillende brandstofcel-configuraties (mee- en tegenstroom, interne en externe reforming, SOFC en MCFC) te evalueren. Het doel van deze berekeningen is, aan te geven welke parameters sterk bepalend

zijn voor het gedrag van de brandstofcel. Twee belangrijke parameters worden geïdentificeerd:

- De effectieve temperatuur geeft de gemiddelde temperatuur aan waarbij de elektrochemische reactie zich afspeelt en blijkt af te hangen van de verdeling van de stroomdichtheid en de temperatuur. De effectieve temperatuur is van grote invloed op de prestaties van de cel (vermogensdichtheid en celspanning);
- De temperatuur approach is het verschil tussen de maximale temperatuur in de cel en de temperatuur van het kathode afgas. Deze parameter is bepalend voor de hoeveelheid lucht die nodig is om de cel te koelen.

Een sterk vereenvoudigd model (isotherm) wordt gebruikt in de systeemberekeningen. In deel II wordt aangetoond dat, door eenvoudige correlaties voor de twee bovenstaande parameters mee te nemen in het isotherme model, de berekeningsresultaten van het vereenvoudigde en het gedetailleerde model goed met elkaar overeenkomen.

Systeemberekeningen

In het laatste deel wordt een groot aantal verschillende systeemconfiguraties geanalyseerd. Eerst worden voor twee basisvarianten van beide typen hoge-temperatuur brandstofcellen, de gesmolten carbonaat brandstofcel (MCFC) en vaste oxide brandstofcel (SOFC), in detail geanalyseerd waar de (exergie)verliezen optreden en waardoor zij veroorzaakt worden. Vervolgens wordt een groot aantal varianten van beide systemen vergeleken, waarbij de nadruk ligt op het vaststellen van de gevolgen van veranderingen in het systeemontwerp. De uitvoerige analyse leidt tot een onderscheid tussen de primaire of beoogde effecten van een ontwerpverandering en de secundaire effecten. De secundaire effecten blijken in dit proefschrift sterk samen te hangen met de 'recycles' van stof- en energiestromen in het systeem. Een verandering van de prestaties van een brandstofcelsysteem is, vanwege de secundaire effecten, veelal te beschouwen als het cumulatieve effect van een aantal primaire en secundaire effecten. Het onderzoek laat zien dat de ontwikkelde methodiek voor exergieanalyse, nuttig is bij het analyseren van verschillende configuraties. De methode biedt daarnaast een systematische methodiek om de verschillen te identificeren. Daarnaast kunnen door de gedetailleerde analyse van de exergieverliezen de verschillende primaire en secundaire verliezen zichtbaar gemaakt worden.

Ook de invloed van de integratie op systeemrendement wordt zichtbaar gemaakt met behulp van de nieuwe methodiek, waarbij onderscheid wordt gemaakt naar de oorzaak van het verlies. De verliezen als gevolg van warmteoverdracht blijken in veel gevallen ongeveer de helft van de totale verliezen uit te maken. Benutting van het overschot aan hoogwaardige warmte in het systeem, is de sleutel tot het verbeteren van het systeemrendement. Interessant is ook te constateren dat de verliezen in die apparaten waar de voornaamste energieconversies optreden (de brandstofcel, de reformer, de verbrandingskamer) op zich relatief gering zijn. Tegelijkertijd blijken veranderingen in de processen in deze apparaten, echter een sterke invloed te hebben op de rest van het systeem en daarmee op het rendement van het totale systeem.

DANKWOORD/ACKNOWLEDGEMENTS

Niet de inspiratie, maar het inspireren is het begin van de wetenschap. Geen wetenschap zonder docenten die, door hun enthousiasme, hun leerlingen of studenten inspireren na te denken over de wereld om hen heen. Ik heb gelukkig zulk onderwijs genoten. Twee docenten wil ik in het bijzonder noemen. Dat de exacte vakken mooi, nee zelfs "elegant", kunnen zijn, heb geleerd van mijn wiskundedocent op het Katholiek Gelders Lyceum, Marius Lehr. Mijn liefde voor de thermodynamica is ontstaan door de boeiende colleges van C.A.A. van Paassen.

Mijn promotor Rob Kouffeld dank ik voor het mogelijk maken van de promotie bij de vakgroep Energievoorziening in Delft. Mijn begeleider bij de vakgroep, Nico Woudstra, heeft mij het belang geleerd van de gedegen thermodynamische onderbouwing van systeemberekeningen en heeft zich door vele versies van het proefschrift heen geworsteld. Van het thermodynamisch inzicht dat professor Van Lier zo mooi wist uit te dragen, heb ik in dit werk dankbaar gebruik gemaakt. Hetzelfde geldt voor Theo Woudstra's kennis van Cycle-Tempo en de bijbehorende "tips en trucs". Teus van der Stelt heeft niet alleen grote delen van Cycle-Tempo gebouwd, maar wist het ook op steeds weer nieuwe (hardware en software) systemen in de lucht te houden. Leuke discussies over het modelleren van brandstofcellen heb ik gehad met Frans Standaert. Verschillende studenten hebben mij geholpen. In het bijzonder het modelleren van de reformer door Otger Cobben is van belang geweest voor het proefschrift.

Met mijn kamergenoten Marianne Meijer en Bart de Melker heb ik plezierig samengewerkt, onder andere aan het uitbouwen van Cycle-Tempo. Bart heeft aan dit proefschrift bijgedragen met zijn Quatro-Pro interface, Marianne met de implementeren van de exergieroutines in Cycle en met haar MCFC systeemberekeningen. Hoewel beiden daarmee een belangrijk aandeel hadden in de totstandkoming van het proefschrift, wil ik ze toch vooral bedanken voor de leuke tijd die ik met hen heb gehad.

Bij mijn huidige werkgever ECN, hebben velen mij met raad en daad bijgestaan. Allereerst natuurlijk mijn promotor Hubert Veringa. Zijn kritische commentaar heeft de kwaliteit van het proefschrift aanzienlijk verbeterd. Met veel plezier denk ik terug aan de sessies waarin ik, stap voor stap, de correctheid van mijn afleidingen mocht bewijzen. Ik dank hem voor de plezierige samenwerking en de loyaliteit. Kees van der Klein heeft mij gestimuleerd door er steeds op aan te blijven dringen, dat ik het proefschrift af zou maken. Maar ook door mij mogelijkheden te geven op kosten van ECN aan mijn proefschrift te werken. Ook Daan Jansen en Jan Willem Erisman hebben mij moreel en financieel gesteund bij de afronding van het proefschrift. Sytze van der Molen heeft waardevol commentaar geleverd op de hoofdstukken over het modelleren van de brandstofcel.
Niets heeft mij in de afgelopen sterker gestimuleerd om het proefschrift toch af te maken, dan de bijzondere groep (in wisselende samenstelling) collega's bij het ECN waar ik de afgelopen jaren mee heb mogen lunchen. Twee problematische projecten wisten mijn collega's op natuurlijke wijze steeds weer in het gesprek te weven: de Haagse Tramtunnel en mijn proefschrift. Het doet mij deugd, dat beide projecten nu toch tot een goed einde zullen komen.

Twee collega's wil ik in het bijzonder bedanken. Ruud van der Woude heeft mij als geen ander aangemoedigd om het karwei af te maken, door mij moed in te spreken als dat nodig was en door mij te vermanen als dát nodig was. Mijn kamergenoot Herman den Uil heeft mijn ups en downs met bewonderenswaardige gelijkmatigheid over zich heen laten komen. "Muziek terwijl u werkt" kwam tijdens dit project van Maarten Bracht (o.a. de Pixies en RadioHead) en mijn broer Siwert, wiens "CD voor Arend" ik grijs heb gedraaid.

Velen hebben groot geduld met mij gehad. Mijn familie en vrienden dank ik voor het geduld waarmee zij mijn verhalen aan hebben gehoord. Maar vooral omdat ze steeds de moed hebben opgebracht om te durven vragen: "hoe gaat het met je ...?". Dat gaf vertrouwen.

Mijn ouders hebben mij op vele manieren gesteund bij het vergaren van al deze kennis. Daarbij is geen geringe aanspraak gedaan op hun geld en geduld. Zij mogen tevreden constateren dat nu de kroon op het lange opleidingstraject is gezet.

Het meeste geduld heeft Myrjam gehad. Van de 15 jaar dat we bij elkaar zijn, ben ik er 12 met mijn proefschrift bezig geweest. Veel heeft zij van mij overgenomen, als ik mij weer eens op mijn proefschrift had gestort, van het verven van het huis tot het in stand houden van ons sociaal leven. Met bewondering zie ik hoe zij het mij de ruimte heeft gegeven het promoveren te combineren met het opvoeden van 2 prachtige kinderen.

CURRICULUM VITAE

Arend de Groot studied Mechanical Engineering at the Polytechnical School in Amsterdam, specializing in Natural Gas Technology. His final work, carried out at the Dutch steel mill Hoogovens (currently Corus), combined experimental and theoretical research on the flame stability of industrial natural gas burners. After completing military service working in an engineering department of the Ministry of Defence (Adviesbureau der Genie), he studied Mechanical Engineering at Delft University of Technology. His Master thesis, written at the Laboratory of Thermal Power Engineering at Delft University, consisted of a thermodynamic analysis of solid oxide fuel cell systems.

Arend de Groot initiated the work described in this thesis at the Laboratory of Thermal Power Engineering in 1992. After working on this study full-time for four years, he was employed by the Systems Assessment group at the Energy research Centre of the Netherlands (ECN), working on fuel cell systems studies. From 1998, the focus of his work has shifted towards hydrogen (and fuel cell) technology, varying in scope from specific technology assessments to developing scenario's for the introduction of hydrogen.

LIST OF SYMBOLS

Contents

General symbols

A	=	area	[m^2]
A_{cs}	=	cross-sectional area	[m^2]
A_t	=	catalyst loading	[kg/m^2]
b	=	cell width	[m]
c_P	=	heat capacity	[kJ/mole K]
e	=	specific or molar exergy	[kJ/mole]
E	=	exergy of a mixture [mole]	[kJ]
E	=	exergy of a process flow [mole/s]	[kW]
E_a	=	activation energy	[kJ/mole]
F	=	Faraday constant ($9.6485 \cdot 10^5$)	[C/mole]
g	=	specific or molar Gibbs energy	[kJ/mole]
$\Delta_r g$	=	specific reaction Gibbs energy	[kJ/mole]
G	=	Gibbs energy for a mixture [mole]	[kJ]
G	=	Gibbs energy for a process flow [mole/s]	[kW]
h	=	specific or molar enthalpy	[kJ/mole]
$\Delta_r h$	=	specific reaction enthalpy	[kJ/mole]
H	=	enthalpy of a mixture [mole]	[kJ]
H	=	enthalpy of a process flow [mole/s]	[kW]
i	=	current density	[A/m^2]
I	=	current	[A]
k_0	=	frequency factor	[-]
K_k	=	equilibrium constant for reaction k	[-]
K^*	=	mass action	[-]
m	=	mass	[kg]
n	=	number of moles	[mole]
n	=	number of moles for each component [vector]	[mole]
N	=	matrix with stoichiometric coefficients	[-]
Nu	=	Nusselt number	[-]
P	=	power	[kW]
p	=	pressure	[bar]
p_i	=	partial pressure of (chemical) component i	[bar]
p^o	=	standard pressure	[bar]
p_o	=	environment pressure (**Section 2.5**)	[bar]
Q	=	heat	[kJ]
Q	=	heat flow	[kW]
q'	=	heat flux	[kW/m^2]
r	=	reaction rate	[$mole/m^2s$]

r'	=	specific reaction rate	[mole/kg s]
R^{ci}	=	area specific resistance (ASR)	[Ωm^2]
R	=	gas constant	[kJ/mole K]
Re	=	Reynolds number	[-]
s	=	specific or molar entropy	[kJ/moleK]
$\Delta_r s$	=	specific reaction entropy	[kJ/mole]
s_i^o	=	specific or molar entropy at standard pressure	[kJ/moleK]
S	=	entropy for a mixture	[kJ/K]
S	=	entropy for a process flow	[kW/K]
ΔS_{irr}	=	entropy production as a result of irreversibility	[kW/K]
T	=	temperature	[K]
T_o	=	environment temperature	[K]
t	=	time	[s]
u	=	specific or molar internal energy	[kJ/mole]
U	=	internal energy of a mixture	[kJ]
U	=	internal energy of a process flow	[kW]
U	=	overall heat transfer coefficient	[kW/m^2K]
U_F	=	fuel utilisation	[-]
U_{OX}	=	oxidant utilisation	[-]
v	=	specific or molar volume	[m^3/mole]
V	=	volume	[m^3]
V	=	volume flow	[m^3/s]
V	=	cell voltage	[V]
V_{rev}	=	reversible voltage or Nernst voltage	[V]
V_{rev}^o	=	reversible voltage at standard conditions	[V]
ΔV	=	voltage loss	[V]
W	=	work	[kJ]
$\Delta \mathbf{W}$	=	lost work	[kJ]
x_i	=	mole fraction for component i	[mole/mole]
$\underline{x}$	=	mole fraction [vector]	[mole]
z	=	number of electrons transferred per mole reacted	[-]

Greek symbols

α	=	heat transfer coefficient	[W/m^2K]
ε	=	reaction coordinate[g]	[mole]
ε	=	reaction coordinate[1] for a flow	[mole/s]
η	=	efficiency	[-]
η	=	overpotential	[-]
λ	=	thermal conductivity	[W/mK]
μ_i	=	thermodynamic potential	[kJ/kg]
$\nu_{i,k}$	=	stoichiometric number[1] for component i in reaction k	[mole/mole]
$\Delta\nu_k$	=	stoichiometric change in number of moles[1] in reaction k	[mole/mole]
ρ	=	density	[kg/m^3]
φ	=	total mole flow	[mole/s]
φ_i	=	mole flow for component i	[mole/s]
$\varphi_{eq.H2}$	=	hydrogen equivalent mole flow ($=\varphi_{H2} + \varphi_{CO} + 4\ \varphi_{CH4}$)	[mole/s]

---

[g] see **Section 2.3** for a definition of the reaction coordinate

Subscripts, superscripts and notations

indices:

i,j	summation over chemical components
k	summation over chemical reactions
ℓ	summation over elements

m	= specific thermodynamic property (per mole)
M	= thermodynamic property of a mixture (for n [mole])
M	= thermodynamic property of a flow (for φ [mole/s])
x	= mole fractions for components i=1,n [mole/mole]
φ	= mole flows for components i=1,n [mole/s]

subscripts

f	=	formation
F	=	fuel
irr	=	irreversible
o	=	environment conditions
OX	=	oxidant
rct	=	reaction
rev	=	reversible

superscripts

o	=	at reference conditions (pressures, temperature)
T	=	transposed matrix or vector (rows and columns are exchanged)
*	=	at reference conditions

Special symbols used in the exergy analysis (**part I**)

e^o_o	=	exergy of the pure environment components at p_o and T_o	[kJ/mole]
e^o_{el}	=	exergy of the pure elements at p_o and T_o	[kJ/mole]
e^o_s	=	exergy of the pure system components at p_o and T_o	[kJ/mole]
E_Q	=	exergy of heat	[kJ]
E_e	=	exergy of an energy flow	[kJ]
E^{ch}	=	chemical energy	[kW]
E^{tm}	=	thermo-mechanical energy	[kW]
ΔE	=	exergy change of a mixture	[kJ]
ΔE_L	=	exergy loss in a process	[kJ]
f	=	Carnot factor (exergy/energy ratio)	[-]
f_e	=	Carnot factor for an energy flow	[-]
f_p	=	Carnot factor for a process flow	[-]
f_Q	=	Carnot factor for a heat flow	[-]

H^{ch}	=	chemical energy	[kW]
H^{tm}	=	thermo-mechanical energy	[kW]
x_o	=	mole fractions components environment	[mole/mole]
x_s	=	mole fractions components system	[mole/mole]

superscripts

ch	=	chemical reaction
el	=	electrical
fr	=	friction
ht	=	heat transfer
mx	=	mixing

Special symbols used in the fuel cell model (**part II**)

general

d	=	(cell) thickness	[m]
i_m	=	average (mean) current density	[A/m^2]
I_F	=	theoretical cell current at U_f =1	[A]
L	=	cell length	[m]
s_k	=	safety factor for carbon deposition through reaction k	[-]
R^{eff}	=	effective temperature cell resistance	[K]
$T_{iso.}$	=	temperature used in the isothermal model	[K]
T^{eff}	=	effective temperature (see **Section 5.3.2**)	[K]
T^{in}_a	=	temperature of anode flow at inlet of the fuel cell	[K]
T^{in}_c	=	temperature of cathode flow at inlet of the fuel cell	[K]
T^{out}_a	=	temperature of anode flow at inlet of the fuel cell	[K]
T^{out}_c	=	temperature of cathode flow at inlet of the fuel cell	[K]
V_o	=	open cell voltage or open circuit voltage	[V]

symbols referring to cross section x

I_x	=	current in cell between x=0 and x=x	[A]
ΔV_x	=	voltage loss in fuel cell in the cross section	[V]

symbols referring to a subcell

$\Delta^j A$	= area of a subcell	[m^2]
I^j	= current generated in the subcell	[K]
P^j	= power generated in the subcell	[K]
Q^j_a	= heat transferred to the anode flow in the subcell	[K]
Q^j_c	= heat transferred to the anode flow in the subcell	[K]
Q^j_e	= heat generated in the electrochemical reaction in the subcell	[K]
Q^j_r	= heat generated in the reforming reaction in the subcell	[K]
Q^j_s	= heat generated in the shift reaction in the subcell	[K]
r^j	= average rate of reaction in the subcell	[mole/m^2 s]
T^j_a	= temperature of anode flow at inlet in the subcell	[K]
T^{j+1}_a	= temperature of anode flow at inlet in the subcell	[K]
ΔT^j_a	= temperature increase of anode flow in the subcell	[K]
T^j_c	= temperature of the cathode flow at the inlet of the subcell	[K]
T^{j+1}_c	= temperature of the cathode flow at the outlet of the subcell	[K]
ΔT^j_c	= temperature increase of the cathode flow in the subcell	[K]
T^j_e	= average temperature of the electrolyte in the subcell	[K]

V^j_{rev}	= average reversible (Nernst) voltage in the subcell	[K]
$\Delta^j\varepsilon_c$	= change in reaction coordinate for the electrochemical reaction	[mole/s]
$\Delta^j\varepsilon_r$	= change in reaction coordinate for the reforming reaction	[mole/s]
$\Delta^j\varepsilon_s$	= change in reaction coordinate for the shift reaction	[mole/s]

Abbreviations: general

A/F-ratio	=	air/fuel ration [kg/kg]
aog(r)	=	anode off-gas (recycle)
CEC	=	compressor/expander combination
CHP	=	combined heat and power
cog(r)	=	cathode off-gas (recycle)
DIR	=	direct internal reforming
ER	=	external reforming
fp	=	fuel processing
IIR	=	indirect internal reforming
MCFC	=	molten carbonate fuel cell
PEN	=	cathode/electrolyte/anode composite[h)]
SOFC	=	solid oxide fuel cell
whb	=	waste heat boiler

[h] PEN = Positive electrode/Electrolyte/Negative electrode